University of Sussex

A University of Sussex PhD thesis

Available online via Sussex Research Online:

http://sro.sussex.ac.uk/

This thesis is protected by copyright which belongs to the author.

This thesis cannot be reproduced or quoted extensively from without first obtaining permission in writing from the Author

The content must not be changed in any way or sold commercially in any format or medium without the formal permission of the Author

When referring to this work, full bibliographic details including the author, title, awarding institution and date of the thesis must be given

Please visit Sussex Research Online for more information and further details

The influence of APOE isoform on everyday memory and the hippocampal c-Fos response

Alexander Cameron Stuart

A thesis submitted for the

degree of DPhil in Neuroscience

at the University of Sussex, United Kingdom

January 2022

Declaration

I hereby declare that this thesis has not been and will not be submitted in whole or in part to another University for the reward of any other degree.

Abstract

Apolipoprotein E (APOE) is a key mediator of lipid homeostasis within the periphery and CNS. Of the primary allelic isoform variants of APOE (APOE2, APOE3, APOE4), APOE4 increases the risk of late-onset Alzheimer's disease (LOAD).

APOE4 is associated with long-term episodic memory dysfunction in mouse models, but there is little investigation of rapid acquisition of 'everyday memory', formed over short timescales (minutes to hours). Further, while evidence suggests that APOE4 disrupts neuronal function via multiple mechanisms, the effect of APOE on the activity of 'neuronal ensembles', sparse groups of activated neurons crucial for behaviour, has yet to be investigated.

This thesis aimed to assess the influence of APOE isoform, age, and sex on trajectories of everyday memory, while in parallel, the influence of these same factors on hippocampal neuronal ensemble activation following behaviour. These questions were addressed using APOE targeted replacement mice, first with longitudinal assessment using an everyday memory maze task, and second via immediate-early gene (IEG) measurements following environmental novelty.

Our results highlighted age, sex, and APOE isoform-dependent interactions in everyday memory, namely with E4-TR mice exhibiting impairments in early-age learning, mid-aged memory accuracy, and late-age learning in female mice. We suggest mild APOE-dependent differences in everyday memory may be superseded by longer-term episodic memory impairments.

In parallel, we observed an enhanced hippocampal CA1 ensemble size in E4-TR mice from young-to-mid age. Further, this was accompanied by genotype-sex interactions in hippocampal IEG network correlations, putative GABAergic innervation, IEG and APOE mRNA expression. Finally, the APOE4 CA1 ensemble size increase was not associated with changes in dendritic spine density or spine 'synaptic occupation'.

We suggest these results reflect early and diverse phenotypic effects of APOE4 on hippocampal function. Further investigation of the underlying cell and circuit-level mechanisms which induce mild cognitive effects decades prior to extensive pathology is needed.

Acknowledgements

Despite being able to write more than 80,000 words about APOE, it is impossible for me to fully put into words the gratitude and admiration I have for those who have made this possible.

First, I would like to thank my supervisor Dr Sarah King. Her continual support throughout my PhD has been fundamental to my development as a researcher. From help with experimental design, data analysis, and writing, your input has been exceptional.

I would like to thank my co-supervisor and assessor Prof Jenny Rusted and Dr Eisuke Koya. Particular mention goes to both Eisuke and Dr Andy Penn for sharing reagents and equipment, providing input on experimental design, advice on working in academia and asking the 'hard questions' to put my work into perspective.

I would like to thank the members of the Hafezparast lab, particularly Dr Greig Joilin, Dr Fabio Simoes, and Dr Matin Hemati for teaching me multiple biochemical techniques without ever once complaining. I want to extend my thanks especially to Dr Greig Joilin, with whom I have only half-jokingly implied should be my second supervisor. Greig is an excellent scientist and an even better friend, and I am truly grateful.

Thank you to my lab partner Cansu and lab-adjacent partner Oli for all your help and friendship across the PhD, you will be writing the equivalent of this sentiment soon, I'm sure. Best of luck and you can do it! Thanks also to Jack for keeping me sane, making me laugh, and being generally a great friend.

I would also like to thank Sussex neuroscience for funding my PhD and providing opportunities for growth. Particular thanks to Ruth Staras on the SN committee, who has never once failed to offer support and put out numerous fires while allowing us to focus on our research. Thank you also to all the animal unit staff who have taken care of our colonies day and night to make our experiments possible.

I would like to thank my parents and family, who have always been there and believed in me. Mum and Dad, thank you for everything.

Last, I would like to dedicate this thesis to my partner, Liane. Liane, you have given me nearly a decade of support and without you, none of this would have been possible. I cannot express how grateful I am for your love, patience, and unfaltering faith. Thank you.

Abbreviations

aBM: Adapted Barnes maze, aCSF: Artificial cerebrospinal fluid, ActB: Beta Actin, AFC: Alternative forced choice, Akt: Akt/Protein kinase B, ANOVA: Analysis of variance, AP-2: Activator protein 2, Ap5: (2R)-amino-5-phosphonovaleric acid, APOCI: Apolipoprotein C1, APOCI': Apolipoprotein C1', APOCII: Apolipoprotein C2, APOCIV: Apolipoprotein C4, APOE: Apolipoprotein E, APOE-KI: Apolipoprotein knock-in mice, Arc: Activity-regulated cytoskeleton-associated protein, Arg-61-APOE: Arginine 61 mAPOE mouse, BP: Base pair, BSN: Bassoon, CA: Cornu ammonis, CAMKII: Calmodulin-dependent protein kinase II, cAMP: cyclic adenosine monophosphate, CD90: Cluster of differentiation 90 (Thy1), cDNA: Complementary DNA, CFC: Contextual fear conditioning task, c-Fos: Fos FBJ osteosarcoma oncogene, c-Jun: JUN proto-oncogene AP-1 transcription factor subunit, Cnqx: cyanquixaline , CPSF4: Cleavage and Polyadenylation Specific Factor 4, CRE: Cre recombinase, CREB: Cyclic adenosine monophosphate response element binding protein, Ct: Threshold cycle, DAPI: 4', 6-diamidino-2-phenylindole, DGH: Dentate gyrus hilus, DGI: Dentate gyrus inferior, DGS: Dentate gyrus superior, DiI: 1, 1'-Dioctadecyl-3, 3, 3', 3'-Tetramethylindocarbocyanine Perchlorate, DiO: DiOC18(3) (3, 3'-Dioctadecyloxacarbocyanine Perchlorate), Dlx: Homeobox protein DLX, DMTP: Delayed match to place, DNA: Deoxyribonucleic acid, E2-TR: APOE2 targeted replacement, e3: APOE3, E3-TR: APOE3 targeted replacement, e4: APOE4, E4-TR: APOE4 targeted replacement, EDTA: Ethylenediaminetetraacetic acid, EHC: Entorhinal cortex, EPSP: Excitatory postsynaptic potential, FDR: False discovery rate, GFP: Green fluorescent protein , GSK-3B: Glycogen synthase kinase 3 beta, hAPOE: Human Apolipoprotein E, HCC: Home cage control, HFS: High frequency stimulation, IEG: Immediate-early gene, IF: Immunofluorescence, IPSP: Inhibitory postsynaptic potential, IR: Immunoreactivity, ITI: Inter-trial interval, LEHC: Lateral entorhinal cortex, L-LTP: Late phase long term potentiation , LRP8: Low density lipoprotein receptor related protein 8, L-VGCC: L-type voltage gated calcium channels, MAPT: Microtubule associated protein tau, mBM: Multi-hole Barnes maze, MGE: Medial ganglionic eminence , mRNA: Messenger RNA, MTO1: Mitochondrial TRNA Translation Optimization 1, MWM: Morris water maze, NCE: Novel context exposure, NGS: Normal goat serum, No-RT: No reverse transcription control, NTC: No template control, PBS: Phosphate buffered saline, PBST: PBS-Triton/Tween, pCAMKII: Phospho-CAMKII, PCR: Polymerase chain reaction, pCREB: Phospho-CREB, pERK: Phosho-ERK, PI3K: Phosphoinositide-3-kinase, PLA: Polylactic acid, PTM: Post translational modification , RFLP: Restriction fragment length polymorphism, RIPA: Radioimmunoprecipitation assay buffer, RNA: Ribonucleic acid, RT-qPCR: Reverse transcription quantitative polymerase chain reaction, SEM: Standard error of the mean, SNP: Single nucleotide polymorphism, SNT: Simple neurite tracer, SOR: Spatial object recognition task, SP-1: Stimulatory protein 1, ssRNA: Single strand RNA, Sub: Subiculum, SWR: Sharp wave ripple, Syn1: Synapsin 1, TAE: Tris acetate EDTA, TBE: Tris borate EDTA, TOMM40: Translocase of outer mitochondrial membrane 40, TRMU: tRNA Mitochondrial 2-Thiouridylase, UV: Ultraviolet, VGLUT1: Vesicular glutamate transporter 1, vLDLR: Very-low density lipoprotein receptor, WT: Wildtype, , Ab: Beta-amyloid; ABCA1: ATP binding cassette transporter 1, AD: Alzheimer's disease, Akt: AKT serine/threonine kinase 1, AMPAR: α-amino-3-hydroxy-5-methyl-4-isoxazolepropionic acid receptor, AP-1: Activator protein 1, APOE-KO: Apolipoprotein E knock-out, ApoER2: APOE receptor 2, APOE-TR: APOE targeted replacement, APP: Amyloid precursor protein, BBB: Blood-brain barrier, CBF: Cerebral blood flow, CBV: Cerebral blood volume, CDS: Coding sequences, CNS: Central nervous system, CSF: Cerebrospinal fluid, DEGs: Differentially expressed genes, DG GCL: Dentate gyrus granule cell layer, DG SGZ: Dentate gyrus sub-granular zone, DG: Dentate gyrus, eEF2: Eukaryotic elongation factor 2, ER: Endoplasmic reticulum , ERK1/2: Extracellular signal regulated kinase 1/2, FAD: Familial Alzheimer's disease, GABA: Gamma aminobutyric acid, GABA-INs: GABAergic interneurons, GAD-67: Glutamic acid decarboxylase 67, GFAP-APOE: Glial fibrillary acidic protein APOE model,

GFP-APOE: Green fluorescent protein APOE model, GluA1: Glutamate receptor ionotropic AMPAR subunit 1, GluA2: Glutamate receptor ionotropic AMPAR subunit 2, GluN1: Glutamate receptor ionotropic NMDAR subunit 1, HDL: High density lipoprotein, HSPG: Heparan-sulphate proteoglycans, IDL: Intermediate density lipoprotein, IPSC: Induced pluripotent stem cells, LDL: Low density lipoprotein, LDLR: Low density lipoprotein receptor, LOAD: Late onset Alzheimer's disease, LPS: Lipopolysaccharide, LRP: Low density lipoprotein receptor related protein, LTP: Long term potentiation, LXR/RXR: Liver X-receptor Retinoid X-receptor, mAPOE: Murine APOE, miR: Micro-RNA, NMDAR: N-methyl-D-aspartate receptor, NSE-APOE: Neuron-specific enolase APOE model, PS1: Presenilin 1, PS2: Presenilin 2, PSD-95: Post-synaptic density 95, RAP: Receptor-associated protein, shRNAs: Short hairpin RNAs, Src: SRC non-receptor tyrosine kinase, TBI: Traumatic brain injury, VLDL: Very low-density lipoprotein, TREM2: Triggering receptor on myeloid 2 cells

Table of Contents

Abstract iii

Acknowledgements iv

Abbreviations v

Table of Contents vii

List of Figures xiv

List of Tables xvii

CHAPTER ONE 1

An introduction to episodic memory, Apolipoprotein E and associated neurocognitive phenotypes. 1

1.1 Episodic memory and the hippocampal memory system 2

1.1.1 Spatial memory and allocentric-egocentric reference frames 3

1.1.2 Hippocampal neuroanatomy 5

1.1.3 The hippocampus and declarative memory 9

1.2 Ageing, episodic memory, and Alzheimer's disease 12

1.2.1 Risk factors for and aetiology of Alzheimer's disease 14

1.3 Introduction to Apolipoprotein E (APOE): gene nomenclature, protein structure, function, and associated model systems 16

1.3.1 APOE allelic isoforms and basic protein structure 16

1.3.2 APOE expression, regulation and function 19

1.3.3 Isoform specific modulation of lipoprotein homeostasis: Structure-function relationships 24

1.3.4 Isoform modulation of APOE expression 25

1.3.5 Murine APOE homology and mouse models of APOE function 26

1.4 Leveraging preclinical models of APOE function to study AD-dependent and AD-independent phenotypic effects. 30

1.5 Influence of APOE isoform on neuronal structure and function in preclinical models of APOE function. 32

1.5.1 Global neuroanatomical changes associated with APOE isoform 33

1.5.2 GABAergic neurodegeneration associated with APOE isoform 34

1.5.3 Neuronal morphological changes associated with APOE isoform 36

1.5.4 APOE isoform modulation of synapse loss 38

1.5.5 APOE isoform and synaptic plasticity..... 40

1.5.6 APOE isoform, ApoE signalling and calcium homeostasis: Implications for synaptic function 42

1.6 Influence of APOE isoform on episodic-like learning and memory in APOE mouse models. 44

1.6.1 Early to mid-age alterations of reference memory in APOE mouse models 49

1.6.2 Late-age alterations of reference memory in APOE mouse models..... 51

1.6.3 Alterations to short-term spatial memory and rapid place learning in APOE mouse models..... 52

1.6.4 Caveats and conclusions from the episodic memory literature in APOE mouse models..... 53

1.7 Summary and primary objectives 57

CHAPTER TWO 59

General methodology 59

2.1 Animals and PCR genotyping 60

2.1.1 Animal maintenance 60

2.1.2 Genotyping of animals 60

2.2 Tissue handling and assay design 66

2.2.1 Processing of tissue for histochemical and biochemical analyses 66

2.2.2 Microscopy..... 72

2.2.3 Tissue preparation for biochemical analyses..... 73

2.2.4 Reverse transcription quantitative PCR (RT-qPCR) 77

CHAPTER THREE 88

Establishing a behavioural assay for the longitudinal assessment of rapid place learning in wildtype and APOE-TR mice 88

3.1 Experiment one 89

3.1.1 Introduction: Experiment one 89

3.1.2 Methods 92

3.1.3 Results 108

3.1.4 Discussion 118

3.1.5 Conclusion 122

3.2 Experiment two 123

3.2.1 Introduction: Experiment two 123

3.2.2 Methods 124

3.2.3 Results 144

3.2.4 Experiment two: Discussion 163

3.2.5 Conclusion 167

3.3 Experiment three 168

3.3.1 Introduction: Experiment three 168

3.3.2 Methods 168

3.3.3 Results 173

3.3.4 Discussion 186

3.3.5 Chapter summary 189

CHAPTER FOUR 190

Characterising the effect of APOE isoform on rapid place learning and memory across the lifespan in the APOE-TR mouse model 190

4.1 Introduction 191

4.2 Methods 192

4.1.1 Design 192

4.1.2 Animals 194

4.1.3 Apparatus 196

4.1.4 Experimental procedures 196

4.1.5 Analysis 196

4.1.6 Statistical analysis 197

4.3 Results 199

4.3.1 Rapid place learning acquisition in APOE-TR mice across the lifespan 199

4.3.2 Rapid place learning retrieval performance in APOE-TR mice across the lifespan.. 211

4.3.3 Rapid place learning reinforcement and extended retrieval delay in APOE-TR mice across the lifespan 218

4.4 Discussion 227

4.4.1 Rapid place learning acquisition performance across the lifespan of APOE-TR mice 227

4.4.2 Rapid place memory retrieval across the lifespan of APOE-TR mice 228

4.4.3 Rapid place learning and memory during variable ITI and reinforcement trials 229

4.4.4 Results summary 230

4.4.5 Interpreting dissociations between measures 233

4.4.6 Normative performance and age-related decline in everyday learning and memory 235

4.4.7 Interpretations within the current framework of the APOE isoform-dependent influence on spatial learning and memory in the APOE-TR mouse model 236

4.4.8 Neurophysiological mechanisms of everyday memory and potential influence of APOE isoform 240

4.4.9 Neuronal ensemble function and susceptibility to pathology 243

4.4.10 Caveats 244

4.5 Chapter four summary and conclusion 246

CHAPTER FIVE 247

The influence of APOE isoform on the hippocampal c-Fos response in APOE-TR mice 247

5.1 Introduction 248

5.2 Methods 253

5.2.1 Design 253

5.2.2 Animals 253

5.2.3 Procedure 256

5.2.4 Experiment one: Immunofluorescence imaging of the hippocampal c-Fos response in APOE-TR mice 256

5.2.5 Experiment two: Analysis of DG hilar interneuron loss across the lifespan of APOE-TR mice 258

5.2.6 Experiment three: Quantification of whole hippocampal c-Fos mRNA response in APOE-TR mice 259

5.2.7 Analysis 259

5.3 Results 261

5.3.1 Experiment one: Immunofluorescence imaging of the hippocampal c-Fos response 261

5.3.2 Hippocampal interneuron c-Fos activation in APOE-TR mice 272

5.3.3 GAD-67 immunoreactivity in APOE-TR mice 276

5.3.4 Experiment two: Analysis of DGH interneuron loss across the lifespan of APOE-TR mice 286

5.3.5 Exploratory analyses: Network correlation analysis of Fos+ neuron density across hippocampal subregions in APOE-TR mice. 289

5.3.6 Experiment three: Quantification of whole hippocampal c-Fos and APOE mRNA response in APOE-TR mice 294

5.4 Discussion 300

5.4.1 Hippocampal c-Fos activity: Potential mechanisms - Local GABAergic disinhibition within the trisynaptic circuit 306

5.4.2 Hippocampal c-Fos activity: Potential mechanisms - Disruption of excitatory inputs to the trisynaptic circuit 308

5.4.3 Hippocampal c-Fos activity: Potential mechanisms - Intrinsic properties and susceptibility of CA1-CA3 to APOE-related pathological processes 310

5.4.4 Alterations to hippocampal c-Fos mRNA expression 312

5.4.5 Alterations to hippocampal APOE mRNA expression 314

5.4.6 Caveats 316

5.5 Chapter five summary and conclusion 318

CHAPTER SIX 319

The influence of APOE isoform on dendritic integrity and synaptic occupation in a CA1 neuronal ensemble in young APOE-TR mice 319

6.1 Introduction 320

6.2 Methods 322

6.2.1 Design 322

6.2.2 Animals 322

6.2.3 Procedure 324

6.2.4 Lipophillic carbocyanine dye labelling 325

6.2.5 Immunofluorescence 327

6.2.6 Microscopy 327

6.2.7 Immunofluorescence image analysis 329

6.2.8 Statistical analysis 333

6.3 Results 334

6.3.1 Experiment one: Validation of enhanced CA1 ensemble size in young E4-TR mice. 334

6.3.2 Experiment two: Assessment of CA1 Bassoon presynaptic protein immunoreactivity 336

6.3.3 Experiment three: Assessment of CA1 dendritic spine density and synaptic occupation in Fos+ and Fos- neurons in young APOE-TR mice 338

6.4 Discussion 342

6.4.1 Variability and age-dependence of CA1 pyramidal neuron dendritic integrity in APOE-TR mice 343

6.4.2 CA1 ensemble dendritic integrity and occupation in APOE-TR mice and the potential role of experience-dependent plasticity 343

6.4.3 Caveats 345

6.5 Chapter six summary and conclusion 347

CHAPTER SEVEN 348

General discussion 348

7.1 Background and scope of the thesis 349

7.2 Summary of findings 350

7.3 Caveats and limitations 354

7.4 Implications, significance, and future work 356

7.5 Conclusions 358

References 359

APPENDIX 391

List of Figures

Figure 1.1: Simplified representation of the rodent hippocampal trisynaptic circuit 8
Figure 1.2: Representation of APOE structure 18
Figure 1.3: Simplified representation of canonical APOE trafficking pathway.. 23
Figure 2.1: Example electropherogram output from the total RNA 76
Figure 2.2: Flow diagram demonstrating qPCR reference gene selection process.. 81
Figure 2.3: Formula used to calculate reaction efficiency for qPCR standard curves 84
Figure 2.4: Standard and dissociation curves for gene targets in qPCR assays 85
Figure 3.1.1: Apparatus design for the adapted Barnes maze (aBM)..... 95
Figure 3.1.2: Diagrammatic example of 1-AFC/5-AFC encoding-retrieval task structure..... 100
Figure 3.1.3: Formula used to calculate performance index (PI) 105
Figure 3.1.4 panel 1: Primary results of performance of WT mice in the aBM task..... 110
Figure 3.2.1: Multi-hole Barnes maze (mBM) design and cue configuration. 127
Figure 3.2.2: mBM task procedure flow diagram.. 129
Figure 3.2.3: Diagrammatic example of mBM standard encoding and retrieval trial structure.. 132
Figure 3.2.4: Formulas used to calculate measure variables..... 139
Figure 3.2.5: Representation of absolute and relative locations of target and foil positions on the mBM task.. 142
Figure 3.2.6: Cross correlation plots of primary measures and velocity 147
Figure 3.2.7: Rapid place learning performance in the mBM task during training, probe, and control trials.. 151
Figure 3.3.1: Characterisation of measure variable relationships in APOE-TR mice during mBM task training 174
Figure 3.3.2: Validation of primary acquisition measures in APOE-TR mice using the mBM ... 179
Figure 3.3.3: Performance during extra-maze occlusion and intra-maze control trials in APOE-TR mice in the mBM task.. 184
Figure 4.1: Average path length to target from 3-18 months of age in APOE-TR mice in the mBM task grouped by genotype and sex. 201
Figure 4.2: Primary search errors to target from 3-18 months of age in APOE-TR mice in the mBM task grouped by genotype and sex. 204
Figure 4.3: Average learning index during training (T2-T4) from 3-18 months of age in APOE-TR mice in the mBM task grouped by genotype and sex..... 209

Figure 4.4: Measures of retrieval performance in APOE-TR mice from 3-18 months in the mBM task. ..... **Error! Bookmark not defined.**
Figure 4.5: Acquisition performance during manipulation trials in APOE-TR mice in the mBM task. 219
Figure 4.6: Retrieval performance during manipulation trials in APOE-TR mice in the mBM task. 222
Figure 4.7: Average movement velocity during training in APOE-TR mice from 3-18-months in the mBM task. 225
Figure 5.1: Average proportion of NeuN+/Fos+ neuron counts, GAD-67+/Fos+ interneuron, and NeuN+ counts in primary hippocampal subregions in APOE-TR mice. 263
Figure 5.2: Average Fos+ neuron counts in the CA1 pyramidal layer grouped by APOE genotype and condition. 265
Figure 5.3: Average Fos+ neuron counts in the CA3 pyramidal layer grouped by APOE genotype, condition, and sex. 267
Figure 5.4: Average Fos+ neuron counts in the DGS granule cell layer grouped by condition, sex, and age. 269
Figure 5.5: Average Fos+ neuron counts in the DGI granule cell layer grouped APOE genotype. 271
Figure 5.6: Average Fos+/GAD+ neuron counts in the CA1 pyramidal layer grouped by condition. 273
Figure 5.7: Average Fos+/GAD+ neuron counts in the CA3 pyramidal layer grouped by APOE genotype and age. 275
Figure 5.8: Average GAD-67 immunoreactivity (IR) in the CA1 pyramidal cell layer of APOE-TR mice grouped by APOE genotype and sex. 277
Figure 5.9: Average GAD-67 immunoreactivity (IR) in the CA3 pyramidal cell layer of APOE-TR mice grouped by age. 279
Figure 5.10: Average GAD-67 immunoreactivity (IR) in the DGS granule cell layer of APOE-TR mice grouped by APOE genotype and sex.. 281
Figure 5.11: Average GAD-67 immunoreactivity (IR) in the DGI granule cell layer of APOE-TR mice grouped by APOE genotype and sex. 283
Figure 5.12: Average GAD-67 immunoreactivity (IR) in the DG hilar (DGH) layer of APOE-TR mice grouped by APOE genotype and sex. 285
Figure 5.13: Average DGH GAD-67+ interneuron density across the lifespan of APOE-TR mice grouped by APOE genotype, age, and sex. 287

Figure 5.14: Correlation matrix heat maps of Fos+ neuron density in CA1-CA3-DG network in APOE-TR mice. 290
Figure 5.15: Correlation matrix heat maps of Fos+ neuron density in CA1-CA3-DG network in APOE-TR mice, grouped by genotype and sex. 292
Figure 5.16: Average DDCt of c-Fos and APOE mRNA from hippocampal samples of APOE-TR mice at 3-12-months 296
Figure 6.1: Example fluorescence images from DiO neuron tracing and immunofluorescent co-labelling of c-Fos and DAPI, grouped by cell type (Fos+/Fos-) in the basal shaft of CA1 pyramidal neurons of APOE-TR mice. 331
Figure 6.2: Average Fos+ neuron density in the CA1 pyramidal layer of APOE-TR mice grouped APOE genotype 335
Figure 6.3: Average Bassoon immunoreactivity in the CA1 pyramidale and oriens layer of APOE-TR mice, grouped APOE genotype. 337
Figure 6.4: Average spine density and spine occupation in Fos+ and Fos- CA1 pyramidal neuron basal dendrites of APOE-TR mice 339

List of Tables

Table 1.1: Table summarising primary APOE mouse models 29
Table 1.2: Table summarising primary findings from the literature in assessments of episodic-like learning (acquisition) and memory (retrieval) in APOE mouse models.. 46
Table 2.1: Details of primers used for individual genotyping reactions in APOE-TR and WT mice. 64
Table 2.2: Thermocycler conditions used for PCR genotyping protocols in APOE-TR and WT mice..... 65
Table 2.3: Reagent details, supplier, dilution/concentration, and incubation times used in experiments 70
Table 2.4: Details of antibody parameters used for immunofluorescence experiments performed in Chapters five and six.. 71
Table 2.5: RNA integrity assessed via Bioanalyser during experiments conducted in Chapter five..... 75
Table 2.6: Details and properties of primers used for RT-qPCR experiments conducted in Chapter five..... 79
Table 2.7: Thermocycler conditions used for each gene target for RT-qPCR experiments conducted in Chapter five..... 84
Table 3.1.1: Individual training phases and trial description for the aBM task. 101
Table 3.1.2: Statistical analyses performed in the aBM task..... 116
Table 3.2.1: Details of trial types and training procedure used in the mBM task in experiment two. 135
Table 3.2.2: Measure variable names and description of variables used in the mBM task in experiment two..... 138
Table 3.2.3: Pearson correlation coefficients and for automated and blind latency ratings ... 145
Table 3.2.4: Correlation between primary measures and velocity..... 148
Table 3.2.5: Statistical analyses performed of mBM performance in WT mice in experiment two. 160
Table 3.3.1: Sample characteristics of APOE-TR mice at 3-months of age during experiment three..... 169
Table 3.3.2: Inter-measure correlations from training data generated at 3-months in APOE-TR mice in experiment three.. 175
Table 3.3.3: Correlations between strategy subtypes and search errors at 3-months in APOE-TR mice in experiment three. 175

Table 3.3.4: Correlations between place preference and search errors from T2 and T5 probe trials at 3-months in APOE-TR mice in experiment three.. 176
Table 3.3.5: Statistical analyses performed in experiment three for primary measures of acquisition and retrieval performance. 181
Table 3.3.6: Statistical analyses performed in experiment three during extra-maze occlusion and intra-maze control trials. 185
Table 4.1: Outline of time points and task design in the experiments in Chapter four. 193
Table 4.2: Sample characteristics of APOE-TR mice across each age during experiments conducted in Chapter four. 195
Table 4.3: Robust linear mixed model of within-day learning in primary path length and search errors from 3-18 months in APOE-TR mice. 206
Table 4.4: Robust linear mixed model analysis of learning index from 3-18 months in APOE-TR mice. 210
Table 4.5.1: Robust linear mixed model analysis of separation accuracy and place preference from 3-18 months in APOE-TR mice. 216
Table 4.5.2: Robust linear mixed model analysis of separation accuracy at individual ages from 3-18-months in APOE-TR mice.. 217
Table 4.6: Robust linear mixed model analysis of learning index during T5 probe and 4/12-hour ITI manipulation trials from 3-18 months in APOE-TR mice. 220
Table 4.7: Robust linear mixed model analysis of place preference and separation accuracy during T5 probe trials from 3-18 months in APOE-TR mice. 223
Table 4.8: Robust linear mixed model analysis of movement velocity during training from 3-18 months in APOE-TR mice. 226
Table 4.9: Summary of results of Chapter four. 232
Table 5.1: Sample characteristics of APOE-TR mice allocated to each condition in experiment one & three from Chapter five. 254
Table 5.2: Outline of animal numbers allocated to each condition in experiment two from Chapter five. 255
Table 5.3: Statistical analyses of hippocampal c-Fos and APOE mRNA in APOE-TR mice in experiment three from Chapter five. 298
Table 5.4: Correlation analysis of hippocampal c-Fos and APOE mRNA in APOE-TR mice in experiment three from Chapter five. 299
Table 5.5: Summary of results from experiments one and two conducted in Chapter five.... 304
Table 5.6: Summary of results from experiment three conducted in Chapter five. 305

Table 6.1: Sample characteristics of APOE-TR mice allocated to each experimental condition comprising experiments 1-3 in Chapter six. 323
Table 6.2: Statistical analyses of CA1 dendritic spine density and occupation in Fos+ and Fos- pyramidal neurons in APOE-TR mice at 3-months of age in experiment three from Chapter six. 341

CHAPTER ONE

An introduction to episodic memory, Apolipoprotein E and associated neurocognitive phenotypes.

1.1 Episodic memory and the hippocampal memory system

The ability to encode, store and retrieve information from a dynamic external environment is a fundamental principle of the evolution of the central nervous system (CNS) across many complex organisms, comprising learning and memory (Otgaar & Howe., 2013). A central feature of memory is the ability to retain relevant experience-dependent information so as to flexibly adapt a behavioural system in the service of a functional outcome such as enhancing probability of survival (Nairne & Pandeirada., 2016; Otgaar & Howe., 2013). Decades of research within the fields of psychology and neuroscience have provided a basic framework for memory system classification which can be viewed simplistically as 'declarative' and nondeclarative or 'procedural' memory systems. However, further subdivisions and the behaviours supported by such are more complex and diverse than a simple dichotomy would suggest (Tulving., 1972; Squire et al., 2004).

Declarative memory is one of the most heavily researched cognitive domains, named so because of its principle meaning of the formation, maintenance and effective retrieval of 'declarable' information often referred to as 'facts and events memory' (Tulving., 1998, 1995, 1972; Squire., 2004). The constructs of declarative memory have largely been characterised as separable from that of procedural or implicit memory, which comprises non-declarative components of memory such as well-trained actions or complex habits, associations between certain forms of stimuli and classically conditioned behaviours (Squire et al., 2004). A central principle of declarative memory as a psychological construct, is its subdivision into components commonly characterised as 'episodic' and 'semantic memory', with episodic representing the retention of consciously experienced information about occurrences, episodes or events, and semantic involving the memory for facts and meaning (Tulving., 2003; Pause et al., 2013).

Further distinctions suggest the dissociations between subcomponents of memory as a function of time and consolidation, namely forming 'working memory', 'short-term' and 'long-term' declarative memory. Short-term memory is encoded over short durations of time such as minutes to hours with a limited capacity and can subsequently be consolidated into long-term memory, a store of seemingly infinite capacity with accurate retrieval possible over an entire lifespan in the absence of perturbation (Baddeley., 2000). Typically, episodic memory is considered to fall within the category of long-term memory, although episodic information can be utilised over short time frames (Baddeley., 2000; Bast., 2007). Working memory, in

contrast, is proposed to comprise the very short term and limited capacity storage and manipulation of information over relatively immediate time scales with an executive function component which allows flexible updating of this information (reviewed in Camina & Guell., 2017; Cowan et al., 2008; Baddeley., 2000).

Rodent spatial navigation is commonly used as a model of 'episodic-like' learning and memory. Learning the probabilistic predictive value of a given contextual factor for a particular outcome, such as a contextual cues for predicting food foraging success is a crucial process for adaptive decision making. Expanding this further, a more complex form of this learning is the learning of the relative spatial location of a given resource or route of escape within a complex environment (Allen & Fortin., 2013). This higher order function of spatial memory, forming the "where" component within episodic memory, is crucial in many organisms in which foraging behaviour and guided predator escape is central to their survival (Pravosudov & Roth., 2013). Thus, spatial foraging and escape behaviours serve as particularly powerful models for the study of declarative memory processes and underlying neurophysiological mechanisms, due to the naturalistic congruency with existing behavioural schemes of rodents (Parvosudov & Roth., 2013).

1.1.1 Spatial memory and allocentric-egocentric reference frames

Spatial information to support navigation can be encoded and implemented in behaviour via multiple strategies which vary in the reference frame said information is encoded. These strategies can be broadly categorised as allocentric and egocentric, relying on somewhat separable but overlapping circuits within the brain (Squire., 1992; Burgess et al., 2006; Grech et al., 2018; Wang et al., 2020). The most well studied, owing to its conduciveness to episodic memory in humans, is allocentric spatial memory. Allocentric spatial learning and memory is defined as the acquisition and recall of environmental information to represent space relative to distal environmental cues such as landmarks and spatial configuration between such cues (e.g., distal landmarks such as buildings or salient objects), particular target locations in space and the self, allowing a 'third person perspective' to support navigation (Ekstrom et al., 2015; Grech et al., 2018; Morris et al., 1990, 1986; O'Keefe & Nadel., 1978). Crucially this is distinct from an 'egocentric' reference frame in which spatial information is specifically gleaned in a self-referent manner. Learning using an egocentric reference frame involves information such as a sequence of directional turns relative to the self to navigate to a spatial target, or path

integration, the ability to compute relative position and possible route based on prior self-referent trajectories or vectors of movement (Ekstrom et al., 2015; Vorhees et al., 2014a; McNaughton et al., 2006). While both forms of learning necessitate the typical encoding, maintenance, and retrieval processes involved in memory, research suggests that spatial information encoded in an allocentric frame is more consistent with episodic memory (Burgess et al. 2001, 2006; Gomez et al., 2009).

Allocentric spatial memory tasks have been widely implemented in rodents to model episodic-like memory, of which maze tasks are particularly common. Maze tasks generally hold a consistent fundamental task principle, which is to successfully navigate a complex environment over the course of single to multiple trials to achieve a particular goal. When studying episodic-like memory in rodents, these tasks are designed to induce allocentric spatial learning by tapping naturalistic tendencies such as foraging or escape behaviours from aversive environmental conditions such as open space, bright light, or water (Vorhees et al., 2014a, 2014b).

The Morris water maze (MWM; Morris., 1984) is one such example in which a rodent is placed in a circular tank filled with opaque water with an escape platform hidden at a specific spatial location. The rodent is forced to navigate to the platform to escape the aversive environment via a number of potential strategies. The task is designed such that learning (encoding or acquisition) the location of the platform within a spatial allocentric reference frame should be the most efficient strategy for escape over repeated trials. Following initial trial and error-based search, performance is expected to improve with increasingly direct navigation to the platform location reflecting successful learning and retrieval of a spatial memory for the platform. Distal cues are used to promote allocentric encoding, while preventing route learning by avoiding a static start position which encourages self-referent egocentric navigation (Vorhees et al., 2014a; Grech et al., 2018). Typically, the rodent is provided a set of repeat trials for acquisition of the spatial memory at a particular inter-trial interval (ITI), before memory retrieval is assessed following a retrieval delay using a 'probe trial' in which the escape platform is removed. Most maze tasks are amenable to quantification of learning and memory performance via measures including improvements in the directness of the path to the platform (or spatial target) and the naturalistic tendency to search in a perseverative manner in the vicinity of the learned platform location (known as a win-stay strategy) as a measure of spatial memory accuracy during unrewarded probe trials (Morris., 1984; Vorhees et al., 2014a).

Many alternative maze tasks have been developed using similar principles to allow flexibility of task design and provide comprehensive assessment over differing task demands in rodent models. Examples of this include the Barnes maze (Barnes., 1973), which has been characterised as a 'dry-land equivalent' of the Morris water maze, radial arm mazes which provide a forced choice element to navigation, and labyrinth mazes which often involve mixed allocentric and egocentric route learning in highly complex spatial environments (for a review see Vorhees et al., 2006, 2014a).

Extensive research in animal and human models has investigated the underpinning neural circuitry of episodic, and more specifically spatial memory for more than 50 years, with rodent maze tasks playing a pivotal role in this. A combination of behavioural, neuroanatomical and neurophysiological techniques has been used to demonstrate both localised and distributed processing of episodic memory and specifically what these neural mechanisms represent in terms of computational function (e.g., Eichenbaum et al., 1999, Rolls et al., 2013). Perhaps the most well characterised system involved in episodic memory processing is the cortico-hippocampal memory system.

1.1.2 Hippocampal neuroanatomy

The hippocampus is a subcortical structure widely conserved across vertebrate species (Amaral et al., 2007). For the purpose of this thesis, the neuroanatomy of the hippocampus is characterised largely within the context of rodents. In rodents, the hippocampus is located toward the dorsal surface of the brain, comprising a 'C-shaped' formation spanning from the parietal aspects of the brain towards the posterior superior colliculi. Due to the curvature, the extent of the hippocampus begins from the midline near the septal nuclei at its anterior-dorsal tip and extends posterior-ventrally into the temporal lobe (Paxinos & Franklin., 2012; Amaral et al., 2007). The hippocampus is characterised both by its anterior-posterior aspects and longitudinal dorso-ventral axis (e.g., Moser & Moser., 1998; Strange et al., 2014; Fanselow & Dong., 2010).

Within the hippocampus (Figure 1.1), there is a stereotyped but complex circuitry, including four primary subfields known as the dentate gyrus (DG), and corn ammonia regions (CA) CA1, CA2, and CA3. The primary CA cell layers (stratum pyramidale) are primarily comprised of densely packed excitatory pyramidal cells, while the DG cell layer known as the granule cell

layer (DG GCL; or stratum granulosum) is composed mainly of larger cell-bodied granule cells. The cell body region of these layers also contains a much sparser population of interneurons (e.g., Klausberger et al., 2009). In the context of their principal excitatory neurons, these layers can be simplistically stated as harbouring largely homogenous cell populations (Amaral et al., 2007; Andersen et al., 2007; Pyapali et al., 1998).

The hippocampal subfields can be further divided according to the anatomical position of the principal neurons and their projections, giving rise to a primary cell layer where neuronal somata are localised (stratum pyramidale and granulosum), the apical dendritic projection site (stratum radiatum and stratum lacunosum moleculare) and the basal dendritic and axonal projection site (in the case of CA1; stratum oriens, alongside the stratum lucidum between CA3 and the DG mossy fibre projections; stratum moleculare in the case of the basal DG GCL dendrites), and the polymorphic or hilar layer of the DG (DGH). Local interneurons of multiple subtypes are localised both inside and outside of the pyramidal and granule cell layers, including positioned within the oriens and radiatum layers, as well as within the DGH layer between the granule cell blades. The organisation of the primary cell layers of the hippocampal circuit into CA and DG subcomponents and their relative connections, in combination with the primary hippocampal input layer the entorhinal cortex (EHC), is referred to as the 'trisynaptic circuit' (Figure 1.1).

Within the trisynaptic circuit, the connectivity is largely unidirectional. The dentate gyrus granule cells receive inputs from the pyramidal cells of the entorhinal cortex (EHC), forming the circuit known as the perforant path, comprising the first synapse in the circuit. Axons from predominantly layer II pyramidal neurons of the EHC innervate the basal dendrites of the DG granule cells, providing excitatory regulation. The DG granule cells subsequently project onto CA3 pyramidal cell dendrites via 'mossy fibres'. CA3 pyramidal neurons have three principal projections, comprising recurrent collateral of self-associating synapses between CA3-CA3 neurons, commissural fibres project to the contralateral portion of the hippocampus, and 'Schaffer collateral' fibres, projecting to both the proximal apical and basal dendrites of CA1 pyramidal neurons. CA1 pyramidal neurons subsequently project predominantly to the subiculum and EHC, providing hippocampal output (Andersen et al., 2007; Schultz & Engelhardt., 2014). Additionally, the temporoammonic path arrives via direct excitatory innervation from layer III of the EHC to the distal apical dendrites of CA1 pyramidal neurons, while some projections from CA1 pyramidal neurons terminate in the entorhinal cortex, primarily within layer Vb, providing some bidirectionality in input-output relationships (Van

Strien et al., 2009; Basu & Siegelbaum., 2015). The complex reality of connectivity patterns extends beyond that stated in the trisynaptic circuit but is beyond the scope of this thesis and has been reviewed extensively elsewhere (e.g., Van Strien et al., 2009; Basu & Siegelbaum., 2015; Scharfman & Myers., 2013; Scharfman., 2016; Muller & Remy., 2014; Van Groen et al., 2003; Amaral & Witter., 1989). On top of this excitatory network, inhibitory regulation via multiple GABAergic interneuron subtypes plays a crucial role in network regulation through both feedforward and feedback inhibition including action across the entire axis of the apical and basal dendrites, and at the soma of CA1 pyramidal neurons, for example (e.g., Klausberger., 2009; Pelkey et al., 2017).

Further modulatory input to the hippocampus originates from multiple cortical and subcortical sites which are thought to form the basis of integration of multisensory information for inputs to the trisynaptic circuit. Examples of these input projections include serotonergic input from the raphe nucleus, cholinergic septal nuclei projections, and dopaminergic input from the locus coeruleus (Takeuchi et al., 2016; Amaral et al., 2007), as well as inputs from the perirhinal cortex, amygdala, and medial prefrontal cortex via the EHC to the ventral portions of the hippocampus (Andersen et al., 2007; Bast et al., 2007; Knierim., 2015).

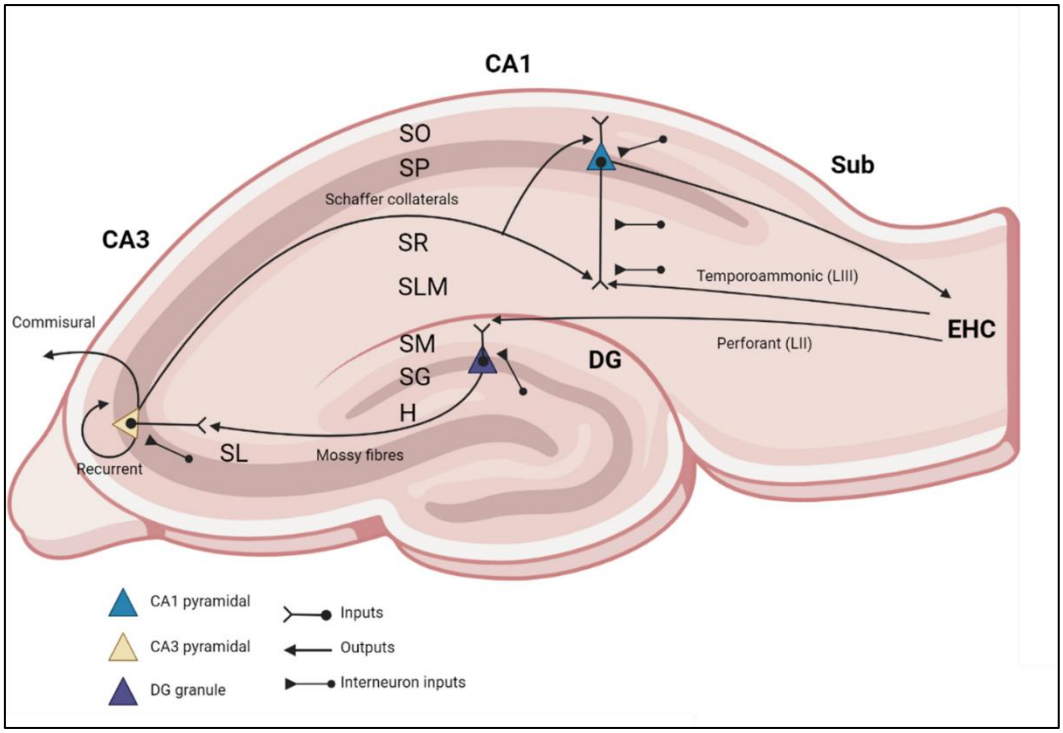

Figure 1.1: Simplified representation of the rodent hippocampal trisynaptic circuit. CA, DG, EHC, and Subiculum (Sub) regions are represented, alongside individual layers. Principal pyramidal and granule neurons are represented in the stratum pyramidale and granulosum by coloured triangles. Arrowheads correspond to output projections, while triangular arrows correspond to inputs. Local inhibitory interneuron inputs are represented by 'ball-and-stick' arrows. In brief, inputs from the entorhinal cortex, primarily layer II, form the perforant path, projecting to the basal dendrites of DG granule neurons. Mossy fibre outputs from the DG granule neurons then project to CA3 pyramidal neurons into the stratum lucidum. CA3 pyramidal neurons project to the apical and basal dendrites of CA1, while also projecting to the contralateral hippocampus via commissural fibres, and to CA3 pyramidal neurons via dense networks of recurrent collaterals. CA1 pyramidal neurons then project to the Subiculum and EHC via the primary output pathway of the hippocampus. The EHC, primarily layer III, also innervates CA1 pyramidal neurons via the temporoammonic pathway. Local interneurons populate all layers of the hippocampus and project to pyramidal and granule neurons. Local interneurons are shown projecting to the cell soma, axon, and dendrites of pyramidal neurons. Within the DG hilus, local interneurons also project to the granule neuron cell body and dendrites. See main text for further details (Figure created using BioRender). SO = stratum oriens, SP = stratum pyramidale, SR = stratum radiatum, SLM = stratum lacunosum moleculare, SM = stratum moleculare, SG = stratum granulosum, H = hilus, SL = stratum lucidum (adapted from Basu & Siegelbaum., 2015).

1.1.3 The hippocampus and declarative memory

Despite debate, theories of the function of the hippocampus generally place emphasis on the processing of integrated multisensory inputs from upstream cortical sites including complex environmental (e.g., visual scene information) and self-referent (e.g., relative body position, spatial location) information to form a mnemonic representation in a spatiotemporal context (i.e., for the encoding of contextual information such as “where am I?”, “where/what is in the environment?”; Eichenbaum et al., 1999a, 1999b, 2014; Knierim., 2015; Bast., 2007; O’Keefe & Nadel., 1978). Further, the hippocampus is proposed to perform processing of this contextually bound information to allow the formation, discrimination, and computation of overlap of memory content known as pattern separation and pattern completion; the distinction between similar representations in a discrete manner (separation) or the generalisation of partial inputs to support recall (completion; Knierim., 2015; Yassa & Stark., 2011; Gilbert et al., 1997; Rolls & Kesner., 2006). Crucially, the outputs of the hippocampus are proposed to allow memory information, particularly episodic, to be used by downstream cortical regions for higher order computations to support executive cognitive functions such as reasoning and decision making (Knierim., 2015; Anderson et al., 2006).

A proposed role for the hippocampus in the formation of new declarative memories is well supported by animal and human neurophysiological and behavioural data. Critically, a dissociation has been established in hippocampal involvement for encoding of novel declarative information and for the utilisation of prior established long-term memory (Steele & Morris., 1999; Morris., 2006; Bast et al., 2007, 2009; Da Silva et al., 2014). Evidence is provided by hippocampal lesion studies in both human patients and rodents. Namely, hippocampal lesions have been associated with a significant disruption of the formation of new declarative memories across multiple tasks such as spatial memory tasks, list learning tasks, and complex figure recall tasks (e.g., Parslow et al., 2005; Squire et al., 2004; Zola-Morgan & Squire., 1986a, 1986b).

In rodents, hippocampal lesion studies support the necessity of the hippocampus, particularly the dorsal and intermediate portions, for the acquisition of novel episodic memory. Lesions of the whole hippocampus cause significant impairments in both the acquisition and retrieval of novel spatial memory in tasks including the Morris water maze (MWM; Bast et al., 2009, Morris et al., 1984, 1990), with similar results following hippocampal white matter tract dissection or disruption of normal transmission (e.g., Barnes maze: Raber et al., 2004, Davis et

al., 2020, McNaughton et al., 1986; discussed in Kennard et al., 2011; adapted tower Barnes maze: Lipatova et al., 2020). However, hippocampal lesions often do not induce episodic memory deficits in their entirety. For example, even with complete hippocampal lesions or extensive pharmacological inactivation, rats trained extensively on the MWM demonstrate eventual acquisition of both relatively direct navigation paths to and preference for a given spatial location. Thus, there is a distinction in the ability to acquire incremental procedural learning, from episodic events, independent of the hippocampal system, even if the principal information has a spatial component (Morris et al., 1990; Packard & McGaugh., 1996; Bast et al., 2009).

Rather, the hippocampal system has been shown to be particularly critical to the updating and consolidation of novel episodic-like information over shorter and less well reinforced timescales. 'Rapid place learning and memory' or 'everyday' memory, requires the acquisition, storage, and retrieval of novel episodic information within a single or few-trial experiences, and requires the intact hippocampus. Importantly, this information often has highly similar content and context between instances, which necessitates the decay or prevention of proactive interference from prior information (Steele and Morris., 1999). Rapid place learning can be measured in tasks such as the "where did I park my car" problem and have been commonly assessed in human patients using the 'Rivermead memory test' (Wilson et al., 1989; Nonaka et al., 2017). A critical aspect of these tasks is the requirement to encode and retrieve novel episodic information over a short time frame, such as within a single day. In rodent models, the task analogues used to assess rapid place learning typically involve adapted maze formats and 'delayed match to sample/place' (DMTS/DMTP) tasks, in which the animal is forced to learn a novel location between days. The intrinsic difference to typical reference memory tasks is both the single experiential demands of the task placing a greater strain on the strength of the given 'memory trace' and requiring subsequent relearning of novel spatial information (e.g., a daily novel spatial location for escape from the maze) often of similar content within a stable context (i.e., prior knowledge or rule learning; Steele & Morris., 1999; Day et al., 2003; Morris et al., 2003; Bast et al., 2005; Wang et al., 2010; De Hoz et al., 2005; Nonaka et al., 2017; Da Silva et al., 2014).

Acquisition of novel memory is suggested to be supported, in part, by long term potentiation (LTP) within the hippocampal circuitry. LTP comprises a synaptic phenomenon which involves the long-lasting potentiation of synaptic transmission typically following persistent stimulation of presynaptic fibres. The perforant path between the EHC input fibres to the DG granule cells

is a well characterised model system for the study of LTP. Typically, presynaptic EHC perforant path fibres project to the DG granule cell basal dendrites (described in section 1.1.3) where presynaptic excitatory inputs to the post synaptic DG dendritic sites (i.e., synapses occupying dendritic spines) induces a post-synaptic excitatory potential (EPSP; Bliss & Collingridge., 1993; Bliss & Lømo., 1973). Persistent high-frequency stimulation (HFS, such as continual trains of 10Hz stimuli) of the perforant path fibres results in the potentiation of the evoked EPSP in the DG granule cells, typically increasing the EPSP amplitude. This persists over a variable time-course dependent on the form of stimulation, typically over several hours (Bliss & Lømo., 1973; Bliss & Collingridge., 1993; Bliss et al., 2018). LTP involves pre- and post-synaptic mechanisms, delineating separable phases of LTP including early and late-phase (or LTP1 and LTP2, respectively; although further denominations and mechanisms have been described, Bliss et al., 2018). General consensus suggests that NMDAR-dependent LTP (N-Methyl D-Aspartate Receptor) involves an early phase activation of the NMDAR and enhancement of AMPA receptor (α-amino-3-hydroxy-5-methyl-4-isoxazolepropionic acid receptor) function such as via enhancing conductance, increased trafficking to the post-synaptic density, and increased presynaptic neurotransmitter release probability to enhance the postsynaptic response.

Late-phase LTP, however, is considered to require the de novo synthesis of synaptic proteins to allow structural plasticity of the synapse to enable persistent functional change over much longer time periods. Stated simply, activation of de novo protein synthesis to support late-phase LTP is induced via activity-dependent signalling pathways, such as activation of calcium sensitive proteins. As an example, increases in intracellular calcium stimulate the Ras-Raf-MEK-ERK kinase (Ras guanosine triphosphatase; Raf kinase, Mitogen-activated protein kinase kinase, Mitogen-activated protein kinase) pathways, which converges on activation of immediate early genes (IEGs), such as CREB (cyclic adenosine monophosphate response element binding protein) and the c-Fos/c-Jun (Fos proto-oncogene/Jun proto-oncogene) heterodimer AP1 (Activator protein 1) which regulate transcriptional activation of downstream synaptic related gene targets (Bliss et al., 2018; Yan et al., 2016; Thomas & Huganir., 2004).

Importantly, NMDAR-dependent LTP has been implicated in the acquisition of novel episodic memory. Pharmacological inhibition of the NMDAR with inhibitors such as AP5 (2R-amino-5-phosphonovaleric acid) has been demonstrated to impair effective establishment of perforant path LTP pre-HFS, but not post-HFS, in vivo (Bliss and Collingridge., 1993; Bast et al., 2005; Morris., 2006). Further, NMDAR inhibition prior to, but not after, acquisition of novel episodic-like memory using rapid place learning tasks including the DMTP MWM and the 'event arena'

appetitive equivalent significantly impairs memory persistence and retrieval in rodents (Steele & Morris., 1999; Bast et al., 2005; Morris et al., 2003). Similar results of NMDAR-dependence of rapid place learning were acquired using a flavour-place paired associate learning task in rats (Day et al., 2003), and in the DMTP MWM following CA3 NMDA NR1 receptor subunit knock-out in mice (Nakazawa et al., 2003).

Partial or whole hippocampal lesions and GABAergic disinhibition similarly impair novel spatial memory formation in the DMTP tasks (Steele & Morris., 1999; Bast et al., 2009; De Hoz et al., 2005; Morris., 2006; McGarrity et al., 2017). Importantly, with the shifting demand of encoding novel episodic information in DMTP tasks, rats failed to achieve significant learning with whole or intermediate region hippocampal lesions over extended training (~40 trials), while successfully acquiring comparable performance to sham lesioned control animals when learning the reference memory task variant (i.e., static location across trials). This implicates the hippocampus in novel episodic-like memory formation rather than well-reinforced procedural learning of spatial information (Bast et al., 2009).

Overall, evidence has established the importance of the hippocampus in rapid acquisition and consolidation of novel episodic experience, which appears supported by LTP within the hippocampus as a function of event reinforcement and stability, with the possibility of learning via incremental means independent of these processes. Therefore, when characterising the influence of hippocampal specific perturbations such as those associated with age-related cognitive decline, the importance of both rapid ‘everyday memory’ and more long-term consolidation should be considered in parallel.

1.2 Ageing, episodic memory, and Alzheimer’s disease

There is a recognised mild decline in cognitive function across the lifespan with normal ageing (e.g., Huppert et al., 2005; Williams et al., 2003), and the degree of decline can vary across cognitive domains. This bias becomes more apparent with age-related pathology and neurodegenerative disease in which particular brain regions exhibit enhanced susceptibility to insult. Declarative memory and executive function have been shown to be particularly vulnerable to both age-related and disease-related pathological processes, with deficits in function disproportionate to other cognitive domains. For example, age-related impairments in episodic/spatial reference and working memory have been reported during normal human

ageing (e.g., Colombo et al., 2017; Olaya et al., 2017; Cohens et al., 1993; Piolino et al., 2002). Similarly, in rodent studies, age-related decline in episodic-like memory performance has been observed in multiple spatial memory tasks (e.g., Barnes et al., 1979, 1980; Bizon et al., 2009, 2012; Feng et al., 2019; Febo et al., 2020). Further, both human and rodent studies have demonstrated a particular susceptibility of the medial temporal lobe and hippocampal formation to age related pathology and age-related neurodegenerative diseases, providing a systems-level explanation for the susceptibility of episodic memory (e.g., Stranahan & Mattson., 2010; Spiegel et al., 2013; Fu et al., 2018; Morrison et al., 2002; Hyman et al., 1984).

Alzheimer's disease (AD), the most common cause of dementia, is one example of an age-related neurodegenerative disease, in which the acquisition of new declarative, particularly episodic, memory is significantly impaired and commonly associated with medial temporal lobe dysfunction (Jahn., 2013; Serino et al., 2014; reviewed in Bastin and Salmon., 2014). Alzheimer's disease is an aggressive neurodegenerative condition which is characterised by both neuropathological hallmarks and progressive cognitive decline. The neuropathological mechanisms of AD have been well-studied, but a complete and explanatory model of AD aetiology remains elusive. The key pathological hallmarks of AD, as noted first by Alois Alzheimer in 1907, are the deposition of extracellular senile plaques and neurofibrillary inclusions (tangles) within neurons. Molecular characterisation of these markers later revealed their identity to be proteinaceous plaque structures predominantly comprised of complex aggregations of the beta-amyloid (Ab) peptide, alongside the accumulation and hyperphosphorylation of the microtubule associated protein tau (MAPT, microtubule associated protein tau), with a propensity to form helical filaments and progress to cause dystrophic, 'tangled' neurites (Hardy & Higgins., 1999; Karran et al., 2011; Binder et al., 2005). Further evidence suggests gliosis as a third hallmark of AD, with a noted chronic activation of glia into pro-inflammatory states which promotes cellular stress and degeneration of neurons at the molecular level (Akiyama et al., 2000).

Understanding the causal pathological mechanisms underpinning AD is essential for both the identification of potential treatment interventions and for the wider scientific understanding of neurological disease-associated processes. As such, the identification of genetic risk factors for AD provides a route for isolation and investigation of the individual mechanisms contributing to the aetiology of AD and age-related cognitive decline.

1.2.1 Risk factors for and aetiology of Alzheimer's disease

Alzheimer's disease comprises two primary aetiologically defined forms: familial AD (FAD) and sporadic AD, with sporadic AD predominantly categorised as non-familial late-onset AD (LOAD), owed to its typical clinical manifestation in late age. FAD is a dominant genetically inherited condition which, while estimates vary, comprises ~1-5% of AD cases (Schott et al., 2002; Shea et al., 2016). FAD is causatively linked to rare mutations in genes associated with Ab processing. These genes include Amyloid Precursor Protein (APP), Presenilin 1 (PS1), and Presenilin 2 (PS2). Briefly, the transmembrane protein APP is associated with amyloidogenic and non-amyloidogenic processing pathways, mediated by families of alpha, beta, and gamma secretases, of which, the amyloidogenic pathway promotes the preferential formation of Ab peptides. Ab peptides formed via this pathway have a greater propensity for aggregation, neurotoxicity and eventual plaque formation than its alternative cleavage counterparts (DeStrooper et al., 1998, 2000, 2003; Thinakaran & Koo, 2008; Karch & Goate., 2015). PS1 and PS2 comprise catalytic subunits of the gamma-secretase complex, and thus mutations in APP, PS1, or PS2 are associated with significant elevation in Ab-related pathology and are causal for FAD.

LOAD, however, is not linked to a single causative mutation any given gene and is often referred to as form of sporadic AD referring to its onset with no clear direct genetic cause, comprising up to ~99% of all AD cases (Schott et al., 2003). While displaying heterogeneity in the extent and regional localisation of AD pathological hallmarks within the brain, LOAD remains characterised by the formation of Ab plaques, neurofibrillary tangles, and neuroinflammation. Thus, considerable research has been devoted to understanding the aetiology of LOAD, in part by investigating the polygenic nature of risk factors associated with LOAD and pathological involvement in LOAD incipience.

Epidemiological and genome-wide analyses have yielded a wide network of genes and single nucleotide polymorphisms (SNPs) associated with risk of development of LOAD (Tilley et al., 1998; Ertekin-Taner., 2010). The mechanistic characterization of the effect of these polymorphisms for gene function, pathology, and neurocognitive function have, and continue to provide, insight into the aetiology of disease (Karch & Goate., 2015). However, by far the most consistent and predictive genetic risk factor for LOAD is that of Apolipoprotein E (APOE) epsilon 4 (APOE4). APOE is primarily implicated in the trafficking and homeostasis of

lipoproteins and associated lipids within the periphery and CNS. APOE, is a polymorphic gene with three primary allelic isoforms, epsilon 2 (e2, APOE2), epsilon 3 (e3, APOE3), and epsilon 4 (e4, APOE4). Critically, possession of APOE4 has been associated with a significant increase in risk for both earlier onset and higher prevalence of LOAD across multiple populations (Corder et al., 1993; Raber et al., 2004). APOE4 has been suggested to account for more than 50% of the variance in AD age of onset and rate of inception (Raber et al., 2004). Further, AD risk has been shown to increase ~3-fold and ~8-fold for the possession of one or two APOE4 alleles, respectively (Corder et al., 1993). This strong linkage disequilibrium provided the basis for extensive research effort toward understanding the role of APOE4 in AD incipience as well as its general function within the periphery and CNS.

Perhaps one of the most intriguing factors driving continued research of APOE, is the association with a range of AD-pathology related processes involving amyloid and tau, alongside pathological processes independent of these hallmarks. Further, APOE4 has been associated with an increased risk of cognitive decline in both AD patients and healthy old age adults (Deary et al., 2002; Small et al., 2004; although see Knight et al., 2014 & O'Donoghue et al., 2018), however with particularly mixed results in young-mid aged adults (reviewed in O'Donoghue et al., 2018). It is therefore a critical challenge to characterise the influence of APOE isoform on cognitive performance across age via both AD-dependent and AD-independent neurobiological pathways to further understand these pathways themselves and their potential as therapeutic targets.

The next section, comprising the predominant focus of this thesis, will describe and discuss the fundamental properties, functions, and phenotypic associations of APOE. This makes the case for the value of extensive phenotyping in preclinical model systems to further address outstanding questions in the field. Additionally, emphasis is placed on the role of APOE isoform in episodic memory and neurobiological dysfunction in the absence of typical AD pathology, to understand how APOE-dependent pathways may contribute to risk of cognitive decline during normative ageing.

1.3 Introduction to Apolipoprotein E (APOE): gene nomenclature, protein structure, function, and associated model systems

1.3.1 APOE allelic isoforms and basic protein structure

The Apolipoprotein E (APOE) gene is located on chromosome 19 of the human genome and is comprised of 4 primary exons and 3 intronic regions. The APOE gene resides within a large multi-gene cluster comprising TOMM40 (Translocase of outer mitochondrial membrane), APOCI (Apolipoprotein C1), APOCI' (APOC1 pseudogene), APOCIV (Apolipoprotein C4), and APOCII (Apolipoprotein C2; Allen et al., 1995, 1995b), which forms a large ~58kB cassette known to be a primary site of apolipoprotein synthesis (Zannis et al., 2001).

The three primary isoform variants of APOE, e2, e3, and e4 arise as a result of three missense SNPs in the APOE gene which have the highest prevalence within the general population (Giau et al., 2015; Ensembl, 2018). Of the isoforms of APOE, APOE3 is the most prevalent allele in the majority of populations, with an estimated at 79% of the European population carrying at least one APOE3 allele. Individual APOE4 and APOE2 alleles have estimated prevalence of 13% and 8%, respectively, again predominantly within European samples, although prevalence varies across populations (Singh et al., 2006; Giau et al., 2015; Raber et al., 2004; Ward et al., 2011). Therefore, the most common genotype combination is homozygosity for APOE3, followed by APOE3/APOE4 heterozygosity (Raber et al., 2004). In the case of APOE2 and APOE4 these SNPs arise in exon 4, consisting of rs429358 which results in T-C substitution associated with APOE4, and rs7412 resulting in a C-T substitution in APOE2. This results in three primary haplotypes, while six genotype combinations are possible (e2/e2, e3/e3, e4/e4, e2/e3, e2/e4, e3/e4; Zannis et al., 1982).

The APOE protein (ApoE) itself comprises a 317 amino acid (aa) glycoprotein (Figure 1.2A), containing an 18aa signalling peptide that is truncated during translation, generating a final protein of 299aa at a primary molecular weight of 34-kDa (from primary transcript APOE-201; Twine et al., 2011; Weisgraber et al., 1981, 1982; Zannis et al., 1982). The function of APOE is primarily in lipoprotein transportation and homeostasis within the CNS and periphery, which is described in more detail in section 1.3.2. The gene structure of APOE is GC rich (~58%) and the primary structure of ApoE protein contains 34 arginine residues, which conferred its original name upon discovery as the 'arginine-rich' gene (Havel & Kane., 1973; Maloney et al., 2007). There are three principal domains within the APOE amino acid sequence which give rise to its

functional properties (Figure 1.2B). The first is the N-terminal portion which is comprised of 191 amino acids, including a receptor binding domain, referred to as the low-density lipoprotein (LDL) receptor (LDLR) binding region (residues 134-150 and R172; Morrow et al., 2000; Mahley et al., 2009). Second, is a flexible 'hinge region' connecting the N and C-terminal domains. Finally, a C-terminal domain, containing the lipid binding region (residues 244-272) at the distal element of the sequence (Flowers & Rebeck., 2020; Mahley & Rall., 2000; Aggerbeck et al., 1988). Additional binding sites have been identified within the primary sequence, including heparan sulphate proteoglycan binding region at residues 136-147 (Li et al., 2020; Futamara et al., 2005).

The missense substitutions induced by the primary isoform SNPs in the APOE gene are at amino acid sites 112 and 158 of the APOE coding sequence. ApoE3, the population norm, possesses a cysteine at site 112 (C112) and an arginine at site 158 (R158), while ApoE4 results in the ApoE4 C112R mutation, switching the final base within the codon from thymine to cytosine, generating two arginine residues at positions 112 and 158. In contrast, ApoE2 results from the switch of cytosine to thymine at position 158, yielding the R158C mutation (Weisgraber et al., 1981; Rall et al., 1982; Zannis et al., 1982; Mahley et al., 2009). The R/C112 site is located in helix three of the N-terminal domain, while residue R/C158 is located in helix 4, both outside of but in proximity of the receptor binding domain (Flowers and Rebeck., 2020; Mahley & Rall., 2000).

The tertiary structure and conformation of ApoE remains an issue of contention. However, multiple models have been suggested and are discussed at length elsewhere and, critically, tertiary conformation may influence both lipid and receptor binding functions of ApoE, alongside the efficacy of trafficking pathways for ApoE itself dependent on isoform. Specifically, it has been suggested that the structural features of ApoE4, such as a putative C-N terminal domain interaction proposed to be introduced via a salt bridge between Glu-255 and Arg-61, may impair lipid, receptor binding, and reduce effective trafficking, although the tertiary features remain somewhat debated (Weisgraber et al., 1994; Dong et al., 1994; 1996; Morrow et al., 2002; Hatters et al., 2006; Mahley et al., 2009; Flowers & Rebeck., 2020; Mahley & Rall., 2000; Aggerbeck et al., 1988; Sakamoto et al., 2008; Chen et al., 2012; Frieden & Garai., 2012, 2013; Raulin et al., 2019). In any case, it is clear that the structural features of APOE isoforms have a propensity to differentially affect overall APOE function.

A

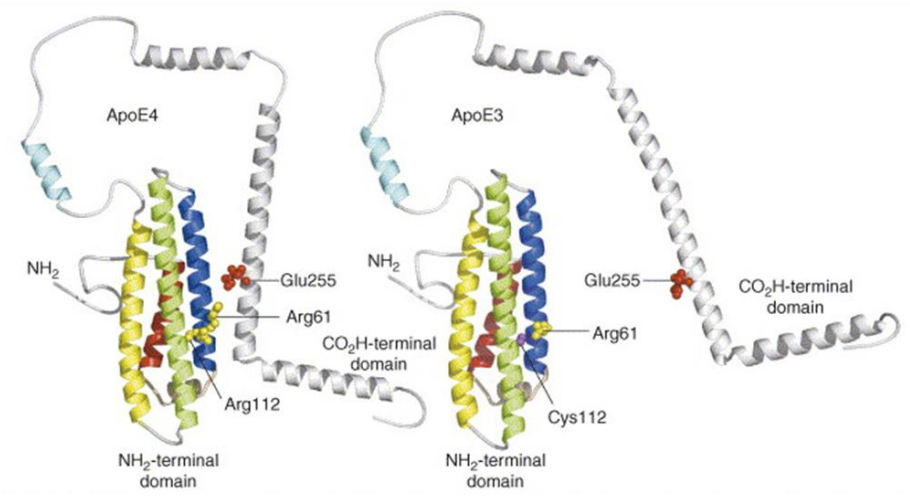

B

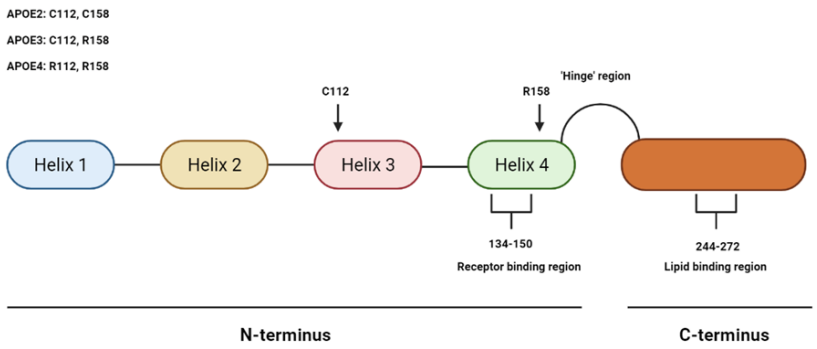

Figure 1.2: Representation of APOE structure. A) Figure taken from Hatters et al. (2006) representing tertiary structure model of ApoE3 and ApoE4 including labelling of N and C-terminal domains, primary mutation sites, and putative 'domain interaction' induced by salt bridge formation between Arg-61 and Glu-255 specific to ApoE4. B) Representation of primary structure of ApoE3, with N-C termini, N-terminus helices, receptor and lipid binding regions, hinge region, and primary isoform SNP sites labelled (adapted from: Flowers & Rebeck., 2020; Figure created using BioRender).

1.3.2 APOE expression, regulation and function

1.3.2.1 Regulation and expression of APOE

Regulation of APOE expression is driven by both transcriptional and post-translational control. At the level of transcription, APOE mRNA expression has been demonstrated to be dependent on the conservation of multiple distal enhancer regions within the APOE multi-gene cluster and has been reviewed elsewhere (Zannis et al., 1990, 2001; Allan et al., 1995, 1997; Maloney et al., 2007, 2010) and some evidence suggests further diversity in APOE transcriptional regulation (Xu et al., 2008; Lee et al., 2020; Mills et al., 2014; Filacek et al., 2012), including upregulation by endogenous stress (Xu et al., 2006, 2009).

APOE has been shown to be widely expressed throughout the body, with RNA sequencing (RNA-seq) data demonstrating expression in a multitude of tissues including liver, kidney, primary sex organs, and brain amongst other tissue types (Uhlén et al., 2015; Peng et al., 2015). The most extensive expression of APOE mRNA and protein is occurs within the liver hepatocytes and macrophages, whilst expression within the CNS occurs primarily within astrocytes (Pitas et al., 1987; Poirier., 1996), and choroid plexus (Xu et al., 2006), and to a lesser extent within in cellular components of the neurovasculature, including smooth muscle cells (Majacek et al., 1988; Mahley et al., 2016; Xu et al., 2006) and pericytes (Bell et al., 2012; Montagne et al., 2021). Neurons and microglia also express low levels of APOE (Xu et al., 1999; Xu et al., 2006) and while ApoE is primarily a secreted protein, evidence suggests that when ApoE is neuronally expressed there is a greater fraction retained intracellularly than secreted (Xu et al., 2006).

Overall, rodent data demonstrates low basal levels of endogenous (mouse or rat homologues) ApoE and human ApoE (hAPOE, such as in humanised APOE targeted replacement mice, APOE-TR; discussed in section 1.3.5) expression in neurons (Huang et al., 2017, 2019; Ignatius et al., 1986; Sullivan et al., 1997), but significant upregulation of ApoE expression occurs following cellular stress events such as kainic acid-induced excitotoxic (Xu et al., 2006) or electrolytic (Poirier et al., 1991) lesions. Expression of ApoE following significant stress events has been shown to be elevated by as much as ~200-300 fold in rat models of spinal cord lesion, accounting for as much as 5% of the total extracellular protein within 3-weeks post injury (Ignatius et al., 1986; Huang et al., 2010). ApoE is thought to retain separate pools between the periphery and CNS, not crossing the blood brain barrier (BBB; Bjorkhem et al., 1998; Huynh

et al., 2019), although ApoE has been shown to be produced in the choroid plexus and secreted into the glymphatic fluid for circulation within the CNS (Achariyar et al., 2016, Xu et al., 2006).

ApoE also undergoes post-translational modification (PTMs) primarily consisting of glycosylation and sialyation, although this appears dependent on the cellular source of APOE and the functional relevance of these modifications are currently under investigation (Rebeck et al., 2017; Lanfranco et al., 2020, 2021; Hu et al., 2020).

1.3.2.2 Canonical functions of APOE within the CNS and periphery: Lipid homeostasis

Lipid homeostasis constitutes the ability of cells to maintain appropriate concentrations of lipids within the cellular environment (Orth & Bellosta., 2012; Rebeck et al., 2017). This function is crucial both in the periphery and within the CNS, which necessitates the transportation of lipid molecules between sites of synthesis and uptake. Within the periphery, the effective metabolic processing of lipid molecules requires transportation both within and between organs. Ultimately the distribution of lipid molecules is required for multiple cellular processes including cellular membrane repair and organelle synthesis (Mahley et al., 1988). In the CNS, this is particularly salient, with a high dependency on transport of lipid molecules to support membrane synthesis and repair underpinning alterations to cellular morphology such as synaptogenesis and neurite growth (Mahley et al., 2016; Bruce et al., 2017; Rebeck et al., 2018).

Cholesterol is a primary component of the lipidome within the CNS and periphery and has important roles in both general membrane synthesis and stability, with a particularly high concentration within myelin sheaths of axons, thought to account for as much as 70% of the brain cholesterol reserves (Dietschy et al., 2001; Mahley et al., 2016). Largely, cholesterol synthesis is suggested to occur de novo and in situ, within glia and neuronal cells of the CNS, with the BBB predominantly preventing cholesterol or lipoprotein infiltration into the CNS from the periphery (Dietschy et al., 2001; Orth et al., 2012). The presence of an effective cellular distribution system for lipids between cells is therefore essential for the CNS to maintain concentrations of lipids and cholesterol within physiologically required levels (Mahley et al., 2016; Mahley & Rall., 2000).

APOE has been primarily implicated in lipid homeostasis in both the periphery and CNS via lipoprotein complex trafficking and clearance (Mahley., 1988; Mahley and Rall., 2000). In the periphery, lipoprotein particles and chylomicron are formed in the intestines via the metabolic processing of dietary lipids, upon which these particles are catabolized into smaller chylomicron remnants which are bound by ApoE to mediate clearance from the plasma to the liver via hepatic APOE receptors (Mahley et al., 1988). The liver subsequently synthesises very-low density lipoprotein (vLDL), which when secreted undergoes further lipolysis to form lipoprotein particles of varying sizes including low density lipoprotein (LDL), intermediate density lipoprotein (IDL), and high-density lipoprotein (HDL), decreasing the overall size of the particles and thus increasing their relative density, hence the sequential naming (Mahley et al., 1988; Havel et al., 1980; Pitas et al., 1987). ApoE binds the processed lipoproteins including chylomicron, vLDL, and HDL and mediates cellular uptake into peripheral tissues via interaction through cell surface receptors-mediated endocytosis with multiple potential receptors including the LDLR family, LDLR related protein (LRP) family, or heparan sulphate proteoglycans (HSPGs) for lipid extraction and use for downstream processes (Mahley et al., 1988., 2016). However, for this thesis the focus is primarily on ApoE function within the CNS.

ApoE is the primary apolipoprotein in the CNS and plays a similar role in lipid homeostasis to the periphery. As primarily a secreted protein, the main fraction of ApoE is extracellular and originates from astrocytes, with a lower concentration retained intracellularly (Zannis et al., 1986), with the exception of neuronally expressed ApoE which is mostly retained intracellularly (Xu et al. 2006). The typical regulatory process for ApoE production and secretion in the CNS is as follows (Figure 1.3). Transcriptional activation of APOE is controlled by numerous factors, but lipid sensitive Liver X Receptor-Retinoid X Receptor (LXR/RXR) binding sites are commonly involved in regulation of APOE transcription (Liang et al., 2004; Courtney & Landreth., 2016). Following transcription, and translation, ApoE is then processed at the endoplasmic reticulum (ER) and Golgi for post-translational modification, before possible retention in vesicular compartments or entering the secretory pathway (although less well characterised in CNS cell types; Dekroon & Armati., 2001; Kockx et al., 2008; Brodbeck et al., 2011; Liao et al., 2017).

Following secretion to the extracellular space from astrocytes, ApoE is lipidated via the ATP binding cassette family (ABC) receptors such as ABCA1, which transports lipid molecules into the extracellular space for lipoprotein formation and binding of ApoE, which exhibits a predominant bias for the formation of HDL-like lipoprotein particles (Pitas et al. 1987; Mahley et al., 2016). After lipidation, ApoE-bound lipoprotein complexes within the extracellular space

typically migrate to their downstream cellular targets, such as neuronal cells, binding via the receptor binding domain of multiple receptor families including the LDLR family, LRP family such as LRP1 and LRP8 (referred to as Apolipoprotein E receptor 2, ApoER2), and HSPGs. This receptor binding initiates the receptor internalisation response, which in turn allows endocytosis of the ApoE-lipoprotein complex (Wang et al., 1997; Bu., 2009; Liao et al., 2017). LRP1 is thought to constitute the primary neuronal cell surface receptor mediating APOE-bound lipoprotein internalisation (Bu., 2009). APOE-bound lipoproteins can also be taken up by microglia via the LDLR/LRP families and also interacts with the microglial TREM2 (triggering receptor on myeloid 2 cells) receptor (Atagi et al., 2015; Damisah et al., 2020). Once within the intracellular milieu, APOE dissociates from its cognate receptor within the early endosomal compartments (Lane-Donovan et al., 2014), before being processed for recycling via recycling endosomes or degradation via various proteases (Basu et al., 1982; Heeren et al., 1999; Kockx et al., 2008, 2012; Tamboli et al., 2014; Xian et al., 2016). The lipoprotein complex can then be processed for extraction of lipids including cholesterol and phospholipids.

This continuous cycle maintains lipid homeostasis with the propensity to respond to lipid poor demands in the cellular environment, such as following neuronal injury (Mahley et al., 1988; Tesseur et al., 2000; Mahley., 2016). Critically, the role of ApoE in supporting neuronal morphology is multifaceted, with the delivery of lipids mediated by ApoE allowing cells to dynamically respond to the demands of various cellular processes during development and in response to stress. These processes include organelle synthesis during mitosis and general organelle maintenance under basal conditions, formation of myelin during development and following injury to support remyelination, clearance of myelin debris, and supporting neurite sprouting during development and axonal pathfinding (Mahley et al., 1988; Tesseur et al., 1998; Nathan et al., 1995; Holtzmann et al., 1995; Demattos et al., 1995; Rebeck et al., 2018; Bruce et al., 2017).

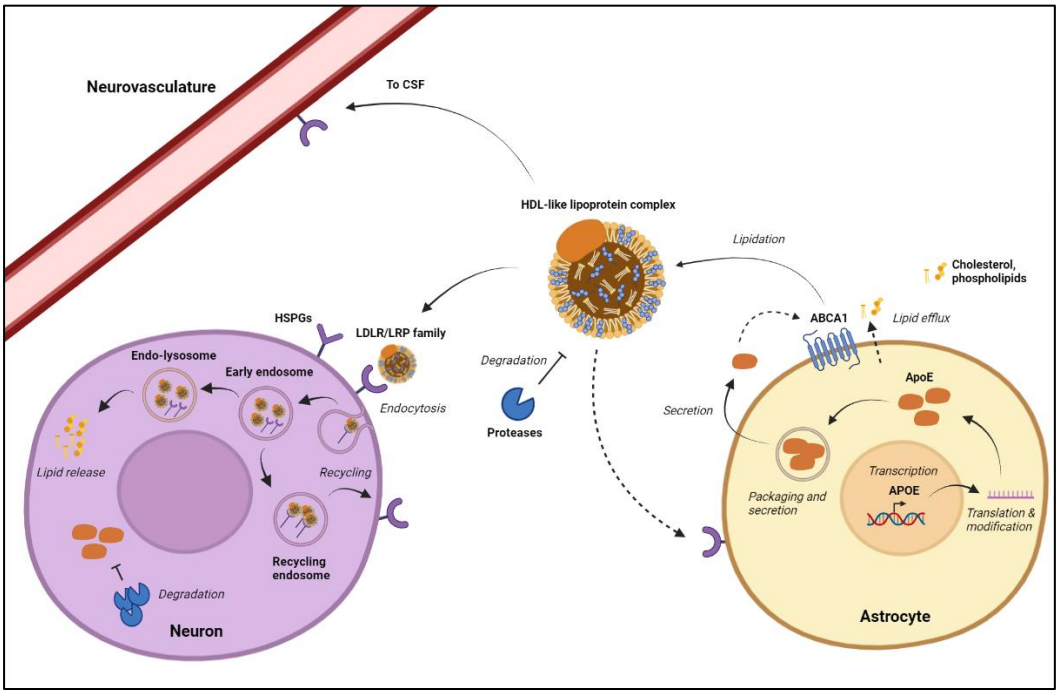

Figure 1.3: Simplified representation of canonical APOE trafficking pathway. For the purpose of simplification, only neuronal, astrocytic, and neurovascular components are shown. APOE gene transcription is initiated in astrocytes and ApoE protein is translated and post-translationally modified. Mature ApoE then is packaged and enters the secretory pathway, before exocytosis to the extracellular space. ApoE forms HDL-like lipoprotein particles via interaction with receptors including the ABCA1 family, which effluxes lipids into the extracellular space where lipoproteins are formed and bound by ApoE. The ApoE-bound lipoprotein complexes can then be trafficked to downstream cellular targets including neurons and microglia (not shown) and may enter the CSF/glymphatic fluid. ApoE binds its receptors, including LDLR and LRP receptor families, on the neuronal cell surface which initiates an endocytic response. The ApoE-lipoprotein-receptor complex is internalised into endosomal compartments where ApoE will dissociate from its receptor and the lipoprotein complex can be further processed for lipid release and use within the cell. The complex can also be processed for recycling via a sorting-recycling endosomal pathway, whereby the ApoE receptor can be trafficked back to the cell surface and ApoE may be secreted. ApoE can also be targeted for degradation via multiple proteases both in the extracellular and intracellular compartments (adapted from: Liao et al., 2013; Kanekiyo et al., 2014). See main text for further details (Figure created using BioRender).

1.3.3 Isoform specific modulation of lipoprotein homeostasis: Structure-function relationships

Functional diversity between APOE isoforms in lipid and receptor binding efficacy has been suggested to occur as a consequence of the alterations at the level of primary sequence and tertiary conformation of ApoE. Firstly, the lipidation of ApoE, comprising the integration into lipoprotein complexes, is altered by the conformation of ApoE (Mahley et al., 2009; Peters et al., 2006). ApoE3 has a greater preference for HDL particles than ApoE4, while showing similar affinity for vLDL particles (Sakamoto et al., 2008; Dong et al., 1994; Mahley et al., 2009). In contrast, other evidence suggests a greater preference of ApoE4 for vLDL particles (Nguyen et al., 2010), as well as a greater cholesterol content and lower clearance rate of these particles in mouse models and in vitro (Knouff et al., 1999; Minigawa et al., 2009). Within the CNS, evidence suggests that APOE4 may be more poorly lipidated, associating with smaller lipid complexes and/or decrease effective phospholipid and cholesterol binding capacity (Rawat and Wang., 2019; Heinsinger et al., 2016; Hu et al., 2015). The putative C-N terminal 'domain interaction' induced specifically in ApoE4 has been proposed to mediate this difference in lipoprotein particle preference (Ramaswamy et al., 2005; Mahley et al., 2006; Xu et al., 2004).

However, in terms of receptor binding, there appear to be minimal differences between ApoE3 and ApoE4 in binding efficacy. ApoE2 demonstrates a remarkable ~2% of the affinity of ApoE3/ApoE4 for the LDLR in vitro, again suggested to be mediated by alterations in the tertiary structure of ApoE2 impairing availability of the receptor binding domain (Dong et al., 1996; Mahley et al., 2009). This results in impaired rate of clearance of lipoprotein particles (Mahley et al., 1999, 2000), thought to underpin the association of APOE2 with type III hyperlipoproteinemia. ApoE3 and ApoE4 have been shown to have similar binding profiles across HSPG (Ji et al., 1998), LDLR family (Kowal et al., 1990), ApoER2 (or LRP8; Li & Kypreos., 2003; Xian et al., 2018), LRP1 and vLDLR (Ruiz & Kouiavskaia et al., 2003) using in vitro binding assays. However, some evidence suggests that there may be cell-type specific alterations in the relative binding efficacy of ApoE to its cognate receptors (e.g., Bell et al., 2012). Further, even if ApoE4 may not exhibit altered binding capacity in its native state or when bound to lipoprotein complexes in vivo, it does not exclude the possibility of alterations to the lipidated:unlipidated ratio of ApoE which subsequently could affect total receptor binding efficacy and subsequent ApoE turnover (Tokuda et al., 2000; Kim et al., 2009). Indeed, poor ApoE lipidation is associated with enhanced degradation (e.g., Warhle et al., 2004; Lanfranco

et al., 2020). This suggests isoform and cell-specific modulations of ApoE may influence effective ApoE action via multiple mechanisms, and as such, reduce effective lipid homeostasis in the case of ApoE4 and ApoE2 (Tokuda et al., 2000; Kim et al., 2009; Mahley., 2016; Li et al., 2020).

1.3.4 Isoform modulation of APOE expression

In addition to direct effects of the structure of APOE on its function, evidence suggests that alterations in the regulation and expression of APOE may also contribute to APOE4 dysfunction. APOE isoforms may undergo differential post-translational modifications, with ApoE4 exhibiting lower levels of sialylation than ApoE3 in human AD cortical samples and APOE4 targeted-replacement mice (E4-TR; DiBattista et al., 2016). Alterations in glycosylation may also occur, with trends observed for a mild reduction in glycosylation in both plasma and CSF of older healthy APOE4 carriers (Hu et al., 2020), and differential glycosylation reported between astrocyte and microglia-derived ApoE dependent on isoform in vitro, which may confer differences in ApoE handling (Lanfranco et al., 2021).

As for expression levels, there is mixed literature which appears particularly dependent on the source of expression. In mouse models there is a suggestion of a reduction of ApoE4 expression, but this appears dependent on brain region with some reports of ApoE4 reductions in the hippocampus and cortex of E4-TR mice (Riddell et al., 2008; Ramaswamy et al., 2005; Sullivan et al., 2011; Lin et al., 2016; Zhang et al., 2021), but not others (Sullivan et al., 2004). Similarly, human patient studies have suggested a reduction in CSF but not plasma ApoE in both AD patients and healthy controls (Ulrich et al., 2016; Cruchaga et al., 2012; Fukomoto et al., 2003), however there is similar discrepancy between brain regions reported (see Bekris et al., 2010). The mechanisms driving possible reductions in ApoE4 expression are not entirely clear, however several possibilities have been highlighted. The structural features of ApoE4, such as a C-N terminal domain interaction and tertiary conformation, are suggested to make it particularly susceptible to abnormal intracellular trafficking, endosomal sequestration in neurons and astrocytes (Morrow et al., 2002; Chen et al., 2010; Xian et al., 2018; Prasad & Rao., 2018), poorer lipidation/lipid efflux (Lanfranco et al., 2020; Heinsinger et al., 2016; Minigawa et al., 2009; Hu et al., 2015), enhanced proteolytic degradation within neurons and the extracellular space, and accumulation (Huang et al., 2001; Chang et al., 2005; Brodbeck et al., 2009; Harris et al., 2003, 2004, 2004b; Brecht et al., 2004; Mahley et al., 2009; Tamboli et

al., 2014; Wang et al., 2018). Further, a reduction in effective microtubule binding has been suggested to result in aberrant cellular distribution of ApoE4 within neurons, away from neurite processes, instead with a preference for cytoplasmic sequestration, possibly in perinuclear areas and within vesicles (Nathan et al., 1995; Mahley & Rall., 2000; Dekroon & Armati., 2001; DiBattista et al., 2016). This evidence demonstrates that APOE isoform can regulate APOE expression levels via multiple pathways which, in the case of APOE4, likely contributes to functional perturbation.

1.3.5 Murine APOE homology and mouse models of APOE function

Understanding the diverse roles of APOE within the periphery and CNS have been contributed to a great deal by the development of multiple mouse models of APOE function. APOE has known orthologs in many species, including primates, rodents, fish, and invertebrates (Ensembl., 2018). In mice (*Mus Musculus*), the mouse APOE (mAPOE) gene encodes eleven splice variants of mAPOE, nine of which are predicted to encode a variant of the mApoE protein. The sequence homology between mAPOE and human APOE (hAPOE) is 77%, with a 70% matched amino acid sequence (Rajavashisth et al., 1985; Maloney et al., 2007).

While mAPOE largely exhibits the same functional roles as hAPOE in vivo, a number of differences in basic properties have been identified. In protein conformation, mAPOE is suggested to be functionally similar to APOE3, although not equivalent (Mahley et al., 2016; Raffai et al., 2001). Notably, the domain interaction observed in APOE4 is not present in mAPOE, however models of the domain interaction have been induced by an R61 mutant model which induces a C-N interaction to model the domain interaction of hAPOE4 (Arg-61 APOE; Raffai et al., 2001; Ramasmamy et al., 2005; Zhong et al., 2009). Thus, in order to study the function and isoform-dependent modulation of hAPOE specifically, ‘humanised’ genetically altered mouse models are an essential platform for research.

A number of mouse models of APOE function have been developed and are listed in Table 1.1. Most relevant to this thesis and perhaps the most commonly used is that of the APOE targeted replacement mouse model (APOE-TR), developed by Sullivan and colleagues (Sullivan et al., 1997; Knouff et al., 1999). The APOE-TR mouse was designed produce a ‘humanised’ model by insertion of the human coding sequences for hAPOE into the mouse locus on a background of mAPOE knock-out (APOE-KO) to entirely replace mAPOE in both the periphery and CNS. The

cassette structure for the APOE-TR model consists of coding exons 2-4 and introns 2-3 alongside 3' and 5' flanking sequence of the hAPOE sequences, with a neomycin resistance gene cassette downstream of exon 4 used for positive clone selection. The mAPOE promoter region is retained within its normal locus in the mouse genome, thereby directing regulatory control of the hAPOE expression under conditions as similar as possible to that of mAPOE. This strategy has generated allelically homozygous animals for the APOE2, APOE3, and APOE4 genotypes.

A large amount of research has been dedicated to characterising the hAPOE function using mouse efficacy of the APOE-TR model as a model of hAPOE function. In initial characterization, both E3-TR and E4-TR mice relative to WT were shown to express similar levels of APOE within multiple organs, including liver, spleen, kidneys, and brain at comparable levels to that of mAPOE (Sullivan et al., 1997; Knouff et al., 1999). However, some work has demonstrated regional differences within the brain between hAPOE isoforms, with the suggestion of decreased expression in the hippocampus and cortex of young E4-TR mice (e.g., Riddell et al., 2008, Yong et al., 2014; see section 1.3.4), while in other reports there is little difference between isoforms (Sullivan et al., 2004), leaving some contention over regional modulation of APOE expression in vivo.

The lipid distribution profiles in the periphery and CNS in the APOE-TR mouse also differ somewhat to that of endogenous mAPOE in several important ways. Firstly, while E3-TR and E4-TR mice display similar fasted cholesterol and triglyceride levels in plasma relative to WT mice, these levels were elevated around 3-fold higher in APOE-TR than WT mice in response to a high fat diet. The distribution of ApoE and lipids in lipoprotein fractions is also affected, with a greater increase in cholesterol within the vLDL particle distribution in E4-TR than E3-TR or WT animals at baseline or following high fat diet exposure. vLDL derived from E4-TR mice exhibited greater affinity for the human LDLR but showed a slower rate of clearance compared to E3-TR-derived vLDL, which was not driven by increased vLDL secretion. Aortic atherosclerotic plaque sizes were also elevated in APOE-TR relative to WT mice. These profiles were suggested to be comparable to those observed in humans with the exception of exaggerated vLDL fraction preference relative to HDL and LDL, as well as exaggerated high-fat diet responses (Sullivan et al., 1997; Knouff et al., 1999).

Notably data from transgenic APOE3 and APOE4 astrocytes with similar origin to the APOE-TR model have demonstrated similar profiles of HDL-like lipoproteins and cholesterol content as

expected in humans, with comparable size to WT mAPOE HDL-like particles, although WT particles exhibited higher lipid:APOE ratios (Fagan et al., 1999). Additionally, viral mediated overexpression delivered to APOE-TR mice demonstrated a decrease in ApoE4-bound lipoprotein particles and decreases in cholesterol levels in the brain, again highlighting potential basal shifts in lipoprotein preference of ApoE4 following acute upregulation in the CNS, which is suggested to mimic that exhibited in humans (Hu et al., 2015; Heinsinger et al., 2016).

Phenotypic differences induced by APOE isoforms have been widely demonstrated using APOE-TR mice, modelling the effects of APOE observed in human patients alongside investigating novel pathways. The targeted replacement mice hold several advantages over other models. Firstly, the APOE-TR model is, by nature, a targeted replacement model, without the potential confound of endogenous mAPOE in the genetic background. Second, the relative expression profiles are very similar to endogenous mAPOE, with the conservation of regulatory sequences, inter-species limitations aside. Third, this combination of conserved expression levels and sites is less likely to result in disruptions to the normal metabolic functions served by mAPOE. Indeed, APOE-TR mice exhibit exceptionally mild general health phenotypic effects with potential alterations in weight gain and atherosclerotic risk as highlighted previously, suggesting the targeted replacement construct serves as a particularly effective substitute for mAPOE (Sullivan et al., 1997; Knouff et al., 1999). Fourth, the APOE-TR model allows for the simultaneous study of APOE in multiple cellular compartments. This is beneficial in comparison to CNS-specific transgenic driver line models, which rely on APOE ectopic expression. Primary examples of these models include specific astrocytic driven expression of APOE in the APOE-GFAP (Glial fibrillary acid protein) model and APOE expression within neurons in the Thy1-APOE (CD90 – Cluster of Differentiation 90) and NSE-APOE (Neuron-specific enolase) models (Sun et al., 1999; Tesseur et al., 2000; Raber et al., 1998). Moreover, the APOE-TR model enables the study of the effect of APOE on these cellular compartments and their interactions simultaneously and under more physiologically relevant conditions.

Table 1.1: Table summarising common APOE mouse models developed and used within the literature. Category of model, model name, APOE promoter, expression sites, sequence, and relevant reference of origin are provided. Note that this list is not comprehensive but does comprise the predominant models used currently.

Model category	Model name	Promoter	Region of expression	Sequence	Reference of origin
Endogenous mouse APOE	**Murine APOE**	Endogenous mAPOE	Endogenous expression sites	Endogenous sequence	N/A
	EGFP(apoE)	Endogenous mAPOE	Endogenous expression sites	Endogenous sequence + EGFP prior to exon 2	Xu et al. (2006)
	APOE-KO (knock-out)	N/A	N/A	Endogenous KO	Piedrahita et al. (1992)
	Arg-61 APOE	Endogenous mAPOE	Endogenous expression sites	Endogenous sequence + missense alteration in exon 4 to introduce Thr61Arg	Raffai et al. (2001)
Transgenic insertion under cell specific or altered promoters	**APOE-TG (APOE-KI)**	Human APOE	Human expression sites, variable	Multi-copy hAPOE sequences	Xu et al. (1996)
	APOEΔ272-299	Thy-1	CNS (and presumed, but unquantified, peripheral tisssue)	hAPOE coding sequence for a.a. 272-299 + signal peptide and FLAG tag	Harris et al. (2003)
	GFAP-APOE	Glial fibrilary acidic protein (GFAP)	Astrocytes	1050bp hAPOE fragment	Sun et al. (1999)
	NSE-APOE	Neuron specific enolase (NSE)	Central and peripheral nervous system neurons	hAPOE 'mini-gene'	Raber et al. (1998)
Targeted replacement of APOE	**APOE-TR**	Endogenous mAPOE	Endogenous expression sites	hAPOE coding exons 2-4	Sullivan et al. (1997); Knouff et al. (1999)
	apoe-fKI	Endogenous mAPOE	Endogenous expression sites	hAPOE coding exons 2-4 + loxP sites between exon 2 and 4	Bien-Ly et al. (2012)

1.4 Leveraging preclinical models of APOE function to study AD-dependent and AD-independent phenotypic effects.

While the primary role of APOE is its involvement in the regulation of lipid homeostasis in the CNS, it has been implicated in a disproportionately large set of functions (Mahley et al., 2006; Huang et al., 2011, 2012, 2014; Dose et al., 2016). As noted in section 1.2.2, APOE4 is most commonly investigated for its strong association with an enhanced risk of LOAD (e.g., Corder et al., 1993; Raber et al., 2004). This has led to the widespread effort to characterise the phenotypic influence of APOE on potential AD-related processes across the lifespan from molecular mechanisms of pathology to behavioural markers of AD-like cognitive decline.

An intriguing theme from this work, is the emergence of both AD-dependent and AD-independent roles of APOE (e.g., Huang et al., 2014; DiBattista et al., 2016; Flowers & Rebeck., 2020). Specifically, a large body of evidence from preclinical models suggests that APOE may modify AD risk by both directly interacting with the molecular level mechanisms underpinning AD, such as amyloid beta and tau pathologies, while also driving separable pathological mechanisms independent of these AD-specific pathways (Huang et al., 2014; Liao et al., 2017). Some pertinent examples of AD-dependent interactions with pathology include the well-established role for APOE4 in enhancing the aggregation of amyloid beta (Aβ; Castellano et al., 2011), impairing its clearance (Wisniewski & Drummond., 2020; Verghese et al., 2013), and potentially promoting amyloid 'seeding'; the early incipience of small, aggregated structures of Aβ (Liu et al., 2017). Additionally, APOE4 has been associated with the hyperphosphorylation of tau, the structural precursor to the paired helical filamentous structures driving neurofibrillary tangle formation, alongside exacerbating tau-dependent neurodegeneration in mice expressing a truncated form of APOE4, mutant human tau, or in neuronal cell lines expressing full length or truncated APOE4 (Andrews-Zwilling et al., 2010; Shi et al., 2017; Brecht et al., 2004; Wang et al., 2018).

However, mouse models face criticism for their ineffective recapitulation of the progression or true pathological representation of Alzheimer's disease due to the lack of conserved pathways (e.g., Sasaguri et al., 2017; Tai et al., 2021). WT mice do possess endogenous forms of tau and amyloid beta, however these murine proteins are typically not driven to pathological states resembling human AD, although neuronal expression and fragmentation of human ApoE4 has been associated with elevated tau phosphorylation in APOE mouse models (Brecht et al., 2004;

Andrews-Zwilling et al., 2010). Even with such manipulations, however, the fundamental fact remains that predominant models of AD pathology in mice require the transgenic or targeted insertion of a mutant human familial AD gene such as APP, PS1, PS2, or P301S mutant tau to induce significant Aβ or tau pathology, respectively (Tai et al., 2017). Put simply, mice do not get Alzheimer's disease. However, AD mouse models have been fundamental in forming a multifaceted and more relevant approach to modelling AD (Tai et al., 2021; Lewandowski et al., 2020). It therefore must be noted when studying APOE mouse models that the hAPOE isoforms induces phenotypic effects in spite of the absence of AD pathology, which justifies the study of its function both in isolation and in combination with AD-related pathways.

Indeed, APOE has been placed at the centre of multiple pathways of CNS dysfunction, and perhaps most convincingly, within pathways which are vulnerable to exacerbation via exogenous or endogenous stressors, which may both contribute to, but may originate independent of, AD pathology. Disruption of these pathways has primarily been established using APOE mouse models, as well as primary, immortalised, or IPSC-derived neuronal or glial cell systems. In each case, APOE4 is generally shown to impair or result in dysfunctional potentiation of a given process. These pathways include: age-related neurodegeneration and a decrease in effective neuronal sprouting/development (e.g., Andrews-Zwilling et al, 2010; Lin et al., 2016; Buttini et al., 1999, 2010; Veinbergs et al., 2000; Nathan et al., 1995), neurovascular dysfunction and inflammatory-mediated breakdown of the BBB via a loss of anti-inflammatory action (e.g., Bell et al., 2012; Koizumi et al., 2018; Montagne et al., 2021), enhanced pro-inflammatory glial activation states and impaired normal glial responsivity (e.g., Dose et al., 2016; Brown et al., 2002; Bell et al., 2012), dysregulation of the oxidative stress response via loss of free radical scavenging ability and reduction in antioxidant enzyme expression (e.g., Miyata & Smith., 1999; Maezawa et al., 2006; Jiang et al., 2019; Shi et al., 2014), enhanced endosomal sequestration of cell surface receptors and impaired intracellular trafficking, recycling, and clearance (e.g., Chen et al., 2010; Xian et al., 2018; Pohlkamp et al., 2021; Prasad & Rao et al., 2020), impaired calcium homeostasis via enhancement of intracellular calcium levels and activation of calcium-dependent signalling pathways (e.g., Tolar et al., 1999; Veinbergs et al., 2002; Jiang et al., 2015; Larramona-Arcas et al., 2020; Ramakrishna et al., 2021), and disruption of transcriptional control of multiple cellular pathways both through direct transcription factor-like activity, and indirectly such as via upstream signalling (e.g., Theendakara et al., 2016, 2018; Lin et al., 2018; Zalocusky et al., 2021). Further, these individual processes appear modulated by 'contextual' biological factors,

which often include exacerbation by cellular/systemic stress, sex, and ageing in a complex manner.

Description of each of these potential roles for APOE are beyond the scope of this thesis, however they highlight the current research landscape and wide scope for further study. Broadly, it is unlikely that each of these processes are drastically and simultaneously dysregulated under normal conditions and the relative contribution of each process is far from known. Characterisation of these pathways has typically been performed in isolation and in in vitro systems, in the presence of some form of systemic insult, or following phenotypic 'exaggeration' via exacerbating the effects by physiologically unrepresentative means (e.g., ectopic ApoE overexpression, ApoE fragment expression etc.). Here, the processes most pertinent to the present thesis are the roles of APOE in synaptic function, neuronal morphology and episodic memory function and will be further explored with a particular emphasis on findings using the APOE-TR mouse model.

1.5 Influence of APOE isoform on neuronal structure and function in preclinical models of APOE function.

Loss of neuronal structural integrity and neuronal cell death are typical pathologies of neurodegenerative disorders, particularly Alzheimer's disease, but is a progressive process that can last decades before mortality (Kanazawa., 2001; LeBlanc et al., 2005; Clare et al., 2010). However, the events preceding gross cell loss include subtle changes to neuronal morphology and synaptic integrity, as well as specific neuronal subtypes demonstrating particular susceptibility to these processes (Najm et al., 2019; Stranahan & Mattson., 2010; Fu et al., 2018).

As discussed in section 1.3.2, APOE is involved in the regulation of neuronal development and morphology via its delivery of lipid molecules to support membrane, organelle, and myelin synthesis, involved in neuronal repair particularly under conditions of stress (Mahley et al., 2016; Boyles et al., 1989; Nathan et al., 1995). Multiple roles have been described for APOE isoform in differentially modulating neuronal structures, which appear mediated by functions extending beyond that of lipoprotein trafficking alone. These include alterations of direct receptor-mediated signalling and downstream signalling pathways, interactions with

mechanisms of synaptic maintenance, and activation of neurotoxic processes. These together converge on APOE isoform-dependent shifts in proliferation, cell fate, damage repair processes, and induction of neurotoxicity.

1.5.1 Global neuroanatomical changes associated with APOE isoform

At the level of global-scale anatomy, structural MRI (magnetic resonance imaging) data indicates volumetric change in several brain regions associated with APOE isoform, sex, and age. Namely, studies have highlighted lower hippocampal, parahippocampal, and striatal volumes in 6-month aged E4-TR female mice, which was exacerbated by treatment with doxorubicin (a chemotherapeutic Topoisomerase 1 inhibitor; Speidell et al., 2019). Similarly, decreases in both hippocampal and cortical volume were observed at 18-24, but not 6-12-month, aged E4-TR male mice relative to WT (Yin et al., 2011) or E3-TR (Yin et al., 2014) controls. Conflicting data was reported by Shang et al. (2020), however, with no change in total brain volume in 16-month aged APOE-TR mice of both sexes, but a greater impairment in the hippocampus proper volume in E3-TR females relative to male, but not female controls.

Histological validation of the gross cell density loss that may underpin global atrophy also provides mixed results. One study reported a reduction in hippocampal pyramidal cell size without a corresponding change in absolute density in 21-month aged GFAP-E4 female mice relative to GFAP-E3 controls (Tan & Zhou., 2009), while another study found a loss of NeuN (Neuronal Nuclei Antigen/RBFOX3) positive pyramidal cells within both the cortex and CA1 of the hippocampus in 18-24-month aged E4-TR mice, with cell density negatively correlating with BBB integrity (Montagne et al., 2021). Similarly, a reduction in CA1 pyramidal cells was reported in 16-month aged E4-TR female mice, which was ameliorated in Syn1-Cre APOE KO mice, reducing neuronal APOE expression (Zalocusky et al., 2021). Reductions in hippocampal and cortical NeuN density in transgenic NSE-E4 mice was also demonstrated relative to NSE-E3 controls following excitotoxic injury at a much earlier age of 5-7-months (Buttini et al., 2010). Conversely, dentate gyrus (DG) granule cell size was reported to increase without a change in total volume in Arg-61 APOE mice relative to WT at 5 (Adeosun et al., 2019), but not 12-months (Zhong et al., 2008), while no differences were detected in DG GCL cell death or volume between E3-TR and E4-TR mice at 5-months either with or without lead exposure (Engstrom et al., 2017). These conflicting results require further characterisation and are likely influenced by the variability in mouse model used and inclusion criteria, namely whether

animals or both sexes were included, variable age-points and relative methodology. For example, histological validation may be more sensitive to low level cell loss or alterations in morphology than whole brain MRI, but often vary in what is actually quantified (e.g., subregion, volume or cell loss etc.). However, these data suggest that APOE4 may contribute to gross late-age neurodegeneration, particularly in the presence of neuronal APOE expression and CNS insult.

1.5.2 GABAergic neurodegeneration associated with APOE isoform

While the preceding findings highlight that APOE4 appears to have an age-dependent neurodegenerative influence in a region-dependent manner, striking findings have arisen from investigations of the DG GABAergic system in APOE4 female mouse models supporting a preferential degenerative risk in these neurons.

Network inhibitory control within the DG is regulated in part by local GABAergic interneurons. Dentate gyrus hilar (DGH) GABAergic interneurons (GABA-INs) are essential for the inhibitory regulation of dentate granule cell activity and DG-CA3 mossy fibre projections (Andrews-Zwilling et al., 2012; Stefanelli et al., 2016; Dudek & Sutula., 2007). Female E4-TR mice, specifically, demonstrate a loss of presynaptic GABAergic terminals in the dentate gyrus granule cell layer (DG GCL) from 6-months of age, as measured by a reduction in perisomal GAD-67 (Glutamic acid decarboxylase 67) immunoreactivity (Li et al., 2009). This reduction in innervation was shown to be followed by a marked linear loss of DGH GABA-INs, of which the somatostatin-positive pool was primarily susceptible. This loss was first detectable at 6-months of age, continuing to 18+ months (Andrews-Zwilling et al., 2010; Leung et al., 2012; Tong et al., 2014, 2016; Knoferle et al., 2014). The specific loss of the DGH GABA-INs in female E4-TR mice is suggested to reflect an inhibitory:excitatory imbalance in cell populations of the DGH, although a significant shift in this ratio when characterising DGH excitatory and inhibitory cell types was observed from 16-months (Leung et al., 2012).

Further, this loss of DGH GABAergic control in E4-TR females was associated with an impairment in neuronal maturation of newborn neurons in the DG GCL, suggesting that APOE4 impairs effective neurogenesis via a network level GABAergic mechanism (Li et al., 2009). Supporting this, the APOE4-mediated GABA-IN loss in the DGH were shown to be ameliorated by systemic treatment with the positive allosteric modulator of $GABA_A$ receptors ($GABA_AR$),

pentobarbital (Tong et al., 2016) as well as transplantation of GABA-IN precursor medial ganglionic eminence (MGE) progenitor cells into the DG (Tong et al., 2014), and neuronal but not glial-specific Cre-dependent knockout of APOE4 (apoe-fKI) using a pan-neuronal Syn1 (Synapsin 1) or the Dlx GABAergic-specific drivers (Knoferle et al., 2014).

Under normal conditions, however, this degenerative effect was not observed in APOE-TR male mice, instead with males demonstrating increasing numbers of DGH GABA-INs across the lifespan independent of APOE isoform (Leung et al., 2012). However, a loss of GABA-INs was noted in both the DGH and prefrontal cortex of 12-month E4-TR male mice following chronic stress exposure (Lin et al., 2016; Zhang et al., 2020). Together this data suggests an important and sex specific role for neuronal APOE4 expression in GABAergic neurodegeneration alongside a possible general enhanced susceptibility of DGH GABA-INs to APOE4-mediated toxicity across both sexes.

A gain of toxic function role for APOE4 may be due to the preferential generation of neurotoxic truncated C-terminal ApoE4 fragments when expressed in neurons. Increased proteolytic fragmentation of ApoE4 has been demonstrated in AD-patient cortical tissue (Huang et al., 2001), in the neuron-specific NSE-E4 mouse cortex (Brecht et al., 2004), alongside preferentially enhanced fragmentation and neurotoxicity in GABA-INs derived from AD patient hIPSCs (Wang et al., 2018), and in cultured primary neurons from E4-TR mice (Li et al., 2009). The elevated ApoE4 proteolytic fragmentation is suggested to be regulated by the ApoE4 domain interaction (Dong et al., 1996; Wang et al., 2018; Mahley et al., 2006; Huang et al., 2010; Amponsah et al., 2020).

ApoE4 fragments have been demonstrated to interact with tau phosphorylation and escape the secretory pathway, localising to mitochondria and ER, causing dysfunction (Zhong et al., 2008; Brodbeck et al., 2011). ApoE4 fragments impair cytochrome oxidase complex expression and function in neurons alongside elevating endoplasmic reticulum (ER) stress in astrocytes (Chang et al., 2005; Zhong et al., 2008; Brodbeck et al., 2011; Chen et al., 2011). Additionally, the simulation of endogenous ApoE4 fragmentation, via expression of the truncated *APOE4*Δ272-299 C-terminal product under the Thy1 promoter in mice exacerbated the GABA-IN degeneration phenotype (Harris et al., 2003; Andrews-Zwilling et al., 2010). An increase in tau phosphorylation was observed both in *APOE4*Δ272-299 mice and an increased proportion of phosphorylated tau positive GABA-INs and cell death in culture. Knockout of endogenous tau in the *APOE4*Δ272-299 model (Andrews-Zwilling et al., 2010), gene editing to convert

APOE4 neurons into isogenic APOE3 neurons, and treatment with a putative ApoE4 domain interaction targeting pharmacological agent PH002 in culture (Wang et al., 2018) reduced ApoE4 fragmentation and consequent GABA-IN loss. Critically, prevention of the ApoE4 domain interaction via mutation of the Arg-61 residue to Thr-61 or pharmacological targeting with PH002 also reduced the toxic effects on mitochondrial function, suggesting that the aberrant domain interaction in ApoE4 may be a conserved mechanism for multiple neurodegenerative pathways (Chen et al., 2011, Mahley & Huang., 2012).

Thus, evidence strongly suggests that ApoE4 fragments generated within neurons are key mediators of hippocampal GABA-IN degeneration via a tau-dependent process and a disruption of mitochondrial/ER function (Muñoz et al., 2018). The question remains, to what extent this process occurs in vivo without transgenic expression or excessive exogenous stress. However, this data makes a strong case for the toxic potential of ApoE4 following neuronal expression, and indeed toxic ApoE4 fragmentation has been reported in the AD brain (Huang et al., 2001).

1.5.3 Neuronal morphological changes associated with APOE isoform

In addition to cell loss, APOE isoform has been associated with changes in the morphological properties of neurons, and alterations in developmental sprouting. Such differences have primarily been reported in dendritic morphology and neurite density as a proxy for innervation and, as such, have implications for neuronal function.

In the cortex, multiple reports have demonstrated a decrease in layer II/III dendritic spine density across the lifespan, from 1-month to 2-years of age in E4-TR mice relative to E3-TR counterparts in male (Neustadl et al., 2018) or mixed sex groups (Dumanis et al., 2009). These APOE4-driven deficits in spine density occurred without a substantial concurrent effect on gross dendritic length, suggesting a reduction in spine-supported synapses in the cortex perhaps without impairments of dendritic extension. However, reductions in overall neurite density have also been reported in E4-TR and E4-KI mice as early as 4-10 months (Bell et al., 2012; Veinbergs et al., 1999)

In the entorhinal cortex (EHC), reductions in both spine density and dendritic length were also observed in the basal dendrites of female E4-TR mice at 3-months (Rodriguez et al., 2013).

Other studies have reported no differences between APOE-TR mice at 8-9-months (Jones et al., 2021), a decrease only in spine density in the EHC of E4-TR females, compared with both spine density and dendritic length/complexity deficits in NSE-E4 female mice at 19-21-months (Jain et al., 2013). Similarly, in the auditory cortex, reductions in spine density were observed in the same NSE-E4 female cohort at 19-21-months, with no differences in GFAP-APOE or APOE-TR mice. Finally, earlier deficits in spine density, particularly mushroom spines density was shown in the EHC, and auditory cortex of NSE-E4 but not E4-TR female mice at 7-8-months (Jain et al., 2013).

Reports are also mixed in the hippocampus, with studies showing no difference in CA1 spine density between APOE-TR genotypes at 4-weeks (Dumanis et al., 2009), 5-months (Klein et al., 2014), 7-8-months (Jain et al., 2013), but reductions in E4-TR females at 19-21 months (particularly basal shaft spines) without changes in dendritic length or complexity (Jain et al., 2013). In contrast, reductions in CA1 dendritic complexity and spine density have also been reported in 4-month E4-TR males (Sun et al., 2017), alongside impaired sprouting and neuropil occupation in 10-month E4-KI mice (Veinbergs et al., 1999), and reduced total and mushroom spines in female NSE-E4 aged 7-8-months (Jain et al., 2013) relative to APOE3 controls. In the dentate gyrus granule cell layer (GCL), one report demonstrated decreased spine density and length at 12-24-months, but not 1-month, in male GFAP-E4 and APOE-KO relative to GFAP-E3 and WT controls (Ji et al., 2003), while another demonstrated no differences in APOE-TR mice from 4-weeks to 1-year (Dumanis et al., 2009). Recent studies have also shown decreased adult-born dentate gyrus granule cell spine density, dendritic length, and complexity in 2-3-month mixed sex E4-TR mice (Tensaouti et al., 2018, 2020), alongside deficits in complexity in 6-7-month E4-TR females relative to E3-TR controls (Li et al., 2009). Crucially this reduction in newborn neuron dendritic complexity in female E4-TR mice is suggested to be driven by an APOE4-dependent loss of GABAergic input onto newborn dentate granule cells (Li et al., 2009), preventing effective maturation and circuit integration. It is unclear, however, what mechanism may explain earlier and sex-independent observations of other reports.

Finally, evidence suggests that APOE4 specifically exacerbates these deficits following systemic stress and reduces effective repair responses following multiple insults including excitotoxic injury (Buttini et al., 1999; 2010), deafferentation (White et al., 2001; Bott et al., 2013, 2016), environmental toxicant exposure (Engstrom et al., 2017), traumatic brain injury (TBI; Tensaouti et al., 2020), and pro-inflammatory stimulation (Maezawa et al., 2006).

Evidence therefore supports the view that ApoE4 in its basal state, particularly when expressed neuronally, mediates disruption of neuronal architecture in a region, age, and sex-dependent manner. These effects may occur through dissociable developmental and neurodegenerative pathways and appear sensitive by cellular/systemic stressors which disrupt recovery.

1.5.4 APOE isoform modulation of synapse loss

Synapse loss is a salient marker of disease progression which is shown to precede that of gross degeneration while predicting impaired neuronal function in multiple neurodegenerative conditions, including AD, and is a strong predictor of cognitive decline (LeBlanc et al., 2005; Burke & Barnes., 2006; Clare et al., 2010). Given the strong association between APOE isoform and neuronal morphology, it would be intuitive that APOE4 may mediate premature synapse degradation prior to larger scale neurodegeneration, although evidence is contentious (Tzioras et al., 2019).

Synaptic integrity in APOE mouse models has typically been proxied via quantification of synaptic protein levels via western blot of brain homogenates or regional immunoreactivity analyses. In protein levels (i.e., western blot), some evidence suggests an age-dependent reduction in whole brain synaptic proteins including synaptophysin and GAP-43 in E4-TR and E4-GFAP mice from as early as 4-months (Bell et al., 2012). Similarly, reductions in PSD-95 and Drebin were reported in 4-month aged E4-TR male mice, with no differences in synaptophysin levels, although all markers were significantly reduced in E4-TR mice following LPS (lipopolysaccharide) administration (Zhu et al., 2012). However, no changes were observed in hippocampal or synaptosome-derived synaptophysin and PSD-95 levels between 3-month male (Lin et al., 2016), 8-months (Zhang et al., 2020) or synaptophysin alone in 12-months mixed sex (Nichol et al., 2009; Chouinard-Watkins et al., 2017) APOE-TR mice. This was modulated by contextual factors however, with hippocampal synaptophysin and PSD-95 levels impaired in 8-12-month aged E4-TR male mice following chronic stress (Lin et al., 2016; Zhang et al., 2020), while synaptophysin was elevated following an exercise intervention (Nichol et al., 2009).

Further, VgluT1 (vesicular glutamate transporter 1) levels were reported to decrease in 12-month aged E4-TR mice, but no differences were detected in Arc (Activity regulated cytoskeletal-associated protein) expression (Chouinard-Watkins et al., 2017). One report also

suggested a reduction in TrkB, the BDNF receptor (Brain-derived neurotrophic factor; Tropomyosin receptor kinase B) in 10-12-month aged E4-TR mice relative to E3-TR controls without any change in BDNF levels itself (Nichol et al., 2009).

Immunoreactivity analysis have also yielded contrasting findings, with young 3-4-month aged NSE-E4 mice exhibiting no difference in synaptophysin immunoreactivity in the cortex and hippocampus, but a deficit at 7-9-months which was exacerbated by excitotoxic injury (Buttini et al., 1999, 2002, 2010). Other reports have suggested no differences in synaptophysin immunoreactivity at 12-months in APOE-KI mice (Veinbergs et al., 1999), but reported losses at the later age of 15-months in E4-TR female mice (Zalocusky et al., 2021) and a delayed recovery of synaptophysin and GAP-43 following EHC-DG deafferentation in E4-KI mice (White et al., 2001). VgluT1 immunoreactivity was also reported to decreased in E4-TR mice at 12-months following chronic stress (Lin et al., 2016).

In terms of higher resolution techniques targeting synaptic structure, evidence is limited. Synaptic size and number were reported to decrease in 19-21-month E4-KI and APOE-KO mice relative to E2-KI and WT controls using electron microscopy methods (Cambon et al., 2000). Some recent evidence also suggested lowered spine formation dynamics and enhanced degenerative susceptibility of GluA2 but not GluN1 containing spines in WT mice primary neurons co-cultured with E4-TR glial cells (Nwasbuisi-Heath et al., 2014) while an overall reduction in both excitatory and inhibitory synaptic density also was observed in APOE-KO mouse neurons incubated with ApoE4 relative to ApoE3 (Konings et al., 2021). In contrast, two recent reports suggest a possible greater synaptogenic influence of both expression and acute action of ApoE4 relative to ApoE3 using hIPSC-derived neuronal cell lines (Huang et al., 2017, 2019; Lin et al., 2018), which may be dependent on an acute signalling role of ApoE. Importantly, this highlights the relevance of expression and action of both neuronal and glial-driven ApoE in the regulation of synapse integrity.

Together this evidence suggests that ApoE can positively modulate neuronal morphological properties by supporting outgrowth and spine dynamics, while ApoE4 specifically impairs or nullifies these processes. These effects appear to be exacerbated by ageing, exogenous stressors and by elevated neuronal APOE4 expression, but are influenced in a region-dependent manner. However, the precise roles of APOE4 in synaptogenesis and synaptic integrity remain unclear and would benefit from both expansion of the phenotyping currently performed in vivo, alongside use of combinatorial approaches to resolve interactions between

pre and postsynaptic structures simultaneously. Additionally, investigation of how APOE may play mechanistically dissociable roles in supporting synaptic structure over acute and chronic timescales is needed, perhaps representing acute signalling and chronic degenerative effects.

1.5.5 APOE isoform and synaptic plasticity

In addition to neuronal morphology, studies have investigated the influence of APOE isoform on both cellular and network level neuronal function and correlates of synaptic plasticity in APOE mouse models. Broadly, APOE isoform has been shown to differentially influence electrophysiological correlates of excitatory:inhibitory balance and synaptic plasticity, including LTP, with a number of potential mechanisms by which these effects may occur.

APOE isoforms have been demonstrated to alter network level neuronal activity within the hippocampus, entorhinal cortex, and amygdala of APOE mouse models. Firstly, as discussed in section 1.5.2, preceding DGH GABA-IN degeneration in 6-7-month aged E4-TR female mice is a reduction in inhibitory control of newborn DG granule cells. Specifically, hippocampal sections from 6-7-month aged E4-TR female mice exhibited a reduction in the frequency of postsynaptic IPSPs (inhibitory postsynaptic potentials) in newborn DG granule cells alongside a reduction in amplitude of spontaneous excitatory currents from DGH GABA-INs following axonal stimulation which was recovered by GABA saturation (Li et al., 2009), suggesting an APOE4-dependent loss of presynaptic DGH-DG granule cell inhibitory control. Further evidence of a late-age APOE4-mediated loss of inhibitory regulation was demonstrated in the lateral EHC (LEHC). A reduction in mIPSC amplitude, increase in field potential amplitude, increase in spontaneous firing, a power spectrum shift towards higher frequencies (>4Hz) and impaired high frequency stimulation-induced (HFS) LTP was detected in 20+ month aged E4-TR male mice relative to E3-TR controls (Nuriel et al., 2017). These two network level effects make the case for an APOE4-dependent disinhibitory phenotype within the trisynaptic circuit although how this is modulated by age and sex is less clear.

Evidence also suggests that APOE4 may affect basal excitatory synaptic transmission and the induction of LTP within the hippocampus, however there is substantial variability in findings and methodology between reports and results vary across components of the trisynaptic circuit. Firstly, application of exogenous ApoE4 prior to HFS in WT rat Schaffer collateral pathway in-vivo resulted in a marked impairment in the magnitude of late-phase LTP (L-LTP)

induction measured using field potentials, while post-HFS ApoE4 application had no effect on L-LTP relative to ApoE3. In addition, application of ApoE4 prior to HFS was associated with reductions in the levels of phospho-CREB (pCREB) and phospho-CAMKII (pCAMKII, Calmodulin-dependent protein kinase II), suggesting a suppressive role for acute action of ApoE4 in the activation of calcium-dependent signalling cascade to support L-LTP induction while having less impact on maintenance (Qiao et al., 2014).

Second, evidence from ex vivo slice preparations using APOE mouse models suggests that induced LTP may either increase or decrease as a result of ApoE4 relative to ApoE3 action. Korwek et al. (2008) demonstrated that Schaffer collateral CA3-CA1 LTP was potentiated in 3-month aged E4-TR hippocampal sections or via acute application of ApoE4 to APOE-KO mouse hippocampal sections, without alterations in input-output relationships. However, there was a specific reduction in NMDAR mediated field potentials and no alteration in NMDAR-independent LTP induction (Korwek et al., 2008). In support of this, increased magnitude of HFS-induced LTP in CA1 preparations were detected in E4-KI mice but not E3-KI at 2-months relative to WT, while E4-KI mice assessed at 6-7-months showed no difference relative to WT (Kitamura et al., 2004). However, Sun et al. (2017) recently demonstrated impaired LTP magnitude, accompanied by increased input-output relationships and short-term plasticity via paired pulse facilitation (PPF) within Schaffer collateral pathway in ~4-month aged E4-TR mice relative to E3-TR controls and an attenuated LTP deficit at 12-months. Similarly, in the perforant path, an impairment in HFS-induced LTP was demonstrated between the EHC and the DG molecular layer in 2-4-month aged E4-TR mice relative to E3-TR controls (Trommer et al., 2004).

Further conflict arises from two recent studies utilising in vitro hIPSC-derived neurons. First, an increase in mEPSC amplitude and frequency was reported following acute ApoE4 application (Huang et al., 2019) while APOE4 expression increased mEPSC frequency alone (Lin et al., 2018). These results were in conjunction with enhanced ERK signalling and synaptogenesis following acute ApoE4 application, suggesting an APOE4-dependent induction of a synaptogenic program to enhance excitatory transmission. Again, the reasons for these conflicts are unclear but appear, in part, driven by model system differences. Indeed, it was noted that the isoform-specific potentiating effect of ApoE4 on the ERK-dependent synaptogenic pathway associated with the increased excitatory transmission became equivalent between isoforms when ApoE was applied via glial conditioned medium. This suggests that while ApoE4 may drive a synaptic potentiating effect in isolation, this effect may

be superseded physiologically when in combination with glial-secreted factors (Huang et al., 2019).

Overall, these findings suggest complex relationships between APOE isoform and modulation of synaptic function, which, mirrored in reports on neuronal morphology, appears dependent on subregion, age, acute versus chronic ApoE action at the synapse, and a possible specific susceptibility of the NMDA receptor. However, between study discrepancies remain largely unexplained. It is also not clear what mechanisms may drive an ApoE4-dependent synaptogenic and enhanced excitatory transmission effect upon acute action or early in the lifespan relative to possible late-life disinhibitory effects of ApoE4 over more chronic time scales.

1.5.6 APOE isoform, ApoE signalling and calcium homeostasis: Implications for synaptic function

One mechanism through which APOE may act on synaptic function is via activation of receptor-mediated signalling cascades and by modulating calcium homeostasis. APOE has been shown to interact with neuronal function indirectly through its action as a putative signalling molecule, via activation of the LDLR, LRP and related receptor families. Activation of multiple members of these families, such as ApoER2 (ApoE receptor 2, also known as LRP8) via their ligands (such as Reelin in the case of ApoER2) are implicated in critical signalling roles to support neuronal growth, axonal pathfinding, and synaptic plasticity (Drakew et al., 2002; D'Arcangelo et al., 2006; Herz., 2006; Durakoglugil et al., 2009; Nakajima et al., 2013; Lane-Donovan et al., 2014; Lane-Donovan & Herz., 2017). Crucially, Reelin action at the ApoER2 via application to hippocampal sections induces LTP at the Schaffer collateral pathway, while APOE isoform has been shown to impact the efficacy of this process. Specifically, ApoE4 supresses the induction of Reelin-dependent LTP in vitro and in vivo, suggested to be mediated by increased endosomal trapping and impaired recycling of these receptors to the cell surface, reducing the chronicity of Reelin signalling (Chen et al., 2010; Xian et al., 2018; Pohlkamp et al., 2021). Further, LDLR family signalling also activate a downstream PI3K-Akt-GSK-3B (Phosphoinositide-3-kinase; Akt/Protein kinase B; Glycogen synthase kinase 3 beta) pathway, which acts at the level of the actin cytoskeleton to stimulate polymerisation for neurite

outgrowth, through which APOE4 may also alter effective neurite growth and synaptogenesis (Lane-Donovan & Herz., 2017; Beffert et al., 2002).

APOE is also implicated in the regulation of calcium-dependent signalling via interaction with its receptors, providing another pathway to influence synaptic plasticity. Regulation of intra and extracellular calcium concentrations via homeostatic mechanisms is crucial for the control of neuronal activity and a number of cellular processes including calcium-sensitive intracellular signalling cascades such as regulation of synaptic gene expression via the transcription factors including CREB and AP-1 (Activator protein 1; Foster et al., 2007).

The direct application of ApoE to neuronal cell lines has been shown to induce a significant increase in intracellular calcium, which is potentiated by ApoE4 relative to ApoE3 (Tolar et al., 1999; Ohkubo et al., 2001; Veinbergs et al., 2002; Qiu et al., 2004; Jiang et al., 2015). Similarly, elevated peak calcium and bursting responses were observed in WT mouse neurons treated with E4-TR astrocyte conditioned medium, suggesting these effects can be mediated by secreted ApoE and at physiological ApoE concentrations (Konings et al., 2021). Pharmacological blockade experiments also have highlighted that this upregulation of cytosolic calcium is dependent on both L-type voltage-gated calcium channels (L-VGCCs) and NMDA receptors, while requiring the interaction between ApoE and its cognate receptors (Ohkubo et al., 2001; Qiu et al., 2003; Veinbergs et al., 2002; Ramakrishna et al., 2021). Evidence also suggests that ApoE4 may potentiate calcium accumulation via efflux from intracellular stores into the cytosol (Larramona-Arcas et al., 2020) or via inhibition of delayed rectifier potassium channels (Qin et al., 2006).

Possibly consequent to ApoE4-mediated impairments in calcium homeostasis are alterations in calcium-dependent signalling proteins. Evidence in vitro, and to a lesser extent in vivo, suggests that ApoE4 potentiates multiple signalling pathways downstream its receptor, including ERK1/2, Akt (AKT serine/threonine kinase 1), Src (SRC non-receptor tyrosine kinase), and eEF2 (Eukaryotic elongation factor 2; Ohkubo et al., 2001; Korwek et al., 2008; Yong et al., 2014; Huang et al., 2017, 2019; Ramakrishna et al., 2021). One study demonstrated that the signalling potentiation effect of ApoE4 may be differentially regulated in vivo by age, with female E4-TR mice exhibiting an early-life (3-4-months) upregulation of calcium signalling pathways (including CREB, ERK, CAMKII [Calmodulin kinase 2], and PKC [Protein kinase C]), while reaching similar levels to E3-TR females at 8-months before showing pathological downregulation at 16-months (Yong et al., 2014). Further, recent evidence has demonstrated a

direct link between acute action of ApoE4 to stimulate of calcium influx via NMDAR/L-VGCC activation, and chronic downstream stimulation of an eEF2-dependent synaptic gene expression pathway (Ramakrishna et al., 2021).

These data suggest that ApoE4 may act through somewhat separable mechanisms through its receptors, driving potentiation of calcium signalling and synaptic gene expression but may have opposing effects on synaptic function via defects in receptor recycling such as impairing Reelin-dependent LTP. The interactions of these effects with age and extent of conservation in vivo remain unclear. Further, given the association between ApoE4 and dysregulation of calcium signalling and network level aberrations in synaptic transmission, one relatively unexplored possibility is that APOE isoforms are differentially associated with immediate early gene (IEG) function in vivo. IEGs are intricately linked to mechanisms underpinning long-term synaptic plasticity, with many IEGs acting as transcription factors (such as CREB, c-Fos, and c-Jun) whose activation is calcium-dependent and drives the expression of synaptic proteins to support activity-dependent modulation of synaptic function (Kim et al., 2018; Minatohara et al., 2016; Chung et al., 2015; Morgan & Curran., 1991). Persistent neuronal activation within neuronal networks is associated with significant increases in IEG expression which have been used to mark 'neuronal ensembles' during and following behaviour. These neuronal ensembles are suggested to represent a distributed network of neurons which are functionally relevant for information processing during various behaviours and prime plasticity-related processes requiring gene expression for supporting consolidation of such behaviours (Tonegawa et al., 2015; Cruz et al., 2015). Therefore, an important question to understand the potential functional network level consequences of APOE isoform in vivo, is whether APOE isoform differentially modulates IEG expression and neuronal ensemble engagement at baseline and following experience-dependent activation. This question encompassed one aim of the present thesis.

1.6 Influence of APOE isoform on episodic-like learning and memory in APOE mouse models.

The characterisation of the effects of APOE isoform on cognition and behaviour has predominantly focussed on episodic-like spatial memory assays in APOE mouse models. This is, in part, due to the association of episodic memory vulnerability with both age-related decline

and as a key cognitive marker and diagnostic criteria for LOAD. Consequently, APOE mouse models have provided evidence for APOE isoform, age, and sex-specific effects on episodic learning and memory function. Assays used to assess these functions in mice have generally relied on classical spatial navigation and discrimination tasks, including the Morris water maze (MWM; Morris 1984; described in section 1.1.2) and Barnes maze reference memory tasks, spatial object recognition (SOR) tasks, alternation tasks such as the Y or T-maze, spatial avoidance learning, and contextual fear conditioning. Table 1.2 provides a summary of key findings in the literature relating to the influence of APOE isoform on episodic memory function across the lifespan in varying mouse models.

Table 1.2: Table (next page) summarising primary findings from the literature in assessments of episodic-like learning (acquisition) and memory (retrieval) in APOE mouse models. Behavioural task, APOE model system, age, sex, and simplified results for acquisition and retrieval performance, and retrieval delay are provided. Note that findings are represented symbolically, with ">" representing greater performance, and "<" representing poorer performance. Colour coding is also provided for each finding with: red = an APOE4-specific impairment, orange = no difference, and green = APOE4-specific advantage or APOE3 impairment. "?" refers to parameters which were unclear or unreported. Blank spaces represent when a parameter is not applicable (e.g., no assessment of retrieval, therefore no retrieval delay). Studies are described in the main text while specific details of parameters are represented here for simplification.

Author	Year	Task	Model	Age	Sex	Acquisition	Retrieval	Retrieval delay
Andrews-Zwilling	2010	MWM	APOE-TR	12m	F	ND	ND	24-120h
		MWM	APOE-TR	16m	F	E4 < E3	ND @ 24-72h, E4 < E3 @ 120h	24-120h
		MWM	APOE-TR	21m	F	E4 < E3	ND @ 24-72h, E4 < E3 @ 120h	24-120h
		MWM	APOE4Δ272-299	12m	F	E4 < WT = E4-TauKO	E4 < WT = E4-TauKO	24h
Basaure	2019	BM	APOE-TR	6m	MF	E4 < E3	E4 < E3	24h
Bour	2008	DMTP MWM	APOE-TR	15-18m	MF	FE4 least improvement; most groups impaired		NA
		SOR	APOE-TR	15-18m	MF		E3 < all groups	15m
		Y-maze avoidance	APOE-TR	15-18m	MF	E3 = E4, F > M	E3F > E4F in avoidance, E4M > E4F in discrimination	48h
		MWM	APOE-TR	15-18m	MF	M>F; FE4 > E3/WT	E4F lowest; E4F & WTF below chance	24h
Harris	2003	MWM	APOE4Δ272-299	6-7m	M	E4 < WT	E4 < WT	72h
Engstrom	2017	NOR	APOE-TR	5-6m	MF		ND	1h
		CFC	APOE-TR	5-6m	MF	ND		
		T-maze	APOE-TR	12-13m	MF	ND		
Grootendorst	2005	DMTP MWM	APOE-TR	4-5 months	MF	E3 & E4 no improvement in trial 2, improved trials 3-4		
		SOR	APOE-TR	4-5 months	MF		FE4 < all groups	15m
		Y-maze avoidance	APOE-TR	4-5 months	MF	E3M most errors	M > F discrimination	48h
		MWM	APOE-TR	4-5 months	MF	FE3 no improvement	E4 lowest	24h
Guardia-Escote	2018	MWM	APOE-TR	9m	F	ND	E4F < E3F	24h
Hartman	2001	Rotating holeboard	GFAP-APOE	5m	M	ND trials to criterion	ND	24h
		MWM	GFAP-APOE	9-12m	M	ND	ND	2h?
		RAM working memory task	GFAP-APOE	11-14m	M	E4 < E3 across days		
		Rotating holeboard	GFAP-APOE	14-17m	M	E4 & WT < E3	ND	24h
Hayley	2012	MWM	APOE-TR	5-6m	M	ND	E4 < E3	1h
Johnson	2014	MWM	APOE-TR/LDLR-/hLDLR+	10-12m	F	ND	ND @ 24h; hLDLR-KI E3 > hLDLR-KI E4 @ 72h	24-72h
Jones	2019	MWM	APOE-TR	6-9m	F	ND		
		MWM	APOE-TR	13-19m	F	E4 < E3		
		Spatial avoidance	APOE-TR	13-19m	F	E4 < E3		
Jones	2021	BM	APOE-TR	9m	MF	E4 < E3 (D1-D2)		
Knoferle	2014	MWM	APOE-TR	17m	F	E4 < E3	ND @ 72h; E4 < E3 @ 120h	72-120h
Leung	2012	MWM	APOE-TR	12m	F	ND	ND	24-72h
		MWM	APOE-TR	16m	F	E4 < E3	ND @ 24h; E4 < E3 @ 72h	24-72h
Maoli	2012	MWM	APOE-TR	6m	?	E4 < E3	ND (on HFD: E4 < E3)	24h
Meng	2015	Y-maze exploration	GFAP-APOE	8m	M		E4 < E3 1h; ND 24h	1h/24h
		NOR	GFAP-APOE	8m	M		ND at 1/24h	1h/24h
Peris-Sampedro	2015	BM	APOE-TR	7-8m	M	E4 < E3	ND	24h

Author	Year	Task	Model	Age	Sex	Acquisition	Retrieval	Retrieval delay
Pontifex	2021	BM	APOE-TR	12m	F	E4 < E3	E4 < E3	24h
		NOR	APOE-TR	12m	F		ND	1h
		Y-maze	APOE-TR	12m	F	E4 < E3		
Raber	1998	MWM	NSE-APOE	3m	MF	FE4 < FE3	ND	?
		MWM	NSE-APOE	6m	MF	FE4 < FE3	FE4 < FE3	?
Raber	2000	MWM	NSE-APOE	6m	MF	ND	E4F < E3F	?
		MWM	NSE-APOE	18m	MF	E4F < E3F	E4F < E3F	?
Raber	2002	NOR	NSE-APOE	6m	MF		E4F < E3F	24h
		MWM	NSE-APOE	6m	MF	E4F < E3F	E4F < E3F	1h
Reverte	2012	MWM	APOE-TR	4-5m	MF	E4 < E3	E4M = E3M; E4F < E3F	72h
Reverte	2013	MWM	APOE-TR	4-5m	MF	E4 < E3	E4 < E3 @ 24h; FE4 < FE3 @ 72h	24/72h
Rodriguez	2013	BM	APOE-TR	3m	MF	E4 < E3	E4 < E3	72h
		BM	APOE-TR	18m	MF	E4 < E3	E4 < E3 (trend)	72h
		MWM	APOE-TR	3m	MF	ND	E4 < E3	72h
Schmitt	2021	Star maze	APOE-TR	6m	M	ND		
		Y-maze	APOE-TR	6m	M	E4 < E3 + reversal deficit		
		Y-maze	APOE-TR	14m	M	ND		
Shinohara	2016	MWM	APOE-TR	7-8m	MF	ND	ND	24/72h
		MWM	APOE-TR	22-24m	MF	E4 < E3	E4 < E3 @ 24h, E4 = E3 @ 72h	24/72h
Siegel	2012	MWM	GFAP-APOE/APOE-TR	6-8m	F	E4 > E3; GFAP-E4 < E4-TR	ND	1h
		MWM	GFAP-APOE/APOE-TR	10-13m	F	E4 > E3; GFAP-E4 < E4-TR	ND	1h
		MWM	GFAP-APOE/APOE-TR	14-22m	F	E4 > E3; GFAP-E4 < E4-TR	ND	1h
Speidell	2019	BM	APOE-TR	6m	F	E4 < E3	E4 < E3 (primary measures)	72h
Van Meer	2007	MWM	GFAP-APOE	6m	F	ND	E4 < E3	1h
Veinbergs	1999	MWM	APOE-KI Xu	12m	M	E4 = WT < E3		
Villasana	2006	MWM	APOE-TR	4-6m	F	ND	E4 < E3	24h
Villasana	2011	MWM	APOE-TR	13m	MF	ND	FE4 < FE3; ME4 = ME3	24h
Villasana	2016	MWM	APOE-TR	5-6m	F	ND	ND	1h
Tong	2014	MWM	APOE-TR	17m	F	E4 < E3	E4 < E3	120h
Tong	2016	MWM	APOE-TR	16m	F	E4 < E3	E4 < E3	72h
Zhang	2019	MWM	APOE-TR	18m	F	E4 < E3	ND	24h

1.6.1 Early to mid-age alterations of reference memory in APOE mouse models

At young to mid age, there has been considerable variability in the reported effects on episodic-like memory in APOE mouse models, which appear influenced by sex, the particular task used, and the methodological differences in parameters related to memory function such as retrieval delay (shown in Table 1.2). In conflict, null differences, performance advantages, and performance impairments by APOE isoform have been reported using reference memory tasks. Additionally, a frequent observation across studies is the dissociation between effects of APOE isoform on encoding (acquisition/learning) and retrieval (memory recall) performance in these tasks.

At the earliest age, studies have demonstrated impairments in 3-6-month aged E4-TR mice during acquisition and both 24-hour (Basaure et al., 2019; Reverte et al., 2012, 2013) and 72-hour (Rodriguez et al., 2013; Speidell et al., 2019; Reverte et al., 2012, 2013) retrieval in the Barnes maze or MWM. However, at the same age, some reports demonstrated only a deficit in 24-hour retrieval but not acquisition and specifically in E4-TR female mice (Grootendorst et al., 2005; Villasana et al., 2011), or only E4-TR deficits in acquisition (Maioli et al., 2012). In further conflict, two studies demonstrated no genotype differences in APOE-TR mice at 5-8-months in either acquisition or 24-72-hour retrieval (Villasana et al., 2016; Shinohara et al., 2016), while another suggested an advantage in acquisition for E4-TR females but no difference following a shorter 1-hour retrieval delay (Siegel et al., 2012). Finally, two studies using passive avoidance memory demonstrated an impairment in E4-TR females (Villasana et al., 2006) or E3-TR mice of both sexes at 4-6-months (Grootendorst et al., 2005).

Towards mid-age, reports are similarly conflicting. From 9-12-months, studies have reported deficits in acquisition in E4-TR females (Jones et al., 2021), deficits in both acquisition and 24-hour retrieval (Pontifex et al., 2021), deficits in 24-hour retrieval and/or no changes in acquisition in E4-TR/E4-KI mice (Guardia-Escote et al., 2018; Veinbergs et al., 1999). No differences in either acquisition or retrieval with between 24-120-hour retrieval delays was also reported in 12-month aged male or female E4-TR mice (Andrews-Zwilling et al., 2010; Leung et al., 2012).

In comparing other transgenic APOE mouse lines with astrocytic or neuronal only hAPOE expression from young to mid-age, evidence is also mixed. One group reported conflicting

findings between ~6-month aged cohorts of GFAP-APOE mice in the MWM, with E4-GFAP (astrocytic hAPOE, see Table 1.1) mice showing impaired acquisition but not 1-hour retrieval (Siegel et al., 2012) or no difference in acquisition and impaired 1-hour retrieval (Van Meer et al., 2007). Further, no differences in acquisition or retrieval were reported between GFAP-APOE mice of mixed sex at mid-age between 9-13-months (Siegel et al., 2012; Hartmann et al., 2001). In contrast, some reports using the APOE-NSE (neuronal hAPOE; see Table 1.1) model are more consistent. NSE-E4 female, but not male, mice were shown to exhibit deficits in acquisition in the MWM at 3-6-months, primarily in later learning blocks, demonstrating an early plateau effect, alongside a 3-4-hour retrieval deficit specifically in the 6-month aged female group (Raber et al., 1998, 2000, 2002).

Intriguingly, one study demonstrated that KO of the endogenous LDLR in mid-aged 10-12-month female APOE-TR mice impaired overall 24-72-hour retention in the MWM. This retrieval deficit was rescued by expression of the human form of the LDLR in E3-TR mice, while E4-TR mice remained impaired in 72-hour retrieval. Further, a positive correlation was observed between levels of ApoE expression in the hippocampus and 72-hour retention accuracy, but only in the presence of hLDLR expression. This suggests that interactions between APOE and the LDLR, and regulation of circulating levels of ApoE, are crucial for supporting long term reference memory, but that this interaction is impaired by ApoE4 (Johnson et al., 2014).

The conclusions that can be drawn from these studies in young-mid aged APOE mouse models are complex given the extensive variability between reports. While it appears that expression of APOE both solely in astrocytes or neurons using the APOE-GFAP or APOE-NSE system, or systematically using the APOE-TR system, can have influences on spatial learning and memory performance, the stark conflict in these results is surprising. However, the overall trend would suggest a deficit in acquisition and retrieval in E4-TR mice, which may be worsened in females. Moreover, neuronal expression of APOE appears to be more detrimental than glial expression to spatial learning and memory performance, as demonstrated by the APOE-NSE model which is consistent with the neuropathological associations of neuronal APOE expression (e.g., Raber et al., 2002; Buttini et al., 1999, 2010; Knoferle et al., 2014; Zalocusky et al., 2021).

1.6.2 Late-age alterations of reference memory in APOE mouse models

At late age, reference memory performance in APOE mouse models is somewhat more consistent but controversy still exists. Reports have demonstrated deficits in E4-TR mice at 15-24-months in acquisition alone (Rodriguez et al., 2013), or in both acquisition and 24-hour retrieval (Shinohara et al., 2016), or a mild advantage in acquisition but mildly poorer 24-hour retrieval (Bour et al., 2008). However, no differences were observed between comparably aged GFAP-APOE mice in 24-hour 'reacquisition' in a holeboard task (Hartmann et al., 2001) or MWM acquisition and 1-hour retrieval in APOE-TR mice (Siegel et al., 2012). Again, as observed at young-mid age, 18-month aged NSE-E4 female mice show more consistent deficits in both acquisition and short-term retrieval in the MWM, with no impairment in males as observed in the younger cohort (Raber et al., 1998, 2000, 2002).

In contrast, a host of reports from the work of the APOE research group at the Gladstone institute have provided robust support for an interaction between sex, APOE isoform, and aging. These results suggest a female-specific E4-TR deficit from 14-16+ months in acquisition and long-term retrieval generally between 48-120-hours in the MWM and a spatial avoidance task across multiple cohorts (Andrews-Zwilling et al., 2010; Leung et al., 2010; Knoferle et al., 2014; Tong et al., 2014, 2016; Jones et al., 2019). Crucially, this deficit in reference memory acquisition and retrieval in aged E4-TR female mice has been specifically linked to an impairment in dentate gyrus hilar (DGH) GABAergic function. As discussed in section 1.5.2, E4-TR mice exhibited strong correlations between DGH GABA-IN loss and reference memory deficits, which were rescued via preventing neuronal APOE expression, GABA-IN degeneration, or by enhancing GABAergic signalling (Andrews-Zwilling et al., 2010; Knoferle et al., 2014; Tong et al., 2014, 2016). This striking set of results have provided strong evidence for a specific deficit in long-term episodic memory in female E4-TR mice at late-age which appears, in part, mediated via DG GABAergic dysfunction. However, this model, while convincing, fails to explain the extensive heterogeneity observed in previous studies of APOE mouse models. Namely why some studies demonstrate earlier spatial reference memory impairments in APOE4-carrying mice preceding reported GABAergic deficits, and particularly why such deficits are sometimes observed in mice of both sexes.

Finally, although beyond the scope of the present work, evidence also suggests that APOE4 is associated with a greater detriment to episodic memory performance following multiple types of endogenous or exogenous stressors across age. Briefly, APOE4 mouse models showed

impaired acquisition or retrieval performance following expression of the truncated APOE4Δ272-299 form (Brecht et al., 2004), controlled cortical impact (Giarratana et al., 2020; although see Mannix et al., 2011. 2013), carotid artery stenosis (Koizumi et al., 2018), high fat diet (Maioli et al., 2012; Jones et al., 2019), ovarian failure or circulating androgen deficits (Pontifex et al., 2021; Raber et al., 1994, 2002, 2008; Acevedo et al., 2008), and chronic stress (Lin et al., 2016). However, there is more contention over the influence of environmental toxicants on performance with some suggestions of an increased susceptibility of E3-TR mice to oxidative stress inducing toxicants (Jiang et al., 2019; Reverte et al., 2013; Peris-Sampedro et al., 2015; Basaure et al., 2019).

At late age, evidence overall points to deficits in both acquisition and retrieval of reference memory in E4-TR mice relative to E3-TR controls, which appear exacerbated in females. These results remain variable across reports, however. There is strong evidence for a GABA-IN-mediated neurodegenerative pathway in E4-TR female mice which may drive spatial memory impairments, while some deficits in aged male E4-TR mice remain unexplained. Further, evidence generally supports a detrimental influence of ApoE4 on episodic memory performance following systemic stress. Together these heterogeneous results highlight the need for further replication and standardisation of task parameters when assessing reference memory performance across age.

1.6.3 Alterations to short-term spatial memory and rapid place learning in APOE mouse models

Other spatial tasks such as the rapid place learning delayed match to place (DMTP) MWM task (Steele and Morris., 1999) have been reported, alongside comparable non-maze rapid or short-term memory tasks, albeit less frequently. The primary difference in task manipulations centre around a reduced number of reinforcement trials and imposing short inter-trial intervals taxing memory formation and retrieval over short time constraints or as few experiences as a single trial (discussed in section 1.1.4).

In the DMTP MWM task, the only two reports in APOE-TR mice showed transient impairment in 1-hour retrieval in both E3-TR and E4-TR mice at 4-5-months relative to WT, while performance at 15-18-months was poor across all groups with the lowest acquisition improvement observed in females (Grootendorst et al., 2005; Bour et al., 2008) possibly

suggesting poor task adherence. In the SOR task, impaired 15-minute retrieval performance was reported in 4-6-month E4-TR female mice (Grootendorst et al., 2005), or no difference between APOE-TR mice at the same age at a delay of 1-hour (Engstrom et al., 2017), while between 15-18-months E3-TR mice were more impaired (Bour et al., 2008). There is also some evidence for an APOE4 impairment in rapid acquisition using spatial alternation tasks with deficits reported in 6-month E4-TR male mice (Schmitt et al., 2021), and mid-aged animals from 9-13-months including, mid-aged female E4-TR mice (Pontifex et al., 2021), and E4-GFAP male mice (Hartmann et al., 2011; Meng et al., 2015), but not mid-aged E4-TR male mice (Schmitt et al., 2021). Additionally, a flexibility deficit was also noted in 6-month aged E4-TR male mice, with poorer reversal learning in an alternation task (Schmitt et al., 2021).

Together, the data surrounding APOE isoform and rapid place learning is limited. The conflicts between reports again appears partly mediated by differences in intrinsic task design and memory parameters such as retrieval delays. Notably the tasks used can be segregated broadly into spatial alternation, spatial recognition, and allocentric place learning, which tap somewhat separable processes. Namely, alternation tasks typically rely on very short-term or working memory, while single trial to short-term acquisition tasks including place learning and recognition tasks are more analogous to everyday memory tasks. The possibility of a dissociation between short- and longer-term recall by APOE isoform is intriguing, with some evidence suggesting that rapid encoding and updating conditions (e.g., 15-minutes versus 1-hour; Grootendorst et al., 2005; Engstrom et al., 2017) may be preferentially impaired by APOE4. This remains to be explored further, however, and it is clear that better characterisation of the lifespan influence of APOE isoform in these mouse models is required.

1.6.4 Caveats and conclusions from the episodic memory literature in APOE mouse models

The literature surrounding the influence of APOE isoform on cognitive performance in mouse models, particularly spatial learning and memory is complex. In young-mid age there is considerable variability in both the directionality and magnitude of reported effects. As discussed, no differences or dissociations between impairments in acquisition and retrieval have been demonstrated, although there appears to be a tendency for a mild deficit in APOE4 mice in both acquisition and retrieval. At old age there is somewhat more consistency, with

evidence supporting an acquisition and long-term retrieval deficit in APOE4 mice, which is more prominent in females and exacerbated following neuronal expression of APOE4. Further, there appears to be more consistency in the directionality of deficits in the presence of exogenous stressors or injury, with APOE4 generally conferring greater injury-induced impairments in learning and memory. However, most relevant to the present thesis is the discrepancy between studies of APOE isoform and spatial learning and memory performance in absence of other perturbations to the CNS.

There are a number of factors which may contribute to these discrepancies. In short, task type, the lack of standardisation and wide variability in memory relevant parameters used such as number of reinforcing 'encoding' acquisition trials, trial spacing (or inter trial-interval, ITI), long-term or short-term retrieval delay in probe trials, and varying habituation/training protocols, poses problems for interpretation. These parameters are known to be critical in rodent memory tasks, with previous literature demonstrating that an increased number of encoding trials, lower ITI, and shorter post-encoding delay predict higher performance, at least in WT rodents (e.g., Wang et al., 2010; Wingard et al., 2015; Takeuchi et al., 2016; Nonaka et al., 2017; Bast et al., 2005).

First, as outlined in the literature above, retrieval delays of between short (e.g., 15-minutes to 1-hour; Grootendorst et al., 2005; Raber et al., 2000; Siegel et al., 2012) to particularly long (e.g., 72-120-hours; Andrews-Zwilling et al., 2010; Leung et al., 2012; Rodriguez et al., 2013) have been used within the same task, which has predominantly been the MWM reference memory variant. While the conclusion from this literature may appear to tend towards the suggestion that APOE4 induces more marked impairment in long-term memory formation, maintenance, and retrieval, at least following extended reinforcement, this is not always the case. Indeed, the majority of studies have used 24-hour or longer retrieval delays (see Table 1.2) with less investigation of shorter delays and rapid place learning. In terms of number of acquisition trials, as few as two (e.g., Andrews-Zwilling et al., 2010), to as many as eight (Hartman et al., 2001) acquisition trials per session have been reported, with varying within-day ITI delay including 5-10-minutes (e.g., Grootendorst et al., 2005) to 2-4-hours (e.g., Andrews-Zwilling et al., 2010; Johnson et al., 2014). Indeed, there is some evidence between studies of impairments as early as 15-minutes but not 1-24-hours in APOE4 mice may suggest differential encoding and consolidation efficacy by APOE isoform (e.g., Hartmann et al., 2001; Meng et al., 2015; Engstrom et al., 2017). Additionally, the days of task administration also varies between 2-5 days (Hartman et al., 2002; Andrews-Zwilling et al., 2010) or longer (e.g.,

Johnson et al., 2014), the contingency of which may complicate the separation of reinforcement and retrieval delay effects. Ultimately these parameters modulate performance while also conferring the possibility of transition between hippocampal-dependent episodic-like memory acquisition and overtrained memory or procedural learning (e.g., Bast et al., 2009; discussed in section 1.1.4).

The diversity of results across different task types may also suggest differing sensitivity of these tasks and involved cognitive processes to APOE-mediated impairments. Notably, deficits reported in the Barnes maze may arguably be more consistent and have been reported earlier in the lifespan than its MWM counterpart (e.g., Rodriguez et al., 2014; Basaure et al., 2019; Peris-Sampedro et al., 2016; Pontifex et al., 2012; Speidell et al., 2019; Jones et al., 2021). This may, in part, driven by differing motivational and stress-related task demands (e.g., Harrison et al., 2006; Youn et al., 2012; Rodriguez et al., 2013).

Overall, the literature investigating episodic-like memory in APOE mouse models highlights both the need for replication and systematic manipulation of memory related parameters (e.g., retrieval delay, trial spacing, reinforcement etc.) to gain a clearer consensus on interactions between APOE isoform, age, and sex in these tasks. The particularly variable age ranges assessed, while allowing inferences to be made in a cross-sectional manner across studies, makes comparisons of animal cognitive trajectories across the lifespan difficult. Further, it is clear that intermediate-long term reference memory via the MWM has been favoured in APOE research, likely due to both its well-established and easily administered nature, and ability to assess fidelity of longer term episodic-like memory.

Rapid place learning or everyday memory has been less well characterised, however, and the potential age-dependent influence of APOE on this domain remains less clear. The development of ‘everyday’ memory analogues in rodents in recent years (as discussed in section 1.1.4) provides an attractive supplement, to allow assessment of rapid updating and retention of novel episodic-like information on the background of prior rule learning. Such tasks provide a powerful platform upon which to assess within and between-subject manipulations, including systematic task parameter manipulation (Nonaka et al., 2017; Broadbent et al., 2020). Additionally, such tasks offer the benefit of repeat testing with, when well controlled, little fatigue or stress-related effects in rodents (e.g., Wang et al., 2010; Takeuchi et al., 2016). This therefore warrants the investigation of the lifespan trajectories of

APOE model mice in rapid place learning and memory as a proxy for everyday memory function, which comprises a primary aim of this current thesis.

1.7 Summary and primary objectives

APOE4 is the primary genetic risk factor for LOAD, yet both animal and cell models demonstrate that APOE4 exhibits a number of AD-pathology independent phenotypes, suggesting separable roles in the incipience of cognitive decline. Animal models of APOE function have primarily focussed on the characterisation of hippocampal-dependent episodic-like reference memory performance. This has demonstrated markedly mixed results, with evidence primarily supporting that APOE4 promotes an age-dependent impairment in learning and reference memory in late-age, with a female bias. However, the relative impact of APOE isoform on 'rapid place' learning and memory (i.e., everyday memory) across the lifespan remains to be assessed. Additionally, evidence highlights complex interactions between APOE4 and impairments in hippocampal neuronal morphology, synaptic plasticity, and dysregulation of multiple signalling pathways, which may contribute to these observed impairments in neuronal and cognitive function. Evidence, predominantly in vitro, also indicates that APOE isoforms may differentially impact signalling including the induction of IEGs, however the influence of APOE on IEG induction and neuronal ensemble activity in vivo following behaviour has not been investigated.

Therefore, the primary questions of the present thesis were:

1. Does APOE isoform and sex impact ageing trajectories of rapid place learning and memory performance across the lifespan of the APOE-TR mouse model?
2. Does APOE isoform, sex, and age impact hippocampal neuronal ensemble activation following behaviour in the APOE-TR mouse model?

The primary hypotheses for these questions were:

1. E4-TR mice would demonstrate earlier impairments in trajectories of rapid learning and memory performance than E3-TR mice, which may be exacerbated in females.
2. E4-TR mice would demonstrate reductions in hippocampal ensemble activation and IEG expression following behaviour, which may again be exacerbated in females and by ageing.

To address our initial research question, we first aimed to establish an effective task for measuring everyday memory (Chapter three) amenable to repeat testing in order to assess APOE-TR mice using a longitudinal design across the lifespan (Chapter four). To address our

second research question aiming to investigate the influence of APOE on neuronal ensemble activation in the hippocampus at baseline conditions and following behaviour, we used IEG imaging and biochemical methods following a contextual novelty paradigm (Chapter five). In final experiments, we further investigated whether an APOE-dependent hippocampal ensemble phenotype was associated with alterations to dendritic structure and putative synaptic occupation using cell tracing and imaging methods (Chapter six).

CHAPTER TWO

General methodology

2.1 Animals and PCR genotyping

2.1.1 Animal maintenance

APOE-TR mice (E3-TR, E4-TR; Sullivan et al., 1997; Knouff et al., 1999), gifted by Dr Nobuyo Maeda (UNC Chapel Hill, USA), were maintained on a C57BL/6J genetic background at the University of Sussex and were backcrossed for at least 8-generations. Experimental mice were derived from colony lines bred to develop mice of E3E3 and E4E4 homozygous genotype, or E3E4 (E3E4-TR) heterozygous genotype. Wildtype-only experiments used C57BL/6J mice purchased from Charles River Laboratories (Harlow, UK).

Animals used for colony maintenance or experiments were kept on a 12h light/dark cycle (lights on: 7am) and provided access to water and regular chow *ad libitum*, with the exception of experiments requiring food restriction which is detailed in subsequent chapters. All stocks were maintained, and experiments conducted in accordance with UK Home Office Animals (Scientific Procedures) Act 1986 (revised 2013) following review and approval by the University of Sussex Animal Welfare and Review Board (AWERB; PPL licence number: PP3378340). Any experiment-specific alterations to holding procedures are outlined in subsequent experimental method sections.

2.1.2 Genotyping of animals

Progeny were regularly genotyped to ensure maintenance of allele purity using standard in-house PCR assays followed by visualisation using gel electrophoresis imaging using an ultra-violet (UV) transilluminator (Syngene). All primer sequences used are presented in Table 2.1 and all relevant reagents are presented Table 2.3.

2.1.2.1 Tissue lysis and DNA extraction

For each animal, small (~1mm^2) samples of ear skin tissue of animals were harvested and lysed overnight at 55°C in 250µl of a sodium chloride lysis buffer (10mM Tris-HCl, 10mM NaCl) and 7.5µl of 10µg/µl Proteinase K (Millipore). Samples were then centrifuged at 13,000RPM for 5 minutes before being stored at -20°C until use.

2.1.2.2 Primer design

All primers were designed in house or adapted from established protocols. In cases where primers were designed in house, PrimerBlast (NCBI) and PREMIER Biosoft PCR guides were typically used to aid primer selection, with use of the UCSC in silico PCR software to assess potential primer pair efficacy. Primers were purchased from Eurofins Genomics (Genomics UK).

2.1.2.3 APOE restriction fragment length polymorphism (RFLP)

A protocol for RFLP PCR with gel electrophoresis targeting hAPOE was adapted from Ossendorf et al. (2000, see for further details). Briefly, two primers were designed to flank the 112 site in exon 4 of the hAPOE genomic sequence, amplifying a 318BP product. The amplicon introduced differing AflIII restriction sites dependent on the presence of the APOE 112 C-T substitution (C112/R112) between isoforms. The amplicon generated from the E4-TR homozygote template introduced a single restriction site, generating a primary product of 295BP, while the E3-TR homozygote template introduced two restriction sites, producing a 232BP primary product. Heterozygous E3E4-TR template introduced both restriction sites, generating both the 232BP and 295BP products (Table 2.1).

2.1.2.4 APOE-TR flanking primers

Due to the associated cost and issue of reliability with the genotyping protocol adapted from Ossendorf et al. (2000) alongside the cost associated with high-resolution melt curves or Sanger sequencing alternatives, we developed and validated an alternative in-house PCR protocol. Two forward primers, and a common reverse primer were designed to flank the exon 4 C112 or R112 site in E3-TR or E4-TR mice, respectively (Table 2.1). The forward primers targeted the 112 site such that the final base of the 3’ end of the forward primer matched or mismatched the respective base in the E3-TR or E4-TR genome, with a T-C substitution. The common reverse primer was downstream in exon 4, generating a 131BP amplicon. This design enabled the detection of either one or both APOE isoforms from lysed tissue, by running two PCR reactions per sample, one using E3-TR forward primer and common reverse, and another

with the E4-TR forward primer and common reverse (Table 2.1). We observed that the 3' single base mismatch was sufficiently sensitive to differentiate E3-TR and E4-TR genotypes based on known results from prior validated samples (see section 2.1.2.8).

2.1.2.5 Neomycin cassette and mAPOE targeting primers (WT/Neo)

To allow for a generic differentiation of the presence of WT or hAPOE alleles independent of isoform, primers were designed to target the neomycin resistance gene cassette within the APOE-TR construct (Sullivan et al., 1997; Knouff et al., 1999), generating a 167BP amplicon. Primers were also designed to target a 270BP region of the mAPOE exon 2, this was paired with the Neo primer set to validate the presence or absence of the targeted replacement construct and/or the presence of the wildtype mAPOE allele (Table 2.1).

2.1.2.6 PCR

Two reactions were typically designated to each sample for PCR in order to assess the presence of either both or a single hAPOE and/or mAPOE allele. Reactions were each 25µl or 50µl total, comprised of premade master mix (MegaMix Blue or MegaMix Blue Double, Clent Life Science) at 25% or 50% of reaction total volume, 1µM final concentration of forward primer, 1µM of reverse primer, 0.5-1µl of DNA template, and the remaining volume in PCR-grade water. In cases where restriction digest of PCR amplicons was required, incubation was typically performed for 1-2-hours at temperatures recommended by the manufacturer (New England Biolabs). Known positive and negative controls, and no template controls (NTC) were included as standard for every PCR batch. Table 2.2 outlines the thermocycler conditions for each primer pair.

2.1.2.7 Gel electrophoresis

Agarose (Fisher) gels of 2% or 4% concentration (4% for APOE RFLP; 2% for all other reactions) were produced using TAE (Tris acetate EDTA) or TBE (Tris borate EDTA) buffer, with $3x10^{-5}$% ethidium bromide (typically 10µl EtBr in 300ml agarose) for labelling. Electrophoresis was performed (MiniSub, BioRad) at 80-120V, at 400mA, for 20/60 minutes dependent on product

size and required resolution. A 100BP DNA ladder, 1kb DNA ladder, or ssRNA standard ladder (during RNA electrophoresis; New England Biolabs) were used as reference for relative product sizes. Gels were then imaged using a UV transilluminator for genotype confirmation (Syngene).

2.1.2.8 Validation of APOE-TR genotyping with Sanger sequencing

In order to validate the specificity and sensitivity of the primer set targeting the hAPOE C112 site, Sanger sequencing was performed using PCR of a 200BP amplicon from exon 4 of the hAPOE gene using predesigned primers (APOE-JAX, primers designed by Jackson Laboratories; Table 2.1) in multiple samples (N = 15). This was performed as described above for DNA extraction, and standard PCR. Amplified DNA was then purified using a post-PCR clean-up kit (Qiagen) following the manufacturer's instructions. The purified PCR product was then submitted to Eurofins Genomics for Sanger sequencing using the Mix2Seq kit (Eurofins) following manufacturer's instructions. All sequenced data was compared to the results generated using the APOE-TR flanking primer system via PCR, which produced a 100% concordance rate across samples. We therefore chose to use the APOE-TR targeting primer system as standard for identification of APOE-TR animal genotypes in cases where breeding was restricted solely to hAPOE/hAPOE (APOE-TR) lines.

Table 2.1: Details of primers used for individual genotyping reactions in APOE-TR and WT mice. Relevant target and reaction (e.g., hAPOE = human APOE CDS, hAPOE (Neo) = human APOE neomycin cassette), sequence, and primer characteristics are provided

Gene target	Primer name	Sequence	Length (BP)	GC content (%)	Tm (°C)	Product size (BP)
hAPOE	E3_F	GCGGACATGGAGGACGTGT	19	63.2	58.8	131
	E4_F	GCGGACATGGAGGACGTGC	19	68.4	60.3	
	E3/E4_R	GAGGAGCCGCTTACGCA				
hAPOE (Neo)	Neo_F	GTTTCGCTTGGTGGTCGAAT	20	50.0	66.1	167
	Neo_R	GTTGTCACTGAAGCGGGAAG	20	55.0	64.8	
mAPOE	mAPOE_F	CCTGAACCGCTTCTGGGATT	20	55.0	67.4	270
	mAPOE_R	GCCAATCGACCAAGCAAGTA	20	50.0	65.0	
hAPOE-RFLP	APOE3_F	ACTGACCCCGGTGGCGGAGGAGACGCGTGC	30	73.3	86.9	232 (e3) / 295 (e4)
	APOE2mut_R	TGTTCCACCAGGGGCCCCAGGCGCTCGCGG	30	76.7	90.7	
hAPOE-JAX	APOE_JAX_F	ACGGCTGTCCAAGGAGCTG	19	63.2	67.9	200
	APOE_JAX_R	CCCCGGCCTGGTACACTG	18	72.2	69.0	

Table 2.2: Details of thermocycler conditions used for each PCR reaction used for genotyping protocols in APOE-TR and WT mice. Phase, temperature, duration, and cycle number is provided in each case, with gene target codes corresponding to that provided in Table 2.1.

Gene target	Step	Phase	Temperature (°C)	Duration (s)	Cycles (N)
hAPOE (hAPOE3)	1	Hot start	95	300	1
	2	Denaturation	95	30	40
	3	Annealing	69	30	40
	4	Extension	72	60	40
	5	Final extension	72	300	1
hAPOE (hAPOE4)	1	Hot start	95	300	1
	2	Denaturation	95	30	40
	3	Annealing	64	30	40
	4	Extension	72	60	40
	5	Final extension	72	300	1
mAPOE/Neo	1	Hot start	95	300	1
	2	Denaturation	95	30	35
	3	Annealing	58	30	35
	4	Extension	72	60	35
	5	Final extension	72	300	1
hAPOE-RFLP	1	Hot start	95	300	1
	2	Denaturation	95	30	40
	3	Annealing	58	30	40
	4	Extension	72	60	40
	5	Final extension	72	300	1
hAPOE-JAX	1	Hot start	95	300	1
	2	Denaturation	95	30	10
	3	Touch-down	65 (-0.5/cycle)	30	10
	4	Extension	72	30	10
	5	Denaturation	95	30	28
	6	Annealing	60	30	28
	7	Extension	72	60	28
	8	Final extension	72	300	1

2.2 Tissue handling and assay design

2.2.1 Processing of tissue for histochemical and biochemical analyses

2.2.1.1 Transcardial perfusion and post-perfusion tissue handling

Tissue used from APOE-TR and WT mice for use in immunohistochemical experiments was collected following one of two protocols using transcardial perfusion, dependent on whether part of the tissue sample was to be allocated to biochemical experiments. These protocols will be referred to as perfusion-fixation or aCSF-perfusion (artificial cerebrospinal fluid), and the protocol used for each experiment is noted within each experimental methods section, respectively.

Perfusion fixation: The first protocol comprised a standard transcardial perfusion-fixation. Animals were terminally anaesthetised with 250mg/kg sodium pentobarbital (Dolethal, Ventoquinol) before being perfused using a peristaltic pump (Cole Parmer) with 1X phosphate buffered saline (PBS, pH 7.4) until clearing of the perfusate (typically 5-minutes at approx. 8ml/minute flow rate). The animal was then perfused with 4% formaldehyde solution in 1X PBS (pH 7.4, Sigma Aldrich or VWR) for 15-minutes. All perfusate reagents were chilled on ice during the perfusion. After completing the perfusion, whole brains were extracted and post-fixed for 24-hours in 30ml of 4% formaldehyde solution at 4°C. After 24-hours, the brain was moved to 30ml of 30% sucrose solution in 1X PBS and stored at 4°C for 24-48 hours, until the tissue sank to the bottom of the container to indicate sufficient sucrose infiltration. The tissue was then removed from the sucrose solution, dried briefly, and flash frozen in powdered dry ice for 1-hour. Tissue was then stored long term at -80°C in sealed containers until use.

aCSF perfusion: This protocol was adapted from Notter et al. (2014) and Dehghani et al. (2018) for perfusion and post-perfusion tissue handling. In short, animals were anaesthetised as described above, before being perfused with oxygenated 1X aCSF (NaCl 125mM, KCl 2.5mM, CaCl2 2.5mM, MgCl2 2mM, NaHCO3 26mM, NaH2PO4 1.25mM, glucose 25mM, pH 7,4; formulation taken from Notter et al., 2014) until the perfusate was clear (typically 2-4 minutes at approx. 10ml/minute). Brain tissue was then extracted and hemisected, before being either post-fixed and processed for long-term cryostorage as described above, processed immediately for biochemical applications (described in section 2.2.3) or snap frozen in liquid nitrogen and stored in sealed containers at -80°C.

The aCSF perfusion protocol was used to allow simultaneous histochemical and biochemical analysis, primarily due to the sensitive nature of RNA and protein to formaldehyde fixation. In addition, common fixatives can impair the viability of RNA for use in multiple assays. For example, RNA and protein analyses (such as RT-qPCR and Western blotting) are difficult to pair with either perfused-fixed-frozen or formalin-fixed paraffin-embedded (FFPE) tissue without specialised treatment and may compromise sample quality.

In some cases, the hippocampus was dissected from freshly aCSF-perfused tissue. First, animals were perfused following the aCSF protocol as described above, brains were then extracted and then hemisected. The hippocampus was manually dissected from one of the hemispheres under a dissection microscope (Leica) and immediately processed for biochemical experiments (section 2.2.3). The remaining tissue from the dissected hemisphere was flash frozen in liquid nitrogen and stored at -80°C. The opposing whole hemisphere was processed for post-fixation, cryoprotection and long-term storage as described above.

2.2.1.2 Preparation of tissue for immunofluorescence

A standardised pipeline was developed for immunofluorescence, used in the experiments comprising Chapters five and six. Assay specific modifications to these general protocols are noted within individual experimental chapters where relevant.

First, single hemispheres were cut into 40µm thick sections using a cryostat (Leica) following established protocols (e.g., Revilla & Jones., 2002). Sections were stored in sealed 24-well cell culture plates (Fisher) in 500µl-1000µl of cryopreservative solution (30% ethylene glycol, Sigma; 30% glycerol, Fisher; 30% distilled water; 10% 2X PBS) at -20°C. Anatomical reference atlases (Paxinos & Franklin., 2001; Allen Adult Mouse Brain Atlas) were used to determine anatomical position relative to key landmarks. For hippocampal sections, the entire length of the hippocampus was taken (approx. bregma = -1.05 to -3.58mm), split into 12 or 24 wells with typically 4-6 sections per well in a given animal. Experiment specific alterations to this procedure are highlighted in subsequent experimental chapters.

To minimise potential confounding batch effects on immunolabelling procedures, tissue was typically processed in batches of predetermined sizes that reflected equivalent proportions of the total sample with matched group characteristics. For example, in cases where mixed APOE genotype and age groups were used, batches of samples would be matched on the number of

samples of each genotype and age to ensure that individual groups have as equal representation as practicable within each batch.

2.2.1.3 Immunofluorescence

Mouse brain sections were then either processed for immunofluorescence within 24-well tissue culture plates or directly mounted onto Superfrost Plus microscope slides (Fisher) at room temperature using 1X PBS, typically producing 6-9 sections per slide/well. For processing tissue on microscope slides, a hydrophobic barrier was manually drawn onto each slide (ImmEdge hydrophobic barrier pen, Vector Labs) to ensure sections were sufficiently covered by reagents during incubations. Sections were then washed three times for 5-minutes in 1x PBS. Solution was aspirated and in cases where sections were slide mounted, they were stored at 4°C for at least 1-hour to allow section adherence. In each case, incubation volumes were typically between 250-500µl dependent on assay.

Following brief rehydration in 1X PBS, heat-induced epitope retrieval (HIER) was performed using sodium citrate buffer (10mM sodium citrate, Fisher; 0.05% Tween 20, Sigma; solution pH 6.0), which was heated to 95°C in a microwaveable slide dish and placed at room temperature. Slides, or free-floating sections were then submerged in the heated citrate buffer for 30-minutes. After 30-minutes, sections were removed from the buffer, and washed three times for 5-minutes with 1X PBS. Sections were then incubated in 3% normal goat serum (NGS, Vector labs) in 1X PBS with 0.02% Triton X100 (Sigma) or 0.2% Tween-20 (Sigma) permeabilization reagent (PBST) for 30-minutes at room temperature with gentle agitation. Sections were then washed three times for 5-minutes in 1X PBS.

Primary antibody incubations were performed for 24 or 48-hours (see Table 2.4 for experiment specific details, assay determined concentration) in 1X PBST with 1% NGS at 4°C in the dark with gentle agitation. After incubation, sections were washed three times for 5-minutes in 1X PBS. Sections were then incubated for 3-hours in secondary antibody solution (see Tables 2.3, 2.4) in PBST at room temperature in the dark, with gentle agitation. Sections were again washed three times for 5-minutes in 1X PBS. In cases where sequential antibody labelling was performed, the steps from primary and secondary antibody incubation were repeated for each epitope as required. In some cases, sections were then incubated in 1µg/ml of DAPI (4',6-diamidino-2-phenylindole, Sigma) for 10 minutes at room temperature in the dark with gentle agitation.

Following final incubation, sections which were processed free-floating were then mounted onto Superfrost Plus microscope slides and washed briefly with 1X PBS. All slides were then cover-slipped with rectangular .15mm coverslips (Fisher) or #1 rectangular coverslips for confocal imaging (Menzel Glazer), using Fluoroshield aqueous mounting media (Sigma). Slides were then sealed with clear varnish and stored at 4°C in the dark prior to use.

In cases where matched host primary antibodies or host-on-host antibody-tissue protocols (i.e., mouse-on-mouse) were used, sequential primary-secondary labelling steps, intermediate NGS blocking and overnight incubation with appropriate monovalent Fab fragment solution (Abcam, Jackson IR) was performed in order to reduce the risk of non-specific binding and cross-reactivity between antibodies. In addition, pilot experiments were conducted with antibody omission controls using pre-post incubation imaging to exclude antibody cross-reactivity, assess potential false positive signal (e.g., channel cross-over), and non-specific antibody binding background within assays (example control images are shown in Supplementary Figure 5.2). During optimisation, we typically observed that extended blocking (24-hours) with Fab fragment/NGS solutions, sequential antibody incubation, extensive wash steps was sufficient to both prevent cross-reactivity in matched host antibody assays and reduce spurious background driven by endogenous mouse-on-mouse IgG binding of secondary antibodies**.**

For validation of immunofluorescence assays and checks of antibody specificity, primary and secondary antibody omission controls were used alongside antibody titration pilot experiments. Omission of primary or secondary antisera typically ablated signal relative to positive control slides. See Supplementary Figures 5.2 for experiment-specific examples.

Table 2.3: Reagent details, supplier, dilution/concentration, and incubation times where appropriate used in experiments conducted supporting this thesis. Experiment specific modifications of application are provided within individual experimental chapters with general protocol use outlined in this chapter.

Category	Reagent	Supplier	Catalogue No	Dilution/concentration	Incubation
Tissue processing					
	Paraformaldehyde (crystalline regeant grade)	Sigma-Aldrich	P6148-1KG	4% (in stock solution)	
	Paraformaldehyde (solution)	VWR	9713.5000	4% (in stock solution)	
	Phosphate buffered saline	NA	NA	1x stock (see section 2.2.1)	
	Artificial CSF	NA	NA	1x stock (see section 2.2.1)	
	Tissue-Tek OCT	VWR	25608-930		
	TWEEN 20	Sigma-Aldrich	P9416	0.2%	
	Triton X-100	Sigma-Aldrich	T8787-250ML	0.2%	
	Sucrose (crystalline)	Fisher	AAA1558336	30%	
	Sodium Chloride	Fisher	10617042	125mM	
	Potassium Chloride	Fisher	10375810	2.5mM	
	Calcium Chloride	Fisher	11301689	2.5mM	
	Magnesium Chloride Hexahydrate	Fisher	10386743	2mM	
	D-Glucose	Fisher	11462858	25mM	
	Monosodium phosphate	Fisher	10133153	1.25mM	
	Sodium Bicarbonate	Fisher	10244683	26mM	
	Ethylene Glycol	Sigma-Aldrich	102466	30%	
	Glycerol	Fisher	10021083	30%	
	Sodium Citrate Dihydrate	Fisher	S279	10mM	
	RIPA Lysis Buffer 10X	Millipore	20-188		
	TRIzol Reagent	Thermo Fisher	15596026		
Immunofluorescence					
	Rabbit anti-c-Fos	Cell Signalling Technology	2250S	1/1000	24h
	Mouse anti-NeuN	Millipore	MAB377	1/1000	24h
	Rabbit anti-NeuN	Millipore	ABN78	1/1000	24h
	Mouse anti-GAD-67	Sigma-Aldrich	G5419-100UG	1/2000	48h
	Guinea pig anti-Bassoon	Synaptic Systems	141 004	1/1000	24h
	Goat anti-rabbit Alexa-Fluor 488	Thermo-Fisher	ab150077	1/500-1/1000	3h
	Goat anti-mouse Alexa-Fluor 568	Abcam	ab175473	1/500-1/1000	3h
	Goat anti-rabbit Alexa-Fluor 568	Thermo-Fisher	A-11011	1/500-1/1000	3h
	Goat anti-rabbit Alexa-Fluor 647	Abcam	ab150083	1/500-1/1000	3h
	Goat anti-guinea pig Alexa-Fluor 647	Thermo-Fisher	A-21450	1/500-1/1000	3h
	Goat F(ab) Anti-Mouse IgG H&L	Abcam	ab6668	1/500	24h
	AffiniPure Fab fragment Goat Anti-Mouse IgG H&L	Jackson Immuno Research	115-007-003	1/500	24h
	Normal goat serum	Vector Laboratories	S-1000-20	1-3%	
	DAPI dihydrochloride	Sigma-Aldrich	268298-10MG	1µg/ml	10m
	DiO(C18)	Thermo Fisher	D275		24h
	Fluoroshield mounting medium	Sigma-Aldrich	F6182-20ML		
Biochemical applications					
	Mega-Mix Blue	Clent Life Sciences	2MMB		
	Mega-Mix Blue Double	Clent Life Sciences	2MMBD		
	Oligonucleotides (primers)	Eurofins Genomics			
	QuantiNova SYBR Green PCR Kit	Qiagen	208052		
	High-Capacity RNA-to-cDNA Kit	Thermo Fisher	4387406		
	QIAquick PCR purification kit	Qiagen	28104		
	RNeasy MinElute Cleanup Kit	Qiagen	74204		
	RNaseZap	Thermo Fisher	AM9780		
	Complete EDTA-Free Protease Inhibitor Cocktail	Roche	4693159001		
	TRIS-HCl (1M)	Sigma-Aldrich	81220	10mM	
	Proteinase K	Millipore	70663	10µg/µl	
	Ethidium Bromide	Sigma-Aldrich	E1510	10µl/300ml	
	Agarose	Fisher	10366603		
	100bp DNA Ladder	New England Biolabs	N3231		
	1kb DNA Ladder	New England Biolabs	N3232		
	ssRNA Ladder	New England Biolabs	N0362		
	Mix2Seq Kit	Eurofins Genomics			
	Phosphatase inhibitor cocktail 2	Sigma-Aldrich	P5726	2%	
	Phosphatase inhibitor cocktail 3	Millipore	P0044	2%	
	Gel Loading Dye SDS-free	New England Biolabs	B7025		

Table 2.4: Details of antibody parameters used for immunofluorescence experiments performed in Chapters five and six. Tissue thickness, processing steps, primary and secondary antibody identity, concentration, and incubation time are provided.

Experimental Chapter	Section (µm)	HIER	Permeabilisation	Procedure	Volume (µl)	Primary antibody (1AB)	1AB concentration	1AB incubation time	Secondary antibody (2AB)	2AB concentration	2AB incubation time
5 - experiment one	40	Citrate	0.02% Triton X100	Free-floating	250	Rabbit anti-c-Fos	1/1000	24h	Goat anti-rabbit Alexa-Fluor 488	1/500	3h
						Rabbit anti-NeuN	1/1000	24h	Goat anti-rabbit Alexa-Fluor 647	1/500	3h
						Mouse anti-GAD-67	1/2000	48h	Goat anti-mouse Alexa-Fluor 568	1/500	3h
						Goat F(ab) Anti-Mouse IgG H&L	1/500	24h		NA	NA
5 - experiment two	40	Citrate	0.02% Triton X100	Slide-adhered	250	Mouse anti-GAD-67	1/2000	48h	Goat anti-mouse Alexa-Fluor 568	1/500	3h
6 - experiment one	100	None	0.2% Tween 20	Free-floating	500	Rabbit anti-c-Fos	1/1000	24h	Goat anti-rabbit Alexa-Fluor 488	1/500	3h
						Rabbit anti-NeuN	1/1000	24h	Goat anti-rabbit Alexa-Fluor 647	1/500	3h
6 - experiment two/three	100	None	0.2% Tween 20	Free-floating	500	Rabbit anti-c-Fos	1/1000	24h	Goat anti-rabbit Alexa-Fluor 568	1/500	3h
						Guinea pig anti-Bassoon	1/1000	24h	Goat anti-guinea pig Alexa-Fluor 647	1/500	3h
						DAPI	1µg/ml	10m	NA	NA	NA

2.2.2 Microscopy

2.2.2.1 Microscopy configuration

For the majority of experiments, unless indicated specifically, imaging was performed using an Olympus BX53 epifluorescent microscope (Olympus) with a 20x magnification objective (Chapter five/six). The microscope was equipped with a standard Halide lamp, motorised stage (Stepper Motorised Stage Controller, Prior Scientific), and CCD camera (FAST-1394, QICAM).

Images were acquired using iVision (Biovision Technologies) software using a custom-made automation scripts for grid-based image acquisition. In cases where multiplex immunofluorescence was performed, individual channels were acquired sequentially to avoid signal bleed-through. Assay-determined acquisition parameters, including exposure time, gain, filter set, and normalisation were standardised within channels and used consistently across samples within experiments.

In other cases (Chapter six), imaging was performed using an SP8 confocal fluorescent microscope (Leica), in which the same principles for standardisation of acquisition parameters were used. The confocal microscope was equipped with 20x and 63x magnification objectives, an automated motorised stage, PMT and hybrid detectors, a standard halide lamp, and excitation lasers across the range of 405-633nm. In cases where z-stack images were required, the z-axis interval between images was set to 0.3µm as standard. Typical image resolution at 63x magnification was 512 x 512px^2 corresponding to 82 x 82µm^2, with a pixel resolution of ~0.16µm/px.

Images were exported in TIFF format and all post-imaging processing was performed using FIJI software. Experiment specific details are provided within each Chapter, however generally images were first stitched using the stitching plugin (Preibisch et al., 2009), before background subtraction, contrast standardisation (standardised across all samples within experiments), and pseudocolouring to generate multi-channel composite images for quantification.

2.2.2.2 Quantification of immunofluorescence images

Experiment-specific details of quantification methods and parameters are provided in each experimental Chapter. Briefly, processed images were quantified for immunoreactivity via

measurement of average fluorescence signal intensity within manually traced regions of interest (ROIs). Cell count measures were similarly performed within individual ROIs from individual sections using standardised counting rules and counting frame sizes. In cases where colocalisation or encapsulation (i.e., subcellular compartment colabelling: nucleus and soma) of images was required, counting was dependent on either clear cellular compartment labelling or clear fluorescence channel overlap and the absence of spurious channel bleed-through, respectively. Quantification was typically performed across replicate sections to generate averages for individual animals which was used for further analysis.

2.2.3 Tissue preparation for biochemical analyses

2.2.3.1 Tissue lysis

In the experiments conducted in Chapter five, dissected hippocampi were manually homogenised with a plastic homogenizer (Fisher) on ice in 300µl of 1X RIPA buffer (RIPA buffer, Millipore; Complete EDTA-free protease inhibitor cocktail, Roche; phosphatase inhibitor cocktails 2 & 3, Sigma). The lysate was then processed through a 1ml syringe (25g needle, Fisher) to shear nucleic acid material. After lysis, the lysate was centrifuged for 5-minutes at 1000g at 4°C. 100µl of supernatant was extracted and aliquoted into 2 x 100µl microcentrifuge tubes, one of which was stored immediately at -80°C for later use, the other was immediately processed for RNA extraction (section 2.2.3.2).

During pilot experiments, aCSF perfusion, hippocampal dissection, and tissue lysis of two APOE-TR mice was performed as described above, with the exception that hemi-hippocampi were extracted from both hemispheres. Of these hemi-hippocampi, one hemi-hippocampi per subject was allocated to lysis with RIPA buffer, the other to lysis with TRIzol reagent (Invitrogen). Lysis with RIPA buffer was performed as described above and lysis with TRIzol was performed according to manufacturers' instructions. 200µl of aqueous phase supernatant was extracted from the TRIzol lysate for use in RNA extraction. It is important to note that, due to the sample splitting performed following lysis with RIPA buffer (i.e., 100µl), the total quantity of lysate for RNA extraction from TRIzol would be double that acquired from the supernatant of RIPA lysate. Therefore, assuming equal homogenisation RNA extraction efficiency, it would be expected that the total RNA quantity extracted from the TRIzol aliquot would be approximately double that of the total RNA extracted from RIPA lysate. This approximation

was therefore used as one qualitative judgement criteria of comparability of the two techniques for total RNA extraction (alongside quantitative comparison, see section 2.2.3.3).

2.2.3.2 RNA extraction

Total RNA extraction was performed on tissue lysates using the RNeasy MinElute kit (Qiagen), following manufacturer's instructions, resulting in elution of total RNA into 14µl of RNAse-free water. Purified RNA was then tested for quality using a Nanodrop 2000 spectrophotometer (Nanodrop, ThermoFisher). Total RNA quantity, A260:A280 and A260:A230 ratios were recorded for reference. Eluted RNA samples were then stored at -80°C until further use.

2.2.3.3 RNA quality validation

To ensure the quality of extracted RNA and viability for biochemical analysis beyond the information provided by spectrophotometer analysis, an initial pilot of 5 samples was performed (see Table 2.5 for details). These samples were electrophoresed on a capillary using a Bioanalyser 2100 (Agilent) system with an RNA Nano chip. RNA integrity numbers (RINs), 28S:18S ribosomal RNA (rRNA) ratios and total RNA estimates were acquired. In addition, 1µl of each RNA sample was electrophoresed in 9µl of SDS-free purple loading dye (New England Biolabs) through a 2% agarose gel with ethidium bromide labelling and ssRNA ladder. Qualitatively we observed visible signs of high-quality RNA extraction when imaging electrophoresed RNA samples, with clear 28S:18S rRNA visible and little to no evidence of RNA degradation indicated by 'smearing'. Validating these observations quantitatively, Bioanalyser RIN values and electropherogram demonstrated that RNA extracted using both RIPA buffer and TRIzol were of high quality (e.g., RIN > 8.0, clear rRNA peaks) and sufficient for biochemical analyses (Table 2.5 and Figure 2.1).

Table 2.5: RNA integrity assessed via Bioanalyser in pilot samples used during experiments conducted in Chapter five. Ratio of 28S/18S rRNA and RNA integrity value (RIN) are provided for individual samples. ID1-2 correspond to assessment of RNA quality using TRIzol and RIPA extraction methods within a matched sample (described in section 2.3.1.1). ID3-5 correspond to additional samples lysed using RIPA extraction method.

Sample	rRNA Ratio [28s / 18s]:	RIN
ID1 (TRIzol)	1.32	8.9
ID2 (RIPA)	1.22	8.7
ID3	1.05	8.6
ID4	1.04	8.6
ID5	0.99	8.3

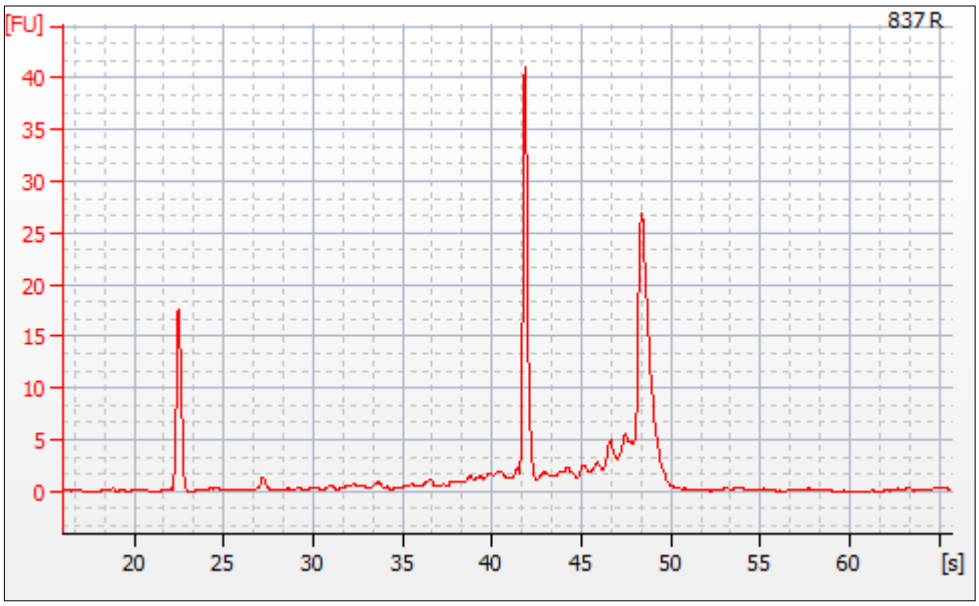

Figure 2.1: Example electropherogram output from the total RNA of a pilot sample (ID3) used in Chapter five. Spike in at 22.5s represents fluorescent marker used in Bioanalyser capillary. 28S and 18S rRNA peaks can be observed at approximately 48s and 42s, respectively.

2.2.3.4 Reverse transcription

RNA aliquots were thawed on ice, prior to undergoing reverse transcription using the High-Capacity RNA-to-cDNA kit (Invitrogen, oligod(T) random octamer priming), following manufacturer's instructions for a 25µl reaction. 500ng of total RNA was used in each reaction according to total RNA concentrations acquired from spectrophotometer analysis. cDNA was synthesised, aliquoted, diluted to 1:50, and stored at -20°C until further use. In 4 samples, the reverse transcription step was performed in the absence of Reverse Transcriptase. This generated 4 no-RT (no reverse transcription) controls matched to the same samples that had undergone reverse transcription in order to confirm the absence of contaminating genomic DNA (gDNA) in the RNA samples by using RT-qPCR and gel electrophoresis (described in section 2.2.4.4).

2.2.4 Reverse transcription quantitative PCR (RT-qPCR)

For experiments conducted in Chapter five, RT-qPCR assays were performed in a standardised manner, retaining an identical processing pipeline between gene targets. Gene targets (mRNA) are listed in Table 2.6, alongside primer design details in each case.

2.2.4.1 Primer design for RT-qPCR

Primers were designed against mouse c-Fos mRNA, transcript splice isoform 1 (Ensembl transcript number: ENSMUST00000021674.6) and human APOE mRNA, transcript splice isoform 201 (Ensembl transcript number: ENSG00000252486.9), following primer design principles provided by the Thermo Fisher, BioRad, and PREMIER Biosoft qPCR technical guides. Primers were generated using the software Primerblast (NCBI), with amplicons spanning exon-exon junctions to ensure specificity to mRNA transcripts, given the intron splicing from mature mRNA (Bustin & Huggett., 2017; Taylor et al., 2010). Primers were also checked for appropriate amplicon size, melting temperature, guanine-cytosine (GC) content between 40-65%, 3'/5' homology and low stability of cross/self-dimerisation products. Finally, primers were cross-referenced against both mouse genome and transcriptome to assess any potential non-specific amplification products due to primer-sequence homology using Primerblast and the UCSC in silico PCR software. Potential non-specific amplicons identified were only tolerated when

meeting the following conditions: a 3’ anchoring point mismatch between primer and sequence, and amplicon size exceeding 1kb which would be untenable under the designed PCR amplification conditions, and/or matching an unvalidated transcript. All primers used in RT-qPCR assays were produced and purchased from Eurofins Genomics or Sigma-Aldrich.

Table 2.6: Details and properties of primers used for RT-qPCR experiments conducted in Chapter five. Relevant gene target, sequence, primer characteristics, and amplicon product size are provided.

Primer target	Primer name	Sequence	Length (BP)	GC content (%)	Tm (°C)	Product size (BP)
c-Fos	Fos_F1	TCC AAG CGG AGA CAG ATC AAC T	22	50.0	60.3	110
	Fos_R1	TCG GTG GGC TGC CAA AAT AA	20	50.0	57.3	
TBP	TBP_F1	CAC GGA CAA CTG CGT TGA TT	20	50.0	57.3	78
	TBP_R1	TGG ATT GTT CTT CAC TCT TGG C	22	45.5	58.4	
CPSF4	CPSF4_F1	TTC GAC TTG GAG ATC GCC GT	20	55.0	59.4	82
	CPSF4_R1	CAG CAG CCC CCG ACT TAT CC	20	65.0	63.4	
Mto1	Mto1_F1	TGC GAT TGT CCT TGA GAA CCT	21	47.6	57.9	81
	Mto1_R1	TCA ATA GAG GGA CAG TAT CGG G	22	50.0	60.3	
TRMU	TRMU_F1	GGA GCA TTT CCT TCT TCA GTA TTT G	25	40.0	59.7	151
	TRMU_R1	CAC GTA CCA GGG CTC TCT CAA	21	57.1	61.8	
ActB	ActB_F1	TGT CCA CCT TCC AGC AGA T	19	52.6	56.7	101
	ActB_R1	AGC TCA GTA ACA GTC CGC C	19	57.9	58.8	
APOE	APOE_F1	GGG TCG CTT TTG GGA TTA CCT G	22	54.5	69.2	124
	APOE_R1	CAA CTC CTT CAT GGT CTC GTC C	22	54.5	67.0	

2.2.4.2 Reference gene target selection

Given the variability in the rigour of prior standards for reporting and designing qPCR assays, reference gene selection has become an issue of contention when interpreting data from diverse sample sets (Taylor et al., 2010). Therefore, in-line with the MIQE guidelines, reference gene selection was held to a set of criteria. This involved choosing multiple reference targets that: approximately match expression levels of the gene of interest, are localised at least to some extent in the matched sub-cellular compartment to the gene of interest, do not have multiple potential isoform targets of matched amplicon size that may artificially alter expression profiles, do not have known direct interactions with the gene of interest, do not possess pseudogenes, and do not vary in expression systematically across given experimental conditions (Taylor et al., 2010; Bustin et al., 2009, 2017). While in practice, dependent on experimental conditions these criteria can be complex to fulfil, the procedural pipeline used to select appropriate reference genes is detailed in Figure 2.2. Briefly, using Genevestigator (Nebion AG) software, microarray data from the AFFYMETRIX database was sampled based on as close to matching parameters to the current samples as possible. We used an available database of >200 mouse hippocampal samples and identified mRNA expression values for one of our genes of interest, c-Fos. Transcriptome wide data from the microarrays was then ranked according to median expression and similarity of coefficient of variation to that of c-Fos using the 'normaliser selection' function. The top 10 ranking genes from this list was then checked for subcellular localisation, no validated direct or clear regulatory interactions with APOE and no pseudogene variants. The final selected reference genes corresponded to: TRMU (tRNA Mitochondrial 2-Thiouridylase; Ensembl transcript number: ENMUST00000023019.12), Mto1 (Mitochondrial TRNA Translation Optimization 1; Ensembl transcript number: ENSMUSG00000034896.13), ActB (Beta actin; Ensembl transcript number: ENSMUST00000100497.11), and CPSF4 (Cleavage and Polyadenylation Specific Factor 4; Ensembl transcript number: ENSMUST00000070487.12).

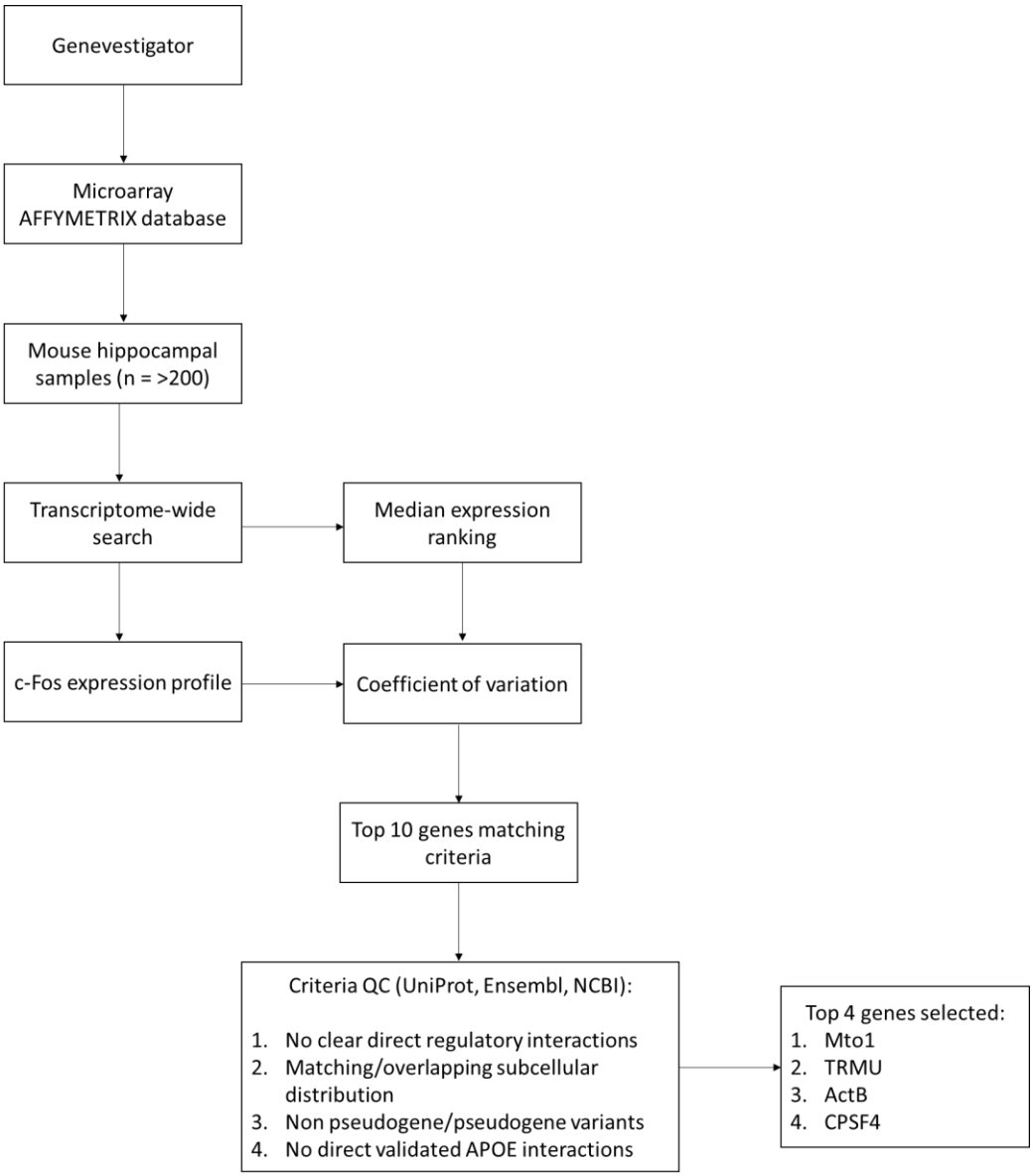

Figure 2.2: Flow diagram demonstrating reference gene selection process for experiments conducted in Chapter five. Criteria QC represents steps for verification of reference gene suitability. Example reference gene targets are provided.

2.2.4.3 SYBR Green RT-qPCR procedure

All RT-qPCR assays were carried out using the QuantiNova SYBR Green qPCR kit (Qiagen) according to manufacturer's instructions. Briefly, 10µl reactions were produced in PCR strip tubes or 96 well plates (Agilent) and were run in triplicate for each sample. Each reaction consisted of 5µl of SYBR Green qPCR master mix, 1µM of each primer, 1µl of ROX fluorescent normaliser dye, 1µl of RNAse free water, and 1µl of template cDNA. Reaction tubes/plates were then sealed, centrifuged briefly, and inserted into an MX4000 multiplex qPCR sampler (Stratagene). Thermocycler conditions and dissociation curve profiles are shown for each target and reference gene in Table 2.7 and Figure 2.4. The detection threshold for all analyses was determined manually based on the median automated threshold selected by Stratagene across plates containing all genes of interest and reference genes. All assays were carried out with a triplicate no template control (NTC) and a standard template on each plate to ensure no reagent contamination, failed reactions or potential degradation of template cDNA.

2.2.4.4 Generating standard curves, optimising annealing temperature, and assessing primer specificity

To assess the efficiency of target and reference gene primer pairs, alongside optimising cDNA concentration to suit the dynamic range of detection, standard curves were performed. For the experiments conducted in Chapter five, standard curves were generated for a mix of 6 cDNA samples from two APOE genotypes and two experimental conditions (see section 5.3, context exposure and home-cage groups). 1µl of each of the sample cDNA was pooled, then diluted in a 1:10 to 1:100000 serial dilution. RT-qPCR for each dilution of the cDNA template standard was then performed in triplicate through the standard cycler conditions described in Table 2.7 for each primer pair.

Raw Ct values were extracted from Stratagene software, after which, R^2 and reaction efficiency were calculated for each dilution of the standard curve across triplicate Ct averages, according to the formula in Figure 2.3. If the efficiency for a given primer pair standard curve was below 90% or above 110% with an R^2 of below .98, the standard curve was repeated for that primer pair at an altered annealing temperature. All primer efficiencies and R^2 values are provided in Supplementary Table 2.1. Based on the results of the standard curves and the dynamic range

suggested by the MIQE guidelines (e.g., Taylor et al., 2010), a dilution factor of 1:50 for cDNA was chosen as appropriate for all gene targets. Dissociation curves were also inspected for evidence of a single peak indicating a probable single amplicon product dissociation, suggesting primer pair specificity for a single target. Example standard curves and dissociation curves are presented in Figure 2.4A-G.

Table 2.7: Thermocycler conditions used for each gene target primer pair for RT-qPCR experiments. Cycle time for denaturation represents 15-minutes heat-induced activation + 30-seconds standard denaturation time per cycle.

Gene target	Step	Phase	Temperature (°C)	Duration (s)	Cycles (N)
c-Fos	1	Hot start	95	900	1
Mto1	2	Denaturation	95	30	40
TRMU	3	Annealing	58	30	40
ActB	4	Extension	72	30	40
CPSF4	1	Hot start	95	900	1
	2	Denaturation	95	30	40
	3	Annealing	60	30	40
	4	Extension	72	30	40
All	1	Denaturation	95	60	1
	2	Dissociation curve	55 (+1.0/Cycle)	30	41

$$Efficiency\ (\%) = \left(10^{\frac{-1}{Slope}} - 1\right) \times 100$$

Figure 2.3: Formula used to calculate reaction efficiency for individual primer sets during standard curve and reaction optimisation procedures. 'Slope' represents the x/y slope of the log of starting template concentration relative to the averaged Ct value of a given reaction triplicate.

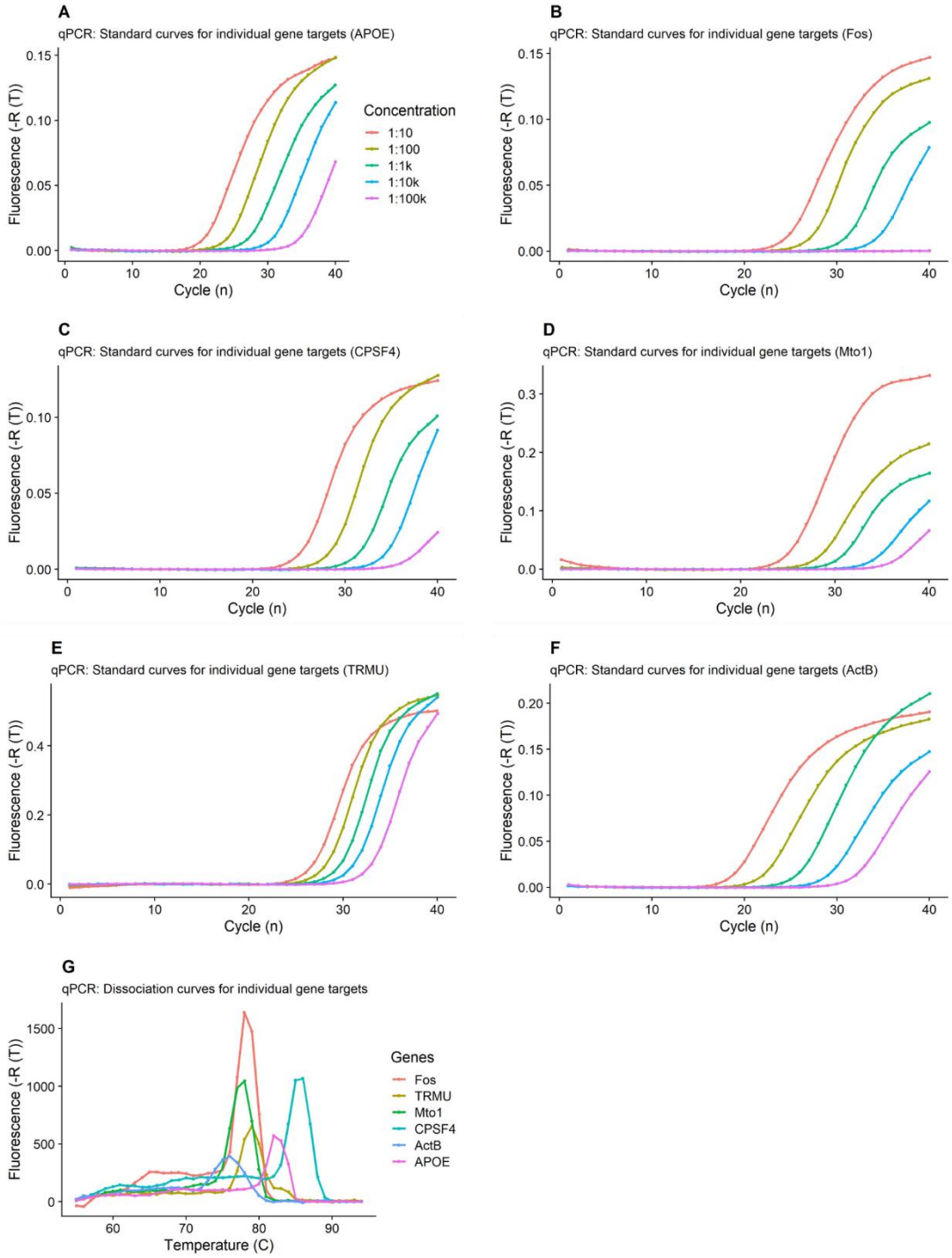

Figure 2.4: Standard and dissociation curves for gene targets in qPCR assays in experiments conducted in Chapter five. Amplification plots across a standard 40-cycle qPCR program, with relative fluorescence -R(T) representing relative amplification, primary genes included A) c-Fos, B) TRMU, C) Mto1, D) CPSF4, E) ActB, and F) APOE. Five step serial dilutions for standard curves are shown over a 1:10 to 1:100000 (1:100k) dilution range. G) Dissociation curves of individual gene targeted performed after standard 40-cycle qPCR. Note singular primary peaks for each target, likely indicating a single amplification product. Individual points in each figure represent

triplicate averages for a multi-sample standard used for assay optimisation (see section 2.4.1.6).

To further validate the specificity of the RT-qPCR assay, post-RT-qPCR products from standard curve reactions were extracted and gel electrophoresis was performed on a 2% agarose gel. None of the no-RT samples showed evidence of amplification when imaged post-electrophoresis, and the lack of gDNA signal in the Bioanalyser results from purified RNA also supports a gDNA contamination free preparation. Additionally, qPCR performed on No-RT controls demonstrated Ct values between 32-35, outside of the normal range expected for amplification, close to that of NTC samples, again supporting a lack of gDNA contamination in the RNA preparations.

2.2.4.5 Reference gene stability analysis

To ensure that expression profiles are accurately captured using RT-qPCR it is crucial to normalise target gene data to a stable reference factor. Two or more reference genes have been suggested as necessary for producing robust qPCR data and as such, reference gene analysis is necessary (Taylor et al., 2010, Bustin et al., 2017). In the experiments conducted in Chapter five, all samples (N = 81) were used for a reference gene stability analysis. RT-qPCR was performed on each sample in triplicate as described in section 2.2.4.3, for the c-Fos and APOE gene targets and all 4 selected reference genes (TRMU, Mto1, CPSF4, ActB) at the set standard template dilution factor. Raw Ct values were extracted and imported into the RefFinder gene analysis software (Xie et al., 2012), compiling algorithms from Genorm, Bestkeeper, and NormFinder software. From this multifaceted analysis, coefficient of variation and inter-gene expression value correlations were assessed. All algorithms ranked each reference gene relative to these criteria, showing that ActB and TRMU comprised the most stable two reference genes (Supplementary Figure 2.1). However, to increase reference factor stability, all four reference genes were averaged to form a single reference factor to normalise gene of interest Ct values.

2.2.4.6 RT-qPCR data analysis

After establishing a stable reference factor, raw Ct values were checked for stability via standard deviation within triplicate reactions (with .25 typically considered an outlier and removing that triplicate Ct value, Rydbirk et al., 2016).

In all cases, triplicate averaged Ct values of the reference factor were subtracted from the triplicate averaged Ct values of the gene of interest (GOI). within each sample to generate normalised dCt (delta Ct) values. dCt values were then imported into analysis software (R and SPSS) for statistical analysis. For graphical representation the ddCt (delta-delta Ct) method was used, normalising individual Ct values to a group average, dependent on the comparison of interest (described in section 5.6). Further details of data handling and analysis are described in section 5.6/5.7.

CHAPTER THREE

Establishing a behavioural assay for the longitudinal assessment of rapid place learning in wildtype and APOE-TR mice

3.1 Experiment one

3.1.1 Introduction: Experiment one

As discussed in Chapter one, it is well established that the hippocampal formation is crucially involved in the processes underlying declarative memory and is particularly implicated in the encoding of novel episodic events in humans and animal models (e.g., Burgess et al., 2002; Bast et al., 2007; Eichenbaum et al., 2014). Disruption of hippocampal function through pharmacological inhibition (e.g., Izquierdo et al., 1995; Pezze et al., 2012), physical lesion (e.g., McCormick et al., 2018; Logue et al., 1997; Morris et al., 1990), functional perturbation of circuitry (e.g., Bast et al., 2018; McGarrity et al., 2017) and multiple neurodegenerative disease processes (e.g., Mariana et al., 2007) substantially impairs behavioural expression of these memory processes in episodic memory tasks. Recent research in the field has led to the development of tasks designed to assess rapid place learning performance in animal models analogous to 'everyday memory' challenges faced by human patients such as the 'car park problem'. These rapid place learning analogues, such as the event arena and delayed-match to place (DMTP) MWM maze tasks developed by the Morris group, have demonstrated the amenability to repeat assessment of episodic-like memory with daily updating of novel episodic information on a background of prior rule learning. These tasks are particularly sensitive to hippocampal function, with both lesions and functional disruption leading to significant impairments in performance (e.g., direct lesions, NMDAR inhibition, disinhibition; Bast et al., 2005; Morris et al., 2006; Wang et al., 2010; McGarrity et al., 2017).

APOE4, the leading genetic risk factor for late-onset Alzheimer's disease (LOAD), has been associated with premature cognitive impairment in both humans and rodent models, with a particular focus on episodic memory tasks (discussed in section 1.6). However, while there appears to be a linear interaction between ageing and APOE4 in impairing cognitive function, findings are somewhat inconsistent. Namely there is less clarity on whether APOE4 may confer impaired cognitive performance at young age and early adulthood. Further, research using APOE rodent models such as the APOE-TR mouse has predominantly focussed on the influence of APOE isoform on long term reference memory; encoding of a well reinforced spatial location followed by long term delayed recall of oftentimes more than 1-2 days. Moreover, there is both a considerable paucity of data surrounding the potential influence of APOE isoform on rapid-place learning, or longitudinal characterisation of the lifespan trajectories of episodic memory in APOE mouse models.

Addressing this gap within the literature formed the first question of the work comprising this thesis:

1. Does APOE isoform and sex impact ageing trajectories of rapid place learning and memory performance across the lifespan of the APOE-TR mouse model?

In order to address this question, we first aimed to develop and establish a task suitable for the repeat assessment of rapid place learning performance in APOE-TR mice. Notably, the majority of prior studies of episodic-like memory in the APOE-TR model have relied on the use of aversive navigation tasks such as the Morris water maze (MWM; e.g., Leung et al., 2012; Reverte et al., 2012; Grootendorst et al., 2005) or the aversive Barnes maze (e.g., Rodriguez et al., 2013; Spiedell et al., 2018; Basaure et al., 2019). These tasks rely on the innate escape behaviours of rodents when exposed to aversive environmental conditions such as water (Morris et al., 1981, 1984) and bright light/open areas in the Barnes maze tasks (Barnes et al., 1979).

Additionally, E4-TR mice have been demonstrated to be susceptible to behavioural impairments following chronic cumulative stress (e.g., Lin et al., 2016; Meng et al., 2015; Zhang et al., 2020), while in some assays demonstrating elevated anxiety (e.g., Siegel et al., 2012; Villasana et al., 2016), which may pose issues for repeat testing under highly aversive conditions. Indeed, one previous study demonstrated null differences in spatial learning in APOE-TR mice using the aversive MWM, while detecting learning impairments in E4-TR mice using the Barnes maze, which may have been due to the particularly aversive nature of the MWM task (Rodriguez et al., 2013). One potentially promising approach is the use of appetitive motivation in tasks such as the Barnes maze and has previously been shown to circumvent strain-specific deficits in aversively motivated spatial learning and reference memory, detecting more robust spatially driven performance than using the MWM alone (Youn et al., 2012).

Therefore, our first experiments sought to design and validate a novel appetitive maze task to assess rapid place learning and memory in wildtype mice of matched background strain to the APOE-TR model (C57BL/6J). The task was adapted on the basis of the Barnes maze (Barnes, 1979; O'Leary et al., 2011, 2013; Youn et al., 2012) and included principles developed in tasks including the delayed match to place (DMTP) MWM (Steele and Morris, 1999; Nakazawa et al., 2003; Bast et al., 2009) and the event arena task (Bast et al., 2005; Wang et al., 2010; Takeuchi et al., 2016; Nonaka et al., 2017; Broadbent et al., 2020). The task itself consisted of a multiple

alternative-forced choice (AFC) DMTP design using a 20-hole Barnes maze modified to fit 'sandwells', named the 'adapted Barnes maze' (aBM). Similar to the event arena task, a single location on the maze is baited with a buried food reward within a sandwell, while a number of other non-target 'foil' locations are unbaited to act as distractors. This induces appetitively-motivated spatial learning to support efficient reward retrieval from the sandwell location, while foil locations serve as controls for chance performance.

In addition, design aspects of the task were developed from the radial arm maze (Clelland et al., 2009) and operant-based task (Oomen et al., 2013) variants which have been adapted to assess putative pattern separation (i.e., the ability to orthogonalize or discriminate between similar competing episodic-like information into discrete memories) in a linearly defined manner. These spatial pattern separation tasks have typically involved encoding of a given spatial configuration, whether corresponding to separated arms on a maze or visual stimuli in space. This is typically followed by a retention delay and a subsequent manipulation of the available spatial configuration at retrieval (i.e., spatial position of open maze arms or visual stimuli) such that the animal is given a forced choice to discriminate between the correct encoded spatial location to match to (i.e., the win-stay rule in DMTP tasks) and incorrect foil locations of varying spatial similarity. Discrimination accuracy varying linearly as a function of 'separation size' (i.e., spatial similarity, with lower spatial similarity between target and foil corresponding to greater likelihood of accurate discrimination and vice versa) is a general feature and prerequisite for demonstration of pattern separation-like performance in such tasks (Oomen et al., 2013; Hvoslef-Eide & Oomen., 2016).

Specifically, to incorporate these principles, the use of a circular maze produces symmetrical and easily definable mathematical relationships between positions in space on the maze by angular separation (e.g., Morales et al., 2020). This motivated the use of a circular maze design, as this approach is hindered by complicated asymmetrical maze design and non-linear spatial relationships such as in the event arena. Moreover, we aimed for the task design to confer flexibility in the assessment of rapid place learning, with the intention of modifying the task parameters to assess performance at varying inter-trial intervals (ITI; encoding-retrieval delay), extent of reinforcement (number of trials), and spatial certainty (varying spatial location of targets and non-target foils).

The procedure required a multi-stage training regimen of increasing task difficulty. Mice were trained to a performance criterion, that enabled daily testing of spatial learning and memory, analogous to 'everyday' episodic memory tasks (Nonaka et al., 2017). Performance was then

assessed using a series of unrewarded 'probe trials' and manipulation/control trials to assess the use of spatial strategies for task performance.

It was hypothesised that C57BL/6J wildtype (WT) mice would demonstrate steady acquisition of rapid place learning and memory performance across task training, which would stabilise above chance to provide an analogous 'everyday memory' condition to test rapid encoding of novel episodic-like information. Secondly, we predicted that, during unrewarded probe trials, animals would demonstrate evidence of accurate spatial memory recall using measures such as place preference. Further, we predicted that spatial recall would be linearly biased by distance from the target location, demonstrating a requisite for pattern separation-like performance (e.g., Oomen et al., 2013; Hvoslef-Eide et al., 2016). Finally, we expected that animals would develop a predominant preference for allocentric place strategy, relying on extra-maze cues and not on idiothetic (egocentric) or odour-based cues for sustained performance, as a prerequisite for measuring episodic-like memory in maze-based navigation tasks.

3.1.2 Methods

3.1.2.1 Design

Experiment one comprised a longitudinal mixed design, with every subject participating in each condition across task training. The task design was that of an appetitive spatial delayed match to place (DMTP) alternative forced choice (AFC) task using the 20-hole Barnes maze design (Barnes et al., 1979; Rodriguez et al., 2013), referred to as the adapted Barnes maze task (aBM). Briefly, the task involved a single encoding trial of navigation to a food reward buried in a 'sandwell' (referred to as sandwells or wells) on the Barnes maze, followed by a 'retrieval' trial to the same location after a fixed interval (10-minutes), to assess rapid place-learning. The structure of the experiment and task design is outlined in Table 3.1.1. The overall experimental structure consisted of repeated task training over 4 phases, totalling 100 days with interleaved probe and control trials. Primary data originated from training phases 3 & 4, at which point training trials were interspersed with probe trials to validate the ability of the task to assess spatial memory in the absence of reward. The general task design for training phases 3 & 4 are shown in Figure 3.2.1 and 3.2.1, although the design for training phases 1-2 is also reflected with only the number of AFCs varying (see Table 3.1.1 for details).

3.1.2.2 Animals

Sixteen (8 male, 8 female) C57BL/6J WT mice at 5 weeks of age were purchased from Charles River laboratories and group housed on a standard 12-hour light/dark cycle (7am lights on, see section 2.1.1). Upon completion of the experiment, animals were aged 6 months (+/- 1 week) prior to culling. Standard chow was provided *ad libitum* prior to food restriction, and water was available *ad libitum* for the duration of the experiment. Mice were handled most days and were regularly weighed throughout the experiment. Experimental testing typically occurred between 9am-5pm. Animals were culled via perfusion-fixation as described in section 2.2.1.

3.1.2.3 Apparatus

Experiment one was performed using a standard 20-hole, 92cm diameter white acrylic mouse Barnes maze (Maze Engineers). The maze holes were located around the periphery of the maze, 5cm from the edge (Figure 3.1.1A/E). The maze was elevated 55cm above ground by a wooden platform. Custom-made 5cm diameter sandwells were 3D-printed (Ultimaker 2+, Ultimaker) in house using black PLA plastic with 5.0mm (days 1-72; training phases 1-3) overhang or white PLA plastic with 0.5mm overhang (days 73-100; training phase 4) at the top of the well. The sandwells were inserted into each hole on the maze to house the food reward. The number of sandwells on the maze at any one trial varied across training phases (see Table 3.1.1 for details). At the final training stage, the standard task was a 5-alternative forced choice (5-AFC) with 6 total sandwells, 5 unbaited (foils) and 1 baited (target). White sandwells (training phase 4) were uniform with the maze floor and therefore no clear visual cue was present. Each well was filled with 'digging medium' either sawdust during training phases 1-3 or bird sand (Jondo Suppliers) during training phase 4. The sandwell content was mixed with 5% weight in powdered food reward (Rewards were Cheerios, Nestle; referred to subsequently as 'rewards' or 'pellets') to control for confounding olfactory cues given by the rewarded sandwell. Further, additional reward pellets were made inaccessible to the animals via perforated inserts within the sandwells during training phase 4. The rewarded sandwell within a given trial contained half pellets during encoding and whole pellets at retrieval, which were buried beneath 2-3cm of digging medium (Takeuchi et al., 2016).

Experiments were conducted in a rectangular room with four large, coloured 2D distal cues (21 x 30cm) placed on each wall: a 2D white triangle (east); a 2D blue cross (south); a 2D grey circle

(west); and a 2D red square (north) shown in Figure 3.1.1D. During training phase 4, four intra-maze cues were added to act as landmarks aiding in allocentric place learning (Bast et al., 2005; Wang et al., 2010): a white pyramid, a black cylinder, one black 'T' shape, and a white hexagonal prism (~8 x 8cm). The diffuse room cues present included: two black curtained walls (south & east), a plastic textured wall (west), a yellow wall (north), and the entrance/exit point of the experimenter/animal (south-west corner). A white PLA 'start box' ($10cm^3$) was used to counterbalance the starting orientation of animals from the centre of the maze via a predetermined pseudorandom sequence. This is analogous to the use of pseudorandom allocation of the starting quadrant in the water maze or start box in the event arena tasks (e.g., Wang et al., 2010), by preventing the animal orienting to the maze entry position which encourages egocentric task solutions. Subject behaviour was captured using an overhead high-fidelity video camera (Kodak), which relayed the video feed to a computer running Ethovision XT9 (Noldus Software) software to record animal locomotion tracks. Manual recordings of latency for animals to locate the target on each trial were also recorded for validation analyses. The testing room was illuminated by a single low-watt bulb (~200 lux average intensity at 2m distance) positioned above the maze in order to provide sufficient light for vision but avoid inducing the aversive state typical of Barnes maze procedures (see Feng et al., 2017 for details on aversive conditions in in DMTP Barnes maze variant).

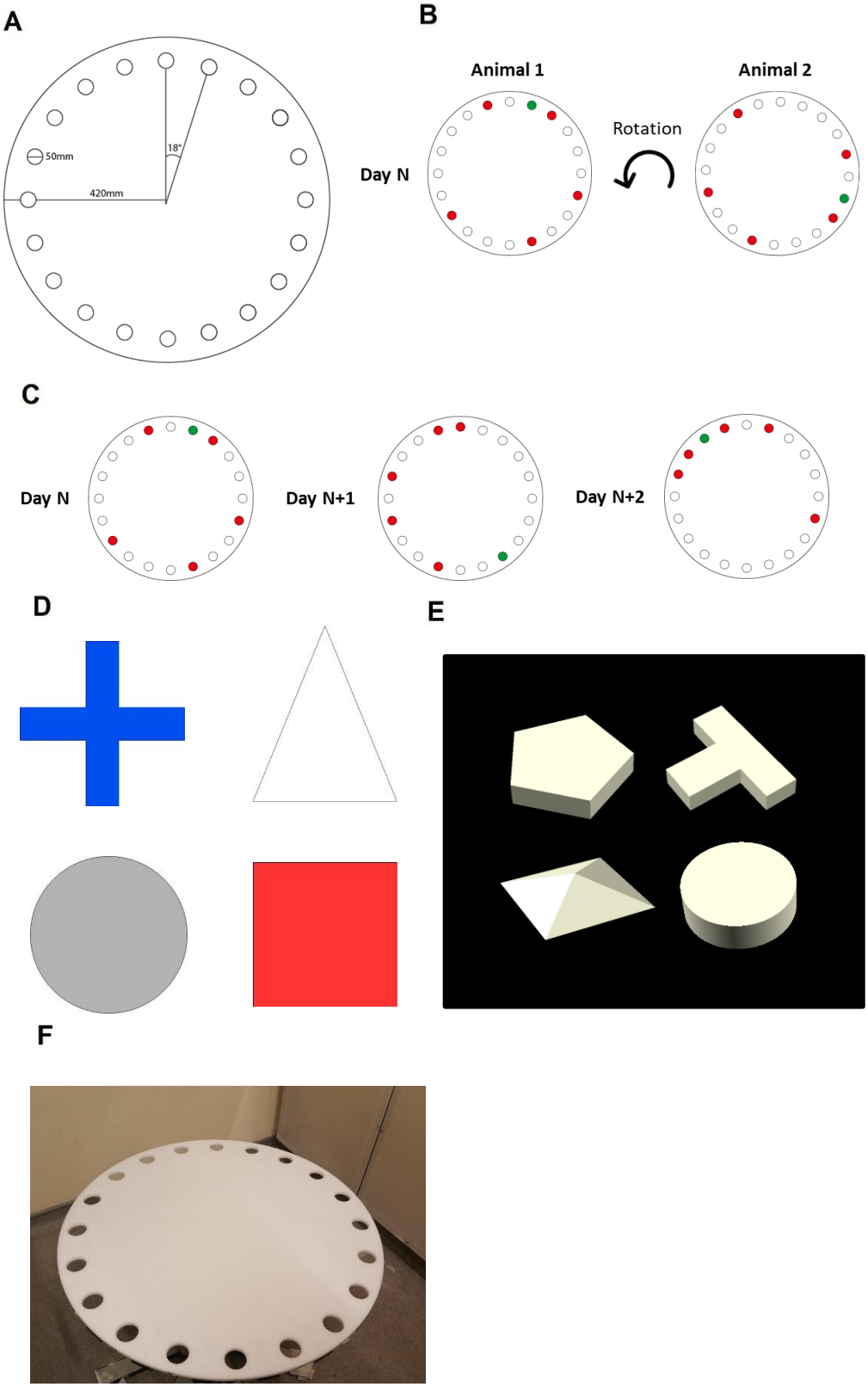

Figure 3.1.1: Apparatus design for the adapted Barnes maze (aBM) used in experiment one. A) Standard 20-hole mouse Barnes maze design, including maze dimensions and reward location position/size. B) Example matching of configurations of target and foils between animals

during the retrieval phase of training phase 3 or 4. C) Example variations of target-foil configurations on a given retrieval trial during training phase 3 and 4. Green coloured positions indicate the target location; red corresponds to non-target foil locations and white represents unavailable locations in B) and C). D) Graphic depicting extra-maze cues used in the aBM. Extra-maze cues corresponded to a blue cross (south), a white triangle (east), a grey circle (west), and a red square (north). E) Graphic 3D render depicting intra-maze cues used in training phase 4 in the aBM. Intra-maze cues corresponded to a white hexagonal prism, a black 'T' shape pyramid, a white pyramid, and a black cylinder. F) Example image of the aBM used during experiment one. Note that the aBM is shown without well inserts.

3.1.2.4 Behavioural procedures

Habituation and shaping

Upon arrival, mice were acclimatised to the laboratory environment for 1-day prior to handling. Animals were then handled daily for 7-days, alongside beginning food restriction to reach 90% of standard expected weight. Animal weights were measured daily, compared to expected developmental weights from the Jackson Laboratory mouse weight database (The Jackson Laboratory), and compared to a within-subject 3-day running average weight. Animals were monitored daily for sudden decline in weight or adverse outcomes. Animals typically reached target weight (+/- 5%) within 7-days before stabilising.

For the second week, all animals were placed into standard single housing home-cages over increasing durations from 30-minutes to 1-hour daily and given access to ½ reward pellets buried in a black sandwell placed in their cage. Feeding behaviour was monitored and animals were given up to 4 whole pellets in a single day. Across these seven days, the ½ rewards were gradually buried deeper in the sandwell, starting on top of the sand, to final depth of 2-3cm below the surface. This process was intended to shape the animals to dig further into the sandwell to retrieve the reward, while providing habituation to both the novel food and environment, handling, and temporary isolation (Takeuchi et al., 2016; Wang et al., 2010).

Pre-training

Animals then underwent a week of pre-training to acclimatise to the testing environment, maze, and task requirements. This extended pre-training protocol was advised by previous studies which indicated the difficulty associated with learning the 1-trial DMTP task in rodents (Wang et al., 2010; Takeuchi et al., 2016). On the first day, animals were placed into individual cages, then placed on the edge of the maze via the start-box. There was a single baited location in one quadrant (opposite side of the maze to start position), with a ½ pellet above and ½ buried shallow beneath the surface. The animals were allowed to acclimatise to the maze for 10-minutes to find and consume the rewards, before being returned to their home-cage. In the subsequent 6-days, animals were progressively exposed to the task design (see

Table 3.1.1 for exact outline), increasing the complexity of the task and shaping towards the planned trial structure of standard training.

Standard training

After all animals were readily consuming the reward on the maze, typically showing stereotyped behaviour of reward retrieval and return to start-box for reward consumption (Takeuchi et al., 2016), standard training commenced. Table 3.1.1 outlines the details of training phases 1-4, which followed the same daily trial structure, with increasing complexity through altering the number of foil locations (increasing the number of possible AFC), relative foil positions, trial duration, and number of encoding trials. Each day, animals were placed into individual cages and transported to the testing room. Animals were then individually placed on the maze via the start-box and given 3-minutes to continually retrieve up to three individual rewards of increasing digging depth from a single sandwell at a set target location (counted as multiple continuous encoding trials). This typical behaviour consisted of a search, retrieval, and consumption phases, in which animals searched for the rewarded sandwell, dug to retrieve the first buried reward, then returned to the start-box to consume the reward. This behaviour was then repeated to retrieve the second and third rewards, generating three retrieve-consume encoding trials. Animals were then returned to the individual housing cage for an ITI of 10-minutes. The maze was cleaned with 70% ethanol solution between trials to reduce the risk of olfactory strategy use. After this delay, animals were placed back on the maze, now with the target well matched to the location of the encoding trial but accompanied by a number of foil wells, which were not baited (Figure 3.1.2). The start-box was opened in a different orientation from that during the encoding phase to discourage egocentric navigation strategies. Following the trial start, animals were given one minute to retrieve the reward from the target location, relative to the foil alternatives (the AFC component of the task). Animals were the removed from the maze upon consumption of the reward or were removed if animals failed to locate the reward during the allotted duration of the retrieval phase.

The number of foil wells, and corresponding number of possible AFCs was dependent on the training phase. In the case of training phase 3, the task was a 5-AFC, with 5 foil wells and a single rewarded well. Performance on training phase 3 was taken as performance on a stable background of learnt task rules, as such primary analyses focussed on data from training phase

3 and 4. The number of days of repeat testing for each phase and relevant details are presented in Table 3.1.1.

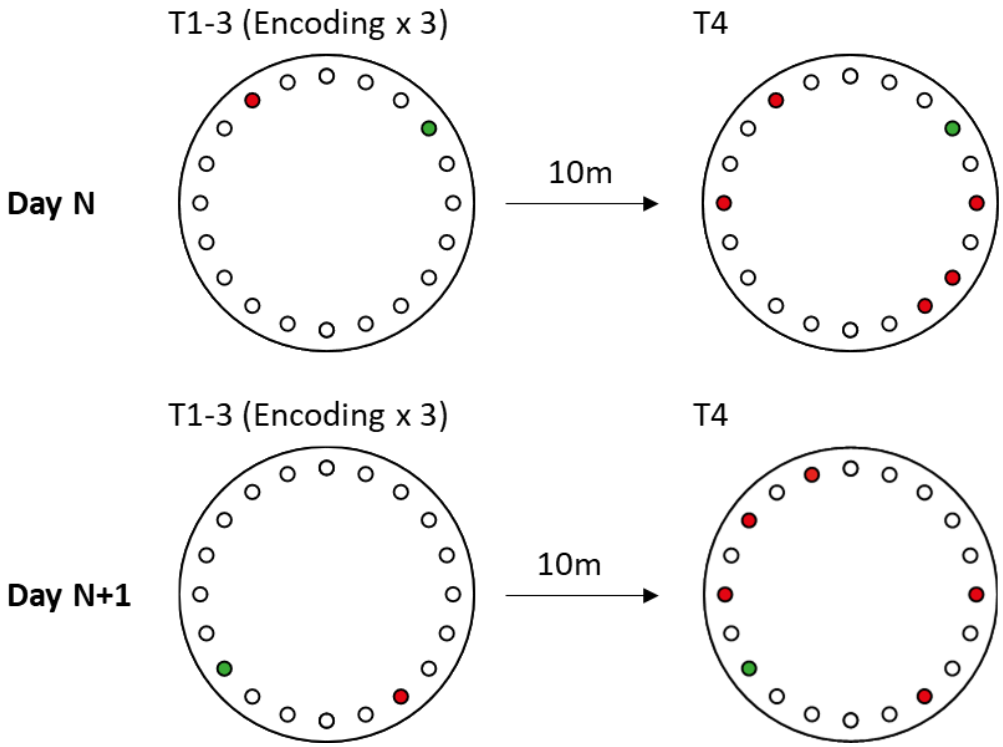

Figure 3.1.2: Diagrammatic example of standard 1-AFC encoding and 5-AFC retrieval trial structure in training phase 4. Green indicates the baited target location, while red and white positions represent non-baited foils and unavailable well locations, respectively. Typical training days involved three continuous encoding trials (T1-3) followed by a separate recall trial (T4). Training phase-specific adjustments to this general task structure are outlined in Table 3.1.1. Arrows represent 10-minute inter-trial intervals (ITI). 'Day N' and 'Day N+1' represent an example of a daily shift of target location and surrounding foil configuration. Note that target location and foil configuration was pseudorandomly varied between days, not allowing repeated target locations on consecutive days.

Table 3.1.1: Individual training phases and brief trial description used for each training day within a given phase. Number of days of training, number of AFC foil wells, sandwell type, and cue types are described for each training phase.

Training phase	Description	Days	AFC (retrieval)	Sandwell type	Cues
Pre-training					
D1	10-minute habituation with 1 pellet buried surface/shallow, no foil wells				
D2	Repeat of D1, 5-minute limit, 2 pellets buried shallow, centre-maze start				
D3	Repeat of D2, 2 pellets buried deep	1-7	NA		
D4	Repeat of D3				
D5	Repeat of D4, 3-minute limit				
D6-7	Repeat of D5				
Training phase 1				Black	Extra-maze
	2 encoding trials, 1 retrieval trial with 1AFC foil at opposite side of maze from target	8-12	1		
Training phase 2					
	2 encoding trials, 1 retrieval trial with 3AFC foils at equal separation angles from target	13-26	3		
Training phase 3					
	3 encoding trials, 1 retrieval trial with 5AFC foils at randomised separation angles from target	27-72	5		
Training phase 4					
	3 encoding trials, 1 retrieval trial with 5AFC foils at randomised separation angles from target	73-100	5	White	Extra-maze + Intra-maze

Retraining: Training phase 4

During training phase 3, data analyses demonstrated high inter and intra-subject variability that may have been driven, in part, by simple visual cued-approach behaviour or mixed strategy learning, possibly including olfactory strategies (see results & discussion of experiment one for further details). As stable use of an allocentric spatial search strategy is a prerequisite for assessing hippocampal-dependent spatial memory on a longitudinal scale, we sought to adapt the design to encourage preference for a spatial strategy. First, given that visual-approach to the sandwells may confound performance, we reduced the available visual cues associated with the sandwells by changing the material from black to white PLA, matching the maze, and ensured the sandwells were level with the maze surface. Second, animals were given an extended encoding phase to 10-minutes to ensure a reward was always obtained, increasing the reinforcement of the win-stay strategy. The digging medium was replaced with bird-sand (Jondo Suppliers) in combination with the addition of further inaccessible foil pellets to increase control of diffuse odour cues (described in apparatus section; Bast et al., 2005; Nonaka et al., 2017). Finally, intra-maze landmark cues were added with the aim of increasing reliance on allocentric spatial learning. Retraining consisted of 5-days of reshaping to consume rewards in the novel white sandwells and digging medium. Animals were then returned to the training procedure as described in training phase 3 (Table 3.1.1). Animals were trained for a further 15-days, before beginning probe and control trials.

Probe trials

‘Probe trial’ in experiment one refers to a trial matched to the structure of a standard training trial in training phase 4, with the omission of the reward from the retrieval phase. Within each probe trial, search performance was measured during the 1-minute retrieval phase, to assess place preference as a measure of effective memory recall. This is analogous to the unrewarded probe trials performed in other maze tasks such as the MWM or Barnes maze which allows assessment of the robustness of spatial memory in the absence of potential olfactory confounds. Three probe trials were performed during training phase 4 on days 87, 90, and 93.

Control trials

On days 96, 98, and 100, odour, intra-maze occlusion, and extra-maze occlusion, control trials were performed, respectively. Control trials were performed to assess reliance on non-spatial strategies for solving the maze task. The intra and extra-maze control trials entailed removal of the 2D extra-maze or intra-maze cues during the retrieval trial, respectively. Under standard conditions, animals should rely on extra-maze cues as spatial landmarks to support allocentric place learning. During extra-maze control trials, removal of these cues should impair normal performance to chance during the retrieval phase if the assumption of the reliance on these cues is met (O'Leary et al., 2011, 2013; Wang et al., 2010). Conversely the intra-maze control trial assessed the reliance on intra-maze cues for navigation. If distal cue (extra-maze) allocentric spatial navigation is being used, retrieval performance should not be impaired to chance by the removal of intra-maze cues (Wang et al., 2010). Finally, the odour control trial was performed as a single rewarded retrieval trial without prior encoding, in order to assess the ability of animals to use olfactory cues to solve the task without prior knowledge of reward location. If odour is made redundant by adulteration of the digging medium, performance should be at or below chance (Bast et al., 2005). These non-spatial strategies of olfactory-based search or response learning (i.e., encoding location relative to egocentric information), are known to be mediated primarily by non-hippocampal structures (e.g., Morris et al., 1990; Bast et al., 2007) and as such would preclude assessment of allocentric place learning.

The experiment ended on day 100 and animals were subsequently culled following the perfusion-fixation procedure detailed in section 2.2.1.

Counterbalancing of rewarded locations

The extensive literature surrounding the use of maze tasks to assess spatial navigation in rodents has emphasised the importance of counterbalancing in assigning rewarded locations (e.g., Bimonte-Nelson et al., 2015; Wang et al., 2010). All maze experiments reported here were designed to adhere to these principles and mitigate confounding factors. The repetition of locations across days in DMTP tasks may result in erroneous results due to perseveration to prior rewarded locations or developing an olfactory-based strategy (Bast et al., 2005). To mitigate this, locations were counterbalanced within subjects across trials to ensure a given subject did not have a rewarded location repeated on subsequent training days. In addition,

foil locations were pseudo-randomised based on matching equal separation sizes (number of positions separated from target) for each day, although the relative configuration was matched between subjects to remove any difficulty confound that may arise within a given trial (demonstrated in Figure 3.1.1B/C). To reduce the likelihood of egocentric search strategies, the start box orientation of animals was varied pseudorandomly between encoding and retrieval phases. Measures were also implemented to control for olfactory biases including intertrial cleaning of the maze and sandwell apparatus using 70% ethanol solution. Finally, each sandwell within the maze contained either a matched number of reward pellets in an inaccessible zone and the digging medium was mixed with powdered reward to avoid directional biases based on any potential intensity difference in olfactory cues originating from the wells.

3.1.2.5 Analysis

Tracking data pre-processing

Raw tracking data was extracted from Ethovision XT9, before removal of frames in which tracking errors occurred. X-Y coordinate tracks were then exported to Excel. Individual track data provided information on distance and latency to individual regions of interest (ROIs) defined on the maze, which corresponded to individual well positions. All raw data was then extracted and processed using custom MATLAB scripts and exported for analysis in R or SPSS analysis software.

Characterisation and statistical analysis of measure variables

A number of variables have been used to quantify spatial learning and memory in maze-based tasks, which often overlap in both appetitive and aversive task variants (Feng et al., 2017; Youn et al., 2012). Common variables include primary latency to reach target (e.g., first platform crossing), primary path length to reach target location, cumulative or mean distance to target, search errors prior to reaching target location, and time spent at target location/quadrant (place preference; probe trials only). It has been noted that it is crucial to characterise these variables from the data in any maze-based task, particularly novel task variants, for sensitivity

and generating normative profiles of performance (Bimonte-Nelson et al., 2015; Vorhees & Williams., 2014a).

The primary measure used to represent training data were search errors and 'performance index'. Search errors were calculated manually for each trial and were defined by an animal nose-poking or digging at a foil sandwell location. Animals could make a maximum of 5 primary errors on training phases 3-4 but could also make additional 'working memory' errors by revisiting a previously searched sandwell. A performance index (PI) was generated on the basis of these search errors (as reported in Takeuchi et al., 2016), for which the formula is outlined in Figure 3.1.3. Performance index was used as a learning criterion for stable background performance, set at an average of 70%, on which to add probe and control trial manipulations (Takeuchi et al., 2016). Performance index produces a value between 0-100 which can be contrasted with the number of errors to reach chance performance (e.g., with 50% chance performance corresponding to 3 errors within a 5AFC task). Average performance index was calculated over 7-day windows for individual animals and were compared to chance performance in each training phase using one-sample t-tests. Additionally, repeated measures t-tests were used in cases where performance index was compared between training phases. In cases where animals failed to retrieve the reward within the allotted time during the retrieval phase, performance index was either omitted or set at zero (see section 3.1.5). Proportion of omissions relative to total trials was calculated, averaged within training phases or weeks and subsequently compared between training phases or weeks respectively, using repeated measures t-tests.

$$PI = 100 - [100 \times \frac{errors}{NumFoils}]$$

Figure 3.1.3: Formula used to calculate performance index (PI) in experiment one. 'NumFoils' corresponds to the number of foil sandwells present in a given trial, corresponding to the maximum number of primary errors, while "errors" corresponds to the given number of errors made by an animal in a given trial.

Search strategy was defined using classification guidelines reported in previous Barnes maze literature (e.g., O'Leary et al., 2013; Bach et al., 1995; Rosenfeld & Fergusson., 2014; Speidell et al., 2019), which broadly separates search paths into three categories, spatial, serial, and random search. Spatial search is typically defined as direct movement to the target location or up to 2-3 adjacent locations either side of the target. In experiment one, due to the limited number of alternative choices, spatial search was defined as direct movement to the target location, with a maximum of 1 error. Serial search is classified as sequential searching at multiple (2+ consecutive) non-target locations. Random search is given when multiple maze crossings are made with no clear directional strategy. Search strategy was expressed as the proportion of trials completed using spatial, serial, or random search within a given training phase (e.g., training phase 4), within subjects. Strategy preference was then compared within subjects by strategy type and between subjects by sex using repeated measures or between-subjects t-tests as appropriate. Further, Pearson's correlation coefficient was calculated between strategy preference during training phase 4 and place preference during subsequent probe trials to assess the predictive validity of prior strategy preference for memory retrieval accuracy.

Finally, time spent at the target relative to foil sandwells (place preference) was calculated for probe trials in lieu of time spent in target relative to non-target quadrants as an approximation of 'dig time' reported in previous experiments (e.g., Wang et al., 2010). Time spent at each open sandwell was calculated using acquired tracking data. During probe and control trials, place preference for the target location was expressed as percentage of time spent at target sandwell and compared to the average foil sandwell using within subject t-tests (Bast et al., 2005). This process was performed across the averaged data for three probe trials or individual control trials. In order to produce a metric of pattern separation-like ability, time spent at individual foil positions was clustered into three discrete categories of separation size: 18-54°, 90-126°, and 144-180° (for reference, see Figure 3.1.1), corresponding to foil sandwell positions: 1-3, 4-6, and 7-9, respectively. Time spent at zones within each of these three foil categories was averaged and compared to preference for the target location using repeated measures t-tests.

Finally, in order to assess the predictive validity of strategy preference during the training phase to the probe phase, animals were grouped according to strategy preference during training phase 4, preceding the probe trials. These groups were defined by a set criterion of equal to or more than 70% spatial strategy preference or <70% spatial strategy preference,

creating ‘spatial’ and ‘non-spatial’ groups, respectively. This data was sourced from the final preceding week of training prior to probe and control trial testing. This post-hoc grouping was only used to predict performance following the period of training used for the categorisation to avoid selection biased (i.e., circular) analyses. Following this grouping, percentage place preference during probe trials between these groups was compared using mixed measures ANOVAs with separation size as within subject and preference group as between subject variables. The results of all statistical tests are presented in Table 3.1.2.

3.1.5 Results

In the first experiment, we aimed to develop a novel appetitive adaptation of the Barnes maze task which was sensitive to putative allocentric rapid place learning and memory as an analogue of 'everyday memory'. We aimed for the aBM task to allow repeat administration and demonstrate suitability for extension to testing APOE-TR mice. Using WT mice, we hypothesised that animals would show steady task acquisition which would become stable above chance (i.e., in our primary measure of performance index) and that animals would demonstrate evidence of spatial memory recall during probe trials such as place preference. We also predicted that animals would demonstrate an allocentric place learning strategy, dependent on extra-maze cues, and lastly that animals would discriminate between the target and non-target foils in a linear fashion, to demonstrate a requisite for pattern separation-like behaviour.

3.1.4.1 Training phases 1 and 2

Firstly, animals readily learnt to dig and consume the food reward in both the home-cage and on the maze after habituation, shaping, and the basic 1-AFC training phase 1. There was, however, some intra-subject variability in the number of rewards consumed on a given day which likely contributed to increased variability in performance. By averaging trials across days within each subject in a given training phase it was possible to decrease this variability and provide more representative data. Animals demonstrated an average performance index significantly greater than chance (50%) during training phase 1 and the first week of training phase 2 upon switching to the 3-AFC task. However, performance index was not significantly above chance in week two of training phase 2 (Figure 3.1.4A, Table 3.1.2).

3.1.4.2 Training phase 3

Upon transitioning to the 5-AFC task in training phase 3, which comprised bulk of standard training across 6-weeks (weeks 4-9), performance index appeared to gradually increase (Figure 3.1.4A). However, while accuracy of performance index increased during completed trials, the number of omitted trials simultaneously increased significantly. This increase in omissions during the retrieval trial totalled 26.8% of retrieval trials over the course of training phase 3 (Figure 3.1.4B) but was observed to increase across weeks of training (Figure 3.1.4C). When

accounting for these trial omissions, performance index was not significantly different from chance during training phase 3 (Figure 3.1.4A). This high rate of omissions and subject variability, despite good performance on completed trials, led to the decision to alter several task parameters, as outlined in section 3.1.3. Briefly, sandwellls were adjusted to be uniform with the maze in colour and visibility, intra-maze cues were introduced, encoding trial duration was extended (3-minutes to 10-minutes) to improve reward contingency, and the digging medium was changed.

3.1.4.3 Training phase 4

Animals again readily shaped to consume food rewards in the novel sandwells in the homecage as well as on the maze. Following reshaping, training phase 4 commenced. During training phase 4, animals demonstrated performance index significantly above chance trials by 7-days (Figure 3.1.4A). Increasing the duration of encoding trials increased the reinforcement regimen and significantly decreased retrieval omissions as compared to training phase 3 to an average of 4.3% (Figure 3.1.4B, C), which was accompanied by a significant increase in performance index between the last week of training phase 3 and the end of the first week of training phase 4 (Figure 3.1.4D).

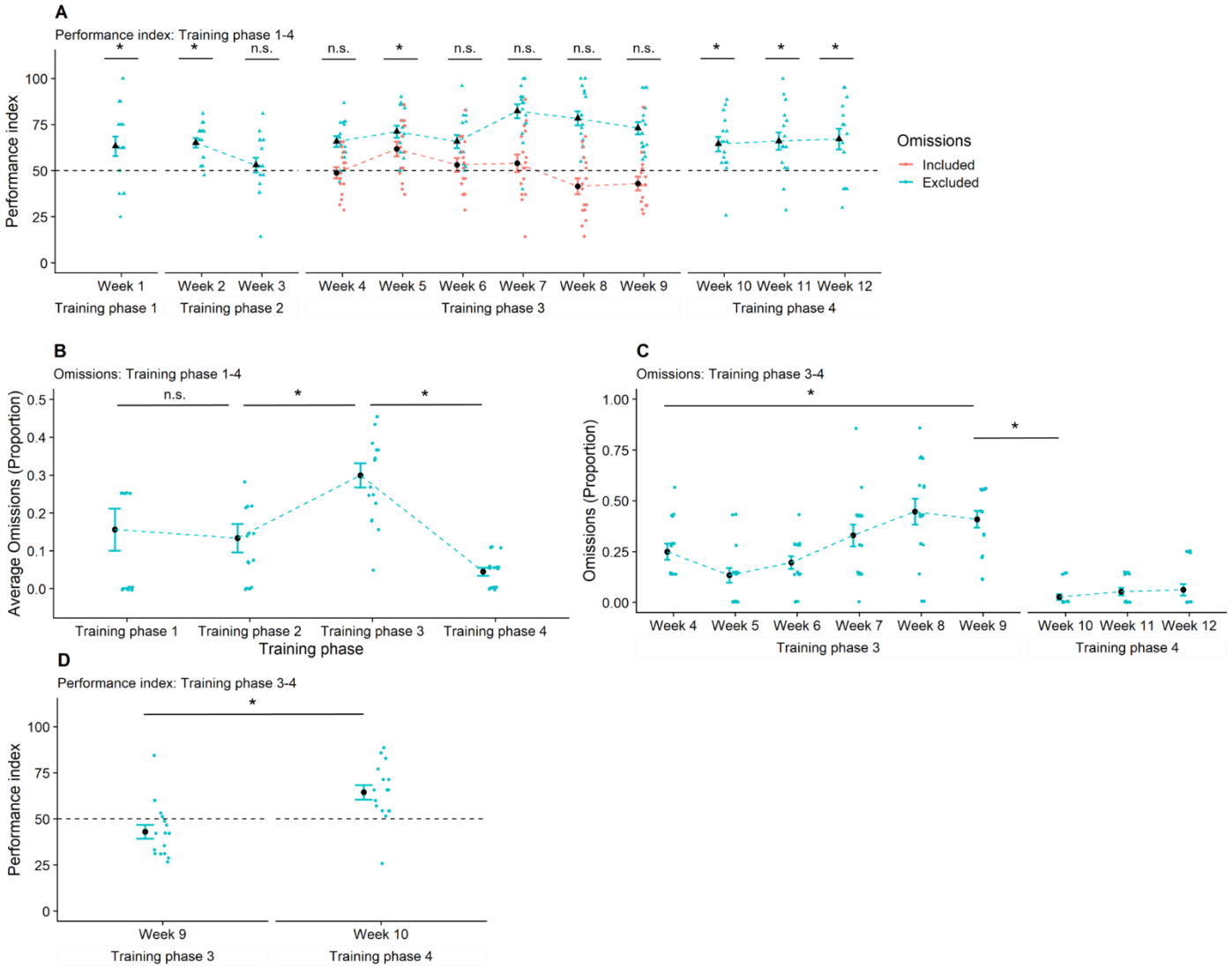

Figure 3.1.4 panel 1: Primary results of performance of WT mice in the aBM task during experiment one. A) Average performance index across 12 weeks of training from training phase 1 to training phase 4. Each weekly within subject average is compared to chance (50%, dotted line) performance. Omission-corrected performance index during training phase 3 is indicated by colour. Statistical comparison during training phase 3 is made between omission

corrected performance index and chance. B) Average proportion of omissions during individual training phases. Statistical comparisons are made between a given training phase average and the subsequent training phase average. C) Average proportion of omissions across individual weeks of training. Statistical comparisons shown are made between week 4 and 9, and week 9 and 10. D) Average performance index between week 9 and 10. In each case, coloured points represent individual subject averages and error bars represent group mean +/-SEM. '' represent significance at p = <.05, and brackets and labels denote relevant comparisons and main effects where appropriate. Corresponding statistical comparisons are presented in Table 3.1.2.*

Spatial search strategy was the most preferred strategy during training phase 4, with significantly higher preference overall for spatial than serial and random search during retrieval (Figure 3.1.4F). However, comparison by sex highlighted an increase in random strategy preference, and a small mean decrease in spatial preference in female mice, although this did not reach significance. Despite the overall spatial strategy preference at the whole group level, analysis across individual animals revealed a clear split in predominant preference. Overall, 7/16 animals showing use of spatial strategies in more than 70% of trials, and 9/16 animals showing relatively uniform preference for serial, spatial, and random strategies. This prompted the use of this criterion to compare the group's performance during probe and control trials, assessing whether strategy preference during training predicted subsequent performance.

3.1.4.4 Training phase 4 probe and control trials

During training phase 4 probe trials, performance index remained significantly above chance (Figure 3.1.4E), however place preference (time spent at the correct reward location) relative to the average foil approached but did not reach significance (Figure 3.1.4G). Place preference (Figure 3.1.4H) and performance index (Table 3.1.2) were not significantly affected by strategy preference during preceding training, however, suggesting strategy use during training did not predict strategy use during probe trials. Strategy preference during probe trials also did not correlate significantly with preference during preceding training (Table 3.1.2).

Despite this there was a significant effect of separation size (foil distance from target) on place preference relative to corresponding foils at the whole group level. Namely, significantly more time was spent at the rewarded location than foils between both 4-6, and 7-9 positions from the target location (Figure 3.1.4I). Therefore, animals showed significant place preference at the target location than foils of a greater than 54° angle separation from the target location. This effect of separation size was, again, independent of strategy preference grouping (Figure 3.1.4J).

The training phase 4 odour control trial revealed no improvement in performance index relative to chance (Figure 3.1.4E), supporting the lack of odour-based task performance. Finally, performance index was not significantly above chance following the occlusion of either intra or extra-maze cues (Figure 3.1.4E). However, animals demonstrated significant place

preference for the target relative to foils above 54-degree separation during extra-maze (Figure 3.1.4K) but not intra-maze occlusion (Figure 3.1.4L) trials.

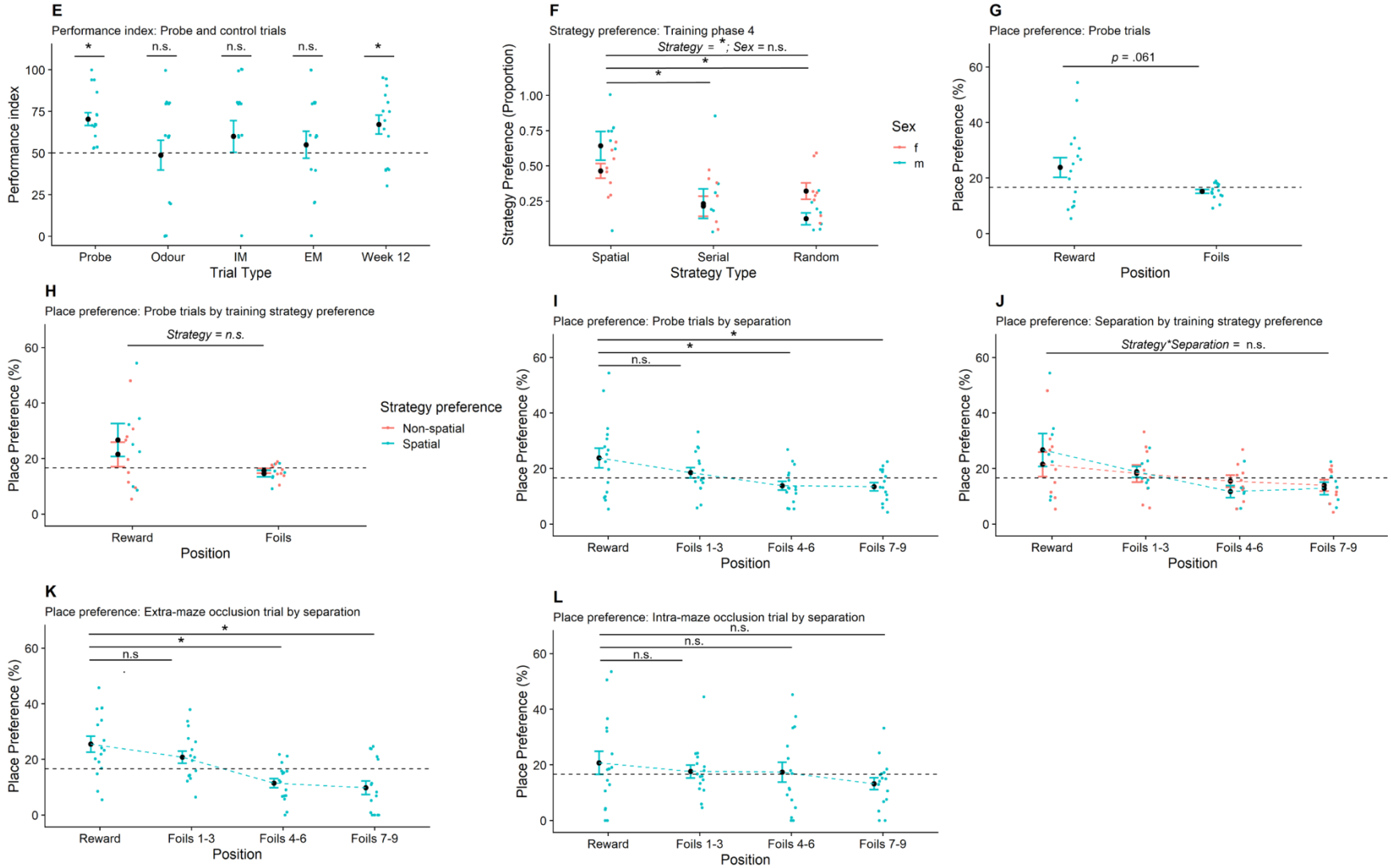

Figure 3.1.4 panel 2: E) Average performance index across probe trials, odour, extra-maze cue occlusion, intra-maze cue occlusion control trials, and week 12 standard training, respectively. Statistical comparisons are relative to chance performance (50%, dotted line). F) Average proportion of spatial, serial, and random strategy preference during retrieval trials in training phase 4. Statistical comparisons are made between sex and within strategy groups. G) Average

place preference for target location compared to average foil during probe trials at the whole group level. H) As Figure G) grouped by strategy preference during training phase 4. I) Average place preference for target location compared to foil separation size during probe trials. Bracket denotes main effect of separation size and individual asterisks denote post-hoc t-tests comparing reward relative to individual foil categories. J) As Figure I) grouped by strategy preference during training phase 4. Statistical comparison represents interaction between strategy preference and separation size. K) As Figure I) during extra-maze cue occlusion trial. L) As Figure I) during intra-maze cue occlusion trial. In each case, coloured points represent individual subject or within-subject averaged data points, black points represent group mean, and error bars represent +/-SEM. '' represent significance at p = <.05, and brackets denote relevant comparisons and labels represent main effect comparisons. Individual accompanying statistical tests and values are presented in Table 3.1.2.*

Table 3.1.2: Statistical comparisons performed in experiment 1. Relevant comparison, measures, training phase, week, statistic and corresponding figures are provided. Analysis corresponds to Figure 3.1.4 panels 1 and 2.

Comparison	Measure	Training phase	Week	Statistic	Figure
Weekly PI Vs Chance					
	PI	1	1	$t(15) = 2.51$, $p = .024$	
		2	2	t(15) = 5.84, p = <.001	
		2	3	t(15) = 0.74, p = .471	
		3	4	t(15) = -0.36, p = 727	
		3	5	t(15) = 2.92, p = .011	
		3	6	t(15) = 0.85, p = .407	3.1.4A
		3	7	t(15) = 0.86, p = .402	
		3	8	t(15) = -1.96, p = .069	
		3	9	t(15) = -1.88, p = .079	
		4	10	t(15) = 3.689, p = .002	
		4	11	t(15) = 3.39, p = .004	
		4	12	t(15) = 3.01, p = .009	
Between/within training phase					
	Omissions	1-2	1-3	t(15) = 0.38, p = .712	
		2-3	2-9	t(15) = -3.70, p = .002	
		3-4	4-12	t(15) = 7.61, p = <.001	3.1.4B-D
		3	4 Vs 9	t(15) = -4.51, p = <.001	
		3/4	9 Vs 10	t(15) = 9.02, p = <.001	
	PI	3/4	9 Vs 10	t(15) = 3.22, p = .006	
Strategy preference					
	Strategy type	4	11	F(2,28) = 8.52, p = .001	
	Spatial Vs Serial	4	11	t(15) = 2.93, p = .010	3.1.4F
	Spatial Vs Random	4	11	t(15) = 3.92, p = .001	
	Strategy type*Sex	4	11	F(2,28) = 2.07, p = .145	
	Training phase 4 Vs Probe trials	4	11	r = 0.186, p = . 491	

Table 3.1.2 continued.

Comparison	Measure	Training phase	Week	Statistic	Figure
Probe trial Vs Chance					
	PI	4	11/12	t(15) = 5.306, p = < .001	
Extra-maze occlusion trial Vs Chance					
	PI	4	12	t(15) = 0.62, p = < .544	3.1.4E
Intra-maze occlusion trial Vs Chance					
	PI	4	12	t(15) = 1.05, p = < .309	
Odour probe trial Vs Chance					
	PI	4	12	t(15) = -0.14, p = < .891	
Probe trial Reward Vs Foil average					3.1.4G
	Place preference	4	11	t(15) = 2.03, p = .061	
Probe trial Reward Vs Foil average (by strategy preference group)					
	Place preference (by strategy preference)	4	11	F(1,14) = 0.51, p = .489	3.1.4H
Probe trial Reward Vs Foil separation					
	Place preference (Target Vs Separation 1)	4	11	t(15) = 1.23, p = .277	
	Place preference (Target Vs Separation 2)	4	11	t(15) = 2.58, p = .021	3.1.4I
	Place preference (Target Vs Separation 3)	4	11	t(15) = 2.25, p = .040	
Probe trial Reward Vs Foil separation (by strategy preference group)					
	Place preference (Separation)	4	11	F(3,42) = 3.71, p = .019	3.1.4J
	Place preference (Strategy preference)	4	11	F(1,14) = 0.50, p = .827	
	Place preference (Separation*Strategy preference)	4	11	F(3,42) = 0.51, p = .681	
Probe trial Reward Vs Foil separation during Extra-maze cue occlusion					
	Place preference (Separation)	4	11	F(3,45) = 7.88, p = <.001	
	Place preference (Target Vs Separation 1)	4	11	t(15) = 1.17, p = .261	3.1.4K
	Place preference (Target Vs Separation 2)	4	11	t(15) = 3.79, p = .002	
	Place preference (Target Vs Separation 3)	4	11	t(15) = 3.51, p = .003	
Probe trial Reward Vs Foil separation during Intra-maze cue occlusion					3.1.4L
	Place preference (Separation)	4	11	F(3,45) = 0.73, p = .537	

3.1.5 Discussion

Experiment one sought to establish the viability of a novel appetitive adaptation of the Barnes maze task, the aBM, for assessing rapid place learning and memory in WT mice. The task design drew from multiple prior task designs which generate stable task performance of episodic-like memory on a background of 'prior knowledge' or rule learning to emulate more ecologically relevant everyday memory tasks. We hypothesised that animals would show evidence of rapid place learning and memory during training, which would stabilise above chance levels and that animals would show place preference to indicate memory recall during probe trials. Finally, we expected that animals would show pattern separation-like discrimination between the target and non-target foils in place preference, which would be reliant on an allocentric spatial strategy.

During training phase 3, we did not observe evidence consistent with our first hypothesis. The high rate of trial omissions during retrieval in training phase 3 prevented stabilisation of task performance and was problematic for intra-subject variability (Figure 3.1.4A-C). Trial omissions continued to increase across training phase 3 and further, performance index showed high day-to-day and inter-subject variability. This confounded the assumption of stable spatial strategy use for repeat and longitudinal testing and prompted task alterations encompassing training phase 4.

The variability in preferred strategy during training phase 3 may have been due, in part, to overshadowing or conflicting information between potential task rule learning strategies. Specifically, during the first three training phases, both target and foil sandwell positions were visible to animals due to the raised edge of each well above the maze floor. While this design was intentional to introduce a forced-choice component to the task, this may have inadvertently introduced a parsimonious visual cued-approach task solution, learnt by simple operant conditioning, where approach to a sandwell visual cue and digging would be intermittently rewarded. Subsequently this may overshadow the more complex strategy of allocentric spatial learning and recall, preventing a reward contingency dependent on spatial memory use. This was in spite of the fact that the number of alternative choices was increased relative to prior studies to decrease the reward contingency associated with random sandwell choice (e.g., Takeuchi et al., 2016). Further, punishment introduced by removal from the maze after failure to retrieve a reward during the retrieval phase may have compounded the strategy variability due to reducing the reward contingency, animal motivation, or promoting extinction.

Training phase 4 was introduced to address these concerns. Switching sandwell inserts to match the colour and uniformity of the maze surface removed the possibility of simple visual-cued approach, while increasing the encoding trial duration improved the reward contingency and reduced trial omissions relative to training phase 3 (Figure 3.1.4B/C). An improvement in performance was observed between training phase 3 and 4 within the first week, suggesting these alterations improved task learning. However, a divide in preferred search strategy during retrieval emerged between animals. Namely, there was a clear split between animals in predominant preference for spatial or non-spatial search strategies. Despite this, performance during probe trials was suggestive of spatially-driven recall given the trend to significance for preference of the target location relative to surrounding foils and that performance index remained significantly above chance in absence of potential odour cues (Figure 3.1.4E/G). Intriguingly, place preference during the probe trials was not predicted by strategy preference during training phase 4 (Figure 3.1.4H), which suggests within-subject variability in day-to-day strategy use. Additionally, there was a significant effect of separation size on place preference relative to surrounding foil groups, independent of preceding strategy preference. Animals failed to differentiate between foils within three positions of the target but spent significantly more time at the target location than foils greater than three positions from the target. This suggests that the pattern separation-like manipulation successfully induced spatial uncertainty, with decreasing separation size intuitively decreasing certainty of the location of the target.

Finally, two patterns of results emerged from the control trials during the experiment. First, performance index was impaired during both extra-maze and intra-maze cue occlusion trials. Second, place preference by separation size was significantly impaired during the intra-maze occlusion trial but not the extra-maze occlusion trial.

Together, this data posits multiple possibilities. Firstly, limited reinforcement due to a low number of encoding trials alongside complex rule learning may have impaired the development of a stable spatial search preference overall. Previous studies have highlighted a ‘typical’ profile of search behaviour which transitions from random to serial to spatial search during reference memory Barnes maze tasks (e.g., Bach et al., 1999; Youn et al., 2012; Illouz et al., 2020). In reference memory tasks, a single target location is typically repeated across multiple trials, often up to or in excess of twelve repeats, while in the current experiment and other rapid place learning DTMP tasks the maximum visits are often limited to four (e.g., Steele and Morris., 1999; Bast et al., 2005). However, the fact that performance index remained

significantly above chance during both training and probe trials but was impaired during either cue removal or the odour control trial make this explanation unlikely.

Second, animals may have solely relied on an intra-maze cue-dependent egocentric strategy. For example, in the case of animals reliant on intra-maze cues a task solution may be to learn to path integrate relative to the position of an intra-maze cue, simply making a given self-referent directional change upon cue approach rather than via allocentric learning. However, the fact that animal starting positions were randomised by the use of the start-box and that performance was impaired across both control trial types also make this unlikely to be the sole explanation. Third, animals may have relied on spatial relational information between the intra-maze and extra-maze cues but the sustained place preference during the extra-maze occlusion trial also makes this unlikely (Broadbent et al., 2020). Fourth, olfactory-based navigation similarly appears unlikely, as performance was at chance during the odour control trial in which prior encoding trials were omitted.

Fifth, it is possible that the extra-maze cues were, in part, lacking salience and were not detrimental to performance when removed, as the global spatial cues remained (i.e., room configuration, distal diffuse cues such as wall texture etc.). Some groups have suggested a combination of complex 2D and 3D cues are more appropriate for maze tasks to support allocentric learning (e.g., Champagne et al., 2002; Wang et al., 2010). Indeed, it has been noted that salient extra-maze cues typically overshadow proximal intra-maze cues in spatial maze tasks (e.g., Wang et al., 2010; Harrison et al., 2006b; Hebert et al., 2017) however this was not the case in this experiment.

Therefore, we suggest that overall performance was sensitive to both intra and extra-maze cue types and that animals may have used a combination of allocentric and egocentric strategies to support task solution. This would be supported by the impairment across both controls in initial search, while sustained preference for the location may have been possible through flexible use of intra-maze cues and diffuse distal cues (O'Leary et al., 2011). Additionally, the fact that search strategy preference during training did not predict probe trial performance also supports intra-subject variability in day-to-day strategy preference. This highlights a need for optimisation of visuo-spatial cue conditions to provide adequate motivation to predominantly rely on allocentric spatial learning.

The successful differentiation between the target location and foils of increasing separation size during probe trials is compatible with previous studies attempting to operationalise pattern separation-like ability in rodents, with a linear decline of accuracy across increasing

spatial similarity in DMTP operant and radial arm maze tasks (Oomen et al., 2013; Creer et al., 2010; Clelland et al., 2009). On the other hand, the task floor effect at small separation sizes in wildtype animals suggests a combination of high task difficulty and variable strategy use may complicate detection of subtle phenotypic effects. Therefore, further alterations to the current task should aim to establish consistent spatial strategy reliance and incorporate more flexible difficulty while maintaining the benefits of a more ecologically valid task for extrapolation than previous established tasks. For example, operant touchscreen-based visual cue separation tasks, while providing similar scope for manipulation and potential for high throughput, lack the more ecological, configural environments typically used for hippocampal-dependent navigation and episodic-like memory tasks (Oomen et al., 2013; Hvoslef-Eide et al., 2016). Additionally, the incorporation of spatial navigation faculties in maze tasks provides a complementary approach to operant tasks and may be used in combination to assess learning and memory performance in differing contexts. Further, it is also possible to dissociate factors such as delay-dependent recall, environmental cue-availability and spatial uncertainty by altering the relative position of target and foil locations to differentiate recall accuracy in both types of tasks. Similarly, dissociating the ‘working memory component’ of task performance from pattern separation may be operationalised by segregating working memory 'revisit’ errors or search from errors or search based on the separation distance from the target over varying retrieval delays (Oomen et al., 2013; Gilbert et al., 2006; Clelland et al., 2009).

3.1.4.1 Caveats

Overall, experiment one failed to generate performance with stability sufficient to justify use in longitudinal repeat testing. Ultimately, while performance on probe trials and prior training were indicative of spatial learning and pattern separation-like performance, the extent to which a spatial strategy was used during retrieval trials was variable. This confounds the assumption of stable spatial memory use for repeat assessment of everyday memory. The impairment of performance following intra-maze cue occlusion is consistent with previous studies highlighting the ability of mice to solve the Barnes maze via both spatial and non-spatial means and the importance of the geometric relationships in configural cues to aid performance (Harrison et al., 2006; O’Leary et al., 2011, 2013). These results also outline the importance of establishing salient extra-maze configural cues which tie reward contingency directly to spatial strategy use. Crucially, the intrinsic concentric design of the Barnes maze, with target locations restricted to only the maze periphery, may induce overshadowing of

distal extra-maze cues lacking salience. Indeed, some recent studies have attempted to ameliorate serial search preference via use of complex maze designs with pseudorandom target locations across the whole maze platform (e.g., Faizi et al., 2012; Illouz et al., 2016; Feng et al., 2017).

Finally, it is also possible that the training history of the animals during experiment one (i.e., training phases 1-3) may have biased their behaviour even following retraining in training phase 4. Therefore, the results of the probe and control trials should be interpreted with caution, and future developments may benefit from a simplified training regime to reduce variability in task adherence.

3.1.5 Conclusion

To conclude, the results from experiment one inform future task designs using appetitive motivation as a driver for assessing rapid place learning and memory. It is clear that, despite the similarities in training protocol and general procedure, the Barnes maze variant holds several important distinctions from event arena tasks previously conducted. While probe trial performance supported spatial memory recall and putative pattern separation-like performance, strategy analyses and cue control trials suggested this was confounded by variable strategy preference. The intrinsic maze design requires optimisation to bias preference towards spatial learning strategies and highlights the necessity of a stable baseline. To achieve this there is a need to reinforce a win-stay strategy while eliminating non-spatial strategies as viable alternatives. Further, the lack of correspondence observed between strategy use and measures of place preference highlights the importance of using multiple metrics of performance to assess task solving, particularly in validation of novel tasks. Moreover, reliance on a sole measure may lead to biased conclusions (e.g., Bimonte-Nelson et al., 2015). Overall, this precludes the usefulness of the design of experiment one for longitudinal repeat testing when prolonged training periods may prevent assessment of normative performance in young animals. This framework may be suitable for cross-sectional design with further optimisation, however.

3.2 Experiment two

3.2.1 Introduction: Experiment two

In order to address several methodological issues and behavioural pitfalls of the aBM task design of experiment one, experiment two was designed with the aim of rectifying these issues and assessing the viability of an adapted task for repeat testing in WT mice from a young age. Each key issue outlined in experiment one is addressed briefly below, and implementation can be found within the experimental methods sections.

Firstly, experiment two aimed to improve the rate of the reliance on an allocentric place strategy by increasing the salience of the visuospatial cues present. This was achieved by increasing the number and visual complexity cues of the testing arena surrounding the maze following guidance from previous protocols (see Wang et al., 2010; Bast et al., 2005 and in the apparatus section for further details). In addition, intra-maze cues were removed, and maze rotation introduced on the basis of the intra-maze control trial used in experiment one which suggested use of a mixed strategy (e.g., non-spatial egocentric, thigmotaxis etc.) during the probe trials. Further, to ensure reliance on both diffuse global and landmark spatial cues, multiple control trials were included to omit local or all visuospatial cues on a given trial. To remove the potential confound of visual cued-approach and thigmotactic behaviour, a maze design was adapted from several prior reports which incorporates pseudo-random hole location to reduce the viability of serial search as an efficient strategy (Youn et al., 2012; Faizi et al., 2012; Feng et al., 2017; Illouz et al., 2020). This adaptation results in task demands more qualitatively comparable to the Morris water maze by increasing the area of the maze where potential target locations are positioned.

Addressing issues identified surrounding training time and ease of administration of the task, the task was adapted to omit digging as a requirement for reward. Potential odour cues were compensated for by using a rotatable maze with large quantities of unreachable reward in each foil location. Finally, stability of learning of the delayed match-to-place rules was also problematic in experiment one. Specifically, the progression of reliance on a serial/random to a spatial strategy was not linear as predicted by reports of performance on the reference memory version of the Barnes maze (e.g., O'Leary et al., 2011; Harrison et al., 2006). Therefore, a 4-trial DMTP design with spaced ITIs was implemented, following task designs from previous reports of success of spaced trials in the event arena (Nonaka et al., 2017). Ultimately, experiment two aimed to overcome these aforementioned issues, improve retest

reliability within subjects, and provide an assay that encouraged the use of allocentric rapid place learning and memory processes on a stable background of prior rule learning.

We hypothesised, based on the results of experiment one, that incorporating the highlighted design and apparatus alterations would improve the rate of task acquisition during training in WT mice, despite the task design differences in number of foils. We further predicted that robust place preference would be demonstrated in the target area during probe trials relative to surrounding foils with a preference for spatial search strategy. Finally, we expected that control trials which omitted extra-maze and visuo-spatial cues would demonstrate reliance on allocentric place learning as opposed to idiothetic or non-spatial learning by impairing performance relative to standard training and probe trials.

3.2.2 Methods

3.2.2.1 Design

Experiment two comprised a similar mixed design to experiment one, with the majority of comparisons being made within-subjects. Each subject took part in each condition across days of task training, therefore making subject-by-session the primary within-subjects factor. All animals took part in a 31-day training regime, which interleaved standard training with multiple probe and control trials. Probe and control trials were used to generate the primary data of interest, while training trials served as control baselines for performance and to characterise task acquisition (e.g., Takeuchi et al., 2016).

3.2.2.2 Animals

A total of 8 (4 males, 4 females) C57BL/6J WT mice were used in experiment two starting at an age of 5 weeks. Animals were aged to approximately 11 weeks (+/- 1 week) by the experimental endpoint. Animals were acquired, maintained, handled, and placed onto a food restriction regimen as listed in section 2.1.2 and 3.1.3. Experimental testing typically occurred between 9am-5pm.

3.2.2.3 Apparatus

Experiment two was conducted on a custom made 40-hole Barnes maze, referred to as the multi-hole Barnes maze (mBM) based on several previous designs reported in the literature (Faizi et al., 2012; Youn et al., 2012; Feng et al., 2017; Illouz et al., 2018). The mBM consisted of a 105cm diameter acrylic disk (Perspex, SimplyPlastics), at 1.5cm thickness. Forty, 5cm diameter holes were cut into the maze, arranged into three concentric rings. The rings were located 15cm, 30cm, and 45cm from the centre-point of the disk, respectively (Figure 3.2.1A). Figure 3.2.1A outlines the maze design, dimensions and distances between hole locations.

The maze was mounted on a rotatable platform elevated to 40cm above ground level. Custom-made 5cm diameter 'wells' were 3D-printed (Ultimaker 2+, Ultimaker) in house using white PLA plastic (RS products), which served as inserts for the maze to house task rewards and olfactory foils. The well inserts were uniform with the maze floor with the depth of the insert extending below the maze surface, therefore providing no visual indication of presence of a reward from a distance. Each well included a grating separating an upper and lower compartment within the well which allowed insertion of retrievable rewards above and irretrievable rewards below the grating. This enabled masking of any reward-based olfactory confound that may alter preferred search strategy during the task. Single rewards were placed above the grating while multiple rewards were placed below in order to further reduce the risk of use of any potential olfactory strategy using distance-based odour cues (Wang et al., 2010; Nonaka et al., 2017). Forty of the custom-made wells filled the holes on the maze, 32 of which comprised potential rewarded locations. The rewarded locations were restricted to the outer and middle rings only to reduce the risk of animals immediately locating the reward by chance (Figure 3.2.1A).

The laboratory room in which behavioural experiments were conducted was a rectangular suite with an array of 2D and 3D cues arranged on the surrounding walls (approx. 30-50cm from any maze edge). Based on the literature and the results of experiment one, to account for the potential poor saliency and varied reliance on visual cues, a wider array of salient cues was included in experiment two. These cues included: one 3D light-blue lampshade (northwest, Figure 3.2.1C), one 3D floral patterned elliptical lantern (southwest), three 2D white repeating diamond shapes (west), three 2D silver circles (north), two 3D red and gold patterned stars, three 3D multicoloured cylinders (east), one 3D multicoloured paper fan (southeast), and two 2D small orange/green paper fans (south) (e.g., Wang et al., 2010). General diffuse room cues

were also present such as: 2 black curtained walls (south & east), 1 plastic textured wall (west), one yellow wall (north), and the entrance/exit point of the experimenter/subject (examples shown in Figure 3.2.1B). A red plastic tube was used to start animals from the centre of the maze and randomise starting orientation, also aiming to reduce anxiety by providing a dimly lit environment with matched lighting conditions to experiment one. This is analogous to the use of pseudorandom allocation of the start quadrant in the Morris water maze or start box used in experiment one and event arena tasks. Animals were rewarded exclusively with one half of a Cheerios cereal pellet (Nestle) (Takeuchi et al., 2016). Animals behaviour on the maze was video recorded and tracked as detailed in section 3.1.2.3.

A

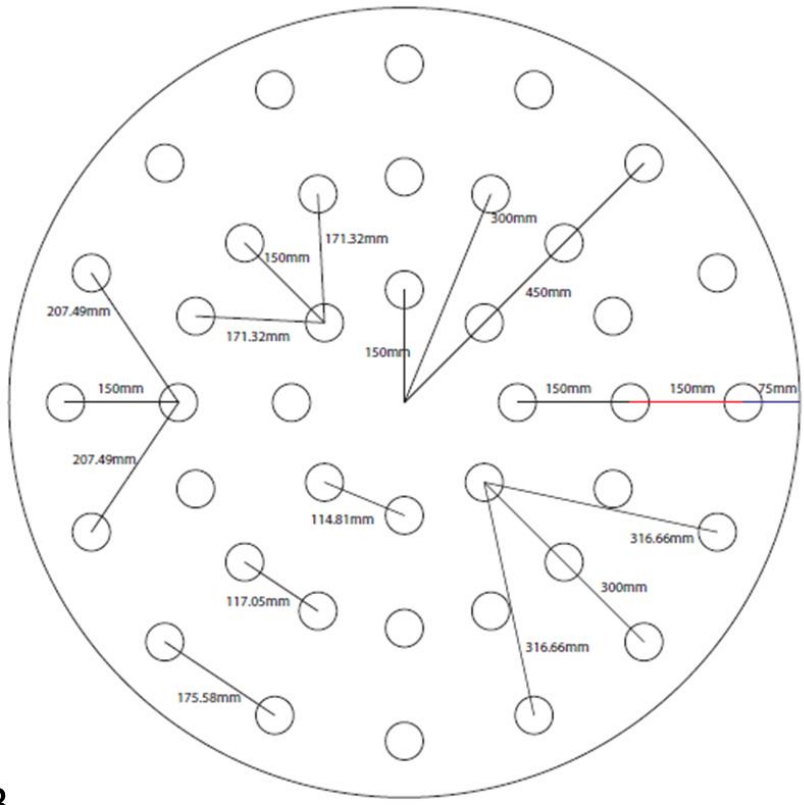

B

Figure 3.2.1: A) Multi-hole Barnes maze (mBM) design including dimensions (in mm) between centre points of bevelled holes and inner, middle, and outer rings. B) Example of maze room configuration including extra-maze cues used during experiment two. Note that mBM is shown without well inserts.

3.2.2.4 Behavioural procedures

Experiment two was comprised of multiple trial types across 31 days. These trials comprised habituation, standard training, probe trials, controls trials, and manipulation (delay-dependence/variable ITI) trials. The overall structure of experiment two is outlined in Figure 3.2.2.

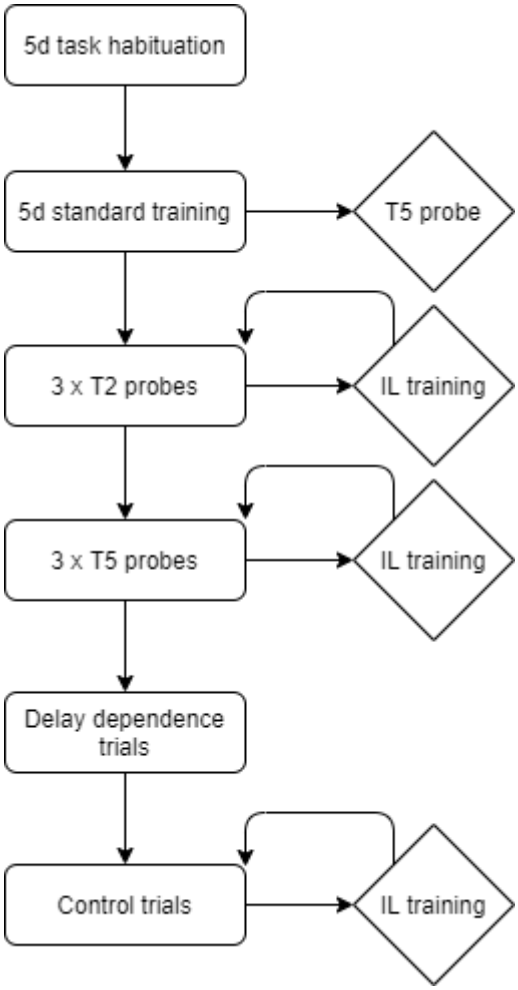

Figure 3.2.2: Flow diagram of trial order used, totalling 26 days plus 5 task habituation days. IL training represents interleaved standard training days between probe and manipulation trials. T2 and T5 probes represent probe trials performed on the 2nd and 5th trials of the day, respectively.

Habituation and shaping

Upon arrival, animals were acclimatised in a procedure identical to described in experiment one, including handling, food-restriction and monitoring. In addition, during the 7-day acclimatisation, all animals were placed into single housing for 1-hour and given access to reward pellets in a single well. Feeding behaviour was monitored and animals were given up to two full pellets per day to emulate the volume of reward that would be consumed in the upcoming training trials. After 7-days all animals reached their target weight (+/- 5%) and readily consumed all food reward from the wells.

Pre-training (task habituation)

Following shaping, animals were exposed to a daily routine of task training, the generic structure of which formed the majority of experiment two. Each day was structured in the same manner: animals were removed from the home cage, placed into individual cages, and transported to the behavioural suite. Pre-training comprised 5-days following the initial habituation/shaping procedure. On the first day, animals were placed in the centre of the maze in the testing room in a start tube, the start tube was removed, and animals were given 5-minutes to habituate to the novel environment. A single well on the maze was baited and animals were guided to the reward using a clear Perspex cylinder if they failed to locate the reward within 5-minutes, where they remained for an additional 1-minute. After each trial, the maze was pseudo-randomly rotated (whilst retaining the relative configuration of the well positions in space) and cleaned with 70% ethanol. After testing, animals were then returned to the home cage in the holding room until the following testing day.

The subsequent 4-days of pre-training consisted of a 4-trial DMTP task, in which animals were placed in the centre of the maze via the start tube and were required to locate a single baited well on the maze within 90-seconds, the location of which was pseudorandomly changed each day. If animals failed to locate the reward, they were guided to the location in the same manner as in pre-training and remained there for 1-minute to consume the reward. Following the completion of a trial, animals were returned to the individual cages for 10-15-minutes, before returning to the maze and repeating the trial process. This process was repeated for 4 trials per subject per day (Figure 3.2.3).

Standard training

Animals then underwent standard training for 26-days with a number of probe, control, and manipulation trials interleaved. Standard training involved a 4-trial-per-day DMTP task (Figure 3.2.3), almost identical to described as pre-training, with the exception of the inter-trial-interval (ITI) being standardised to 15-minutes. A 15-minute ITI was chosen based on procedures used by previous DMTP maze studies in both rats and mice, with the aim of allowing sufficient delay to involve hippocampal-dependent processes while allowing scope for manipulating the retention delay intervals in subsequent trials (Steele and Morris., 1999; Bast et al., 2005; Wang et al., 2010; Takeuchi et al., 2016; Nonaka et al., 2017). This process was repeated daily for the first 5-days to characterise acquisition performance, prior to beginning manipulation and probe trials.

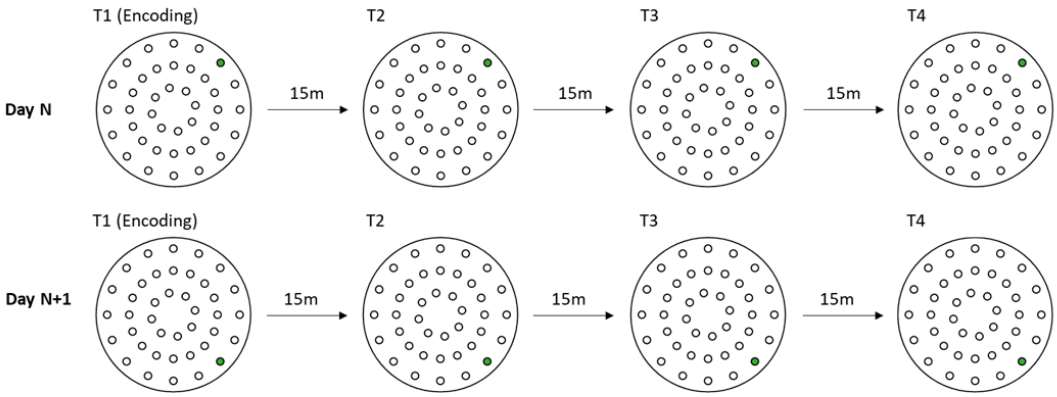

Figure 3.2.3: Diagrammatic example of standard encoding and retrieval trial structure in experiment two. Green indicates the baited target location, while white positions represent non-baited foils. Arrows represent 15-minute intertrial intervals (ITI). Example randomisation of target location between days represented by starting 'Day N' and following day 'Day N+1'. Trial-type specific adjustments to this general task structure are outlined in Table 3.2.1.

Probe trials

On the fifth day of standard training, a probe trial was performed after animals had completed the fourth reinforced trial of the day. This entailed including a 90-second trial without the reward present at the target location. Probe locations were restricted solely to the middle ring of well positions to control for variability in potential difficulty, cue salience, and travel distance between locations across animals. Performance was monitored and analysed to test for successful spatial memory in the absence of any potential olfactory cue. Subsequent probe trials were performed as described in the standard training procedure, with the exception of replacing one of the trials with an unrewarded probe. On days 6, 8, and 10, a probe trial replaced trial 2 of training (T2 probe trials) and on days 12, 13, and 14, a probe trial was added after trial 4 (T5 probe trials). These two trial positions were chosen based on previous literature and data from experiment one, which highlight the variability of 1-trial place learning performance in mice. Therefore, a trial 5 probe was included to assess spatial memory after robust reinforcement had occurred but with still relatively few trials compared to typical reference memory maze procedures (e.g., 2-4 trials per day for several days with reward at a static spatial location).

Control trials

Control trials included one extra-maze occlusion control trial (O'Leary et al., 2013), two delay-dependence variable ITI trials (Takeuchi et al., 2016), and a full visual occlusion trial (Bast et al., 2005; see table 3.2.1 for details). Briefly, the extra-maze occlusion trial involved occlusion of the surrounding cues on the walls with black polythene on trial 2 to trial 4, performed on training day 25. This enabled assessment of the animals' reliance on these landmark cues which have been demonstrated to be essential for successful allocentric, hippocampal-dependent place learning. These trials are typically driven by the hypothesis that an impairment in performance during an extra-maze occlusion trial, relative to a standard training, indicates reliance on extra-maze cues for optimal navigation. While this is subject to inter and intra-subject variability, significant deviation in performance from an established stable baseline provides convincing evidence for the effect of removal of these extra-maze cues on spatial navigation (O'Leary et al., 2011).

Delay-dependence trials are typically used to demonstrate the time-dependent nature of the fidelity of rapidly encoded ‘one-shot’ episodic memory. This is achieved by manipulating the ITI between the first and second trial, with the hypothesis that performance should decrease as a function of increasing ITI. In this experiment, an ITI of 1-hour or 30-seconds were used as the manipulation compared to the 10-15 minutes used as standard. These delay dependence trials were carried out on training days 16 and 18, respectively.

A full visual occlusion trial was an additional control included at the end of the experimental timeline in order to ascertain whether diffuse global visuospatial cues contributed to sustained performance following impairment on the second and third trials of the extra-maze occlusion control day (see section 3.2.3). In this instance, after the initial encoding trial, the light source is removed from the arena, preventing the subject from using any visual information. The assertion is that animals relying solely on tactile, olfactory, or other non-visuospatial strategies (including self-referent egocentric response learning) should not be impaired by the removal of visual information, while animals reliant on global visuospatial information will be unable to sustain task performance (e.g., Bast et al., 2005; Vorhees & Williams., 2014a).

Table 3.2.1: Details of trial types used in experiment two including trial type, total number of replicates, trial ITI, and a brief description of the procedure for each trial type.

Trial type	Replicates (days per type)	ITI (minutes)	Manipulation
Standard training	20	15	A 4-trial repetition of the DMTP task on the Barnes maze, typically with an inter-trial-interval (ITI) of 15 minutes.
Probe (T2/T5)	3	15	Matched to a standard training trial with the exception that the reward is not present in order to assess spatial memory in the absence of any potential olfactory cue. In experiment two, probe trials were performed on either the second (T2) or fifth (T5) trial of designated days.
Delay dependence	1	0.5/60	Matched to a standard training trial with the exception that the ITI between the first and second trial is manipulated (increased to 1 hour or decreased to 30 seconds in this experiment).
Extra-maze occlusion	1	15	Matched to a standard training trial with the exception that the extra-maze cues are occluded in trials 2 to 4.
Visual occlusion	1	15	Matched to a standard training trial with the exception that all visual cues are removed on trials 2-4 by removing all light sources from the maze.

3.2.2.5 Analysis

Tracking data pre-processing

Raw tracking data was extracted using Ethovision XT9 as detailed in experiment one. Tracks were then smoothed using a 10-frame sample shifting window Lowess function. Tracks were then exported to Excel. All measures were extracted from raw XY coordinate tracking data using custom MATLAB scripts and exported for analysis in R or SPSS.

Characterisation of variables

Measure variables collected in experiment two were similar to that reported in experiment one and are outlined in Table 3.2.2. Typically, custom MATLAB scripts were used to extract variables from raw animal tracking data to ensure reproducibility and high throughput. Latency to reach the target location was collected both manually and by automated analysis on all trials. Primary latency was defined by the time taken from the start of the trial to reach the target location for the first time. Primary measures have been reported to be more reliable than measures dependent on retrieval of the reward/escape itself, as in occasional trials animals may locate the reward/escape location but continue exploratory behaviour (O'Leary et al., 2013; Feng et al., 2017). This use of primary measures is sustained for all subsequent performance measures on rewarded trials. In each case, these primary measures are considered indicators of within-day task learning, and as such should decrease as a function of increasing trial number (Vorhees & Williams., 2006).

To validate the accuracy of automated tracking analyses in calculating performance measures, blinded manual latency ratings were performed on a subset of days (N = 3 days, 12 trials per animal) and correlated with the corresponding automated latency ratings. Pearson's correlation was performed across all subjects nested within trials. To characterise the within day variability of trial latency and the influence of animal velocity, further Pearson's correlation analyses performed between primary measures and average trial velocity within individual trials across a subset of training and probe trials per animal (N = 5-days, 20 total trials per animal). Additionally, primary measures of 'path length', 'search errors', and latency, were cross-correlated to establish the relationships between measures variables.

Path length to target location was defined as the sum of the distance travelled (expressed as Euclidean distance) from tracking start point to the first video frame when the subject tracking centre-point was within 2cm of the target location or entering the sandwell (standardised threshold determined relative to manual classification, not shown). The general formula for this calculation is shown in Figure 3.2.4A (adapted from Illouz et al., 2016). In order to standardise path length to the minimum distance from the start position to the target for comparison across differing trial types, a distance correction ratio was generated. Briefly, the observed path length to the target was divided by the minimum direct path length, which for each trial is always either 25cm or 50cm based on the centre point distance to the middle or outer maze rings, respectively. This transforms data to comparable scales, removing minimum travel distance as a confound in measuring path length (e.g., Gawel et al., 2019).

Table 3.2.2: Measure variable names and brief description of variables used in experiment two. Details of calculation can be found in Figure 3.2.4.

Variable name	Description
Primary latency to target (latency)	Duration of time to reach target from trial start
Primary path length to target (path length)	Distance of path covered to reach target
Search errors (errors)	Number of non-target foil entries to reach target
Search strategy	Categorical pattern of search paths to reach target
Perseveration ratio	Ratio of average distance of animal from current and previous target location
Quadrant occupation	Relative percentage of time spent in each maze quadrant
Place preference	Relative percentage of time spent at target location relative to surrounding foils
Velocity	Average movement velocity across trials

A

$$PathLength = \sum_{i=1}^{length(x)} \sqrt{(x_{i+1} - x_i)^2 + (y_{i+1} - y_i)^2}$$

B

$$PerseverationRatio = \frac{[D1]\mu \sum_{i=1}^{length(x)} \sqrt{(x_{i+1} - x_i)^2 + (y_{i+1} - y_i)^2}}{[D2]\mu \sum_{i=1}^{length(x)} \sqrt{((x_{i+1} - x_i)^2 + (y_{i+1} - y_i)^2}}$$

C

$$QuadrantOccupation = \frac{\sum t(qT)}{\sum t(qT, q2, q3, q4)}$$

D

$$PlacePreference = \frac{\sum t(P1)}{\sum t(P1 : P9)}$$

Figure 3.2.4: General formulas used in experiment two to calculate measure variables. A) Formula used to calculate path length to reach the target, where 'x' and 'y' represent coordinate positions of tracking centre point, 'i' represents the frame of the raw tracking data, resulting in the sum of the Euclidean distance between sequential tracking points. B) Formula used to calculate perseveration ratio. D1 and D2 represent sequential training days. Bracketed formula represents mean path distance from the target over two sequential training days, 'D1' and 'D2'. C) Formula used to calculate the proportion of time spent in the target quadrant relative to all maze quadrants. 't' represents the time that animal x-y coordinates occupy a given quadrant space, 'q' represents a given quadrant of positions from target quadrant 'T' to opposite quadrant 'q4' and adjacent quadrants 'q2' and 'q3'. D) Formula used to calculate the proportion of time spent in target zone 'P1' relative to all 9 position separation groups. 't' represents the time that animal XY coordinates occupy a given well position, 'P1:P9' represents each of the given 9 position separations.

Primary errors were extracted using a custom MATLAB script, defining errors as the centre tracking point of the animal crossing any unbaited foil well prior to reaching the target position and were summed across the trial. Search strategy was defined according to modified criteria described in previous studies (e.g., Bach et al., 1995; Youn et al., 2012), classified into spatial, serial, or unclassified/random strategies, similar to described in experiment one. Spatially directed search was defined by direct movement to the target location, with no more than 3-hole deviation errors from the target in the path trajectory. Serial search was classified by thigmotaxis-like behaviour following the path of the well rings with >3 hole-deviation errors from the target. Finally, random search was defined by no clear search pattern with >1 maze crossing in the search path. The proportion of trials in which each search strategy was used was counted by manually rating the path pattern of each subject for each trial in training and probe trials according to the above criteria. This semi-quantitative approach was further standardised by the use of a custom MATLAB script to plot subject XY path coordinates for each trial, counting intersections between subject paths and with foil wells, as well as rating maze crossing and direct or indirect path trajectories to the target.

As a measure of preference for the target location and proactive learning interference, search perseveration ratio was calculated following the procedure described by Nakazawa et al. (2003), outlined in Figure 3.2.4B. Perseveration ratio comprises the ratio of mean distance of the subject from the target location of the current and previous test days. Therefore, the expected pattern of performance with increasing trial number is a decrease in perseveration ratio due to an increase in preference for the current and decrease for the preceding target.

Measures of ‘place preference’ were calculated in probe trials using the proportion of time the search path of animals remained within a particular location on the maze. In the case of quadrant preference, percentage time spent in the target quadrant during probe trials was calculated by the formula presented in Figure 3.2.4C.

Preference for the target location (referred to directly as place preference) was calculated as the percentage of time spent within a 2cm criteria of the target location and expressed relative to non-target foils. This data was clustered as a function of relative ‘separation size’ from the target in a similar manner described in experiment one (outlined in Figure 3.2.5).

First, probe trial data was trimmed into a ‘post-target’ period, representing the majority of the trial following reaching the target location. The time spent (place preference) at each well position was then grouped by relative separation distance from the target, which resulted in 8 potential foil sites grouped across both inner and outer rings of the maze, plus the single target

location. Data for all positions were then 'rotated' such that trials with differing reward locations were no longer orthogonal, ensuring the target position always corresponded to 'position 1', while the relative spatial relationships between well positions were retained. Following rotation, data was then averaged across both 'sides' of the maze relative to the target position to ensure equal representation of the maze area for all trials, which also controlled for the absolute number of foils comprising a given separation category. This resulted in a place preference (proportion of time) for each foil category normalised to the absolute number of foils. This prevented artificial inflation of measures due to unequal foil representation (see Figure 3.2.5). To reduce the potential elevated number of multiple comparisons and generate an overall preference score, individual separation points were then clustered into 'close' and 'far' categories by averaging error and place preference data for the relative well positions P2:5 and P6:9. Finally, data was averaged within subjects across the 3 replicate days of probe trials of matched type (T2 and T5 probe trials). Thus, place preference for the target location was expressed as a percentage of total time spent at the target relative to non-target foils.

In order to ensure that data handling and clustering did not artificially elevate place preference measures in the target location, data extraction and analysis was also repeated on randomised non-target locations. This randomised target data was compared to randomised 'non-target' foils and chance in the same manner as the true data and was then compared directly to the true data itself. In addition, place preference data were generated unaveraged across each of the 32 well locations on the maze and analysed for target-specific place preference to assess whether potential clustering artificially inflated place preference. Both clustered and non-clustered data were handled and analysed in an identical manner, with the assertion that matched effects should be observed in both sets of data, if the relationships between target and foils are not artificially inflated by the clustering process itself.

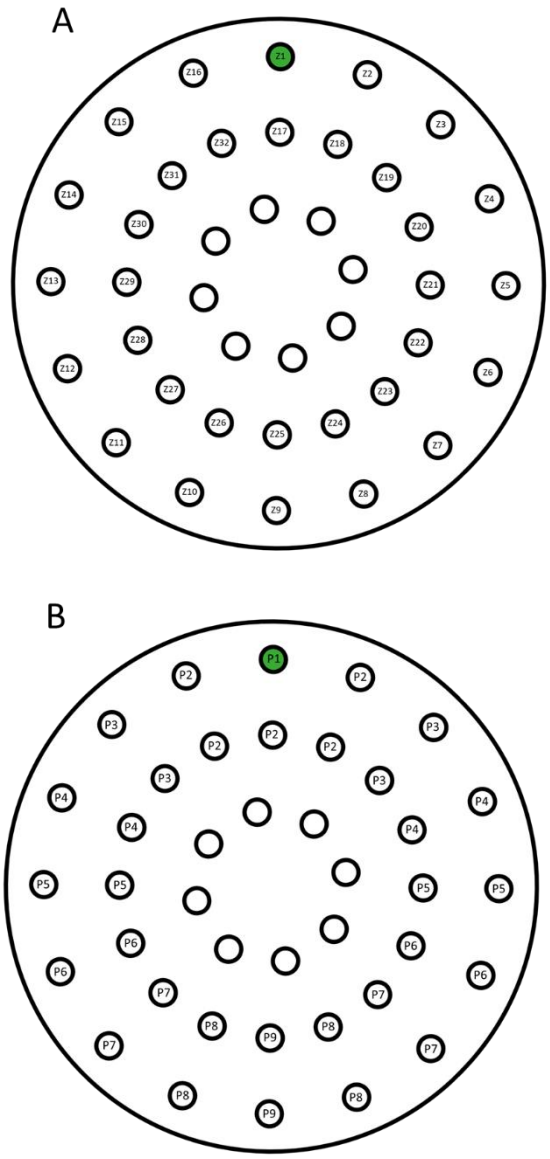

Figure 3.2.5: Representation of absolute and relative locations of target and foil positions on the mBM task in experiment two. A) Represents absolute position identifiers (Z1-32 = Zones 1-32), while B) represents relative positions (P1-P9) following data rotation. Values 'P2-P9' represent relative separation positions for each foil (white) relative to the target location 'P1' (green). Note that the number of wells within each separation category is normalised after clustering to prevent artificial inflation of scores at separations comprising a greater number of wells (e.g., there are five P2 positions, four P3 positions etc.).

Statistical analysis

Primary data (e.g., path length, latency, errors etc.) was averaged within subjects for either: the first 5 training days, the 3 days of each probe trials type (3 days per probe trial type: T2, and T5 probes, respectively), and control trials where applicable. The general structure of analysis for most trial-dependent measures (i.e., measure variables with which the hypothesis predicts will change dependent on the number of trials within-day) consisted of repeated or mixed ANOVAs followed by post-hoc t-tests, or repeated measures/one-sample t-tests. For example, repeated measures ANOVA and post-hoc t-tests were performed on primary path length to compare the first trial to all subsequent trials within a day to indicate improvement at the retrieval phase. This analysis structure was performed for the 5 training days, probe trials, and control trials. Search strategy count data was converted into the proportion of trials in which each strategy was used within a subject, which was then averaged across days and analysed as above.

In control trials (extra-maze/visual occlusion trials), performance was analysed both within trial type across trials as well as being compared to matched trials from previous training days (interleaved training) as typical 'expected performance' at that time during training. Primary latency to target was used in lieu of path length on the visual occlusion day, due to the tracking software being unable to resolve subject paths without a light source.

Quadrant occupation was analysed only on probe trials themselves, relative to chance (25%) and non-target quadrants across an average of the replicates of both T2 and T5 probe trials (i.e., 6 trials) using one sample (relative to chance) or repeated measures t-tests (between quadrants). Place preference measures were calculated as described in 'characterisation of variables' (section 3.2.4), and analysed with repeated measures t-tests, comparing foil positions to the target location. In the case of the randomised place preference data, analysis was performed in the same manner as for the true data using repeated measures t-tests. In addition, the 'P1' target place preference was directly compared between the randomised and true data in the same way. Unaveraged place preference across all 32 zones was analysed using one sample t-tests relative to chance and Holm-Bonferroni (HB) correction was applied to control for multiple comparisons.

Pearson's correlation was calculated between a number of variables including errors, latency, and path length for characterisation, *r* and *p*-values are reported subsequently. Finally, primary measure variables were compared by animal sex incorporating a between subjects term in

repeated measures ANOVAs as outlined above. Alpha was set at a criterion of 0.05 for statistical significance in all tests.

3.2.3 Results

3.2.3.1 Pre-analysis checks: Variable selection

Pearson correlation performed on manually rated and automated latency metrics across 3-days of exemplar training data were significantly correlated (nested within trials across all subjects), with coefficients ranging between $r = .84$ to $r = .99$, with a global average of $r = .98$. Table 3.2.3 shows the individual coefficients and associated p-value, all of which were below the criteria of $p = < .05$. This high degree of consistency between manual and automated measures gave suitable evidence for the use of automated metrics in further analyses.

Table 3.2.3: Pearson correlation coefficients and associated p-values for latency to reach target location between blinded manual and automated calculation for individual trials.

Trials	*r*	*p*
1	0.99	< .001
2	0.84	.002
3	0.99	< .001
4	0.93	<.001
5	0.89	.007
6	0.99	< .001
7	0.99	< .001
8	0.99	< .001
9	0.94	<.001
10	0.99	< .001
11	0.98	< .001
12	0.98	< .001

Primary path length, latency, and errors were compared for mean and variability to determine which metric was most informative of performance. Latency to reach the target location can be affected by a number of behavioural confounds including variability in movement velocity, the frequency and duration of stops made during traversal, and delay before initiating search. Primary path length, however, overcomes these issues with the calculation invariant to velocity as only frames in which the subject is moving contribute to the metric in a cumulative manner (Bimonte-Nelson et al., 2015; Harrison et al., 2006; Patil et al., 2009).

To assess the potential of non-performance behaviours (i.e., stops, alterations in velocity etc.) to influence the primary measures, Pearson' correlation analyses were performed between each primary measure and movement velocity. Notably, within an average trial there was variability both between animals and within trials in animal movement velocity, which we predicted would ultimately bias latency (example shown in Figure 3.2.6B). An increase in velocity across trials within days between trials 1 and 4/5(Figure 3.2.6D) and across training days (Figure 3.2.6C) was also seen, with increasing average velocity between initial training, T2, and T5 probe trials. From this, despite an expected bias in the performance of latency relative to velocity, we observed significant correlations between all primary measures and velocity (Figure 3.2.6A). There were also significant inter-measure correlations between errors, path length, and latency (Figure 3.2.6A, Table 3.2.4). This is similar to relationships in primary measures previously reported in the literature (e.g., Vorhees., 2006; Maei et al., 2009). While in the case of this experiment, latency bias did not appear significant, the reported differences in sensitivity of primary measures and the invariance of path length and errors to velocity led to the decision to use primary path length and errors as the main outcome measures for trial performance (Bimonte-Nelson et al., 2015).

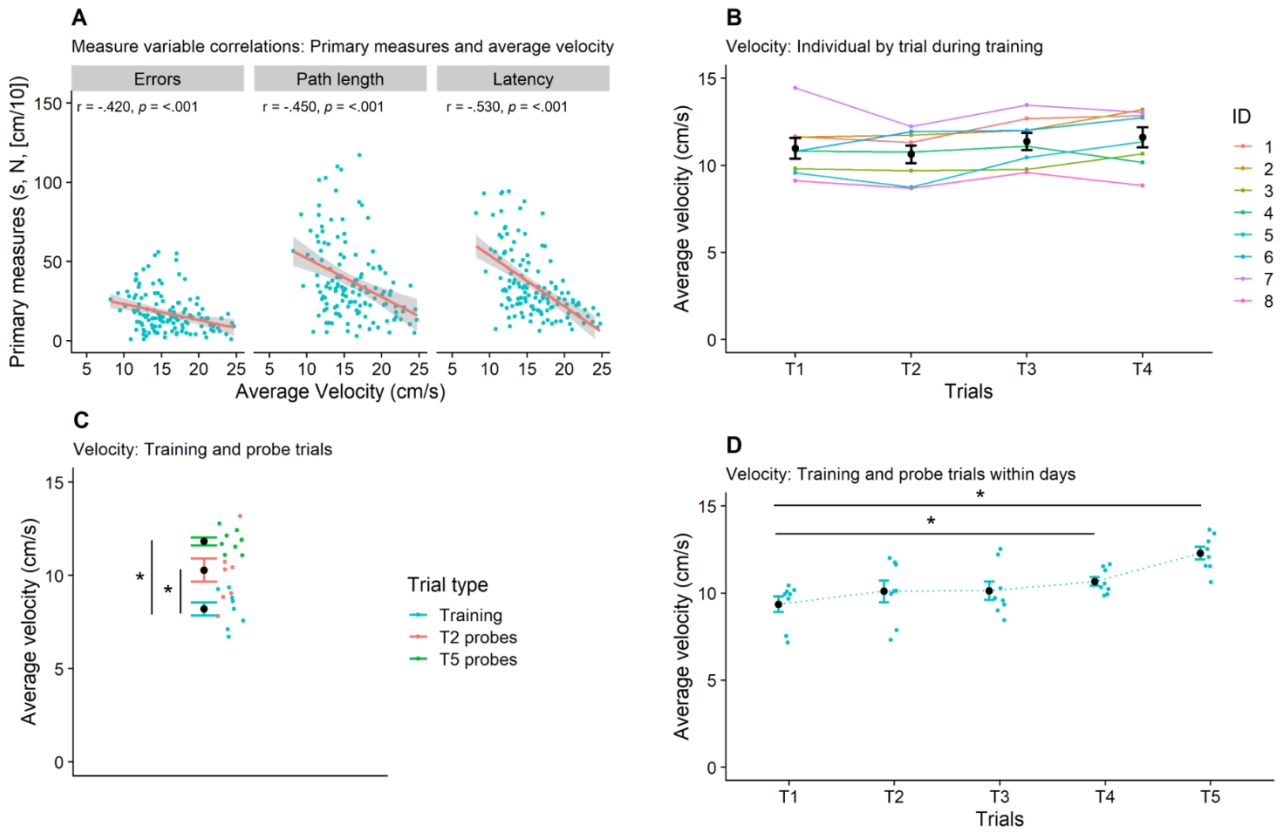

Figure 3.2.6: A) Scatter plot of primary measures: latency, path length, and errors plotted against average velocity across a sample of trials (N = 20, animal N = 8). Note that path length has been normalised relative to optimal path length to allow representation of each variable on a comparable scale. Each point represents a single trial for an individual animal. B) Average velocity of individual animals across 4 trials collapsed across standard training days 1-5. Individual animals (ID) are represented by coloured points and connecting lines across trials. C) Average velocity across trial types within animals. D) Average velocity grouped across training and probe trials for each within-day trial. In each case error bars represent group mean +/- SEM. Individual subject averages are represented by single-coloured points in C) and D). '' represent statistical significance at p = <.05 relative compared trial type in C) and to trial 1 in D). See Table 3.2.5 for details.*

Table 3.2.4: Pearson's correlations between primary measures and velocity. r and p-values are shown for each correlation. Refer to Figure 3.2.6A for relevant data.

Variable	Statistic	Errors	Path length	Latency	Velocity
Errors	*r*	1	0.97	0.90	-0.42
	p		<.001	<.001	<.001
Path length	*r*	0.97	1	0.94	-0.45
	p	<.001		<.001	<.001
Latency	*r*	0.90	0.94	1	-0.53
	p	<.001	<.001		<.001
Velocity	*r*	-0.42	-0.45	-0.53	1
	p	<.001	<.001	<.001	

3.2.3.2 Training

On average, across the 5 days of training, animals significantly decreased their path length to reach the target location between trial 1 and trial 3/4, but not trial 1 and trial 2 (Figure 3.2.7A, Table 3.2.5). Results were similar when compared to error and latency metrics (Figure 3.2.7B/E, Table 3.2.5), therefore path length was selected as the primary variable of interest given these results and aforementioned confounds of latency. Further, the use of a spatial search strategy improved across days from 25% to 46% in the first week but did not reach significance (Table 3.2.5). There was, however, a significant within-day effect, with an increasing proportion of trials in which a spatial strategy was used between the first and all subsequent trials, typically reaching ~50% spatial preference by trial 4 (Figure 3.2.7F). There was no significant effect of sex on each of these variables (Table 3.2.5).

3.2.3.3 Probe trials

Across the three T2 probe trials there was, as in the training data, a clear effect of decreasing errors, while path length was more variable with increasing number of trials. Animals significantly decreased path lengths between trial 1 and trial 2, but not trial 1 and trials 3 while trending between trial 1 and 4 (Figure 3.2.7C). However, errors significantly decreased between trial 1 and trials 3/4. In the three T5 probe trials, path length significantly decreased between trial 1 and 3/4/5, while errors decreased between trial 1 and all subsequent trials (Figure 3.2.7E). The consistent decrease in path length and errors across trials within each day is indicative of improved performance with consistent with increasingly accurate recall of the target location. Additionally, there was no significant difference path length between T5 probe trials and interleaved training, suggesting that unrewarded probe trials did not result in a refractory impairment in within-day performance (Figure 3.2.7D). Importantly, sustained performance in the absence of the food reward during probe trials was also observed, acting as a control for the possible use of odour-based navigation strategy. This improvement was independent of subject sex, with no significant effect of sex on performance during training or probe trials (Table 3.2.5).

The proportion of trials in which a spatial strategy was used increased significantly between the first training week and the subsequent probe trials, which was specifically observed during trial 2. There was a clear transition from serial/random to predominant spatial strategy use,

with an average of ~60% spatial search use by the first probe trial (Table 3.2.5). This was again mediated by trial within a given day, with a significant increase in spatial search use from the encoding to the first retrieval trial, showing ‘one-trial’ spatial strategy use (Figure 3.2.7G). There was no significant effect of sex on strategy preference across all both training and probe trials (Table 3.2.5).

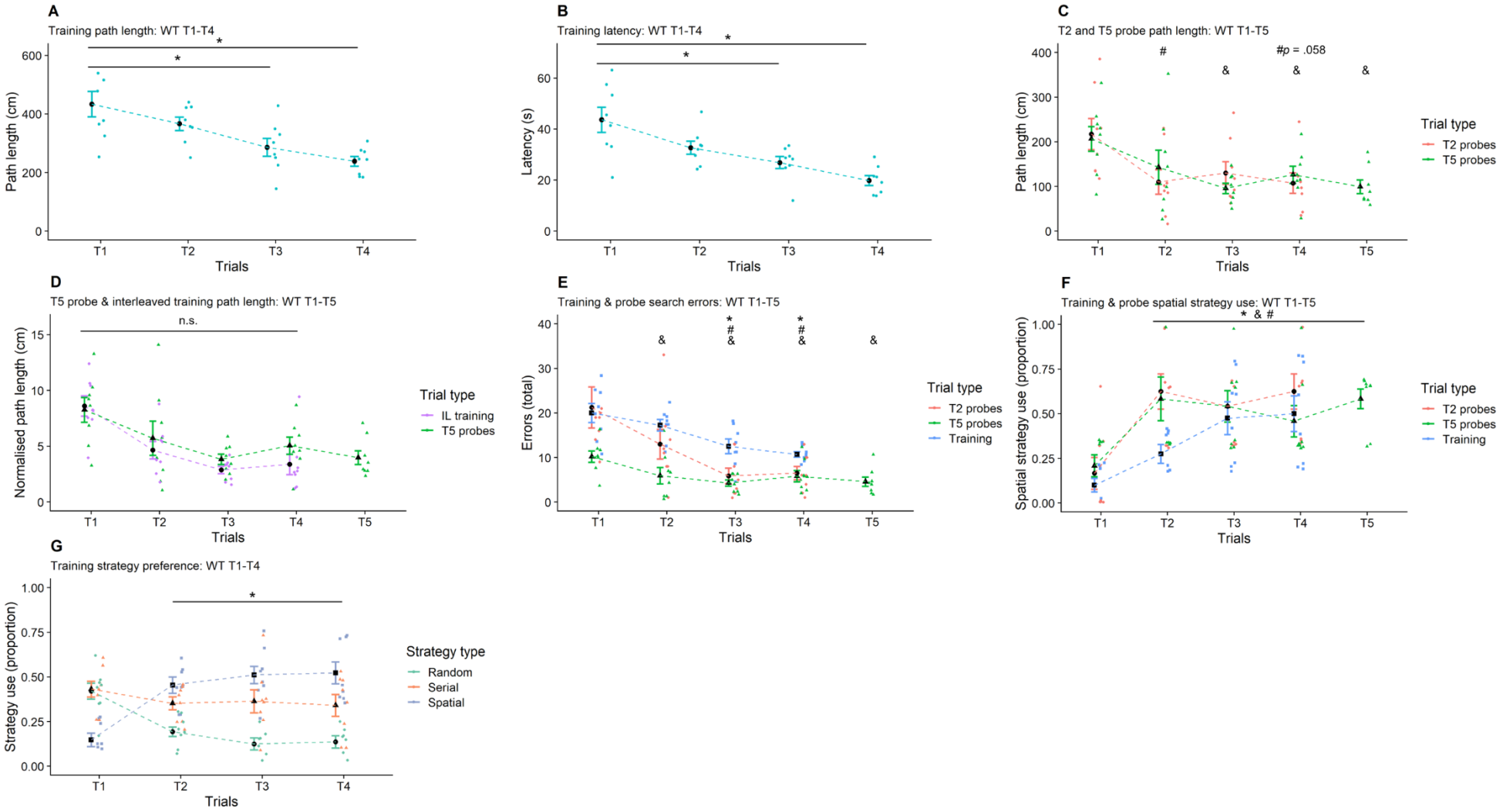

Figure 3.2.7 panel 1: Experiment two rapid place learning performance in the mBM task during training, probe, and control trials. Average A) path length and B) latency, on each trial across all animals during the first 5 training days. C) Average path length on probe trials 1-6, including 3 x T2 probe trials and 3 x T5 probe trials. D) Average path length normalised to optimal path length in probe trials 4-6, relative to interleaved training days (D15, D17, and D19). E)

Average errors during training, T2, and T5 probe trials. F) Proportion of spatial strategy preference across all animals during training, T2, and T5 probe trials. G) Proportion of strategy type preference averaged across training, T2, and T5 probe trials. IL = interleaved. Error bars represent mean +/- SEM. '', '#', '&' represents statistical significance at alpha = < .05 in contrasts between the given trial and T1 during training (*), T2 probe trials (#), and T5 probe trials (&), respectively. In G) '*' represents significant difference in spatial strategy use during T2-4 relative to T1. In each case, individual points represent either single trial or multi-trial within-subject average of individual animals.*

3.2.3.4 Place preference during probe trials

Typical measures of place preference in maze tasks measure search perseveration in the vicinity of the target location during unrewarded probe trials, reflecting successful recall of the encoded spatial memory (Vorhees., 2006; Sharma et al., 2010). Quadrant preference is one particularly popular measure of place preference. The time spent in the target and non-target quadrants during T2 and T5 probe trials was compared but intriguingly, animals showed little preference for the target maze quadrant (quadrant occupation, Table 3.2.5; Figure 3.2.7H panel 2). Average target quadrant preference was slightly above chance (28%) and was above all non-target quadrants on average, but high variability was apparent, and this did not approach significance. This was accompanied by the observation that the perseveration ratio (ratio of distance to the current target relative to the previous day's target) decreased during rewarded trials but increased during probe trials to comparable levels observed during the encoding trial (T1) in both T2 and T5 probes (Figure 3.2.7I). This suggested multiple possibilities. Firstly, the task may have failed to provide sufficient demand to drive allocentric place memory. However, the improvement in primary measures within days, increase in direct strategy use, and the performance impairment induced during control trials (see section 3.2.3.5) made this unlikely. Second, quadrant preference may lack sensitivity in this task, either due to low level of reinforcement with few trials or due to continual animal mobility with wandering-reapproach revisiting behaviour to the target as previously reported (Vorhees et al., 2006; Maiei et al., 2009; Illouz et al., 2016). Alternatively, the absence of a reward in the expected target location may have driven animals to diversify their search strategy, further limiting the sensitivity of quadrant preference.

To investigate the latter possibilities, we separated probe trials into epochs consisting of the duration of trials prior to and after locating the target, avoiding the initial approach period skewing the data. Place preference was then derived from the post-target period by grouping the proportion of time spent at the target relative to non-target foil positions. Foil positions were spatially categorised by absolute position and relative separation size from the target location (see Figure 3.2.5B) and place preference was compared between the target, foils, and chance (see section 3.2.2.5 for details).

The average post-target epoch duration was ~55-seconds during T2, and ~66-seconds during T5 probe trials. This indicated that animals would generally locate the target quickly, spending the remaining majority of the probe trial searching. Importantly, with within-subject, between-

replicate averaging, the post-target epoch duration was reasonably stable across animals (Figure 3.2.7J). The duration was significantly shorter during T2 probe trials by an average of ~10-seconds, likely reflecting a greater initial latency to reach the reward, owed to the lower number of reinforcements from preceding trials relative to T5 probes. This aside, the majority of sampled trials were between 40-70s in duration reducing the likelihood of spurious results from an undersampled trial period, and data was expressed as a proportion of time.

Subsequently, during both T2 and T5 probe trials, despite the lack of sensitivity of quadrant preference, we observed a significant preference specifically for the target location relative to chance. Expressing place preference data by relative position on the maze with or without clustering provided similar results when comparing within probe trial type (T2 or T5; Figure 3.2.7M/N). When place preference was expressed without averaging across foils, yielding 32 locations, we found that variability was more evident, due to providing multiple representations for each possible foil separation. Preference for search at the target within the inner ring was notable, more so in T5 than T2 probe trials, while a bias towards a target-adjacent foil was observed in T2 probe trials (Figure 3.2.7K/L). Surprisingly, despite this variability, preference for the target remained significantly above chance in both T2 and T5 probe trials, while preference for surrounding foils was either not different to, or significantly below chance, with the exception of a single target-opposite position during T5 probe trials (Figure 3.2.7L). When HB correction was applied, only target preference in T5 but not T2 probe trials remained significantly above chance, however the number of comparisons made for 32 locations substantially elevated test stringency. Results were comparable when data was clustered by relative separation size into 8 foil categories, target preference remained significantly above chance with a generally linear decrease in preference when compared to surrounding foils by separation distance during both T2 and T5 probe trials (Figure 3.2.7M/N).

Quantifying preference based on separation was then performed by further reducing the dimensionality of the data into ‘close’ and ‘far’ foil categories based on the closest and farthest 4 foils from the target. During T2 probe trials, animals successfully distinguished between the target and the furthest 4-foil average but failed to discriminate the target from the closest 4-foil average (Figure 3.2.7M, Table 3.2.5). In contrast, animals significantly discriminated between the target location and both close and far foils categories during T5 probe trials (Figure 3.2.7N). Therefore, given that during both T2 and T5 probe trials, target preference was consistently above chance, comparison of target to close and far category foils effectively

distinguished performance based on extent of reinforcement, while avoiding unnecessarily excessive post-hoc comparisons and inflating type 1 error risk.

To control for spurious results which may have arisen during the clustering process, this analysis was repeated on randomised or 'shuffled' data (see section 3.2.2.5), in which the true target data is replaced with a non-target foil and subsequently data is rotated and clustered relative to this non-target position (thus effectively disrupting the spatial congruency of the positions). This abolished the effects observed in the true data, with the shuffled 'target' preference at chance during T2 and below chance during T5 probes trials. Further, shuffled target preference was significantly below the close foil category in T5 probe trials. Data shuffling also removed the spatial relationships observed between target and foils of increasing separation sizes, with the target no longer significantly above foils in a linear fashion (Figure 3.2.7O/P). Finally, target preference calculated from the true data was significantly higher than shuffled target preference during both T2 and T5 probe trials (Table 3.2.5). This specific decrease observed in shuffled 'target' preference, accompanied by the upward shift in shuffled foils suggests that the effects observed are specific to the true target location and are unlikely due to data clustering or chance.

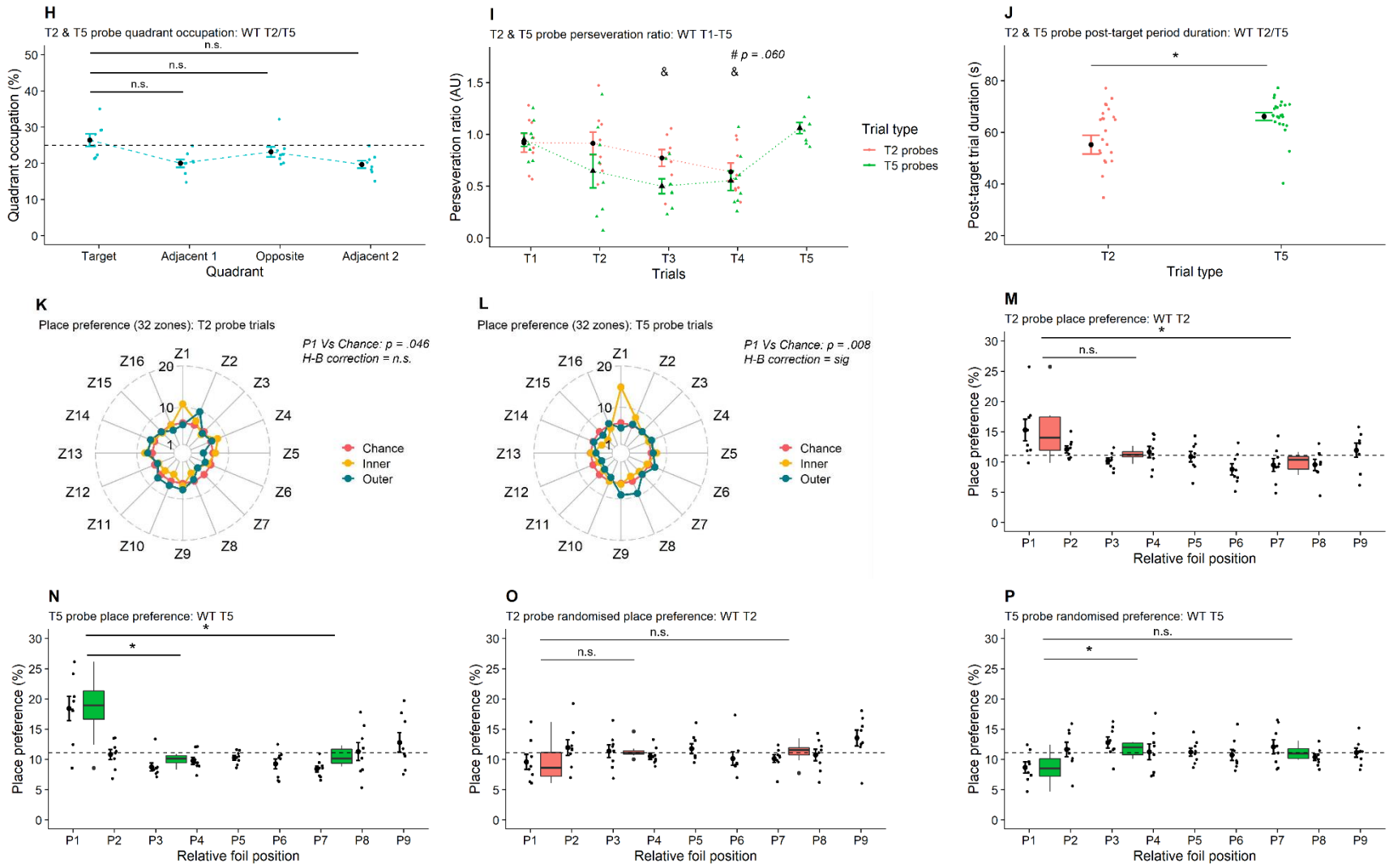

Figure 3.2.7 panel 2: Experiment two rapid place learning and memory performance in the mBM task during probe trials. H) Average target quadrant preference (%) relative to non-target quadrants in all animals across T2 and T5 probe trials. I) Average perseveration ratio during T2 and T5 probe trials. J) Average duration of 'post-target' period used to comprise place preference analysis epochs. Radar plot representation of average target (Z1) and non-target

zone preference (%) across all animals during K) T2 and L) T5 probe trials across all possible target/foil locations, relative to chance with Holm-Bonferroni correction applied. Colour code indicates the position of the wells in the inner or outer category on the maze, while chance performance (3.25%) is shown in red. Average place preference in target and non-target foils clustered by relative position in M) T2 and N) T5 probe trials. Black bars and points represent data from individual clustered positions, coloured (red/green) boxplots represent the target, close, and far foil category data, respectively. Average place preference in randomised (shuffled) data taken from O) T2 and P) T5 probe trials. Annotations and figure components represent identical features to those described for Figure 3.2.7M/N. Error bars represent mean +/- SEM. '#', '&' represents statistical significance at alpha = < .05 in contrasts between the given trial and T1 during T2 probe trials (#), and T5 probe trials (&), respectively. In Figure 3.2.7 M-P, '' represents statistical significance at alpha = < .05 in contrasts between the target and non-target locations. In each case, individual points represent either single trial or multi-trial within-subject average of individual animals.*

3.2.3.5 Control and manipulation trials

During control trials, path lengths were subsequently compared within trials and between interleaved training days to assess effects on within-day performance relative to recent prior normal training. Removal of the extra-maze cues resulted in acute impairment of acquisition performance, with only a significant improvement in path length observed between trial 1 and 4 but no significant difference was observed relative to interleaved training, which may be attributable to the high inter-subject variability seen (Figure 3.2.7Q, Table 3.2.5). Full visual occlusion had a more pronounced effect than obscuring overt landmark cues alone, with animals failing to improve their latency to locate the target reward between trial 1 and any subsequent trial. Animals were also significantly impaired during the visual occlusion trials relative to interleaved training, supporting reliance on both landmark cues and global visuospatial information (Figure 3.2.7R). Performance was less clear during delay dependence trials, however. An extended ITI of 1-hour between the first and second trial impaired performance improvement across trials, with no significant improvement of path length on trial 2 or 3 and higher path length relative to interleaved training on trial 3. Finally, performance on the 30-second ITI trial showed a low trial 1 baseline relative to interleaved training but no subsequent improvement across trials (Figure 3.2.7S/T; Table 3.2.5).

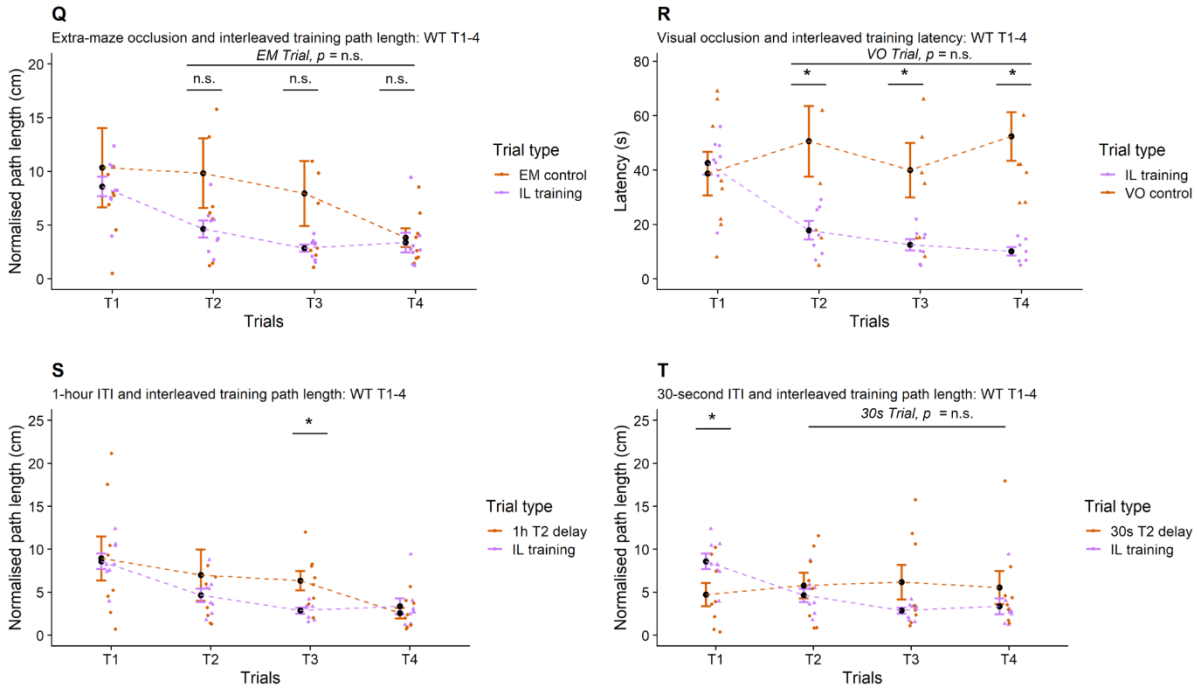

Figure 3.2.7 panel 3: Experiment two rapid place learning performance during control and manipulation trials. Average normalised path length across trials during Q) extra-maze occlusion trials, S) 1-hour T1-T2 ITI trials, and T) 30-second T1-T2 ITI trials each relative to interleaved training. Note that normalised path length corresponds to total path length / optimal path length e.g., 500cm total / 50cm optimal = 10cm normalised. R) Average latency during visual occlusion control trials relative to interleaved training. IL = interleaved, EM = extra-maze occlusion, VO = visual occlusion. Error bars represent mean +/- SEM. '' represents statistical significance at alpha = < .05 in contrasts between a given trial and T1. In the case of Figure 3.2.7S, T4 path length at during both 1-hour and IL training is significantly different from that of T1. The effect of trial in EM and VO control trials is shown above individual comparisons between interleaved training and relative training type comparison. In each case, individual points represent either single trial or multi-trial within-subject averages from individual animals.*

Table 3.2.5: Statistical comparisons performed in experiment two. Trial type, measure variable, independent variable, statistics, and corresponding figure are provided. Corresponds to Figure 3.2.7.

Trial type	Measure	Variable	Statistic	Paired comparison	Statistic	Figure
Training (D1-D5)						
	Latency	Trial	F(3,21) = 11.69, p = <.001			
				T1 vs T2	t(7) = 2.11, p = .073	**3.2.7B**
				T1 vs T3	t(7) = 3.51, p = .010	
				T1 vs T4	t(7) = 4.71, p = .002	
		Sex	F(1,6) = 0.011, p = .920			
	Path length	Trial	F(3,21) = 8.44, p = .001			
				T1 vs T2	t(7) = 1.36, p = .216	**3.2.7A**
				T1 vs T3	t(7) = 2.71, p = .030	
				T1 vs T4	t(7) = 4.48, p = .003	
		Sex	F(1,6) = 0.22, p =.659			
	Errors	Trial	F(3,21) = 9.90, p = < .001			
				T1 vs T2	t(7) = 1.22, p = .262	**3.2.7E**
				T1 vs T3	t(7) = 3.30, p = .013	
				T1 vs T4	t(7) = 4.64, p = .002	
		Sex	F(1,6) = 0.007, p = .936			
	Strategy	Trial	F(3,18) = 5.70, p = .006			
				T1 vs T2	t(7) = -2.50, p = .041	**3.2.7G**
				T1 vs T3	t(7) = -3.91, p = .006	
				T1 vs T4	t(7) = -3.35, p = .012	
		Sex	F(1,6) = 1.80, p = .228			
Probe trials (T2)						
	Path length	Trial	F(3,21) = 3.32, p = .039			
				T1 vs T2	t(7) = 2.73, p = .029	**3.2.7C**
				T1 vs T3	t(7) = 1.71, p = .131	
				T1 vs T4	t(7) = 2.26, p = .058	
		Sex	F(1,6) = 0.022, p =.886			
	Errors	Trial	F(3,21) = 6.07, p = .004			
				T1 vs T2	t(7) = 1.36, p = .210	**3.2.7E**
				T1 vs T3	t(7) = 3.95, p = .006	
				T1 vs T4	t(7) = 3.48, p = .010	
		Sex	F(1,6) = 4.95, p = .068			
	Perseveration ratio	Trial		T1 vs T2	t(7) = 0.04 p = .969	
				T1 vs T3	t(7) = 1.01, p = .343	**3.2.7K**
				T1 vs T4	t(7) = 2.24, p = .060	
	Place preference (relative proportion)					
				Target vs chance (32 categories	t(7) = 2.32, p = .049, n.s. HB	
				Target vs chance (9 categories)	t(7) = 2.43, p = .046	
				Target vs close foils	t(7) =2.19, p = .065	
				Target vs far foils	t(7) =2.47, p = .043	**3.2.7M,O,Q**
				Randomised target vs close foils	t(7) = -1.40, p = .204	
				Randomised target vs far foils	t(7) = -0.92, p = .387	
				Randomised target vs chance	t(7) = -1.11, p = .304	
				Randomised target vs true target	t(7) = -2.76, p = .028	

Table 3.2.5 continued - 1

Trial type	Measure	Variable	Statistic	Paired comparison	Statistic	Figure
Probe trials (T5)						
	Path length	Trial	F(4,21) = 3.40, p = .023			
				T1 vs T2	t(7) = 1.16, p = .284	
				T1 vs T3	t(7) = 4.88, p = .002	**3.2.7C**
				T1 vs T4	t(7) = 3.17, p = .016	
				T1 vs T5	t(7) = 3.10, p = .017	
		Sex	F(1,6) = 0.281, p =.615			
	Errors	Trial	F(4,28) = 3.19, p = .028			
				T1 vs T2	t(7) = 1.76, p = .122	
				T1 vs T3	t(7) = 4.82, p = .002	**3.2.7E**
				T1 vs T4	t(7) = 2.95, p = .021	
				T1 vs T5	t(7) = 3.19, p = .015	
		Sex	F(1,6) = 0.642, p = .453			
	Perseveration ratio					
				T1 vs T2	t(7) = 1.54 p = .167	
				T1 vs T3	t(7) = 6.42 p = < .001	
				T1 vs T4	t(7) = 3.66 p = .008	**3.2.7K**
				T1 vs T5	t(7) = -1.55, p = .165	
	Place preference (proportion)					
				Target vs chance (32 categories)	t(7) = 3.61, p = .009, sig HB	
				Target vs chance (9 categories)	t(7) = 3.68, p = .008	
				Target vs close foils	t(7) =3.94, p = .006	
				Target vs far foils	t(7) =3.28, p = .014	**3.2.7N,P,R**
				Randomised target vs close foils	t(7) = -2.96, p = .021	
				Randomised target vs far foils	t(7) = -2.11, p = .073	
				Randomised target vs chance	t(7) = -2.55, p = .038	
				Randomised target vs true target	t(7) = -4.50, p = .003	
Probe trials (T2 & T5)						
	Quadrant occupation	Target vs chance	t(7) = .851, p = .423			**3.2.7J**
Training and probe trials (T2 & T5)						
	Average velocity	Trial type				
				Training vs T2 probes	t(7) = -5.04, p = .001	**3.2.6C**
				Training vs T5 probes	t(7) = -8.80, p = < .001	
				T2 vs T5 probes	t(7) = -2.58, p = .037	
		Trial	F(4,28) = 7.42, p = .<.001	T1 vs T2	t(7) = -1.24, p = .257	
				T1 vs T3	t(7) = -1.39, p = .206	**3.2.6D**
				T1 vs T4	t(7) = -3.13, p = .017	
				T1 vs T5	t(7) = -5.09, p = .001	
	Strategy					
		Day (training vs probe)				
				T1 vs T1	t(7) = -0.98, p = .359	
				T2 vs T2	t(7) = -2.74, p = .029	**3.2.7F**
				T3 vs T3	t(7) = -0.53, p = .613	
				T4 vs T4	t(7) = -0.82, p = .439	

Table 3.2.5 continued – 2

Trial type	Measure	Variable	Statistic	Paired comparison	Statistic	Figure
Interleaved training (D15-19)						
	Path length	Trial	F(3,21) = 15.87, p = < .001			
				T1 vs T2	t(7) = 3.78, p = .007	**3.2.7D**
				T1 vs T3	t(7) = 6.14, p = < .001	
				T1 vs T4	t(7) = 4.73, p = .002	
	Errors	Trial	F(3,21) = 13.65, p = <.001			
				T1 vs T2	t(7) = 3.46, p = .011	
				T1 vs T3	t(7) = 5.61, p = .001	
				T1 vs T4	t(7) = 4.58, p = .003	
Delay dependence 1 (1 hour)						
	Path length	Trial	F(3,21) = 1.70, p = .197			
				T1 vs T2	t(7) = .50, p = .630	
				T1 vs T3	t(7) = .74, p = .490	
				T1 vs T4	t(7) = 2.66, p = .033	
						3.2.7S
		DD1 vs IL				
				T1 vs T1	t(7) = -.108, p = .917	
				T2 vs T2	t(7) = -.810, p = .444	
				T3 vs T3	t(7) = -3.42, p = .011	
				T4 vs T4	t(7) = .618, p = .556	
Delay dependence 2 (30 seconds)						
	Path length	Trial	F(3,21) = .162, p = .921			
				T1 vs T2	t(7) = -.53, p = .610	
				T1 vs T3	t(7) = -.54 p = .610	
				T1 vs T4	t(7) = .28, p = .790	
						3.2.7T
		DD2 vs IL				
				T1 vs T1	t(7) = 3.70, p = .008	
				T2 vs T2	t(7) = -.672, p = .523	
				T3 vs T3	t(7) = -1.66, p = .141	
				T4 vs T4	t(7) = -.981, p = .359	
EM control						
	Path length	Trial	F(3,21) = 1.05, p = .392			
				T1 vs T2	t(7) = -1.92, p = .096	
				T1 vs T3	t(7) = 1.57, p = .160	
				T1 vs T4	t(7) = 2.40, p = .048	
						3.2.7H
		EM vs IL				
				T1 vs T1	t(7) = -.420, p = .685	
				T2 vs T2	t(7) = -1.56, p = .163	
				T3 vs T3	t(7) = -1.70, p = .133	
				T4 vs T4	t(7) = -.346, p = .740	
	Errors	Trial	F(3,21) = 1.44, p = .259			
				T1 vs T2	t(7) = 0.56, p = .592	
				T1 vs T3	t(7) = .420, p = .688	
				T1 vs T4	t(7) = 2.50, p = .041	
VO control						
	Latency	Trial	F(3,21) = .653, p = .590			
				T1 vs T2	t(7) = -.98, p = .362	
				T1 vs T3	t(7) = -.11, p = .914	
				T1 vs T4	t(7) = -1.30, p = .234	
						3.2.7I
		VO vs IL				
				T1 vs T1	t(7) = 1.92, p = .096	
				T2 vs T2	t(7) = 3.02, p = .019	
				T3 vs T3	t(7) = 3.27, p = .014	
				T4 vs T4	t(7) = 4.87, p = .002	

3.2.4 Experiment two: Discussion

Experiment two demonstrated a proof-of-concept for using a novel appetitive adaptation of a Barnes maze, the mBM, for assessing rapid place learning and memory. We hypothesised that a number of manipulations to the intrinsic maze and task design from that of experiment one would result in improved rate of task acquisition, with animals demonstrating place preference, a preference for spatial search, and extra-maze cue reliance. The results of experiment two largely satisfied these predictions.

Animals demonstrated within-day learning across multiple measures including path length, search errors, and latency. Improvement of task acquisition was also observed across days, with improvements between the first 5 training days and subsequent probe trials, likely indicating improved task rule learning. For example, significant improvement on the first retrieval trial (T2) of the T5 probes and interleaved training, but not training or T2 probes, appears indicative of such learning. This is analogous to results reported in rodent models in which prior knowledge of everyday task requirements is shown with decreasing errors and increasing accuracy across blocks of trials (e.g., Takeuchi et al., 2016; Nonaka et al., 2017; Nakazawa et al., 2003). The increasing reliance on a spatial search strategy further supports this assertion, with the trial-to-trial effect on spatial search preference becoming more pronounced between training and the later probe trials. Comparable performance in primary measures between training and unrewarded probe trials also suggests that an olfactory-based strategy was not used to distinguish between rewarded and unrewarded locations.

There were, however, some unexpected results when assessing place preference during probe trials. Namely, quadrant occupation did not appear to be an informative measure for recall of target location, with no significant differences between target and non-target quadrants. This is despite conserved improvements in other spatial recall measures during the probe trial itself (path length, errors etc.), suggesting this is likely not caused by olfactory artefacts. However, further investigation revealed that this was likely due to an insensitivity of quadrant occupation to preference for the target location relative to unrewarded foils. Specifically, we observed that preference for the specific target location during T2 and T5 probe trials was significantly above chance, while foil location preference decreased generally as a linear function of distance from the target, remaining at or below chance. Further, a graded preference for the target and foils close to the target was observed when clustering place preference data by relative separation. Notably this preference was substantially more robust during T5 probe trials, which we attribute to a greater number of reinforcements from

preceding recall trials, enhancing spatial certainty of the reward location. The increase in spatial certainty was reflected in that animals were able to significantly distinguish the target from both 'close' and 'far' categories of 4-foil averages during T5 but only from far foils during T2 probe trials. Comparable results were obtained irrespective of whether data was clustered by location. Meanwhile the target-specific place preference effects were abolished by data shuffling to randomise the target location, supporting the specificity of the effect as a true preference for the spatial location of the target and not an artefactual consequence of data clustering. The insensitivity of quadrant preference may be explained by approach-wander-reapproach behaviours which have been previously demonstrated in variants of the Barnes maze task, with initial direct path to the target followed by a diversification of search before spatially oriented re-approach behaviour (Illouz et al., 2016; 2020).

The extra-maze and full visual occlusion control trials demonstrated reliance on both the global visuospatial configuration of the environment and the complex spatial landmark cues, with a reduction in within-day learning in trials 1-3 or 1-4 in extra-maze or visual occlusion trials, respectively. These results, in combination with improvements in primary measures and place preference during normal probe trials, support the likely use of allocentric spatial learning for task solution. During manipulation of the trial ITI, the impairment in trial 3 following a 1-hour delay, alongside a failure to improve in any trials at a 30-second delay was surprising. Typically, significant trial-trial performance improvements have been reported in unimpaired rats in the DMTP MWM with 30-second to 20-minute ITIs, while delay dependent 'forgetting' is typically observed at delays exceeding 6-hours (e.g., Bast et al., 2005; Takeuchi et al., 2016; Nonaka et al., 2017; Broadbent et al., 2020). Task difficulty may have resulted in premature deficits in delay-dependent recall at 1-hour, however a lack of improvement during 30-second ITIs may be attributable to a reduction in effective learning following massed training (e.g., Nonaka et al., 2017) or repetitive stress induced by significantly increasing trial frequency. In addition, to further validate the ability of this task to generate stable, rapid place learning, the ITI may be extended further than 1-hour (e.g., Da Silva et al., 2014; Bast et al., 2005).

In addition to demonstrating robust task learning across animals, we did not detect any sex differences in performance, however this was likely limited by our small sample size and as such should be interpreted with caution. Sex differences in rodents are commonly reported in maze tasks, often with a split in the use of a spatial or serial search strategy (e.g., Locklear et al., 2014).

In comparison to experiment one (the aBM), experiment two (mBM) in general generated a more consistent profile of performance. Namely, the robust within-day learning effects across multiple measures accompanied by the consistent increase in spatial search preference with increasing trials and between day task learning in the mBM task was more reliable than the fluctuations in trial omissions and inconsistent strategy use observed using the aBM task. Further acquisition of the mBM task required significantly less training time than the aBM task, with a training duration of ~2-weeks as compared to more than 5-weeks in the aBM. Addressing the key issues with task design identified in the aBM appears likely to explain this improvement in task viability. Alterations including changing the maze design itself to reduce the efficacy of non-spatial task solving, segregation of recall trials to standardised intervals, and further control of potential olfactory and spatial cue salience appear likely contributors to this improvement. Indeed, we observed a much more rapid acquisition of direct navigation during training and probe trials than observed in the aBM, although note the qualitative differences in task design make quantitative comparison of measures difficult.

Despite the variability in acquisition observed using the aBM, the observations in place preference were somewhat comparable between the aBM and mBM tasks, with probe trials revealing preference for the target relative to foils varying as a function of separation distance. In the case of the mBM, animals appeared to successfully distinguish between spatially contiguous foils as a function of the number of preceding recall trials. Specifically, in the mBM, preference for the target itself was above chance in both cases, while distinction from foil categories was significantly more accurate at >90 degrees (far) during T2 and <90 degrees (close) during T5 probe trials. During T5 probe trials, comparison between the preference for the target and all individual surrounding foils surpassed Holm-Bonferroni correction, suggesting animals were able to distinguish foils even at a single position separation from the target with sufficient prior reinforcement. In contrast, data from the aBM indicated limited discrimination of the target relative to foils with accuracy only significant relative to foils of more than >54 degrees despite three preceding ‘encoding’ trials.

The task design of the mBM and associated pattern of results is largely in-line with that reported in the DTMP water maze and event arena, both of which have been demonstrated to be hippocampal-dependent. Namely reducing errors as a function of reinforcement, reliance on visuospatial cues, and perseveration within the vicinity of the target location during memory retrieval probe trials (e.g., Steele & Morris., 1999; Bast et al., 2005; Wang et al., 2010; Da Silva et al., 2014). Further, previous studies have similarly demonstrated putative pattern

separation in spatial memory using maze-based and operant tasks (e.g., Clelland et al., 2009; Morales et al., 2020; Oomen et al., 2013). While the current data suggest that the design used in experiment two may be applicable for this purpose, it remains to be seen whether the present task is sufficiently sensitive to resolve pattern separation-like ability differences when replicated in a larger cohort.

3.2.4.1 Limitations of experiment two

While the results of experiment two provided a proof of principle for the use of the mBM task for assessing rapid place learning and memory, there are notable limitations. First and foremost, this experiment comprised a particularly small (N=8) sample size, and as such is likely underpowered to detect subtle behavioural differences that may be detectable between groups at the population level. Particularly in the case of potential sex effects, the group size of 4 for each group is likely too small. Further, the data handling and generation of metrics of place preference, while developed on the basis of well-established measures of performance, are novel in the context of this experimental design. Therefore, results should be interpreted with caution and validation in both larger cohorts of animals and multiple rodent species would be beneficial.

Further, while we interpret the results presented as good evidence for performance driven by spatial learning and memory, namely allocentric place learning, these findings have not been validated in the context of systems-specific dependence. Specifically, classical pharmacological lesion/inactivation manipulations of the hippocampal circuitry (e.g., ibotenate lesions of the whole hippocampal complex; Bast et al., 2009) would be predicted to disrupt both acquisition and place preference performance in the mBM task if it holds hippocampal-dependence. These manipulations will need to be performed for future validation. Finally, the use of multiple modes of assessments of spatial memory is advisable, with a single assay not precluding gold standard practices. However, we note the current design likely permits flexibility to assess both reference memory and rapid place memory in parallel experiments in a similar manner to the MWM by simply retaining a static target location across training days.

3.2.5 Conclusion

Overall, experiment two demonstrated the viability of the appetitive mBM task to assess putative rapid place learning and spatial memory, generating reliance on spatial cues and visuo-spatial strategy use. Additionally, the re-testability and flexibility of this task makes it a potentially useful candidate for future studies to investigate rapid place learning and pattern separation-like ability, particularly in cases where water maze testing is problematic. The ability of animals to acquire within-day spatial learning and between-day task rule learning may provide multiple levels for probing learning and memory processes, including both everyday memory and cognitive flexibility in rule learning (e.g., reversal learning; Feng et al., 2017). Practically, the use of a dry land maze may provide a platform for pairing with pharmacological or imaging techniques (e.g., Morales et al., 2020). However, there is a clear need for replication and longitudinal follow-up to assess the replicability of these results and efficacy of task relearning in a larger cohort. Further, validation of hippocampal dependence of this task via systems interference such as pharmacological inactivation and/or lesions will be crucial for future characterisation. Crucially, the results of experiment two provided superior task adherence to that observed using the aBM and provides justification for task validation using APOE-TR mice.

3.3 Experiment three

3.3.1 Introduction: Experiment three

In experiment two, we established the efficacy of the mBM task to assess rapid place learning using repeat testing in WT mice. Animals successfully showed rapid within-day learning of a given spatial location, without substantial pre-training. The learning was robust to odour confounds and was dependent on global visuospatial and distal cues, with preference for direct spatial search strategy becoming increasingly predominant in across trials. Finally, animals demonstrated place preference for reward location during unrewarded probe trials, supporting accurate recall of allocentric spatial memory.

Importantly the results of experiment two confirmed the expected patterns of performance in WT mice and provided a basis for assessing rapid place learning and memory in APOE-TR animals longitudinally, across the lifespan. Firstly, we aimed to establish baseline performance in a cohort of mixed sex homozygous APOE-TR mice of E3-TR and E4-TR genotype at 3-months of age, with the goal of replicating findings observed in WT mice using the mBM.

We hypothesised that APOE-TR mice would demonstrate, as observed in WT mice, characteristic within and between day learning in the mBM task, showing decrements in primary measures of path length and errors. Further we hypothesised that APOE-TR mice would also exhibit reliable place preference for the target location relative to non-target foils and performance would be disrupted by occlusion of extra-maze cues, indicative of reliance on visuospatial cue information. At this stage only whole group analyses were performed, agonistic to sex and genotype groups.

3.3.2 Methods

3.3.2.1 Animals

A total of 36 APOE-TR mice (16 E3-TR [8M,8F], 20 E4-TR [9M,11F]) mice were used in experiment three (see Table 3.3.1), on a C57BL/6J background, maintained as outlined in section 2.1.1. Animals entered the experiment at 2-3 months of age. These animals were later used for experiments described in Chapter four, comprising longitudinal repeat-testing.

Table 3.3.1: Sample characteristics of APOE-TR mice grouped by sex and genotype at 3-months of age during experiment three.

Age	Total sample	Sex	Genotype	
			E3-TR	E4-TR
3-months	36	M	8	9
		F	8	11

3.3.2.2 Apparatus

The apparatus used for all aspects of experiment three were identical to that listed in experiment two (Figure 3.2.1A), see section 3.2.2.3 for details.

3.3.2.3 Experimental procedures

Animals were acclimatised and habituated with pre-training as listed in section 3.2.3, including matched food restriction, handling, and maze exposure as performed in experiment two. Following pre-training, a similar training regime to experiment two was used, with a standard 4-trial daily shifting DMTP task. Only minor modifications to the content of the training were made, while retaining the general task design. First, the overall training regime was shortened to 12-13 days, with 5 standard training days and T2 and T5 probe trials integrated without interleaved standard training trials. Second, an extra-maze occlusion control trial was performed at the end of the experiment which included cue occlusion on all four of the day's trials in order to reduce the likelihood of carry-over effects of orienting to cues based on the first trial of the day. Last, an egocentric control trial was conducted when animals were 6-months of age. The egocentric control trial consisted of a standard training day with the exception that the start position was altered to the maze periphery at a pseudorandomised distance and entry orientation from the target location, to test the possibility of egocentric navigation based on initial starting position. Although it is of note that the use of an opaque starting container occludes visual orientation and thus makes egocentric navigation unlikely (e.g., Dudchenko et al., 1997).

3.3.2.4 Analysis

Measure variables and data extraction

Processing of raw tracking data from Ethovision was performed as described for experiment two. Briefly, raw tracking data with Lowess smoothing was exported to excel, processed with a custom MATLAB script for variable extraction and analysed in R or SPSS.

The primary measure variables used in the analysis were primary path length to target, search errors, search strategy, velocity, and place preference as described in experiment two. Identical variable formulae and data extraction pipelines were used to that described for experiment two (section 3.2.2.5). Search strategy was also manually determined based on criteria described for experiment two. Briefly, raw tracks were plotted, superimposed onto a maze template and were rated as direct, serial, or random. Direct paths required no multiple maze crossings and no more than two crossings of sequential wells. Serial paths were defined as three or more incorrect sequential well crossings, while random paths involved multiple maze crossings with no clear strategic search trajectories.

Based on observations of a linear decrease in preference for foils of increasing distance from the target, a measure of target-foil separation ('separation accuracy') was generated from place preference data. Three categories of ratios of separation, 'close' (P2:P4), 'mid' (P5:P7), and 'far' (P8:P9) relative to the preference for the target were used. Separation accuracy was calculated by taking a ratio of preference for the target location relative to each of the three foil categories. Therefore, an index of above one indicates a greater preference for the target location than foils of a given separation from the target. Moreover, if place preference data follows a linear distribution in which preference for the target is generally highest and above chance, ratios would be expected to increase proportionally to the foil category dependent on distance of separation. This follows the formulation of similar discrimination or separation ratios generated in operant (Oomen et al., 2014), maze-based (Clelland et al., 2009), and object recognition (Ces et al., 2018) pattern-separation tasks. Therefore, alterations in these ratios would reflect decreasing certainty of the relative spatial relationships between the target and surrounding foil categories over the duration of a probe trial.

Statistical analysis

Measure variables were cross-correlated using Pearson's correlation analysis across all training and probe trials performed in all animals. This included latency, path length, errors, velocity, search strategy preference, and place preference.

For the main analysis, data for each primary measure variable was averaged across days, within subjects for the five training days, and three probe trial days of each type (T2 and T5). For single day trial manipulations, data was handled without within-subject averaging and analysed within subjects.

Place preference data was handled as described in experiment two, averaging across probe trial replicates, followed by clustering data by relative separation and across 'close/far' categories of a 4-foil average. Similarly, the generation of separation accuracy from place preference data was performed as described above, with 'close, mid or far' separation categories classed as a within subjects factor. Additionally, place preference data was shuffled to generate randomised 'target' data as described in experiment two and compared to true data, to control for data handling artefacts skewing preference values.

All primary analyses were conducted using repeated measures ANOVAs or paired t-tests. Pairwise comparisons were used for whole group level comparisons of within-day between-trial effects and between separation effects. Fisher's least significant difference (no correction) were used in these cases. Multiple one-sample t-test comparisons performed on place preference data across 32 individual zones were corrected using the Holm-Bonferroni procedure. Alpha was set at a criterion of 0.05 for significance in all tests.

3.3.3 Results

3.3.3.1 Relationships between measure variables in APOE-TR mice

First, we sought to test and validate whether data from primary measures generated in APOE-TR mice cross-correlated in the same manner as observed in WT animals during experiment two. During training at the three-month baseline, there were significant correlations between primary errors, latency, path length, and movement velocity. Velocity showed significant but moderate negative correlations with errors, path length, and latency, with the strongest relationship observed between velocity and latency (Figure 3.3.1A, Table 3.3.1). There were markedly stronger positive correlations between measure variables, with the largest correlation observed between latency and path length (Figure 3.3.1B/C).

Similarly, correlations were observed between search strategy preference and primary errors. A strong positive correlation between errors and random preference and a negative correlation with spatial preference indicated that a reduction in errors predicted direct spatial navigation paths to the target during training and a decrease in random preference (Figure 3.3.1D, Table 3.3.2). The lack of a significant correlation between errors and serial search strategy suggested that errors were primarily sensitive to the shift from random to spatially-directed search. Correlations were also performed between primary acquisition measures and measures of place preference during probe trials to assess the relationships between acquisition and recall performance. There was a reinforcement-dependent influence on correlation strength between errors and place preference. During T2 probe trials, a significant but weak negative correlation was observed between errors and relative place preference, this correlation increased somewhat with further reinforcement in T5 probe trials (Figure 3.3.1E/F, Table 3.3.3).

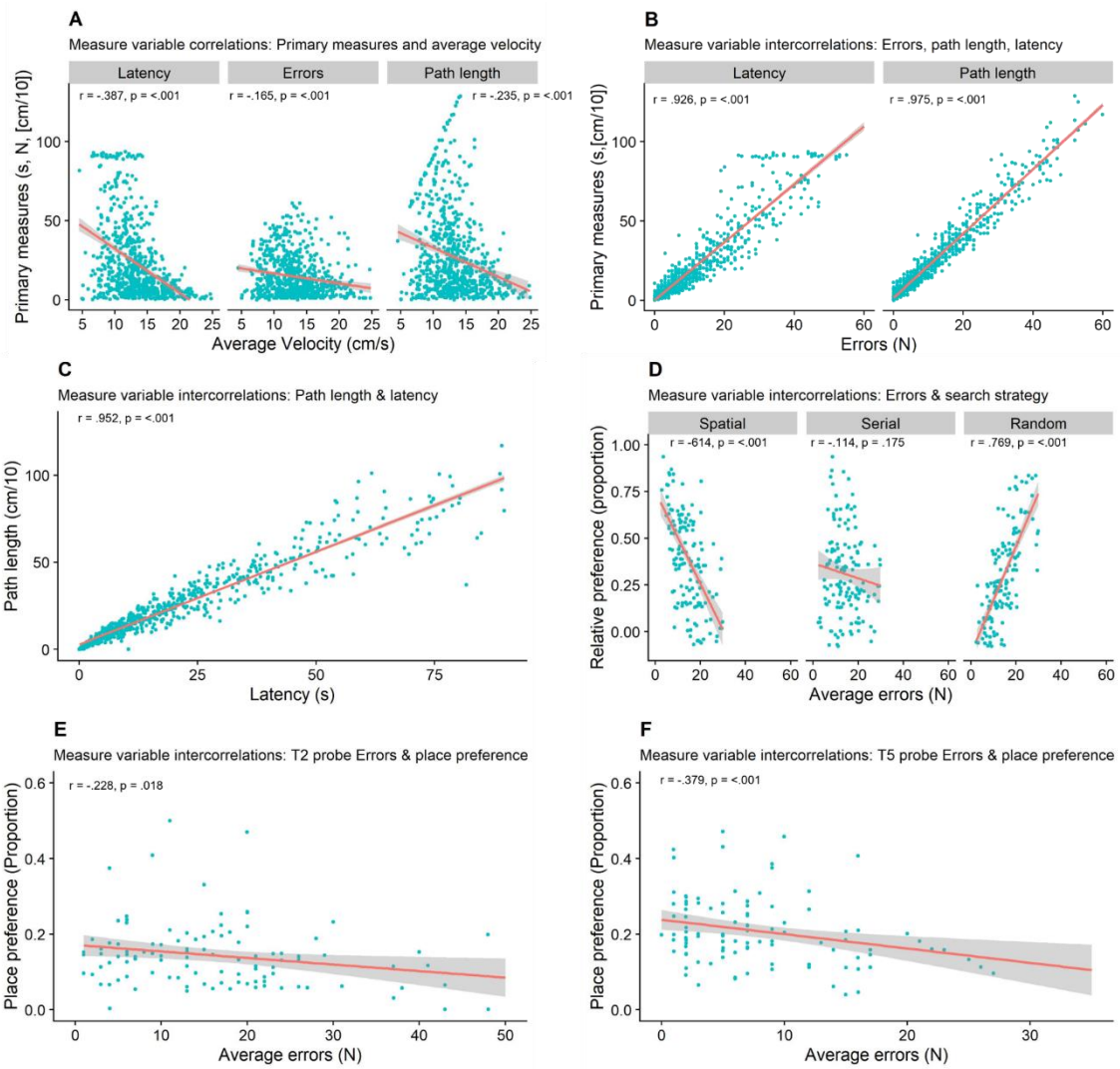

Figure 3.3.1: Characterisation of measure variable relationships in experiment three in APOE-TR mice during task training. Correlations of A) average movement velocity with latency, errors, and path length, B) errors with latency and path length and C) path length and latency. Measure variables are normalised to comparable scales for representation. Linear best fit is represented in red, while individual data points represent single trials replicated for individual animals across training days. D) Correlation between search errors and proportion of strategy preference during training, subdivided by strategy type including spatial, serial, and random search. Correlation between E) T2 and F) T5 probe trial place preference and primary errors. Individual data points represent individual animal averages across trials and training days. Line plot 'windows' represent 95% CIs. Pearson's correlation coefficient (r) and associated p-values are presented for each measure.

Table 3.3.2: Inter-measure correlations from training data generated at 3-months in APOE-TR mice at the group level in experiment three. Pearson's correlation (r) and associated p-value are represented for each measure. Corresponds to Figures 3.1A-C.

Measure		Velocity	Errors	Path length	Latency	Figure
Velocity	*r*	1	-0.221	-0.236	-0.387	
	p		<.001	<.001	<.001	
Errors	*r*	-0.221	1	0.975	0.926	
	p	<.001		<.001	<.001	
Path length	*r*	-0.236	0.975	1	0.952	**3.1A-C**
	p	<.001	<.001		<.001	
Latency	*r*	-0.387	0.926	0.952	1	
	p	<.001	<.001	<.001		

Table 3.3.3: Correlations between strategy subtypes and search errors from training data generated at 3-months in APOE-TR mice at the group level in experiment three. Pearson's correlation (r) and associated p-value are represented for each measure. Corresponds to Figure 3.1D.

	Strategy				
Measure		Spatial	Serial	Random	Figure
Spatial	*r*	1	-0.520	-0.582	
	p		<.001	<.001	
Serial	*r*	-0.520	1	-0.392	
	p	<.001		<.001	
Random	*r*	-0.582	-0.392	1	**3.1D**
	p	<.001	<.001		
Errors	*r*	-0.614	-0.114	0.769	
	p	<.001	0.175	<.001	

Table 3.3.4: Correlations between place preference and search errors from T2 and T5 probe trial data generated at 3-months in APOE-TR mice at the group level in experiment three. Pearson's correlation (r) and associated p-value are represented for each measure. Corresponds to Figure 3.1E-F.

Trial type		Errors	Figure
Place preference (T2)	*r*	-0.228	
	p	.018	
Place preference (T5)	*r*	-0.379	**3.1E-F**
	p	<.001	

3.3.3.2 Task replication and baseline performance in APOE-TR mice.

To confirm the replicability of performance in the mBM, comparisons in primary measures performed in experiment two were replicated in the APOE-TR cohort at the 3-month baseline. APOE-TR mice demonstrated similar patterns of performance relative to WT mice in both task rule learning and within-day learning of the target reward location. In terms of task rule learning, we observed that path length and primary errors during retrieval trials (T2-T4) decreased over the course of training in APOE-TR mice in a similar manner to that observed in WT mice (Table 3.3.5).

In within-day learning, APOE-TR mice significantly improved performance, with decreasing average path length and errors between T1 and T3-T4 during training and T2-T4/T5 during T2/T5 probe trials, respectively (Figure 3.3.2A/B). Across days, APOE-TR mice also demonstrated a significant increase in the within-day improvement in the summed path length and errors across recall trials (T2-T4) between the first and last day of training (Figure 3.3.2G/H), suggestive of between-day rule learning.

Analysis of strategy preference from paths during training revealed that APOE-TR mice acquired similar preference for a direct spatial search strategy across training and probe trials, demonstrating a significant increase in spatial search following T1 (Figure 3.3.2C). APOE-TR mice showed a significant increase in average spatial strategy preference between days during training from ~28-46% across the first week, and the largest average increase was seen between trials one and two, typically reaching ~40% by trial two (Figure 3.3.2C). Overall, within-day average spatial search preference increased from 18-51% by trial four (Figure 3.3.2C).

In measures of place preference during probe trials, time spent at target zone was significantly above chance in APOE-TR mice during both T2 and T5 probe trials, as observed in WT mice during experiment two (Figure 3.3.2D, Table 3.3.6), while we noted that APOE-TR mice showed significant preference for the target over both close and far foils during both T2 and T5 probe trials. These effects were also robust to data clustering, with target but not foil preference significantly above chance across the 32 possible zones without cross-foil averaging (Supplementary Table 3.1). Shuffling place preference data to control for data clustering effects, completely abolished the target preference effect in both T2 and T5 probe trials, with no positions significantly different to chance (Figure 3.3.2E). Target preference from ‘true’ data was also significantly above target preference from the shuffled data in both T2 and T5 probe

trials (Table 3.3.6), again demonstrating specificity of the preference effect for the target location.

Despite the demonstration of the specificity of the place preference effect to the target, we noted that the ratios of place preference of non-target foils varied linearly as a function of distance from the target and better reflected discrimination performance than averaging of absolute proportions alone. To further investigate the relative accuracy of place preference relative to the target at increasing separation distance, these ratios were clustered in a similar manner to absolute proportion, generating 'close', 'mid', and 'far' categories, respectively. A significant increase in 'separation accuracy' was observed between close, mid, and far foil categories (described in section 3.3.3), indicating a greater discrimination of non-target foils as a function of distance from the target (i.e., preference for the target is greater than foils, the ratio of this preference increases with increasing distance between the target and a given foil; Figure 3.3.2F). During both T2 and T5 probe trials there was a significant main effect of separation, with animals significantly preferring near over mid and far foils (Figure 3.3.2F, Table 3.6). Further, there was a significant increase in separation accuracy between close and mid foils following the extended reinforcement of T5 probe trials relative to T2 probe trials, suggesting more accurate discrimination between target and foils dependent on extent of reinforcement (Figure 3.3.2F, Table 3.3.6). Some animals demonstrated particularly notable separation accuracy at mid to far foil categories, in some cases with between 3 to 5-fold greater preference for the target than the respective foil (Figure 3.3.2F)

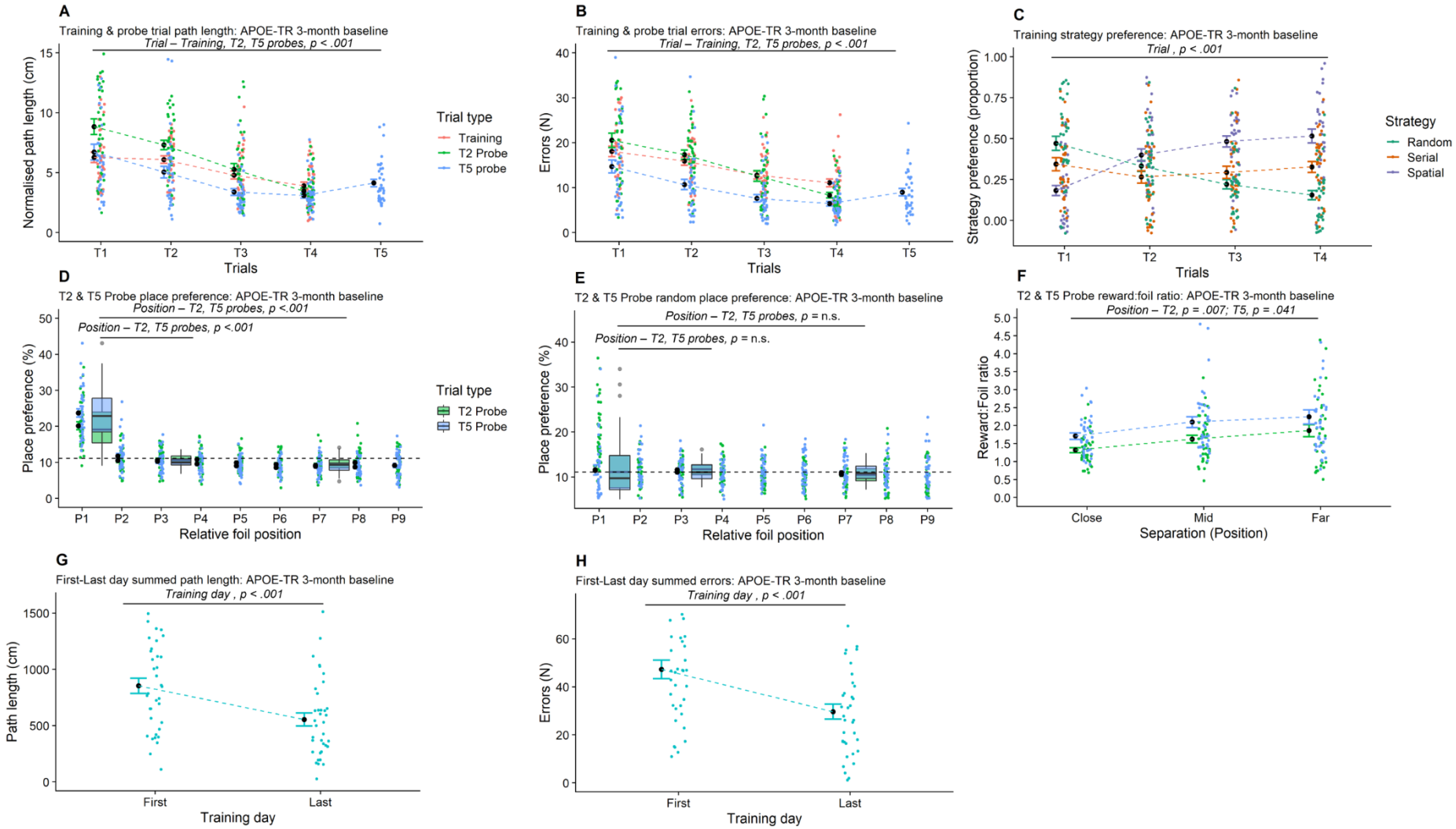

Figure 3.3.2: Validation of primary acquisition measures at whole group level in 3-month aged APOE-TR mice using the mBM in experiment three. A) Average normalised primary path length to target across trials from five days of training and T2/T5 probe trials. Path length is normalised to the optimum distance to the target to control for intrinsic differences in distance between start position and inner or outer position targets on the maze. B) Average search errors to

target across trials from five days of training and T2/T5 probe trials. C) Relative proportion of spatial strategy preference across trials during five days of training. D) Average percentage place preference during T2 and T5 probe trials for the target and non-target foil positions (P1:P9) clustered by separation (relative foil position) from the target. Box plots represent place preference for the target, and close/far four-foil averages, while coloured points and error bars represent average place preference at individual foil separations. E) Figures represent same data as presented in D with shuffling algorithm applied to randomise target location during T2 and T5 probe trials. Dashed black line represents chance performance (11.1%). F) Relative separation accuracy represented by reward:foil discrimination ratio across close, mid, and far categories of foil separations from the target during T2 and T5 probe trials. Sum of G) path length and H) search errors across recall trials (T2-T4) during the first and last day of training. Brackets with accompanying relevant main effect or pairwise comparison and associated p-values are presented. All black points represent mean, while error bars represent mean +/- SEM. Individual coloured data points represent multiple day averages within-trial type, for a single subject. See Table 3.3.5 for details.

Table 3.3.5: Statistical comparisons performed in experiment three for primary measures of acquisition and retrieval performance. Trial type, measure variable, independent variable, statistics, and corresponding figure are provided. Corresponds to Figure 3.3.2.

Measure	Trial type	Variable	Statistic	Paired comparison	Statistic	Figure
Path length						
	Training	Trial	F(3,105) = 10.41, p = <.001			
				T1 vs T2	MD = 9.76, p = .732	
				T1 vs T3	MD = 72.63, p = .009	
				T1 vs T4	MD = 118.99, p = <.001	
	T2 probe trials	Trial	F(2.63,91.93) = 32.53, p = <.001			
				T1 vs T2	MD = 85.51, p = .012	
				T1 vs T3	MD = 180.53, p = <.001	**3.3.2A**
				T1 vs T4	MD = 279.06, p = <.001	
	T5 probe trials	Trial	F(2.71,103.51) = 13.54, p = <.001			
				T1 vs T2	MD = 83.16, p = .009	
				T1 vs T3	MD = 166.37, p = <.001	
				T1 vs T4	MD = 180.79, p = <.001	
				T1 vs T5	MD = 128.85, p = <.001	
	Training (D1-8)	Training day		Training day (First Vs Last)	t(35) = 3.99, p = <.001	**3.3.2G**
Errors						
	Training	Trial	F(3,105) = 13.54, p = <.001			
				T1 vs T2	MD = 2.23, p = .098	
				T1 vs T3	MD = 5.31, p = <.001	
				T1 vs T4	MD = 7.06, p = <.001	
	T2 probe trials	Trial	F(3,105) = 24.61, p = <.001			
				T1 vs T2	MD = 3.38, p = .026	
				T1 vs T3	MD = 7.38, p = <.001	**3.3.2B**
				T1 vs T4	MD = 11.86, p = <.001	
	T5 probe trials	Trial	F(3.25,103.11) = 13.75, p = <.001			
				T1 vs T2	MD = 4.01, p = .006	
				T1 vs T3	MD = 7.07, p = <.001	
				T1 vs T4	MD = 8.28, p = <.001	
	Training (D1-8)			Training day (First Vs Last)	t(35) = 5.00, p = <.001	**3.3.2H**
Strategy (spatial)						
	Training (D1-8)	Trial	F(3,105) = 19.39, p = <.001			
				T1 vs T2	MD = -.22, p = <.001	**3.3.2C**
				T1 vs T3	MD = -.30, p = <.001	
				T1 vs T4	MD = -.33, p = <.001	

Table 3.3.5 continued.

Measure	Trial type	Variable	Statistic	Paired comparison	Statistic	Figure
Place preference						
	T2 probe trials					
				Target vs close foils	t(35) = 8.21, p = <.001	
				Target vs far foils	t(35) = 8.15, p = <.001	
				Close vs far foils	t(35) = 1.74, p = .091	**3.3.2D**
	T5 probe trials					
				Target vs close foils	t(35) = 10.36, p = <.001	
				Target vs far foils	t(35) = 10.98, p = <.001	
				Close vs far foils	t(35) = 3.18, p = .003	
	T2 probe trials (target randomised)					
				True vs Random target	t(35) = 5.93, p = <.001	
				Random target vs close foils	t(35) = -0.12, p = .904	
				Random target vs far foils	t(35) = 0.75, p = .457	**3.3.2E**
	T5 probe trials (target randomised)					
				True vs Random target	t(35) = 7.25, p = <.001	
				Random target vs close foils	t(35) = 0.40, p = .693	
				Random target vs far foils	t(35) = 0.44, p = .664	
Reward:foil ratio (separation accuracy)						
	T2 probe trials	Separation	F(1.56,54.58) = 9.28, p = .001			
				Close vs Mid	MD = -.306, p = .001	
				Close vs Far	MD = -.544, p = .001	
				Mid vs Far	MD = -.238, p = .086	
	T5 probe trials	Separation	F(1.57,56.87) = 10.29, p = <.001			
				Close vs Mid	MD = -.391, p = .001	**3.3.2F**
				Close vs Far	MD = -.537, p = .001	
				Mid vs Far	MD = -.146, p = .161	
	T2 vs T5 probe trials					
				T2 Vs T5: Close	t(35) = -3.67, p = .001	
				T2 Vs T5: Mid	t(35) = -2.72, p = .01	
				T2 Vs T5: Far	t(35) = -1.56, p = .124	

3.3.3.3 Extra-maze occlusion and egocentric strategy control trials

An extra-maze cue occlusion control trial was performed in all animals to attempt to replicate findings observed in experiment two and validate reliance on extra-maze visual cues for spatial task performance. During extra-maze occlusion trials, while errors decreased across trials there was no significant effect of trials on errors, with performance only improving significantly between T1 and T4 (Figure 3.3.3A, Table 3.3.6). Further, to test whether place preference accuracy during acquisition itself was impaired, we compared the search preference within a more lenient 10cm boundary of the target prior to locating the reward. This allowed characterisation of the search phase during the rewarded T2 trial to compare relative to preceding probe trials. Place preference accuracy (i.e., search within the vicinity of the reward) during the extra-maze occlusion T2 trial was significantly decreased relative to the preceding probe trials and was not significantly different from chance (Figure 3.3.3B).

Additionally, an egocentric strategy control trial was included as a further control for potential use of allothethic cues such as entry direction and body orientation during transport to the maze. Starting animals from a pseudo-randomised and counterbalanced alternative position on the maze, alongside forcing an entry orientation did not significantly impair performance in errors. Animals demonstrated a significant effect of trial, with improvements between T1 and all subsequent trials (Figure 3.3.3A). Further, in contrast to the extra-maze cue occlusion day, animals demonstrated a significant preference for the vicinity of the target during initial search in T2, comparable to that observed during preceding probe trials (Figure 3.3.3B, Table 3.3.6).

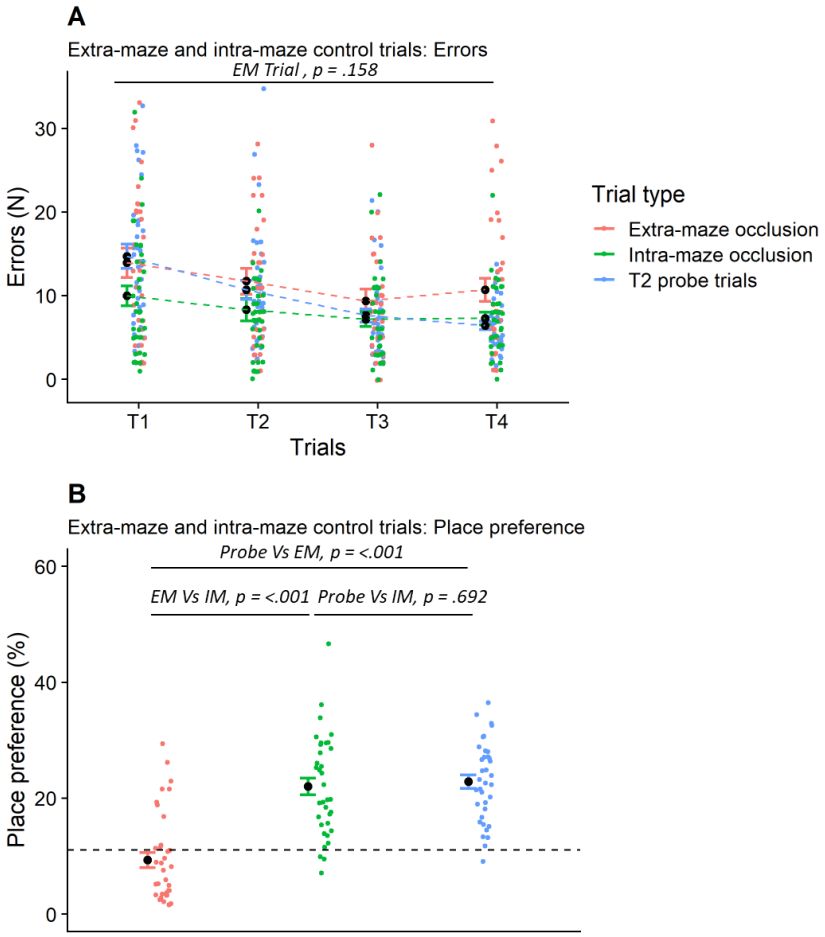

Figure 3.3.3: Performance during extra-maze occlusion and intra-maze control trials. A) Average search errors and B) place preference for the target across trials during control trials and T2 probe trials at 3-months at the whole group level. Individual points represent individual subject performance during each trial type. Error bars represent group mean +/- SEM. Brackets and labels denote p-values of main effects, interactions or pairwise comparisons (see main text and Table 3.3 for details). Dashed black line in B) represents chance performance (11.1%).

Table 3.3.6: Statistical comparisons performed in experiment three during extra-maze occlusion and intra-maze control trials. Trial type, measure variable, independent variable, statistics, and corresponding figure are provided. Corresponds to Figure 3.3.3.

Measure	Trial type	Age	Variable	Statistic	Paired comparison	Statistic	Figure
Errors							
	Extra-maze cue occlusion	**3-months**	Trial type	F(2.78,72.281) = 1.78, p = .158			
					T1 vs T2	MD = 3.23, p = .237	
					T1 vs T3	MD = 4.82, p = .065	
					T1 vs T4	MD = 4.81, p = .021	
							3.3.3A
	Intra-maze control	**6-months**	Trial type	F(3,90) = 3.24, p = .026			
					T1 vs T2	MD = 2.77, p = .032	
					T2 vs T3	MD = 3.68, p = .027	
					T3 vs T4	MD = 3.13, p = .048	
Place preference							
	Control trials Vs Probe	**3-months**	Trial type				
					Probe Vs Extra-maze	t(34) = -4.97, p = <.001	**3.3.3B**
					Probe Vs Intra-maze	t(34) = -0.40, p = .692	
					Extra-maze Vs Intra-maze	t(35) = -6.44, p = <.001	

3.3.4 Discussion

Experiment three aimed to assess baseline rapid place learning and memory performance in the mBM task using young APOE-TR mice, with the aim of replicating and expanding findings observed in WT mice during experiment two. We hypothesised that APOE-TR mice would exhibit a comparable profile of performance to WT mice, with robust within and between-day learning reflected in improvements in primary acquisition measures, alongside demonstration of accurate spatial recall indicated by measures of place preference. Overall, the results of experiment three are largely consistent with these hypotheses. APOE-TR mice demonstrated comparable performance to WT mice, exhibiting putative rapid place learning acquisition and retrieval, which was dependent on the availability of configural extra-maze cues.

Firstly, characterisation of the measure variables in APOE-TR mice demonstrated similar relationships as observed in WT mice in experiment two, with strong positive inter-measure correlations in path length, search errors, latency. Search errors were also demonstrated to correlate strongly with spatial search strategy preference during training, while negatively correlating with random search, suggesting search errors were a reasonable proxy for a transition to spatial strategy preference. In conjunction, errors correlated negatively, albeit weakly, with place preference during probe trials, supporting a moderate predictive validity for fewer errors preceding finding the target to greater preference for the target zone itself. This negative correlation was stronger during T5 probe trials, supporting the effect of reinforcement across trials in promoting both direct navigation to and preference for the spatial location of the target.

APOE-TR mice at 3-months demonstrated within and between-day learning. There were significant within-day improvements in path length and search errors from T1 to T3-T4 during training and from T1 to all subsequent trials during probe trials, also demonstrating between day improvements. Between the first and last two training days there was a significant reduction in overall path length and errors in T2-T4, indicating improvements in the magnitude of acquisition across days, likely reflecting task rule learning. Further, there was a clear acquisition of preference for a spatial search strategy, with significant improvements between T1 and all subsequent trials, with the most pronounced increase occurring between T1 and T2.

Measures of one-trial (T2) and four-trial (T5) place memory retrieval indexed by relative place preference during unrewarded probe trials was also comparable between APOE-TR and WT mice, with both cohorts showing significant target location place preference. Place preference

was significantly above chance in both probe trial types and again, place preference was enhanced during T5 probe trials, supporting the effect of reinforcement on accuracy of memory recall. APOE-TR mice demonstrated preference for the target location relative to both the closest and furthest foil categories during T2 and T5 probe trials. Repeating this analysis with raw data from individual zones on the maze provided comparable results to cross-foil averaging, further supporting preference specificity for the target (Supplementary Table 3.1). Applying a shuffling algorithm to the place preference data, randomising the target location, resulted in a complete loss of the place preference effect in APOE-TR mice as observed during experiment two. This again suggests that, in both APOE-TR and WT mice, the place preference effect was specific to the target location and not a spurious result of cross-foil averaging. Additionally, the specificity of recall accuracy was demonstrated for foils near to the target, with greater discrimination of foils of greater separation distance from the target. This is again consistent with pattern-separation-like behaviour observed in similar tasks such as the radial arm maze pattern-separation task (e.g., Clelland et al, 2009).

Finally, APOE-TR mice demonstrated retrieval performance dependent on extra-maze cue availability. Occlusion of extra-maze cues attenuated acquisition performance, with no significant effect of trial on errors, while no such effect was observed during standard T2 probe trials or egocentric control trials. Additionally, measuring place preference relative to a more lenient criteria during the rewarded T2 trials demonstrated a significant impairment in place preference during extra-maze cue occlusion relative to both T2 probe and egocentric trials, suggesting reliance on extra-maze cues for expression of accurate preference for the target location. Despite not reaching significance, errors did decrease across extra-maze occlusion trials, which is consistent with the results observed during experiment two and suggests the use of both specific extra-maze cues and global visuospatial cues may be used for spatial orienting (e.g., lighting, approximate room dimensions etc.). The impairment following extra-maze occlusion, but not egocentric strategy controls is comparable to demonstrations of visuospatial cue reliance during the reference memory version of the Barnes maze (O'Leary et al., 2011).

Overall, the results of experiment three supported the robust replication of effects observed in WT mice in an APOE-TR cohort using the mBM task, with evidence demonstrating comparable within-day rapid place learning and reinforcement-dependent spatial memory retrieval. The demonstration of spatial place preference, and putative pattern separation-like discrimination of non-target foils, in combination with the reliance on extra-maze cues, supports the use of

allocentric spatial strategies to sustain task performance. This provided sufficient evidence for the use of the mBM task framework for longitudinal assessment of performance in APOE-TR mice.

3.3.5 Chapter summary

The experiments conducted in Chapter three sought to establish the validity of an appetitive adapted Barnes maze task to assess rapid place learning and memory in WT and APOE-TR mice with the aim of using the task for repeat longitudinal testing in APOE-TR mice across the lifespan. Experiment one and two comprised the development and testing of two adapted Barnes maze task designs in WT mice, the aBM and the mBM tasks. Experiment one using the aBM task highlighted several intrinsic design limitations for appetitively-driven rapid place learning, with animals showing high day-to-day variability in performance which appeared driven by parsimonious task solutions such as cued approach and non-spatial serial search strategies. Amendments to the task design improved performance somewhat, but memory retrieval performance was inconsistent and confounded the requirement of a stable baseline of spatial strategy use on which to assess learning and memory performance longitudinally.

In experiment two, multiple task design alterations were made, generating the mBM task, which aimed to ameliorate the limitations raised during experiment one and assess performance again in WT mice. Task performance during experiment two revealed more consistent performance, with animals demonstrating robust within day learning, supported by reliance on spatial search strategies and place preference during probe trials, classical indicators of spatial memory retrieval in maze tasks. Control trials demonstrated that the predominant strategy use relied on extra-maze cues and global visuo-spatial cues, consistent with allocentric place learning.

Finally, experiment three sought to replicate these findings at baseline in a larger cohort of young APOE-TR mice. APOE-TR mice demonstrated robust improvements in performance both in between-day task learning and within-day acquisition of novel spatial memory, while place preference for the spatial location during probe trials demonstrated accurate memory recall. These results, alongside reliance on extra-maze cues, were consistent with that observed in WT mice during experiment two. Overall, the experiments in Chapter three provided the validation of a novel appetitive spatial memory task variant for the assessment of ‘everyday memory’ or rapid place learning through repeat testing with daily updating of episodic-like spatial information. This task can subsequently be used for the longitudinal assessment of everyday memory in APOE-TR mice.

CHAPTER FOUR

Characterising the effect of APOE isoform on rapid place learning and memory across the lifespan in the APOE-TR mouse model

4.1 Introduction

In the experiments conducted in Chapter three, we established the efficacy of the modified Barnes maze (mBM) delayed match to place (DMTP) task to assess rapid place learning and memory in WT and APOE-TR mice. Animals successfully showed rapid within-day learning of daily updated spatial locations, without substantial pre-training. This learning was robust to odour or egocentric navigation confounds and reliance on extra-maze cues alongside place preference for the rewarded location supported a predominant use of allocentric spatial learning. These findings were replicated in a larger cohort of APOE-TR mice, providing a baseline on which to perform longitudinal repeat testing to characterise cognitive performance across the lifespan.

Using homozygous APOE-TR mice of both sexes, we aimed to assess the influence of APOE genotype, sex, and age on rapid place learning using the mBM task. We hypothesised that E4-TR mice would demonstrate an impairment in the age-dependent trajectory of rapid spatial learning and memory performance, which would decline prior to that of E3-TR mice. We also predicted that this trajectory would be differentially influenced by sex, with greater impairments in female E4-TR mice, as multiple previous studies have highlighted that E4-TR female mice exhibit exaggerated deficits in spatial reference memory (e.g., Leung et al., 2012; Andrews-Zwilling et al., 2010; Jones et al., 2019).

We predominantly focussed on measures validated in Chapter three alongside some novel measures. In order to allow characterisation of acquisition performance across age, agnostic to initial finding phase (T1) which does not reflect spatial memory, while retaining sensitivity to the incremental learning of the task within a given day, we calculated a 'learning index' (Pereira et al., 2015). The use of a summative metric of acquisition performance such as learning index in the spatial memory literature have proven useful in providing an individual value for performance which can be tracked across time both within and between individuals (Gallagher et al., 1993, 2015; Pereira et al., 2015). A learning index has frequently been used by weighting and summing primary measures such as path length error (i.e., path deviation) or search errors to comprise a single score of learning performance with greater weighting assigned to early trials, based on their predictive value to acquisition. The rationale for this is to firstly exclude the influence of baseline effects in strategy preference which may confer an initial benefit to the animal during the first trial without necessitating spatial learning per-se; while second to incorporate the cumulative learning component of the task reflected in the measures themselves. Moreover, given the generally supported assumption of initial

exponential learning phase during single or multiple trial encoding followed by a shallowing of the acquisition curve, a weighting is assigned to trials which increases as a function of increasing trial number. The result of this weighting is that errors in later encoding trials produce a greater effect on the index and thus favours profiles of more rapid acquisition. For the purpose of Chapter four, we generated a learning index on the basis of search errors during retrieval trials (T2-T4).

4.2 Methods

4.1.1 Design

A three-way mixed design was used, with APOE genotype (E3-TR, E4-TR) and sex (male, female) as between subject variables, and age (3-18-months at 3-month intervals, comprising 6 levels) as the primary within-subject variable. A testing regime was designed for repeated testing at 3-month intervals between 3-18-months, including training, probe, and manipulation trials, resulting in an approximate two-week training period every 3 months. Experiments were performed in two batches of 20 and 16 animals respectively, resulting in approximately four-to-five weeks of testing per experiment at each time point. Table 4.1 outlines the experiment design across time-points. Age-specific alterations to the training regime are noted subsequently.

Table 4.1: Outline of time points and task design in the experiments in Chapter four. Each animal underwent the training regime outlined below. Each trial type used is described and typical number of repeats and ITI are provided for each time point.

Trial type	Replicates (days per type)	ITI (minutes)	Age	Manipulation
Standard training	5	15	3-18-months	A 4-trial repetition of the DMTP task on the mBM, with an inter-trial-interval (ITI) of 15 minutes.
Probe (T2)	3	15	3-18-months	Matched to standard training trial with absent reward on trial 2.
Probe (T5)	3	15	3-months, 18-months	Matched to standard training trial with absent reward on trial 5.
Extended ITI	1	240/720 (4/12-hours)	6-18-months	Matched to standard training trial with the ITI between trial 1 and 2 is extended to 4/12-hours.

4.1.2 Animals

A total of 36 APOE-TR mice (16 E3-TR [8M,8F], 20 E4-TR [9M,11F]) mice were used in Chapter four (see Table 4.2), on a C57BL/6J background, maintained as outlined in section 3.1.2. These animals comprised the same cohort used for 3-month baseline characterisation in experiment three of Chapter three. Animals were 18-19 months of age at the end of testing. Animals were acquired, maintained and handled as listed in section 3.1.2. Experimental testing typically occurred between 9am-5pm, with the exception of delay-dependence manipulation trials due to the necessity of extended inter-trial intervals. Age-related attrition of animals in each group can be noted in Table 4.2.

Table 4.2: Sample characteristics of APOE-TR mice grouped by sex and genotype across each age of longitudinal testing during experiments conducted in Chapter four.

Age	Total sample	Sex	Genotype	
			E3-TR	E4-TR
3-months	36	M	8	9
		F	8	11
6-months	36	M	8	9
		F	8	11
9-months	36	M	8	9
		F	8	11
12-months	36	M	8	9
		F	8	11
15-months	35	M	8	9
		F	7	11
18-months	29	M	5	9
		F	4	11

4.1.3 Apparatus

The apparatus used for all aspects of the experiments in Chapter four were identical to that described in section 3.2.2.

4.1.4 Experimental procedures

Animals were acclimatised and habituated with pre-training as listed in section 3.2.2.4, including matched food restriction, handling, and maze exposure. Following pre-training, a similar training regime to described in section 3.3.2.3 was used, with a standard 4-trial daily shifting DMTP task. Further modifications to the training were made dependent on animal age and are outlined in Table 4.1. These changes were as follows:

1) The overall training regime was again retained at the shortened 12-13 days, with 5 standard training days and three T2 probe trials integrated without interleaved standard training trials.

2) T5 probe trials were conducted at 3-month and 18-month time points based on the observation that acquisition performance plateau was generally achieved by the fourth trial

3) Finally, from 6-months onwards, additional manipulation trials were included as noted in Table 4.1. Namely, 4-hour and 12-hour T1-T2 ITI trials were added to probe delay-dependent forgetting, again with the assumption that longer retention intervals would result in attenuated performance as previously demonstrated (e.g., Dunnet et al., 1988; Bast et al., 2005; Wang et al., 2010; da Silva et al., 2014; Takeuchi et al., 2016).

At the end of the experiment (18-months age), remaining animals were sacrificed, perfused, and tissue handled using the aCSF perfusion protocol detailed in section 2.2.1.

4.1.5 Analysis

4.2.1.1 Tracking data pre-processing & variable selection

Processing of raw tracking data from Ethovision was performed as described in section 3.2.2.5. Briefly, raw tracking data with Lowess smoothing was exported to excel, processed with a custom MATLAB script and analysed in R or SPSS.

The primary variables used in the analysis were primary path length to target, search errors, learning index, velocity, place preference, and separation accuracy as described in section 3.2.3. Variable formulae used were identical to that described in section 3.2.3.

4.2.1.2 Learning Index

We developed a learning index to provide a single acquisition score independent of performance on the initial finding trial (T1), based on the principles outlined in section 4.1. Briefly, a baseline dataset of search errors was generated from the average performance of the E3-TR control cohort at 3-months of age. This baseline comprised the average errors between T2-T4 during training, from which a multiplier was generated, modelled on the average improvement in errors between trials (e.g., Perieira et al., 2015). The total search errors for a given trial were then differentially weighted according to these multipliers, with increasing trial number corresponding to a greater weight. A single final index score was then generated by summing the individual weighted values from recall trials T2-4. The index score was generated for each animal at each time point for use in statistical analysis. Assuming acquisition performance improves between subsequent trials, the net effect on learning index is that search errors in later trials receive greater weighting than early errors, favouring effective early acquisition performance to result in lower scores, reflecting better acquisition performance.

4.1.6 Statistical analysis

Data for each measured variable was averaged across days, within subjects. For primary acquisition data including path length, errors, and learning index, performance scores were averaged across 8-days of training and T2 probe trials within each time point. To compare between day learning, ‘early’ and ‘late’ phases were defined by extracting acquisition data from the first two and last two days of training to form averaged early and late category data, respectively.

For measures of retrieval (place preference and separation accuracy), which corresponds only to probe trials, data was averaged across the number of replicates of a given trial type (typically three). For single day trial manipulations, data was handled without within-subject averaging and was analysed within time point. Place preference data was handled as described

in Chapter three, extracting time spent within a stringent 2cm criteria of the target and averaging across probe trial replicates. Similarly, the generation of separation indices from place preference data was performed as described in Chapter three, with ratios generated reflecting the relative preference for the target over foils of 'close, mid or far' separation distance, reflecting foil positions 2-4, 5-7, and 8-9 separated from the target (e.g., see Figure 3.2.5), respectively.

All primary analyses were conducted using a mixed linear modelling approach. Generally, mixed linear models with robust parameter estimation were generated for each measure variable. In each case, age was included as a repeated-measures variable, as was trial number in cases where data structure was nested within trials (data was also nested within subjects across age, forming a random factor). APOE genotype and sex were included as primary between groups variables in each model. Each model was constructed sequentially, assessing model fit improvement between iterations using the log-likelihood method. Models were checked for satisfaction of the assumptions of linearity, homogeneity of residuals, independence of errors, and normality of residuals. QQ-plots, plots of standardised residuals versus fitted values, and Cook's distance plots revealed that generally data was linear and free from substantial influential values. Levene's tests demonstrated that in each case residuals held relatively homogenous variance, with no significant result in any basic model of the measure variables. Histogram plots of model residuals demonstrated weak negative skew in errors, path length, and separation accuracy as well as weak positive skew in place preference. However, Durbin-Watson tests revealed significant dependence of error terms in search errors, learning index, and separation accuracy. Therefore, to reduce the likely impact on model parameter estimates, all model parameter estimates were performed using the robust 'HC3' method (e.g., Field & Wilcox., 2017). Intercepts but not slopes were allowed to randomly vary, which improved model fit in all cases.

To follow-up significant interaction terms from mixed linear models, a simple main effects (SME) analysis approach was taken, generating models at individual levels of a given variable within the interaction term. In cases where this interaction comprised at least one repeated measures variable (e.g., age), subsequent models were also mixed linear models to allow modelling of dependence. In cases where only between-subjects variables were present at a fixed level of a repeated measures variable (e.g., modelling effect of genotype at a single level of age), standard linear models were used, again using robust parameter estimation. Alpha was set at a criterion of 0.05 for significance in all tests. In the case of each model, false

discovery rate (FDR) correction is provided, in which *p*-values were corrected within measures for the number of test terms used (e.g., within a given linear model, FDR-corrected *p*-values are generated relative to the number of variables and interaction terms within the model).

4.3 Results

Across age, performance of APOE-TR mice in the mBM task demonstrated a complex set of genotype and sex dependent effects in primary measures of spatial memory acquisition and retrieval. Measures of acquisition and retrieval performance were modelled across the lifespan using mixed linear modelling methods and are presented sequentially.

4.3.1 Rapid place learning acquisition in APOE-TR mice across the lifespan

Primary acquisition measures of path length, errors and learning index were modelled longitudinally during the training and probe trial period using mixed linear models with robust parameter estimation. In each case of path length, errors, and learning index, we observed that models were best fit by allowing random intercepts, but not slopes, and fit was significantly improved by inclusion of all primary variables and their compound interactions (Supplementary Table 4.1). Random intercepts account for the dependence in measurements within matched individuals across time (i.e., not independent measurements as they are repeated within subjects across time), with a significant effect of random intercept indicating variability across individuals when the value of the repeated measures variable is zero, in this case the age baseline of 3-months.

4.3.1.1 Path length

A linear mixed model demonstrated that there was significant variability in baseline path length, as demonstrated by the significant random intercept (Table 4.2). Both age and trials were the most significant predictors with increasing trial number and age predicting an overall improvement in performance reflected in a decrease in path length, although this was mediated by a significant interaction between age and trial. Neither sex nor genotype significantly predicted path length but there were trends for two-way interactions between

genotype and age, and sex and age, with a trend for a three-way interaction between age, genotype, and trial (Table 4.3). These indicated that APOE genotype only trended towards and did not significantly influence path length in combination with age, sex, or trials. Path length data are shown for each individual time point in Figure 4.1, grouped by APOE genotype and sex although note no significant differences were detected by these factors. Follow-up linear models of the significant interaction between age and trial number showed that age predicted a significant decrease in path length in during trials T1 and T2, but not T3/T4, suggesting a decrease in both baseline and the second daily trial path length with increasing age (Figure 4.1G, Table 4.3), with animals taking a shorter path to the reward in both the first and second trial of the day.

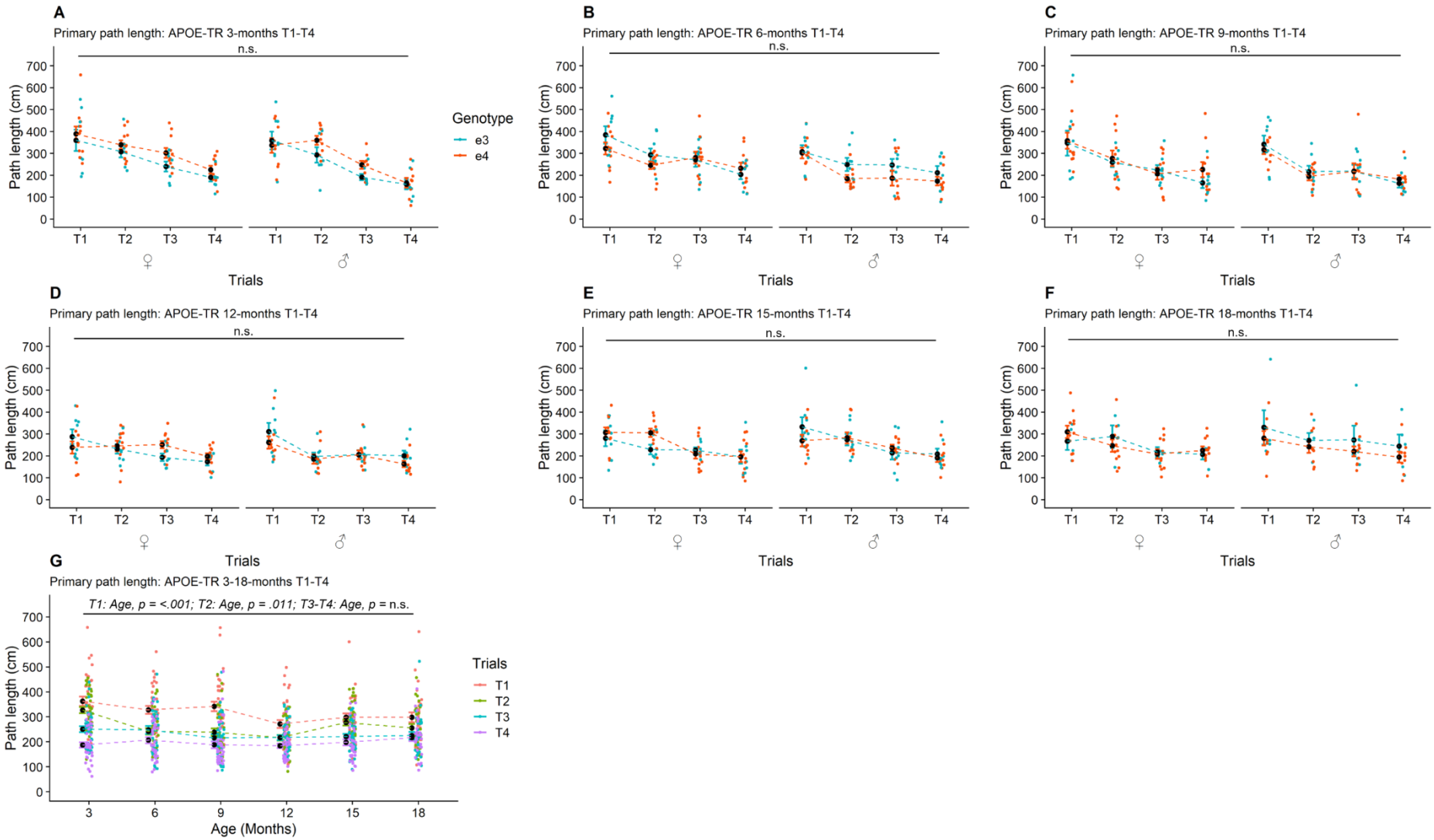

Figure 4.1: Average primary path length to target from 3-18 months of age in APOE-TR mice grouped by genotype and sex. Individual points represent average path length within trials from T1-T4 across days of training for individual animals. Individual age points are represented in figures A) 3-months, B) 6-months, C) 9-months, D) 12-months, E) 15-months, F) 18-months. G) Average path length across 3-18-months grouped by trial number. Effect of age can be

observed on baseline encoding (T1) and retrieval trials (T2-T4), with the most pronounced decrease occurring in T1. Individual points in G) represent average path length for individual animals across training and probe trials, with points replicated by colour according to trial number. Error bars represent group mean +/- SEM. Brackets and labels denote p-values of main effects, interactions or pairwise comparisons (see main text and Table 4.3 for details). "n.s." denotes no statistically significant effects of any comparison within a given time point. Sex grouping is represented by "♀" and "♂" overlay.

4.3.1.2 Search errors

Search errors demonstrated a markedly different profile of results, however, appearing more sensitive to interactions between the primary variables of interest. Again, as in path length, there was a significant effect of the random intercept indicating baseline variability across animals in overall errors. There were main effects of age and trials, indicating a significant decrease in overall errors with both increasing trial number (i.e., within-day learning) and across age. There were also significant main effects of genotype, and sex, with E4-TR mice and male mice making fewer errors than their E3-TR and female counterparts overall. However, there were also three significant two-way interactions between age and genotype, trials and genotype, and age and sex, as well a three-way interaction between age, genotype, and sex (Table 4.3). Although the significant two-way interaction between trials and genotype did not pass FDR correction, exploratory analysis highlighted a significant effect of genotype overall at T1, with E4-TR mice making fewer errors during the initial trial, T1, compared to E3-TR mice (Figure 4.2G, Table 4.3).

Individual models were used to explore the three-way interaction, modelling the effects of sex and genotype on search errors at each level of age. This analysis revealed a significant effect of sex at 3 and a trend at 6-months with female mice making more errors overall than male mice. Additionally, there was a significant two-way sex by genotype interactions at 12-months and 15-months, although the interaction at 15-months was marginally above the FDR correction threshold. Post-hoc analysis of this interaction at 12-months revealed a main effect of genotype in female mice, with E4-TR female mice making more errors than E3-TR female controls, the directionality of which was conserved at 15-months but only trended towards significance. In contrast, male E4-TR mice trended to make fewer errors than male E3-TR controls at 12-months. Finally, there were no significant group differences detected in errors at either 9 or 18-months (Figure 4.2A-F).

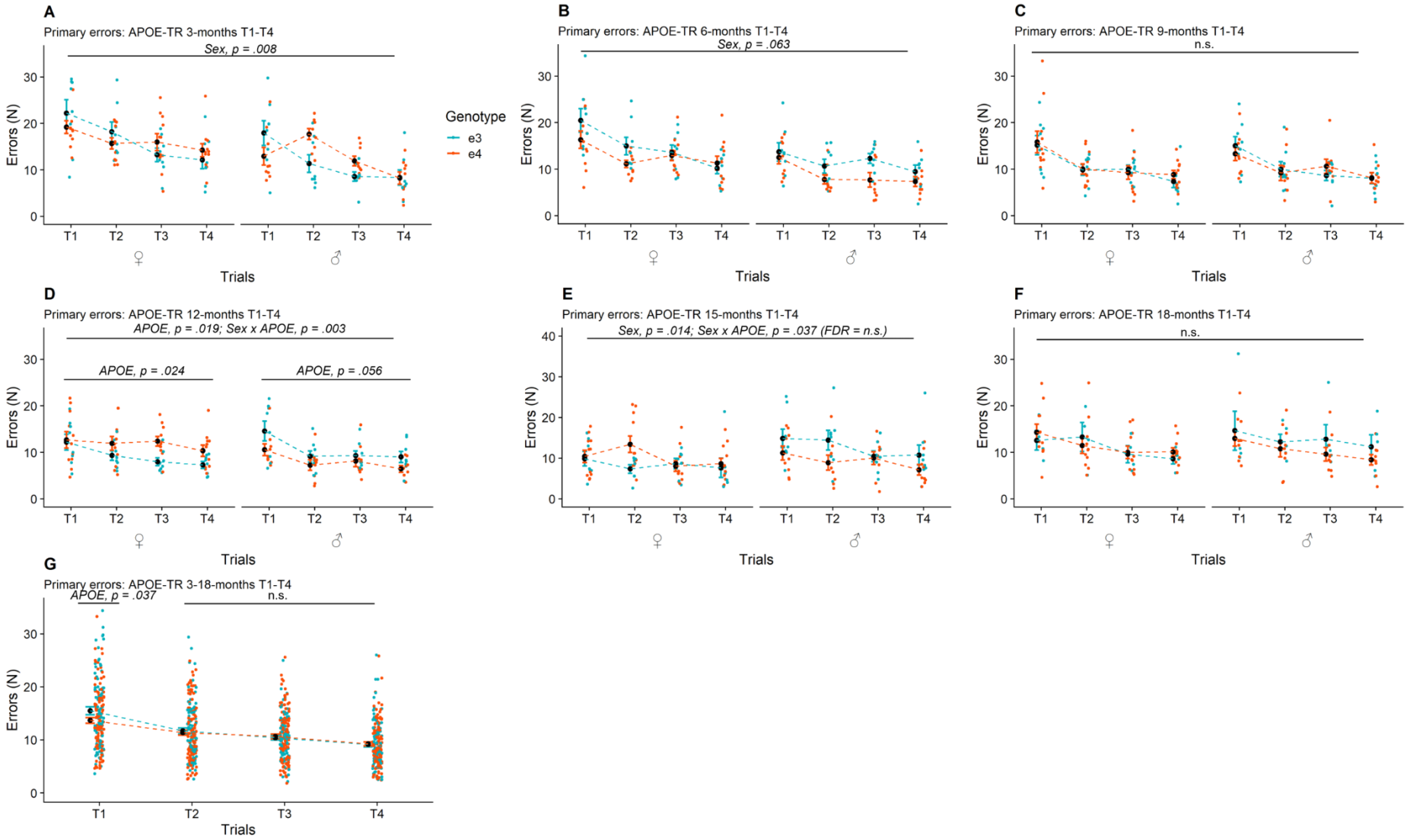

Figure 4.2: Primary search errors to target from 3-18 months of age in APOE-TR mice grouped by genotype and sex. Individual points represent average errors within trials from T1-T4 across days of training for individual animals. Individual age points are represented in figures A) 3-months, B) 6-months, C) 9-months, D) 12-months, E) 15-months, F) 18-months. G) Average search errors across 3-18-months grouped by trial number and genotype. Individual points in

G) represent average path length for individual animals across training and probe trials, with points replicated for each age point to demonstrate distribution. Statistical analysis in G) was nested within subject and not represented by replicate points for each age. Error bars represent group mean +/- SEM. Brackets and labels denote p-values of main effects, interactions or pairwise comparisons (see main text and Table 4.3 for details). "n.s." denotes no statistically significant effects of any comparison within a given time point. Sex grouping is represented by "♀" and "♂" overlay.

Table 4.3: Robust linear mixed model analyses of within-day learning in primary path length and search errors from 3-18 months in APOE-TR mice. Trial type, measure variable, independent variable, statistic, and corresponding figure are provided. Corresponds to Figures 4.1/4.2.

Measure	Trial type	Age	Variable	Coefficient	SE	CI lower	CI upper	*t*	*p*	SME	Statistic	FDR	Figure
Path length													
	Training (D1-8)	3-18-months	Random intercept	16.51		10.28	26.54						
			Age	-31.94	8.53	-48.67	-15.20	-3.33	<.001			s	
			Trials	-71.08	11.61	-93.87	-48.29	-5.63	<.001			s	
			Age*Trials	7.90	2.27	3.45	12.35	2.26	0.001			s	
										T1: Age	t(171) = -3.32, p = <.001	s	
										T2: Age	t(171) = -2.56, p = .011	s	**4.1/4.3**
										T3: Age	t(171) = -1.97, p = .077	ns	
										T4: Age	t(171) = 1.11, p = .300	ns	
			Trials*Genotype	26.84	14.06	-0.77	54.44	1.65	0.057			ns	
			Age*Sex	21.26	11.90	-2.10	44.63	1.60	0.074			ns	
			Age*Trials*Genotype	-5.11	3.08	-11.16	0.93	-1.17	0.097			ns	
Errors													
	Training (D1-8)	3-18-months	Random intercept	1.25		0.86	1.80						
			Age	-9.97	2.60	-15.03	-4.91	-3.83	<.001			s	
			Trials	-9.68	3.47	-16.44	-2.93	-2.79	0.005			s	
			Genotype	-14.19	5.87	-26.03	-2.35	-2.42	0.022			s	
			Sex	-16.00	6.18	-28.47	-3.54	-2.59	0.014			s	
			Age*Trials	1.80	0.95	-0.04	3.65	1.90	0.058			ns	
			Age*Genotype	4.22	1.54	1.23	7.20	2.75	0.006			s	
			Trials*Genotype	4.16	2.09	0.10	8.22	1.99	0.047			ns	
										T1: Genotype	t(34) = -2.07, p = .032	s	
										T2: Genotype	t(34) = -0.36, p = .713	ns	
										T3: Genotype	t(34) = 0.33, p = .714	ns	
										T4: Genotype	t(34) = 0.09, p = .925	ns	**4.2/4.3**
			Age*Sex	4.84	1.63	1.66	8.01	2.96	0.003			s	
			Age*Genotype*Sex	-2.19	0.97	-4.09	-0.30	-2.25	0.025			s	
										3-months: Sex	t(32) = -3.31, p = .008	s	
										6-months: Sex	t(32) = -2.17, p = .063	ns	
										12-months: Genotype	t(32) = 2.16, p = .019	s	
										12-months: Sex*Genotype	t(32) = -2.85, p = .003	s	
										12-months males: Genotype	t(15) = -1.95, p = .056	ns	
										12-months females: Genotype	t(17) = 2.10, p = .024	s	
										15-months: Sex	t(32) = 2.19, p = .014	s	
										15-months: Sex*Genotype	t(32) = -1.97, p = .037	ns	

4.3.1.3 Learning index

The effect of age on T1 in path length (Figure 4.1G), and APOE genotype on T1 in search errors (Figure 4.2G) is problematic for measures of learning. Namely, these shifts in T1 performance are not indicative of within-day learning performance and likely rather reflects initial search strategy efficiency, which has the potential to bias parameter estimates. To circumvent this issue, we developed a learning index that is agnostic to performance during T1 (described in sections 4.1 and 4.2.5), instead reflecting performance only during retrieval trials (T2-T4/T5). Importantly, as the learning index was developed based on search errors, greater scores indicate poorer performance and vice versa.

Mixed modelling of learning index demonstrated that the overall effect of age during retrieval trials was best explained by a quadratic, rather than a linear term (Table 4.4, Figure 4.3). Thus, a significant quadratic effect of age predicted an initial decrease (improvement) in young age and a plateau-to-increase (impairment) towards old age at the whole group level. There were no main effects of genotype or sex but instead a significant two-way interaction between age and sex, and a three-way interaction between age, sex, and genotype (Table 4.4). To explore these interactions, linear models were again generated at individual levels of age, modelling the interaction between sex and genotype.

At 3-months, there were significant effects of sex and genotype, with female and E4-TR mice showing higher learning index, indicating poorer performance relative to male and E3-TR mice, respectively. At 6-months, only the effect of sex persisted, with male mice outperforming female controls. At 9-months, there was equivalent performance between groups, with no main effects or interactions between sex and genotype observed. There was a significant sex by genotype interaction at 12-months and a close trend at 15-months. In both cases these interactions reflected poorer performance in female E4-TR mice than sex-matched E3-TR controls, with a trend for enhanced performance in male E4-TR mice relative to E3-TR controls. Finally, no differences were detected by sex or genotype in learning index at 18-months, with equivalent performance across groups (Figure 4.3, Table 4.4).

4.3.1.4 Between-day learning

To investigate the possibility that between-day learning (i.e., decrements in overall errors, likely reflecting enhanced task-rule learning across days), 'early' and 'late' phase performance was characterised by comparing learning index during the first and last two days during training at each timepoint (Early: Day 1-2; Late: Day 7-8). A difference score between early and late phase learning index was generated, with positive values indicating an improvement in performance between phases, therefore reflecting more effective learning later in training. These phases are at the extremes of the testing period and, as such, differences in task performance would be expected to be most clear. This data was again analysed using a robust mixed linear modelling approach across age.

Comparing early and late phase performance showed overall main effects of age and sex, with a two-way interaction between age and sex, and a three-way interaction between age, sex, and genotype (Table 4.4). To assess whether ageing trajectories of between-day learning were influenced by genotype, the three-way interaction was followed up with individual models grouped by sex. In both males and females, there was a significant effect of age but in opposing directions, reflecting an improvement with age in male mice and an impairment with age in female mice. There was also a close trend for an interaction between genotype and age in male but not female mice. Exploratory analysis of this interaction, splitting the models by APOE genotype revealed that E3-TR but not E4-TR male mice demonstrated a significant effect of age, with increasing between-day learning across age (Figure 4.3B, Table 4.4). Of note, the slopes for E4-TR mice of both sexes were centred near zero suggesting small effects of age on between day learning, however this interaction was only a trend when tested statistically.

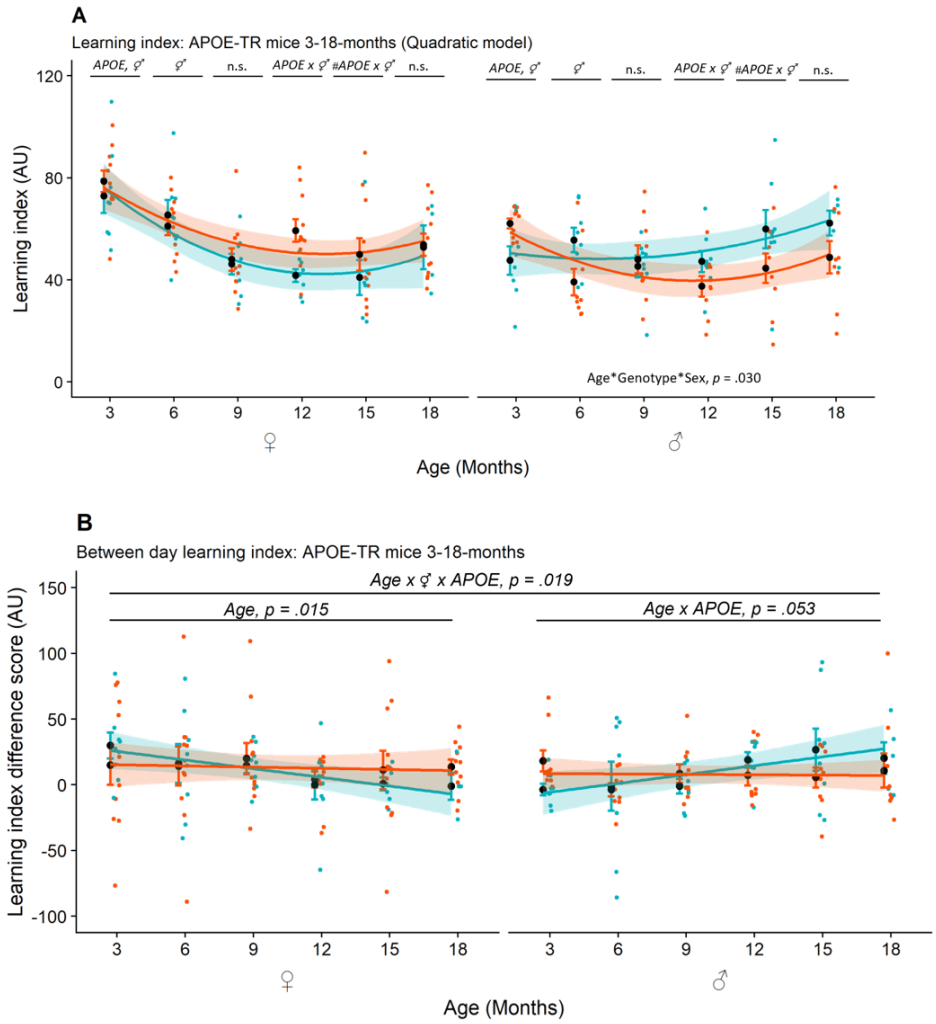

Figure 4.3: A) Average learning index during training (T2-T4) from 3-18 months of age in APOE-TR mice grouped by genotype and sex. Modelled quadratic effect is represented in best fit lines for each group respectively, with 'windows' representing 95% confidence intervals (CIs) of parameter estimates. For clarity, significant main effects and interactions are represented by abbreviations and symbols: APOE = main effect of APOE genotype, ⚥= main effect of sex, APOE x ⚥= interaction between APOE genotype and sex, # = marginal trend. B) Learning index difference score across early and late phase training (Early: D1/2 T2-T4; Late: D7/8 T2-T4) to represent between day learning across 3-18 months of age in APOE-TR mice grouped by genotype and sex. Linear model fits and accompanying 95% CI windows are shown. Error bars represent group mean +/- SEM. Brackets and labels denote p-values of main effects, interactions or pairwise comparisons. "n.s." denotes no statistically significant effects of any comparison within a given time point. See main text and Table 4.4 for details. Sex grouping is represented by "♀" and "♂" overlay.

Table 4.4: Robust linear mixed model analysis of learning index from 3-18 months in APOE-TR mice. Trial type, measure variable, independent variable, statistic, and corresponding figure are provided. Relevant simple main effect (SME) analysis of significant interaction terms is shown. Corresponds to Figure 4.3.

Measure	Trial type	Age	Variable	Coefficient	SE	CI lower	CI upper	*t*	*p*	SME	Statistic	FDR	Figure
Learning index (LI)													
	Training (D1-8)	3-18-months	Random intercept	15.21		13.69	16.91						
			Age (Quadratic)	-6.04	1.46	-8.91	-3.16	-3.90	<.001			s	
			Sex	-29.02	8.71	-46.77	-11.28	-3.51	0.002			s	
			Age*Sex	8.39	2.32	3.81	12.98	3.93	<.001			s	
			Age*Genotype*Sex	-5.96	2.73	-11.35	-0.57	-2.17	0.030			s	
										3-months: Sex	F(1,32) = 15.58, p = <.001	s	
										3-months: Genotype	F(1,32) = 4.99, p = .020	s	**4.3A**
										6-months: Sex	F(1,32) = 9.87, p = .001	s	
										9-months: Sex*Genotype	F(1,32) = 0.19, p = .653	ns	
										12-months: Sex*Genotype	F(1,32) = 9.95, p = .001	s	
										12-month females: Genotype	F(1,32) = 8.05, p = .003	s	
										12-month males: Genotype	F(1,32) = 2.91, p = .082	ns	
										15-months: Sex*Genotype	F(1,31) = 3.49, p = .057	ns	
										18-months: Sex*Genotype	F(1,25) = 0.89, p = .336	ns	
	Early Vs Late (D1-2/D7-8)	3-18-months	Random intercept	5.70		1.11	29.31						
			Age	-6.64	2.71	-11.99	-1.29	-2.27	0.015			s	
			Sex	-46.03	14.02	-74.58	-17.48	-3.06	0.002			s	
			Age*Sex	13.44	3.69	6.14	20.73	3.32	0.000			s	
			Age*Genotype*Sex	-12.76	5.38	-23.37	-2.14	-2.45	0.019			s	**4.3B**
										Females: Age	t(88) = -2.00, p =.015	s	
										Males: Age*Genotype	t(80) = -2.12, p =.053	ns	
										Male E3-TR: Age	t(36) = 2.34, p =.010	s	
										Male E4-TR: Age	t(44) = 1.12, p =.248	ns	

4.3.2 Rapid place learning retrieval performance in APOE-TR mice across the lifespan

Following standard training, probe trials were conducted to assess accuracy of single or multiple trial spatial memory retrieval using measures of place preference and separation accuracy. Briefly, place preference was measured as the proportion of time spent in the close vicinity (~2cm) of the target location relative to all non-target foils, categorised according to distance (separation) from the target. Effectively, chance performance for place preference is 11.11%, corresponding to a single target and 8 possible categories of non-target foil by separation (discussed in section 3.2.3). As for separation accuracy, place preference across the non-target foils was categorised by distance from the target into three categories of 'close', 'mid', and 'far'. Using this, a ratio was generated to represent the ratio of time spent at the target relative to each of these foil categories, with an increase in the ratio indicating more accurate preference for the target and discrimination of the target from that particular non-target foil category. As such, separation accuracy was expected to increase linearly as a function of distance (separation), with more accurate discrimination the further away the foil was from the target.

As with measures of acquisition, linear mixed models were used to model changes in retrieval measures across age. Again, there was significant baseline individual variability across animals, indicated by the significant random intercept. In place preference alone, there were no significant main effects of age, genotype, or sex, and no significant interactions across the lifespan (Figure 4.4A). Notably, at the whole group level, at each timepoint target preference remained significantly above chance performance (11.11%) relative to surrounding foil locations (Figure 4.4A, Table 4.5.1/2, Supplementary Table 4.2).

In contrast, separation accuracy (expressed as 'reward:foil ratio', the relative ratio of time spent between the target and non-target locations of varying 'separation' or distance from the target) was modulated by primary variables across the lifespan, with significant main effects of separation, age, and sex. Increasing separation size predicted greater accuracy at the whole group level, while increasing age predicted a significant decrease in separation accuracy and female mice showed lower separation accuracy overall. Modelling the coefficients for the effect of separation at each age demonstrated a decrease in the coefficient for the effect of separation from 12-18-months, indicating that animals showed less accurate discrimination of further foils from the target at the whole group level from mid to late-age (Figure 4.4E).

However, multiple three-way interactions between age, genotype, sex, and separation indicated that the data was better suited to individual models grouped by levels of age. We therefore retained the analysis structure used for follow-up analysis of acquisition measures after initial mixed modelling (Table 4.5.1/2). Therefore, the effect of genotype, sex, and separation were modelled within individual ages, using linear models with robust parameter estimation as outlined for acquisition measures.

At 3-months there was a significant main effect of separation, indicating that preference (time spent) decreased for the foils as a function of increasing distance (i.e., animals showed greater preference for foils closer to the target than those further away). There was also an interaction between genotype and sex, and a three-way interaction between genotype, sex, and separation. Follow-up analysis of the three-way interaction showed an interaction between genotype and sex at far but not close or mid foil categories, with male E4-TR, but not female E4-TR mice showing greater separation accuracy relative to E3-TR controls (i.e., E4-TR male mice spent less time at the furthest foils and a greater proportion of time at closer foils). At 6-months there was only a trend to a main effect of separation, with a weaker discrimination of non-target foils as a function of distance from the target. We noted that E4-TR mice showed poorer mean discrimination at each foil category, but this did not reach significance. At 9-months, however, there were main effects of genotype, sex, and separation, alongside an interaction between genotype and sex. The main effect of separation again demonstrated greater discrimination of the target from foils with increasing separation distance from the target. The interaction between genotype and sex was underpinned by a main effect of genotype in male but not female mice, whereby E4-TR males showed poorer separation accuracy at all foil categories than E3-TR male controls, suggesting less accurate discrimination between target and foil irrespective of distance from the target. There was also a significant interaction between genotype and separation, with E3-TR but not E4-TR mice showing a trend to a significant effect of separation across sexes, suggesting greater overall separation accuracy in E3-TR mice at 9-months (Figure 4.4A-C; Table 4.5.1/4.5.2).

From 12-18-months, performance between genotype groups appeared to converge, with no main effects of genotype or interaction with separation, although a trend for an interaction between genotype and sex was observed at 15-months. Finally, an interaction between sex and separation was observed at 12-months and a trend at 18-months, with female mice exhibiting reduced separation accuracy relative to male mice (Figure 4.4B-D, Table 4.5.1/2). As discussed above, at the whole group level the effect of separation decreased markedly at 12-

months with poorer discrimination between foil categories of varying distance between 12-18-months, suggesting a reduction in preference for foils closer than further from the target (i.e., a loss of distinction of foils as a function of distance, Figure 4.4E).

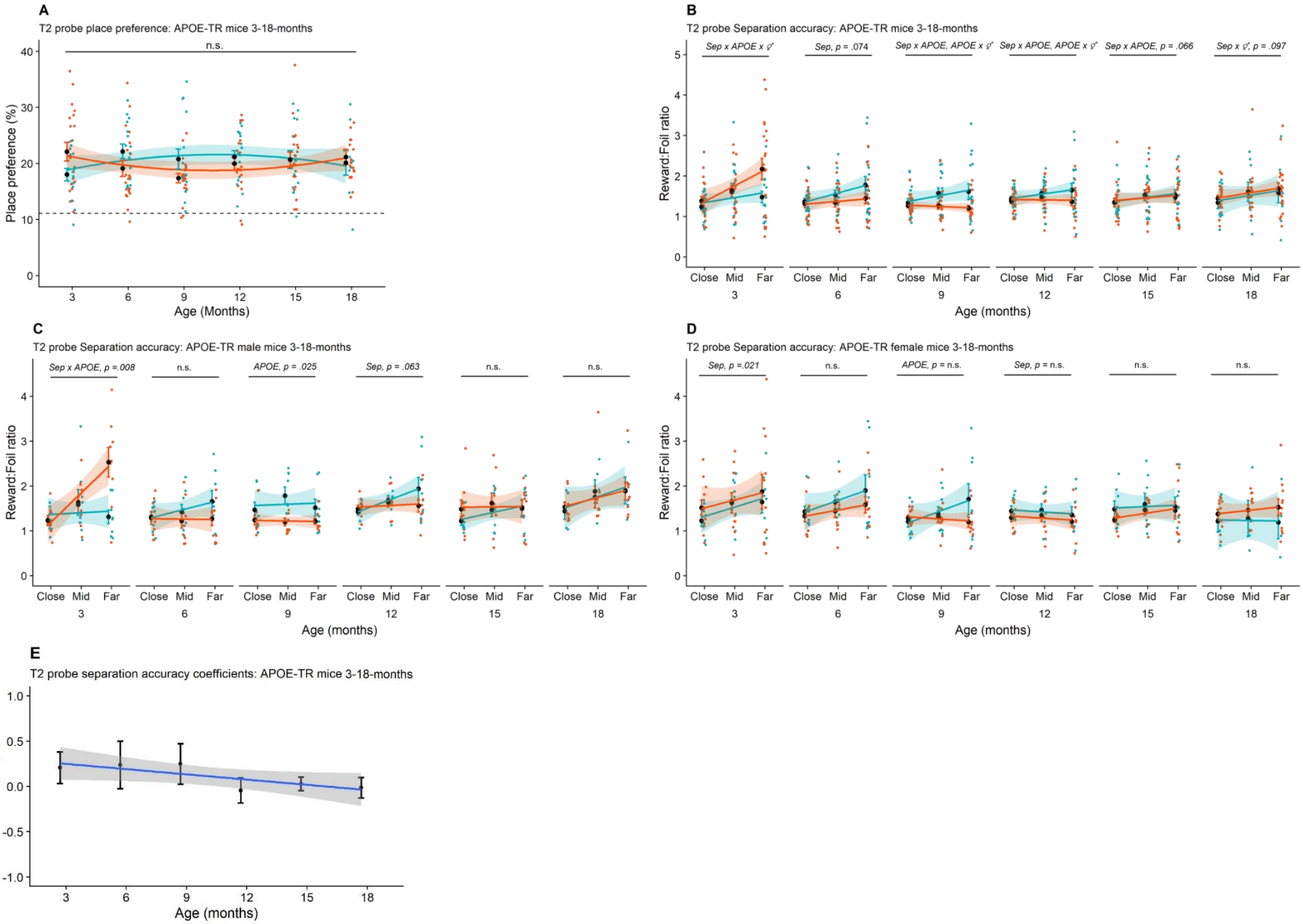
A
T2 probe place preference: APOE-TR mice 3-18-months
n.s.
Place preference (%)
Age (Months)
B
T2 probe Separation accuracy: APOE-TR mice 3-18-months
Sep x APOE x ♀
Sep, p = .074
Sep x APOE, APOE x ♀
Sep x APOE, APOE x ♀
Sep x APOE, p = .066
Sep x ♀, p = .097
Reward:Foil ratio
Close Mid Far
Age (months)
C
T2 probe Separation accuracy: APOE-TR male mice 3-18-months
Sep x APOE, p =.008
n.s.
APOE, p = .025
Sep, p = .063
n.s.
n.s.
Reward:Foil ratio
Close Mid Far
Age (months)
D
T2 probe Separation accuracy: APOE-TR female mice 3-18-months
Sep, p =.021
n.s.
APOE, p = n.s.
Sep, p = n.s.
n.s.
n.s.
Reward:Foil ratio
Close Mid Far
Age (months)
E
T2 probe separation accuracy coefficients: APOE-TR mice 3-18-months
Coefficient (ß)
Age (months)

Figure 4.4: Measures of retrieval performance in APOE-TR mice from 3-18 months. A) Average target place preference during T2 probe trials from 3-18 months grouped by APOE genotype. Individual points represent averages of three T2 probe trials for individual animals in preference for the target location. Dashed black line in A) represents chance performance (11.1%). B) Average reward:foil ratio (separation accuracy) during T2 probes from 3-18 months grouped by APOE genotype. Close, mid, and far foil categories are represented for each age. Individual points represent averages across three T2 probe trials for each measure within individual animals. Sex-specific grouping is shown for C) male, and D) female mice to represent analysis results of interaction terms. For clarity, significant main effects and interactions are represented by abbreviations and symbols: APOE = APOE genotype, ⚥= Sex, Sep = Separation. E) Whole group coefficient values for the effect of separation on reward:foil ratio (separation accuracy). Note the general reduction from 12-18-months of age. Error bars represent group mean +/- SEM or 95% CIs in E). Brackets and labels denote p-values of main effects, interactions or pairwise comparisons. "n.s." denotes no statistically significant effects of any comparison within a given time point. See Table 4.5.1 and 4.5.2 for details.

Table 4.5.1: Robust linear mixed model analysis of separation accuracy and place preference from 3-18 months in APOE-TR mice. Trial type, measure variable, independent variable, statistic, and corresponding figure are provided. Corresponds to Figure 4.4. Modelling of interaction terms at individual levels of age is presented in Table 4.5.2.

Measure	Trial type	Age	Variable	Coefficient	SE	CI lower	CI upper	*t*	*p*	FDR	Figure
Reward:foil ratio (separation accuracy)											
	T2 probe trials	3-18-months	Random intercept	0.19		0.13	0.26				
			Separation	0.32	0.09	0.14	0.50	2.57	0.001	s	
			Age (Quadratic)	0.09	0.04	0.02	0.16	1.26	0.008	s	
			Genotype	0.35	0.21	-0.07	0.78	0.99	0.101	ns	**4.4B-D**
			Sex	0.41	0.16	0.07	0.74	1.04	0.019	s	
			Separation*Age*Sex	0.09	0.02	0.05	0.14	1.93	<.001	s	
			Separation*Genotype*Sex	0.53	0.18	0.18	0.89	2.32	0.003	s	
			Age*Genotype*Sex	0.28	0.09	0.11	0.46	2.14	0.001	s	
Place preference (Target)											
	T2 probe trials	3-18-months	Random intercept	1.74		0.90	3.35				
			Age	-0.03	0.54	-1.10	1.05	-0.05	0.959	ns	**4.4A**
			Genotype	-0.72	2.19	-5.17	3.74	-0.27	0.745	ns	
			Sex	-1.55	1.98	-5.57	2.48	-0.54	0.440	ns	

Table 4.5.2: Robust linear mixed model analysis of separation accuracy at individual ages from 3-18-months in APOE-TR mice. Trial type, measure variable, independent variable, statistic, and corresponding figure are provided. Individual models are presented for each age, alongside relevant simple main effect (SME) follow-up of significant interaction terms. Corresponds to Figure 4.4.

Measure	Trial type	Age	Variable	Coefficient	SE	CI lower	CI upper	*t*	*p*	SME	Statistic	FDR	Figure
Reward:foil ratio (separation accuracy)													
	T2 probe trials	3-months	Intercept	1.09	0.13	0.83	1.36	3.40	0.000				
			Separation	0.21	0.09	0.03	0.38	1.68	0.020			s	
			Genotype*Sex	-1.07	0.35	-1.79	-0.35	-1.75	0.005			s	
			Separation*Genotype	0.65	0.24	0.17	1.12	2.74	0.008			s	
										Males-Far: Genotype	F(1,15) = 11.69, p = <.001	s	
										Females: Separation	t(51) = 1.77, p = .021	ns	
		6-months	Intercept	1.18	0.17	0.84	1.52	5.10	0.000				
			Separation	0.24	0.13	-0.02	0.50	2.79	0.074			ns	
		9-months	Intercept	0.93	0.06	0.81	1.05	4.65	0.000			s	
			Separation	0.25	0.11	0.03	0.47	3.46	0.029			s	
			Genotype	0.43	0.09	0.25	0.61	1.64	0.000			s	
			Sex	0.61	0.23	0.14	1.08	2.16	0.013			s	
			Genotype*Sex	-0.72	0.29	-1.31	-0.14	-1.91	0.016			s	
										Males: Genotype	t(47) = -2.28, p = .025	s	**4.4B-D**
										Females: Genotype	t(53) = -0.77, p = .456	ns	
			Genotype*Separation	-0.30	0.12	-0.53	-0.06	-3.11	0.015			s	
										E3s: Separation	t(44) = 2.13, p = .082	ns	
										E4s: Separation	t(56) = -0.89, p = .407	ns	
		12-months	Intercept	1.51	0.14	1.23	1.79	8.60	0.000				
			Sex*Separation	0.30	0.15	0.01	0.59	3.27	0.045			ns	
										Males:Separation	t(47) = 2.50, p = .063	ns	
										Females:Separation	t(53) = -1.37, p = .243	ns	
		15-months	Intercept	1.48	0.19	1.10	1.86	6.43	0.000				
			Genotype*Sex	0.71	0.37	-0.05	1.47	1.70	0.066			ns	
		18-months	Intercept	1.26	0.18	0.89	1.63	3.94	0.000				
			Sex*Separation	0.24	0.14	-0.05	0.53	1.71	0.097			ns	

4.3.3 Rapid place learning reinforcement and extended retrieval delay in APOE-TR mice across the lifespan

4.3.3.1 Acquisition during manipulation trials

T5 probe trials were performed at the 3 and 18-month time points, and the learning index was analysed to assess the influence of extended reinforcement on performance across groups and age. During T5 probe trials at both 3 and 18-months, there was no significant effect of genotype or sex on learning index and no significant interactions, with near identical performance between both genotypes and sexes, indicating extended reinforcement from a single trial to four did not discriminate between groups (Figure 4.5A).

Investigating the influence of retrieval delay on acquisition performance following single trial experience, extended ITI trials between T1 and T2 at 4-hours and 12-hours were performed at 6-18-month time points. Analysis of T2 errors during variable ITI trials allowed the effect of delayed retrieval on the first recall trial to be studied. Linear models for T2 errors after a 4-hour ITI demonstrated a significant main effect of genotype, a sex by genotype interaction, and a genotype by age interaction (Table 4.6). These interactions did not pass FDR correction, although exploratory analysis demonstrated a significant effect of genotype in male but not female mice, with E4-TR males generally making fewer errors during T2 following a 4-hour ITI than E3-TR male controls independent of age (Figure 4.5B, Table 4.6).

With a 12-hour delay between T1 and T2, there were no significant main effects or interactions between APOE genotype, sex, and ageing on T2 errors (Figure 4.5C, Table 4.6). However, exploratory analyses comparing search errors across 4-hour and 12-hour ITI trials revealed a general age-dependent deficit in overall within-day learning. Specifically, analysing search errors at individual time points revealed a failure to improve within-day performance, with a lack of a main effect of trial number at 12 and 18-months following a 4-hour ITI and 9, 12, and 18-months following a 12-hour ITI delay (Supplementary table 4.4). This suggests that extension of the ITI to 4-12-hours resulted in an overall reduction in within-day learning at later time points at the whole group level but did not distinguish between genotype and sex groups.

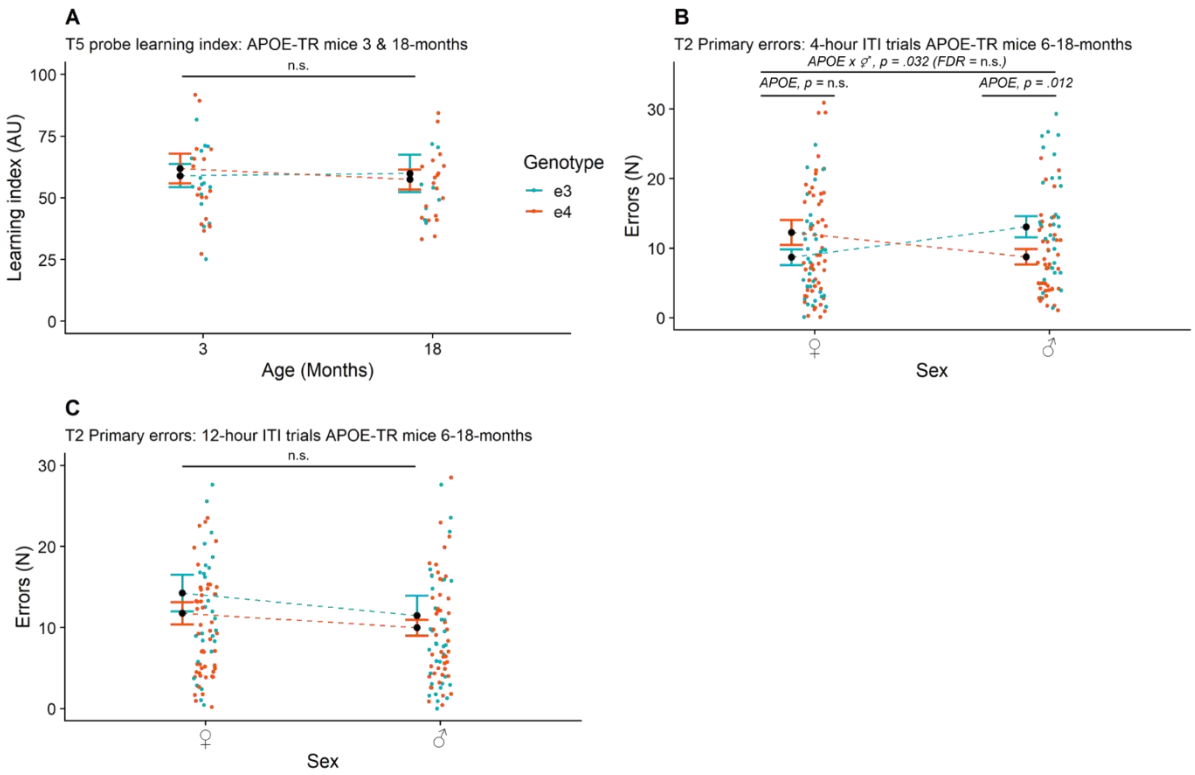

Figure 4.5: Acquisition performance during manipulation trials in APOE-TR mice. A) Average learning index across T2-T5 during T5 probe trial days conducted at 3 and 18-months. B) Errors during T2 only in 4-hour ITI trials and C) 12-hour ITI trials from 6-18-months. Individual points in A) represent learning index scores of individual animals averaged across trial replicates while individual points in B) and C) represent errors across replicates for individual animals at each time point from 6-18-months (note that statistical analysis itself was nested by subject but data is represented unnested here to demonstrate distribution). Error bars represent group mean +/- SEM. Brackets and labels denote p-values of main effects, interactions or pairwise comparisons (see main text and Table 4.6 for details). "n.s." denotes no statistically significant effects of any comparison within or a given time point. Sex grouping is represented by "♀" and "♂" overlay.

Table 4.6: Robust linear mixed model analysis of learning index and T2 errors during T5 probe and 4/12-hour ITI manipulation trials from 3-18 months in APOE-TR mice. Trial type, measure variable, independent variable, statistic, and corresponding figure are provided. Corresponds to Figure 4.5.

Measure	Trial type	Age	Variable	Coefficient	SE	CI lower	CI upper	*t*	*p*	SME	Statistic	FDR	Figure
Learning index (LI)													
	T5 probe trials	3-months	Random intercept	10.58		2.34	47.85						
			Age	0.89	6.06	-11.59	13.38	0.08	0.884			ns	**4.5A**
			Genotype	16.34	16.99	-18.28	50.95	0.83	0.344			ns	
			Sex	-15.72	15.40	-47.10	15.65	-0.73	0.315			ns	
Errors (T2)													
	4-hour ITI trials	6-18-months	Random intercept	-1.05		5.01	11.07						
			Genotype	8.53	3.80	0.79	16.27	2.10	0.032			ns	
			Age*Genotype	-2.22	0.93	-4.06	-0.37	-1.77	0.019			ns	**4.5B**
			Genotype*Sex	-10.61	4.74	-20.26	-0.95	-1.82	0.032	Males: Genotype	t(15) = -2.81, p = .012	ns	
										Females: Genotype	t(17) = 1.14, p = .204	ns	
	12-hour ITI trials	6-18-months	Random intercept	1.83		0.19	17.52						
			Age	1.09	2.05	-2.97	5.15	0.92	0.597			ns	**4.5C**
			Genotype	3.41	5.31	-7.40	14.23	0.74	0.525			ns	
			Sex	1.63	6.56	-11.74	14.99	0.32	0.806			ns	

4.3.3.2 Retrieval during manipulation trials

Place preference and separation accuracy during the T5 probe trials was analysed to establish potential retrieval effects between groups following extended reinforcement. Linear modelling of place preference during T5 probe trials revealed main effects of both sex and age, and two-way interactions between age and genotype, age and sex, and genotype and sex. A significant three-way interaction was also observed between age, genotype, and sex (Table 4.7). Post-hoc analysis, generating robust linear models at individual age points, demonstrated significant sex by genotype interactions in place preference at both 3 and 18-months, and main effects of sex and genotype at 18-months, although the interaction at 3-months did not pass correction (Figure 4.6A, Table 4.7). At 18-months, the sex by genotype interaction was driven by a significant effect of genotype in female but not male mice, with E4-TR females showing greater place preference than their E3-TR counterparts (Figure 4.6B, Table 4.7)

Separation accuracy during T5 probe trials demonstrated a significant effect of separation, with animals showing greater discrimination between foils further from the target at both 3 and 18-month time points. Additionally, there was a significant interaction between age and sex, but this did not pass FDR correction. Analysis by individual time points demonstrated no effect of sex at 3-months and only a trend to an effect of sex at 18-months, with male mice discriminating non-target foils more accurately than female controls. (Figure 4.6C, Table 4.7).

Importantly, we noted that the age-dependent reduction in the effect of separation observed in T2 probe trials from 12-18-months (described in section 4.3.2) was ameliorated in 18-month aged mice by increasing the number of encoding trials prior to the probe trial. Namely, during T5 probe trials, mice significantly discriminated foils dependent on distance from the target with an increase in the effect separation (coefficient), while they did not during T2 probe trials (Figure 4.6D; Supplementary Table 4.3).

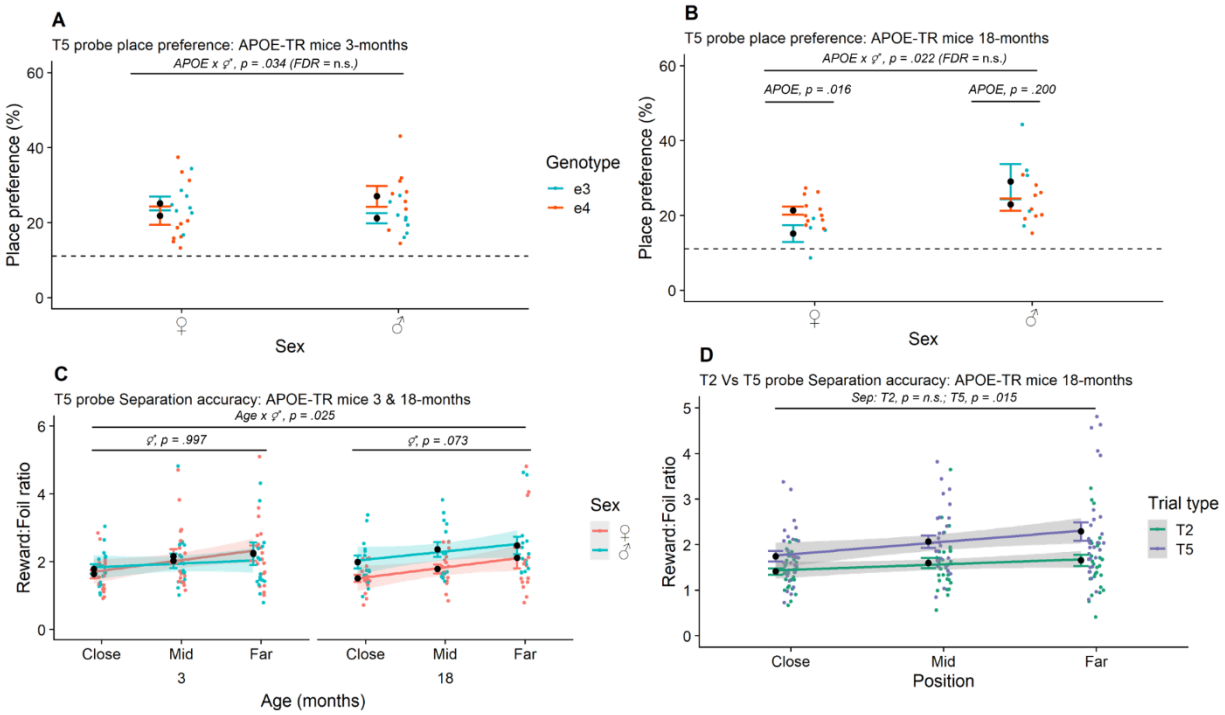

Figure 4.6: Retrieval performance during manipulation trials in APOE-TR mice. A) Average place preference during T5 probe trials conducted at 3-months and B) 18-months grouped by genotype and sex. C) Average Reward:Foil ratio (separation accuracy) during T5 probe trials at 3 and 18-months grouped by sex and age. D) Average separation accuracy during T2 and T5 probe trials at 18-months, grouped by trial type. Individual points represent averages of three T2 or T5 probe trials for each measure within individual animals. Error bars represent group mean +/- SEM. Brackets and labels denote p-values of main effects, interactions or pairwise comparisons (see main text and Table 4.7 for details). "n.s." denotes no statistically significant effects of any comparison within or between time points. Black dashed line represent chance performance (11.1%) Age grouping is represented by overlay in C).

Table 4.7: Robust linear mixed model analysis of place preference and separation accuracy during T5 probe trials from 3-18 months in APOE-TR mice. Trial type, measure variable, independent variable, statistic, and corresponding figure are provided. Corresponds to Figure 4.6.

Measure	Trial type	Age	Variable	Coefficient	SE	CI lower	CI upper	*t*	*p*	SME	Statistic	FDR
Reward:foil ratio (separation accuracy)												
	T5 probe trials	3-18-months	Random intercept	0.47		0.34	0.65					
			Separation	0.47	0.20	0.06	0.87	1.11	0.023			ns
			Sex	-0.99	0.50	-2.00	0.02	-0.76	0.055			ns
			Age*Sex	0.95	0.42	0.12	1.78	1.07	0.025			ns
										3-months: Sex	t(34) = 0.01, p = .997	ns
										18-months: Sex	t(27) = 1.85, p = .073	ns
Place preference (Target)												
	T5 probe trials	3-18-months	Random intercept	1.70		0.20	14.49					
			Age	-10.17	2.91	-16.17	-4.18	-2.65	0.002			s
			Genotype	-12.88	6.60	-26.32	0.56	-1.88	0.060			ns
			Sex	-22.07	5.70	-33.67	-10.46	-2.93	0.001			s
			Age*Genotype	9.62	3.98	1.42	17.81	2.07	0.023			s
			Age*Sex	18.11	4.75	8.32	27.90	3.46	0.001			s
			Genotype*Sex	30.83	9.20	12.10	49.56	3.15	0.002			s
			Age*Genotype*Sex	-21.69	6.16	-34.38	-9.00	-3.32	0.002			s
										3-months: Genotype*Sex	t(34) = 1.97, p = .034	ns
										18-months: Genotype*Sex	t(34) = -2.62, p = .022	s
										18-months males: Genotype	t(12) = -1.50, p = .200	ns
										18-months females: Genotype	t(13) = 2.70, p = .016	s

4.3.3.3 Locomotion speed during training

Finally, to control for potential differences in general ambulatory behaviour and locomotion capacity, we compared movement velocity across age. A mixed linear model was generated based on average velocity during training trials for each age. Overall, male mice showed faster locomotion, with a main effect of sex, however this did not pass FDR correction. There was also a significant interaction between age and sex, whereby age in male, but not female APOE-TR mice, predicted a significant increase in movement velocity (Figure 4.7, Table 4.8). This age-dependent skew in movement velocity provided further support for using path length and errors as primary measures as opposed to latency. Although significant, the increase in movement velocity in male mice was small, increasing by only an average of ~2cm/s across the lifespan (Figure 4.7, Table 4.8).

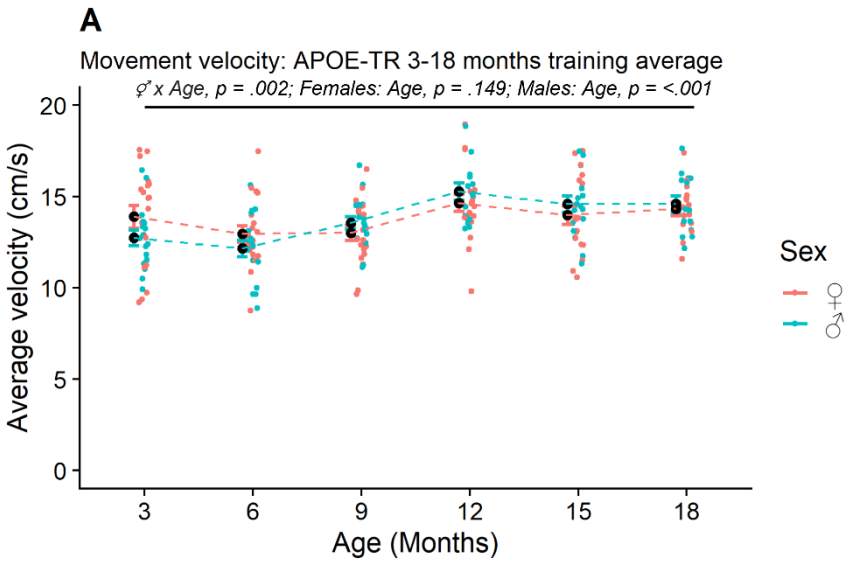

Figure 4.7: A) Average movement velocity during training in APOE-TR mice from 3-18-months. Individual points represent averages across days of training within a time point for individual animals. Error bars represent group mean +/- SEM. Brackets and labels denote p-values of main effects, interactions or pairwise comparisons (see main text and Table 4.8 for details). "n.s." denotes no statistically significant effects of any comparison within or between time points.

Table 4.8: Robust linear mixed model analysis of movement velocity during training from 3-18 months in APOE-TR mice. Trial type, measure variable, independent variable, statistic, and corresponding figure are provided. Corresponds to Figure 4.7.

Measure	Trial type	Age	Variable	Coefficient	SE	CI lower	CI upper	*t*	*p*	SME	Statistic	FDR	Figure
Movement velocity													
	Training (D1-8)	3-18-months	Random intercept	1.09		0.75	1.60						
			Sex	-2.05	0.84	-3.75	-0.34	-2.06	0.020			s	
			Age*Sex	0.65	0.20	0.25	1.05	2.88	0.002			s	**4.7**
										Males: Age	t(81) = 6.57, p = <.001	s	
										Females: Age	t(89) = 1.81, p = .149	ns	

4.4 Discussion

Chapter four aimed to assess the effect of APOE isoform on rapid place learning and memory performance, analogous to 'everyday memory', in APOE-TR mice across the lifespan. Using the mBM task, developed in Chapter three, we assessed APOE-TR mice from 3 to 18-months of age at 3-month intervals, thus characterising trajectories of rapid place learning and memory performance longitudinally in a single cohort of animals.

We hypothesised that E4-TR mice would demonstrate trajectories of earlier decline in both acquisition and retrieval of rapid place memory relative to E3-TR controls, which would be exacerbated in female mice. The results of the longitudinal assessment predominantly do not support these hypotheses, demonstrating complex sex and genotype interactions across age in measures of acquisition and retrieval. A summary of the results of these experiments is provided in Table 4.9.

4.4.1 Rapid place learning acquisition performance across the lifespan of APOE-TR mice

Linear mixed models were conducted on acquisition measures of path length and search errors during training and probe trials. Errors but not path length, appeared sensitive to our primary variables of age, sex, and APOE genotype. Namely, while there was only significant effects of age and trial number in path length, for errors there were significant main effects of age, trial number, sex, and genotype, alongside multiple two-way interactions and a three-way interaction between age, genotype and sex. These interactions in errors were investigated by generating individual linear models for each age. This revealed an effect of sex at 3-months and a trend at 6-months, where male mice outperformed females, making fewer errors across all trials. While no differences were observed at 9-months, at 12 months a significant interaction between genotype and sex, revealed impairments in female E4-TR mice making a greater number of errors relative to female E3-TR controls, which was only a trend at 15 months. In contrast, male mice displayed opposing trends at 12-15-months, with E4-TR male mice slightly outperforming E3-TR male controls. No group differences were observed at 18-months, however.

Comparing errors and path length across trials to measure learning was confounded by changes in the performance in the first trial of the day (T1), where animals initially search for

the rewarded location. T1 path length significantly decreased across age and T1 errors were significantly lower overall in E4-TR mice. This may indicate changes in initial search strategy between groups, however it confounds inclusion of T1 in measures of learning. To avoid the confound of unequal T1 trial path length and errors, we developed a learning index. The learning index comprised search errors from T2-T4 reflecting retrieval trials, which were weighted in a linear fashion, such that the learning index was sensitive to errors early during acquisition. Analyses of the learning index revealed similar results to that observed in overall search errors. Age and sex impacted performance, with overall higher learning index (reflecting poorer performance) in female mice, while showing a quadratic function across age, initially decreasing then increasing from mid-old age. These effects were mediated by a three-way interaction between genotype, age, and sex. Modelling at individual ages revealed female mice and E4-TR mice performed poorer at 3-months relative to male and E3-TR mice, while at 6-months only the effect of sex persisted with male mice outperforming female mice. Performance then converged at 9-months, with no differences in learning index between groups. At 12-months there was an interaction between genotype and sex, driven by poorer performance in female but not male E4-TR mice relative to E3-TR controls, with a similar trend observed at 15-months. Finally, at 18-months there were no main effects or interactions between genotype and sex in learning index.

When analysing potential between-day learning effects, we observed differences between early and late learning index (Days 1-2 Vs Days 7-8). Specifically, there were effects of age, and sex on learning index, alongside the three-way interaction between age, genotype, and sex. Increasing age predicted an increase in between day learning in E3-TR but not E4-TR male but not female mice. We noted that despite no interaction with genotype in female mice, that between day learning in both female and male E4-TR mice was relatively static across age whereas E3-TR mice appeared to decrease or increase in females and males respectively. This likely reflects mild differences task learning between groups across age.

4.4.2 Rapid place memory retrieval across the lifespan of APOE-TR mice

Across all ages, APOE-TR mice demonstrated robust place preference for the target location during T2 probe trials that was significantly above chance, demonstrating consistent retrieval of the reward location from a single trial experience. However, preference for the target alone during T2 probe trials was not significantly affected by age, sex, or genotype, suggesting that,

at the least, preference for specifically the target location did not differ between groups. However, we observed that groups did differ in the relative accuracy of this preference relative to non-target foils as a function of separation (distance) from the target. Separation accuracy (or Reward:Foil ratio) was calculated as a ratio of the accuracy of spatial memory retrieval for the reward relative to surrounding foils. Multiple three-way interactions in separation accuracy led us to model the effects at individual ages. At 3-months, male, but not female, E4-TR mice showed increased separation accuracy at the furthest foil category, suggesting greater discrimination of the target from far foils relative to E3-TR male controls. At 6-months this effect was no longer present, with equivalent performance across groups. At 9-months a significant interaction between genotype and sex became apparent, with male but not female E4-TR mice showing an overall deficit in discrimination across all foil categories (a trend which we had observed at 6 months). By 12-months, genotype differences were no longer observed but a sex by separation interaction became apparent, with greater separation accuracy for far versus near foils in male but not female mice. At 15-18-months some trends remained but there were no significant differences between groups.

Importantly, modelling the coefficients of the separation effect across the lifespan demonstrated that separation accuracy decreased with age, and from 12-18-months, the effect of separation was weak or non-significant. This may suggest a general effect of ageing on separation accuracy performance following single trial learning, with decreasing accuracy from mid age. Supporting this, we observed a significant effect of separation (i.e., greater discrimination of close from far foils) on separation accuracy during T5 probe trials at both 3 and 18-months (Supplementary Table 4.3), with an increase in the coefficients. This suggested that the age-dependent deficit in separation accuracy could be ameliorated by increasing the number of preceding encoding events (or ‘reinforcements’).

4.4.3 Rapid place learning and memory during variable ITI and reinforcement trials

During acquisition in T5 probe trials there were no significant age, sex or genotype differences at 3 or 18-months, as measured by learning index. However, in retrieval measures, alongside the overall increase in separation accuracy during T5 probe trials at the whole group level, there was an interaction between age and sex. Post-hoc analysis revealed a trend for male mice to outperform female mice at 18-months. In place preference, however, there were

multiple two-way interactions and a three-way interaction between genotype, sex, and age in place preference for the target alone during T5 probe trials. This interaction was driven by significant sex and genotype interactions at 3 and 18-months, although the effect at 3-months did not pass correction. At 18-months, female E4-TR mice showed significantly higher place preference for the target than E3-TR female controls, although we note the caveat that the E3-TR female group size was particularly reduced at 18-months due to attrition.

Between 6-18 months, we introduced trials varying the ITI between T1 and T2 to 4 and 12-hours to assess potential delay-dependent effects of APOE genotype, sex, and age on performance. Following a 4-hour ITI, there was a significant sex by genotype interaction independent of age in T2 errors, with overall E4-TR males outperforming E3-TR controls on average (across the 6-18-month average), but no effect in female mice. After an extended 12-hour ITI, there were no effects of primary variables on acquisition performance, however.

Finally, we observed mild effects of sex and age on average velocity during training and probe trials, with male mice significantly increasing running speed on the maze across age but no difference in female mice. We note that this difference, while significant, is particularly small and with the use of latency-independent measures likely has negligible impact on the present results.

4.4.4 Results summary

Overall, these findings highlight complex interactions between APOE genotype, sex, and ageing in acquisition and retrieval of rapid place memory. Number of errors during search for the target and a learning index composite of retrieval trials held sensitivity to detect these effects. The results generally suggest a mild early life impairment in rapid acquisition but not retrieval in E4-TR mice, predominantly in males, which is not present following extended reinforcement. Despite this, at 6-months this genotype difference was no longer present, and at late-age (12-15 months) E4-TR males began to trend towards advantages in acquisition whereas female E4-TR mice showed impairments. These deficits may represent a premature ageing-like phenotype in E4-TR female mice, however by 18-months performance across genotypes was again similar. Notably E3-TR but not E4-TR male mice demonstrated a linear increase in performance across days of training (between day learning) as they age. This may suggest differences in task rule between groups.

In contrast, when analysing memory retrieval measures, place preference following single trial experience was consistently above chance across the lifespan of APOE-TR mice. However, performance by separation accuracy varied across groups and age, with E4-TR male mice showing a transient advantage at a young age, before a specific deficit in mid age and group convergence from 12-18-months with overall poor separation accuracy following single trial experience.

Table 4.9: Summary of results of Chapter four. Phase (acquisition, retrieval, trial type and ITI) is provided across primary measure variables, represented across age from 3-18-months, with main effects/interactions of interest represented symbolically. In each case ">" represents greater performance than or "<" poorer performance than, across metrics. Therefore, in all measures 'X > Y' corresponds to performance of group 'X' was greater than performance of group 'Y'.

Phase	Measure	Age					
		3m	6m	9m	12m	15m	18m
Acquisition (15m ITI)							
	Path	ND	ND	ND	ND	ND	ND
	Errors	M > F	M > F	ND	E3F > E4F; trend E4M > E3M	trend E3F > E4F; trend E4M > E3M	ND
	Learning index	M > F; E3 > E4	M > F	ND	E3F > E4F; trend E4M > E3M	trend E3F > E4F; trend E4M > E3M	ND
Acquisition (4-hour ITI)							
	Errors (T2)		E4M > E3M	E4M > E3M	E4M > E3M	E4M > E3M	E4M > E3M
Acquisition (12-hour ITI)							
	Errors (T2)		ND	ND	ND	ND	ND
Retrieval (T2, 15m ITI)							
	Place preference	ND	ND	ND	ND	ND	ND
	Separation accuracy	E4M > E3M	ND	E4M < E3M		Age decrease from 12-18m	
Retrieval (T5, 15m ITI)							
	Place preference	trend E4M > E3M					E4F > E3F
	Separation accuracy	ND					T5 > T2 accuracy; trend M > F

4.4.5 Interpreting dissociations between measures

4.4.5.1 Dissociation between path length and errors

Several key patterns of performance between measures and across age were particularly of note and complicate interpretation. Firstly, the dissociation between path length and errors during acquisition across age was surprising. While search errors were sensitive to sex and genotype effects across age, path length was not. This may be accounted for by the search behaviour of animals, in which while similar path efficiencies may occur, changes in the number of local search errors made may increase in a given trajectory. This suggests that errors reflect inaccurate search during target approach and overall reduced certainty of the spatial location of the reward.

4.4.5.2 Dissociation of acquisition and recall measures

The dissociation between measures of acquisition and recall between groups was also unexpected. While a correlation was observed at the whole group level between errors and place preference at 3-months, defects in multi-trial acquisition did not co-occur with deficits in one-trial place memory and vice versa across groups. Namely in E4-TR males, at 3-months a deficit in acquisition was accompanied by an advantage in separation accuracy, whereas at 9-months comparable acquisition accompanied a deficit in separation accuracy. Also, an acquisition deficit in E4-TR females at 12-months and a trend at 15-months were observed without cooccurring changes in retrieval measures. These results may suggest the measures hold sensitivity to different spatial learning processes, that are differentially affected by APOE genotype, such as the accuracy of spatial recall across multiple trials relative to single-trial learning.

Specifically, the accuracy of initial wayfinding (navigation), as measured by errors and learning index during rewarded trials, did not always appear predictive of certainty of spatial location, as measured by place preference and separation accuracy, during the probe trials. Place preference requires target reapproaching and local search, which is better supported by allocentric place representations, while initial wayfinding can be supported by a combination of allocentric and egocentric representations or more diffuse allocentric information such as relative distance from a starting position (Buckley & Bast., 2018; Gallagher et al., 2015;

Vorhees et al., 2014; Illouz et al., 2020). Therefore, a deficit in separation accuracy but conserved initial wayfinding may reflect conserved relative spatial path information from the start point such as the distance to the target, but an impairment of the allocentric representation. This may explain a reduced accuracy in recall and thus poorer distinction between foil separation categories during revisiting behaviour following single-trial experience, but preserved initial navigation across multiple reinforced trials.

Indeed, research in rodent and human models of spatial memory and navigation have suggested that wayfinding acquisition and place preference accuracy during recall may represent behaviourally and neurophysiologically distinct components of memory. Specifically, place preference has been shown to be more sensitive to hippocampal function than primary wayfinding measures, with hippocampal lesions having a greater impact on place preference measures (e.g., McGarrity et al., 2017; Bast et al., 2009; De Hoz et al., 2005; Zhang et al., 2004; Sprague et al., 2003; Morris et al., 1990). This behavioural dissociation may suggest that APOE genotype differentially affects rapid place recall and navigation functions across age.

Thus, APOE4 may mediate early impairments in multi-trial wayfinding (e.g., search errors and learning index) followed by similar performance at adult maturity, before mild deficits in female mice at mid-age and similar performance in males. APOE4 may, in contrast, confer advantages in one-trial separation accuracy in young male mice, followed by premature age-related deficits in separation accuracy at mid age, and comparable performance in old age which may reflect a generic ageing effect.

Additionally, the lack of APOE genotype differences in separation accuracy following increased reinforcement during T5 probe trials at 3-months suggest that rapid place memory retrieval differences between E3-TR and E4-TR mice are particularly subtle and likely dependent on the challenging condition provided by single trial encoding. This explanation may account or some variability in findings in APOE-TR mice which use single or multiple trial acquisition approaches (e.g., single trial spatial object recognition or multi trial alternation tasks; see section 1.6). The question remains whether increasing reinforcement to the point of sustaining task performance but increasing retrieval delay would differentially affect the forgetting function in APOE-TR mice, although we note that studies of reference memory retention in APOE-TR mice suggest deficits after 24-72-hour delays in well reinforced reference memory (e.g., five days with up to four trials per day; Leung et al., 2012). Further study should focus on the replication and expansion of the present results particularly at early-mid age in the context of the effect of encoding reinforcement and recall delay in APOE-TR mice.

4.4.6 Normative performance and age-related decline in everyday learning and memory

The results at the whole group level from Chapter four are predominantly consistent with previous research investigating everyday memory using rapid place learning and memory maze tasks across age in rodent models. For example, robust one-trial acquisition and recall has been observed in rodents in the appetitive event arena and aversive Barnes maze, MWM, and radial arm mazes following matched or comparably short delays of 15-60 minutes, which is typically thought sufficient to involve hippocampal function (Steele and Morris et al., 1999; Diamond et al., 1999; Shukkit-Hale et al., 2004; Bast et al., 2005; Bast et al., 2009; Wang et al., 2010; Faizi et al., 2012; Takeuchi et al., 2016; Feng et al., 2017; Broadbent et al., 2020). Further, the reinforcement-dependent effect on memory strength was also observed in the mBM task, consistent with demonstrations in both the event arena and MWM (Nonaka et al., 2017; Wang et al., 2010; Bast et al., 2009), for example with increasing trial numbers and reward pellets enhancing recall accuracy. Delay dependent forgetting of one trial experience is also reported in such tasks, albeit in the current experiment 4-hour and 12-hour ITIs were only sufficient to induce deficits in within-day learning at 12+ months at the whole group level, suggesting the need to extend the ITI probe tests to 24-hours to assess everyday forgetting in younger animals (e.g., Takeuchi et al., 2016; Da Silva et al., 2014).

Multiple studies have demonstrated age-dependent deficits spatial reference memory tasks such as the Barnes maze task in WT rodents (Barnes et al., 1979, 1985; Bach et al., 1999; Kennard et al., 2011; Feng et al., 2017), with some demonstrations of age-dependent deficits in acquisition as early as 12-months (Bach et al., 1999). In DMTP rapid place variants, acquisition deficits have also been reported across age from 12-20 months in WT rodents (Frick et al., 1995; Magnusson et al., 2003; Feng et al., 2017; Krukowski et al., 2020; Febo et al., 2020) or AD transgenic mice (Faizi et al., 2012). One study demonstrated only a mild age-dependent impairment in rapid place learning in the MWM DMTP task which was delay-dependent, with appreciable deficits in acquisition between 6-12-18-months most apparent at short 5-minute rather than 30-minute delays (Febo et al., 2020). Notably, when comparing performance at the whole group level in the mBM, we observed age-dependent deficits in one-trial place learning and overall acquisition following 4-12-hour ITI delays, but relatively stable within-day learning with a standard 15-minute ITI. This highlights the importance of characterisation of delay-dependent forgetting as a manipulation of task demand or difficulty to achieve more comprehensive assessments of episodic-like memory in rodent models.

Further characterisation studies of normative ageing in wild-type mice will be needed to assess baseline, delay-dependent and age-dependent effects on acquisition and retrieval performance in the mBM task.

Age-dependent deficits in pattern separation-like ability have also been reported in WT mice, with deficits observable as early as 11-months in C57-WT mice using a spatial separation object preference task and object similarity tasks (Ces et al., 2018), 17-months in a contextual separation task (Wu et al., 2015) and 22-months in an operant spatial separation task (Creer et al., 2010). Additionally, object pattern separation tasks have been suggested to be particularly sensitive to MCI-related cognitive impairments in aged human patients (e.g., Yassa et al., 2011; Stark et al., 2013; Tran et al., 2017). In the present study, we typically observed that APOE-TR mice exhibited stable place preference but an age-dependent deficit in distinguishing close from far foils from 12-18-months which we propose represents a putative measure of pattern separation-like performance. The positive influence of reinforcement on overall accuracy and strength of separation is also important to consider and further characterisation of responses across increasing acquisition trials in WT animals in the mBM is needed, although notably we observed a similar trial enhancement effect in WT and APOE-TR mice at the 3-month baseline. For a greater detailed profile of separation accuracy in the APOE-TR model, further work should aim to assess a range of encoding-retrieval schedules. Additionally, characterisation of proactive interference in separation accuracy and flexibility could also plausibly be assessed using the adapted Barnes maze, with similar adaptations to previous reports (e.g., Prut et al., 2007; O'Leary et al., 2009; Riedel et al., 2018).

4.4.7 Interpretations within the current framework of the APOE isoform-dependent influence on spatial learning and memory in the APOE-TR mouse model

In the literature surrounding performance of APOE-TR mice in maze tasks probing spatial reference memory and rapid place learning, there is significant variability in findings. Both co-occurring and dissociated deficits in acquisition and retrieval have been observed in E4-TR mice during reference memory tasks (e.g., Andrews-Zwilling et al., 2010; Leung et al., 2012; Rodriguez et al., 2013; Speidell et al., 2019; Peris-Sampedro et al., 2015; see section 1.6 for a summary and discussion).

Our results suggest that E4-TR mice may be impaired in multiple trial raid learning of a novel spatial location at 3-months, which is consistent with previous reports of reference memory acquisition deficits at the similar ages in the Barnes maze (Rodriguez et al., 2013; Speidell et al., 2019) although there were conflicting findings in the MWM (Reverte et al., 2012, 2013; Grootendorst et al., 2005). However, we did not observe an APOE4-dependent deficit in retrieval measures as sometimes reported, instead we observed a mild advantage in E4-TR males in recall accuracy of the target from further foils, at least following single trial experience as opposed to reference memory. Our results also contrast with that reported at a similar age (~4-months) using the rapid place learning DMTP MWM task, which found no overall T1-T2 task learning in APOE-TR mice across genotypes at a shorter delay (5-minutes) than that used in the current experiments (15-minutes), although notably this previous study did not assess retrieval performance using probe trials following single-trial experience (Grootendorst et al., 2005). This, in combination with our observations, suggests that E4-TR at young age show deficits in spatial learning across single-day rapid learning or multiple days reference learning, while retention and retrieval of this spatial memory may only be impaired by APOE4 over longer retention periods (i.e., reference memory; 24-hours and above).

Additionally, the lack of genotype differences at 6-9-months in acquisition is comparable to some recent reports showing no differences between APOE-TR mice using both the Barnes maze and MWM reference memory tasks (Guardia-Escote et al., 2018; Shinohara et al., 2016; Villasana et al., 2016; Hayley et al., 2012), while some others show E4-TR specific deficits others (e.g., Speidell et al., 2019; Peris-Sampedro et al., 2015). Further, the lack of overall deficit in E4-TR mice in place preference at 6-9-months in the current data consistent with a host of reports suggesting an E4-TR female deficit in long term retrieval only at later age (e.g., Leung et al., 2012; Knoferle et al., 2014; Tong et al., 2013, 2016) or across sexes (Shinohara et al., 2016), while other reports suggest earlier APOE4-specific retrieval deficits (e.g., Villasana et al., 2006; Guardia-Escote et al., 2018; Basaure et al., 2019). However, the deficit we observed in separation accuracy at 9-months in E4-TR males may support a premature ageing effect of APOE4 on spatial memory retrieval accuracy. One interpretation of the conflict in findings between reports at this age point is that it reflects variability in the detectability of an age-dependent 'tipping point' between sustained spatial learning and memory performance and APOE4-related impairment.

At later age, the deficit we observed in acquisition in E4-TR female mice at 12-15 months is also mostly consistent with reference memory data (e.g., Rodriguez et al., 2013; Pontifex et al.,

2021; Leung et al., 2012), however we did not detect this effect at 18-months which may have been due to limited power by our reduced group size at this time point. In contrast, the lack of place preference differences we reported between 12-18-months in APOE-TR mice is less consistent with the reference memory literature, with late-age deficits in long-term retrieval suggested to be predominantly observed in E4-TR female mice (e.g., Grootendorst et al., 2005; Leung et al., 2012; Knoferle et al., 2013; Jones et al., 2019), although sometimes in E4-TR mice of both sexes (e.g., Shinohara et al., 2016). However, the size of the impairment in rapid acquisition we observed in E4-TR females appears subtle and therefore suggests that the influence of APOE4 on long term reference memory consolidation is greater than that of rapid place learning, at least with our current experimental design (i.e., with four-five trials at 15-minute trial delays).

In conjunction, we observed an overall deficit in separation accuracy from 12-18 months at the whole group level in the present data. Further, with the extension of reinforcement to four trials preceding the memory recall probe trial, we observed recovery of the separation effect in 18-month aged mice, but there were no differences observed by APOE genotype at 18-months. We suggest that this reflects comparable rapid place memory retrieval accuracy and putative pattern separation-like behaviour at late age between APOE-TR mice following relatively low reinforcement. The question remains, however, whether separation accuracy may be altered in APOE-TR mice following multi-day reference memory reinforcement regimes requiring long term consolidation. In any case, our results, in conjunction with prior literature, appears to suggest that APOE4-dependent deficits in episodic-like memory are more pronounced in long term reference memory than and only subtle in 'everyday memory' across the lifespan.

The present study is the first, to the authors knowledge, to systematically address rapid place learning and memory ability across the lifespan of APOE-TR mice. The results therefore contribute towards the characterisation of the influence of APOE genotype, sex, and ageing within APOE mouse models on spatial cognition and everyday memory. Additionally, the measures of putative spatial pattern separation assessed longitudinally support that memory retrieval accuracy varies as function of age.

It is difficult to dissect the specific cognitive component of rapid place learning and memory that may be affected by APOE genotype. However, the contrasting results between the present study and the long-term retrieval deficits in E4-TR mice observed previously may suggest that APOE4 results in an impairment in the consolidation of spatial episodic-like

memory in an allocentric (i.e., third-person spatial) reference frame, but may not impair encoding or updating of similar information over the short-term time frame such as one-to-four trial experience. However, it is not possible to definitively dissociate these possibilities from the current data, as it is possible that an APOE4-dependent impairment in either effective information encoding, consolidation or retrieval may underpin the observed effects. Such deficits may be expected to be characterised by proactive interference or simply a loss of the accuracy of encoded information necessary to support performance.

A recent study described a paradigm able to dissociate specific impairments in retrieval from encoding in multiple AD-mouse models using contextual fear conditioning, demonstrating recovery of fear memory upon optogenetic activation of a genetically tagged neuronal ensemble (Roy et al., 2016). Similarly, partial context reinstatement paradigms using brief retraining in the MWM demonstrated recovery of a spatial reference memory trace (place preference) despite preceding deficits in long-term retrieval in aged PDAPP (human APP-695Indiana) transgenic mice, suggesting retrieval impairment as opposed to loss or decay of the memory trace per-se. Additionally these mice demonstrated enhanced proactive interference across novel spatial locations in the DMTP MWM variant (Daumas et al., 2008). Future studies may dissect these possibilities in APOE-TR mice with use of such contextual fear conditioning paradigms and partial reinstatement paradigms.

Some studies have demonstrated advantages in healthy young human E4-carriers in a continuous performance attention and working memory task (Rusted et al., 2013) as well as greater working memory updating performance when under low but not high executive function demand by requiring repeated task switching in a word categorisation task (Atkinson et al., 2019). Additionally, faster responses in a visual working memory ‘N-back’ task have been observed in E3E4-heterozygous young adults but accompanied by overall reduced working memory accuracy (Sinclair et al., 2015). Further investigation of the influence of executive function demand on rapid place learning in the APOE-TR model may demonstrate whether this effect is conserved across species and whether performance differences in working memory extend beyond rapid place learning alone.

Finally, we note that the conflicting findings in previous studies of the cognitive performance of APOE-TR mice may be in part contributed to by a vast range of inconsistencies in behavioural testing parameters. Namely, the manipulation of trial reinforcement, ITIs, source of task motivation and ages tested are primary contributors to this inter-report variability. As the experiments in Chapter four have demonstrated, it is possible that such parameters alter

performance in APOE-TR mice and as such these parameters should be systematically explored when characterising spatial learning and memory performance in APOE mouse models in both rapid place learning and reference memory tasks.

4.4.8 Neurophysiological mechanisms of everyday memory and potential influence of APOE isoform

As discussed in section 1.1.4, the neurophysiological underpinnings of everyday memory, proxied in rapid place learning tasks are not fully understood (Bast et al., 2005; McGarrity et al., 2017; Bast et al., 2018). However, the importance of both hippocampal NMDA/AMPA receptor function has been demonstrated and appear somewhat dissociable in their role in encoding and retrieval, with hippocampal NMDAR function required for encoding of novel episodic experience and perforant path LTP (Steele & Morris., 1999; Day et al., 2003; Bast et al., 2005; Nai et al., 2010; Morris et al., 2012). Rapid acquisition of one trial place memory also appears dependent on effective dopaminergic modulation of hippocampal circuitry. Blockade of hippocampal dopaminergic D1 receptors induced impairment of one-trial place memory in the DMTP MWM task at short delays (Pezze et al., 2012). The impairment of hippocampal LTP following NMDA/AMPA blockade and requirement of D1 receptor function for early LTP and similarly impairing rapid place memory recall implicate hippocampal LTP as necessary for the formation of rapid place memory even at short delays of 15-30 minutes.

Notably, enhancement of perforant path LTP (Trommer et al., 2004) and deficits in NMDAR-dependent Schaffer collateral path LTP over 10-minutes to 1-hour (Korwek et al., 2008; Sun et al., 2017) have been observed in ex vivo hippocampal preparations from young E4-TR mice, as well acute ApoE4 inhibition of Reelin-mediated LTP in WT rat hippocampal neurons (Xian et al., 2018; as discussed in section 1.5.5). These results may predict that in young APOE-TR animals, the net effect of ApoE4 would be a suppression of stimulus-responsive short term synaptic plasticity. How these effects would account for the present results are unclear, however, and necessitates in vivo electrophysiological and behavioural experiments in APOE-TR mice to assess the hypothesis that impaired propensity for hippocampal LTP may relate to performance in one-trial rapid place learning. For example, field potential recording during place learning tasks of varying reinforcement in APOE-TR mice may address this question.

Evidence also suggests dissociable roles of hippocampal subregions underpinning encoding and retrieval processes of spatial information between CA3 and CA1/DG. Lesions of CA3 have

been shown to preferentially impair encoding performance in spatial and contextual learning tasks, while DG or CA1 lesions have a greater impact on retrieval (Jerman et al., 2006; Kesner et al., 2008; Ji et al., 2008). Further, pattern separation ability, is primarily thought to be mediated by the DG and 'pattern completion' by CA3 (Morris et al., 2012; Lee et al., 2020; Yassa et al., 2016; McAvoy et al., 2015; Kesner., 2008; Gold & Kesner., 2005; Nakazawa et al., 2003), particularly with lesions (Morris et al., 2012; Hunsaker et al., 2008) and inhibition of neurogenesis (Clelland et al., 2009; Pan et al., 2012) in the DG impairing spatial and non-spatial pattern separation ability. Previous evidence highlights impaired neurogenesis in E4-TR female mice (Li et al., 2009; Koutseff et al., 2014; Engstrom et al., 2017), enhanced CA3-DG hyperactivity in mid aged MCI E4-carriers (Tran et al., 2017), and in some cases behavioural defects in pattern separation aged E4-carriers (Shepard et al., 2016). Our current data do not suggest specific late-age deficits in pattern separation-like ability in E4-TR mice, although we note that a more detailed characterisation of pattern separation ability at longer retrieval delays and the possible involvement of APOE4-mediated impairments in neurogenesis is warranted.

Prefrontal cortical function and modulation of hippocampal activity is also implicated in the task demands of rapid place learning. There is a requirement to update spatial memory information while preventing proactive interference, alongside a function of rapid re-learning and 'forgetting' of previous spatial information which no longer is behaviourally relevant (Bast et al., 2018; McDonald et al., 2008; Kesner et al., 1996). Additionally, hippocampal GABAergic control has been shown to be critical for formation of rapid place memory, with hippocampal but not prefrontal hyperactivity induced by picrotoxin-mediated $GABA_AR$ disinhibition impairing rapid place learning performance in adult rats, enhancing aberrant hippocampal bursting activity (McGarrity et al., 2017). Further, DG hilar (DGH) GABAergic interneuron activity is also thought to be critical for mediating accurate reference memory recall in the MWM task, with optogenetic inhibition of DGH interneurons resulting in impaired reference memory recall without loss of the memory trace itself, with normal recall observed without DGH IN inhibition (Andrews-Zwilling et al., 2010). Notably GABA-IN neurodegeneration has been shown to be linked to long term reference memory deficits in aged female E4-TR mice (Andrews-Zwilling et al., 2010; Knoferle et al., 2014), which is plausibly via disruption of normal hippocampal synaptic transmission and aberration of plasticity mechanisms such as LTP and LTD contributing to long term memory formation and stability. Additionally, impairment in GABAergic control of the EHC has been shown to drive EHC hyperactivity in very late age (~20 months) E4-TR male mice (Nuriel et al., 2017). However, these late-stage and sex-dependent

deficits and their associated degenerative correlates appear unlikely to explain earlier alterations in performance observed in APOE-TR mice in the present experiment or others reporting early APOE4-dependent impairments in spatial learning and memory (e.g., Rodriguez et al., 2013; Grootendorst et al., 2005; Speidell et al., 2019).

In parallel, there is recently emerging evidence for a hippocampal network level deficit in 'sharp wave' ripple population events, associated with the hippocampal-dependent memory consolidation deficit in E4-TR female mice. 'Sharp wave ripple' (SWR) events are high frequency electrophysiological network events detected within the hippocampal circuitry during sleep and wakeful rest which have been suggested to be critical for 'memory replay' events supporting consolidation of recent experience (Buzsaki et al., 2015; Jadhav et al., 2012), and require local GABAergic interneuron function (Gillespie et al., 2016; Mann and Paulson et al., 2005). SWRs are suggested to be underpinned by CA3 recurrent collateral activation which generate a population level, large amplitude, sharp wave excitation event which subsequently leads to a short, high-frequency ripple event in CA1 pyramidal cells (Buzsaki et al., 2015), and has been associated with a slow gamma oscillation (30-120Hz frequency) power component thought to be important for organisation of replay events. CA3 SWRs appear involved in encoding rewarded locations in a spatial working memory radial arm maze and M-maze tasks (Sasaki et al., 2018; Fernandez-Ruiz et al., 2019). Accurate SWR temporal ordering of replay 'reactivation' also has been shown to predict MWM memory recall performance in aged animals (Gerrard et al., 2008), while disruption of SWR events using on-line in vivo electrophysiology results in impairment in the M-maze spatial working memory task (Jadhav et al., 2012).

Critically, reductions in overall SWR abundance in hippocampal CA1 have been detected as early as 4-5 months in E4-TR female mice, while slow gamma power during SWR events appears to decline more markedly from 12-18 months of age (Gillespie et al., 2016). The early reductions in SWR abundance occur prior to the detectable loss of DGH GABAergic INs and may represent mild physiological disruption of IN function prior to marked pathology. Further, slow gamma power but not SWR abundance decrements in E4-TR female mice was shown to be dependent on GABAergic interneuron expression of ApoE4, with conditional-KO of APOE4 in Dlx+ interneurons partially rescuing gamma oscillation power. GABA-IN KO of APOE4 has previously been shown to ameliorate GABA-IN neurodegeneration and long-term reference memory recall deficits in aged E4-TR female mice (Knoferle et al., 2014). Further, reference memory deficits in acquisition and retrieval in the MWM and a spatial avoidance task at 15-18

months in E4-TR female mice were predicted by SWR and slow gamma function during SWR events, respectively. Specifically, reductions in SWR abundance at 12-months predicted poorer acquisition scores at 18-months within the same animals, while CA3 slow gamma power during SWR events positively predicted recall accuracy across the same time points (Jones et al., 2019).

Together these results highlight the possibility that a similar mechanism may influence rapid place learning and memory in APOE-TR mice. How such predictions would map to the present results are unclear, however, as SWR alterations and GABA-IN deficits have only previously been reported in female, but not male, E4-TR mice and similarly only have predicted late-stage reference memory deficits and not deficits at the time of SWR event recording in APOE-TR mice (Jones et al., 2019). Therefore, we may not predict, given the current evidence, that deficits in these mechanisms would fully account for the present results, particularly the dissociation in encoding and retrieval and potential early-age advantage in separation accuracy. This is speculative, however, and future work may aim to characterise the involvement of SWR function on rapid place learning and recall in the mBM, alongside the relationship of APOE genotype and performance in young to mid-aged animals.

In any case, it is unclear how much of the evidence of neuronal structure and function in early life, which suggest an E4-TR specific deficit (reviewed in section 1.5), would translate into an early life switch between impairment to comparable rapid place learning and memory performance and investigation of the neurophysiological underpinnings of this are required. Particularly, the dissociation between primary acquisition measures and measures of recall accuracy leaves open questions about dissociable cognitive processes and underlying neural mechanisms.

4.4.9 Neuronal ensemble function and susceptibility to pathology

Intriguing alternative possibilities arise from recent research in the field of neuronal ensemble and engram cell function. For example, specific deficits in short- and long-term memory recall have been linked to impairments in neuronal ensemble function across multiple AD mouse models (Roy et al., 2016). Specifically, a reduction in engram cell activity (or engram size) was observed in APP/PS1 and 3xTg-AD (APP/PS1/MAPT) transgenic mice following long term (24h) contextual fear conditioning recall, alongside deficits in the spine density of engram cells within the DG.

Genetic tagging and capture of these engram neurons encoding a context associated with fear (shock-induced) was performed using an immediate-early gene-dependent (IEG) optogenetic viral labelling system (c-Fos-tTA [tetracycline transactivator complex] + TRE-ChR2 [Channelrhodopsin 2]), through which persistent neuronal activation was marked by expression of the activity-dependent IEG c-Fos. Subsequent activation of these labelled engram neurons in the DG led to short term rescue of contextual fear memory retrieval, while an 'optogenetic LTP' protocol between labelled entorhinal cortex and DG engram cells led to a persistent (48h) rescue of the memory trace and increased associated engram cell spine density (Roy et al., 2016). The specificity of the retrieval deficit induced by FAD mutations via impairment of engram cell functional activity may represent a general mechanism by which age dependent deficits in memory retrieval may occur, weakening synaptic connectivity or outputs of engram cells upon 'reactivation' of a given memory trace (Roy et al., 2016; Poll et al., 2020).

APOE-TR mice demonstrate age-dependent impairments in dendritic spine density in multiple subregions, including in the cortex, entorhinal cortex, and hippocampus, with deficits in CA1/DG/EHC reported as early as 3-months although with some contention (e.g., Jiang et al., 2003; Dumanis et al., 2009; Klein et al., 2014; Sun et al., 2017; Rodriguez et al., 2013). Further, acute action of ApoE4 in vitro has been demonstrated to potentiate ERK and immediate early gene (IEG) signalling (Ohkubo et al., 2001, Qiu et al., 2004; Huang et al., 2019), although there is less data to these effects in vivo (e.g., Yong et al., 2014, Korwek et al., 2008). However, the possibility of alterations to neuronal ensemble activation and IEG expression following behaviour as a consequence of APOE isoform remains unexplored. Given these questions, in Chapter five we therefore aimed to establish whether APOE isoform, sex, and age were associated with alterations in hippocampal neuronal ensemble engagement at baseline levels and following behaviour using an immediate-early gene imaging approach in young to mid-aged APOE-TR mice.

4.4.10 Caveats

There are a number of caveats notable in the experiments conducted in Chapter four. Firstly, animal attrition in the 15-18-month time points reduced the overall sample size, reducing statistical power. While only one animal was lost from the 15-month group, the group size for

18-months was 29. This was unevenly distributed across groups, with a greater loss of E3-TR animals. Therefore, the results at 18-months should be interpreted with more caution.

Second, as noted in section 4.3.1, our cohort of APOE-TR mice demonstrated an influence of age, sex, and genotype on between day learning. Repeat testing across age may have differentially influence on groups by APOE genotype and as such may have masked effects such that would be detectable without repeat testing (e.g., see Salomon-Zimri et al., 2015 for an example). Further, it is possible that repeat testing may also serve as an environmental/cognitive enrichment, which may reduce rate of cognitive decline (e.g., Mora et al., 2013).

Third, manipulation trials were performed in a single replicate at individual time points to avoid extinction effects and potential disruption of task rule learning. This may have contributed to greater variability in the manipulation trials, however. The ability to detect significant improvements in performance in young but not mid-old age in both 4-hour and 12-hour ITI trials appears to support a more specific effect of the manipulation rather than a substantial influence of between-day variability. In any case, replication of the current results with a more specific focus on trial delays with greater number of replicates would be beneficial.

Finally, as noted in Chapter three, while our present findings are consistent with the predominant use of allocentric place memory for task solving, dependence on the hippocampal circuitry remains to be validated. Therefore, pharmacological and lesion experiments of the hippocampus are necessary to assess the role of the hippocampus in the measures reported in the adapted Barnes maze. We predict that manipulations such as dorsal hippocampal and DG pharmacological lesion would lead to marked impairments, particularly in one trial place recall and separation accuracy, as well as attenuation of acquisition measures including errors and learning index. The results of Chapter four should therefore be interpreted with this caveat noted, as while the effects of APOE genotype in APOE-TR mice appear consistent with alterations to everyday memory performance, the underpinning neural mechanisms are unclear.

4.5 Chapter four summary and conclusion

In summary, the experiments carried out in Chapter four comprise the longitudinal assessment of rapid place learning and memory ability in APOE-TR mice across the lifespan as a proxy for everyday memory, using the mBM task. We demonstrated complex interactions between APOE genotype, sex, and age in both acquisition and retrieval of putative rapid place memory. We suggest that there may be a dissociation in early age in APOE-TR mice, with E4-TR mice demonstrating deficits in wayfinding acquisition but advantages in pattern separation-like retrieval accuracy following single trial experience, predominantly in male mice. Second, we suggest that a mild deficit in E4-TR male mice at 9-months but not subsequent ages in place separation may reflect a premature ageing effect in place memory accuracy following one trial experience, after which point E3-TR and E4-TR mice perform equivalently in recall accuracy. Finally, the defect in female E4-TR mice from 12-15 months in acquisition again appear to reflect wayfinding deficits across trials in the absence of significant impairments to place memory accuracy following single-trial encoding. However, we suggest that, at least under these conditions, that effects of APOE on long term reference memory in the APOE-TR model may exceed that of rapid place learning. Overall, these results highlight the complexity of interactions between ageing, rapid spatial learning and APOE genotype, and further study particularly of early age points is warranted in APOE models for detailed investigation of these interactions and the relative memory processes underlying these behaviours.

CHAPTER FIVE

The influence of APOE isoform on the hippocampal c-Fos response in APOE-TR mice

5.1 Introduction

In the experiments conducted in Chapter four, we investigated the influence of APOE isoform, sex, and ageing on rapid place learning in a novel adapted delayed match to place task using the APOE-TR mouse model. We demonstrated a complex profile of APOE genotype, age, and sex dependent modulations of spatial learning and memory, including a subtle early life deficit in acquisition but mild advantage in rapid recall in E4-TR mice. Given the generally ageing-centric study of APOE, relatively less is known about the phenotypic effects of APOE isoforms in early to mid-life.

Extensive evidence also suggests that there are both structural and functional alterations to the hippocampal circuitry in APOE mouse models in an age and sex dependent manner (discussed in section 1.5). Generally, APOE4 has been associated with neurodegeneration in late age but also more subtle reductions in dendritic morphology and possible synaptic integrity defects in adulthood in APOE mouse models. Less is known, however, about how APOE isoform may modulate hippocampal function during early to mid-life in vivo, particularly during and following hippocampal-dependent behaviour (as discussed in section 1.6). Therefore, in parallel studies comprising Chapter five, we investigated whether APOE isoform and sex alter hippocampal 'neuronal ensemble' activation at rest and following behaviour in young to mid-aged APOE-TR mice.

Within the field of learning and memory, neuronal ensembles are proposed to be critically involved in the representation and consolidation of memory processes and to represent one of the substrates of 'memory engrams', the long-lasting physiological changes which underpin a physical mechanism of information or memory storage (e.g., Semon., 1921; reviewed in Whitaker & Hope., 2015; Bogoch., 1968; Tonegawa et al., 2015a; Ryan et al., 2021). Neuronal ensembles are sparse, distributed groups of neurons which are specifically activated by a stimulus or, for example, in response to environmental demands that require goal-directed behaviour (Mountcastle., 1957; Buzsáki., 2004; Guzowski & Knierim., 2004; Cruz et al., 2015; Tonegawa et al., 2015a, 2015b; Minatohara et al., 2016). Typically, neuronal ensembles are not spatially correlated, and the individual nodes of an ensemble are not necessarily directly synaptically connected, however their role in learning and memory has become a topic of increasing interest (Tonegawa et al., 2015a). Importantly, distinction has been made between ongoing neuronal network activity in the representation of information as distinct from mechanisms which underpin the ability to represent this information over time. That is, online representation and consolidation can be dissociated, with consolidation proposed to require

lasting morphological and physiological changes, such as the mechanisms underpinning long term synaptic plasticity such as activity-dependent gene expression (e.g., Whitaker & Hope., 2015; Buzsáki., 2004; Morris., 2006).

The ability to spatially resolve regionally distributed ensembles has been particularly informative. Crucially, multiple lines of evidence have highlighted the behavioural and physiological relevance of the dynamic expression of immediate-early genes (IEGs) as markers of neuronal and neuronal ensemble activity (Morgan et al., 1987; Morgan & Curran., 1991; Chung et al., 2015; Cruz et al., 2013; Cohen & Greenberg, 2008). IEGs such as c-Fos (Fos proto-oncogene AP-1 subunit in humans or FBJ osteosarcoma gene in mice) and Arc (Activity regulated cytoskeleton associated protein) have been demonstrated to be upregulated in response to persistent neuronal activity. Moreover, IEG expression has been shown to be crucial for the expression and maintenance of certain behaviours such as contextual fear conditioning, spatial memory, and drug-cue sensitisation behaviour in rodent models, with ablation or inactivation of these IEG expressing ensembles (e.g., Koya et al., 2009; Cruz et al., 2013; Liu et al., 2012; Tonegawa et al., 2015a; Tanaka et al., 2014), or inhibition of IEG expression (e.g., He et al., 2002; Katche et al., 2010, 2017) impairing the specific behaviour. For example, optogenetic inhibition of CA1 ensembles using the tetracycline transactivator genetic construct under an IEG promoter for 'tag and capture' of c-Fos expressing neurons, significantly impaired freezing responses proxying memory retrieval performance following a contextual fear conditioning paradigm (Tanaka et al., 2014). Similarly, the ablation of neurons overexpressing CREB following fear conditioning in the lateral amygdala using a CREB-Cre Diphtheria toxin receptor (DTXR) system, impaired fear memory retrieval (Han et al., 2009). In parallel, reducing excitability of c-Fos expressing neurons following paired exposure of an environment with cocaine, using the 'Daun02' method in c-Fos-lacZ rats, reduced the locomotor sensitising effects of cocaine-paired environment re-exposure (Koya et al., 2009). This provides strong evidence for the importance of specifically activated neuronal ensembles in multiple forms of learning and memory, and their susceptibility to disruption.

These ensembles are proposed to be activated in a specific spatiotemporal pattern by processes pertaining to that given memory content, such as reactivation for memory retrieval (Tonegawa et al., 2015a, 2015b; Clayton et al., 2000). Additionally, the temporal dynamics of expression of various IEGs has been proposed to underpin the activation of distinct signalling pathways and selective activation of certain genes (e.g., Lacar et al., 2016) to support structure-function correlates of synaptic plasticity within neuronal networks. The study of

neuronal ensembles, their relevance to behaviour, and the functional outcomes of neuronal perturbation, such as by disease processes, is crucial to gain insight into how behaviour may be disrupted at the network level. Indeed, a number of studies have highlighted changes in the intrinsic functional properties of neurons within behaviourally relevant ensembles and how interference, such as by hyperexcitation, inhibition, and neuropathology, prior to gross neurodegeneration may also impair expression of given behaviours (Garner et al., 2012; Roy et al., 2016; Stefanelli et al., 2016; Cai et al., 2016; Brebner et al., 2020).

There is little data on the potential effect of APOE isoform on neuronal ensemble responses or IEG expression, despite evidence suggesting APOE-dependent aberrations in hippocampal neuronal network activity (e.g., Gillespie et al., 2016; Jones et al., 2019). In vitro studies show APOE isoform specific differences in the expression of signalling pathways that drive IEG expression (see section 1.5.6). Specifically, ApoE4 acutely stimulates the canonical ERK pathway in WT rat hippocampal neurons to a greater extent than ApoE3 likely via inducing calcium influx, converging on downstream increases in c-Fos and CREB expression. These effects were blocked both by RAP-mediated APOE-receptor inhibition and inhibition of NMDAR or voltage-gated calcium channelS (VGCC), highlighting an acute signalling role for ApoE in potentiating neuronal calcium and IEG responses (Ohkubo et al., 2001; see section 1.5.6). In addition, ApoE4 application (full length or truncated) to neurons, increases intracellular calcium, suggesting increased neuronal excitability with acute ApoE4 exposure (Ohkubo et al., 2001; Tolar et al., 1999; Veinbergs et al., 2002; Qiu et al., 2004). However, these cell culture studies do not preserve relevant in vivo signals, network structure, or physiologically relevant chronic, rather than acute, expression of ApoE. Thus, it is important to determine the effect of chronic APOE expression on neuronal ensemble and network IEG activity in vivo.

A single study by Zhong et al. (2008) showed, in contrast, a reduction in both Arc (Arc+) and c-Fos (Fos+) expressing neurons in the DG granule cell layer (DG-GCL) in the Arg-61 APOE mouse at 12-months, relative to WT controls following exposure to a novel environment. However, these results do not pertain to the specific effects of hAPOE isoforms, rather an incorporation of a point mutation into endogenous mAPOE in the Arg-61 mouse model to putatively model the APOE4 domain interaction (Zhong et al., 2008; Raffai et al., 2001). Therefore, there is a clear need to establish first whether hAPOE isoform alters neuronal ensemble engagement and IEG expression in-vivo at baseline and in response to stimulation. The APOE-TR model is well suited to this, given the endogenous genomic regulatory control of hAPOE expression in

place of mAPOE (discussed in section 1.3.5) as well as allowing the study of possible interacting factors such as sex and ageing.

Ensemble-level activity may be expected to vary between isoforms in the APOE-TR mouse model due to known structural and functional differences in the hippocampal circuitry. For example, ageing E4-TR female mice show a neurodegenerative phenotype of GABAergic DGH interneurons alongside a sex-independent impairment of dendritic complexity and morphology within the hippocampal complex (e.g., Leung et al., 2012; discussed in section 1.5.2). In addition, cellular and circuit level electrophysiological evidence demonstrates that the application or expression of ApoE4 alters synaptic plasticity including impairments in NMDA-dependent field potentials, reduced LTP in the perforant path, and potentiation of LTP in the Schaffer collateral pathway (Trommer et al., 2004; Korwek et al., 2008), as well as mid-late age sex-modulated inhibitory deficits in the hippocampal-entorhinal circuitry (e.g., impairments in GABA-dependent mIPSCs, Andrews-Zwilling et al., 2010; Nuriel et al., 2017).

Thus, there is an emerging image that APOE4 mediates disruptions in synaptic transmission, which may be preferentially exacerbated in females and become pathological with ageing. However, the results across studies, which commonly differ in age, sex, APOE genotypes, and brain region investigated are variable. Although the hippocampus is the most well investigated, how APOE isoforms impact its function still remains unclear, particularly at young to mid age. Further, how this impact may be modulated by behavioural state is unknown. In order to characterise whether APOE isoforms differentially modulate neuronal ensemble responses, it is crucial to account for any interactions with age and sex.

Here, using APOE-TR mice, we aimed to establish how APOE isoform, age, and sex alter hippocampal neuronal ensemble responses under basal and behaviourally activating conditions. A second aim was to characterise neuronal ensemble activation in parallel with markers of inhibitory neurons to determine whether specific excitatory and/or inhibitory ensemble activity preceded previously reported hippocampal inhibitory defects (e.g., Li et al., 2009; Andrews-Zwilling et al., 2010; Leung et al., 2012). These aims were addressed through three experiments.

Experiment one: Firstly, young (3-months) and mid-aged (12-months) APOE-TR mice of mixed sex (male, female) and APOE genotype (heterozygous E3E4-TR and homozygous E3-TR, E4-TR), were tested using a novel context exposure/home-cage control paradigm with post-mortem quantification of the IEG c-Fos as a marker of neuronal ensemble activity in both excitatory and inhibitory neurons. Further, quantification of the inhibitory interneuron marker GAD-67 was

performed to assess possible loss of putative GABAergic innervation. Subregions of the hippocampal complex comprising the CA1, CA3, DG superior and inferior (DGS/DGI) were selected as primary regions of interest, due to their relevance in learning and memory processes and the extensive evidence in cellular, animal, and human systems associating APOE with hippocampal structural, physiological, and pathological change (Najim et al., 2019). Exposure to a novel context is commonly used to robustly induce hippocampal and cortical neuronal ensemble activation and IEG expression (e.g., VanElzakker et al., 2008; Mendez et al., 2016). c-Fos was chosen as the metric of neuronal activation and IEG induction as a well characterised gene and with strong evidence supporting c-Fos as a marker for behaviourally relevant neuronal ensembles (e.g., Chung et al., 2015; Morgan & Curran., 1991; Kovacs et al., 1998).

Experiment two: Within the same cohort and an additional aged (18-months) cohort of APOE-TR mice, the previously reported potential neurodegenerative loss of GABAergic interneurons within the DGH was investigated, to assess inhibitory function and possible co-occurrence with hippocampal ensemble changes (e.g., Andrews-Zwilling et al., 2010; Leung et al., 2012).

Experiment three: Finally, in parallel experiments, hemi-hippocampi from the same animals used in experiment one were used for c-Fos and APOE mRNA quantification to assess whether our primary variables were associated with transcriptional-level alterations in IEG and APOE expression at the whole hippocampal level.

We first hypothesised that exposure to the novel context would robustly increase c-Fos expressing (Fos+) neuron and interneuron network activity or ‘ensemble size’, in CA1, CA3, and the DGS regions of the hippocampus, and similarly increase whole hippocampal c-Fos mRNA expression. Further, we predicted that possession of one or two copies of APOE4 in the APOE-TR model, compared to E3-TR controls, would be associated with an overall reduction in both pyramidal and interneuron Fos+ ensemble size throughout the hippocampus both in baseline and novel conditions. We also predicted that these effects would be replicated in decreases in c-Fos and APOE mRNA expression within the whole hippocampus. We expected that these changes would be exacerbated with ageing and would be greater in female mice. Finally, we predicted that these changes would precede a potential loss of DGH GABA-INs, which we expected to detect in mid-old aged (12-18-month) E4-TR female mice.

5.2 Methods

5.2.1 Design

Three primary experiments were performed in Chapter five, using tissue from two cohorts of APOE-TR mice:

1. Experiment one: Immunofluorescence imaging of the hippocampal c-Fos response.
2. Experiment two: Immunofluorescence imaging of the GABA-IN population in the dentate gyrus hilus.
3. Experiment three: Assessment of whole hippocampal c-Fos and APOE mRNA expression.

Experiments one and three were conducted in a cross-sectional, four-way between groups design. APOE genotype (E3-TR, E3E4-TR, and E4-TR mice), age (3 and 12-months of age), sex (male and female), and behavioural condition (novel context exposure or home cage control) were the primary independent variables of interest. Experiment two was a three-way between groups design with age (3, 12, or 18-months), sex (male and female), and APOE genotype (E3-TR and E4-TR) as the primary independent variables.

5.2.2 Animals

81 APOE-TR mice (see Table 5.1) were used in experiments one and three. 71 APOE-TR mice were used in experiment two, including appropriate tissue from the 3-12-month aged E3-TR and E4-TR mice (experiments one and three) alongside tissue from a further 16 mice aged 18-months (see Table 5.2 for details). All animals were maintained and handled as described in section 2.1.1.

Table 5.1: Outline of animal numbers allocated to each condition in experiment one & three. Condition allocation of home-cage control 'HCC' and novel context exposure 'NCE' are shown.

Age	Condition	Genotype	Sex	N
3-months	HCC			
		E3	Male	3
			Female	3
		E3/E4	Male	3
			Female	3
		E4	Male	3
			Female	4
	NCE			
		E3	Male	3
			Female	3
		E3/E4	Male	3
			Female	4
		E4	Male	3
			Female	5
12-months	HCC			
		E3	Male	3
			Female	4
		E3/E4	Male	3
			Female	3
		E4	Male	3
			Female	3
	NCE			
		E3	Male	4
			Female	3
		E3/E4	Male	4
			Female	3
		E4	Male	3
			Female	5

Table 5.2: Outline of animal numbers allocated to each condition in experiment two.

Age	Genotype	Sex	N
3-months			
	E3	Male	6
		Female	6
	E4	Male	9
		Female	6
12-months			
	E3	Male	7
		Female	7
	E4	Male	8
		Female	6
18-months			
	E3	Male	3
		Female	4
	E4	Male	4
		Female	5

5.2.3 Procedure

Animals were split into two primary conditions, exposure to a novel environmental context (NCE, novel context exposure), or a home-cage control (HCC). All animals were acclimated to experimenter handling one day prior to the experiment. On the day of testing, animals were placed in either a novel context chamber (a 30cm x 30cm x 30cm open field chamber with two novel objects: one Lego tower, one red and gold bauble) for 30-minutes or remained in their home cage for the same period. After 30-minutes, the novel context group were removed from the chamber and returned to their home-cage. Once returned to the home cage, after a delay of 60-minutes, animals were anaesthetised and rapidly perfused with aCSF as described in section 2.2.1. Brains were then extracted, and the tissue was pre-processed for IHC and biochemical experiments, including RNA extraction, as described in section 2.2.3. Home-cage control subjects were treated in the same manner, without exposure to the novel context.

5.2.4 Experiment one: Immunofluorescence imaging of the hippocampal c-Fos response in APOE-TR mice

Post-fixed frozen hemibrains were cryosectioned at 40µm as described in section 2.2.1.2. Hippocampal sections were acquired across the entire dorsal-ventral axis in the coronal plane, from approximate coordinates B = -1.05 to -3.50 (Paxinos & Franklin., 2012), anterior to the point at which the CA1 and CA3 regions recess and the DG GCL forms the posterior tail. Observing co-staining patterns with a general neuronal marker, NeuN, enabled identification of these key landmarks during imaging and analysis. Tissue sampling was performed using principles similar to that described in Andrews-Zwilling et al. (2010). In 24-well culture plates, 1 in 6 wells of sections were sampled, taking three sections from each well, yielding nine sections across the anterior-posterior extent of the hippocampus for each animal. Three sections were pseudorandomly sampled (allowing representation of anterior to posterior hippocampus) from this pool per animal for whole section imaging.

Immunofluorescence was performed as described in section 2.2.1.3 in 24-well culture plates, with primary antibodies targeting c-Fos, NeuN, and GAD-67, paired with Alexa-fluor conjugated IgG targeting secondary antibodies with fluorophores at 488nm, 568nm, and 647nm (Alexa-Fluor series), respectively (see Tables 2.3 & 2.4). Sections were imaged as described in section 2.2.2., using an Olympus BX53 upright fluorescent microscope with a

motorised stage controller at 20x magnification. In order to improve signal to noise ratio and cell nuclei visibility, 9µm z-stacks were acquired at 3µm intervals for the c-Fos fluorescence channel for max intensity projection. Imaging generated large, 10 x 10 tiles of 1392 x 1040px^2 images per tile, encompassing the extent of the hippocampal formation in a given coronal section.

Images were analysed in Fiji, using custom-made scripts to overlay counting grids for manual cell counting with a grid size of 100µm x 100µm. Stitched images (Stitching plugin, Preibisch et al., 2009) underwent background subtraction for each channel, using a 50-pixel rolling ball radius function, before contrast values were set to a standardised value within each channel. Image were then pseudocoloured and channels were merged into dual channel composites containing either: GAD-67 (568 - Green) and c-Fos (488 – Magenta), or c-Fos and NeuN (647 – Cyan).

Counts of Fos+ nuclei were performed for each subregion within each section according to the principles described in section 2.2.2.2. Counting grids were overlayed onto individual sections and grids colliding with the region of interest (ROI; corresponding to a given subregion present within a coronal section), which was manually traced, were quantified. Immunoreactive Fos+ nuclei which colocalised with NeuN+ nuclei were counted as Fos+ neurons. Immunoreactive cell structures were counted in cases where immunoreactivity satisfied the criteria of clear cellular boundaries, intensity of staining above background, and within the boundaries of the region of interest (ROI) covered by the counting grid. In cases where colocalisation or encapsulation (i.e., subcellular compartment labelling within the same cells: nucleus and soma) of images was required, cells were counted in cases where fluorescence channel overlap or compartment labelling was present with clear cellular boundaries within the focal plane.

c-Fos+ cell counts were produced for 4 subregions within the hippocampus for each subject, corresponding to the principal cell layers of CA1, CA3, DGS, and the DGI. Individual counts of Fos+ nuclei colocalized with NeuN+ signal within a subregion were normalised to the estimated NeuN+ cells within each given ROI, expressed as a percentage. The estimated number of NeuN+ cells for each subregion ROI was based on counts generated from placement of a 150 x 150µm cell counting window within the cell layer for each image, which was then scaled to the total ROI area (similar to Adeosun et al., 2019). GAD-67+/Fos+ colocalization and cell quantification was performed using the same criteria described above within the principle pyramidal/granule cell layers of CA1, CA3, DGS, and the DGI but requiring both GAD-67+ somal labelling and Fos+ nuclei labelling within clear cellular compartments within the same cell.

GAD-67+/Fos+ cell counts were expressed as density/mm^2 and data handling is described in section 5.7. Finally, for total GAD-67 immunoreactivity, mean fluorescence intensity was calculated within each subregion ROI, with an additional ROI included of the DG hilar layer (DGH).

5.2.5 Experiment two: Analysis of DG hilar interneuron loss across the lifespan of APOE-TR mice

Tissue from 3-12-month APOE-TR mice collected during experiment one and additional tissue from 18-month aged APOE-TR (collected via perfusion-fixation, see section 2.2.1) was subsampled. This comprised 71 animals of E3-TR and E4-TR genotype (Table 5.2).

Immunofluorescence staining for GAD-67 was performed as reported in section 2.2.1.2 (Table 2.4), with 6 sections sampled per animal across the anterior-posterior axis of the hippocampus. Microscopy and image acquisition was performed similarly to described to experiment one, using identical microscopy hardware with some minor acquisition adjustments. Each section was imaged using 5 x 5 tiles at 1392 x 1040px^2 before stitching. As performed for c-Fos immunofluorescence, 3 x 3µm z-stacks were taken for max intensity projection to improve cell boundary resolution. Background subtraction was then performed before standardised contrast values were set across all samples.

DGH GAD-67+ interneurons were counted within each section within 100µm x 100µm counting grids. Criteria for counting inclusion were as follows: position within the DG hilar layer or on the close boundary between the DG granule cell layer and the hilus, between the DG granule cell blades and not beyond this boundary (i.e., excluding non-pyramidal layer CA3 interneurons), clear somal and non-nuclear GAD-67 immunoreactivity with defined cellular boundaries (i.e., excluding cells with solely perisomal labelling more likely reflecting presynaptic termini). The DGH ROI for each section was manually traced and cell counts were then normalised to this ROI size and scaled to reflect cell density/mm^2.

5.2.6 Experiment three: Quantification of whole hippocampal c-Fos and APOE mRNA response in APOE-TR mice

Hemi-hippocampi were dissected fresh from the opposing hemisphere of the same animals used for immunofluorescence experiments as described in section 2.2.1. Hemi-hippocampi were then homogenised in ice cold RIPA lysis buffer, before total RNA was extracted and 500ng was converted to cDNA and diluted 1:50 in RNAse free water as described in section 2.2.3.

RT-qPCR was performed as described in section 2.2.4, using 96-well reaction plates. Briefly, c-Fos and APOE were the primary genes of interest (GOI), with a 4-gene reference factor comprising the average Ct of targets: Mto1, TRMU, CPSF4, and ActB used for GOI dCt normalisation (see section 2.2.4.6). Each reaction plate contained an equal balance of the primary conditions of interest where possible for each subject. For example, 2-3 subjects for each condition were included in triplicate on the same plates for a given gene as much as possible, including all APOE-TR genotypes, both age groups, and home-cage/novel context conditions alongside relevant controls (standard, and no template control). This plate design was chosen in-line with the MIQE guidelines to avoid potential Ct/background drift between plate reactions (Taylor et al., 2019). A standardised fluorescence detection threshold was selected based on the median threshold across all plates used within the experiment. The set threshold and standard sample used for each plate ensured that raw Ct values were not artificially skewed by between-plate drift or reagent contamination.

5.2.7 Analysis

Data from c-Fos imaging was handled by averaging area-normalised Fos+ cell density for pyramidal and interneuron populations separately. Each cell population was grouped by subregion and averaged across the number of sections sampled for each subject. ROI area and estimated total NeuN+ count data were also analysed using univariate ANOVAs to test for potential confounds in the normalisation factor used between conditions of interest. Analysis revealed biases in ROI area sizes under some variable conditions, but no such biases were observed in scaled estimated NeuN+ count. Therefore, to avoid introducing potential bias, Fos+ cells as a percentage of estimated NeuN+ count was chosen for analysis. Normalised

counts for GABA-INs from experiment two were expressed per mm^2 and we observed no significant effects of conditions on DGH ROI size.

Fos+ cell count data was then grouped by experimental condition and tested for homogeneity of variance using the Levene's test. This revealed violations of homogeneity of variance in each subregion analysed. In order to reduce parameter biases introduced by such violations, univariate general linear models with robust parameter estimation were used. Fos+ cell density data from each subregion for each cell type (Fos+/NeuN+ or Fos+/GAD+) was used as the measure variable, with all predictor variables and interaction terms included. Briefly, data for each subregion was characterised using diagnostic plots of Cook's distance, standardised residual-leverage, Q-Q distributions, and co-linearity plots to check for influential cases and indications or skewness or non-normal distribution before modelling. No outliers exceeding a Cook's distance of 0.5 were observed and IQR-based trimming had a negligible effect on model parameter estimates. Therefore, no data was removed prior to analysis. Robust F-ratios and *p*-values were calculated for each individual model. Simple main effects analysis was used to follow up significant interaction terms and pairwise comparisons were performed in cases where a significant main effect in variables with more than two levels were present. Univariate models were generated using R (lm, lmRob packages, see CRAN repositories for details).

In the case of Fos+/GAD+ (interneurons) cell counts in the primary cell body layers, we observed that the population size was particularly low across subregions. This resulted in significant data compression when normalised to estimated NeuN+ counts. To avoid this, we opted instead to correct to the ROI size occupying the subregion cell layer. Following this, standard univariate linear models were generated for each subregion, in which we observed consistent positive skew in residual-fitted value plots, suggesting non-homogenous variance at higher values, likely caused by a moderate proportion of zero values (i.e., average of zero for Fos+/GAD+ cells within a subregion for a given animal). Therefore, the Fos+/GAD+ count results should be interpreted with caution.

GAD-67 immunoreactivity and DGH GAD-67+ IN count data was analysed as above, averaging data across sections for each subregion, followed by fitting a linear model and using robust F-ratio estimation with identical pre-analysis checks to that described above.

RT-qPCR raw Ct values were handled as described in section 2.2.4.6. Briefly, raw Ct values for each GOI and reference gene were averaged across replicates (triplicate per sample), while triplicate values above one cycle variance (i.e., 0.5 SD) were removed in cases where remaining duplicate values were within one cycle. Ct averages for the reference factor was generated by

averaging across the four reference genes, before the GOI Ct was normalised to the reference factor to form delta-Ct (dCT) for each subject for both c-Fos and APOE. The dCt for c-Fos and APOE were analysed using a three-way between groups ANOVA with main effects and interaction analyses. Homogeneity of variance was assessed with Levene's test and was not statistically significant ($F(23,57) = 1.67$, $p = .061$). Simple main effects analyses were performed to follow up significant interaction terms, accompanied by Sidak adjusted pairwise comparisons. In all cases, the alpha criterion for significance was set at 0.05.

Exploratory post-hoc network correlation analysis was performed using Fos+ neuron densities from CA1, CA3, and the DGS calculated during experiment three. Pearson's correlation coefficient was calculated between Fos+ neuron densities between subregions using primary variables to cluster data prior to correlation. Alpha was again set at 0.05 in each case and Bonferroni corrected *p*-values are provided in Supplementary Table 5.2.

5.3 Results

5.3.1 Experiment one: Immunofluorescence imaging of the hippocampal c-Fos response in APOE-TR mice

5.3.1.1 Hippocampal neuron c-Fos activation in APOE-TR mice

c-Fos+ neurons within the primary hippocampal pyramidal and granule cell layers were counted and categorised based on NeuN/c-Fos or soma-nuclear GAD-67/c-Fos colocalisation into excitatory and inhibitory neuron populations, respectively. Two categories of cells comprised the majority of Fos+ cells encountered in the pyramidal and granule cell layers. NeuN+/Fos+ representing total Fos+ neurons (referred to as Fos+ neurons), and GAD+/Fos+ representing Fos+ GABAergic interneurons (referred to as Fos+ interneurons). A rare NeuN-/Fos+ category likely represented unsuccessfully labelled neuronal cells or glia, which were not counted.

Initial observations indicated that, as expected, the vast majority of Fos+ cells were NeuN+ within the pyramidal and granule cell layers, while Fos+ interneurons were sparse, comprising <1% of estimated number of NeuN+ putative pyramidal neurons (Figure 5.1A/B). Fos+ interneurons were more common in the CA1 and CA3 than the blades of the DG (Figure 5.1B). A univariate analysis of Fos+ neuron density by hippocampal subregion revealed a significant

effect of condition, with a significantly higher Fos+ neuron density in CA1 ($F(1,57) = 25.75$, $p = <.001$), CA3 ($F(1,57) = 52.71$, $p = <.001$), and DGS ($F(1,57) = 22.70$, $p = <.001$), but not the DGI ($F(1,57) = 0.55$, $p = .450$), following novel context exposure compared to the home cage controls (Figure 5.1A).

Additionally, we quantified the estimated NeuN density of each subregion. We observed no significant effect of genotype, sex, or age on the estimated cell density of any of the principal hippocampal layers (Figure 5.1C; Supplementary Table 5.1; Supplementary Figure 5.1).

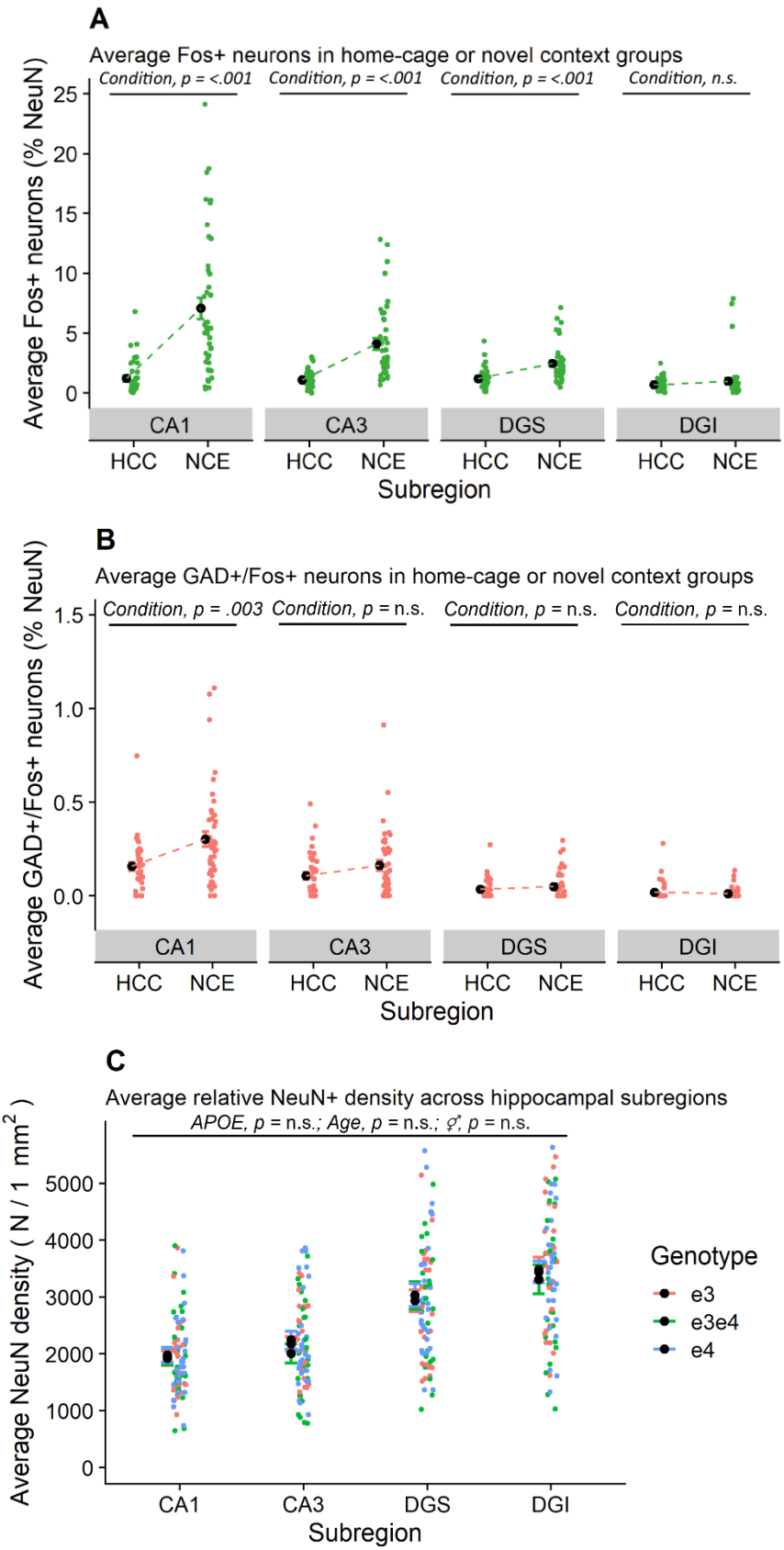

Figure 5.1: Average percentage of A) NeuN+/Fos+ pyramidal/granule neurons and B) GAD-67+/Fos+ interneurons in primary hippocampal subregions, grouped by condition. C) Average

estimated NeuN+ density per mm^2 across CA1, CA3, DGS, and DGI grouped by APOE genotype. Individual points represent averages across replicate sections for individual animals. Note the axes in A) and B) are scaled relative to overall proportion, with interneurons comprising a smaller percentage than pyramidal neurons. Error bars represent mean +/- SEM. Brackets and labels represent relevant statistical main effects, interactions and pairwise comparisons where appropriate.

5.3.1.2 Fos+ neuron density in CA1

In CA1 there was both a significant main effect of APOE genotype ($F(2,57) = 4.29$, $p = .030$) and a significant interaction between genotype and condition ($F(2,57) = 6.41$, $p = .009$) on the Fos+ neuron density but no significant effect of sex ($F(1,57) = 0.58$, $p = .448$). Simple main effects analysis revealed a significant effect of genotype in novel context ($F(2,38) = 4.70$, $p = .030$) but not home-cage control ($F(2,33) = 1.74$, $p = .190$) animals. Pairwise comparisons demonstrated a significant increase in Fos+ neurons in E4-TR mice relative to both E3-TR (MD = 4.96, SE = 2.00, $p = .019$) and E3E4-TR (MD = 4.34, SE = 2.05, $p = .036$) controls in the novel context condition. There were no differences between E3-TR and E3E4-TR mice (MD = -0.65, SE = 2.11, $p = .760$); Figure 5.2A/B). Importantly there was no significant interaction with age, and while we noted the magnitude of the effect appeared greater in the 3-month aged mice, the pattern of results was preserved at 12-months.

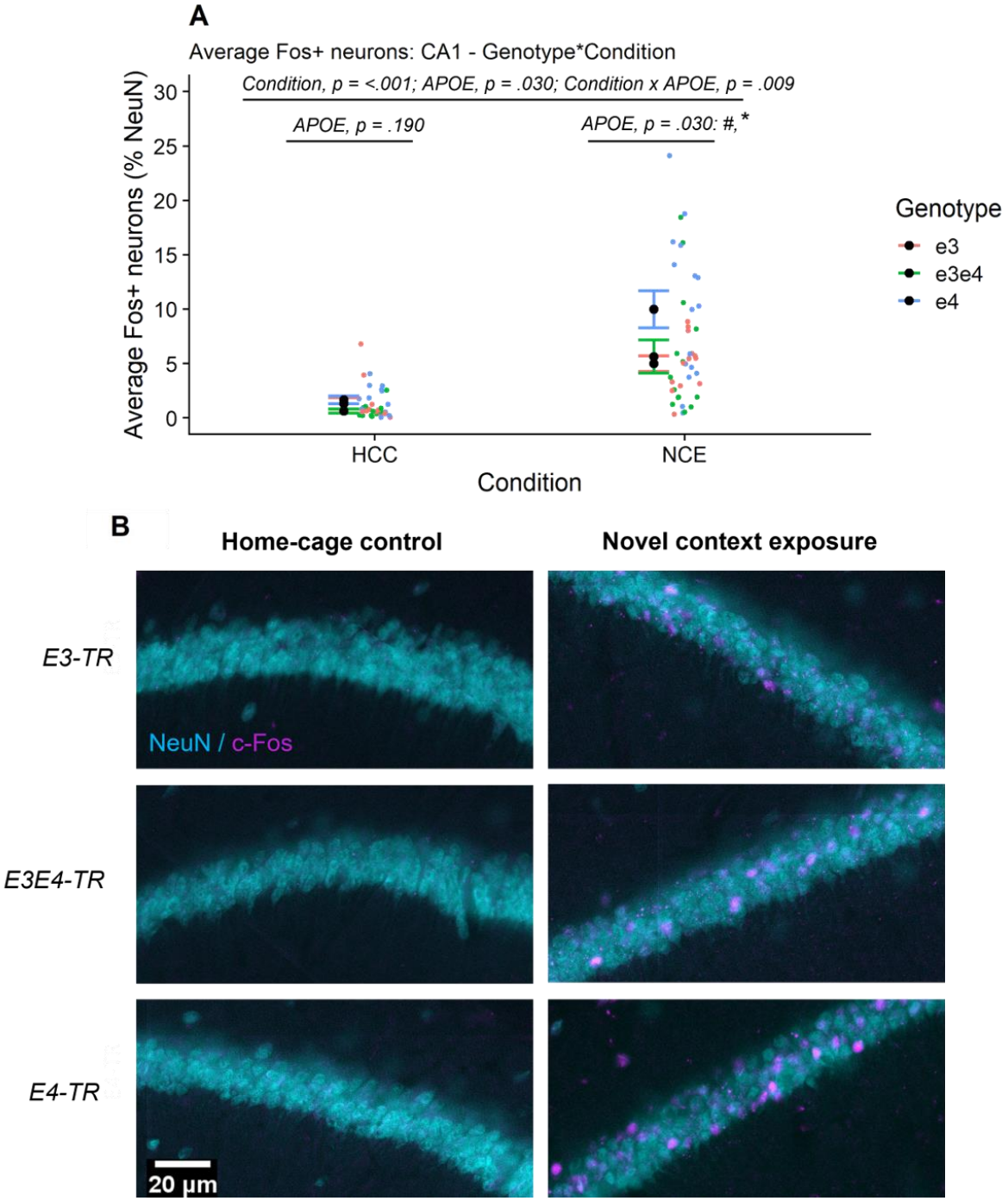

Figure 5.2: A) Average Fos+ neuron counts in the CA1 pyramidal layer expressed as the percentage of estimated NeuN+ neurons, grouped by APOE genotype and condition. Brackets and labels represent relevant statistical main effects, interactions and pairwise comparisons where appropriate. Individual points represent the average of each count across sections within a single animal. Error bars represent mean +/- SEM. Symbols represent significant comparisons at p = <.05: '' represents E3-TR Vs E4-TR, '#' represents E3E4-TR Vs E4-TR, '$' represents E3-TR*

Vs E3E4-TR. B) Representative example immunofluorescence images of labelled Fos (magenta) and NeuN (cyan) neurons in the CA1 pyramidal layer grouped by APOE genotype and condition.

5.3.1.3 Fos+ neuron density in CA3

In CA3, there was a significant interaction between sex and genotype on Fos+ neuron density ($F(1,38) = 5.28$, $p = .010$). Simple main effects analysis showed a main effect of genotype in female ($F(1,38) = 5.28$, $p = .010$), but not male ($F(1,38) = 0.25$, $p = .773$), mice. Pairwise comparisons showed that this effect was driven by significantly elevated Fos+ neurons in female E4-TR mice compared to E3E4-TR female controls (MD = 2.11, SE = 0.98, $p = .038$) and a trend relative to E3-TR female controls (MD = 1.94, SE = 0.98, $p = .055$; Figure 5.3A). Again, there was no significant difference in CA3 Fos+ neuron density between E3-TR and E3E4-TR female mice (MD = 0.17, SE = 0.96, $p = .859$; Figure 5.3A/B).

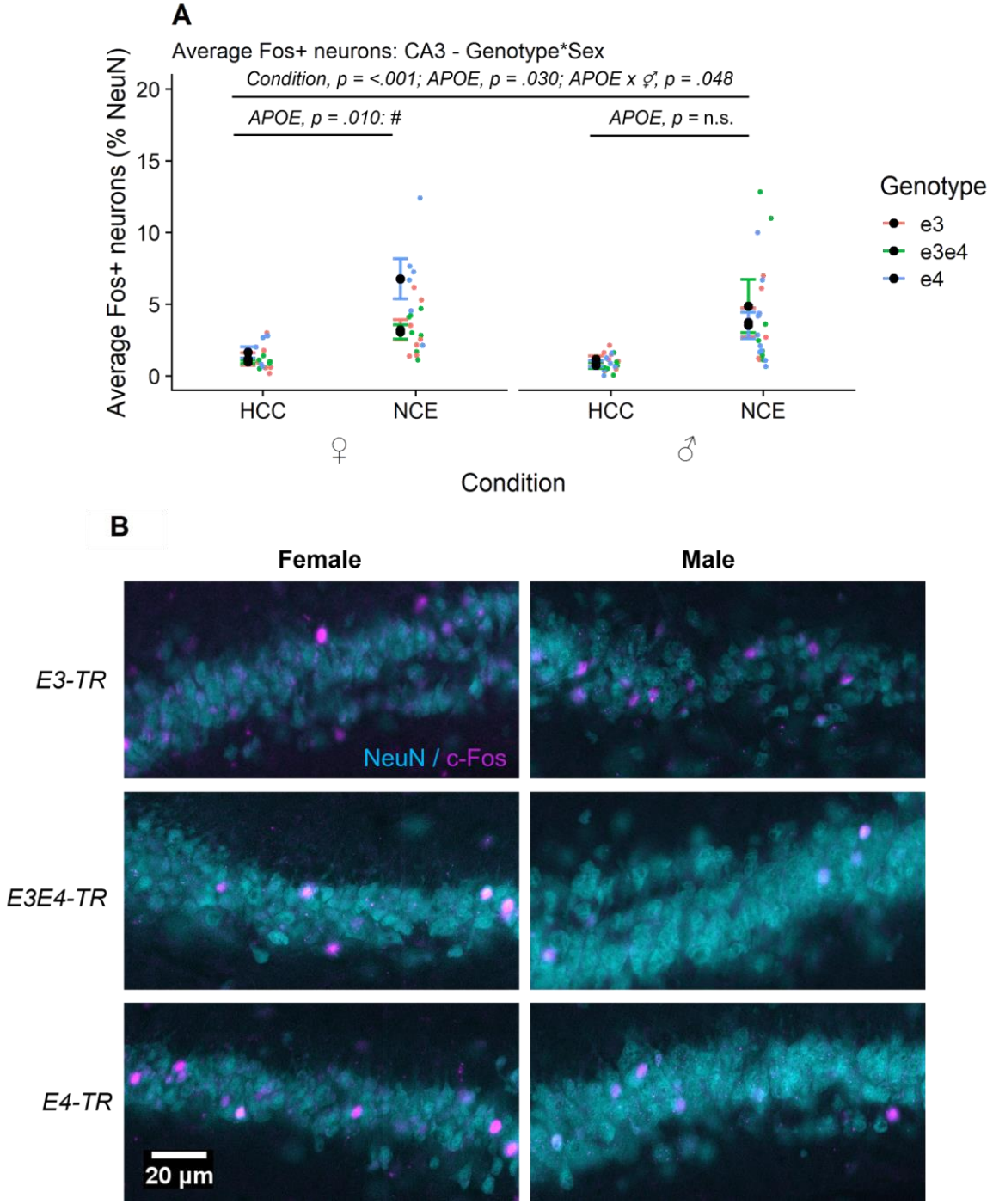

Figure 5.3: A) Average Fos+ neuron counts in the CA3 pyramidal layer expressed as the percentage of estimated NeuN+ neurons, grouped by APOE genotype, condition, and sex. Brackets and labels represent relevant statistical main effects, interactions and pairwise comparisons where appropriate. Individual points represent the average of each count across sections within a single animal. Error bars represent mean +/- SEM. Symbols represent significant comparisons at p = <.05: '' represents E3-TR Vs E4-TR, '#' represents E3E4-TR Vs E4-*

TR, '$' represents E3-TR Vs E3E4-TR. B) Representative example immunofluorescence images of labelled Fos (magenta) and NeuN (cyan) neurons in the CA3 pyramidal layer grouped by APOE genotype and sex.

5.3.1.4 Fos+ neuron density in the DGS

In the DGS there was a main effect of sex ($F(1,57) = 4.12$, $p = .039$) on Fos+ neuron density with female APOE-TR mice exhibiting greater Fos+ neuron density than male mice overall. The DGS was also the only region in which Fos+ neuron density varied with age, with a significant decrease observed in 12-month compared to 3-month aged mice ($F(1,57) = 4.40$, $p = .032$; Figure 5.4A/B). There were no main effects or interactions with APOE genotype, however.

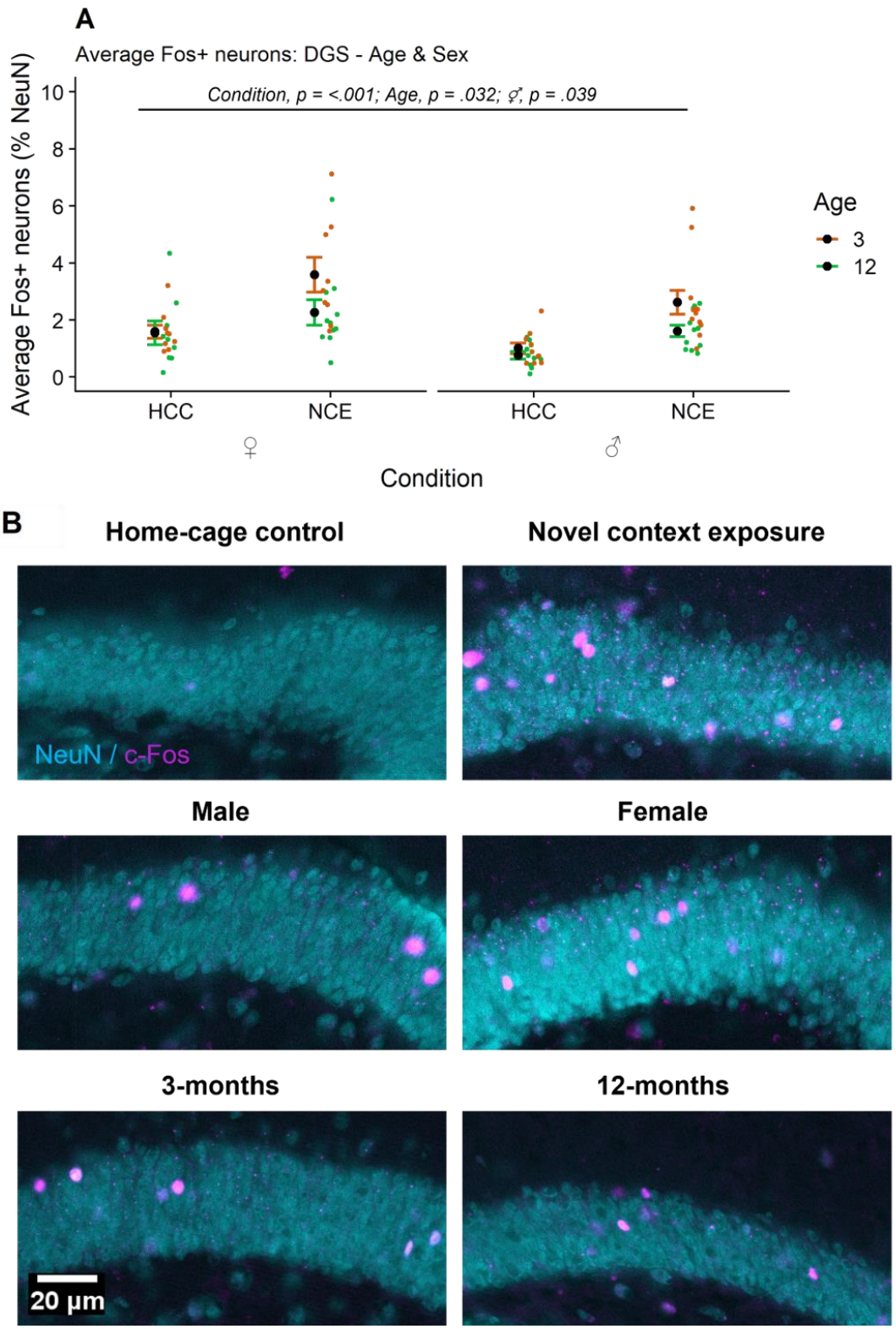

Figure 5.4: A) Average Fos+ neuron counts in the DGS granule cell layer expressed as the percentage of estimated NeuN+ neurons, grouped by condition, sex, and age. Brackets and labels represent relevant statistical main effects, interactions and pairwise comparisons where

appropriate. Individual points represent the average of each count across sections within a single animal. Error bars represent mean +/- SEM. B) Representative example immunofluorescence images of labelled Fos (magenta) and NeuN (cyan) neurons in the DGS granule cell layer grouped by condition, sex, and age.

5.3.1.5 Fos+ neuron density in the DGI

In the DGI, a main effect of genotype was apparent ($F(2,57) = 4.82$, $p = .025$). However, pairwise comparisons revealed no significant differences between the genotypes (E3-TR Vs E3E4-TR: MD = -0.41, SE = 0.36, $p = .260$; E3-TR Vs E4-TR: MD = 0.19, SE = 0.35, $p = .580$; E3E4-TR Vs E4-TR: MD = 0.21, SE = 0.35, $p = .550$), with high levels of variability observable within both E3E4-TR and E4-TR groups (Figure 5.5A/B). No other main effects of or interactions were significant.

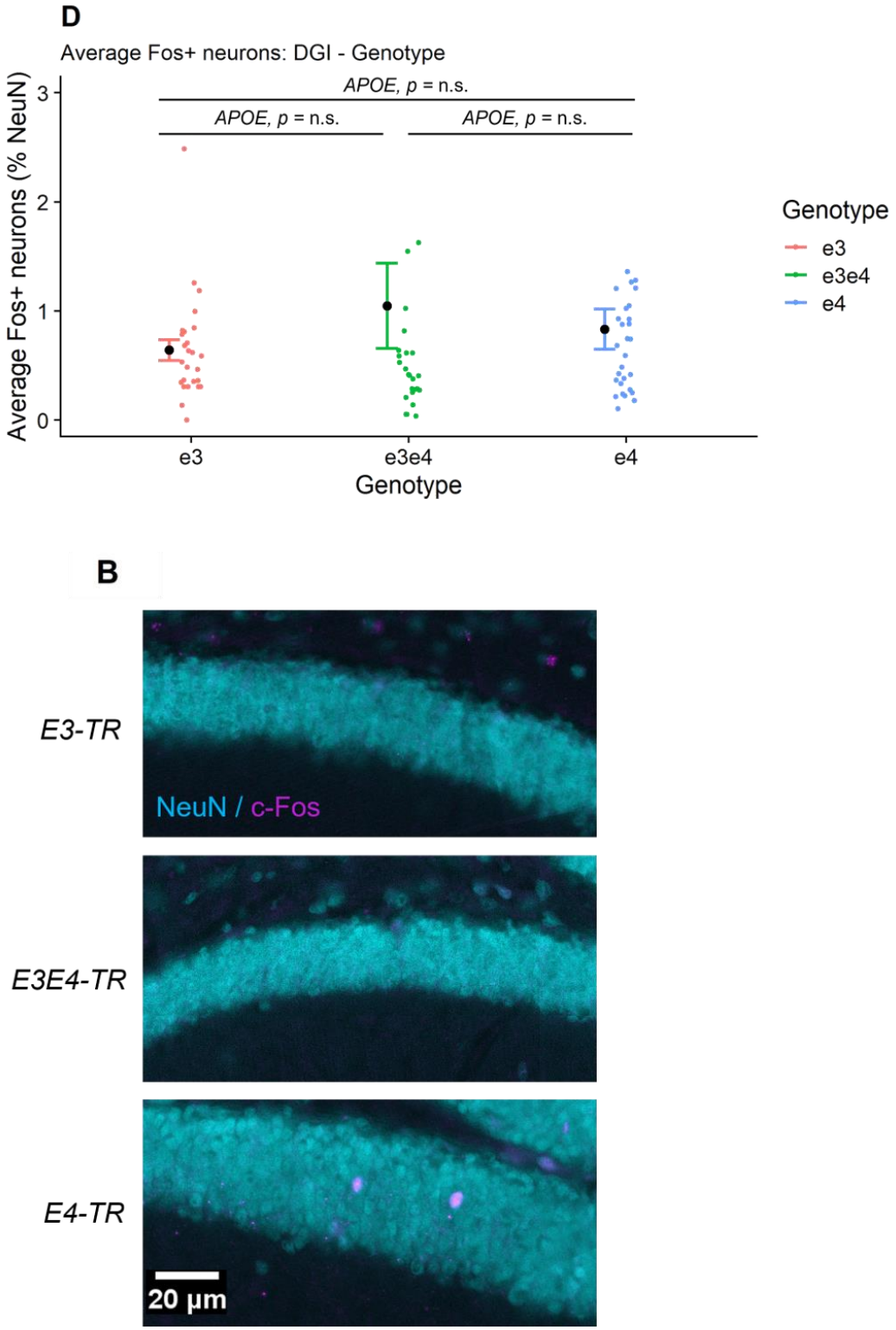

Figure 5.5: A) Average Fos+ neuron counts in the DGI granule cell layer expressed as the percentage of estimated NeuN+ neurons, grouped APOE genotype, across both home-cage and novel context conditions. Brackets and labels represent relevant statistical main effects, interactions and pairwise comparisons where appropriate. Individual points represent the average of each count across sections within a single animal. Error bars represent mean +/-

SEM. B) Representative example immunofluorescence images of labelled Fos (magenta) and NeuN (cyan) neurons in the DGI granule cell layer grouped by APOE genotype.

5.3.2 Hippocampal interneuron c-Fos activation in APOE-TR mice

Overall, the proportion of double-labelled Fos+/GAD+ interneurons within the principal pyramidal and particularly granule cells layers was sparse. This resulted in some cases having null values across all sampled sections for a given subregion. In the case of the DGS and DGI this was particularly apparent, with a mean value near floor, with influential cases resulting in significant deviations from the mean. Therefore, the DGS and DGI were excluded from analysis.

5.3.2.1 Fos+ interneuron density in CA1

There was a significant effect of condition in CA1, with significantly more Fos+ interneurons in the novel context than home-cage condition ($F(1,67) = 5.77$, $p = .019$, Figure 5.6A). There was no significant impact of APOE genotype ($F(2,67) = 0.95$, $p = .391$), sex ($F(1,67) = 0.02$, $p = .890$), or age ($F(1,67) = 0.61$, $p = .436$), on Fos+ interneuron density, however.

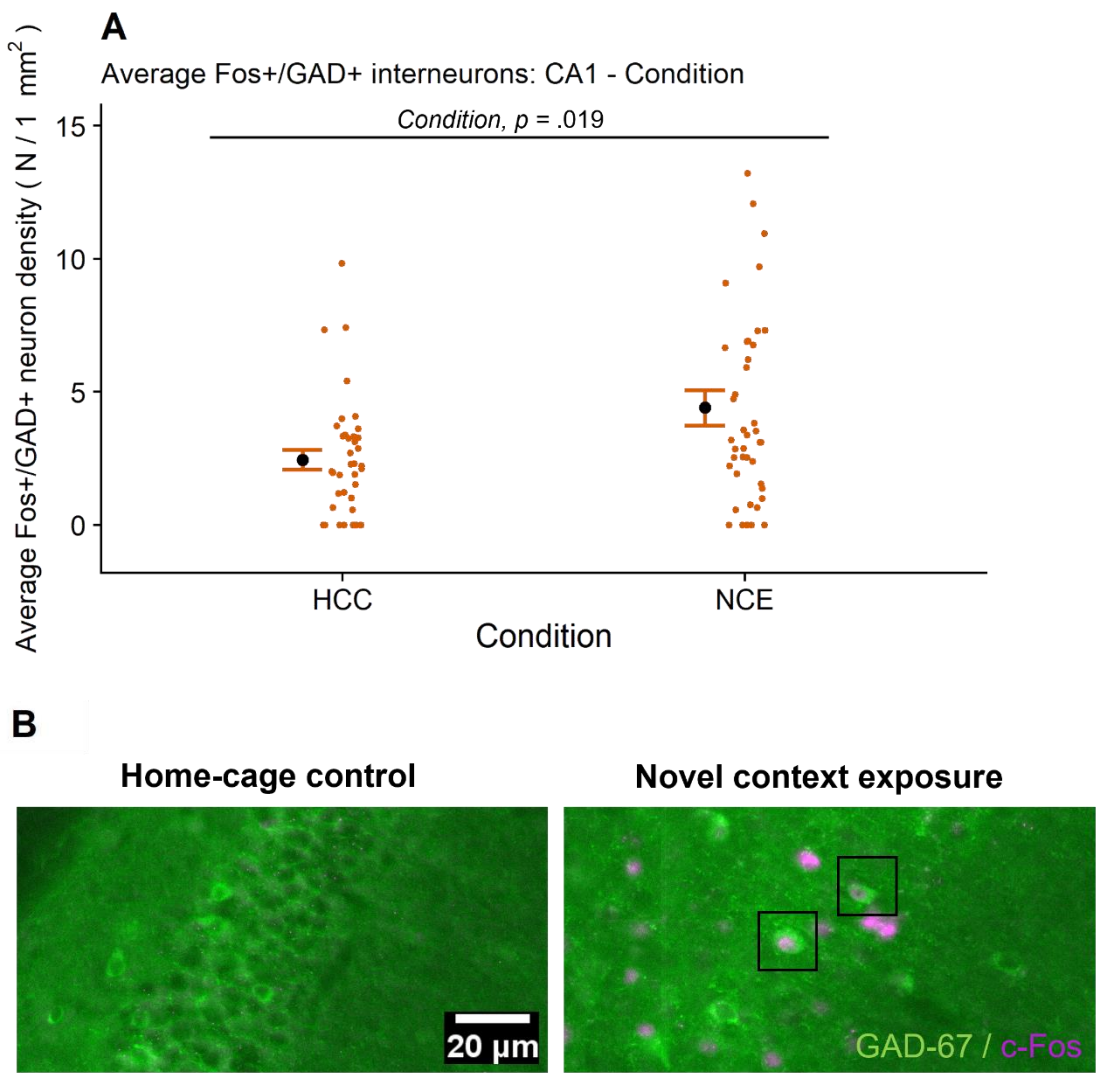

Figure 5.6: A) Average Fos+/GAD+ neuron counts in the CA1 pyramidal layer expressed as relative density per millimetre, grouped by condition. Brackets and labels represent relevant statistical main effects, interactions and pairwise comparisons where appropriate. Individual points represent the average of each count across sections within a single animal. Error bars represent mean +/- SEM. B) Representative example immunofluorescence images of labelled Fos (magenta) and GAD-67 (green) neurons in the CA1 pyramidal layer grouped by condition. Black boxes outline example double-labelled Fos+/GAD-67+ interneurons within the CA1 pyramidal layer.

5.3.2.2 Fos+ interneuron density in CA3

In CA3, there was no significant effect of condition ($F(1,67) = 1.64$, $p = .205$) or sex ($F(1,67) = 0.01$, $p = .937$), but a significant effect of age ($F(1,67) = 6.87$, $p = .011$) and a two-way interaction between genotype and age ($F(2,67) = 3.20$, $p = .047$). Overall, there was a greater density of Fos+ interneurons at 12-months relative to 3-month aged animals, while the interaction was driven by a main effect of age in E3E4-TR ($F(1,24) = 9.37$, $p = .005$) and E4-TR mice ($F(1,27) = 5.00$, $p = .034$), but not E3-TR mice ($F(1,24) = 0.47$, $p = .499$; Figure 5.7A/B).

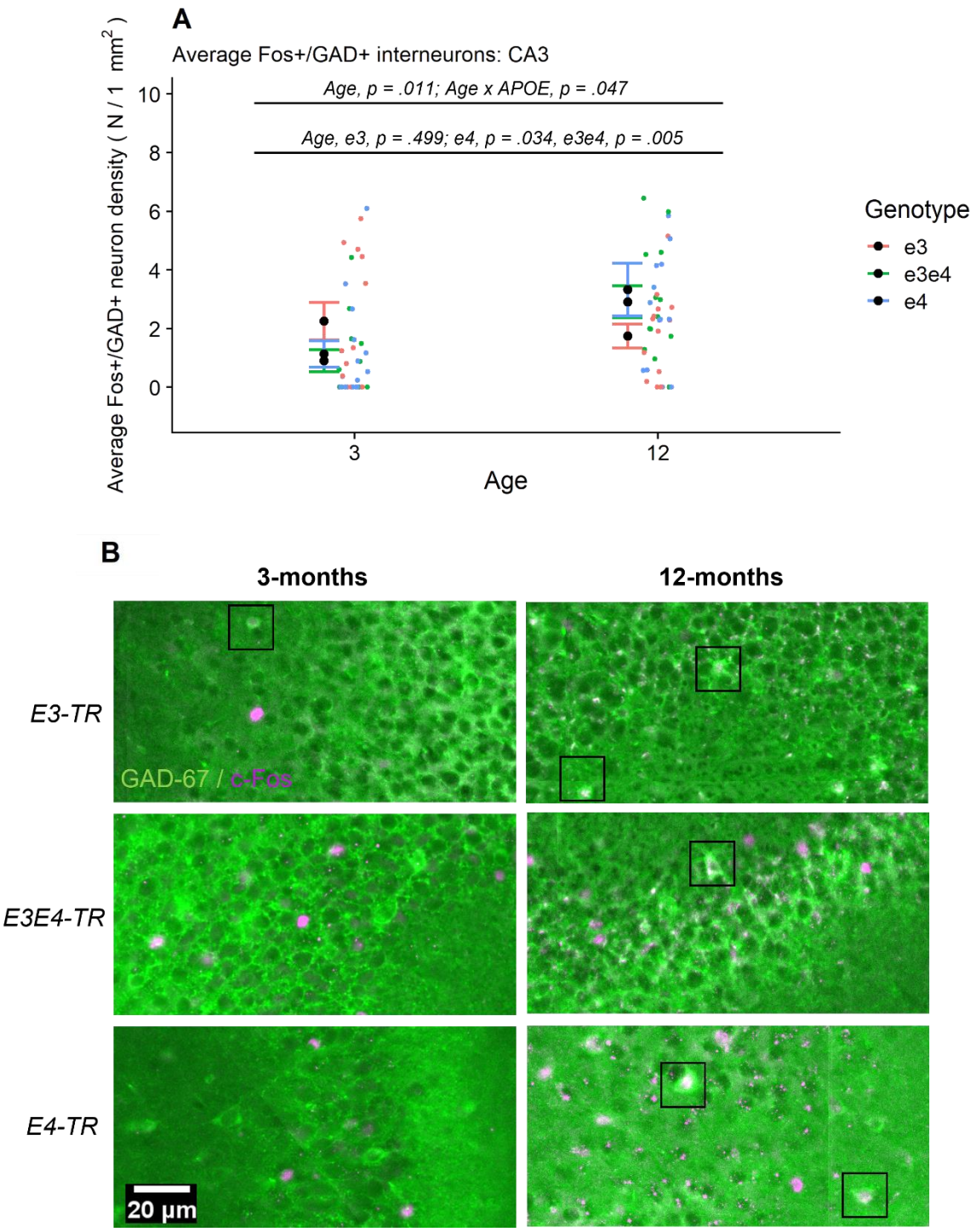

Figure 5.7 A) Average Fos+/GAD+ neuron counts in the CA3 pyramidal layer expressed as relative density per millimetre, grouped by APOE genotype and age. Brackets and labels represent relevant statistical main effects, interactions and pairwise comparisons where appropriate. Individual points represent the average of each count across sections within a single animal. Error bars represent mean +/- SEM. B) Representative example immunofluorescence images of labelled Fos (magenta) and GAD-67 (green) neurons in the CA3

pyramidal layer grouped by APOE genotype and age. Black boxes outline example double-labelled Fos+/GAD-67+ interneurons within the CA3 pyramidal layer.

5.3.3 GAD-67 immunoreactivity in APOE-TR mice

To investigate whether APOE genotype was associated with alterations in putative perisomal GABAergic termini, we quantified GAD-67 immunoreactivity within primary pyramidal and granule cell layers, and the hilar layer (e.g., Li et al., 2009; Andrews-Zwilling et al., 2010).

5.3.3.1 GAD-67 immunoreactivity in CA1

Univariate analysis revealed a main effect of APOE genotype ($F(2,57) = 3.95$, $p = .043$) and a significant interaction between genotype and sex in CA1 ($F(2,57) = 6.25$, $p = .011$). However, simple main effects analysis of the interaction demonstrated only trends towards a main effect of genotype in male ($F(2,35) = 2.86$, $p = .070$) and female ($F(2,32) = 2.53$, $p = .096$) APOE-TR mice, with the lowest immunoreactivity in E4-TR female and E3-TR male mice (Figure 5.8A/B).

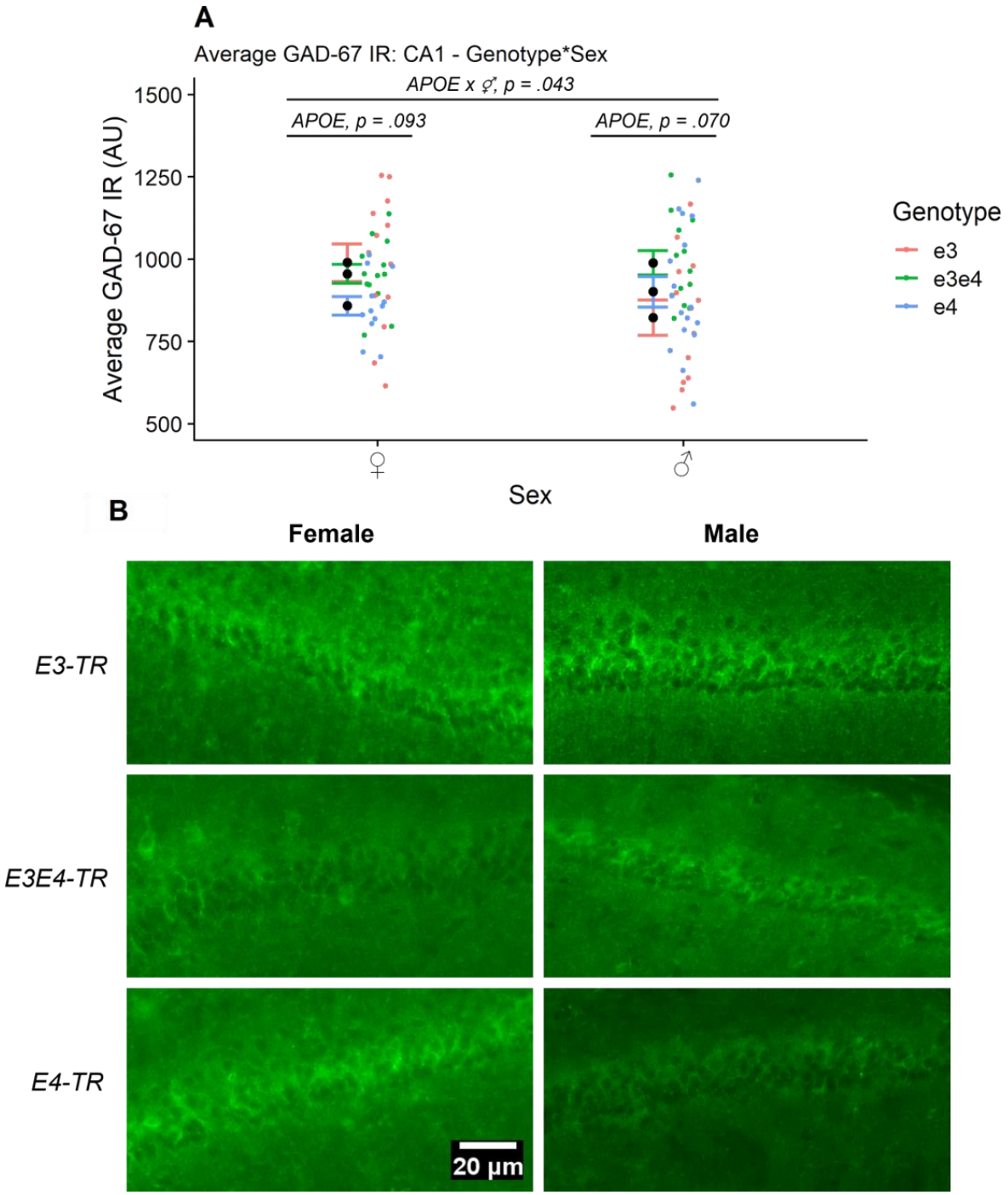

Figure 5.8: A) Average GAD-67 immunoreactivity (IR) in the CA1 pyramidal cell layer of APOE-TR mice, expressed as the mean fluorescence intensity, grouped by APOE genotype and sex. Brackets and labels represent relevant statistical main effects, interactions and pairwise comparisons where appropriate. Individual points represent the IR measurement averaged across sections within a single animal. Error bars represent mean +/- SEM. B) Representative

example immunofluorescence images of labelled GAD-67 (green) immunoreactivity in the CA1 pyramidal layer grouped by APOE genotype and sex.

5.3.3.2 GAD-67 immunoreactivity in CA3

In CA3, there was only a main effect of age on GAD-67 immunoreactivity ($F(2,57) = 4.95$, $p = .023$), with the 12-month aged group showing significantly higher immunoreactivity than 3-month aged animals (Figure 5.9A/B). There were no other significant main effects or interactions (Supplementary Figure 5.3).

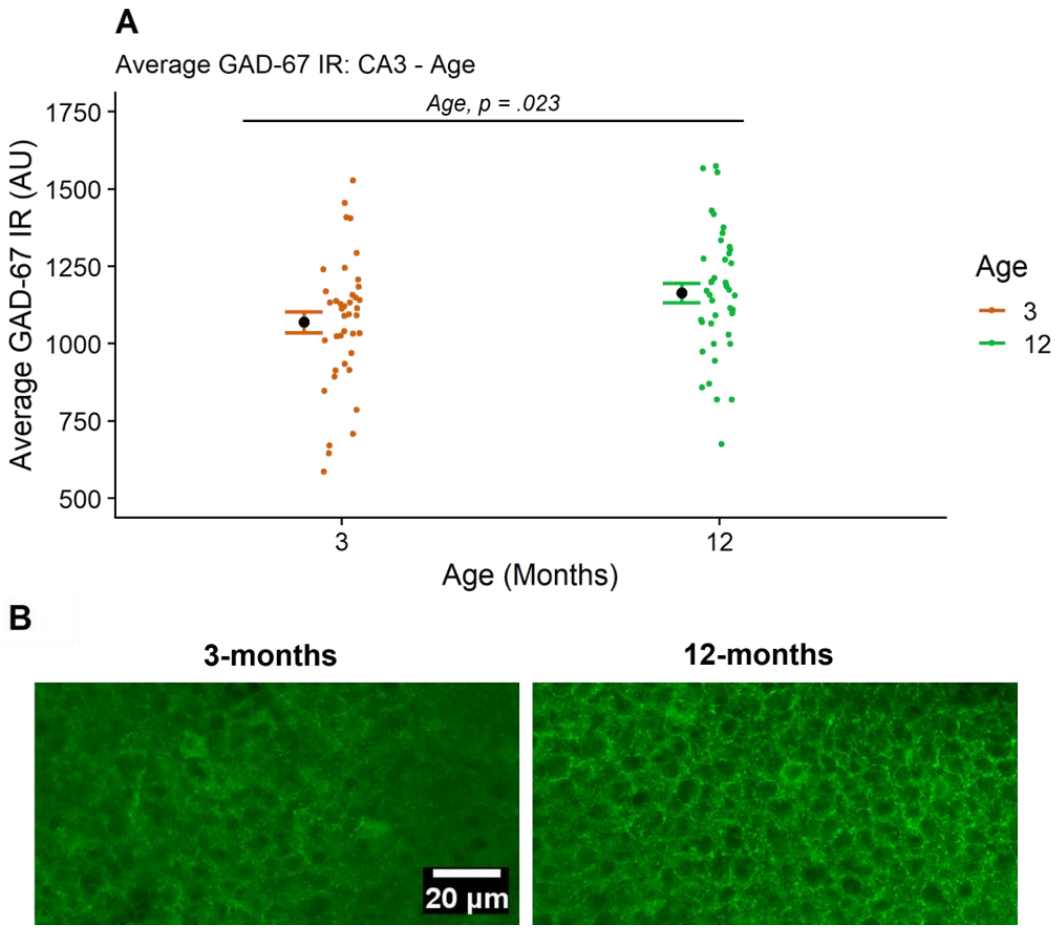

Figure 5.9: A) Average GAD-67 immunoreactivity (IR) in the CA3 pyramidal cell layer of APOE-TR mice, expressed as the mean fluorescence intensity, grouped by age independent of APOE genotype and sex. Brackets and labels represent relevant statistical main effects, interactions and pairwise comparisons where appropriate. Individual points represent the IR measurement averaged across sections within a single animal. Data grouped by APOE genotype and sex can be seen in Supplementary Figure 5.3. Error bars represent mean +/- SEM. B) Representative example immunofluorescence images of labelled GAD-67 (green) immunoreactivity in the CA3 pyramidal layer from E3-TR mice (matched genotype) grouped by age.

5.3.3.3 GAD-67 immunoreactivity in the DGS

Similar to CA1, there was a significant interaction between APOE genotype and sex in DGS GAD-67 immunoreactivity ($F(2,57) = 5.39$, $p = .018$), however there were no significant main effects of genotype in either males ($F(2,35) = 2.00$, $p = .148$) or females ($F(2,32) = 1.31$, $p = .282$) upon follow-up analysis (Figure 5.10A/B). There were no further significant main effects of interactions.

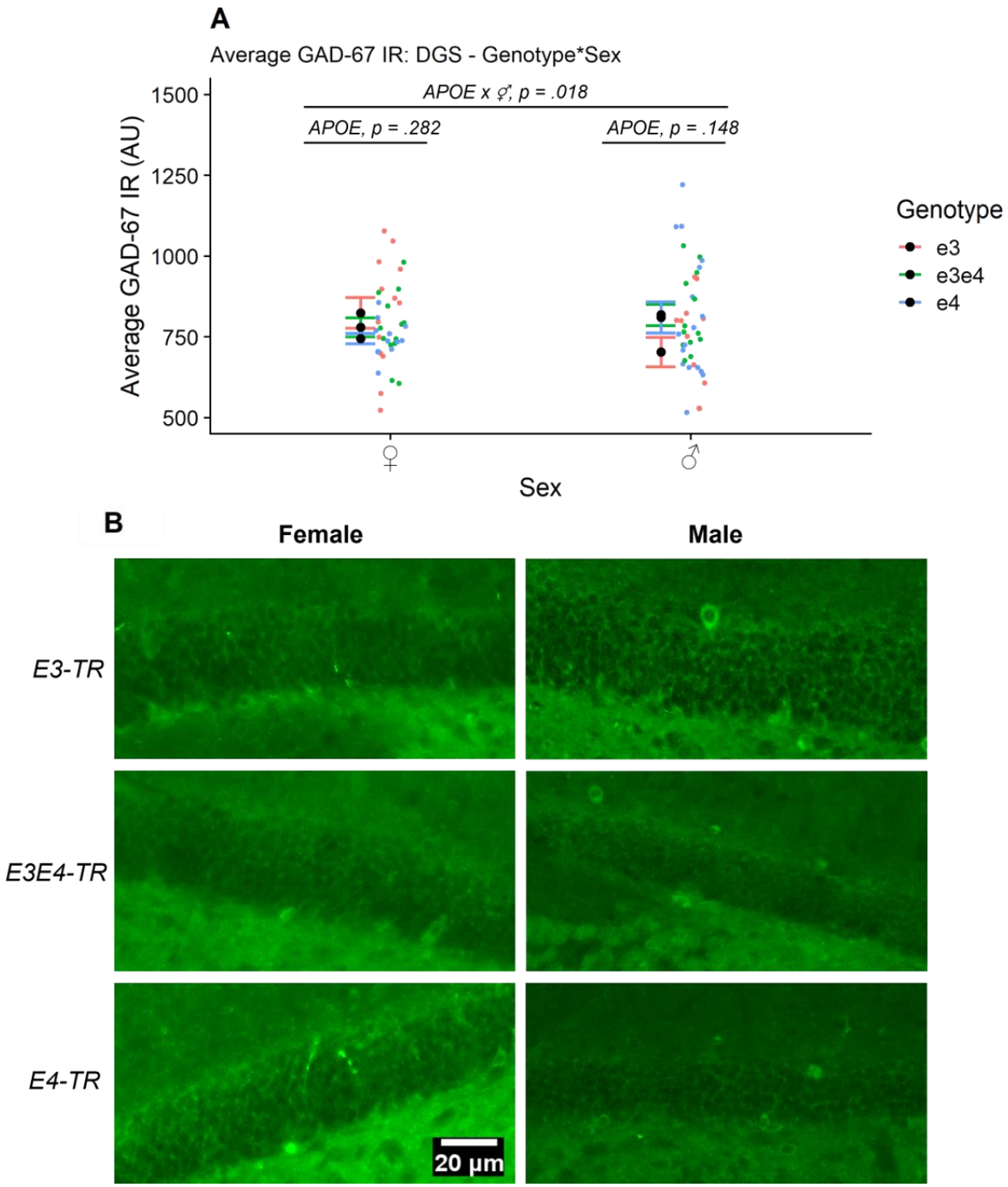

Figure 5.10: A) Average GAD-67 immunoreactivity (IR) in the DGS granule cell layer of APOE-TR mice, expressed as the mean fluorescence intensity, grouped by APOE genotype and sex. Brackets and labels represent relevant statistical main effects, interactions and pairwise comparisons where appropriate. Individual points represent the IR measurement averaged across sections within a single animal. Error bars represent mean +/- SEM. B) Representative

example immunofluorescence images of labelled GAD-67 (green) immunoreactivity in the DGS granule cell layer grouped by APOE genotype and sex.

5.3.3.4 GAD-67 immunoreactivity in the DGI

There was again a significant interaction between genotype and sex in DGI GAD-67 immunoreactivity ($F(2,57) = 7.23$, $p = .006$), with a main effect of genotype in female ($F(2,32) = 3.42$, $p = .045$), but not male ($F(2,35) = 2.14$, $p = .132$), APOE-TR mice. E4-TR female mice had significantly reduced GAD-67 immunoreactivity relative to E3-TR controls (MD = 119.29, SE = 49.81, $p = .022$) and a similar trend to a reduction in E3E4-TR mice (MD = 85.80, SE = 48.81, $p = .088$), while there was comparable immunoreactivity between E4-TR and E3E4-TR mice (MD = 33.48, SE = 49.81, $p = .510$; Figure 5.11A/B). There was also a significant main effect of age, with the 12-month aged group showing higher GAD-67 immunoreactivity than 3-month aged mice ($F(1,57) = 3.90$, $p = .044$).

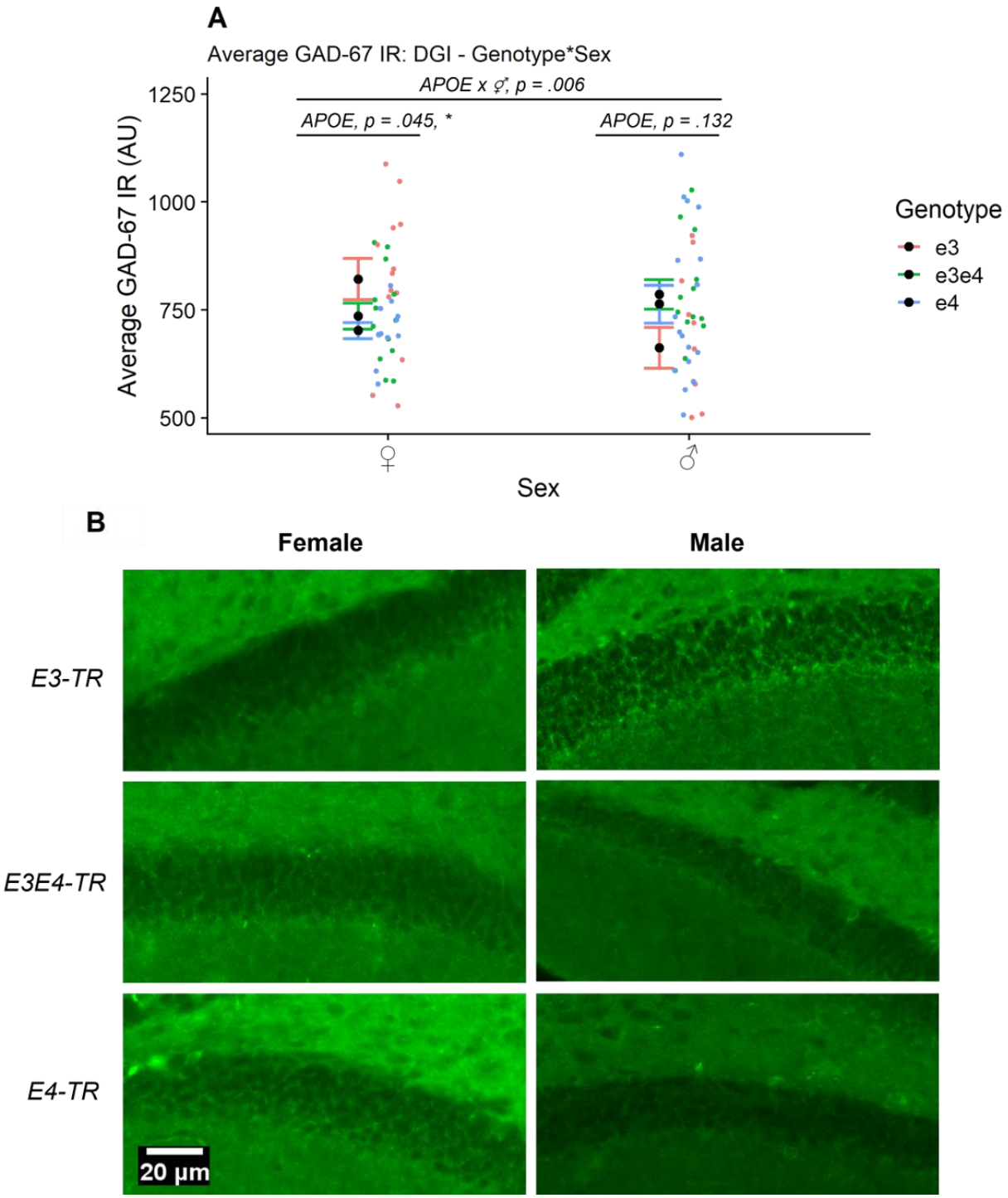

Figure 5.11: A) Average GAD-67 immunoreactivity (IR) in the DGI granule cell layer of APOE-TR mice, expressed as the mean fluorescence intensity, grouped by APOE genotype and sex. Main effect of age is also represented in figure inset. Brackets and labels represent relevant statistical main effects, interactions and pairwise comparisons where appropriate. Individual points represent the IR measurement averaged across sections within a single animal. Error bars represent mean +/- SEM. Symbols represent significant comparisons at p = <.05: ''*

represents E3-TR Vs E4-TR, '#' represents E3E4-TR Vs E4-TR, '$' represents E3-TR Vs E3E4-TR. B) Representative example immunofluorescence images of labelled GAD-67 (green) immunoreactivity in the DGI granule cell layer grouped by APOE genotype and sex.

5.3.3.5 GAD-67 immunoreactivity in the DGH

GAD-67 immunoreactivity was also quantified in the DG hilar layer (DGH), revealing near identical results to that observed in the DGI. Namely, there was a significant interaction between genotype and sex ($F(2,57) = 2.32$, $p = .020$), which was driven by a main effect of genotype in female ($F(2,32) = 3.49$, $p = .041$) , but not male ($F(2,35) = 1.19$, $p = .315$) mice. Both E3E4-TR (MD = 148.51, SE = 68.20, $p = .036$) and E4-TR (MD = 165.03, SE = 69.61, $p = .023$) female mice exhibited significantly lower GAD-67 immunoreactivity than female E3-TR controls, while there was no significant difference between E3E4-TR and E4-TR mice (MD = 16.52, SE = 68.61, $p = .814$; Figure 5.12A/B).

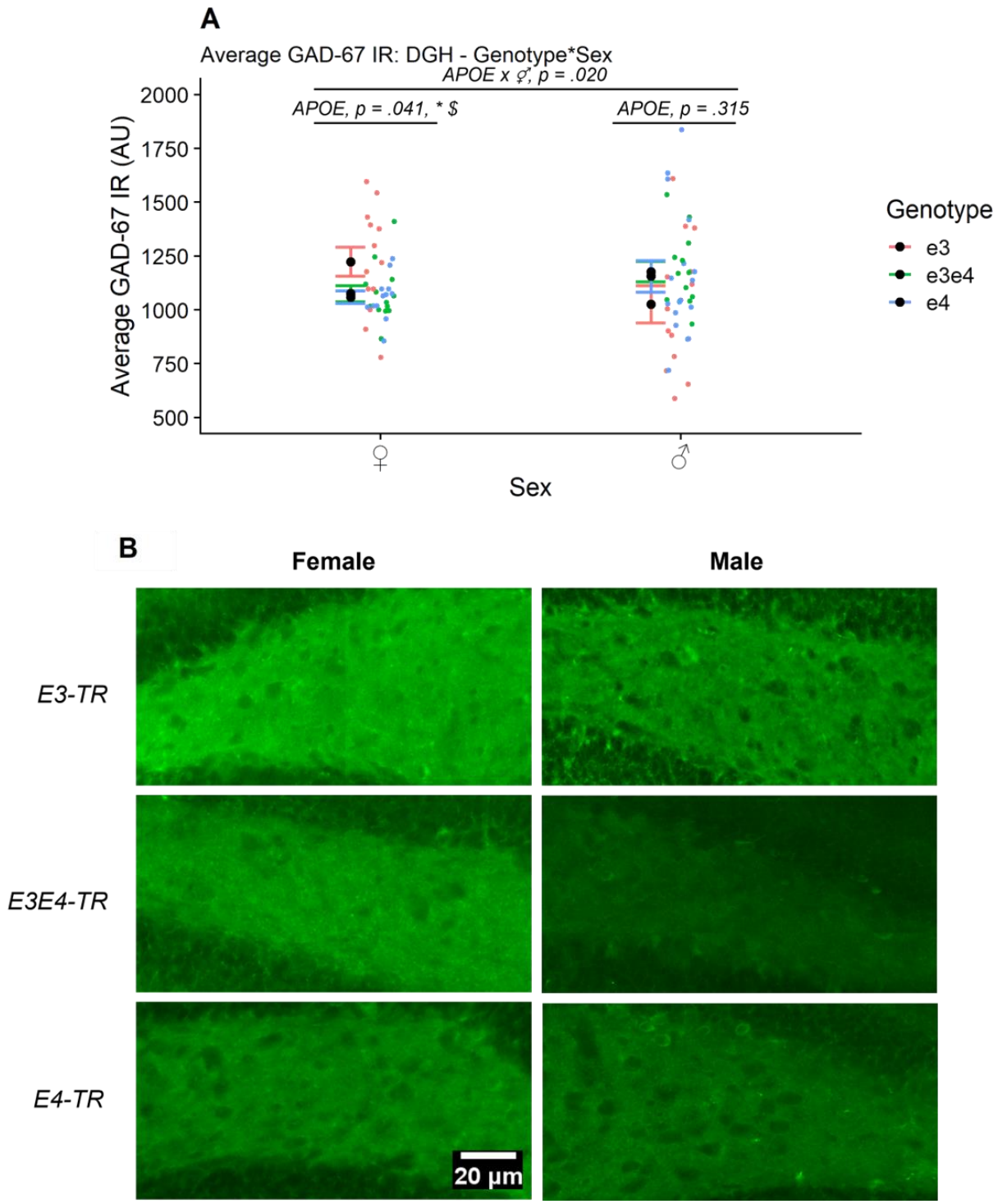

Figure 5.12: A) Average GAD-67 immunoreactivity (IR) in the DG hilar (DGH) layer of APOE-TR mice, expressed as the mean fluorescence intensity, grouped by APOE genotype and sex. Brackets and labels represent relevant statistical main effects, interactions and pairwise comparisons where appropriate. Individual points represent the IR measurement averaged across sections within a single animal. Error bars represent mean +/- SEM. Symbols represent significant comparisons at p = <.05: '' represents E3-TR Vs E4-TR, '#' represents E3E4-TR Vs E4-*

TR, '$' represents E3-TR Vs E3E4-TR. B) Representative example immunofluorescence images of labelled GAD-67 (green) immunoreactivity in the DG hilar layer grouped by APOE genotype and sex.

5.3.4 Experiment two: Analysis of DGH interneuron loss across the lifespan of APOE-TR mice

We next investigated the possibility that loss of GABAergic interneurons within the DGH may occur and be associated with changes in hippocampal network activity. The relative densities of GAD-67+ DGH interneurons was quantified in the present cohort (3-12-months) as well as an additional cohort of aged (18-months) APOE-TR mice which were processed without exposure to a novel context.

We observed a significant main effect of age ($F(2,59) = 15.70$, $p = <.001$), with DGH GABA-IN density decreasing across the lifespan, however this was mediated by a three-way interaction between age, sex, and APOE genotype ($F(2,59) = 6.21$, $p = .011$). Follow-up simple main effects analysis of the three-way interaction revealed a genotype by age interaction in female ($F(2,28) = 6.19$, $p = .011$) but not male ($F(2,32) = 0.89$, $p = .336$) APOE-TR mice. Follow-up of the genotype by age interaction in female APOE-TR mice revealed no significant main effect of genotype at any level of age, however (3-months: $F(1,10) = 2.68$, $p = .095$; 12-months: $F(1,11) = 1.87$, $p = .160$; 18-months: $F(1,7) = 0.44$, $p = .500$; Figure 5.11). Male APOE-TR mice, however, demonstrated a main effect of age ($F(2,31) = 4.33$, $p = .034$), with GAD-67+ DGH interneuron density decreasing significantly at 18-months relative to 3-months (MD = -8.12, SE = 3.04, $p = .038$) but not 12-months (MD = -6.28, SE = 3.00, $p = .132$; Figure 5.13A-C).

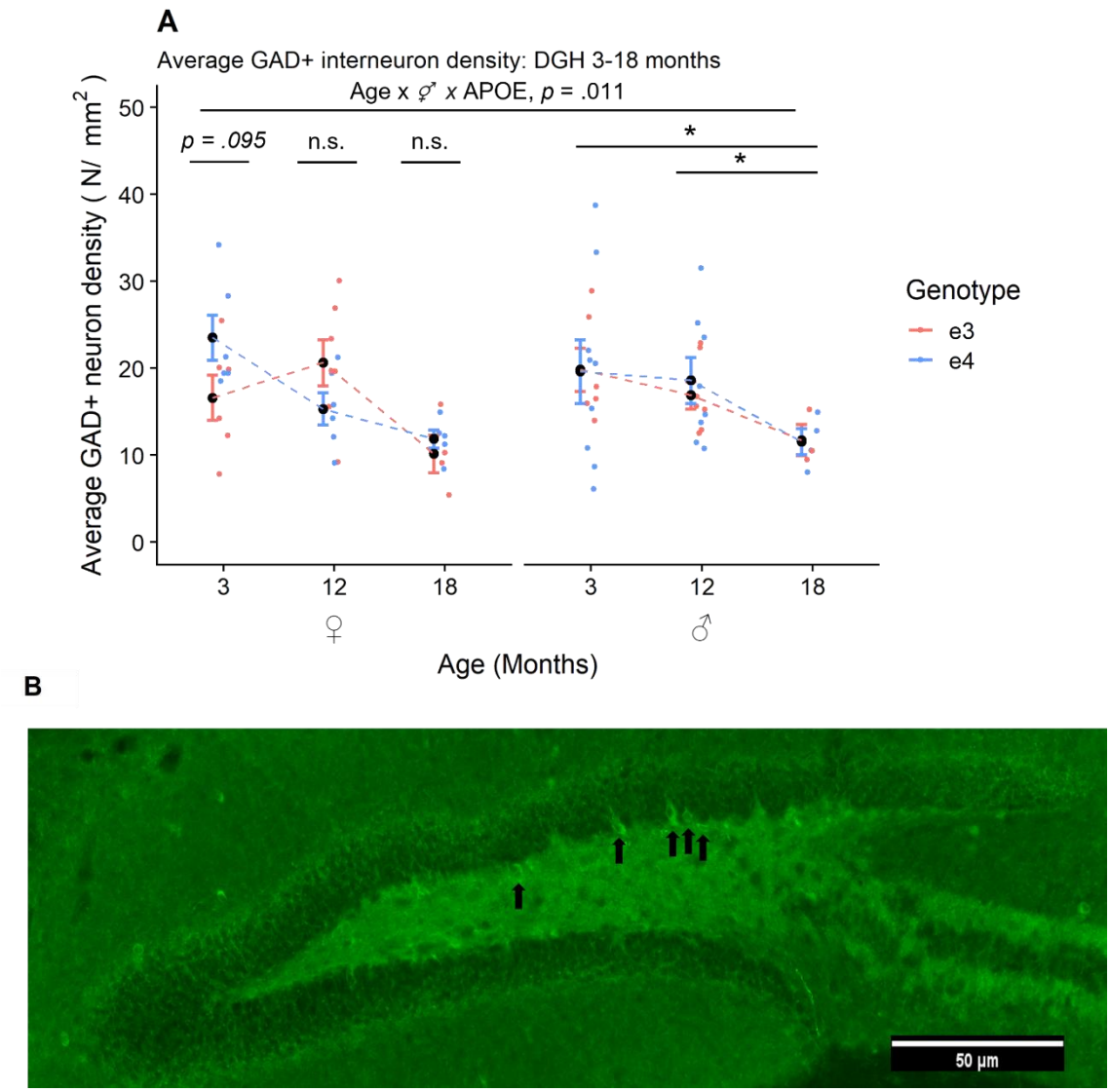

Figure 5.13 panel 1: A) Average DGH GAD-6 7+ interneuron density expressed as cell/mm^2 across the lifespan of APOE-TR mice grouped by APOE genotype, age, and sex. Individual points represent densities averaged across sections within a single animal. Error bars represent mean +/- SEM. Brackets and labels represent relevant statistical main effects, interactions and pairwise comparisons where appropriate. B) Example representative magnified image of DG granule and hilar region showing GAD-67 immunoreactivity and labelled GAD-67+ interneurons. Black arrows highlight GAD-67+ interneurons within the DGH that meet quantification criteria. Note that both interneurons within the hilus proper and at the borders of but not within the deep granule cell layer are included.

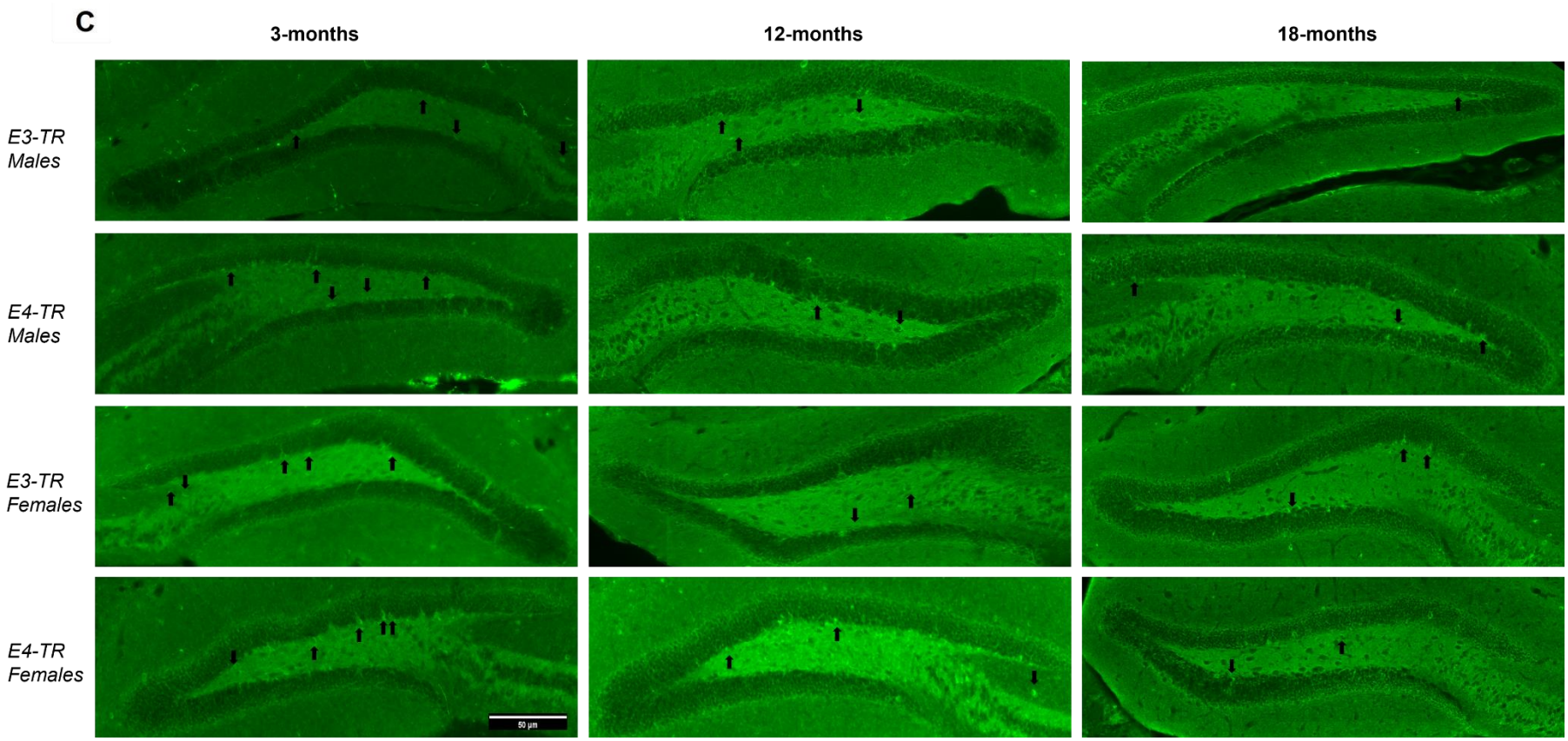

Figure 5.13 panel 2: C) Individual representative example images of DG granule and hilar region for GAD-67 immunoreactivity and GAD-67+ interneurons. Black boxes again highlight GAD-67+ interneurons within the DGH. Examples are shown for each relevant condition shown in A), grouped by APOE genotype, sex, and age. Black arrows represent GAD-67+ interneurons within the DGH meeting quantification criteria.

5.3.5 Exploratory analyses: Network correlation analysis of Fos+ neuron density across hippocampal subregions in APOE-TR mice.

Following these observations of subregion-dependent effects on hippocampal neuronal activity, we performed exploratory correlational analyses between subregions using Fos+ neuron density as a proxy for network coactivation, as has been reported previously (e.g., George et al., 2012; Moench et al., 2019; Haberman et al., 2019). Cross-correlating Fos+ neuron density (referred to in the context of regional cross-correlations as network activity) between principal hippocampal regions CA1, CA3 and DG, we generated correlation matrices across conditions, comparing the profiles of network correlation. Given the general observations that E4-TR mice exhibited a greater shift in Fos+ neuron density than heterozygous E3E4-TR mice, we made comparisons of the extreme genotypes, E3-TR and E4-TR mice. DGI Fos+ neuron density was also excluded from this analysis due to the observation of a lack of significant novelty response and a low baseline activity.

Firstly, examining the effect of novel context exposure, we observed that at the whole group level, there were moderate positive correlation between all regions, presumably due to a relatively quiescent state and low basal neuronal activity, insufficient to induce substantial detectable c-Fos expression. Following exposure to the novel context, these network correlations decreased, but with significant correlations remaining between each region (Figure 5.14A/B). We next investigated the influence of age on the network, observing a conserved pattern of correlations between 3 and 12-month aged animals, with particularly strong positive correlations between CA1-CA3 and more moderate correlations between CA3-DG and CA1-DG at both ages (Figure 5.14C/D). Finally, we observed significant correlations between each subregion in both male and female mice, with somewhat stronger correlations observed in females between CA1-CA3 and CA1-DGS (Figure 5.14E/F).

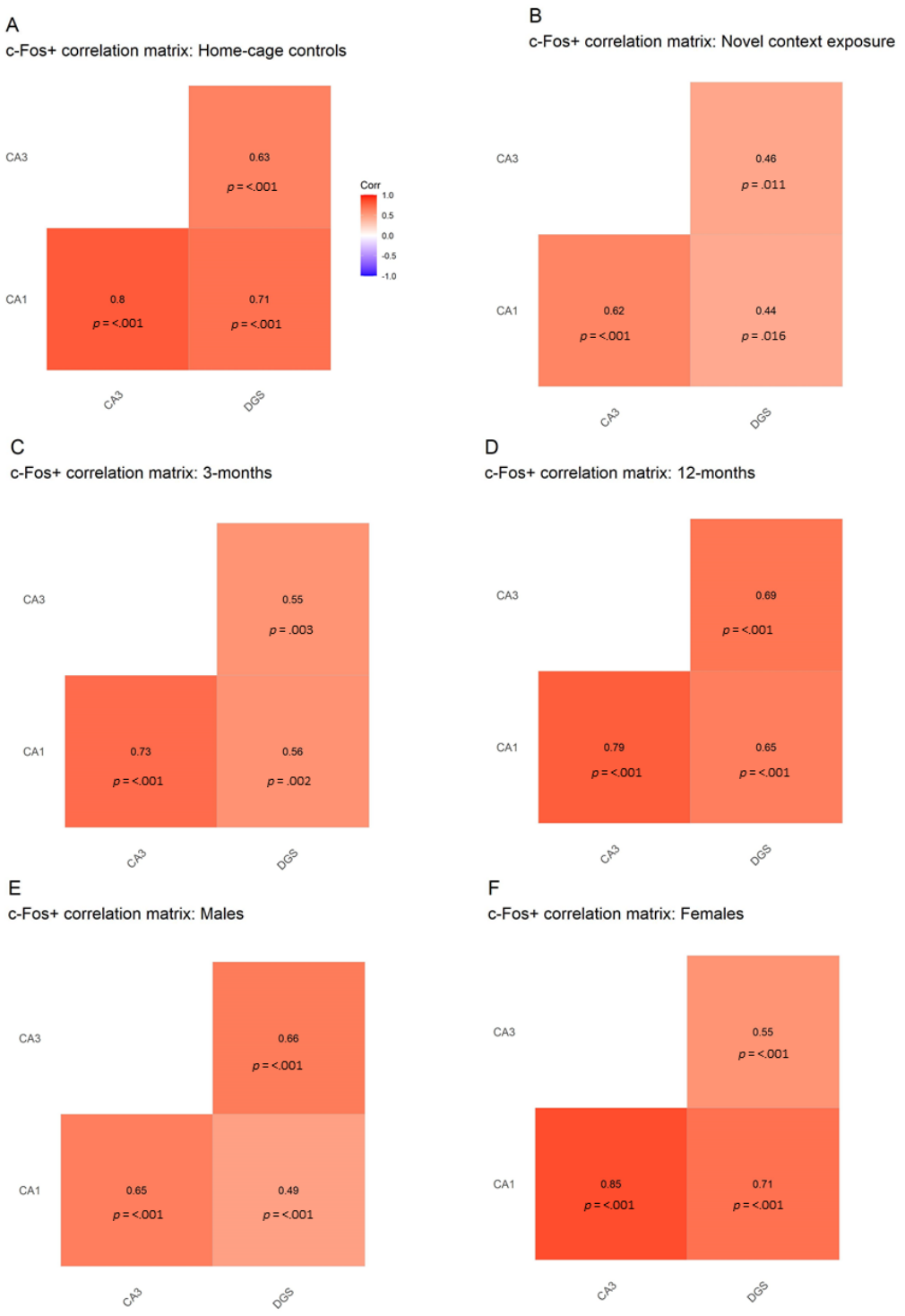

Figure 5.14: Correlation matrix heat maps of Fos+ neuron density in CA1-CA3-DG network in APOE-TR mice, grouped by A) home-cage control, B) novel context exposure, C) 3-months age group, D) 12-months age group, E) male mice, F) female mice. Individual cells represent individual correlation between subregions on the X and Y axis frame, while individual values represent the Pearson's correlation coefficient and corresponding p-values. Colour 'warmth' represents directionality and strength of individual correlations. "X" within individual cells of

the matrix represents a correlation above an alpha threshold of 0.05 (note in the case of Figure 5.14, all are below this threshold).

Further analysis demonstrated that network correlations were modulated by APOE genotype and sex. We collapsed the groups across age and exposure condition to increase power and given the similar correlation patterns observed between 3 and 12-month groups (Figure 5.14C/D). Doing so, we observed sex specific differences in strength of network correlations between genotypes. Firstly, E4-TR females demonstrated significant strong positive correlations between CA1-CA3, DG-CA1, and a moderate correlation between DG-CA3, while E3-TR females exhibited only a strong positive correlation between CA1-CA3 and no significant correlations between CA1/CA3-DG (Figure 5.15A/B). Conversely, we observed almost the inverse pattern of results in male APOE-TR mice, with significant strong correlations between CA1-CA3, DG-CA1, and DG-CA3 in E3-TR male mice, but only moderate correlations between CA1-CA3 and DG-CA3 and no significant correlation between DG-CA1 in male E4-TR mice (Figure 5.15C/D). Together, this demonstrated an overall increase in between region correlations in E4-TR female and E3-TR male mice relative to their sex-matched controls, with a more pronounced increase in female E4-TR mice (Figure 5.15E-G).

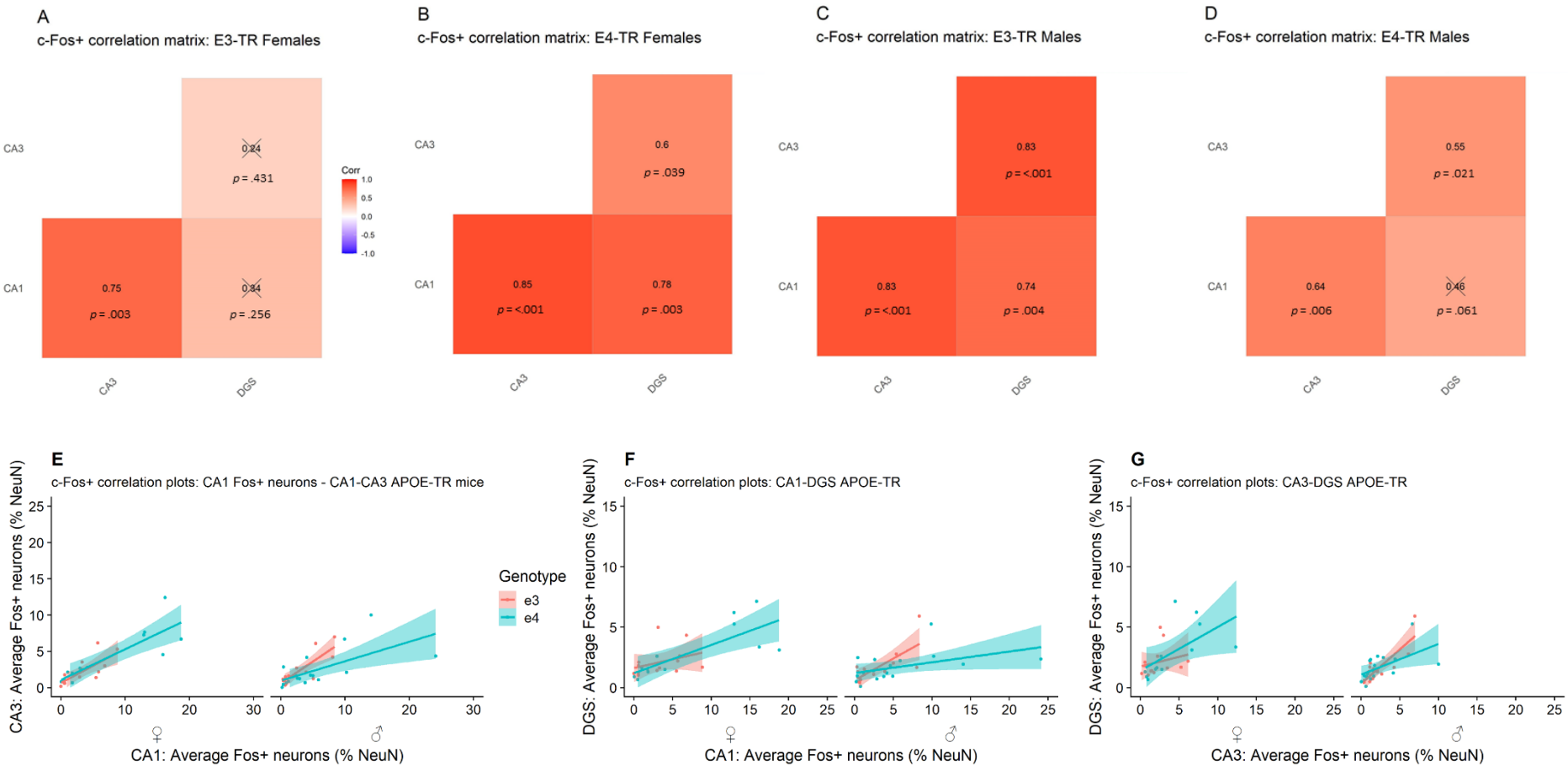

Figure 5.15: Correlation matrix heat maps of Fos+ neuron density in CA1-CA3-DG network in APOE-TR mice, grouped by A) female E3-TR mice, B) female E4-TR mice, C) male E3-TR mice, D) male E4-TR mice. Individual cells represent individual correlation between subregions on the X and Y axis frame, while individual values represent the Pearson's correlation coefficient and corresponding p-values. Colour 'warmth' represents directionality and strength of individual correlations. "X" within individual cells of the matrix represents a correlation above an alpha threshold of .05. G) Plots of Fos+ neuron density data

comprising correlation matrices, grouped by sex and genotype across individual network components: E) CA1-CA3, F) CA1-DGS, G) CA3-DGS. Individual points represent the average of each Fos+ density count across sections within a single animal. Line plots represent linear model fit and 95% confidence interval 'window' within each relevant group.

5.3.6 Experiment three: Quantification of whole hippocampal c-Fos and APOE mRNA response in APOE-TR mice

As described in section 2.2.3 hemi-hippocampi from the opposing hemisphere to that used for immunofluorescence was processed for qPCR analysis of c-Fos and APOE mRNA. Analysis was performed on the delta Ct (dCT) values, representing GOI Ct normalised to the multi-gene reference factor as described in section 2.2.4.6. For clarity of representation in figures the delta-delta Ct (DDCt) method was used, which represents the difference in threshold cycle between the experimental and control groups. For the purpose of experiment three, the reference group used was the E3-TR home-cage control group. For reference, a 2-fold change corresponds to a DDCt of 1.0, 4-fold to a DDCt of 2.0 etcetera.

5.3.6.1 Whole hippocampal c-Fos mRNA

Quantification of whole hippocampal c-Fos mRNA revealed a number of interactions between APOE genotype, sex, and age. As expected, a univariate analysis demonstrated a significant main effect of environmental novelty, with exposure to the novel environment inducing a significant increase in hippocampal c-Fos mRNA (Figure 5.16A, Table 5.3). Further there was a main effect of age, with a reduction in c-Fos mRNA expression at 12-months relative to 3-months (Fig 5.16B, Table 5.3). A significant three-way interaction between genotype, sex, and age mediated these effects, however (compound two-way interactions also shown in Table 5.3). Simple main effects analysis demonstrated that the three-way interaction was driven by differential sex by genotype interactions between age groups.

Namely, at 3-months, there was a significant sex by genotype interaction. Male mice showed a dose dependent effect of APOE4 on c-Fos expression, with a significant decrease in c-Fos mRNA in E4-TR mice relative to both E3-TR and E3E4-TR mice. Female mice, however, did not show this pattern, with E3E4-TR mice showing lower c-Fos expression than E4-TR mice and a similar trend relative to E3-TR mice. At 12-months, however, these effects were no longer apparent, with equivalent expression across all genotype and sex groups (Figure 5.16C, Table 5.3). Notably, there was no significant interactions between condition and any other variable.

5.3.6.2 Whole hippocampal APOE mRNA

In contrast, whole hippocampal APOE mRNA demonstrated an expression profile dependent only on age and genotype. Firstly, as would be expected, there was no main effect of condition, with comparable expression levels across home-cage and novel context conditions ($F(1,56) = 0.00$, $p = .967$). Thus, these groups were combined for further analysis. There were significant main effects of age, genotype, but not sex, and a significant age by genotype interaction (Figure 5.16D, Table 5.3). Simple main effects analysis demonstrated this age by genotype interaction was driven by main effects of genotype at both 3 and 12-months, with a differential influence of APOE4 dosage on expression.

Specifically, at 3-months there was significant reduction in APOE mRNA in E4-TR mice, relative to both E3-TR and E3E4-TR mice, but no difference between E3-TR and E3E4-TR mice. In contrast, at 12-months, this expression profile reversed, with similar expression of APOE between E3-TR and E4-TR mice, while E3E4-TR mice had significantly elevated APOE mRNA expression relative to both E3-TR and E4-TR mice. Notably, the expression profile of E4-TR mice appeared equivalent between 3-12 months, while E3-TR mice decreased over this period and E3E4-TR mice retained equivalent APOE mRNA levels to that observed at 3-months (Figure 5.16D, Table 5.3). Finally, correlations between APOE and c-Fos mRNA revealed no significant overall correlation, or any modulation by genotype or sex (Table 5.4).

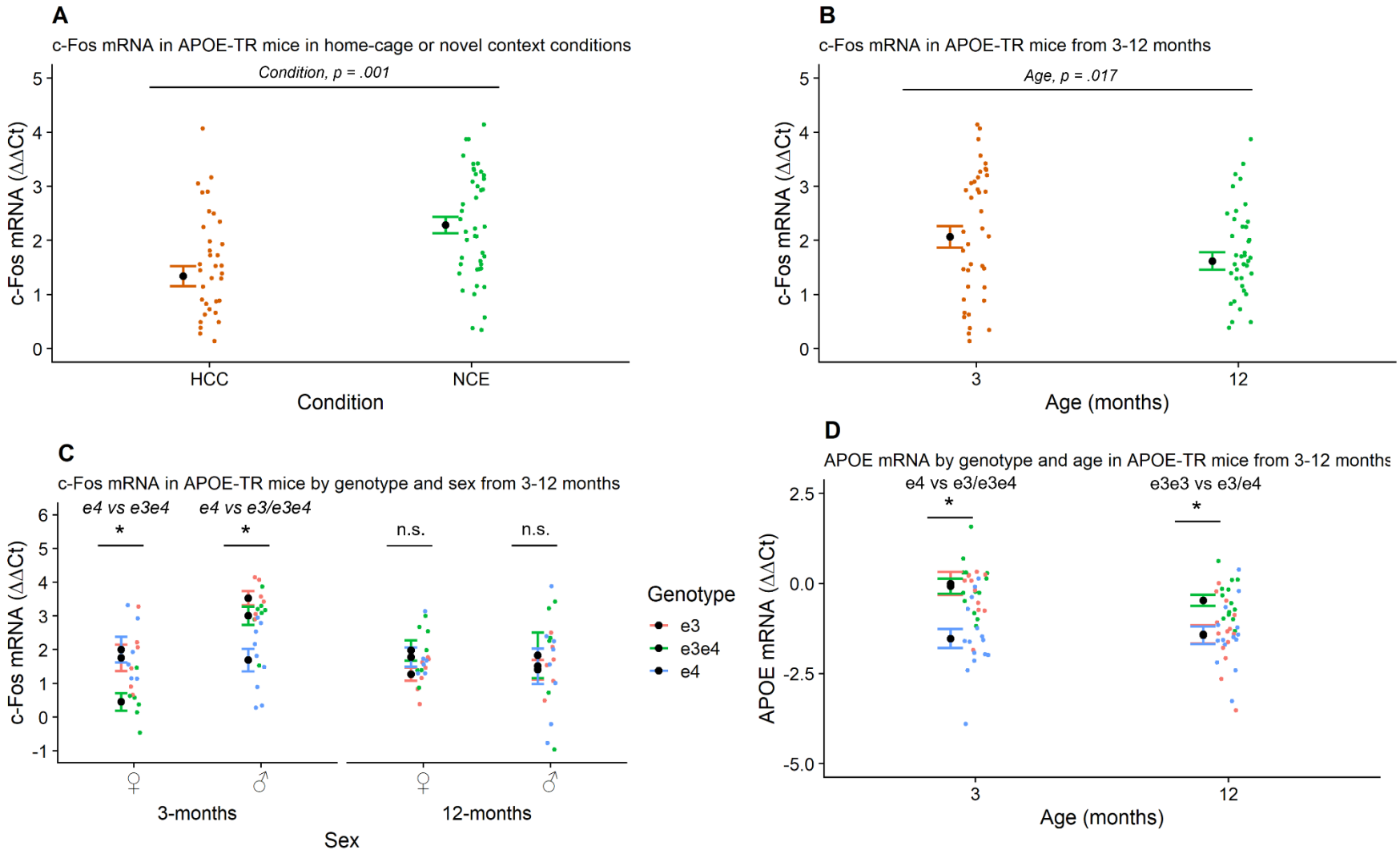

Figure 5.16: Average ddCt of c-Fos and APOE mRNA from hippocampal samples of APOE-TR mice at 3-12-months, normalised to a multi-gene reference gene factor with the reference group set as the E3 home-cage control (HCC). c-Fos mRNA grouped by A) home-cage (HCC) or novel context exposure (NCE) conditions or B) age from 3-12 months. C) c-Fos mRNA ddCt grouped by APOE genotype, age, and sex. D) APOE mRNA ddCt grouped by APOE genotype and

age. Individual points represent the average of a triplicate technical repeat for an individual animal, normalised relative to a multi-gene reference factor converted to ddCt relative to the E3-HCC group. Error bars represent mean +/- SEM of individual subject ddCt. Brackets and labels represent relevant statistical main effects, interactions and pairwise comparisons where appropriate. Symbols represent significant relevant genoptye comparisons at p = <.05. In C) age is represent by "3" and "12" overlay.

Table 5.3: Statistical analysis of hippocampal c-Fos and APOE mRNA dCt values in APOE-TR mice in experiment three. Relevant main effects, interactions, and follow-up simple main effects and pairwise comparisons are represented. Results correspond to Figure 5.117A-D.

Measure	Variable	Statistic	Interaction simple main effect	Statistic	Pairwise comparison	MD	SE	*p*
c-Fos mRNA (dCT)								
	Condition	F(1,68) = 26.06, p = .001						
	Sex	F(1,68) = 11.01, p = .001						
	Age	F(1,68) = 4.08, p = .017						
	Genotype*Sex	F(2,68) = 7.37, p = .001						
	Genotype*Age	F(2,68) = 3.78, p = .006						
	Sex*Age	F(1,68) = 9.21, p = <.001						
	Genotype*Sex*Age	F(2,68) = 4.00, p = .023						
			3-months: Sex*Genotype	F(2,34) = 10.50, p = <.001				
					3-months female E3 vs E3E4	-1.31	0.49	0.053
					3-months female E3E4 vs E4	1.55	0.49	0.020
					3-months female E3 vs E4	0.24	0.49	0.951
					3-months male E3 vs E3E4	-0.52	0.45	0.600
					3-months male E3E4 vs E4	-1.31	0.41	0.014
					3-months male E3 vs E4	-1.84	0.43	0.001
			12-months: Sex*Genotype	F(2,54) = 0.13, p = .883				
APOE mRNA (dCT)								
	Genotype	F(1,56) = 8.75, p = <.001						
	Age	F(1,56) = 12.42, p = .001						
	Genotype*Age	F(2,56) = 3.79, p = .029	3-months: Genotype	F(2,36) = 9.92, p = <.001	E3 vs E3E4	-0.70	0.36	0.836
					E3E4 vs E4	-1.28	0.34	0.001
					E3 vs E4	-1.36	0.35	<.001
			12-months: Genotype	F(2,38) = 6.01, p = .005	E3 vs E3E4	0.94	0.32	0.005
					E3E4 vs E4	-0.97	0.32	0.004
					E3 vs E4	0.03	0.30	0.934

Table 5.4: Correlation analysis of hippocampal c-Fos and APOE mRNA in APOE-TR mice in experiment three. Pearson's r and p-values are provided for each corresponding comparison.

Measure	Variable	*r*	*p*
c-Fos-APOE mRNA (dCt)	Whole-group	0.15	.187
	E3-TR female	0.12	.690
	E4-TR female	0.07	.824
	E3-TR male	0.31	.289
	E4-TR male	0.13	.624

5.4 Discussion

Chapter five investigated whether APOE isoform, sex, and age influenced hippocampal network activity in APOE-TR mice under basal and behaviourally activating conditions using environmental novelty exposure. This was investigated in experiments one and three via immunofluorescence and biochemical analyses of the hippocampal c-Fos response as a proxy for the historical activity of a hippocampal neuronal ensemble. Experiment two in parallel sought to assess whether such effects may be accompanied by GABAergic interneuron degeneration within the DGH, a region noted for susceptibility to APOE4-related pathology in female E4-TR mice (e.g., Andrews-Zwilling et al., 2010).

We first hypothesised that novel context exposure would increase overall Fos+ neuron density, or 'ensemble size', in CA1, CA3, and the DGS. Additionally, we expected that E4-TR mice would exhibit reductions in the number of both Fos+ pyramidal and interneurons throughout the hippocampus, which would be exacerbated at mid-age and furthered in E4-TR female mice. In the case of E4-TR female mice, we predicted that these changes would precede a reduction in GABAergic innervation and loss of DGH GABA-INs, which we expected to detect in mid-old aged (12-18-month) mice.

The results of the c-Fos imaging did not confirm the hypotheses relevant to APOE genotype, sex, and age. Instead, the findings demonstrating mixed region, sex, and genotype-dependent effects in Fos+ neuron and interneuron density. These results are summarised in Table 5.5. A univariate linear model approach with robust parameter estimation within individual regions indicated that exposure to the novel context induced an increase in Fos+ neurons in CA1, CA3, DGS, but not the DGI, which is consistent with previous reports detailing hippocampal subregion responses to environmental novelty (e.g., Bernstein et al., 2019; Arias et al., 2015; Hoffman et al., 2013; VanElzakker et al., 2008). We observed that this response was robust across age, sex, and APOE genotype. The overall influence of APOE genotype was primarily observed in CA1 with an interaction between condition and genotype demonstrating that E4-TR mice exhibited significantly elevated Fos+ neurons than E3-TR and E3E4-TR mice following environmental novelty. In CA3, female, but not male, E4-TR mice also exhibited greater Fos+ neuron density than E3E4-TR mice and a trend relative to E3-TR controls. In the DGS, 12-month aged mice showed a reduction in c-Fos neuron density relative to 3-month aged mice, while females showed increased Fos+ neuron density relative to male mice. There was no further effect of APOE genotype in the DGS and a mild effect of genotype in the DGI, although follow-up analysis showed no significant differences between genotype groups.

GAD+/Fos+ interneurons within the principle pyramidal and granule cell layers were sparse and results only proved quantifiable within CA1-CA3 due to data compression effects in the particularly sparse population within the DGS and DGI. This aside, a significant effect of condition was observed in CA1, with a significant increase in GAD+/Fos+ interneurons following environmental novelty relative to home-cage controls but was not modulated by APOE genotype, sex, or age. An age by genotype interaction was observed in CA3, with the 12-month aged E3E4-TR and E4-TR mice showing a significantly higher GAD+/Fos+ interneuron density than 3-month aged genotype-matched controls, while E3-TR mice retained comparable levels between 3-12-months. We also observed significant interactions between genotype and sex in GAD-67 immunoreactivity (GAD IR) as a proxy for GABAergic terminal innervation in the hippocampal cell layers, with general trends towards reduced GAD IR in female E4-TR mice in CA1, while there was a significant reduction in female E4-TR mice in the DGI and in both E3E4-TR and E4-TR female mice in the DGH relative to E3-TR controls. We observed no significant alterations in estimated NeuN cell density, suggesting no group differences in the overall neuron density in each subregion.

In experiment two, we characterised the GAD-67+ interneuron population within the DGH of a wider cohort of 3, 12, and 18-month aged APOE-TR mice to assess age-related degeneration. We observed no significant association between APOE genotype, sex, and interneuron loss as previously reported (e.g., Andrews-Zwilling et al., 2010; Leung et al., 2012; Knoferle et al., 2014). We did, however, observe a significant age-dependent decline at 18-months in DGH GAD-67+ interneurons, relative to both 3 and 12-month groups. Additionally, a significant three-way interaction between age, sex, and genotype was found, although no significant effect of genotype was observed at individual time points.

Exploratory network correlation analysis as a measure of hippocampal subregion coactivation demonstrated differential network correlations amongst subregions, which were predominantly dependent on APOE genotype and sex. While we observed similar correlation patterns between ages, we observed a near inverted pattern of low and high network correlations between sex and genotypes. Specifically, E4-TR female mice and E3-TR male mice demonstrated significant strong positive correlations between CA1-CA3, CA1-DGS, and CA3-DGS which in all cases were above that of sex matched controls. This was particularly notable in E4-TR female mice relative to E3-TR female controls, in which E3-TR females exhibited weak non-significant correlations between the DGS-CA3 and DGS-CA1, while retaining a similar strong positive correlation between CA1-CA3.

In whole-hippocampal c-Fos mRNA expression, a similarly complex picture emerged. We hypothesised that E3E4-TR and E4-TR mice would exhibit a reduction in c-Fos mRNA expression in whole hippocampi and, in line with predictions made for the c-Fos activity data, predicted that the reductions in c-Fos mRNA would be more extreme in female mice and decrease with age. Firstly, exposure to the novel context successfully induced a significant upregulation of c-Fos mRNA. Subsequent results only partially confirmed our hypotheses, however, with a significant 3-way interaction between APOE genotype, sex, and age. There was a reduction in hippocampal c-Fos mRNA expression in E4-TR male, but not female, mice at 3-months. Female mice instead demonstrated equivalent c-Fos expression between E3-TR and E4-TR groups, with a decrease only in E3E4-TR mice at 3-months. A significant effect of age also showed that c-Fos expression decreased overall between 3 and 12-months. However, the effects of genotype observed at 3-months were not conserved at 12-months with no differences between APOE genotype groups. Intriguingly, there was no interaction between condition and other primary variables, suggesting that the influence of APOE genotype and sex at 3-months and may reflect overall shift in basal expression of c-Fos mRNA.

Finally, we predicted that APOE mRNA would be significantly reduced in E3E4-TR and E4-TR mice across age. APOE mRNA levels were differentially modulated by both APOE genotype and age, however. There was a significant reduction in APOE mRNA in 3-month aged E4-TR mice relative to E3-TR and E3E4-TR mice, while at 12-months APOE expression in E3-TR mice appeared to decrease to match levels in E4-TR mice. In contrast, E3E4-TR mice demonstrated similar levels of APOE mRNA between 3 and 12-month groups. Expression of APOE mRNA did not correlate significantly with c-Fos expression at the whole group level, or when grouped by genotype or sex.

Together, we suggest these results point towards an early to mid-life hyperactivity phenotype, with an increased hippocampal ensemble size following environmental novelty in homozygous E4-TR mice, predominantly in pyramidal neurons of CA1, extending into CA3 in female E4-TR mice. The enhancement of network correlations in E4-TR female mice and reduction in E3-TR male mice is intriguing and may indicate an increase in hippocampal subregion co-activation following novelty exposure in female E4-TR mice and a contrasting decrease in male E4-TR mice. Further, possession of homozygous APOE4 results in a deficit in both basal and induced c-Fos mRNA expression in male APOE-TR mice, while heterozygous but not homozygous expression of APOE4 impairs c-Fos mRNA expression in female APOE-TR mice. Additionally, homozygous APOE4 appears to result in an early but not mid-life deficit in APOE mRNA

expression in E4-TR mice, while E3E4-TR mice retain sustained APOE mRNA levels across early-mid-life.

Table 5.5: Summary of results from experiments one and two conducted in Chapter five. Measure, effect of condition, and main effects/interaction of interest are presented in each case by subregion with a brief symbolic description of the directionality of each result. In each case, ">" represents greater than, while "=" represents equal to.

Measure	Variable	CA1	CA3	DGS	DGI	DGH
Fos+ neurons						
	Condition	NCE > HCC	NCE > HCC	NCE > HCC	NCE = HCC	
	Main effect/interaction	Genotype: NCE: E4 > E3 = E3E4	Genotype: E4F > E3E4F = E3F	Sex: F > M; Age: 3m > 12m	ND	
Fos+ interneurons						
	Condition	NCE > HCC	ND			
	Main effect/interaction	ND	Genotype: Age: E3E4 = E4 > E3			
GAD-67 IR						
	Main effect/interaction	ND	Age: 12m > 3m	ND	Age: 12m > 3m; Genotype: E3F = E3E4F > E4F	Genotype: E3 > E3E4F = E4F
GAD-67+ IN count						
	Main effect/interaction					Age: 3m = 12m > 18m; Genotype: ND
c-Fos correlations						
	Main effect/interaction	CA1-CA3-DGS: Females: E4 > E3; Males: E3 > E4				

Table 5.6: Summary of results from experiment three conducted in Chapter five. Measures, effect of condition, and main effects/interaction of interest are presented in each case with a brief symbolic description of the directionality of each result. In each case, ">" represents greater than, while "=" represents equal to. Whole HPC = whole hippocampus

Measure	Variable	Whole HPC
c-Fos mRNA		
	Condition	NCE > HCC
	Main effect/interaction	Age: 3m > 12m
		12m: Genotype: ND
		3m: Genotype: E3M = E3E4M > E4M; E3F = E4F > E3E4F
APOE mRNA		
	Main effect/interaction	Age: 3m > 12m
		3m: Genotype: E3 = E3E4 > E4
		12m: Genotype: E3E4 > E3 = E4

5.4.1 Hippocampal c-Fos activity: Potential mechanisms - Local GABAergic disinhibition within the trisynaptic circuit

One possible mechanism that may drive the observed increase in hippocampal activity is the local dysregulation of inhibitory function within the trisynaptic circuit. We observed a reduction in GAD-67 immunoreactivity (GAD-67 IR), as a proxy for GABAergic terminal innervation within the primary cell layers, particularly in the DGH and in the DGI of female E4-TR mice, with no changes in male APOE-TR mice. This raises the possibility that hippocampal hyperactivity in female E4-TR mice may be contributed to by a loss of DG inhibitory action onto the CA3-CA1 network, although the lack of conservation of this effect in male E4-TR mice, despite retaining CA1 hyperactivity, makes this explanation unlikely to fully account for these observations.

Prior reports also have demonstrated a reduction in miniature spontaneous synaptic currents (mSSCs) in DGH GABA-INs, reduced post-synaptic IPSCs in DG granule neurons, and a reduction in DG granule cell GAD-67 IR in 6-7-month female E4-TR mice. These, in combination with age-related degeneration of DGH GAD-67+ interneurons, particularly SOM+ (Somatostatin) in female E4-TR are consistent with a loss of local inhibition of dentate granule cells at the cell body (Leung et al., 2012; Andrews-Zwilling et al., 2010; Li et al., 2009). Our observation of reduced GAD-67 IR within the DGI/DGH of in E4-TR females is consistent with these reports (Andrews-Zwilling et al., 2010; Li et al., 2009), although we observed a reduction in a cohort 3-months younger.

However, we failed to observe any significant loss of GAD-67+ interneuron numbers in the DGH of E4-TR female mice across the lifespan as previously reported (e.g., Andrews-Zwilling et al., 2012; Leung et al., 2012). Further, how local disinhibition of DG granule cells may extend to induce hyperactivity in both CA1 and CA3 in E4-TR female is not entirely clear, and was not previously investigated (Li et al., 2009; Andrews-Zwilling et al., 2010). Moreover, simulation of DG granule cell disinhibition by acute optogenetic inhibition of DGH interneuron function successfully induced DG granule cell hyperactivity measured by c-Fos but failed to increase CA1 and CA3 Fos+ neuron densities in WT mice (Andrews-Zwilling et al., 2012). Further, recent evidence suggests that the inhibitory function of SOM+ (somatostatin) DGH interneurons onto DG granule cells is crucial for regulation of the DG Fos+ ensemble size following contextual fear conditioning (Stefanelli et al., 2018). This suggests, that at the least, induced disinhibition via loss of acute inhibitory inputs of DGH GABA-INs onto dentate granule cells may be insufficient

to induce CA1-CA3 activity to levels sufficient to impact c-Fos expression. However, following this line of reasoning (and assuming that acute disinhibition as achieved by optogenetic models as in Andrews-Zwilling et al., [2012] is a reasonable proxy for chronic, neurodegenerative-induced disinhibition), we may have expected to observe elevated DG granule cell c-Fos activity in E4-TR females, which was not the case in the present experiment.

A counter explanation may be that DG granule cell c-Fos activation is generally relatively sparse (e.g., Hainmueller & Bartos., 2020; Chawla et al., 2005) yet DG granule cells possess particular powerful excitatory 'detonator' synapses with CA3 pyramidal cells via the mossy fibre pathway (e.g, Vyleta et al., 2016). Via this pathway, it is plausible that local disinhibition of DG granule cells may induce increases in excitability which is subthreshold to induce detectable changes in c-Fos within granule cells themselves but may induce detectable increases in c-Fos expression in CA3 pyramidal neurons via excitatory input from mossy fibre synapses. Indeed, the relative activity 'thresholds' for the induction of c-Fos are poorly characterised and remain a valid criticism of IEG-based approaches. Further, while we observed reductions in GAD-67 IR primarily in the DG of female E4-TR mice, trends to the same pattern of results were also observed in CA1. This may suggest an overall low-level reduction in GABAergic innervation across hippocampal subregions, which may contribute to a more global disinhibitory phenotype of hippocampal pyramidal neurons. These possible explanations are speculative and will require investigation via multiple approaches. For example, dual recording electrophysiological approaches within the CA3-CA1 network, alongside concurrent manipulation of DG/CA3 excitatory outputs in APOE-TR mice may help delineate the possible network-level effects underpinning the results observed in Chapter five.

It is not clear why c-Fos network correlations were differentially affected by APOE genotype and sex, with overall greater cross-region correlations in E4-TR female and E3-TR male mice relative to sex-matched controls. Zerbi et al. (2014) previously demonstrated significant reductions in functional connectivity across multiple regions including the dorsal-ventral hippocampus and dorsal hippocampus-auditory cortex (Wiesmann et al., 2016) in E4-TR male mice across 12-18-months. Limitations of imaging resolution prevented comparison of hippocampal subregions; however, we suggest these results are consistent with the current findings of reduced hippocampal subregion c-Fos activity correlations in male E4-TR mice, albeit comparing novel context-related activity relative to resting functional connectivity assessed by Zerbi et al. The opposing results in female APOE-TR mice in the present study, with overall increased hippocampal subregion c-Fos correlations in female E4-TR mice and a

decrease in female E3-TR mice is surprising, however. The increase in corelation in E4-TR females may be attributable to an overall increase in network activity, predominantly driven by CA1 and CA3. Although, given that an increase in CA1 activity was observed in E4-TR mice of both sexes, it is unclear why similar correlation patterns were not conserved between sexes.

Further, the reason for the discrepancy between current and previous results in GAD-IN loss in E4-TR female mice is unclear. However, while well-reported, this phenotype has almost entirely been shown by a single research group. Further, a recent report also failed to demonstrate any basal loss of GABA-INs in the DGH of 5-6 month aged female E4-TR mice, with GAD-IN loss only occurring following lead exposure stress (Engstrom et al., 2017). Similarly, cumulative stress has been shown to induce DGH GABA-IN loss in E4-TR male mice, while unstressed mice showed unaltered profiles of DGH GABA-INs (Lin et al., 2016). One possibility is that differences in methodological procedures may also contribute to detectability. For example, while we used comparable approaches for sample preparation and quantification of cell densities, previous reports have performed quantification using adapted stereological principles (e.g., Leung et al., 2012). This may have conferred increased sensitivity to subtle APOE genotype-associated changes. On the other hand, we note that the reported GAD-67+ IN deficit in the DGH of female E4-TRs is particularly marked at 18-months, with levels approximately half that of E3-TR female controls. This perhaps makes issues surrounding assay sensitivity less likely, as we would expect across our sampling design to observe a similar magnitude of effect within cell density estimates. Alternatively, as we did not delineate interneuron subtypes by typical expression markers (such as SOM or Parvalbumin, PV), we cannot exclude the possibility that SOM+ GABA-INs may have been specifically susceptible to degeneration and not detected in our E4-TR cohort. However, we suggest that this factor does not supersede the expected effect size in overall interneuron number indexed using the general interneuron marker GAD-67 as previously reported.

5.4.2 Hippocampal c-Fos activity: Potential mechanisms - Disruption of excitatory inputs to the trisynaptic circuit

An alternative potential network-level mechanism underpinning the increase in hippocampal activity in E4-TR mice may be alterations at the levels of excitatory input into the hippocampal circuitry. One particular candidate for this possibility is the entorhinal cortex, with perforant path layer three and two projections predominantly providing excitatory innervation to CA1

and DG, respectively (e.g., Van Groen et al., 2003; Amaral et al., 2007). Some evidence provides precedent for an APOE-dependent effect on EHC function, with a very-late age deficit in E4-TR male mice in inhibitory control reported in the lateral-medial entorhinal cortex. Specifically, elevated cerebral blood volume, increased intrinsic excitability (reduced IPSP amplitude), and network hyperactivity during field potential recordings, alongside impaired LTP was detected in 20+ months aged E4-TR male mice (Nuriel et al., 2017). Further a younger cohort of animals at 8-months was also used, in which a hypermetabolic state was observed in E4-TR mice, with shifts towards purine/ATP overproduction were observed in the EHC without significant changes in cerebral blood flow. These effects were not investigated in female mice, however, which leaves an unanswered question of potential sexual dimorphisms in APOE genotype effects of the EHC circuitry. Indeed, previous studies have demonstrated a reduction in high-frequency stimulation induced LTP of the perforant path in young E4-TR male mice (2-4 months; Trommer et al., 2004) and no change in aged female E4-TR mice (24-27 months; Sung et al., 2007), without changes in input-output relationships in both cases. This may suggest sexual dimorphism in the influence of APOE isoform on EHC function, impairing perforant path LTP across the lifespan in male E4-TR mice, while the effect in females is less clear. Further, reductions in EHC dendritic spine density in layer II/III basal dendrites as well as a reduction in overall length has also been reported in younger, 3-month aged female E4-TR mice (Rodriguez et al., 2013). This reduction in EHC spine density may reflect altered intrinsic excitability of EHC pyramidal neurons in young E4-TR female mice, although this remains to be investigated.

From this evidence, a possible hypothesis would be that low-level EHC disinhibition and hyperexcitability in E4-TR mice from a young age may contribute to the incipience of increased excitability of the trisynaptic network, particularly in CA1. It is unclear whether effects at the level of excitatory input and local disinhibition via loss of GABAergic innervation may be synergistic or perhaps represent separable pathological actions of APOE4 at different stages of the lifespan. One possibility is that the hyperactivity in CA1 which extends to CA3 in female, but not male E4-TR mice represents a local disinhibition due to the loss of GABAergic innervation, while in males E4-TR mice, EHC excitatory drive may be a predominant factor. This is speculative and future experiments may similarly target this question with dual recording approaches between the entorhinal inputs and hippocampal circuitry ex vivo and in vivo. Indeed, several lines of evidence suggest that entorhinal pathology and dysfunction are amongst the earliest pathological events in neurodegenerative diseases including AD (Olajide et al., 2021; Stranahan & Mattson., 2010; Khan et al., 2014; Small et al., 2002).

5.4.3 Hippocampal c-Fos activity: Potential mechanisms - Intrinsic properties and susceptibility of CA1-CA3 to APOE-related pathological processes

CA1 has been shown to be particularly susceptible to multiple types of insults including excitotoxicity (Jinde et al., 2009; Davolio et al., 1995) and hypoxia (Shaw et al., 2021; Dehghani et al., 2018; Kawasaki et al., 1990). Additionally, intrinsic excitability is likely modulated by age with debates around hyper/hypoexcitability in normal ageing (Oh et al., 2016) and CA1 hyperexcitability reported in AD models such as the APP-PS1 mouse (Vitale et al., 2021). CA3 hyperexcitability has also been demonstrated in aged rodents (Oh et al., 2016; Robitsek et al, 2015; Lee et al., 2021). This possible dissociation from normal ageing observed in young-mid aged E4-TR mice raises the possibility of alterations to the intrinsic functional properties of CA1 pyramidal neurons. Indeed, recent evidence has shown enhanced input-output relationships and short-term plasticity via paired pulse facilitation (PPF) observed in the Schaffer collateral pathway, accompanied by reductions in dendritic length, apical spine density and volume in young (~4 month) E4-TR mice relative to E3-TR controls (Sun et al., 2017). Interestingly, this enhancement was associated with an impairment in long term potentiation in the same animals without alterations in synaptic vesicle recycling, with the enhanced short-term plasticity interpreted as increased CA1 excitability in young E4-TR mice (Sun et al., 2017). In contrast, 12-month aged E4-TR mice exhibited reductions in PPF, LTP, and input-output relationships relative to the young E4-TR cohort, although comparison to E3-TR mice was not performed in these later experiments.

The present results are somewhat consistent with this. While we observed an increased Fos+ ensemble size possibly reflecting increased CA1 excitability across 3-12 months, it is notable that the mean difference between APOE genotypes appeared reduced in 12-month aged animals. One study has also reported abnormally enhanced power in the theta frequency during EEG recordings in E4-TR mice relative to E3-TR, E2-TR and WT controls, which was associated with enhanced seizure frequencies in aged (21-months) but not young (6-month) aged mice (Hunter et al., 2012). This may suggest that lower level CA1 hyperactivity may precede more marked susceptibility of the hippocampal network to APOE4-mediated hyperexcitation and seizure-like events.

Mechanistically, Sun et al. (2017) proposed that CA1 hyperexcitability may represent an attempted compensation for impaired dendritic morphology. While synaptic vesicle recycling

was unaltered between APOE genotypes, it is possible that presynaptic CA3 glutamate release or postsynaptic CA1 responsivity may be altered, for example via altering glutamatergic vesicle loading proposed to be impaired by APOE4 (e.g., Dumanis et al., 2013), or by changes in postsynaptic receptor density or function. These possibilities warrant further investigation, although notably some evidence suggests little to no change in NMDA/AMPA receptor subunit expression in 3-12-month aged E4-TR male CA1 or whole hippocampal samples (Korwek et al., 2008; Lin et al., 2016), which may suggest a presynaptic origin of dysregulation of the Schaffer collateral pathway by APOE4.

Given that c-Fos expression is highly dependent on intracellular calcium and NMDA receptor function, an elevation in c-Fos+ neurons by APOE4 may also represent a calcium-dependent pathway. As discussed in section 1.5.6, acute action of ApoE4 is associated with elevated calcium influx in neurons, which is suggested to be dependent on NMDAR and L-VGCC activation (e.g., Ohkubo et al., 2001; Qiu et al., 2004) with subsequent elevation of synaptic gene expression (Ramakrishna et al., 2021). This also raises the possibility of a general susceptibility of CA1 to ApoE4-mediated calcium influx. Indeed, some evidence indicates that CA1 pyramidal neurons are particularly susceptible to elevated calcium influx with ageing (e.g., Oh et al., 2013, 2016). This may be investigated in the future using techniques such as simultaneous calcium and IEG reporter imaging in vivo and ex vivo, allowing correspondence between calcium handling and IEG expression to be measured in the context of varying APOE isoforms.

Finally, given prior evidence for the vulnerability of IEG expressing neuronal hippocampal ensembles to dendritic impairments (Pignatelli et al., 2019; Roy et al., 2016, Ryan et al., 2015) and correlations between impaired CA1 spine density and hyperexcitability in AD mouse models (Šišková et al., 2014; Zott et al., 2018), the question arises whether alterations in morphological characteristics (e.g., spine density and synaptic inputs) of CA1 neurons may be associated with an increased propensity for ensemble recruitment in E4-TR mice. Therefore, subsequent experiments conducted in Chapter six aimed to address this question.

Together, the results from c-Fos immunofluorescence imaging experiments conducted here suggest an increased CA1 neuronal ensemble size in response to novelty in early to mid-aged E4-TR mice which extends to CA3 in females, alongside specific reductions in putative local DG GABAergic innervation in female E4-TR mice. These deficits in GABAergic innervation in the DG may contribute to enhanced CA3-CA1 hyperactivity in E4-TR female mice, although potential causal relationships remain to be validated. However, we failed to replicate previous findings

of a specific loss of DGH GABA-INs in E4-TR female mice. Candidate network level mechanisms include local GABAergic disinhibition, excitatory modulation at the level of hippocampal inputs such as the EHC, and alterations to the intrinsic properties of CA1-CA3 pyramidal neurons. Multiple avenues are therefore open for future investigation to further understanding of the complex influence of APOE isoform on the hippocampal circuitry during behaviour.

5.4.4 Alterations to hippocampal c-Fos mRNA expression

The age, sex, and genotype-dependent shifts in whole hippocampal c-Fos mRNA expression are intriguing. While we hypothesised that E4-TR mice would exhibit reductions in c-Fos expression, this was only observed in male E4-TR mice at 3-months. In addition, a reduction was also observed in 3-month female E3E4-TR mice, but not E4-TR homozygous mice. Further, the lack of significant differences between genotypes at 12-months suggests that there may be some compensatory processes to restore c-Fos mRNA levels or alternatively that age-dependent decline in c-Fos expression results in equivalent profiles across APOE genotypes in APOE-TR mice. Indeed, ageing in rodents has been associated with reductions in the expression of mRNA of some IEGs in the hippocampus, including c-Fos and Arc, with some demonstrations in AD mouse models (Burke & Barnes., 2006; Penner et al., 2011; Chawla et al., 2013; Christensen et al., 2013), although c-Fos mRNA expression has also been suggested to increase with age in some cases (e.g., Burke & Barnes., 2006; Haberman et al., 2017).

Recent results support our findings, at least in male APOE-TR mice, with a reduction in c-Fos mRNA expression reported in 2-3-month aged E4-TR male mice in the hippocampus (Li et al., 2021). This reduction in c-Fos was suggested to be a downstream consequence of a loss of histone acetylation and regulation of cholesterol biosynthesis. Histone acetylation reductions were shown to be driven by a reduction of ApoE4 function to downregulate cholesterol biosynthesis pathways via lipoprotein-mediated delivery of micro-RNAs (miRs) specifically targeting cholesterol synthesis mRNAs, delineated in vitro. This impaired downregulation of these pathways subsequently fails to allow increase of free acetyl-CoA, which then reduced normal histone acetylation at multiple IEG promoter regions (Li et al., 2021). Similarly, knockdown (KD) of endogenous APOE using shRNA in the hippocampus of WT mice reduced histone acetylation, IEG expression, CA1 pyramidal spine density, and impaired acquisition latency and retrieval in the MWM task (Li et al., 2021). Whether these effects are conserved in female E4-TR mice is unknown, although if this were the case, we would likely expect to

observe a sex-independent reduction in c-Fos mRNA expression in E4-TR mice, which we did not. This again suggests that there may be sexually dimorphic mechanisms through which APOE isoform influences signalling pathways upstream of IEG expression. One other prior study in vivo, however, suggests age-dependent modulation of ERK signalling, with E4-TR female mice exhibiting an elevation of pERK and pCREB signalling (amongst others, see section 1.5.5) were observed relative to E3-TR females at 3-months, before matched expression between genotypes at 7-8 months, and finally a reduction at 15-months (Yong et al., 2014).

In contrast, evidence in vitro suggests that the acute action of ApoE4 induces an increase in activation of the ERK signalling pathway and consequent IEG expression, including c-Fos (e.g., Ohkubo et al., 2001; Huang et al., 2019), rather than suppression of c-Fos as presently reported. Additionally, work in vitro has shown that acute ApoE application and signalling can induce c-Fos and CREB expression via an acute DLK-MKK7-ERK pathway in hIPSC-derived neurons and mouse embryonic fibroblasts (MEFs) in an E4 > E3 > E2 isoform potency manner (Huang et al., 2017, 2019). This activation of c-Fos and CREB led to transcriptional and translational upregulation of APP (c-Fos mediated) and upregulation of multiple synaptic genes (CREB-mediated; Huang et al., 2017, 2019), which may be consequent to an acute APOE-receptor-dependent signalling pathway, enhancing calcium influx (Ramakrishna et al., 2021). These discrepancies highlight the need for greater characterisation of the influence of APOE on IEG signalling in vivo, including investigating possible mechanisms which may underpin age-dependent interactions between APOE isoform and these pathways.

As for the transcriptional and translational regulation of c-Fos, it is not possible to dissociate from the present data whether our findings may be contributed to by alterations in levels of transcription factor activation, translation rate, post-transcriptional degradation etcetera. Indeed, Fos protein is known to have autoregulatory functions, alongside the transrepressive features of other IEGs within the c-Fos family (Tuckwell et al., 2019; Chung et al., 2015), which may repress c-Fos expression at the transcriptional level. In terms of the regulation of c-Fos, APOE may alter the time course of c-Fos induction and as such may shift the peak of the time window of expression. For example, in the early study by Ohkubo et al., (2001), ApoE4 application to rat hippocampal neurons induced an increase in ERK phosphorylation after 1-hour, returning to baseline between 4-8-hours before showing a transient reduction relative to baseline from 8-12-hours, while ApoE3 induced no change. Levels of c-Fos, however, remained elevated for 2-12-hours after ApoE peptide application (note ApoE4 itself was not used for c-Fos induction; Ohkubo et al., 2001). Further, recent evidence also suggests that acute ApoE4

action at its receptor may alter translational control of gene targets by altering ribosomal occupancy states via a calcium and p-eEF2-dependent signalling pathway, differentially favouring higher occupancy states synaptic-related gene mRNAs (such as PTEN and PSD-95) while exhibiting lower global translation of non-synaptic gene mRNAs in neuronal cells and rat synaptosomes (Ramakrishna et al., 2021).

These complex findings highlight the need for greater characterisation of the effect of APOE isoform on the molecular mechanisms of IEG expression, particularly whether these mechanisms are underpinned by more than a single pathway concurrently such as via activation of upstream signalling cascades or via alteration at the transcriptional-translational level. We would speculate, therefore, that our current observations may be driven by both APOE isoform-dependent aberrations in signalling upstream of c-Fos, alongside shifts in transcription-translational regulation of c-Fos itself, which require delineation.

5.4.5 Alterations to hippocampal APOE mRNA expression

We observed an age-dependent shift in APOE expression by isoform, with lower hippocampal APOE mRNA levels in E4-TR mice at 3-months but matched between E3-TR and E4-TR mice at 12-months. On the contrary, heterozygous expression of APOE in E3E4-TR mice was associated with retained APOE mRNA levels across 3-12 months in the hippocampus. This may represent some potential functional compensation for earlier inductions of reduced APOE mRNA expression originating from the APOE4 allele, with similarly lower expression of the ApoE4 than ApoE3 at the level of protein reported in heterozygous E3E4-TR mice (Riddell et al., 2008), although this is speculative.

Our present findings are largely not consistent with previous reports, however, with generally no regional differences reported in mRNA expression in the brain of APOE-TR mice (e.g., Sullivan et al., 2004; Riddell et al., 2008; Hu et al., 2015 following viral mediated APOE expression). Discrepancies have been reported in human patients, however, with no change in APOE mRNA in human brain tissue of mixed APOE genotype (Bekris et al., 2010), an increase in APOE mRNA in all-cause AD (Akram et al., 2012) or APOE4-carrier AD patients (Yamagata et al., 2001), or no change in APOE4 AD patients (Growdon et al., 1999). Perhaps the most comparable study to present is that of Riddell et al. (2008) who demonstrated significant ApoE protein reductions in E4-TR mouse hippocampus and cortex, but no differences in mRNA. Notably these animals were 4-5-months of age, comparable to the present study, but with

somewhat smaller group sizes (4-10 per group Vs 12-15 per group within age, by APOE genotype) and only used male APOE-TR mice, although we note that we did not observe an effect of sex on APOE mRNA expression. The reason for this discrepancy is therefore not clear and environmental novelty was not associated with any effect on APOE mRNA expression, making environmental differences appear an unlikely candidate explanation.

Evidence generally suggests that APOE isoform-specific modulation of expression levels is primarily attributable to post-translational protein handling mechanisms such as sequestration, and intra or extra-cellular proteolytic fragmentation. In the case of ApoE4, reductions in expression levels are suggested to occur due to a greater propensity for fragmentation and endosomal sequestration (Prasad & Rao., 2018; Xian et al., 2018; Morrow et al., 2002), which appears attributable to the C-N terminal domain interaction observed only in ApoE4 (Weisgraber et al., 1996; Dong et al., 1996; Raffai et al., 2001).

The potential mechanism underpinning our observed decrease in APOE4 mRNA is therefore unclear. However, debate is still ongoing and species differences or previously unknown transcriptional-translational regulatory mechanisms may be involved in control of APOE expression. For example, neuronal expression of hAPOE in mice has been shown to induce intron 3 retention (APOE-I3), with a shift to mature mRNA for rapid translation upon excitotoxic injury (Xu et al., 2008). Additionally, recent evidence suggests that APOE may form circular RNA species in human patients which may modulate expression levels (Lee et al., 2020). There has generally been less characterisation of the transcriptional consequences of APOE isoform for APOE expression itself in mouse models, perhaps partly attributable to the generally protein-centric approaches.

APOE4 has also been associated with dysregulation of transcriptional machinery in some RNA-sequencing experiments (e.g., Zhao et al., 2020; Zalocusky et al., 2021), and it has been suggested from recent in vitro studies that APOE itself may act as a putative transcription factor (Theendakara et al., 2016, 2018) but remains a relatively unexplored topic. A recent single-cell RNA-sequencing study of hippocampal samples from APOE-TR mice and AD/healthy patient cortical samples highlighted that APOE mRNA expression levels within neurons significantly predicted the expression of a wide range of genes across multiple cellular processes, while glial expression did not but was independent of APOE genotype. Namely, cellular metabolism, DNA damage-repair and transcriptional machinery, immune responses, and neurodegenerative disease-associated pathways amongst others (Zalocusky et al., 2021). This posits a potential crucial role for relative APOE expression levels within neurons. However,

given that the majority of APOE is glial in origin, which is likely what was primarily reflected in the present study, the translatability between findings is likely limited. The present results therefore appear likely to reflect APOE isoform and age-related modulation of glial APOE mRNA expression within the hippocampus, the mechanism of which requires further investigation.

5.4.6 Caveats

There are a few notable caveats to the experiments conducted in Chapter five. Firstly, the technical limitations of IEG-based immunohistochemical methods for assessment of neuronal activity apply. While c-Fos is a robust marker for elevated neuronal activity at the single cell to network level (e.g., Curran & Morgan., 1995; Cruz et al., 2015; Mintohara et al., 2016; Chung et al., 2015), it provides only a temporally static 'snapshot' and undynamic image of intrinsically dynamic processes. From this data, it is not possible to delineate from where such hyperactivity and network correlations may originate, or the relative contribution of excitatory and inhibitory synaptic inputs as may be determined via in-vivo or ex-vivo electrophysiological approaches. Indeed, the electrophysiological underpinnings of IEG expression in terms of a relative activity 'threshold' for induction of c-Fos expression is not fully understood, although NMDAR and other calcium channels are directly implicated, with a requirement of sustained intracellular calcium increases (Cheng et al., 2015, Hudson et al., 2018). Further, while analysis between electrophysiological and IEG immunohistochemical measures are generally complementary (e.g., Segev et al., 2018), it is possible that we were unable to detect lower-level alterations in intrinsic cellular excitability properties.

Correlational network analysis was performed as exploratory analysis and as such, should be interpreted with caution. While significance testing was performed with all correlation analyses, it should be noted that an alpha threshold of 0.05 may enhance the likelihood of false positives. However, we note that with a Bonferroni post-hoc correction applied based on within groups type one error rate, the general pattern of results described were still observed, albeit with fewer correlations passing the significance threshold (Supplementary Figure 5.2). Further, as these results are purely correlational, without direct manipulation of processes involved to assess causal dependence, extrapolation is limited.

Additionally, the environmental novelty paradigm does not involve direct control or manipulation of goal directed behaviour, and while environmental novelty has been

specifically associated with induction of c-Fos expression in the hippocampus (VanElzakker et al., 2008) we cannot control for potential differences in goal-directed behaviour across groups. In order directly to assess the relevance of the identified phenotypes in c-Fos activity, further investigation is needed. For example, manipulation of c-Fos ensemble activity with the use of IEG-dependent genetic tagging methods, such as the c-Fos-tTA TRE-channelrhodopsin system (e.g., Ramirez et al., 2013) for optogenetic interference on the ensemble during goal-oriented behaviour (e.g., spatial navigation or contextual fear learning, as discussed in section 5.9.3), would enable assessment of the potential relevance of the putative ensemble alterations observed in Chapter five.

It is also notable that the characterisation of Fos+/GAD-67+ interneurons did not reveal any marked APOE genotype-dependent effects and that the population itself was extremely sparse. This may, in part, be due to the restriction of quantification to only pyramidal layer neurons. We cannot rule out potential APOE genotype-dependent alterations to activation of other interneuron subtypes residing in the other hippocampal sublayers such as the stratum oriens and radiatum, which house a wide diversity of interneuron types (e.g., Klausberger et al., 2009). More comprehensive characterisation of hippocampal interneuron function in APOE-TR mice following behavioural experience will be required.

Finally, as for experiment three, due to the differing spatial resolution between the histochemical and biochemical methods, direct quantitative comparison is limited. For example, potential subregional variation in both c-Fos and APOE mRNA expression may be masked by whole structure lysis and therefore would be complemented by in situ hybridisation approaches. While the positive correlation between c-Fos mRNA and protein induction has been demonstrated (e.g., Zangenehpour & Chaudhuri., 2002), and the present results suggest transcriptional dysregulation at some level, we cannot delineate the mechanisms underpinning this and the possibility of changes in translation are not assessed. Moreover, we cannot exclude additional post-translational alterations in both c-Fos and ApoE protein and future assessments will benefit from combined assessment of both protein and mRNA concurrently. Additionally, basal alterations in signalling pathways upstream of c-Fos, as discussed in section 5.5.4, may occur that we did not assess in the present experiments, and which may contribute to the present findings.

5.5 Chapter five summary and conclusion

Ultimately the results of Chapter five demonstrate complex relationships between APOE isoform, sex, and ageing in the regulation of hippocampal ensemble activity in response to environmental novelty. Particularly, we observed an elevation of Fos+ neuronal ensemble size in CA1, which may suggest hyperactivity in young-mid aged E4-TR mice following environmental novelty, which extended to CA3 in E4-TR females. This was accompanied by a profile of increased CA1-CA3-DG network correlations in female E4-TR and male E3-TR mice relative to sex matched controls. Further, a reduction in putative DG GABAergic innervation in female E4-TR mice was not accompanied by significant GABA-IN degeneration in the DGH in contrast to previous reports.

We speculate that this increase in hippocampal ensemble size may be a general feature of the APOE4 hippocampal network during behaviour and future studies should delineate whether this phenotype is functionally relevant for other hippocampal-dependent behaviours, particularly episodic memory. We suggest that local disinhibition, elevated excitatory input from extra-hippocampal structures, and intrinsic CA1 excitability changes are candidate network-level sources for this APOE4-dependent increase in ensemble size from a young age in APOE-TR mice and should be further investigated.

Further we observed reductions in hippocampal APOE4 expression at young age, alongside reductions in c-Fos mRNA in E4-TR male and E3E4-TR female mice, which may suggest dysregulation of transcriptional-translational control of IEGs and/or altered signalling cascade activation in early life. Finally, in mid-aged APOE-TR animals we observed comparable profiles of hippocampal c-Fos expression alongside similar APOE mRNA expression levels between E3-TR and E4-TR but not E3E4-TR mice. Together these results suggest that early in life, prior to extensive pathology, APOE4 may drive hippocampal network hyperactivity alongside shifts in IEG expression following novel experience in E4-TR mice. Future work should aim to further characterise the driving forces of these phenotypes in early life and assess the potential relevance for neuronal ensembles involved in behaviour.

CHAPTER SIX

The influence of APOE isoform on dendritic integrity and synaptic occupation in a CA1 neuronal ensemble in young APOE-TR mice

6.1 Introduction

In Chapter five, we demonstrated that E4-TR mice exhibit an enhanced novelty-induced CA1 pyramidal neuronal ensemble size at young to mid age, extending into CA3 in females, which we suggested may reflect hippocampal hyperactivity. Additionally, c-Fos neuron network correlations suggested an enhancement of network correlation between the CA1-CA3-DG in female E4-TR and male E3-TR mice. To further explore these findings, we sought to determine whether alterations to dendritic structure and synaptic innervation in young E4-TR mice might be present that may contribute to a hyperactive CA1 ensemble.

Neuronal ensembles within CA1 exhibiting IEG expression following exposure to a novel environment are thought to reflect the processing and representation of contextual and novelty-related information within the environment, with a somewhat linear relationship between ensemble reactivation (or overlap) and environmental contiguity across experiences (Vazdarjanova & Guzowski., 2006; VanElzakker et al., 2008; Cai et al., 2016; Milczarek et al., 2015). Previous research has demonstrated morphological and electrophysiological alterations to IEG expressing ensemble neurons following exposure to multiple behavioural paradigms, including contextual fear conditioning (Roy et al., 2016; Pignatelli et al., 2019; Ryan et al., 2015), appetitive Pavlovian conditioning (Brebner et al., 2020), and contextual drug-cue learning (Singer et al., 2016; Koya et al., 2012).

For example, enhanced dendritic spine density and volume was demonstrated specifically in c-Fos expressing (Fos+) neurons in the nucleus accumbens recruited during amphetamine drug-context pairing in WT rats, suggesting experience-dependent structural plasticity in the formation of the drug-context association (Singer et al., 2016). Additionally, increased mean firing rates and theta burst probability was observed in Fos+ CA1 pyramidal neurons during exploration of a novel environment, while decreasing firing rate upon exposure to a second context. Decoding of firing rate showed greater predicative validity for discriminating between novel contexts in Fos+ neurons than non-expressing (Fos-), demonstrating that Fos expression was associated with modification of cell firing properties as a function of representing contextual information (Tanaka et al., 2018).

As discussed in section 1.5, there are conflicting findings surrounding the influence of APOE isoform on both the structure and function of CA1 pyramidal neurons and little to no investigation of these effects in neuronal ensembles following behaviour. Recent work has shown CA1 hyperactivity in APP/PS1 AD model mice, that was linked to cellular excitability and

dendritic degeneration (Šišková et al., 2014), while DG ensemble recruited neurons following contextual fear conditioning demonstrated spine loss in multiple AD mouse models (Roy et al., 2016; as discussed in section 4.4.9). We therefore speculated that early age network level disruptions driven by APOE4 in CA1 following contextual novelty, may be accompanied by changes in dendritic morphology and synaptic occupation which may enhance the probability of ensemble recruitment. More specifically, we asked whether APOE isoform in young APOE-TR mice differentially influences the dendritic spine density, and synaptic innervation to post-synaptic spines in Fos+ relative to Fos- CA1 neurons of an environmental novelty-recruited ensemble. This would provide insight as to the potential morphological underpinnings of an APOE4-mediated increase in CA1 ensemble size and indicate whether such changes were accompanied by structural correlates of synaptic input at the level of individual spines.

These questions and hypotheses were addressed in three experiments in a single cohort of 3-month aged APOE-TR mice of both sexes following exposure to contextual novelty:

Experiment one: In the first experiment, we aimed to replicate the observed increased Fos+ CA1 ensemble size observed in Chapter five. We addressed this first aim with a near identical pipeline as described previously, specifically focussing on characterising Fos+ neuron density in CA1 of young 3-month aged APOE-TR mice of homozygous genotype (E3-TR and E4-TR) using immunofluorescence imaging following exposure to the contextual novelty paradigm.

Experiment two: Second, we aimed to assess whether young APOE-TR mice exhibited isoform-dependent baseline changes in presynaptic integrity/density within CA1, as an overall reduction in presynaptic integrity may preclude specific alterations at the level CA1 of Fos+ or Fos- neurons, which we addressed via immunofluorescence and confocal imaging of the presynaptic scaffolding protein, Bassoon.

Experiment three: Finally, using combined cell tracing and immunofluorescence techniques, we assessed whether young APOE-TR mice demonstrated alterations in basal shaft CA1 dendritic morphology and spine synaptic occupancy as measured by colocalization with Bassoon in both c-Fos expressing (Fos+) and non-expressing (Fos-) neurons.

We first hypothesised that E4-TR mice would again demonstrate an increased CA1 increased Fos+ ensemble size following exposure to a novel context, as we observed in Chapter five. Second, we predicted that there would be no overall difference by APOE genotype in presynaptic integrity, indexed by immunofluorescence analysis of a presynaptic scaffolding protein, Bassoon. However, we expected that E4-TR mice would exhibit an overall deficit in

CA1 dendritic spine density and synaptic occupation, which would be more pronounced in c-Fos expressing ensemble recruited neurons following exploration of a novel environmental context.

6.2 Methods

6.2.1 Design

The experiments were conducted within a single cohort of animals. Experiment one and two were cross-sectional two-way between subjects with APOE genotype (E3-TR and E4-TR) and sex (male & female) as the primary between group variables. Experiment three was a four-way mixed design with APOE genotype and sex as between groups variables and cell type (Fos+ & Fos-) and spine occupation (Bassoon positive, BSN+ = occupied; Bassoon negative, BSN- = unoccupied) as within-subjects variables. All animals underwent a novel context exposure condition as described in section 5.3.

6.2.2 Animals

20 APOE-TR mice were used. All animals were maintained and handled as described in section 2.1.1. Subjects were divided into experimental groups as outlined in Table 6.1.

Table 6.1: Outline of animals (total N = 20) allocated to each experimental condition comprising experiments one-three in Chapter six, grouped by APOE genotype and sex. Note that each animal was used for experiments 1-3, with the exception of a loss of 3 animals in experiment 3 due to attrition.

Genotype	Sex	N	
		Experiment 1-2	Experiment 3
E3-TR	Male	5	4
	Female	5	4
E4-TR	Male	5	4
	Female	5	5

6.2.3 Procedure

6.2.3.1 Environmental novelty exposure and tissue preparation

As we previously characterised baseline c-Fos expression in home-cage controls during experiments in Chapter five and given that our focus was the characterisation of a novelty-activated Fos+ neuronal ensemble, home-cage control animals were omitted from the present experiment.

Animals were handled, habituated, and exposed to environmental novelty as described in section 5.3, with minor differences in tissue handling prior to processing for immunofluorescence. Briefly, all animals were exposed to a novel environment for 30-minutes in a 30cm x 30cm x 30cm open field chamber containing two novel objects. After 30-minutes animals were removed and returned to the home-cage where they remained for a further 60-minutes to allow robust induction of c-Fos expression (e.g., Kovacs et al., 1998). Following this delay, animals were anesthetised, and underwent rapid aCSF transcardial perfusion as outlined in section 2.2.1. Brains were then extracted, hemisected and one hemisphere was allocated to a modified light fixation protocol via submersion in 30ml of 1.5% PFA for 24-hours, while the other hemisphere was flash frozen in liquid nitrogen before storage at -80°C. Following fixation, hemi-brains were cryopreserved in 30% sucrose solution in 1X PBS for 24-hours. Hemi-brains were visibly sucrose infiltrated following 24-hour incubation, sinking to the bottom of the solution as described in section 2.2.1. Hemi-brains were then dissected, removing the cerebellum and frontal cortex, and chilled to 4°C in 1X PBS. 100µm thick sections were then taken throughout the extent of the hippocampus using a vibratome (Leica 1200VTS, Leica). Sections were then stored in cryopreservant solution (see section 2.2.1.2) in 24-well cell culture plates (Corning) and kept at -20°C until use. The subsequent three experiments comprising Chapter six were conducted using tissue within the same animals processed via this pipeline.

6.2.3.2 Experiment one: Validation of enhanced CA1 ensemble size in young E4-TR mice.

In order to validate the effects of APOE isoform on CA1 hyperactivity observed in experiments conducted in Chapter five, we performed a replication experiment in a new cohort of 3-month aged APOE-TR mice. c-Fos and NeuN immunofluorescence was performed via a slightly modified protocol in all animals (see section 6.2.9) within the cohort and images were acquired and quantified exactly as reported in section 5.4. Specific modifications to this protocol are outlined subsequently.

6.2.3.3 Experiments two and three: Assessment of synaptic integrity, dendritic spine density and synaptic occupation of ensemble-recruited CA1 pyramidal neurons in APOE-TR mice

To assess whether APOE isoform influenced baseline synaptic integrity CA1 at young age, tissue from the same animals was processed for confocal immunofluorescence analysis of the presynaptic scaffolding protein Bassoon, as a proxy for presynaptic innervation in CA1 stratum pyramidale and oriens. Concurrently, to investigate potential differences in dendritic spine density and synaptic innervation in a CA1 pyramidal neuron ensemble specifically recruited or unrecruited during environmental novelty in APOE-TR mice, matched tissue sections were processed for neuronal tracing and immunofluorescence analysis. Neuronal tracing was performed using a fluorescent lipophilic carbocyanine dye, while immunofluorescence was performed for Bassoon to colocalise pre-and post-synaptic structures, and c-Fos to identify ensemble recruited neurons from the CA1 population. Specific details of each procedure are provided in the subsequent sections.

6.2.4 Lipophillic carbocyanine dye labelling

Carbocyanine dyes are a group of fluorescence dyes commonly used for neuronal tracing and morphological analysis of cells both in vitro and in vivo. Carbocyanine dyes are highly lipophilic and function by binding and integrating within the membrane lipid bilayer, increasing fluorescent significantly upon lipid binding. These dyes then typically mobilise across the

extent of the membrane surface moving both anterogradely and retrogradely. Following dye diffusion, fluorescence imaging can be performed for high fidelity resolution of cellular morphology, which is suited to the resolution of dendrites and individual spines (Fritzsch et al., 2005; Singer et al., 2016; Rasia-Filho et al., 2018). The carbocyanine dyes include multiple variants with differing spectral properties, allowing multiplexing alongside combination with immunofluorescence methods. We used DiOC18(3) (3,3'-Dioctadecyloxacarbocyanine Perchlorate, DIO), a variant with a green shifted emission spectrum.

6.2.4.1 Application of crystalline DiO microparticles to the CA1 hippocampal pyramidal layer

For DiO labelling, DiO crystals (Thermo Fisher) were prepared and applied using an adapted protocol from reported in two recent publications (Trivino-Paredes et al., 2019; Rasia-Filho et al., 2018). DiO crystals were first aliquoted into microcentrifuge tubes before 3-hour sonication to reduce the crystals to smaller microparticles suitable for tissue application.

Subsequently, 100µm thick, fixed dorsal hippocampal sections were prepared as described above. Sections were washed briefly in 1X PBS before being placed into the chamber of an electrophysiology recoding rig, equipped with an upright BX53 microscope (Olympus) fitted with 4X air and 40X water-immersion objectives. Sections were affixed using small tungsten wire coils before being submerged in 1X PBS.

Sharp microelectrode pipettes of ~15 megaohm resistance (mOhms) and a thin tapered tip (~1-2µm) were pulled from thin walled 1.5mm width x 7.5cm length filamented borosilicate glass capillaries (Harvard instruments) with a pipet puller (Model P97, Sutter instruments). Pipettes were then coated in a thin layer of DiO microparticles, before affixation to a motorised micromanipulator (Scientifica) to allow precise pipet manipulation for DiO application.

DiO crystals were then gently deposited onto the stratum pyramidale layer of CA1, at approximately 200-400µm intervals across the extent of the dorsal CA1. This process typically resulted in reliable small microparticle deposits spanning the pyramidal cell layer which would readily adhere to the tissue. Sections were then rehydrated in 1X PBS before being transferred to a humidified chamber. Sections were then encased in Parafilm (Bemis, Fisher) with a small volume (50-100µl) of 1X PBS to apply pressure and promote adherence of DiO crystals to the

tissue for continual diffusion as previously reported (Trivino-Paredes et al., 2019). Humified chambers were then stored overnight at 4°C.

6.2.5 Immunofluorescence

For co-labelling experiments, immunofluorescence was typically performed after DiO labelling. The general protocol is similar to that described in section 2.2.1.2. Minor protocol adjustments were made to avoid excessive membrane permeabilisation which typically renders carbocyanine dyes ineffective (e.g., Matsubayashi et al., 2008). Firstly, light permeabilisation was achieved using 0.2% Tween 20 in all permeabilising solutions. Second, antigen retrieval was not performed to avoid reported loss of carbocyanine labelling. Incubation volumes were also increased to 500µl to increase antibody availability for effective labelling in thicker sections.

Sections were first washed three times for 5-minutes in 1X PBS before undergoing 30-minutes blocking with 3% NGS in 1X PBS with 0.2% Tween 20 (PBST-20). Sections were washed again (three times, 5-minutes), before primary antibody incubations were performed. Rabbit anti-c-Fos (1:1000) and Guinea pig anti-Bassoon (1:1000) were diluted in PBST20 and applied to the sections with incubation with gentle agitation for 24-hours at 4°C (as described in Table 2.4). Following primary antibody labelling, sections were washed, and then incubated in secondary antibody solution for 3-hours at room temperature with gentle agitation. Goat anti-rabbit Alexa-Fluor 568 (1:500), and goat anti-guinea-pig Alexa-Fluor 647 were used (1:500), avoiding blue-green emission spectra due to the wide emission spectra of DiO and the potential for fluorescence channel bleed through. Sections were washed again before incubation in 1µg/ml DAPI in PBST-20 for 10-minutes at room temperature with gentle agitation. Finally, sections were washed, mounted, coverslipped, and varnish sealed for confocal imaging.

6.2.6 Microscopy

Fluorescence microscopy was performed using a Leica SP8 confocal microscope as reported in section 2.2.2. Sequential channel acquisition and laser intensity settings were optimised to minimise channel bleed through or photobleaching, while maximising sensitivity. Variable spectra emission filters allowed conservative control of individual channel spectral size, preventing bleed through from DiO labelling which exhibited particularly marked fluorescence

from approximately ~350-600nm wavelengths. Excitation was provided by an argon laser with excitation wavelengths of 405nm, 488nm, 561nm, and 633nm for DAPI, DiO, c-Fos, and Bassoon labelling, respectively. Standardised acquisition settings were determined based on initial pilot experiments and retained for all subsequent experiments. These parameters included excitation laser power, emission wavelength filter spectra, contrast, gain, offset, pixel resolution, and scan speed.

Images were acquired using a 63x 1.4NA oil-immersion objective at a resolution of 512 x 512 pixels, corresponding to 82.17 x 82.17µm^2 (0.16µm/pixel). Using the DiO fluorescence channel, individual CA1 pyramidal neurons were isolated and the basal tuft dendrites and soma were imaged. Sequential acquisition of Z-stack images across channels was then performed across the DiO (488nm) and Bassoon (647nm) channels for the full visible plane of neuronal processes. This typically ranged between 10-30µm in depth. Nuclear images of c-Fos immunolabelling (568nm) and DAPI (405nm) staining were acquired in single plane images corresponding to the Z-plane position at which the cell soma boundary and nucleus was most clearly visible, allowing clear confirmation of Fos+ or Fos- cellular identity during reconstruction. Images were then exported for analysis. Identical imaging parameters were used for the acquisition of images for the quantification of Bassoon immunoreactivity for experiment two, with the exception of standardising Z-depth to 10µm.

Typically, images were acquired for 1-2 cells per section, grouped by Fos+ or Fos- status of a given pyramidal cell, with 2-3 sections quantified per animal. Three animals were excluded from experiment three due to poor quality of DiO penetrance, adjusted animal numbers are provided in Table 6.1.

For experiment one, acquisition of images of c-Fos and NeuN labelled sections was performed identically to described in section 2.2.2, with minor modifications. Briefly, images were acquired using an Olympus BX53 epifluorescence microscope at 20x magnification with a halide fluorescent lamp with excitation filters at 488nm (c-Fos) and 647nm (NeuN). 5 x 5 grids of images at 1392 x 1040px^2 per tile were acquired of the dorsal hippocampus for each channel sequentially at standardised exposure values set from experiments conducted in Chapter five, set within each channel and used consistently across each sample.

6.2.7 Immunofluorescence image analysis

For experiment one, analysis of Fos+ neuron density in CA1, 5 x 5 images at 1392 x 1040px^2 were processed using FIJI as described in section 5.4. Briefly, images from individual channels were stitched using the stitching plugin (Preibisch et al., 2009), before background was subtracted, pseudocolour applied, and colour channels merged. Whole CA1 ROIs were manually outlined for each section, and 100 x 100µm counting grids were overlaid onto the image. Neurons showing clear Fos+/NeuN+ colocalisation were counted within the ROI and normalised to the estimated NeuN density, calculated as described in section 5.4.

In experiments two and three, immunofluorescence analysis of confocal images was performed using an adapted general pipeline with similar principles to that described in section 2.2.2.2. Confocal images were segregated by individual channels and reconstructed for max intensity projection before contrast standardisation, pseudocolouring, and re-merging colour channels. For analysis of Bassoon immunoreactivity, average whole image fluorescence intensity was calculated. This included both perisomatic pyramidal cell layer and stratum oriens basal dendrite labelled portions of CA1 pyramidal neurons. Average fluorescence intensity was averaged across 4-6 individual imaged fields per section with three sections per animal.

For dendritic reconstruction, quality checks were first performed on max intensity projected DiO images to inspect relative dendritic and somal labelling quality for further use. Additionally, Fos+ or Fos- status of individually imaged cells was confirmed by colocalisation between DAPI and c-Fos immunolabelling, alongside encapsulation of the nuclear signals within the somal DiO labelling by alignment to individual Z-stack images of the DiO channel (Figure 6.1A). Following quality checks, DiO labelled dendritic image stacks were reconstructed using the FIJI plugin SNT (simple neurite tracer). Dendritic branches were traced using the default parameters for detection, which proved accurate in distinguishing DiO labelling from low background, resolving single dendritic branches and attached spines. Basal dendritic branches were traced for the entirety of visible labelling from the base at the cell soma to the tip of the dendrite segment, excluding any dendrites showing clear branch disruption or an unclear soma. Dendritic branching was allowed and were processed as attached but secondary segments. We generally observed that while DiO labelling provided sufficient quality for visualisation of dendritic structures and individual spines, entire cell filling was generally not observed, which may be attributable to the reduced affinity and diffusion constant of DiO through lipid membranes as compared to DiI (Fritsch et al., 2005). Example single plane partial

trace images with overlaid DAPI and c-Fos signal are shown in Figure 6.1A, demonstrating targeting of Fos+ and Fos- CA1 pyramidal neurons.

Selected dendrite segments were then reconstructed across the entire Z-plane of the images. For quantification of spine occupation, max intensity projected Bassoon immunofluorescence images were overlaid onto reconstructed segments (adapted from Schachtele et al., 2011), before both were binarized using a standardised threshold (Huang method, FIJI). The binarized DiO channel was then used as a mask to isolate signal from the Bassoon channel in the vicinity of the DiO-labelled dendrite segment to improving visibility and ease of quantification (Figure 6.1B/C). Binarised Bassoon signal was then overlayed onto reconstructed DiO (non-binarised) segments which was then exported for quantification.

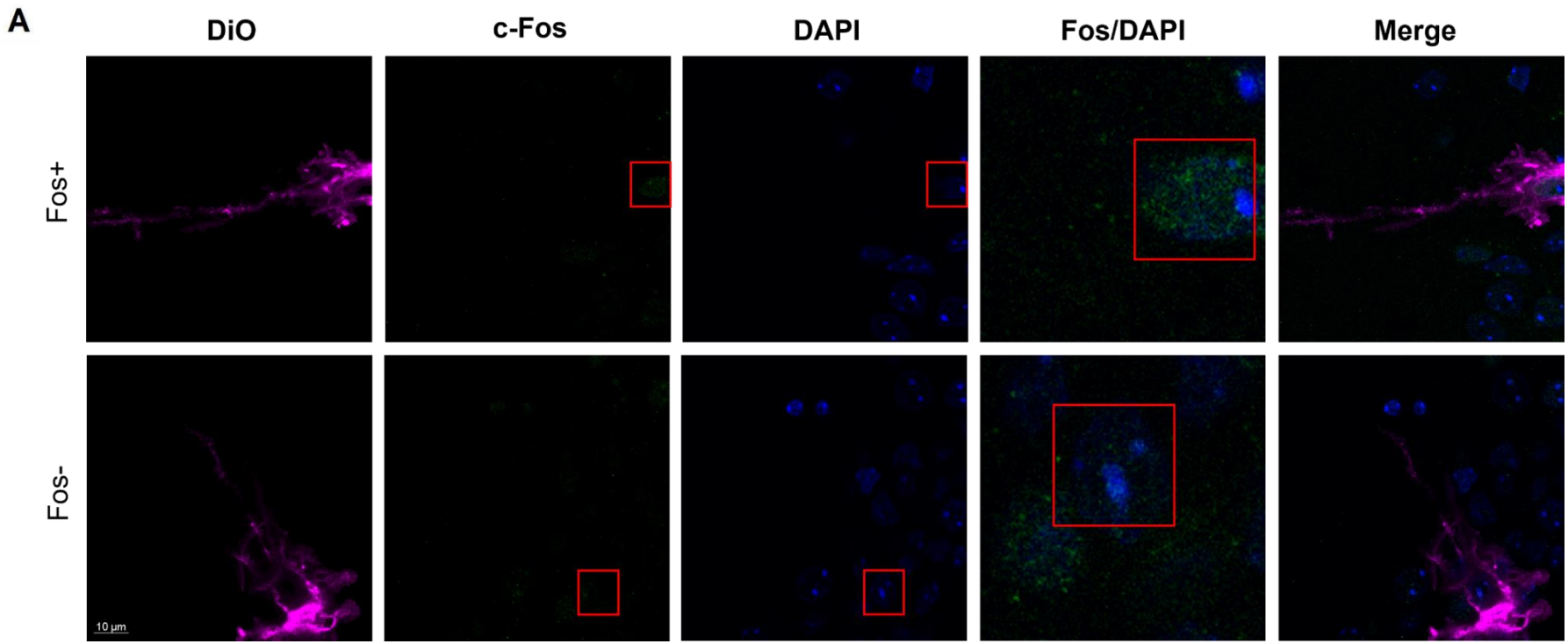

Figure 6.1 panel 1: A) Example fluorescence images (63x magnification) from DiO neuron tracing and immunofluorescent co-labelling of c-Fos and DAPI, grouped by cell type (Fos+/Fos-) in the basal shaft of CA1 pyramidal neurons. Red boxes highlight cell nucleus with or without colocalization with c-Fos, respectively. Each image is in a single Z-plane to best demonstrate somal encapsulation of nuclear signals and dendritic protrusions from each given cell. Inset shows magnified DAPI and c-Fos labelled nuclei from example Fos+ and Fos- cells. Note the high intensity signal in the DiO channel localised near the base of the soma is due to the site of contact of targeted DiO microparticles in the stratum pyramidale and subsequent multidirectional diffusion.

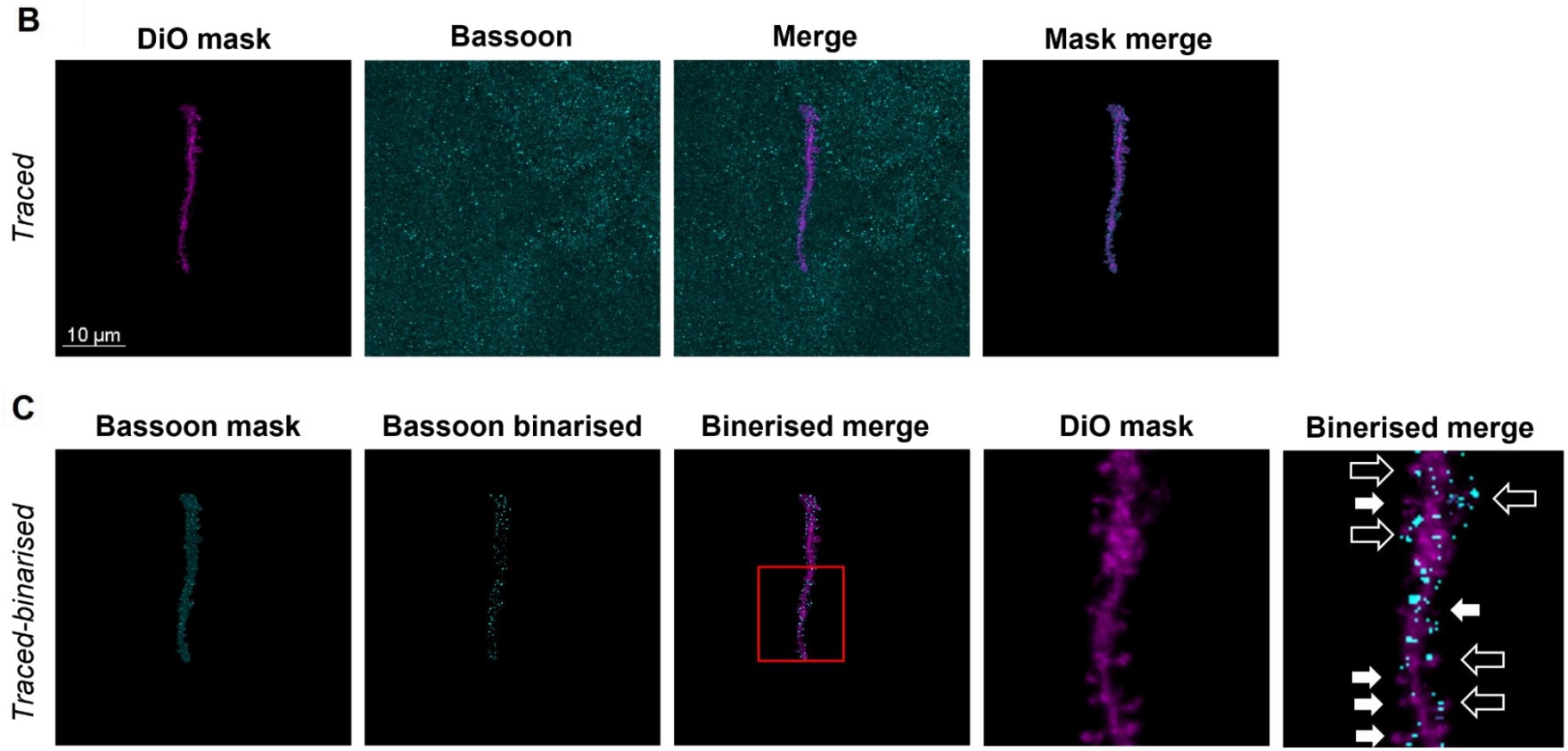

Figure 6.1 panel 2: B) Example of processing pipeline for an individual traced dendritic segment. Traced dendrite with DiO labelling is first isolated before overlay of full field Bassoon immunoreactivity. A binarized version of the DiO image is used to mask the raw Bassoon signal. C) Example of conversion of DiO-masked Bassoon signal into binarized signal for colocalization with DiO and quantification of Bassoon occupied spines. Example of magnified image of DiO and overlayed binarized Bassoon signal from inset shows dendrite segments and visible individual spines. White arrows indicate spine heads without Bassoon signal colocalization, while black filled arrows indicate spine heads with Bassoon colocalization.

For quantification of dendritic length, spine density, and spine occupancy, analysis was performed in FIJI. Firstly, reconstructed dendrite segments were measured in length by tracing the dendritic segment from the base at the soma to the furthest tip of the primary dendrite. Second order branches were also quantified, with dendritic length measured from the point of branching to the observable tip of the branched segment. Spine number was counted agnostic to spine subtype, while excluding any noticeably dysmorphic spines or those with no clear connection to the primary dendrite. Spine occupancy was counted when individual spines had clear colocalisation signal with Bassoon immunolabelling within the spine head. Spine number for occupied (Bassoon+/BSN+) and unoccupied (Bassoon-/BSN-) spines (example in Figure 6.2D) was then converted to density by dividing total spines in each category over the dendrite segment length. Measurements for individual cells were then grouped by cell type (Fos+ or Fos-) and averaged across cells and sections, yielding average spine density and occupied spine density for both Fos+ and Fos- cells within each animal.

6.2.8 Statistical analysis

For experiments one and two, analysis of Fos+ neuron density and Bassoon immunoreactivity was performed using univariate between groups ANOVAs, including APOE genotype and sex as primary independent variables. For experiment three, a four-way mixed ANOVA was used to assess dendritic spine density, with APOE genotype and sex as between subject factors and cell type (Fos+/Fos-) and occupation (BSN+/BSN-) as repeated measures variables. Alpha criterion was set at 0.05 for all tests performed. Homogeneity of variance or sphericity was assessed using the Levene’s and Mauchly’s tests as appropriate, with corrected statistical values provided in each case.

6.3 Results

6.3.1 Experiment one: Validation of enhanced CA1 ensemble size in young E4-TR mice.

First, we attempted to replicate the finding of an increase in CA1 ensemble size in 3-month aged E4-TR, as reported in Chapter five. Univariate analysis of Fos+ neuron density in CA1 revealed a significant main effect of genotype, with E4-TR mice demonstrating significantly elevated Fos+ neuron density relative to E3-TR controls ($F(1,15) = 6.78$, $p = .020$). There was no main effect of sex ($F(1,15) = 1.75$, $p = .206$) or interaction with APOE genotype ($F(1,15) = 0.18$, $p = .681$; Figure 6.2A/B). We therefore replicated the increased ensemble size observed in Chapter five, although we noted that the relative average size of the ensemble was smaller overall than previously observed.

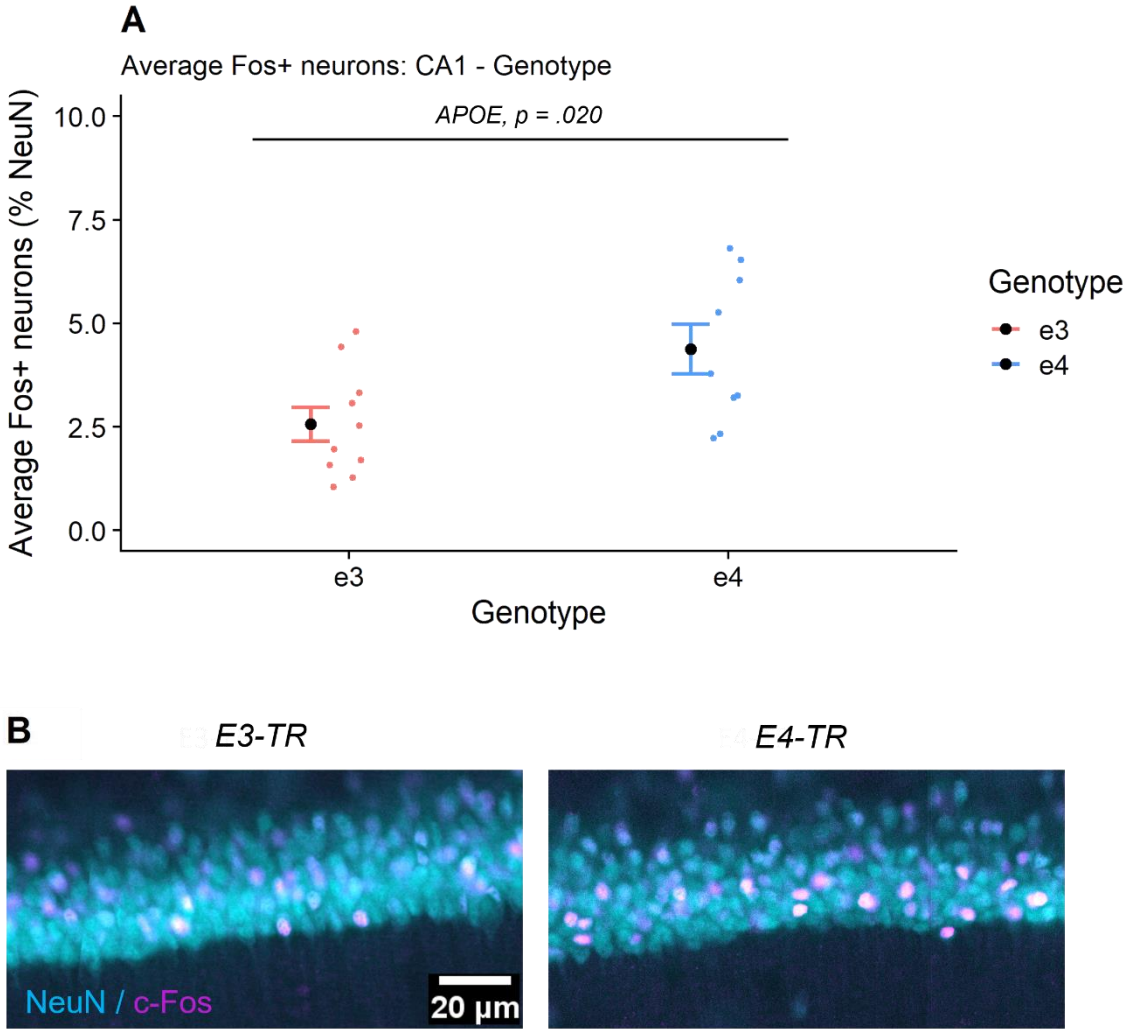

Figure 6.2: A) Average Fos+ neuron density in the CA1 pyramidal layer expressed as percentage of estimated NeuN+ neurons, grouped APOE genotype. Brackets and labels represent relevant statistical main effects, interactions and pairwise comparisons where appropriate. Individual points represent the average of each count across sections within a single animal. Error bars represent mean +/- SEM. B) Representative example immunofluorescence images of labelled Fos (magenta) and NeuN (Cyan) neurons in the CA1 pyramidal layer grouped by APOE genotype.

6.3.2 Experiment two: Assessment of CA1 Bassoon presynaptic protein immunoreactivity

Second, to assess whether APOE-TR mice demonstrated basal differences in overall presynaptic integrity, immunofluorescence analysis was performed on the presynaptic protein Bassoon within the stratum pyramidale and oriens fields of CA1. Univariate analysis of Bassoon immunoreactivity demonstrated no significant baseline differences between groups, with no main effect APOE genotype ($F(1,14) = 0.32$, $p = .583$), a trend for an effect of sex with females showing lower mean immunoreactivity ($F(1,14) = 3.45$, $p = .084$), and no significant interaction ($F(1,14) = 1.42$, $p = .253$) in 3-month aged APOE-TR mice (Figure 6.3A/B).

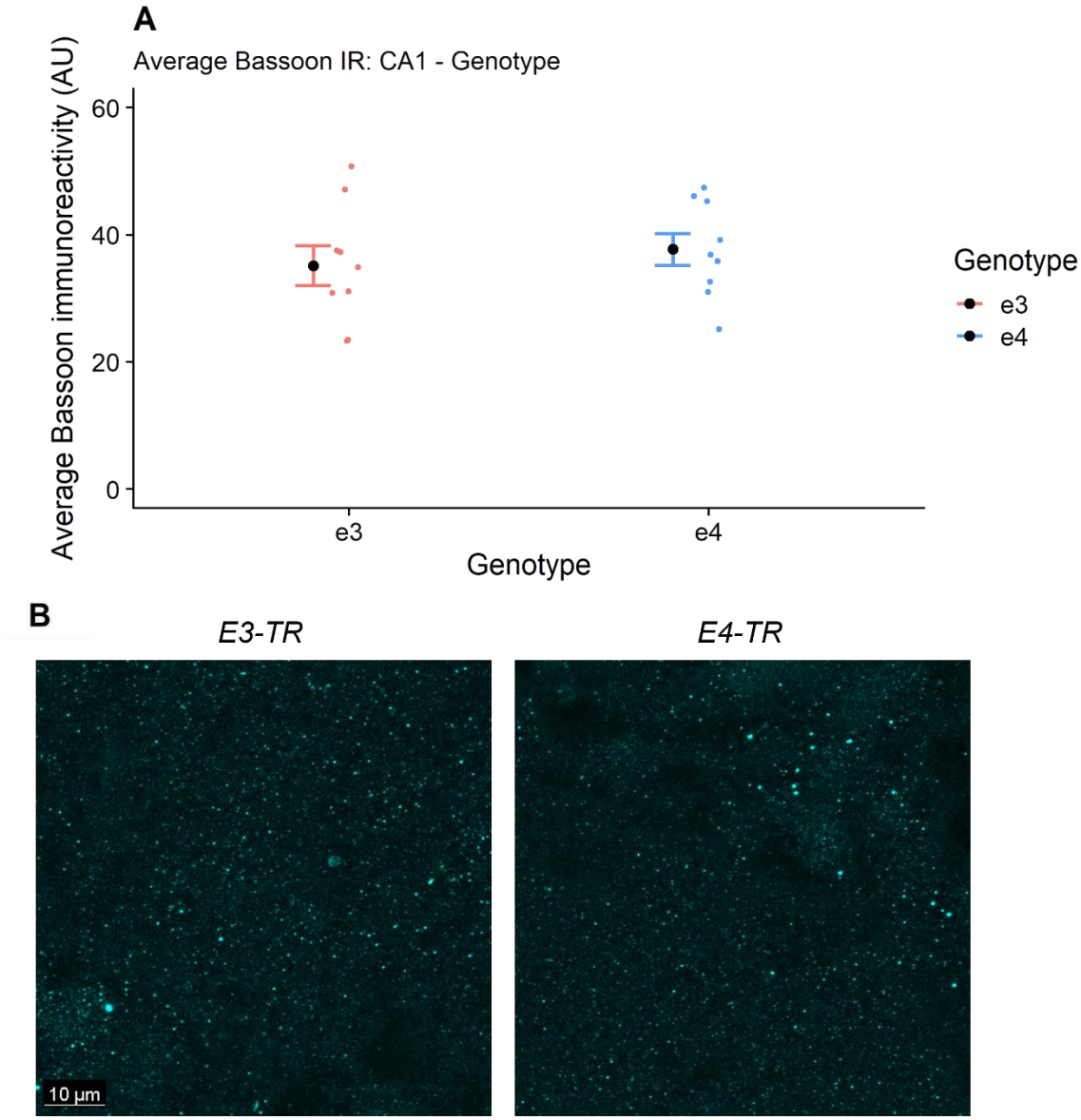

Figure 6.3: A) Average Bassoon immunoreactivity in the CA1 pyramidale and oriens layer, grouped by APOE genotype. Brackets and labels represent relevant statistical main effects, interactions and pairwise comparisons where appropriate. Individual points represent the average immunoreactivity across 4-6 fields within three hippocampal sections within a single animal. Error bars represent mean +/- SEM. B) Representative example immunofluorescence images (63x magnification) of labelled Bassoon (cyan) neurons in the CA1 pyramidale and oriens layer grouped by APOE genotype.

6.3.3 Experiment three: Assessment of CA1 dendritic spine density and synaptic occupation in Fos+ and Fos- neurons in young APOE-TR mice

After establishing the replication of the increase in CA1 ensemble size in E4-TR mice at 3-months of age without basal differences in overall Bassoon immunoreactivity as a proxy for synaptic integrity, we next assessed the possibility that APOE4 was associated with decrements in dendritic spine density and synaptic occupation with a particular susceptibility of neurons activated in response to environmental novelty as indexed by c-Fos expression. Using direct application of the lipophilic carbocyanine dye DiO in combination with multiplex immunofluorescence, we were able to isolate and trace basal dendritic protrusions from Fos+ and Fos- CA1 pyramidal neurons. Colocalization was performed between post-synaptic DiO labelled dendritic spines and putative presynaptic terminals using Bassoon immunofluorescence. Bassoon generally demonstrated a punctate diffuse immunolabelling throughout the neuropil and demonstrated colocalization with a subset of dendritic spines on each dendritic segment, allowing generation of spine density for occupied and unoccupied spine sites, referred to as Bassoon positive (BSN+) and Bassoon negative (BSN-), respectively (e.g., Figure 6.D).

A mixed ANOVA demonstrated that there was no significant main effect of c-Fos expression (cell type) on dendritic spine density for either BSN+ or BSN- spines (Table 6.2). There was a main effect of occupation on overall spine density, as expected, with a significantly lower spine density of occupied BSN+ spines than total spines at the whole group level. There was no significant interaction between spine occupation or c-Fos expression, with equivalent BSN+ spine density between Fos+ and Fos- neurons, however (Figure 6.4A, Table 6.2).

As for APOE genotype and sex, there were no significant main effects, although we noted a slightly lower mean for both BSN+/BSN- spine density in E4-TR mice (Figure 6.4B/C, Table 6.2). Finally, there were no significant interactions between APOE genotype, sex, and either spine occupation or cell type on spine density (Table 6.2).

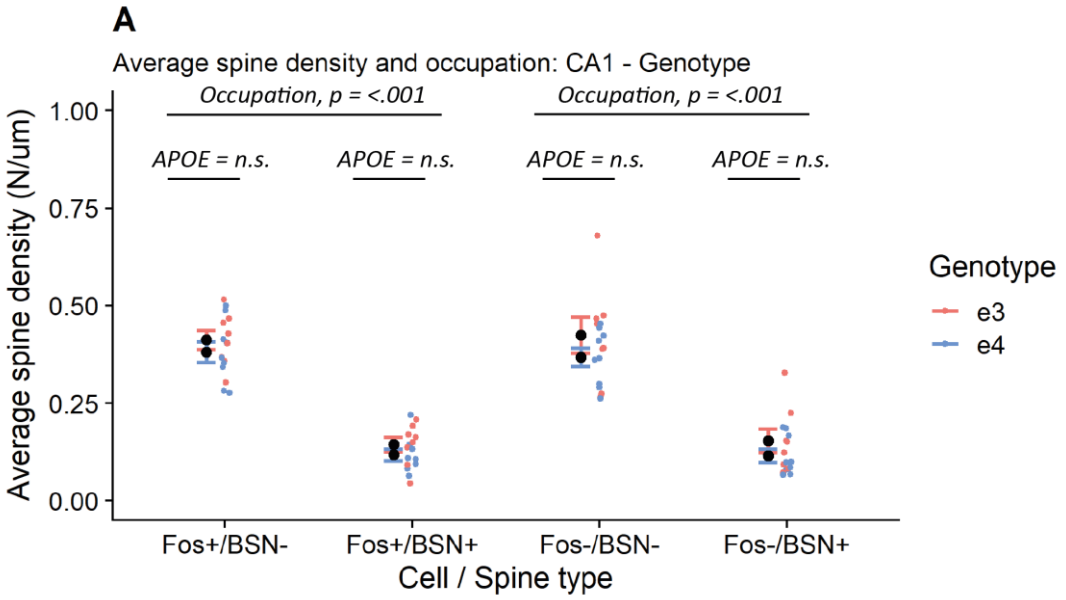

Figure 6.4 panel 1: Average spine density in Fos+ and Fos- CA1 pyramidal neuron basal dendrites in 3-month aged APOE-TR mice. A) Average occupied (BSN+) and unoccupied (BSN-) dendritic spine densities grouped by cell type into Fos+ and Fos- neurons, by APOE genotype. Brackets and labels represent relevant statistical main effects, interactions and pairwise comparisons where appropriate. Individual points represent the average spine density for a single animal, representing the average across multiple dendritic segments and cells. Error bars represent mean +/- SEM.

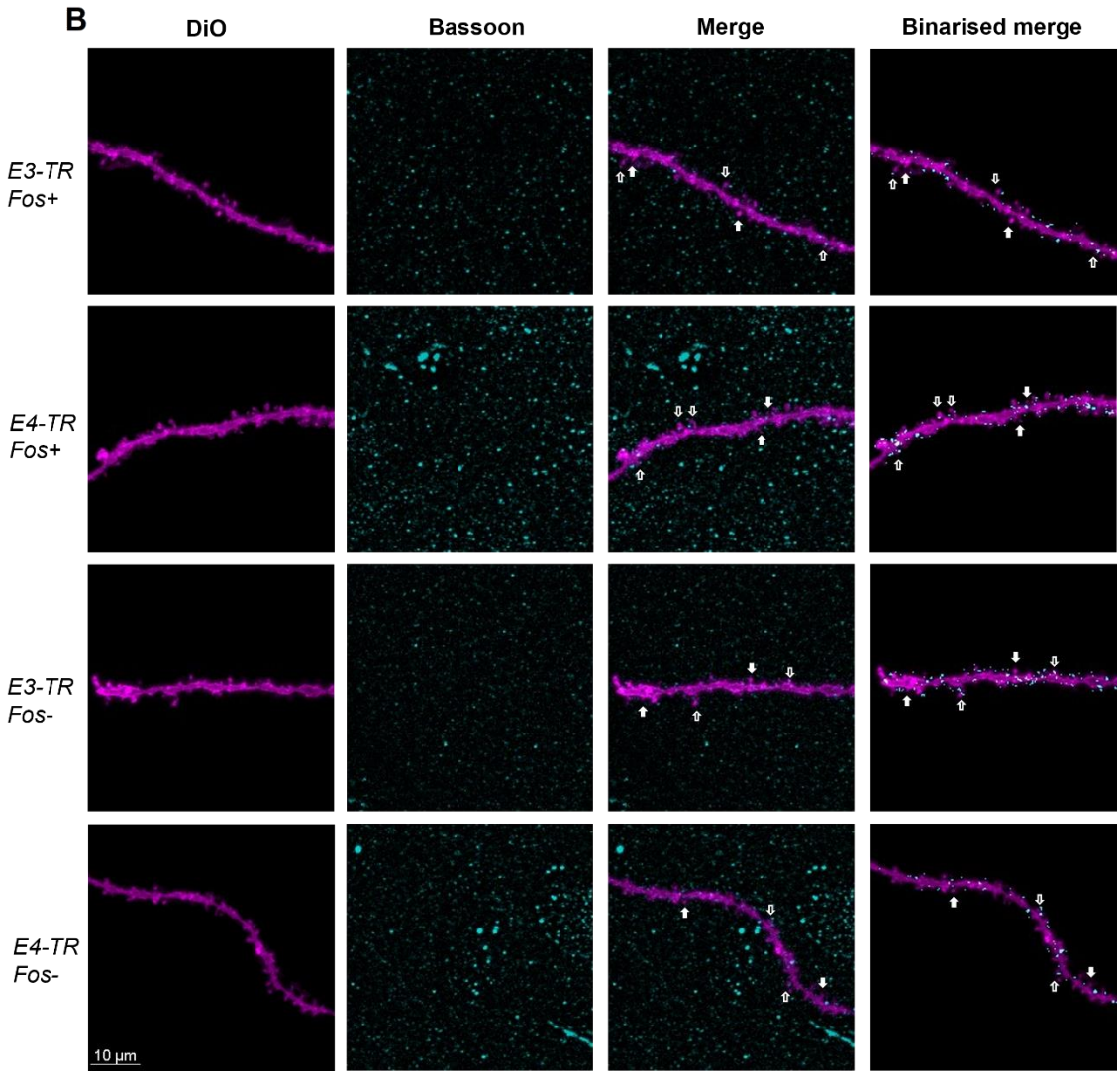

Figure 6.4 panel 2: B) Representative example DiO fluorescence and Bassoon immunofluorescence (63x magnification) images of individual DiO traced dendritic segments and Bassoon immunoreactivity shown in isolation and merged, grouped by APOE genotype and cell type. Examples of unoccupied dendritic spines are outlined by white arrows, while occupied spines are shown by white arrows with black fill. Note that occupation criteria required presence of Bassoon puncta within the fluorescent signal of a given spine head. Masked and binarized example images are provided.

Table 6.2: Statistical analysis of CA1 dendritic spine density and occupation in Fos+ and Fos- pyramidal neurons in APOE-TR mice at 3-months of age in experiment three. Relevant main effects and interactions are provided. Results correspond to Figure 6.4.

Measure	Variable	Statistic	Figure
Dendritic spine density			
	Cell type	F(1, 13) = 0.02, p = .899	
	Occupation	F(1, 13) = 403.04, p = <.001	
	Cell type*Occupation	F(1, 13) = 0.12, p = .751	
	Genotype	F(1, 13) = 1.62, p = .225	
	Sex	F(1, 13) = 0.04, p = .839	**6.4**
	Genotype*Sex	F(1, 13) = 0.02, p = .891	
	Cell type*Genotype	F(1, 13) = 0.19, p = .673	
	Cell type*Sex	F(1, 13) = 1.54, p = .237	
	Occupation*Genotype	F(1, 13) = 0.20, p = .663	
	Occupation*Sex	F(1, 13) = 1.40, p = .258	

6.4 Discussion

In the final experiments conducted in Chapter six, we investigated whether an increased CA1 neuronal ensemble size observed following exposure to environmental novelty in young E4-TR mice was associated with alterations in dendritic spine density and spine occupation specifically in ensemble 'recruited' and 'unrecruited' neurons. Carbocyanine DiO dye labelling was performed in dorsal hippocampal CA1 following environmental novelty exposure in 3-month aged APOE-TR mice, before immunofluorescence analysis with the presynaptic marker Bassoon to enable quantification of postsynaptic dendrites and putative presynaptic innervation or spine occupation (e.g., Schachtele et al., 2011). Dendritic tracing was performed in the basal shaft in both c-Fos expressing and non-expressing (Fos+/Fos-) CA1 pyramidal neurons to mark ensemble recruitment.

We hypothesised that E4-TR mice would exhibit an increased ensemble size in dorsal CA1, indexed by enhanced Fos+ neuron density, as observed in experiments conducted in Chapter five. Further we predicted that E4-TR mice would exhibit a significant reduction in both overall spine density and Bassoon occupied spine density in the basal shaft of CA1 pyramidal neurons, without a significant overall loss of presynaptic Bassoon immunoreactivity within CA1. Finally, we predicated that this deficit would be enhanced in an ensemble recruited population of Fos+ neurons.

Our results confirmed the first hypothesis, with 3-month aged E4-TR demonstrating a significantly larger CA1 ensemble than E3-TR controls following environmental novelty exposure and was additionally independent of sex. Analysis of presynaptic Bassoon immunoreactivity revealed no significant differences in overall immunoreactivity in the pyramidal/oriens layer of CA1, suggesting no overall reduction in presynaptic integrity as predicted. Analysis of reconstructed dendrites colocalised with Bassoon revealed that Bassoon occupied spines were significantly less dense than unoccupied. However, there was no significant effect of ensemble recruitment on total density of Bassoon occupied spine density, with equivalent densities between Fos+ and Fos- CA1 pyramidal neurons. Finally, there were no main effects or interactions between APOE genotype and sex in either occupied or unoccupied spines.

Together these results support the replicability of an elevated CA1 ensemble size in response to environmental novelty in E4-TR mice at young age, without substantial changes in a general presynaptic marker. However, there appears to be no substantial baseline influence of APOE

isoform in young APOE-TR mice on CA1 pyramidal neuron basal spine density or occupation in either an ensemble-recruited or unrecruited neuronal population.

6.4.1 Variability and age-dependence of CA1 pyramidal neuron dendritic integrity in APOE-TR mice

The lack of an APOE4-dependent deficit in overall dendritic spine density, while contrary to our hypotheses, is perhaps not surprising. As discussed in the introductory Chapter, there is substantial variability between reports assessing dendritic integrity in APOE mouse models in terms of model, technique used, and variable coverage of age points across the lifespan. While some evidence appears to suggest that APOE4 is detrimental to spine density in late age in the APOE-TR model (e.g., Jain et al., 2013), the extent of this difference is unclear and appears to vary by region. For example, reports have suggested no APOE isoform dependent changes in apical or basal CA1 spine density in APOE-TR mice at 1-month (Dumanis et al., 2009), 5-months in female mice, and 7-8 months (Jain et al., 2013), while some suggest apical CA1 spine deficits in E4-TR mice as early as 4-months (Sun et al., 2017). Even between hippocampal subregions there may be variability in vulnerability to APOE-mediated dendritic impairment with no change in DG granule cell spine density at 12-24-months (Dumanis et al., 2009) or reductions reported at the same age by different groups (Ji et al, 2003). Our results are consistent with the suggestion that E4-TR mice of both sexes do not demonstrate significant impairments in CA1 basal shaft dendritic spine density at young age and further, our results also suggest that the density of these spines occupied by putative presynaptic innervation is also unaffected by APOE isoform. This may suggest equivalent structural correlates of synaptic innervation from input regions to the CA1 basal shaft, such as the prevalent inputs from CA3 and the EHC. However, we cannot rule out functional alterations at these sites, although spine metrics are suggested to strongly correlate with glutamatergic function (e.g., Matsuzaki et al., 2001; Kasai et al., 2003; Lee et al., 2012).

6.4.2 CA1 ensemble dendritic integrity and occupation in APOE-TR mice and the potential role of experience-dependent plasticity

In the present experiments, our results did not support the speculation that an increased size of a novelty responsive c-Fos expressing neuronal ensemble in E4-TR mice would be

specifically associated with deficits in dendritic integrity and synaptic occupation relative to unrecruited (Fos-) neurons. Our present question and hypotheses rather made the case for a lack of differences in spine density and occupation between ensemble recruited and unrecruited neurons following acute environmental novelty exposure.

The Fos+ ensemble recruited during novel context exposure is thought to represent multiple components of information processing, with hippocampal CA1 particularly responsive and implicated in the encoding of novel environmental features (e.g., Vazdarjanova & Guzowski., 2006; Cai et al., 2016; Leutgeb et al., 2004). Indeed, recent evidence suggests that c-Fos expressing ensemble neurons, particularly neurons expressing place fields, during exploration of a novel environment show elevated firing rates, including elevated theta bursting, larger place fields but less information spatial information per spike than Fos- neurons in mice, and are suggested to represent general contextual memory-relevant information rather than spatial information specifically (Tanaka et al., 2018).

However, as discussed in section 5.4, novel context exposure does not control for specific goal-oriented behaviour and does not involve overt learning of a hippocampal-dependent task. This therefore raises the question of whether differences in dendritic spine integrity may be observed specifically in 'engram-like' cell populations, which are specifically activated over the course of learning and are involved in the representation of a memory trace (e.g., Roy et al., 2016; Ryan et al., 2015). Indeed, spine density increases have been shown to be induced in CA1 and the DG, alongside mossy fibre terminal expansion onto CA3 pyramidal neurons following maze task learning (Uriarte et al., 2017; Ruediger et al., 2011, 2012), while specific increases in Fos+ nucleus accumbens neuron spine density was observed following drug-context learning (Singer et al., 2016). This raises the question of whether at baseline and following experience, such neuronal plasticity mechanisms may be preferentially affected by APOE-dependent mechanisms and requires further investigation. One possible hypothesis would be that the induction of IEG-dependent activation of downstream synaptic effector genes to support structural learning-related plasticity (i.e., spine density and related changes) may be differentially influenced by APOE isoform as opposed to a single experience evoked ensemble as measured in the present experiment. In contrast, the present results are unlikely to involve experience-dependent learning and rather reflect a lack of basal differences in the dendritic properties of acutely activated hippocampal ensembles. Extension of the present experiments to paradigms such as contextual fear conditioning or reference memory maze tasks would be suitable to assess this possibility, with the prediction that APOE4 would be

associated with attenuated spine parameter increases in ensemble-recruited neurons following learning.

In spite of this consideration, it remains an open question as to the potential origins of the APOE4-dependent increase in CA1 ensemble size. Given our results, it appears unlikely to be due to basal alterations in dendritic spine density or spine occupation. We would therefore speculate that alternative explanations such as elevations in intrinsic CA1 pyramidal cell excitability such as via pre- or postsynaptic mechanisms (e.g., altered post synaptic receptor density or presynaptic release) and/or network disinhibition may be more likely, and require further investigation.

6.4.3 Caveats

The predominant caveats of the experiments conducted for Chapter six are centred on experiment three. Namely, some methodological constraints limit extrapolation. Firstly, we noted that optimisation of neuronal labelling with DiO was particularly challenging. DiO has a particularly high propensity for precipitation and a slower diffusion constant than other carbocyanine dyes (Fritzsch et al., 2005) and therefore the current protocol may be better suited by acute live section preparation followed by direct cell filling or fixed cell filling with an alternative dye. This would likely also ameliorate the second limitation of throughput, with successful labelling of Fos+ cells proving somewhat sparce with direct DiO application to fixed sections. Due to these limitations, the animal number used for experiment three was also reduced from 20 to 17, reducing power.

Further, analysis focussed on basal shaft dendrites of CA1 pyramidal neurons due to their input from both CA3 and the EHC. We cannot therefore rule out that changes in spine integrity may occur in the apical tuft dendrites of APOE-TR mice. Additionally, analyses were agnostic to spine type and thus we are unable to distinguish the possible selective differences between spine types (e.g., stubby and mushroom subtypes). Further we exclusively targeted CA1 pyramidal cells on the basis of the findings in Chapter five that CA1 pyramidal neurons, but not GAD-67+ interneurons, showed preferentially increased c-Fos activity in E4-TR mice. We additionally therefore cannot rule out interneuron-specific changes in dendritic integrity which also warrants investigation.

Finally, as discussed above and in Chapter five, the novel context paradigm used to induce CA1 ensemble activity is inherently not directly linked to a goal-directed task or involve measurable

learning. As such we are unable to dissociate potential differences in learning and task-related neuronal ensembles from those ‘online’ during exploration of a novel context. Further, multiple behaviours are common in rodents during novel environmental exposure such as locomotion, grooming, escape behaviour, and idle rest. Therefore, our current methodology cannot dissect which components of behaviour the c-Fos expressing neuronal ensemble may represent and as such should be interpreted with this in mind.

6.5 Chapter six summary and conclusion

In Chapter six, we aimed to further investigate the increased CA1 c-Fos expressing neuronal ensemble size following contextual novelty in young E4-TR mice established in Chapter five. There was a particular focus on the possibility of impaired dendritic structure in ensemble recruited neurons, indexed by c-Fos, in E4-TR mice. Neuronal tracing using a lipophilic carbocyanine dye in combination with multiplex immunofluorescence imaging of CA1 neurons following exposure to environmental novelty allowed the assessment of dendritic spine density and measurement of a proxy for synaptic occupation in both ensemble-recruited and unrecruited neurons. We successfully replicated the increase CA1 ensemble size phenotype in E4-TR mice, while demonstrating no overall change in the abundance of the presynaptic marker Bassoon as a proxy for presynaptic integrity. Dendritic analysis revealed no differences in spine density or occupation between c-Fos expressing ensemble neurons and unrecruited neurons, alongside no significant influence of APOE genotype or sex. We suggest that the present results support a null or negligible effect of APOE isoform on basal CA1 pyramidal neuron spine density and occupation at young age and that, at least under the current circumstances, no substantial influence of acute environmental novelty exposure on these metrics. Critically, further investigation may focus on establishing whether APOE isoform may modulate the effect of experience-dependent plasticity, such as following tasks taxing episodic learning and memory, on these measures. Moreover, we would speculate that APOE4 may have a detrimental impact on the induction of mechanisms necessary to support long-term experience-dependent spine growth within ensemble recruited neurons which warrants investigation beyond one-trial experience.

CHAPTER SEVEN

General discussion

7.1 Background and scope of the thesis

APOE4 has persistently been identified as the greatest genetic risk factor for sporadic late-onset Alzheimer's disease (LOAD) in the general population and has been associated with both cognitive decline and neurophysiological defects, primarily in the aged population. However, while extensively investigated, the phenotypic influence of APOE isoforms in the CNS on structure-function relationships and consequent cognitive performance remain incompletely characterised, particularly at young age and in the absence of cooccurring pathologies. Importantly, evidence from preclinical models implicates APOE4 in numerous neurobiological processes which contribute to CNS dysfunction without necessitating interaction with AD-dependent pathways such as amyloid beta or tau pathogenesis.

In studies of cognitive performance using APOE mouse models, primary focus has been dedicated to hippocampal-dependent long-term episodic memory. The data from these studies generally suggest that APOE4 impairs episodic memory acquisition and long-term retrieval in an age-dependent manner, with an enhanced susceptibility of females. In contrast, little focus has been given to the rapid episodic learning and memory, more akin to 'everyday memory', which typically requires learning of novel episodic information over single to a few experiences on a stable background of prior 'rule learning'. Additionally, most studies using APOE mouse models have used cross-sectional designs at varying ages and as such, trajectories of performance across the lifespan within animals is sparsely characterised.

Further, evidence in vitro and in vivo suggests that APOE4 induces age-dependent defects in neuronal morphology including deficits in dendritic complexity and spine density, aberrations in synaptic plasticity such as via high-frequency stimulation or Reelin-dependent LTP, calcium homeostasis, and calcium-dependent signalling activation. However, there has been no investigation of the potential influence of APOE isoform on the behaviour-related activation of neuronal ensembles and related immediate early gene expression in vivo, which has been shown to be crucial for experience-dependent synaptic plasticity, learning, and memory in animal models.

Therefore, the work comprising the present thesis aimed to assess the influence of APOE isoform and sex on the lifespan trajectories of everyday learning and memory performance using the APOE-TR mouse model and a novel adaptation of an 'everyday memory' rapid place learning task. In parallel, we aimed to assess the impact of APOE isoform on the hippocampal neuronal ensemble response at baseline and following behaviour in young and mid-aged

APOE-TR mice. Finally, following up on our findings, we investigated whether APOE isoform may be associated with alterations in the morphological properties of an environmental novelty-recruited hippocampal CA1 ensemble.

We hypothesised that E4-TR mice would show premature age-related cognitive decline in rapid place learning and memory performance, which would be accelerated in females. In parallel we predicted that E4-TR mice would demonstrate impairments in overall hippocampal ensemble recruitment alongside reductions in IEG expression and of APOE expression itself, which would be worsened with ageing and similarly exacerbated in females. In final experiments, we hypothesised that E4-TR mice would exhibit a deficit in dendritic spine density and spine occupation in CA1 neurons, which would be enhanced in neurons comprising a novelty-recruited ensemble.

7.2 Summary of findings

In Chapter three, we first conducted two experiments in WT mice with the aim to establish the validity of novel appetitive adaptations of the delayed match to place (DMTP) Barnes maze task. The task was designed to measure everyday learning and memory performance across repeat administrations, using a rapid place learning task design. We implemented design principles from multiple existing maze tasks, including the Barnes maze, Morris water maze, event arena, and appetitive holeboard task, with the aim of adapting the Barnes maze for repeatable testing, flexibility in encoded spatial locations, and minimal environmental stress (i.e., without explicit aversive components such as bright lights, water, shock etc.). We predicted that WT mice would readily learn these tasks and demonstrate allocentric spatial learning and memory, a prerequisite of assessing everyday episodic memory.

In the first task, the adapted Barnes maze (aBM), we observed a number of limitations which impaired acquisition and induced variable spatial and non-spatial task solving strategies. We subsequently addressed these limitations in a second experiment following manipulation of several intrinsic task parameters that had limited performance, including reward contingency, intrinsic maze design, and parsimonious task solutions. Following these changes to task design, a multi-hole Barnes maze (mBM) was tested in a new cohort of WT animals. We observed robust within-day learning and consistent preference for a spatial strategy to support task solution, with performance reliant on extra-maze and global visuospatial cues, consistent with allocentric rapid place learning. Further, we observed place preference for the learned location

during unrewarded probe trials, supporting successful recall of the spatial memory. Retrieval accuracy was also graded as a function of prior reinforcement and distance from the target itself, which we suggest reflects putative spatial pattern separation-like behaviour. In the final experiment of Chapter three, we replicated these findings in a cohort of 3-month aged APOE-TR mice, with analyses agnostic to APOE genotype. At the whole group level, we again observed robust within-day learning across multiple measures, alongside accurate place preference for the target location with control trials suggesting this again reflected allocentric place learning.

In Chapter four, we aimed to apply the novel mBM task to a cohort of APOE-TR mice across the lifespan to assess the trajectories of rapid place learning and memory performance, using longitudinal repeat-testing methods. APOE-TR mice were trained on the mBM task from 3-18-months of age at 3-month intervals, during which, learning and memory performance was measured during training, memory retrieval probe trials, and manipulations of retrieval delay. We observed complex interactions between age, sex, and APOE genotype in both measures of spatial learning acquisition and memory retrieval. Namely, E4-TR mice exhibited an early life deficit in acquisition, while male E4-TR mice showed a mild advantage in spatial recall accuracy following single trial experience. We observed that at adult maturity there were little differences in acquisition performance. At mid age, we observed that E4-TR male mice, while demonstrating an advantage at 3-months, showed a premature deficit in memory accuracy, failing to distinguish non-target foil locations as a function of distance from the target. From mid to late age, we observed that at the whole group level, while animals demonstrated evidence of memory for the target location, their overall ability to distinguish between foils of increasing distance from the target was impaired, suggesting a general age-dependent impairment in pattern separation-like ability. This was recovered at 18-months, however, by extending the number of preceding acquisition trials to four, although this did not distinguish between APOE genotype groups. We also observed impairments in E4-TR females in rapid acquisition at mid-late age, while there were trends to advantages in E4-TR males. Finally, we observed no group differences at the oldest age, however this may have been limited by reduced power due to animal attrition. We further demonstrated a mild advantage in acquisition following an extended delay (4-hours, but not 12-hours) between the first and second trial in E4-TR male mice, independent of age.

Overall, from these results we suggested that APOE4 may lead to subtle early life impairments and mid-late life female-specific impairments in rapid spatial learning, while male mice show

similar learning from mid-late age. However, rapid place memory accuracy was dissociated from that of acquisition, with APOE4 appearing to confer an early advantage to males in single trial spatial memory but premature age-related impairments in this capacity. We suggested that this dissociation between acquisition and retrieval may reflect differences in initial wayfinding ability (acquisition) and accuracy of encoded allocentric place memory (retrieval). Further, we highlighted that these APOE4-dependent effects were subtle and as such, detrimental effects of APOE4 may be more pronounced in long-term reference memory than rapid place learning. Moreover, this may suggest specific impairments in the neural mechanisms underpinning long-term memory maintenance and retrieval which requires further investigation.

In Chapter five, we investigated the possibility that APOE isoform, sex, and ageing alters hippocampal neuronal ensemble activity and IEG expression following behaviour. To do this we used parallel biochemical and immunofluorescent techniques across a cohort of early-mid aged APOE-TR mice following a contextual novelty paradigm. Characterising hippocampal ensemble activation using c-Fos immunofluorescence in both excitatory and inhibitory neurons, we observed an increase in Fos+ CA1 pyramidal neuron ensemble size in E4-TR mice relative to both E3-TR and E3E4-TR mice following environmental novelty, independent of sex. We also observed a similar effect in CA3, specifially in female E4-TR mice. In both cases these effects occurred across young to mid-age, although were more pronounced in young animals. We also observed a mild APOE genotype effect on CA3 interneuron activation, with E4-TR and E3E4-TR mice showing an increase from young to mid age. Female E4-TR mice also demonstrated mild deficits in GAD-67 immunoreactivity, particularly in the inferior and hilar regions of the DG, and a trend in CA1. However, we did not observe significant changes in overall DG hilar interneuron number as previously reported. We suggest this may represent a reduction in putative GABAergic innervation within the primary hippocampal cell layers, detectable from young age in E4-TR female mice. In exploratory analyses, we observed sex-genotype dissociations in hippocampal c-Fos network correlations. Specifically, E4-TR female and E3-TR male mice exhibited enhanced inter-region correlations between CA1-CA3-DG than their sex matched counterparts. We suggested that these results could reflect a combination of an APOE4-mediated network-level disinhibitory phenotype within the trisynaptic circuit, and possible enhanced excitatory inputs from extra-hippocampal regions, which requires further investigation. Further, the possible role of intrinsic cellular excitability and calcium homeostasis should be assessed. We speculated that increases in neuronal ensemble size may

be a general feature across varying hippocampal-dependent behaviours, a possibility and the functional consequences of which, also warrants study.

In parallel biochemical experiments in the same cohort, we characterised whole hippocampal c-Fos and APOE mRNA expression levels to investigate possible transcription-level shifts in expression that may be associated with APOE isoform. In c-Fos mRNA expression we similarly observed complex sex, age, and APOE genotype-dependent effects. At young age, male, but not female, E4-TR mice showed drastic reduction in c-Fos mRNA both at baseline and following environmental novelty. Young female E3E4-TR mice showed minor reductions in c-Fos mRNA, but levels were comparable between E3-TR and E4-TR females. At mid-age, however, these effects were lost, and expression was equivalent across all groups. APOE mRNA expression was also modulated by isoform and age, and we observed a reduction in APOE mRNA in young E4-TR mice relative to both E3-TR and E3E4-TR mice. At mid age, E4-TR and E3-TR mice exhibited similar levels of APOE mRNA, which were below that observed in young animals, while heterozygous E3E4-TR mice retained levels comparable to young controls. We suggested that these results may reflect differential c-Fos mRNA induction profiles between sexes and altered transcriptional activation of c-Fos by APOE isoform. It is unclear however at what mechanistic level this may be occurring, with multiple possibilities including an indirect signalling effect of APOE isoform to induce c-Fos program activation, or interference with transcriptional mechanisms such as post-transcriptional degradation. Additionally, we suggested that the age-dependent modulation of hippocampal APOE mRNA may represent shifts in the available APOE mRNA pool in the hippocampus, which is impaired during young adulthood by homozygous possession of APOE4, but further study of the transcription-translation programmes of APOE are required.

In the final experiments of Chapter six, we investigated whether the APOE4-dependent increase in CA1 ensemble size observed in Chapter five was associated with impairments in the morphological properties of CA1 pyramidal neurons recruited into a novelty-stimulated ensemble. Young APOE-TR mice were again exposed to the contextual novelty paradigm and were processed for cell tracing and immunofluorescence. First, we replicated the increased CA1 ensemble size phenotype in young E4-TR mice in a new cohort using the near identical methods applied during Chapter five. We also observed no basal differences between groups in immunoreactivity for the presynaptic scaffolding protein Bassoon as a marker for synapses, suggesting no overall gross loss of synaptic integrity in CA1 of young APOE-TR mice. Subsequently, CA1 pyramidal neurons were traced using the lipophilic fluorescent dye DiO and

dendritic branches were reconstructed from both c-Fos expressing (Fos+) and non-expressing (Fos-) neurons. Immunolabelling for Bassoon, we quantified Bassoon-DiO colocalisation within post-synaptic spines to quantify occupied spines. We observed no overall differences between APOE genotypes or sexes in CA1 basal shaft dendritic spine density or putative synaptic occupation in either Fos+ or Fos- neurons. We suggest that this first reflects no overall significant differences between APOE-TR mice in CA1 basal shaft spine densities at a young age, in the absence of insult. Further, this suggests that the APOE-associated increase in size of a transient novelty-recruited CA1 ensemble, does not exhibit a basal shift in spine density or putative synaptic occupation. However, we posited that while this study demonstrated that APOE4 can influence transient ensemble recruitment, further studies should investigate the possibility that APOE4 may alter both recruitment and experience-dependent plasticity, such as following learning, within the hippocampal ensemble.

7.3 Caveats and limitations

Interpretation of the findings from this present work should be considered in the context of several general caveats. Notably, the present work was carried out in its entirety within the APOE-TR model system. While the APOE-TR mouse is widely considered an effective model of APOE function (see section 1.3.5 for a discussion), there are some notable interspecies differences in the regulation of APOE between humans and mice which may contribute to our observed effects and limit translatability.

Firstly, in regulatory sequences, the entire multi-gene cluster in which APOE resides is not entirely conserved in mice. Specifically, the APOCI' pseudogene is not conserved and instead APOE is followed by APOCI, APOCIV and APOCII, while upstream TOMM40 is conserved (Allan et al., 1995; Maloney et al., 2007; Balu et al., 2019). Therefore, the distal regulatory elements show interspecies differences in control of APOE expression, with the inclusion of only a single hepatic control and multi enhancer region in the mAPOE gene cluster. The promoter has been shown to hold only ~40% homology with human sequences beyond the first 180bp of the transcription start site. Additionally, the proximal and distal regulatory regions exhibit similarities and differences in conservation of transcription factor binding sites. For example, mouse and human sequences show conservation of multiple AP-1 and AP-2 binding sites across the distal regions, while Sp1 (stimulatory protein 1) sites are far more abundant in the human sequences across the promoter (Maloney et al., 2007). Importantly for CNS APOE

expression, human and mouse regulatory sequences exhibit different numbers and positions of glial and neuronal positive and negative regulatory elements in a complex manner. For example, the more distal region of the hAPOE flanking region contains negative neuronal regulatory elements, while the analogous region in mAPOE does not. In any case the complexity of these differences extends beyond this and is reviewed in Maloney et al. (2007, 2010). Crucially, it has been suggested that it would be beneficial to use models of both human and mouse APOE regulatory sequences to understand potential differences in regulatory control of APOE expression in vivo. Moreover, these differences may contribute to interspecies variation in both APOE transcription, relevant for our findings in Chapter five, and circulating ApoE protein levels.

Second, as a general problem for the expression of human proteins in the mouse system, species differences in the interaction between the functional hApoE protein, murine ApoE receptors, and downstream signalling pathways may also vary. While in vitro studies in rodent and human cell lines indicate homology between human and mouse APOE receptors (Herz., 2009) and a general conservation of hApoE or ApoE receptor induced signalling activation such as the ERK pathway (e.g., Ohkubo et al., 2001; Qiu et al., 2004; Huang et al., 2017, 2019), we cannot rule out the possibility that such differences may affect our results. For example, whether our observed effects of APOE isoform on c-Fos expression may be influenced by interspecies differences in such signalling pathways is unknown.

Third is the general reliance on a homozygous APOE system, rather than the more common heterozygous E3E4 allele configuration in the human population. While a reasonable argument to support this approach is the possible compensatory action of APOE3 for APOE4 dysfunction and that homozygous expression provides a ‘purer’ system to study APOE4, the extrapolation to phenotypic effects in presence of a single APOE4 allele is limited.

As for general limitations in our experimental approaches, behavioural experiments conducted in Chapter three and four were performed using a novel task adaptation and limited parameter manipulations (e.g., retrieval delay) and requires replication and extension to assess normative performance and task dependence on the hippocampus. Further, the post-mortem approaches used in Chapters five and six are inherently outside of the physiological context and would benefit from comparative replication using in vivo measurement techniques to validate the physiological relevance of these findings. Additionally, as discussed in Chapter five, the identification of neuronal ensembles using IEG labelling approaches, while widely used, provides only limited insight into dynamic neuronal activity. This limits potential

identification of electrophysiological correlates of such activity and again would benefit from in vivo approaches.

7.4 Implications, significance, and future work

Given that the studies comprising this thesis were largely conducted in parallel across cohorts of animals, it is not possible to ascertain direct association between the reported phenotypes (i.e., between alterations in rapid place learning and memory, neuronal ensemble recruitment, APOE expression, spine density etc.). However, an important common feature between these studies is the coincident factor of age. We have noted several phenotypes associated with APOE4 at a particularly young age of 3-months, namely with E4-TR mice exhibiting a mild impairment in rapid place learning acquisition, elevated CA1 neuronal ensemble size, without a concurrent change in dendritic spine density or putative synaptic occupation, decreased APOE mRNA expression, and c-Fos mRNA expression in males, and a reduction in DG GABAergic innervation in females.

These concurrent phenotypes point to an early multifaceted dysregulation at the neuronal circuit level, which may culminate in combination with other associated actions of APOE4 (e.g., impaired immunoregulation, lipid trafficking etc.) to contribute to subtle cognitive dysfunction in the absence of gross pathology. We suggest that counterintuitive to the ageing-centric view of cumulative APOE4 dysfunction, further focus should be given to the exploration of young-age phenotypes which may be predictive of later impairments, or alternatively indicate variable trajectories of neurobiological processes across the lifespan. Indeed, some evidence suggests that cellular-systems level APOE4-mediated dysfunction may be detectable from early age (e.g., neurovascular function: Bell et al., 2012; Montagne et al., 2012; synaptic function: Korwek et al., 2008; Trommer et al., 2004; Sun et al., 2017; signalling activation: Yong et al., 2014; Korwek et al., 2008 etc.). Further, while complicating interpretation, the variability in reported phenotypes and modulation of such effects by sex and age is perhaps one the most surprising aspects of APOE function. Our work therefore also reinforces the importance of inclusion, or at least acknowledgement, of mixed sex groups to models the effects of APOE, with particular attention paid to the age investigated.

The mechanistic underpinnings of our findings in the experiments conducted during Chapter five and six are unclear. However, there are a number of potential APOE4-dependent mechanisms that have been outlined in the literature which may contribute to our observations. With a multifaceted role for APOE isoform in regulation of neuronal function,

future studies should further dissect the individual pathways which may underpin these changes. For example, three predominant but not mutually exclusive potential molecular mechanisms which may be involved in the present findings include: a gain of neurotoxic proteolytic fragmentation for neuronally expressed ApoE4 and subsequent proapoptotic signalling (e.g., Huang et al., 2001; Brecht et al., 2004; Zhong et al., 2008; Brodbeck et al., 2011), a loss of function for ApoE4 to mediate effective lipid delivery and distribution to support the membrane and organelle synthesis necessary for neuronal structural integrity and regulation of synaptic function (e.g., Holtzmann et al., 1998, 2012; Tesseur et al., 2000; Mahley & Rall., 2000; Mahley et al., 2016), and altered calcium-dependent signalling activation via acute action at the APOE receptors (e.g., Ohkubo et al., 2001; Tolar et al., 2002; Huang et al., 2017, 2019; Ramakrishna et al., 2021). Of these pathways, we suggest that, with relevance to our findings, the influence of APOE isoform on calcium-dependent signalling across both acute and chronic timescales may be informative, particularly in the context of neuronal network function.

A combination of both in vitro and in vivo cellular and network level approaches will be necessary to dissect these possibilities. For example, this could be assessed by combination of calcium imaging or field electrophysiological recordings with genetic reporters for calcium-dependent gene expression (e.g., c-Fos/CREB-GFP) either in vivo or using ex vivo organotypic systems following APOE expression in the APOE-TR model and/or acute APOE application. This would allow measurement of the relationships between network excitability, cellular-level calcium events, and consequent IEG expression to examine the correlates of IEG induction and both the acute and chronic influence of APOE on these relationships. Further, the possibility of differential induction of activity-dependent IEGs and downstream gene expression could be screened using RNA sequencing approaches following acute APOE stimulation or APOE expression and LTP induction ex vivo. Additionally, manipulation of APOE expression in vivo and in vitro such as via cell-type specific knock-out (e.g., Knoferle et al., 2014) would allow investigation of whether such observed results were directly as a consequence of APOE4 expression of neuronal or glial origin as well as the time-course of these effects (e.g., developmental in origin or during maturity; time-course of signalling induction etc.). These possible approaches may help delineate how APOE isoforms modulate the relationships between calcium homeostasis, network activity, synaptic plasticity, and ultimately may dictate effects on cognitive function.

In any case, ‘to what extent’, ‘in what combination’, and ‘when’ are key questions that challenge the field currently to understand how isoform differences in the molecular mechanisms of APOE function act to give rise to superordinate phenotypes within the CNS.

7.5 Conclusions

Overall, the work comprising this thesis has provided further evidence for a multifaceted influence of APOE isoform on cognitive and neuronal function within the APOE-TR mouse model. Specifically, our results demonstrate complex interactions between APOE isoform, sex, and age in rapid acquisition of episodic-like memory, with E4-TR mice demonstrating mild early life impairments and mid-life sex dependent effects in acquisition and memory retrieval accuracy. However, these differences are mild and appear likely superseded by long-term memory deficits. Further, we have shown that APOE4 is associated with enhanced hippocampal ensemble activation following environmental novelty particularly in CA1 at young to mid-age, alongside age-dependent shifts in both APOE and IEG mRNA expression levels. However, this early life increase in CA1 ensemble size in E4-TR mice was not associated with spine density or synaptic occupation changes in either ensemble-recruited or unrecruited CA1 neurons. Together, this work has contributed to characterisation of both lifespan trajectories and early life effects of APOE isoform in vivo and suggest avenues for further research to improve understanding of cell to network phenotypic effects of APOE4 in the absence of marked disease-related pathology.

References

Acevedo, S., Gardell, L., Bradley, S., Piu, F., & Raber, J. (2008). Selective Androgen Receptor Modulators Antagonize Apolipoprotein E4-Induced Cognitive Impairments. *Letters in Drug Design & Discovery*, *5*(4), 271–276. https://doi.org/10.2174/157018008784619898

Achariyar, T. M., Li, B., Peng, W., Verghese, P. B., Shi, Y., McConnell, E., … Deane, R. (2016). Glymphatic distribution of CSF-derived apoE into brain is isoform specific and suppressed during sleep deprivation. *Molecular Neurodegeneration*, *11*(1). https://doi.org/10.1186/S13024-016-0138-8

Adeosun, S. O., Hou, X., Shi, L., Stockmeier, C. A., Zheng, B., Raffai, R. L., … Wang, J. M. (2019). Female mice with apolipoprotein E4 domain interaction demonstrated impairments in spatial learning and memory performance and disruption of hippocampal cyto-architecture. *Neurobiology of Learning and Memory*, *161*, 106–114.

Aggerbeck, L. P., Wetterau, J. R., Weisgraber, K. H., Wu, C. S. C., & Lindgren, F. T. (1988). Human apolipoprotein E3 in aqueous solution. II. Properties of the amino- and carboxyl-terminal domains. *Journal of Biological Chemistry*, *263*(13), 6249–6258. https://doi.org/10.1016/S0021-9258(18)68779-4

Akiyama, H., Barger, S., Barnum, S., Bradt, B., Bauer, J., Cole, G. M., … Wyss-Coray, T. (2000). Inflammation and Alzheimer's disease. *Neurobiology of Aging*, *21*(3), 383–421. https://doi.org/10.1016/S0197-4580(00)00124-X

Akram, A., Schmeidler, J., Katsel, P., Hof, P. R., & Haroutunian, V. (2012). Association of ApoE and LRP mRNA levels with dementia and AD neuropathology. *Neurobiology of Aging*, *33*(3), 628.e1. https://doi.org/10.1016/J.NEUROBIOLAGING.2011.04.010

Allan, C. M., Taylor, S., & Taylor, J. M. (1997). Two hepatic enhancers, HCR.1 and HCR.2, coordinate the liver expression of the entire human apolipoprotein E/C-I/C-IV/C-II gene cluster. *Journal of Biological Chemistry*, *272*(46), 29113–29119. https://doi.org/10.1074/jbc.272.46.29113

Allen, T. A., & Fortin, N. J. (2013). The evolution of episodic memory. *Proceedings of the National Academy of Sciences of the United States of America*, *110*(Suppl 2), 10379. https://doi.org/10.1073/PNAS.1301199110

Amaral, D. G., & Witter, M. P. (1989). The three-dimensional organization of the hippocampal formation: A review of anatomical data. *Neuroscience*, *31*(3), 571–591. https://doi.org/10.1016/0306-4522(89)90424-7

Amponsah, A. E., Feng, B., Guo, R., Zhang, W., He, J., Kong, D., … Cui, H. (2020). Fragmentation of brain apolipoprotein e (ApoE) and its relevance in Alzheimer's disease. *Reviews in the Neurosciences*, *31*(6), 589–603. https://doi.org/10.1515/revneuro-2019-0115

Andersen, P., Morris, R., Amaral, D., Bliss, T., & O' Keefe, J. (2009). *The Hippocampus Book*. *The Hippocampus Book*. https://doi.org/10.1093/acprof:oso/9780195100273.001.0001

Andrews-Zwilling, Y., Bien-Ly, N., Xu, Q., Li, G., Bernardo, A., Yoon, S. Y., … Huang, Y. (2010). Apolipoprotein E4 Causes Age- and Tau-Dependent Impairment of GABAergic Interneurons, Leading to Learning and Memory Deficits in Mice. *Journal of Neuroscience*, *30*(41), 13707–13717. https://doi.org/10.1523/JNEUROSCI.4040-10.2010

Arias, N., Méndez, M., & Arias, J. L. (2015). The recognition of a novel-object in a novel context leads to hippocampal and parahippocampal c-Fos involvement. *Behavioural Brain Research*, *292*, 44–49. https://doi.org/10.1016/J.BBR.2015.06.012

Atagi, Y., Liu, C. C., Painter, M. M., Chen, X. F., Verbeeck, C., Zheng, H., … Bu, G. (2015). Apolipoprotein E Is a Ligand for Triggering Receptor Expressed on Myeloid Cells 2 (TREM2) *. *Journal of Biological Chemistry*, *290*(43), 26043–26050. https://doi.org/10.1074/JBC.M115.679043

Atkinson, R., Gaysina, D., & Rusted, J. M. (2019). Responses to executive demand in young adulthood differ by APOE genotype. *Behavioural Brain Research*, *360*, 158–168. https://doi.org/10.1016/J.BBR.2018.11.033

Bach, M. E., Hawkins, R. D., Osman, M., Kandel, E. R., & Mayford, M. (1995). *Impairment of spatial but not contextual memory in CaMKII mutant mice with a selective loss of hippocampal ltp in the range of the ϑ frequency*. *Cell* (Vol. 81). https://doi.org/10.1016/0092-8674(95)90010-1

Baddeley, A. (2000). The episodic buffer: a new component of working memory? *Trends in Cognitive Sciences*, *4*(11), 417–423. https://doi.org/10.1016/S1364-6613(00)01538-2

Balu, D., Karstens, A. J., Loukenas, E., Maldonado Weng, J., York, J. M., Valencia-Olvera, A. C., & LaDu, M. J. (2019). The role of APOE in transgenic mouse models of AD. *Neuroscience Letters*, *707*, 134285. https://doi.org/10.1016/J.NEULET.2019.134285

Barnes, C. A. (1979). Memory deficits associated with senescence: A neurophysiological and behavioral study in the rat. *Journal of Comparative and Physiological Psychology*, *93*(1), 74–104. https://doi.org/10.1037/H0077579

Barnes, C. A., Nadel, L., & Honig, W. K. (1980). Spatial memory deficit in senescent rats. *Canadian Journal of Psychology*, *34*(1), 29–39. https://doi.org/10.1037/H0081022

Basaure, P., Guardia-Escote, L., Cabré, M., Peris-Sampedro, F., Sánchez-Santed, F., Domingo, J. L., & Colomina, M. T. (2019). Learning, memory and the expression of cholinergic components in mice are modulated by the pesticide chlorpyrifos depending upon age at exposure and apolipoprotein E (APOE) genotype. *Archives of Toxicology*, *93*(3), 693–707. https://doi.org/10.1007/S00204-019-02387-9

Bast, T. (2007). Toward an integrative perspective on hippocampal function: From the rapid encoding of experience to adaptive behavior. *Reviews in the Neurosciences*, *18*(3–4), 253–281. https://doi.org/10.1515/REVNEURO.2007.18.3-4.253

Bast, T., Da Silva, B. M., & Morris, R. G. M. (2005). Distinct Contributions of Hippocampal NMDA and AMPA Receptors to Encoding and Retrieval of One-Trial Place Memory. *Journal of Neuroscience*, *25*(25), 5845–5856. https://doi.org/10.1523/JNEUROSCI.0698-05.2005

Bast, T., Pezze, M., & McGarrity, S. (2017). Cognitive deficits caused by prefrontal cortical and hippocampal neural disinhibition. *British Journal of Pharmacology*, *174*(19), 3211–3225. https://doi.org/10.1111/BPH.13850

Bast, T., Wilson, L. A., Witter, M. P., & Morris, R. G. M. (2009). From Rapid Place Learning to Behavioral Performance: A Key Role for the Intermediate Hippocampus. *PLOS Biology*, *7*(4), e1000089. https://doi.org/10.1371/JOURNAL.PBIO.1000089

Bastin, C., & Salmon, E. (2014). Early neuropsychological detection of Alzheimer's disease. *European Journal of Clinical Nutrition 2014 68:11*, *68*(11), 1192–1199. https://doi.org/10.1038/ejcn.2014.176

Basu, J., & Siegelbaum, S. A. (2015). The corticohippocampal circuit, synaptic plasticity, and memory. *Cold Spring Harbor Perspectives in Biology*, *7*(11). https://doi.org/10.1101/cshperspect.a021733

Beffert, U., Morfini, G., Bock, H. H., Reyna, H., Brady, S. T., & Herz, J. (2002). Reelin-mediated Signaling Locally Regulates Protein Kinase B/Akt and Glycogen Synthase Kinase 3β *. *Journal of Biological Chemistry*, *277*(51), 49958–49964. https://doi.org/10.1074/JBC.M209205200

Bekris, L. M., Galloway, N. M., Montine, T. J., Schellenberg, G. D., & Yu, C. E. (2010). APOE mRNA and Protein Expression in Postmortem Brain are Modulated by an extended Haplotype Structure. *American Journal of Medical Genetics. Part B, Neuropsychiatric Genetics: The Official Publication of the International Society of Psychiatric Genetics*, *153B*(2), 409. https://doi.org/10.1002/AJMG.B.30993

Bekris, L. M., Yu, C.-E., Bird, T. D., & Tsuang, D. W. (2010). Review Article: Genetics of Alzheimer Disease. *Journal of Geriatric Psychiatry and Neurology*, *23*(4), 213–227. https://doi.org/10.1177/0891988710383571

Bell, R. D., Winkler, E. A., Singh, I., Sagare, A. P., Deane, R., Wu, Z., … Zlokovic, B. V. (2012). Apolipoprotein e controls cerebrovascular integrity via cyclophilin A. *Nature*, *485*(7399), 512–516. https://doi.org/10.1038/nature11087

Bernstein, H. L., Lu, Y.-L., Botterill, J. J., & Scharfman, H. E. (2019). Novelty and Novel Objects Increase c-Fos Immunoreactivity in Mossy Cells in the Mouse Dentate Gyrus. *Neural Plasticity*, *2019*, 1815371. https://doi.org/10.1155/2019/1815371

Bimonte-Nelson, H. A. (2015). *The maze book: Theories, practice, and protocols for testing rodent cognition*. *The Maze Book: Theories, Practice, and Protocols for Testing Rodent Cognition*. Springer New York. https://doi.org/10.1007/978-1-4939-2159-1

Binder, L. I., Guillozet-Bongaarts, A. L., Garcia-Sierra, F., & Berry, R. W. (2005). Tau, tangles, and Alzheimer's disease. *Biochimica et Biophysica Acta (BBA) - Molecular Basis of Disease*, *1739*(2–3), 216–223. https://doi.org/10.1016/J.BBADIS.2004.08.014

Björkhem, I., Lütjohann, D., Diczfalusy, U., Ståhle, L., Ahlborg, G., & Wahren, J. (1998). Cholesterol homeostasis in human brain: Turnover of 24S- hydroxycholesterol and evidence for a cerebral origin of most of this oxysterol in the circulation. *Journal of Lipid Research*, *39*(8), 1594–1600. https://doi.org/10.1016/s0022-2275(20)32188-x

Bliss, T. V. P., & Collingridge, G. L. (1993). A synaptic model of memory: Long-term potentiation in the hippocampus. *Nature*, *361*(6407), 31–39. https://doi.org/10.1038/361031a0

Bliss, T. V. P., & Lømo, T. (1973). Long-lasting potentiation of synaptic transmission in the dentate area of the anaesthetized rabbit following stimulation of the perforant path. *The Journal of Physiology*, *232*(2), 331–356. https://doi.org/10.1113/JPHYSIOL.1973.SP010273

Bliss, T. V. P., Collingridge, G. L., Morris, R. G. M., & Reymann, K. G. (2018). Long-term potentiation in the hippocampus: Discovery, mechanisms and function. *Neuroforum*, *24*(3), A103–A120. https://doi.org/10.1515/nf-2017-A059

Bogoch. (1968). The Future of the Brain Sciences. Proceedings of a Conference held at the New York Academy of Medicine, May 2-4, 1968. *Journal of Medical Genetics*, *7*(1), 102–103. https://doi.org/10.1136/jmg.7.1.102-b

Bott, J. B., Cosquer, B., Héraud, C., Zerbinatti, C., Kelche, C., Cassel, J. C., & Mathis, C. (2013). Reduced plasticity and mild cognitive impairment-like deficits after entorhinal lesions in hAPP/APOE4 mice. *Neurobiology of Aging*, *34*(11), 2683–2693. https://doi.org/10.1016/J.NEUROBIOLAGING.2013.04.018

Bott, J. B., Héraud, C., Cosquer, B., Herbeaux, K., Aubert, J., Sartori, M., … Mathis, C. (2016). APOE-sensitive cholinergic sprouting compensates for hippocampal dysfunctions due to reduced entorhinal input. *Journal of Neuroscience*, *36*(40), 10472–10486. https://doi.org/10.1523/JNEUROSCI.1174-16.2016

Bour, A., Grootendorst, J., Vogel, E., Kelche, C., Dodart, J. C., Bales, K., … Mathis, C. (2008). Middle-aged human apoE4 targeted-replacement mice show retention deficits on a wide range of spatial memory tasks. *Behavioural Brain Research*, *193*(2), 174–182. https://doi.org/10.1016/J.BBR.2008.05.008

Brebner, L. S., Ziminski, J. J., Margetts-Smith, G., Sieburg, M. C., Reeve, H. M., Nowotny, T., … Koya, E. (2020). The Emergence of a Stable Neuronal Ensemble from a Wider Pool of Activated Neurons in the Dorsal Medial Prefrontal Cortex during Appetitive Learning in Mice. *The Journal of Neuroscience: The Official Journal of the Society for Neuroscience*, *40*(2), 395–410. https://doi.org/10.1523/JNEUROSCI.1496-19.2019

Brecht, W. J., Harris, F. M., Chang, S., Tesseur, I., Yu, G. Q., Xu, Q., … Huang, Y. (2004). Neuron-Specific Apolipoprotein E4 Proteolysis Is Associated with Increased Tau Phosphorylation in Brains of Transgenic Mice. *Journal of Neuroscience*, *24*(10), 2527–2534. https://doi.org/10.1523/JNEUROSCI.4315-03.2004

Broadbent, N., Lumeij, L. B., Corcoles, M., Ayres, A. I., Bin Ibrahim, M. Z., Masatsugu, B., … Tse, D. (2020). A stable home-base promotes allocentric memory representations of episodic-like everyday spatial memory. *European Journal of Neuroscience*, *51*(7), 1539–1558. https://doi.org/10.1111/EJN.14681

Brodbeck, J., McGuire, J., Liu, Z., Meyer-Franke, A., Balestra, M. E., Jeong, D. E., … Huang, Y. (2011). Structure-dependent impairment of intracellular apolipoprotein E4 trafficking and its detrimental effects are rescued by small-molecule structure correctors. *Journal of Biological Chemistry*, *286*(19), 17217–17226. https://doi.org/10.1074/JBC.M110.217380/ATTACHMENT/31A8EF4E-E19E-433F-8C58-F1E7A63D124A/MMC1.ZIP

Brown, C. M., Wright, E., Colton, C. A., Sullivan, P. M., Laskowitz, D. T., & Vitek, M. P. (2002). Apolipoprotein E isoform mediated regulation of nitric oxide release. *Free Radical Biology and Medicine*, *32*(11), 1071–1075. https://doi.org/10.1016/S0891-5849(02)00803-1

Bruce, K. D., Zsombok, A., & Eckel, R. H. (2017). Lipid processing in the brain: A key regulator of systemic metabolism. *Frontiers in Endocrinology*, *8*(APR), 60. https://doi.org/10.3389/FENDO.2017.00060/BIBTEX

Bu, G. (2009). Apolipoprotein e and its receptors in Alzheimer's disease: Pathways, pathogenesis and therapy. *Nature Reviews Neuroscience*, *10*(5), 333–344. https://doi.org/10.1038/nrn2620

Buckley, M. G., & Bast, T. (2018). A new human delayed-matching-to-place test in a virtual environment reverse-translated from the rodent watermaze paradigm: Characterization of performance measures and sex differences. *Hippocampus*, *28*(11), 796–812. https://doi.org/10.1002/HIPO.22992

Burgess, N., Becker, S., King, J. A., & O'Keefe, J. (2001). Memory for events and their spatial context: models and experiments. *Philosophical Transactions of the Royal Society of London. Series B: Biological Sciences*, *356*(1413), 1493–1503. https://doi.org/10.1098/RSTB.2001.0948

Burgess, N. (2006). Spatial memory: how egocentric and allocentric combine. *Trends in Cognitive Sciences*, *10*(12), 551–557. https://doi.org/10.1016/J.TICS.2006.10.005

Burgess, N., Maguire, E. A., & O'Keefe, J. (2002). The Human Hippocampus and Spatial and Episodic Memory. *Neuron*, *35*(4), 625–641. https://doi.org/10.1016/S0896-6273(02)00830-9

Burke, S. N., & Barnes, C. A. (2006). Neural plasticity in the ageing brain. *Nature Reviews Neuroscience*, *7*(1), 30–40. https://doi.org/10.1038/nrn1809

Bustin, S. A., Benes, V., Garson, J. A., Hellemans, J., Huggett, J., Kubista, M., … Wittwer, C. T. (2009). The MIQE guidelines: Minimum information for publication of quantitative real-time PCR experiments. *Clinical Chemistry*, *55*(4), 611–622. https://doi.org/10.1373/clinchem.2008.112797

Bustin, S., & Huggett, J. (2017). qPCR primer design revisited. *Biomolecular Detection and Quantification*. Elsevier GmbH. https://doi.org/10.1016/j.bdq.2017.11.001

Buttini, M., Akeefe, H., Lin, C., Mahley, R. W., Pitas, R. E., Wyss-Coray, T., & Mucke, L. (2000). Dominant negative effects of apolipoprotein E4 revealed in transgenic models of neurodegenerative disease. *Neuroscience*, *97*(2), 207–210. https://doi.org/10.1016/S0306-4522(00)00069-5

Buttini, M., Masliah, E., Yu, G. Q., Palop, J. J., Chang, S., Bernardo, A., … Mucke, L. (2010). Cellular Source of Apolipoprotein E4 Determines Neuronal Susceptibility to Excitotoxic Injury in Transgenic Mice. *The American Journal of Pathology*, *177*(2), 563–569. https://doi.org/10.2353/AJPATH.2010.090973

Buttini, M., Orth, M., Bellosta, S., Akeefe, H., Pitas, R. E., Wyss-Coray, T., … Mahley, R. W. (1999). Expression of human apolipoprotein E3 or E4 in the brains of Apoe(-/-) mice: Isoform-specific effects on neurodegeneration. *Journal of Neuroscience*, *19*(12), 4867–4880. https://doi.org/10.1523/jneurosci.19-12-04867.1999

Buzsáki, G. (2015). Hippocampal sharp wave-ripple: A cognitive biomarker for episodic memory and planning. *Hippocampus*, *25*(10), 1073–1188. https://doi.org/10.1002/HIPO.22488

Cai, D. J., Aharoni, D., Shuman, T., Shobe, J., Biane, J., Song, W., … Silva, A. J. (2016). A shared neural ensemble links distinct contextual memories encoded close in time. *Nature*, *534*(7605), 115–118. https://doi.org/10.1038/nature17955

Cambon, K., & Stewart, M. G. (2000). *Influence of ApoE polymorphism on synaptic morphom- etry during aging in the dentate gyrus of ApoE knock- out and human ApoE transgenic mice Thesis on synaptic morphometry during aging*. *Processing*. Retrieved from https://oro.open.ac.uk/19118/1/pdf38.pdf

Camina, E., & Güell, F. (2017). The neuroanatomical, neurophysiological and psychological basis of memory: Current models and their origins. *Frontiers in Pharmacology*, *8*(JUN), 438. https://doi.org/10.3389/FPHAR.2017.00438/BIBTEX

Castellano, J. M., Kim, J., Stewart, F. R., Jiang, H., DeMattos, R. B., Patterson, B. W., … Holtzman, D. M. (2011). Human apoE isoforms differentially regulate brain amyloid-β peptide clearance. *Science Translational Medicine*, *3*(89), 89ra57. https://doi.org/10.1126/scitranslmed.3002156

cell, T. F.-A., & 2007, undefined. (2007). Calcium homeostasis and modulation of synaptic plasticity in the aged brain. *Wiley Online Library*, *6*(3), 319–325. https://doi.org/10.1111/j.1474-9726.2007.00283.x

Cès, A., Burg, T., Herbeaux, K., Héraud, C., Bott, J. B., Mensah-Nyagan, A. G., & Mathis, C. (2018). Age-related vulnerability of pattern separation in C57BL/6J mice. *Neurobiology of Aging*, *62*, 120–129. https://doi.org/10.1016/J.NEUROBIOLAGING.2017.10.013

Champagne, D., Dupuy, J. B., Rochford, J., & Poirier, J. (2002). Apolipoprotein E knockout mice display procedural deficits in the Morris water maze: Analysis of learning strategies in three versions of the task. *Neuroscience*, *114*(3), 641–654. https://doi.org/10.1016/S0306-4522(02)00313-5

Chang, S., Ma, T. R., Miranda, R. D., Balestra, M. E., Mahley, R. W., & Huang, Y. (2005). Lipid- and receptor-binding regions of apolipoprotein E4 fragments act in concert to cause mitochondrial dysfunction and neurotoxicity. *Proceedings of the National Academy of Sciences*, *102*(51), 18694–18699. https://doi.org/10.1073/PNAS.0508254102

Chawla, M. K., Guzowski, J. F., Ramirez-Amaya, V., Lipa, P., Hoffman, K. L., Marriott, L. K., … Barnes, C. A. (2005). Sparse, environmentally selective expression of Arc RNA in the upper blade of the rodent fascia dentata by brief spatial experience. *Hippocampus*, *15*(5), 579–586. https://doi.org/10.1002/HIPO.20091

Chawla, M. K., Penner, M. R., Olson, K. M., Sutherland, V. L., Mittelman-Smith, M. A., & Barnes, C. A. (2013). Spatial behavior and seizure-induced changes in c-fos mRNA expression in young and old rats. *Neurobiology of Aging*, *34*(4), 1184–1198. https://doi.org/10.1016/J.NEUROBIOLAGING.2012.10.017

Chen, H. K., Liu, Z., Meyer-Franke, A., Brodbeck, J., Miranda, R. D., McGuire, J. G., … Mahley, R. W. (2012). Small molecule structure correctors abolish detrimental effects of apolipoprotein E4 in cultured neurons. *Journal of Biological Chemistry*, *287*(8), 5253–5266. https://doi.org/10.1074/JBC.M111.276162/ATTACHMENT/393EECF6-1DE9-45E2-A65C-5375ADC0B846/MMC1.PDF

Chouinard-Watkins, R., Vandal, M., Léveillé, P., Pinçon, A., Calon, F., & Plourde, M. (2017). Docosahexaenoic acid prevents cognitive deficits in human apolipoprotein E epsilon 4-targeted replacement mice. *Neurobiology of Aging*, *57*, 28–35. https://doi.org/10.1016/J.NEUROBIOLAGING.2017.05.003

Christensen, D. Z., Thomsen, M. S., & Mikkelsen, J. D. (2013). Reduced basal and novelty-induced levels of activity-regulated cytoskeleton associated protein (Arc) and c-Fos mRNA in the cerebral cortex and hippocampus of APPswe/PS1ΔE9 transgenic mice. *Neurochemistry International*, *63*(1), 54–60. https://doi.org/10.1016/J.NEUINT.2013.04.002

Chung, L. (2015). A Brief Introduction to the Transduction of Neural Activity into Fos Signal. *Development & Reproduction*, *19*(2), 61–67. https://doi.org/10.12717/dr.2015.19.2.061

Clare, R., King, V., … M. W.-J. of neuroscience, & 2010, undefined. (2010). Synapse loss in dementias. *Wiley Online Library*, *88*(10), 2083–2090. https://doi.org/10.1002/jnr.22392

Clayton, D. F. (2000). The genomic action potential. *Neurobiology of Learning and Memory*, *74*(3), 185–216. https://doi.org/10.1006/nlme.2000.3967

Clelland, C. D., Choi, M., Romberg, C., Clemenson, G. D., Fragniere, A., Tyers, P., … Bussey, T. J. (2009). A functional role for adult hippocampal neurogenesis in spatial pattern separation. *Science*, *325*(5937), 210–213. https://doi.org/10.1126/science.1173215

Cohen, S., & Greenberg, M. E. (2008). Communication between the synapse and the nucleus in neuronal development, plasticity, and disease. *Annual Review of Cell and Developmental Biology*, *24*, 183–209. https://doi.org/10.1146/ANNUREV.CELLBIO.24.110707.175235

Cohens, G. (1993). Memory and ageing. *Advances in Psychology*, *100*(C), 419–438. https://doi.org/10.1016/S0166-4115(08)61118-8

Colombo, D., Serino, S., Tuena, C., Pedroli, E., Dakanalis, A., Cipresso, P., & Riva, G. (2017). Egocentric and allocentric spatial reference frames in aging: A systematic review. *Neuroscience & Biobehavioral Reviews*, *80*, 605–621. https://doi.org/10.1016/J.NEUBIOREV.2017.07.012

Corder, E. H., Saunders, A. M., Strittmatter, W. J., Schmechel, D. E., Gaskell, P. C., Small, G. W., … Pericak-Vance, M. A. (1993). Gene dose of apolipoprotein E type 4 allele and the risk of Alzheimer's disease in late onset families. *Science*, *261*(5123), 921–923. https://doi.org/10.1126/SCIENCE.8346443

Courtney, R., & Landreth, G. E. (2016). LXR Regulation of Brain Cholesterol: From Development to Disease. *Trends in Endocrinology and Metabolism*, *27*(6), 404–414. https://doi.org/10.1016/j.tem.2016.03.018

Cowan, N. (2008). What are the differences between long-term, short-term, and working memory? *Progress in Brain Research*, *169*, 323. https://doi.org/10.1016/S0079-6123(07)00020-9

Creer, D. J., Romberg, C., Saksida, L. M., Van Praag, H., & Bussey, T. J. (2010). Running enhances spatial pattern separation in mice. *Proceedings of the National Academy of Sciences of the United States of America*, *107*(5), 2367–2372. https://doi.org/10.1073/pnas.0911725107

Cruchaga, C., Kauwe, J. S. K., Nowotny, P., Bales, K., Pickering, E. H., Mayo, K., … Goate, A. M. (2012). Cerebrospinal fluid APOE levels: an endophenotype for genetic studies for Alzheimer's disease. *Human Molecular Genetics*, *21*(20), 4558. https://doi.org/10.1093/HMG/DDS296

Cruz, F. C., Javier Rubio, F., & Hope, B. T. (2015). Using c-fos to study neuronal ensembles in corticostriatal circuitry of addiction. *Brain Research*, *1628*, 157–173. https://doi.org/10.1016/J.BRAINRES.2014.11.005

Curran, T., & Morgan, J. I. (1995). Fos: An immediate-early transcription factor in neurons. *Journal of Neurobiology*, *26*(3), 403–412. https://doi.org/10.1002/NEU.480260312

Da Silva, B. M., Bast, T., & Morris, R. G. M. (2014). Spatial memory: Behavioral determinants of persistence in the watermaze delayed matching-to-place task. *Learning and Memory*, *21*(1), 28–36. https://doi.org/10.1101/lm.032169.113

Damisah, E. C., Rai, A., & Grutzendler, J. (2020). TREM2: Modulator of Lipid Metabolism in Microglia. *Neuron*, *105*(5), 759–761. https://doi.org/10.1016/J.NEURON.2020.02.008

D'Arcangelo, G. (2006). Reelin mouse mutants as models of cortical development disorders. *Epilepsy & Behavior*, *8*(1), 81–90. https://doi.org/10.1016/J.YEBEH.2005.09.005

Daumas, S., Sandin, J., Chen, K. S., Kobayashi, D., Tulloch, J., Martin, S. J., … Morris, R. G. M. (2008). Faster forgetting contributes to impaired spatial memory in the PDAPP mouse: Deficit in memory retrieval associated with increased sensitivity to interference? *Learning & Memory*, *15*(9), 625. https://doi.org/10.1101/LM.990208

Davis, E. A., Liu, C. M., Décarie-Spain, L., Lauer, L. T., Gianatiempo, I. H., Suarez, A. N., … Kanoski, S. E. (2021). Ventral hippocampus-lateral septum circuitry mediates foraging-related spatial memory. *BioRxiv*, 2020.06.16.155721. https://doi.org/10.1101/2020.06.16.155721

Davolio, C., & Greenamyre, J. T. (1995). Selective vulnerability of the CA1 region of hippocampus to the indirect excitotoxic effects of malonic acid. *Neuroscience Letters*, *192*(1), 29–32. https://doi.org/10.1016/0304-3940(95)11600-2

Day, M., Langston, R., & Morris, R. G. M. (2003). Glutamate-receptor-mediated encoding and retrieval of paired-associate learning. *Nature 2003 424:6945*, *424*(6945), 205–209. https://doi.org/10.1038/nature01769

De Hoz, L., Moser, E. I., & Morris, R. G. M. (2005). Spatial learning with unilateral and bilateral hippocampal networks. *European Journal of Neuroscience*, *22*(3), 745–754. https://doi.org/10.1111/J.1460-9568.2005.04255.X

De Strooper, B. (2003). Aph-1, Pen-2, and Nicastrin with Presenilin generate an active γ-Secretase complex. *Neuron*, *38*(1), 9–12. https://doi.org/10.1016/S0896-6273(03)00205-8

De Strooper, B., & Annaert, W. (2000). Proteolytic processing and cell biological functions of the amyloid precursor protein. *Journal of Cell Science*, *113*(11), 1857–1870. https://doi.org/10.1242/jcs.113.11.1857

De Strooper, B., Saftig, P., Craessaerts, K., Vanderstichele, H., Guhde, G., Annaert, W., … Van Leuven, F. (1998). Deficiency of presenilin-1 inhibits the normal cleavage of amyloid precursor protein. *Nature*, *391*(6665), 387–390. https://doi.org/10.1038/34910

Deary, I. J., Whiteman, M. C., Pattie, A., Starr, J. M., Hayward, C., Wright, A. F., … Whalley, L. J. (2002). Cognitive change and the APOE ε4 allele. *Nature 2002 418:6901*, *418*(6901), 932–932. https://doi.org/10.1038/418932a

Dehghani, A., Karatas, H., Can, A., Erdemli, E., Yemisci, M., Eren-Kocak, E., & Dalkara, T. (2018). Nuclear expansion and pore opening are instant signs of neuronal hypoxia and can identify poorly fixed brains. *Scientific Reports*, *8*(1). https://doi.org/10.1038/s41598-018-32878-1

DeKroon, R. M., & Armati, P. J. (2001). The Endosomal Trafficking of Apolipoprotein E3 and E4 in Cultured Human Brain Neurons and Astrocytes. *Neurobiology of Disease*, *8*(1), 78–89. https://doi.org/10.1006/NBDI.2000.0362

DeMattos, R. B., Curtiss, L. K., & Williams, D. L. (1998). A minimally lipidated form of cell-derived apolipoprotein E exhibits isoform-specific stimulation of neurite outgrowth in the absence of exogenous lipids or lipoproteins. *Journal of Biological Chemistry*, *273*(7), 4206–4212. https://doi.org/10.1074/jbc.273.7.4206

Diamond, D. M., Park, C. R., Heman, K. L., & Rose, G. M. (1999). Exposing rats to a predator impairs spatial working memory in the radial arm water maze. *Hippocampus*, *9*(5), 542–552. https://doi.org/10.1002/(SICI)1098-1063(1999)9:5<542::AID-HIPO8>3.0.CO;2-N

DiBattista, A. M., Dumanis, S. B., Newman, J., & Rebeck, G. W. (2016). Identification and modification of amyloid-independent phenotypes of APOE4 mice. *Experimental Neurology*, *280*, 97–105. https://doi.org/10.1016/J.EXPNEUROL.2016.04.014

Dietschy, J. M., & Turley, S. D. (2001). Cholesterol metabolism in the brain. *Current Opinion in Lipidology*, *12*(2), 105–112. https://doi.org/10.1097/00041433-200104000-00003

Dose, J., Huebbe, P., Nebel, A., & Rimbach, G. (2016, July 25). APOE genotype and stress response - A mini review. *Lipids in Health and Disease*. BioMed Central Ltd. https://doi.org/10.1186/s12944-016-0288-2

Dragunow, M. (1996). A Role for Immediate-Early Transcription Factors in Learning and Memory. *Behavior Genetics*, *26*(3).

Drakew, A., Deller, T., Heimrich, B., Gebhardt, C., Del Turco, D., Tielsch, A., … Frotscher, M. (2002). Dentate Granule Cells in Reeler Mutants and VLDLR and ApoER2 Knockout Mice. *Experimental Neurology*, *176*(1), 12–24. https://doi.org/10.1006/EXNR.2002.7918

Dudchenko, P. A., Goodridge, J. P., Seiterle, D. A., & Taube, J. S. (1997). Effects of repeated disorientation on the acquisition of spatial tasks in rats: Dissociation between the appetitive radial arm maze and aversive water maze. *Journal of Experimental Psychology: Animal Behavior Processes*, *23*(2), 194–210. https://doi.org/10.1037/0097-7403.23.2.194

Dudek, F. E., & Sutula, T. P. (2007). Epileptogenesis in the dentate gyrus: a critical perspective. *Progress in Brain Research*, *163*, 755–773. https://doi.org/10.1016/S0079-6123(07)63041-6

Dumanis, S. B., DiBattista, A. M., Miessau, M., Moussa, C. E. H., & Rebeck, G. W. (2013). APOE genotype affects the pre-synaptic compartment of glutamatergic nerve terminals. *Journal of Neurochemistry*, *124*(1), 4–14. https://doi.org/10.1111/j.1471-4159.2012.07908.x

Dumanis, S. B., Tesoriero, J. A., Babus, L. W., Nguyen, M. T., Trotter, J. H., Ladu, M. J., … Hoe, H. S. (2009). ApoE4 decreases spine density and dendritic complexity in cortical neurons in vivo. *Journal of Neuroscience*, *29*(48), 15317–15322. https://doi.org/10.1523/JNEUROSCI.4026-09.2009

Dunnett, S. B., Evenden, J. L., & Iversen, S. D. (1988). Delay-dependent short-term memory deficits in aged rats. *Psychopharmacology*, *96*(2), 174–180. https://doi.org/10.1007/BF00177557

Durakoglugil, M. S., Chen, Y., White, C. L., Kavalali, E. T., & Herz, J. (2009). Reelin signaling antagonizes β-amyloid at the synapse. *Proceedings of the National Academy of Sciences*, *106*(37), 15938–15943. https://doi.org/10.1073/PNAS.0908176106

Eichenbaum, H., Otto, T., Biology, N. C.-B. and neural, & 1992, U. (1992). The hippocampus—what does it do? *Behavioral and Neural Biology*, *57*(1), 2–36. Retrieved from https://www.sciencedirect.com/science/article/pii/016310479290724I?casa_token=z8Ma-fIm_D8AAAAA:x4CKoe0BykcfWGheZVtDIOMBaFB-NVLG79N297ukrkyvgqeNdO_Wf052Z4NA7Mo9IibRyDs

Eichenbaum, H. (1999). The hippocampus and mechanisms of declarative memory. *Behavioural Brain Research*, *103*(2), 123–133. https://doi.org/10.1016/S0166-4328(99)00044-3

Eichenbaum, H., & Cohen, N. J. (2014). Can We Reconcile the Declarative Memory and Spatial Navigation Views on Hippocampal Function? *Neuron*, *83*(4), 764–770. https://doi.org/10.1016/j.neuron.2014.07.032

Ekstrom, A. D., Arnold, A. E. G. F., & Iaria, G. (2014). A critical review of the allocentric spatial representation and its neural underpinnings: Toward a network-based perspective. *Frontiers in Human Neuroscience*, *8*(OCT), 803. https://doi.org/10.3389/fnhum.2014.00803

Engstrom, A. K., Snyder, J. M., Maeda, N., & Xia, Z. (2017). Gene-environment interaction between lead and Apolipoprotein E4 causes cognitive behavior deficits in mice. *Molecular Neurodegeneration*, *12*(1), 1–23. https://doi.org/10.1186/S13024-017-0155-2/FIGURES/16

Ertekin-Taner, N. (2010). Genetics of Alzheimer disease in the pre- and post-GWAS era. *Alzheimer's Research and Therapy*, *2*(1), 1–12. https://doi.org/10.1186/ALZRT26/TABLES/3

Fagan, A. M., Holtzman, D. M., Munson, G., Mathur, T., Schneider, D., Chang, L. K., … LaDu, M. J. (1999). Unique Lipoproteins Secreted by Primary Astrocytes From Wild Type, apoE (−/−), and Human apoE Transgenic Mice *. *Journal of Biological Chemistry*, *274*(42), 30001–30007. https://doi.org/10.1074/JBC.274.42.30001

Faizi, M., Bader, P. L., Saw, N., Nguyen, T.-V. V, Beraki, S., Wyss-Coray, T., … Shamloo, M. (2012). Thy1-hAPP(Lond/Swe+) mouse model of Alzheimer's disease displays broad behavioral deficits in sensorimotor, cognitive and social function. *Brain and Behavior*, *2*(2), 142–154. https://doi.org/10.1002/brb3.41

Fanselow, M. S., & Dong, H. W. (2010). Are the Dorsal and Ventral Hippocampus Functionally Distinct Structures? *Neuron*, *65*(1), 7–19. https://doi.org/10.1016/j.neuron.2009.11.031

Febo, M., Rani, A., Yegla, B., Barter, J., Kumar, A., Wolff, C. A., … Foster, T. C. (2020). Longitudinal Characterization and Biomarkers of Age and Sex Differences in the Decline of Spatial Memory. *Frontiers in Aging Neuroscience*, *12*, 34. https://doi.org/10.3389/FNAGI.2020.00034/BIBTEX

Feng, X., Krukowski, K., Jopson, T., & Rosi, S. (2017). Delayed-matching-to-place Task in a Dry Maze to Measure Spatial Working Memory in Mice. *Bio-Protocol*, *7*(13). https://doi.org/10.21769/bioprotoc.2389

Fernández-Ruiz, A., Oliva, A., de Oliveira, E. F., Rocha-Almeida, F., Tingley, D., & Buzsáki, G. (2019). Long-duration hippocampal sharp wave ripples improve memory. *Science*, *364*(6445), 1082–1086. https://doi.org/10.1126/science.aax0758

Flowers, S. A., & Rebeck, G. W. (2020). APOE in the normal brain. *Neurobiology of Disease*, *136*, 104724. https://doi.org/10.1016/j.nbd.2019.104724

Frick, K. M., Baxter, M. G., Markowska, A. L., Olton, D. S., & Price, D. L. (1995). Age-related spatial reference and working memory deficits assessed in the water maze. *Neurobiology of Aging*, *16*(2), 149–160. https://doi.org/10.1016/0197-4580(94)00155-3

Frieden, C., & Garai, K. (2012). Structural differences between apoE3 and apoE4 may be useful in developing therapeutic agents for Alzheimer's disease. *Proceedings of the National Academy of Sciences of the United States of America*, *109*(23), 8913. https://doi.org/10.1073/PNAS.1207022109

Frieden, C., & Garai, K. (2013). Concerning the structure of apoE. *Protein Science*, *22*(12), 1820–1825. https://doi.org/10.1002/pro.2379

Fritzsch, B., Muirhead, K. A., Feng, F., Gray, B. D., & Ohlsson-Wilhelm, B. M. (2005). Diffusion and imaging properties of three new lipophilic tracers, NeuroVue Maroon, NeuroVue Red and NeuroVue Green and their use for double and triple labeling of neuronal profile. *Brain Research Bulletin*, *66*(3), 249–258. https://doi.org/10.1016/J.BRAINRESBULL.2005.05.016

Fu, H., Hardy, J., & Duff, K. E. (2018). Selective vulnerability in neurodegenerative diseases. *Nature Neuroscience*, *21*(10), 1350–1358. https://doi.org/10.1038/s41593-018-0221-2

Fukumoto, H., Ingelsson, M., Gårevik, N., Wahlund, L. O., Nukina, N., Yaguchi, Y., … Irizarry, M. C. (2003). APOE ε3/ε4 heterozygotes have an elevated proportion of apolipoprotein E4 in cerebrospinal fluid relative to plasma, independent of Alzheimer's disease diagnosis. *Experimental Neurology*, *183*(1), 249–253. https://doi.org/10.1016/S0014-4886(03)00088-8

Futamura, M., Dhanasekaran, P., Handa, T., Phillips, M. C., Lund-Katz, S., & Saito, H. (2005). Two-step Mechanism of Binding of Apolipoprotein E to Heparin: IMPLICATIONS FOR THE KINETICS OF APOLIPOPROTEIN E-HEPARAN SULFATE PROTEOGLYCAN COMPLEX FORMATION ON CELL SURFACES. *Journal of Biological Chemistry*, *280*(7), 5414–5422. https://doi.org/10.1074/JBC.M411719200

Gallagher, M., Burwell, R., & Burchinal, M. (2015). Severity of Spatial Learning Impairment in Aging: Development of a Learning Index for Performance in the Morris Water Maze. *Behavioral Neuroscience*, *129*(4), 540. https://doi.org/10.1037/BNE0000080

Gallagher, M., & Nicolle, M. M. (1993). Animal models of normal aging: Relationship between cognitive decline and markers in hippocampal circuitry. *Behavioural Brain Research*, *57*(2), 155–162. https://doi.org/10.1016/0166-4328(93)90131-9

Garner, A. R., Rowland, D. C., Hwang, S. Y., Baumgaertel, K., Roth, B. L., Kentros, C., & Mayford, M. (2012). Generation of a synthetic memory trace. *Science*, *335*(6075), 1513–1516. https://doi.org/10.1126/science.1214985

Gawel, K., Gibula, E., Marszalek-Grabska, M., Filarowska, J., & Kotlinska, J. H. (2019). Assessment of spatial learning and memory in the Barnes maze task in rodents—methodological consideration. *Naunyn-Schmiedeberg's Archives of Pharmacology*, *392*(1), 1–18. https://doi.org/10.1007/s00210-018-1589-y

George, O., Sanders, C., Freiling, J., Grigoryan, E., Vu, S., Allen, C. D., … Koob, G. F. (2012). Recruitment of medial prefrontal cortex neurons during alcohol withdrawal predicts cognitive impairment and excessive alcohol drinking. *Proceedings of the National Academy of Sciences of the United States of America*, *109*(44), 18156–18161. https://doi.org/10.1073/pnas.1116523109

Gerrard, J. L., Burke, S. N., McNaughton, B. L., & Barnes, C. A. (2008). Sequence reactivation in the hippocampus is impaired in aged rats. *Journal of Neuroscience*, *28*(31), 7883–7890. 10.1523/JNEUROSCI.1265-08.2008

Giarratana, A. O., Zheng, C., Reddi, S., Teng, S. L., Berger, D., Adler, D., … Alder, J. (2020). APOE4 genetic polymorphism results in impaired recovery in a repeated mild traumatic brain injury model and treatment with Bryostatin-1 improves outcomes. *Scientific Reports*, *10*(1), 1–17. https://doi.org/10.1038/s41598-020-76849-x

Giau, V. Van, Bagyinszky, E., An, S. S. A., & Kim, S. Y. (2015). Role of apolipoprotein E in neurodegenerative diseases. *Neuropsychiatric Disease and Treatment*, *11*, 1723. https://doi.org/10.2147/NDT.S84266

Gilbert, P. E., & Kesner, R. P. (2006). The role of the dorsal CA3 hippocampal subregion in spatial working memory and pattern separation. *Behavioural Brain Research*, *169*(1), 142–149. https://doi.org/10.1016/J.BBR.2006.01.002

Gilbert, P. E., Kesner, R. P., & Decoteau, W. E. (1997). Memory for Spatial Location: Role of the Hippocampus in Mediating Spatial Pattern Separation. *The Journal of Neuroscience*, *13*(2), 804–810.

Gillespie, A. K., Jones, E. A., Lin, Y. H., Karlsson, M. P., Kay, K., Yoon, S. Y., … Huang, Y. (2016). Apolipoprotein E4 Causes Age-Dependent Disruption of Slow Gamma Oscillations during Hippocampal Sharp-Wave Ripples. *Neuron*, *90*(4), 740–751. https://doi.org/10.1016/J.NEURON.2016.04.009

Gold, A. E., & Kesner, R. P. (2005). The role of the CA3 subregion of the dorsal hippocampus in spatial pattern completion in the rat. *Hippocampus*, *15*(6), 808–814. https://doi.org/10.1002/HIPO.20103

Gomez, A., Rousset, S., & Baciu, M. (2009). Egocentric-updating during navigation facilitates episodic memory retrieval. *Acta Psychologica*, *132*(3), 221–227. https://doi.org/10.1016/J.ACTPSY.2009.07.003

Grech, A. M., Nakamura, J. P., & Hill, R. A. (2018). The Importance of Distinguishing Allocentric and Egocentric Search Strategies in Rodent Hippocampal-Dependent Spatial Memory Paradigms: Getting More Out of Your Data. *The Hippocampus - Plasticity and Functions*. https://doi.org/10.5772/intechopen.76603

Grootendorst, J., Bour, A., Vogel, E., Kelche, C., Sullivan, P. M., Dodart, J. C., … Mathis, C. (2005). Human apoE targeted replacement mouse lines: h-apoE4 and h-apoE3 mice differ on spatial memory performance and avoidance behavior. *Behavioural Brain Research*, *159*(1), 1–14. https://doi.org/10.1016/J.BBR.2004.09.019

Growdon, W. B., Cheung, B. S., Hyman, B. T., & Rebeck, G. W. (1999). Lack of allelic imbalance in APOE ϵ3/4 brain mRNA expression in Alzheimer's disease. *Neuroscience Letters*, *272*(2), 83–86. https://doi.org/10.1016/S0304-3940(99)00557-1

Guardia-Escote, L., Basaure, P., Peris-Sampedro, F., Biosca-Brull, J., Cabré, M., Sánchez-Santed, F., … Colomina, M. T. (2019). APOE genetic background and sex confer different vulnerabilities to postnatal chlorpyrifos exposure and modulate the response to cholinergic drugs. *Behavioural Brain Research*, *376*, 112195. https://doi.org/10.1016/j.bbr.2019.112195

Guzowski, J. F., Knierim, J. J., & Moser, E. I. (2004). Ensemble dynamics of hippocampal regions CA3 and CA1. *Neuron*. Cell Press. https://doi.org/10.1016/j.neuron.2004.11.003

Haberman, R. P., Branch, A., & Gallagher, M. (2017). Targeting Neural Hyperactivity as a Treatment to Stem Progression of Late-Onset Alzheimer's Disease. *Neurotherapeutics*, *14*(3), 662–676. https://doi.org/10.1007/s13311-017-0541-z

Haberman, R. P., Colantuoni, C., Stocker, A. M., Schmidt, A. C., Pedersen, J. T., & Gallagher, M. (2011). Prominent hippocampal CA3 gene expression profile in neurocognitive aging. *Neurobiology of Aging*, *32*(9), 1678–1692. https://doi.org/10.1016/J.NEUROBIOLAGING.2009.10.005

Haberman, R. P., Koh, M. T., & Gallagher, M. (2017). Heightened cortical excitability in aged rodents with memory impairment. *Neurobiology of Aging*, *54*, 144–151. https://doi.org/10.1016/j.n

Haberman, R. P., Monasterio, A., Branch, A., & Gallagher, M. (2019). Aged rats with intact memory show distinctive recruitment in cortical regions relative to young adults in a cue mismatch task. *Behavioral Neuroscience*, *133*(5), 537. https://doi.org/10.1037/BNE0000332

Hainmueller, T., & Bartos, M. (2020). Dentate gyrus circuits for encoding, retrieval and discrimination of episodic memories. *Nature Reviews Neuroscience*, *21*(3), 153–168. https://doi.org/10.1038/s41583-019-0260-z

Haley, G. E., Villasana, L., Dayger, C., Davis, M. J., & Raber, J. (2012). Apolipoprotein E Genotype-Dependent Paradoxical Short-Term Effects of 56Fe Irradiation on the Brain. *International Journal of Radiation Oncology, Biology, Physics*, *84*(3), 793. https://doi.org/10.1016/J.IJROBP.2011.12.049

Han, J. H., Kushner, S. A., Yiu, A. P., Hsiang, H. L., Buch, T., Waisman, A., … Josselyn, S. A. (2009). Selective erasure of a fear memory. *Science*, *323*(5920), 1492–1496. https://doi.org/10.1126/SCIENCE.1164139/SUPPL_FILE/HAN.SOM.PDF

Hardy, J. A., & Higgins, G. A. (1992). Alzheimer's disease: The amyloid cascade hypothesis. *Science*, *256*(5054), 184–185. https://doi.org/10.1126/science.1566067

Hardy, J., & Selkoe, D. J. (2002). The amyloid hypothesis of Alzheimer's disease: Progress and problems on the road to therapeutics. *Science*, *297*(5580), 353–356. https://doi.org/10.1126/SCIENCE.1072994

Harris, F. M., Brecht, W. J., Xu, Q., Mahley, R. W., & Huang, Y. (2004). Increased tau Phosphorylation in Apolipoprotein E4 Transgenic Mice Is Associated with Activation of Extracellular Signal-regulated Kinase: MODULATION BY ZINC *. *Journal of Biological Chemistry*, *279*(43), 44795–44801. https://doi.org/10.1074/JBC.M408127200

Harris, F. M., Brecht, W. J., Xu, Q., Tesseur, I., Kekonius, L., Wyss-Coray, T., … Huang, Y. (2003). Carboxyl-terminal-truncated apolipoprotein E4 causes Alzheimer's disease-like neurodegeneration and behavioral deficits in transgenic mice. *Proceedings of the National Academy of Sciences of the United States of America*, *100*(19), 10966–10971. https://doi.org/10.1073/pnas.1434398100

Harris, F. M., Tesseur, I., Brecht, W. J., Xu, Q., Mullendorff, K., Chang, S., … Huang, Y. (2004). Astroglial regulation of apolipoprotein E expression in neuronal cells: Implications for Alzheimer's disease. *Journal of Biological Chemistry*, *279*(5), 3862–3868. https://doi.org/10.1074/jbc.M309475200

Harrison, F. E., Hosseini, A. H., & McDonald, M. P. (2009). Endogenous anxiety and stress responses in water maze and Barnes maze spatial memory tasks. *Behavioural Brain Research*, *198*(1), 247–51. https://doi.org/10.1016/j.bbr.2008.10.015

Harrison, F. E., Reiserer, R. S., Tomarken, A. J., & McDonald, M. P. (2006). Spatial and nonspatial escape strategies in the Barnes maze. *Learning and Memory*, *13*(6), 809–819. https://doi.org/10.1101/lm.334306

Hartman, R. E., Wozniak, D. F., Nardi, A., Olney, J. W., Sartorius, L., & Holtzman, D. M. (2001). Behavioral phenotyping of GFAP-ApoE3 and -ApoE4 transgenic mice: ApoE4 mice show profound working memory impairments in the absence of Alzheimer's-like neuropathology. *Experimental Neurology*, *170*(2), 326–344. https://doi.org/10.1006/EXNR.2001.7715

Hatters, D. M., Peters-Libeu, C. A., & Weisgraber, K. H. (2006). Apolipoprotein E structure: insights into function. *Trends in Biochemical Sciences*, *31*(8), 445–454. https://doi.org/10.1016/J.TIBS.2006.06.008

Havel, R. J., & Kane, J. P. (1973). Primary dysbetalipoproteinemia: predominance of a specific apoprotein species in triglyceride-rich lipoproteins. *Proceedings of the National Academy of Sciences of the United States of America*, *70*(7), 2015–2019. https://doi.org/10.1073/PNAS.70.7.2015

He, J., Yamada, K., & Nabeshima, T. (2002). A Role of Fos expression in the CA3 region of the hippocampus in spatial memory formation in rats. *Neuropsychopharmacology*, *26*(2), 259–268. https://doi.org/10.1016/S0893-133X(01)00332-3

Heeren, J., Grewal, T., Jäckle, S., & Beisiegel, U. (2001). Recycling of Apolipoprotein E and Lipoprotein Lipase through Endosomal Compartments in Vivo. *Journal of Biological Chemistry*, *276*(45), 42333–42338. https://doi.org/10.1074/jbc.M107461200

Heinsinger, N. M., Gachechiladze, M. A., & Rebeck, G. W. (2016). Apolipoprotein e genotype affects size of ApoE complexes in cerebrospinal fluid. *Journal of Neuropathology and Experimental Neurology*, *75*(10), 918–924. https://doi.org/10.1093/jnen/nlw067

Herz, J., & Chen, Y. (2006). Reelin, lipoprotein receptors and synaptic plasticity. *Nature Reviews Neuroscience*, *7*(11), 850–859. https://doi.org/10.1038/nrn2009

Hoe, H. S., Harris, D. C., & Rebeck, G. W. (2005). Multiple pathways of apolipoprotein E signaling in primary neurons. *Journal of Neurochemistry*, *93*(1), 145–155. https://doi.org/10.1111/J.1471-4159.2004.03007.X

Hoffman, A. N., Anouti, D. P., Lacagnina, M. J., Nikulina, E. M., Hammer, R. P., & Conrad, C. D. (2013). Experience-dependent effects of context and restraint stress on corticolimbic c-Fos expression. *Stress*, *16*(5), 587–591. https://doi.org/10.3109/10253890.2013.804505

Holtzman, D. M., Herz, J., & Bu, G. (2012). Apolipoprotein E and apolipoprotein E receptors: Normal biology and roles in Alzheimer disease. *Cold Spring Harbor Perspectives in Medicine*, *2*(3). https://doi.org/10.1101/cshperspect.a006312

Holtzman, D. M., Pitas, R. E., Kilbridge, J., Nathan, B., Mahley, R. W., Bu, G., & Schwartz, A. L. (1995). Low density lipoprotein receptor-related protein mediates apolipoprotein E-dependent neurite outgrowth in a central nervous system-derived neuronal cell line. *Proceedings of the National Academy of Sciences of the United States of America*, *92*(21), 9480–9484. https://doi.org/10.1073/pnas.92.21.9480

Hu, J., Liu, C. C., Chen, X. F., Zhang, Y. W., Xu, H., & Bu, G. (2015). Opposing effects of viral mediated brain expression of apolipoprotein E2 (apoE2) and apoE4 on apoE lipidation and Aβ metabolism in apoE4-targeted replacement mice. *Molecular Neurodegeneration*, *10*(1), 1–11. https://doi.org/10.1186/s13024-015-0001-3

Hu, Y., Meuret, C., Go, S., Yassine, H. N., & Nedelkov, D. (2020). Simple and Fast Assay for Apolipoprotein E Phenotyping and Glycotyping: Discovering Isoform-Specific Glycosylation in Plasma and Cerebrospinal Fluid. *Journal of Alzheimer's Disease*, *76*(3), 883. https://doi.org/10.3233/JAD-200203

Huang, Y. (2011). Roles of apolipoprotein E4 (ApoE4) in the pathogenesis of Alzheimer's disease: lessons from ApoE mouse models. *Biochemical Society Transactions*, *39*(4), 924–932. https://doi.org/10.1042/BST0390924

Huang, Y. (2010). Aβ-independent roles of apolipoprotein E4 in the pathogenesis of Alzheimer's disease. *Trends in Molecular Medicine*, *16*(6), 287–294. https://doi.org/10.1016/J.MOLMED.2010.04.004

Huang, Y., Liu, X. Q., Wyss-Coray, T., Brecht, W. J., Sanan, D. A., & Mahley, R. W. (2001). Apolipoprotein E fragments present in Alzheimer's disease brains induce neurofibrillary tangle-like intracellular inclusions in neurons. *Proceedings of the National Academy of Sciences of the United States of America*, *98*(15), 8838–8843. https://doi.org/10.1073/pnas.151254698

Huang, Y., & Mahley, R. W. (2014). Apolipoprotein E: Structure and function in lipid metabolism, neurobiology, and Alzheimer's diseases. *Neurobiology of Disease*, *72*(Part A), 3–12. https://doi.org/10.1016/J.NBD.2014.08.025

Huang, Y., & Mucke, L. (2012). Alzheimer Mechanisms and Therapeutic Strategies. *Cell*, *148*(6), 1204–1222. https://doi.org/10.1016/J.CELL.2012.02.040

Huang, Y. W. A., Zhou, B., Nabet, A. M., Wernig, M., & Südhof, T. C. (2019). Differential Signaling Mediated by ApoE2, ApoE3, and ApoE4 in Human Neurons Parallels Alzheimer's Disease Risk. *Journal of Neuroscience*, *39*(37), 7408–7427. https://doi.org/10.1523/JNEUROSCI.2994-18.2019

Huang, Y. W. A., Zhou, B., Wernig, M., & Südhof, T. C. (2017). ApoE2, ApoE3, and ApoE4 Differentially Stimulate APP Transcription and Aβ Secretion. *Cell*, *168*(3), 427–441.e21. https://doi.org/10.1016/j.cell.2016.12.044

Hudson, A. E. (2018). Genetic Reporters of Neuronal Activity: c-Fos and G-CaMP6. *Methods in Enzymology*, *603*, 197–220. https://doi.org/10.1016/bs.mie.2018.01.023

Hugo, J., & Ganguli, M. (2014). Dementia and Cognitive Impairment: Epidemiology, Diagnosis, and Treatment. *Clinics in Geriatric Medicine*, *30*(3), 421. https://doi.org/10.1016/J.CGER.2014.04.001

Hunter, J. M., Cirrito, J. R., Restivo, J. L., Kinley, R. D., Sullivan, P. M., Holtzman, D. M., … Paul, S. M. (2012). Emergence of a seizure phenotype in aged apolipoprotein epsilon 4 targeted replacement mice. *Brain Research*, *1467*, 120–132. https://doi.org/10.1016/j.brainres.2012.05.048

Huppert, F. A., Cabelli, S. T., & Matthews, F. E. (2005). Brief cognitive assessment in a UK population sample - Distributional properties and the relationship between the MMSE and an extended mental state examination. *BMC Geriatrics*, *5*(1), 1–14. https://doi.org/10.1186/1471-2318-5-7/TABLES/9

Huynh, T. P. V., Wang, C., Tran, A. C., Tabor, G. T., Mahan, T. E., Francis, C. M., … Holtzman, D. M. (2019). Lack of hepatic apoE does not influence early Aβ deposition: Observations from a new APOE knock-in model. *Molecular Neurodegeneration*, *14*(1), 1–23. https://doi.org/10.1186/S13024-019-0337-1/FIGURES/9

Hvoslef-Eide, M., & Oomen, C. A. (2016). Adult neurogenesis and pattern separation in rodents: A critical evaluation of data, tasks and interpretation. *Frontiers in Biology*, *11*(3), 168–181. https://doi.org/10.1007/s11515-016-1406-2

Hyman, B. T., Van Hoesen, G. W., Damasio, A. R., & Barnes, C. L. (1984). Alzheimer's disease: Cell-specific pathology isolates the hippocampal formation. *Science*, *225*(4667), 1168–1170. https://doi.org/10.1126/science.6474172

Ignatius, M. J., Gebicke-Harter, P. J., Skene, J. H. P., Schilling, J. W., Weisgraber, K. H., Mahley, R. W., & Shooter, E. M. (1986). Expression of apolipoprotein E during nerve degeneration and regeneration. *Proceedings of the National Academy of Sciences of the United States of America*, *83*(4), 1125–1129. https://doi.org/10.1073/pnas.83.4.1125

Illouz, T., Madar, R., Clague, C., Griffioen, K. J., Louzoun, Y., & Okun, E. (2016). Unbiased classification of spatial strategies in the Barnes maze. *Bioinformatics*, *32*(21), 3314–3320. https://doi.org/10.1093/BIOINFORMATICS/BTW376

Illouz, T., Madar, R., & Okun, E. (2020). A modified Barnes maze for an accurate assessment of spatial learning in mice. *Journal of Neuroscience Methods*, *334*. https://doi.org/10.1016/j.jneumeth.2020.108579

Izquierdo, I., & Medina, J. H. (1995). Correlation between the pharmacology of long-term potentiation and the pharmacology of memory. *Neurobiology of Learning and Memory*, *63*(1), 19–32. https://doi.org/10.1006/nlme.1995.1002

Jadhav, S. P., Kemere, C., German, P. W., & Frank, L. M. (2012). Awake hippocampal sharp-wave ripples support spatial memory. *Science*, *336*(6087), 1454–1458. https://doi.org/10.1126/science.1217230

Jahn, H. (2013). Memory loss in Alzheimer's disease. *Dialogues in Clinical Neuroscience*, *15*(4), 445. https://doi.org/10.31887/DCNS.2013.15.4/HJAHN

Jain, S., Yoon, S. Y., Leung, L., Knoferle, J., & Huang, Y. (2013). Cellular Source-Specific Effects of Apolipoprotein (Apo) E4 on Dendrite Arborization and Dendritic Spine Development. *PLoS ONE*, *8*(3), e59478. https://doi.org/10.1371/journal.pone.0059478

Janssen, C. I. F., Jansen, D., Mutsaers, M. P. C., Dederen, P. J. W. C., Geenen, B., Mulder, M. T., & Kiliaan Kiliaan, A. J. (2016). The effect of a high-fat diet on brain plasticity, inflammation and cognition in female ApoE4-knockin and ApoE-knockout mice. *PLoS ONE*, *11*(5), e0155307. https://doi.org/10.1371/journal.pone.0155307

Jerman, T., Kesner, R. P., & Hunsaker, M. R. (2006). Disconnection analysis of CA3 and DG in mediating encoding but not retrieval in a spatial maze learning task. *Learning & Memory*, *13*(4), 458. https://doi.org/10.1101/LM.246906

Ji, J., & Maren, S. (2008). Differential roles for hippocampal areas CA1 and CA3 in the contextual encoding and retrieval of extinguished fear. *Learning and Memory*, *15*(4), 244–251. https://doi.org/10.1101/lm.794808

Ji, Y., Gong, Y., Gan, W., Beach, T., Holtzman, D. M., & Wisniewski, T. (2003). Apolipoprotein E isoform-specific regulation of dendritic spine morphology in apolipoprotein E transgenic mice and Alzheimer's disease patients. *Neuroscience*, *122*(2), 305–315. https://doi.org/10.1016/J.NEUROSCIENCE.2003.08.007

Ji, Z. S., Pitas, R. E., & Mahley, R. W. (1998). Differential Cellular Accumulation/Retention of Apolipoprotein E Mediated by Cell Surface Heparan Sulfate Proteoglycans: APOLIPOPROTEINS E3 AND E2 GREATER THAN E4 *. *Journal of Biological Chemistry*, *273*(22), 13452–13460. https://doi.org/10.1074/JBC.273.22.13452

Jiang, C., Stewart, L. T., Kuo, H. C., McGilberry, W., Wall, S. B., Liang, B., … Liu, R. M. (2019). Cyclic O3 exposure synergizes with aging leading to memory impairment in male APOE ε3, but not APOE ε4, targeted replacement mice. *Neurobiology of Aging*, *81*, 9–21. https://doi.org/10.1016/J.NEUROBIOLAGING.2019.05.006

Jiang, L., Zhong, J., Dou, X., Cheng, C., Huang, Z., & Sun, X. (2015). Effects of ApoE on intracellular calcium levels and apoptosis of neurons after mechanical injury. *Neuroscience*, *301*, 375–383. https://doi.org/10.1016/j.neuroscience.2015.06.005

Jinde, S., Belforte, J. E., Yamamoto, J., Wilson, M. A., Tonegawa, S., & Nakazawa, K. (2009). Lack of kainic acid-induced gamma oscillations predicts subsequent CA1 excitotoxic cell death. *European Journal of Neuroscience*, *30*(6), 1036–1055. https://doi.org/10.1111/J.1460-9568.2009.06896.X

Johnson, L. A., Olsen, R. H. J., Merkens, L. S., DeBarber, A., Steiner, R. D., Sullivan, P. M., … Raber, J. (2014). Apolipoprotein E-low density lipoprotein receptor interaction affects spatial memory retention and brain ApoE levels in an isoform-dependent manner. *Neurobiology of Disease*, *64*, 150–162. https://doi.org/10.1016/j.nbd.2013.12.016

Jones, E. A., Gillespie, A. K., Yoon, S. Y., Frank, L. M., & Huang, Y. (2019). Early Hippocampal Sharp-Wave Ripple Deficits Predict Later Learning and Memory Impairments in an Alzheimer's Disease Mouse Model. *Cell Reports*, *29*(8), 2123–2133.e4. https://doi.org/10.1016/J.CELREP.2019.10.056

Jones, N. S., Watson, K. Q., & Rebeck, G. W. (2019). Metabolic Disturbances of a High-Fat Diet Are Dependent on APOE Genotype and Sex. *ENeuro*, *6*(5). https://doi.org/10.1523/ENEURO.0267-19.2019

Jones, N. S., Watson, K. Q., & Rebeck, G. W. (2021). High-fat diet increases gliosis and immediate early gene expression in APOE 3 mice, but not APOE4 mice. *Journal of Neuroinflammation*, *18*(1), 1–13. https://doi.org/10.1186/S12974-021-02256-2/FIGURES/7

Kanazawa, I. (2001). How do neurons die in neurodegenerative diseases? *Trends in Molecular Medicine*, *7*(8), 339–344. https://doi.org/10.1016/S1471-4914(01)02017-2

Kanekiyo, T., Xu, H., & Bu, G. (2014). ApoE and Aβ in Alzheimer's disease: accidental encounters or partners? *Neuron*, *81*(4), 740. https://doi.org/10.1016/J.NEURON.2014.01.045

Karch, C. M., & Goate, A. M. (2015). Alzheimer's Disease Risk Genes and Mechanisms of Disease Pathogenesis. *Biological Psychiatry*, *77*(1), 43–51. https://doi.org/10.1016/J.BIOPSYCH.2014.05.006

Karran, E., Mercken, M., & Strooper, B. De. (2011). The amyloid cascade hypothesis for Alzheimer's disease: An appraisal for the development of therapeutics. *Nature Reviews Drug Discovery*, *10*(9), 698–712. https://doi.org/10.1038/nrd3505

Kasai, H., Matsuzaki, M., Noguchi, J., Yasumatsu, N., & Nakahara, H. (2003). Structure–stability–function relationships of dendritic spines. *Trends in Neurosciences*, *26*(7), 360–368. https://doi.org/10.1016/S0166-2236(03)00162-0

Katche, C., Bekinschteina, P., Slipczuk, L., Goldin, A., Izquierdo, I. A., Cammarota, M., & Medina, J. H. (2010). Delayed wave of c-Fos expression in the dorsal hippocampus involved specifically in persistence of long-term memory storage. *Proceedings of the National Academy of Sciences of the United States of America*, *107*(1), 349–354. https://doi.org/10.1073/pnas.0912931107

Katche, C., & Medina, J. H. (2017). Requirement of an Early Activation of BDNF/c-Fos Cascade in the Retrosplenial Cortex for the Persistence of a Long-Lasting Aversive Memory. *Cerebral Cortex*, *27*(2), 1060–1067. https://doi.org/10.1093/CERCOR/BHV284

Kawasaki, K., Traynelis, S. F., & Dingledine, R. (1990). Different responses of CA1 and CA3 regions to hypoxia in rat hippocampal slice. *Journal of Neurophysiology*, *63*(3), 385–394. https://doi.org/10.1152/jn.1990.63.3.385

Kennard, J. A., & Woodruff-Pak, D. S. (2011). Age sensitivity of behavioral tests and brain substrates of normal aging in mice. *Frontiers in Aging Neuroscience*, *3*(MAY), 1–22. https://doi.org/10.3389/FNAGI.2011.00009/BIBTEX

Kesner, R. P., Hunsaker, M. R., & Warthen, M. W. (2008). The CA3 Subregion of the Hippocampus Is Critical for Episodic Memory Processing by Means of Relational Encoding in Rats. *Behavioral Neuroscience*, *122*(6), 1217–1225. https://doi.org/10.1037/A0013592

Kesner, R. P., Hunt, M. E., Williams, J. M., & Long, J. M. (1996). Prefrontal Cortex and Working Memory for Spatial Response, Spatial Location, and Visual Object Information in the Rat. *Cerebral Cortex*, *6*(2), 311–318. https://doi.org/10.1093/CERCOR/6.2.311

Khan, U. A., Liu, L., Provenzano, F. A., Berman, D. E., Profaci, C. P., Sloan, R., … Small, S. A. (2014). Molecular drivers and cortical spread of lateral entorhinal cortex dysfunction in preclinical Alzheimer's disease. *Nature Neuroscience*, *17*(2), 304–311. https://doi.org/10.1038/nn.3606

Kim, J., Basak, J. M., & Holtzman, D. M. (2009). The Role of Apolipoprotein E in Alzheimer's Disease. *Neuron*, *63*(3), 287–303. https://doi.org/10.1016/j.neuron.2009.06.026

Kitamura, H. W., Hamanaka, H., Watanabe, M., Wada, K., Yamazaki, C., Fujita, S. C., … Nukina, N. (2004). Age-dependent enhancement of hippocampal long-term potentiation in knock-in mice expressing human apolipoprotein E4 instead of mouse apolipoprotein E. *Neuroscience Letters*, *369*(3), 173–178. https://doi.org/10.1016/J.NEULET.2004.07.084

Klausberger, T. (2009). GABAergic interneurons targeting dendrites of pyramidal cells in the CA1 area of the hippocampus. *European Journal of Neuroscience*, *30*(6), 947–957. https://doi.org/10.1111/j.1460-9568.2009.06913.x

Klein, R. C., Mace, B. E., Moore, S. D., & Sullivan, P. M. (2010). Progressive loss of synaptic integrity in human apolipoprotein E4 targeted replacement mice and attenuation by apolipoprotein E2. *Neuroscience*, *171*(4), 1265–1272. https://doi.org/10.1016/J.NEUROSCIENCE.2010.10.027

Klein, R. C., Saini, S., Risher, M. L., Acheson, S. K., Fleming, R. L., Sexton, H. G., … Moore, S. D. (2014). Regional-specific effects of ovarian hormone loss on synaptic plasticity in adult human APOE targeted replacement mice. *PLoS ONE*, *9*(4), e94071. https://doi.org/10.1371/journal.pone.0094071

Knierim, J. J. (2015). The hippocampus. *Current Biology*, *25*(23), R1116–R1121. https://doi.org/10.1016/J.CUB.2015.10.049

Knight, R. G., Tsui, H. S. L., Abraham, W. C., Skeaff, C. M., McMahon, J. A., & Cutfield, N. J. (2014). Lack of effect of the apolipoprotein E ε4 genotype on cognition during healthy aging. *Journal of Clinical and Experimental Neuropsychology*, *36*(7), 742–750.

Knoferle, J., Yoon, S. Y., Walker, D., Leung, L., Gillespie, A. K., Tong, L. M., … Huang, Y. (2014). Apolipoprotein E4 produced in GABAergic interneurons causes learning and memory deficits in mice. *Journal of Neuroscience*, *34*(42), 14069–14078. https://doi.org/10.1523/JNEUROSCI.2281-14.2014

Knouff, C., Hinsdale, M. E., Mezdour, H., Altenburg, M. K., Watanabe, M., Quarfordt, S. H., … Maeda, N. (1999). Apo E structure determines VLDL clearance and atherosclerosis risk in mice. *The Journal of Clinical Investigation*, *103*(11), 1579–1586. https://doi.org/10.1172/JCI6172

Kockx, M., Dinnes, D. L., Huang, K. Y., Sharpe, L. J., Jessup, W., Brown, A. J., & Kritharides, L. (2012). Cholesterol accumulation inhibits ER to Golgi transport and protein secretion: Studies of apolipoprotein E and VSVGt. *Biochemical Journal*, *447*(1), 51–60. https://doi.org/10.1042/BJ20111891

Kockx, M., Jessup, W., & Kritharides, L. (2008). Regulation of endogenous apolipoprotein e secretion by macrophages. *Arteriosclerosis, Thrombosis, and Vascular Biology*, *28*(6), 1060–1067. https://doi.org/10.1161/ATVBAHA.108.164350

Koizumi, K., Hattori, Y., Ahn, S. J., Buendia, I., Ciacciarelli, A., Uekawa, K., … Iadecola, C. (2018). Apoε4 disrupts neurovascular regulation and undermines white matter integrity and cognitive function. *Nature Communications*, *9*(1), 1–11. https://doi.org/10.1038/s41467-018-06301-2

Konings, S. C., Torres-Garcia, L., Martinsson, I., & Gouras, G. K. (2021). Astrocytic and Neuronal Apolipoprotein E Isoforms Differentially Affect Neuronal Excitability. *Frontiers in Neuroscience*, *15*, 1190. https://doi.org/10.3389/FNINS.2021.734001/BIBTEX

Korwek, K. M., Trotter, J. H., Ladu, M. J., Sullivan, P. M., & Weeber, E. J. (2008). Apoe isoform-dependent changes in hippocampal synaptic function. *Molecular Neurodegeneration*, *4*(1), 1–18. https://doi.org/10.1186/1750-1326-4-21/FIGURES/10

Koutseff, A., Mittelhaeuser, C., Essabri, K., Auwerx, J., & Meziane, H. (2014). Impact of the apolipoprotein E polymorphism, age and sex on neurogenesis in mice: Pathophysiological relevance for Alzheimer's disease? *Brain Research*, *1542*, 32–40. https://doi.org/10.1016/J.BRAINRES.2013.10.003

Kovács, K. J. (1998). Invited review c-Fos as a transcription factor: a stressful (re)view from a functional map. *Neurochemistry International*, *33*(4), 287–297. https://doi.org/10.1016/S0197-0186(98)00023-0

Kowal, R. C., Herz, J., Weisgraber, K. H., Mahley, R. W., Brown, M. S., & Goldstein, J. L. (1990). Opposing effects of apolipoproteins E and C on lipoprotein binding to low density lipoprotein receptor-related protein. *Journal of Biological Chemistry*, *265*(18), 10771–10779. https://doi.org/10.1016/S0021-9258(18)87014-4

Koya, E., Cruz, F. C., Ator, R., Golden, S. A., Hoffman, A. F., Lupica, C. R., & Hope, B. T. (2012). Silent synapses in selectively activated nucleus accumbens neurons following cocaine sensitization. *Nature Neuroscience*, *15*(11), 1556–1562. https://doi.org/10.1038/nn.3232

Koya, E., Golden, S. A., Harvey, B. K., Guez-Barber, D. H., Berkow, A., Simmons, D. E., … Hope, B. T. (2009). Targeted disruption of cocaine-activated nucleus accumbens neurons prevents context-specific sensitization. *Nature Neuroscience*, *12*(8), 1069–1073. https://doi.org/10.1038/nn.2364

Krukowski, K., Nolan, A., Frias, E. S., Boone, M., Ureta, G., Grue, K., … Rosi, S. (2020). Small molecule cognitive enhancer reverses age-related memory decline in mice. *ELife*, *9*, 1–22. https://doi.org/10.7554/ELIFE.62048

Lacar, B., Linker, S. B., Jaeger, B. N., Krishnaswami, S., Barron, J., Kelder, M., … Gage, F. H. (2016). Nuclear RNA-seq of single neurons reveals molecular signatures of activation. *Nature Communications*, *7*(1), 1–13. https://doi.org/10.1038/ncomms11022

Lane-Donovan, C., & Herz, J. (2017). ApoE, ApoE Receptors, and the Synapse in Alzheimer's Disease. *Trends in Endocrinology & Metabolism*, *28*(4), 273–284. https://doi.org/10.1016/J.TEM.2016.12.001

Lane-Donovan, C., Philips, G. T., & Herz, J. (2014). More than Cholesterol Transporters: Lipoprotein Receptors in CNS Function and Neurodegeneration. *Neuron*, *83*(4), 771–787. https://doi.org/10.1016/J.NEURON.2014.08.005

Lanfranco, M. F., Ng, C. A., & Rebeck, G. W. (2020). ApoE lipidation as a therapeutic target in Alzheimer's disease. *International Journal of Molecular Sciences*, *21*(17), 1–19. https://doi.org/10.3390/ijms21176336

Lanfranco, M. F., Sepulveda, J., Kopetsky, G., & Rebeck, G. W. (2021). Expression and secretion of apoE isoforms in astrocytes and microglia during inflammation. *Glia*, *69*(6), 1478–1493. https://doi.org/10.1002/GLIA.23974

Larramona-Arcas, R., González-Arias, C., Perea, G., Gutiérrez, A., Vitorica, J., García-Barrera, T., … Masgrau, R. (2020). Sex-dependent calcium hyperactivity due to lysosomal-related dysfunction in astrocytes from APOE4 versus APOE3 gene targeted replacement mice. *Molecular Neurodegeneration*, *15*(1). https://doi.org/10.1186/s13024-020-00382-8

LeBlanc, A. (2005). The Role of Apoptotic Pathways in Alzheimers Disease Neurodegeneration and Cell Death. *Current Alzheimer Research*, *2*(4), 389–402. https://doi.org/10.2174/156720505774330573

Lee, C. H., & Lee, I. (2020). Impairment of Pattern Separation of Ambiguous Scenes by Single Units in the CA3 in the Absence of the Dentate Gyrus. *Journal of Neuroscience*, *40*(18), 3576–3590. https://doi.org/10.1523/JNEUROSCI.2596-19.2020

Lee, E. G., Tulloch, J., Chen, S., Leong, L., Saxton, A. D., Kraemer, B., … Yu, C. E. (2020). Redefining transcriptional regulation of the APOE gene and its association with Alzheimer's disease. *PLoS ONE*, *15*(1), e0227667. https://doi.org/10.1371/journal.pone.0227667

Lee, H., Wang, Z., Zeger, S. L., Gallagher, M., & Knierim, J. J. (2021). Heterogeneity of age-related neural hyperactivity along the CA3 transverse axis. *Journal of Neuroscience*, *41*(4), 663–673. https://doi.org/10.1523/JNEUROSCI.2405-20.2020

Lee, K. F. H., Soares, C., & Béïque, J. C. (2012). Examining form and function of dendritic spines. *Neural Plasticity*, *2012*. https://doi.org/10.1155/2012/704103

Leung, L., Andrews-Zwilling, Y., Yoon, S. Y., Jain, S., Ring, K., Dai, J., … Huang, Y. (2012). Apolipoprotein E4 Causes Age- and Sex-Dependent Impairments of Hilar GABAergic Interneurons and Learning and Memory Deficits in Mice. *PLoS ONE*, *7*(12), e53569. https://doi.org/10.1371/journal.pone.0053569

Leutgeb, S., Leutgeb, J. K., Treves, A., Moser, M. B., & Moser, E. I. (2004). Distinct ensemble codes in hippocampal areas CA3 and CA1. *Science*, *305*(5688), 1295–1298. https://doi.org/10.1126/science.1100265

Lewandowski, C. T., Maldonado Weng, J., & LaDu, M. J. (2020). Alzheimer's disease pathology in APOE transgenic mouse models: The Who, What, When, Where, Why, and How. *Neurobiology of Disease*, *139*, 104811. https://doi.org/10.1016/J.NBD.2020.104811

Li, G., Bien-Ly, N., Andrews-Zwilling, Y., Xu, Q., Bernardo, A., Ring, K., … Huang, Y. (2009). GABAergic Interneuron Dysfunction Impairs Hippocampal Neurogenesis in Adult Apolipoprotein E4 Knockin Mice. *Cell Stem Cell*, *5*(6), 634–645. https://doi.org/10.1016/J.STEM.2009.10.015

Li, J., Kanekiyo, T., Shinohara, M., Zhang, Y., LaDu, M. J., Xu, H., & Bu, G. (2012). Differential Regulation of Amyloid-β Endocytic Trafficking and Lysosomal Degradation by Apolipoprotein E Isoforms. *Journal of Biological Chemistry*, *287*(53), 44593–44601. https://doi.org/10.1074/JBC.M112.420224

Li, X., Zhang, J., Li, D., He, C., He, K., Xue, T., … Liu, Q. (2021). Astrocytic ApoE reprograms neuronal cholesterol metabolism and histone-acetylation-mediated memory. *Neuron*, *109*(6), 957–970.e8. https://doi.org/10.1016/J.NEURON.2021.01.005

Li, X., Kypreos, K., Zanni, E. E., & Zannis, V. (2003). Domains of apoE required for binding to apoE receptor 2 and to phospholipids: Implications for the functions of apoE in the brain. *Biochemistry*, *42*(35), 10406–10417. https://doi.org/10.1021/BI027093C

Li, Z., Shue, F., Zhao, N., Shinohara, M., & Bu, G. (2020). APOE2: protective mechanism and therapeutic implications for Alzheimer's disease. *Molecular Neurodegeneration*, *15*(1), 1–19. https://doi.org/10.1186/S13024-020-00413-4/FIGURES/3

Liang, Y., Lin, S., Beyer, T. P., Zhang, Y., Wu, X., Bales, K. R., … Paul, S. M. (2004). A liver X receptor and retinoid X receptor heterodimer mediates apolipoprotein E expression, secretion and cholesterol homeostasis in astrocytes. *Journal of Neurochemistry*, *88*(3), 623–634. https://doi.org/10.1111/j.1471-4159.2004.02183.x

Liao, F., Yoon, H., & Kim, J. (2017). Apolipoprotein E metabolism and functions in brain and its role in Alzheimer's disease. *Current Opinion in Lipidology*, *28*(1), 60. https://doi.org/10.1097/MOL.0000000000000383

Lin, L. Y., Zhang, J., Dai, X. M., Xiao, N. A., Wu, X. L., Wei, Z., … Chen, X. C. (2016). Early-life stress leads to impaired spatial learning and memory in middle-aged ApoE4-TR mice. *Molecular Neurodegeneration*, *11*(1), 1–16. https://doi.org/10.1186/S13024-016-0107-2/FIGURES/10

Lin, Y. T., Seo, J., Gao, F., Feldman, H. M., Wen, H. L., Penney, J., … Tsai, L. H. (2018). APOE4 Causes Widespread Molecular and Cellular Alterations Associated with Alzheimer's Disease Phenotypes in Human iPSC-Derived Brain Cell Types. *Neuron*, *98*(6), 1141–1154.e7. https://doi.org/10.1016/J.NEURON.2018.05.008

Lipatova, O., Campolattaro, M. M., & Picone, J. A. (2020). Fornix lesions impair place-, but not response-learning in the open-field tower maze. *Neurobiology of Learning and Memory*, *167*, 107134. https://doi.org/10.1016/J.NLM.2019.107134

Liu, C. C., Zhao, N., Fu, Y., Wang, N., Linares, C., Tsai, C. W., & Bu, G. (2017). ApoE4 Accelerates Early Seeding of Amyloid Pathology. *Neuron*, *96*(5), 1024–1032.e3. https://doi.org/10.1016/J.NEURON.2017.11.013

Liu, X., Ramirez, S., Pang, P. T., Puryear, C. B., Govindarajan, A., Deisseroth, K., & Tonegawa, S. (2012). Optogenetic stimulation of a hippocampal engram activates fear memory recall. *Nature*, *484*(7394), 381–385. https://doi.org/10.1038/nature11028

Locklear, M. N., & Kritzer, M. F. (2014). Assessment of the effects of sex and sex hormones on spatial cognition in adult rats using the Barnes maze. *Hormones and Behavior*, *66*(2), 298–308. https://doi.org/10.1016/J.YHBEH.2014.06.006

Logue, S. F., Paylor, R., & Wehner, J. M. (1997). Hippocampal lesions cause learning deficits in inbred mice in the Morris water maze and conditioned-fear task. *Behavioral Neuroscience*, *111*(1), 104–113. https://doi.org/10.1037//0735-7044.111.1.104

Maei, H. R., Zaslavsky, K., Teixeira, C. M., & Frankland, P. W. (2009). What is the most sensitive measure of water maze probe test performance? *Frontiers in Integrative Neuroscience*, *3*(MAR), 4. https://doi.org/10.3389/NEURO.07.004.2009/BIBTEX

Maezawa, I., Zaja-Milatovic, S., Milatovic, D., Stephen, C., Sokal, I., Maeda, N., … Montine, K. S. (2006). Apolipoprotein E isoform-dependent dendritic recovery of hippocampal neurons following activation of innate immunity. *Journal of Neuroinflammation*, *3*(1), 21. https://doi.org/10.1186/1742-2094-3-21

Magnusson, K. R., Scruggs, B., Aniya, J., Wright, K. C., Ontl, T., Xing, Y., & Bai, L. (2003). Age-related deficits in mice performing working memory tasks in a water maze. *Behavioral Neuroscience*, *117*(3), 485–495. https://doi.org/10.1037/0735-7044.117.3.485

Mahley, R. W. (2016). Central nervous system lipoproteins: ApoE and regulation of cholesterol metabolism. *Arteriosclerosis, Thrombosis, and Vascular Biology*, *36*(7), 1305–1315. https://doi.org/10.1161/ATVBAHA.116.307023

Mahley, R. W. (1988). Apolipoprotein E: Cholesterol Transport Protein with Expanding Role in Cell Biology. *Science*, *240*(4852), 622–630. https://doi.org/10.1126/SCIENCE.3283935

Mahley, R. W., & Huang, Y. (2012). Apolipoprotein E Sets the Stage: Response to Injury Triggers Neuropathology. *Neuron*, *76*(5), 871–885. https://doi.org/10.1016/j.neuron.2012.11.020

Mahley, R. W., & Rall, S. C. (2000). Apolipoprotein E: Far more than a lipid transport protein. *Annual Review of Genomics and Human Genetics*, *1*(2000), 507–537. https://doi.org/10.1146/annurev.genom.1.1.507

Mahley, R. W., Weisgraber, K. H., & Huang, Y. (2009). Apolipoprotein E: structure determines function, from atherosclerosis to Alzheimer's disease to AIDS. *Journal of Lipid Research*, *50*(SUPPL.), S183–S188. https://doi.org/10.1194/JLR.R800069-JLR200

Mahley, R. W., Weisgraber, K. H., & Huang, Y. (2006). Apolipoprotein E4: A causative factor and therapeutic target in neuropathology, including Alzheimer's disease. *Proceedings of the National Academy of Sciences of the United States of America*, *103*(15), 5644–5651. https://doi.org/10.1073/pnas.0600549103

Maioli, S., Puerta, E., Merino-Serrais, P., Fusari, L., Gil-Bea, F., Rimondini, R., & Cedazo-Minguez, A. (2012). Combination of apolipoprotein E4 and high carbohydrate diet reduces hippocampal BDNF and Arc levels and impairs memory in young mice. *Journal of Alzheimer's Disease*, *32*(2), 341–355. https://doi.org/10.3233/JAD-2012-120697

Majacek, R. A., Castle, C. K., Goodman, L. V., Weisgraber, K. H., Mahley, R. W., Shooter, E. M., & Gebicke-Haerter, P. J. (1988). Expression of apolipoprotein E by cultured vascular smooth muscle cells is controlled by growth state. *Journal of Cell Biology*, *107*(3), 1207–1213. https://doi.org/10.1083/jcb.107.3.1207

Maloney, B., Ge, Y. W., Alley, G. M., & Lahiri, D. K. (2007). Important differences between human and mouse APOE gene promoters: Limitation of mouse APOE model in studying Alzheimer's disease. *Journal of Neurochemistry*, *103*(3), 1237–1257. https://doi.org/10.1111/j.1471-4159.2007.04831.x

Maloney, B., Ge, Y. W., Petersen, R. C., Hardy, J., Rogers, J. T., Pérez-Tur, J., & Lahiri, D. K. (2010). Functional characterization of three single-nucleotide polymorphisms present in the human APOε promoter sequence: Differential effects in neuronal cells and on DNA-protein interactions. *American Journal of Medical Genetics, Part B: Neuropsychiatric Genetics*, *153*(1), 185–201. https://doi.org/10.1002/AJMG.B.30973

Mann, E. O., & Paulsen, O. (2005). Mechanisms underlying gamma ('40 Hz') network oscillations in the hippocampus - A mini-review. *Progress in Biophysics and Molecular Biology*, *87*(1 SPEC. ISS.), 67–76. https://doi.org/10.1016/j.pbiomolbio.2004.06.004

Mannix, R. C., Zhang, J., Park, J., Zhang, X., Bilal, K., Walker, K., … Whalen, M. J. (2011). Age-dependent effect of apolipoprotein E4 on functional outcome after controlled cortical impact in mice. *Journal of Cerebral Blood Flow and Metabolism*, *31*(1), 351–361. https://doi.org/10.1038/jcbfm.2010.99

Mannix, R., Meehan, W. P., Mandeville, J., Grant, P. E., Gray, T., Berglass, J., … Whalen, M. (2013). Clinical correlates in an experimental model of repetitive mild brain injury. *Annals of Neurology*, *74*(1), 65–75. https://doi.org/10.1002/ANA.23858

Matsubayashi, Y., Iwai, L., & Kawasaki, H. (2008). Fluorescent double-labeling with carbocyanine neuronal tracing and immunohistochemistry using a cholesterol-specific detergent digitonin. *Journal of Neuroscience Methods*, *174*(1), 71–81. https://doi.org/10.1016/J.JNEUMETH.2008.07.003

Matsuzaki, M., Ellis-Davies, G. C. R., Nemoto, T., Miyashita, Y., Iino, M., & Kasai, H. (2001). Dendritic spine geometry is critical for AMPA receptor expression in hippocampal CA1 pyramidal neurons. *Nature Neuroscience*, *4*(11), 1086–1092. https://doi.org/10.1038/nn736

McCormick, C., Ciaramelli, E., De Luca, F., & Maguire, E. A. (2018). Comparing and Contrasting the Cognitive Effects of Hippocampal and Ventromedial Prefrontal Cortex Damage: A Review of Human Lesion Studies. *Neuroscience*, *374*, 295–318. https://doi.org/10.1016/J.NEUROSCIENCE.2017.07.066

McDonald, R. J., King, A. L., Foong, N., Rizos, Z., & Hong, N. S. (2008). Neurotoxic lesions of the medial prefrontal cortex or medial striatum impair multiple-location place learning in the water task: evidence for neural structures with complementary roles in behavioural Xexibility. *Exp Brain Res*, *187*, 419–427. https://doi.org/10.1007/s00221-008-1314-z

McGarrity, S., Mason, R., Fone, K. C., Pezze, M., & Bast, T. (2017). Hippocampal Neural Disinhibition Causes Attentional and Memory Deficits. *Cerebral Cortex*, *27*(9), 4447–4462. https://doi.org/10.1093/CERCOR/BHW247

McNaughton, B. L., Barnes, C. A., Rao, G., Baldwin, J., & Rasmussen, M. (1986). Long-term enhancement of hippocampal synaptic transmission and the acquisition of spatial information. *Journal of Neuroscience*, *6*(2), 563–571. https://doi.org/10.1523/jneurosci.06-02-00563.1986

McNaughton, B. L., Battaglia, F. P., Jensen, O., Moser, E. I., & Moser, M. B. (2006). Path integration and the neural basis of the "cognitive map." *Nature Reviews Neuroscience*, *7*(8), 663–678. https://doi.org/10.1038/nrn1932

Meng, F. T., Zhao, J., Fang, H., & Liu, Y. J. (2015). The influence of chronic stress on anxiety-like behavior and cognitive function in different human GFAP-ApoE transgenic adult male mice. *Stress*, *18*(4), 419–426. Retrieved from https://www.tandfonline.com/doi/abs/10.3109/10253890.2015.1040986

Milczarek, M. M., & Vann, S. D. (2020, April 1). The retrosplenial cortex and long-term spatial memory: from the cell to the network. *Current Opinion in Behavioral Sciences*. Elsevier Ltd. https://doi.org/10.1016/j.cobeha.2020.01.014

Mills, J. D., Sheahan, P. J., Lai, D., Kril, J. J., Janitz, M., & Sutherland, G. T. (2014). The alternative splicing of the apolipoprotein E gene is unperturbed in the brains of Alzheimer's disease patients. *Molecular Biology Reports*, *41*(10), 6365–6376. https://doi.org/10.1007/S11033-014-3516-8

Minagawa, H., Gong, J. S., Jung, C. G., Watanabe, A., Lund-Katz, S., Phillips, M. C., … Michikawa, M. (2009). Mechanism underlying apolipoprotein E (ApoE) isoform-dependent lipid efflux from neural cells in culture. *Journal of Neuroscience Research*, *87*(11), 2498–2508. https://doi.org/10.1002/jnr.22073

Minatohara, K., Akiyoshi, M., & Okuno, H. (2016). Role of immediate-early genes in synaptic plasticity and neuronal ensembles underlying the memory trace. *Frontiers in Molecular Neuroscience*, *8*(JAN2016), 78. https://doi.org/10.3389/FNMOL.2015.00078/BIBTEX

Moench, K. M., Breach, M. R., & Wellman, C. L. (2019). Chronic stress produces enduring sex- and region-specific alterations in novel stress-induced c-Fos expression. *Neurobiology of Stress*, *10*, 100147. https://doi.org/10.1016/j.ynstr.2019.100147

Montagne, A., Nikolakopoulou, A. M., Huuskonen, M. T., Sagare, A. P., Lawson, E. J., Lazic, D., … Zlokovic, B. V. (2021). Author Correction: APOE4 accelerates advanced-stage vascular and neurodegenerative disorder in old Alzheimer's mice via cyclophilin A independently of amyloid-β. *Nature Aging*, *1*(7), 624–624. https://doi.org/10.1038/s43587-021-00090-y

Mora, F. (2013). Successful brain aging: plasticity, environmental enrichment, and lifestyle. *Dialogues in Clinical Neuroscience*, *15*(1), 45. https://doi.org/10.31887/DCNS.2013.15.1/FMORA

Morales, L., Tomàs, D. P., Dalmau, J., de la Rocha, J., & Jercog, P. E. (2020). High-Throughput Task to Study Memory Recall During Spatial Navigation in Rodents. *Frontiers in Behavioral Neuroscience*, *14*, 64. https://doi.org/10.3389/FNBEH.2020.00064/BIBTEX

Morgan, J. I., Cohen, D. R., Hempstead, J. L., & Curran, T. (1987). Mapping patterns of c-fos expression in the central nervous system after seizure. *Science*, *237*(4811), 192–197. https://doi.org/10.1126/science.3037702

Morris, A. M., Churchwell, J. C., Kesner, R. P., & Gilbert, P. E. (2012). Selective lesions of the dentate gyrus produce disruptions in place learning for adjacent spatial locations. *Neurobiology of Learning and Memory*, *97*(3), 326–331. https://doi.org/10.1016/J.NLM.2012.02.005

Morris, R. G. M. (2006). Elements of a neurobiological theory of hippocampal function: the role of synaptic plasticity, synaptic tagging and schemas. *European Journal of Neuroscience*, *23*(11), 2829–2846. https://doi.org/10.1111/J.1460-9568.2006.04888.X

Morris, R. G. M., Hagan, J. J., & Rawlins, J. N. P. (1986). Allocentric Spatial Learning by Hippocampectomised Rats: A Further Test of the "Spatial Mapping" and "Working Memory" Theories of Hippocampal Function. *The Quarterly Journal of Experimental Psychology Section B*, *38*(4), 365–395. https://doi.org/10.1080/14640748608402242

Morris, R. G. M., Moser, E. I., Riedel, G., Martin, S. J., Sandin, J., Day, M., & O'Carroll, C. (2003). Elements of a neurobiological theory of the hippocampus: The role of activity-dependent synaptic plasticity in memory. *Philosophical Transactions of the Royal Society B: Biological Sciences*, *358*(1432), 773–786. https://doi.org/10.1098/rstb.2002.1264

Morris, R. G. M., Schenk, F., Tweedie, F., & Jarrard, L. E. (1990). Ibotenate Lesions of Hippocampus and/or Subiculum: Dissociating Components of Allocentric Spatial Learning. *European Journal of Neuroscience*, *2*(12), 1016–1028. https://doi.org/10.1111/j.1460-9568.1990.tb00014.x

Morris, R. (1984). Developments of a water-maze procedure for studying spatial learning in the rat. *Journal of Neuroscience Methods*, *11*(1), 47–60. https://doi.org/10.1016/0165-0270(84)90007-4

Morris, R. G. M., Inglis, J., Ainge, J. A., Olverman, H. J., Tulloch, J., Dudai, Y., & Kelly, P. A. T. (2006). Memory Reconsolidation: Sensitivity of Spatial Memory to Inhibition of Protein Synthesis in Dorsal Hippocampus during Encoding and Retrieval. *Neuron*, *50*(3), 479–489. https://doi.org/10.1016/J.NEURON.2006.04.012

Morrison, J. H., & Hof, P. R. (2002). Selective vulnerability of corticocortical and hippocampal circuits in aging and Alzheimer's disease. *Progress in Brain Research*, *136*, 467–486. https://doi.org/10.1016/S0079-6123(02)36039-4

Morrow, J. A., Hatters, D. M., Lu, B., Höchtl, P., Oberg, K. A., Rupp, B., & Weisgraber, K. H. (2002). Apolipoprotein E4 forms a molten globule: A potential basis for its association with disease. *Journal of Biological Chemistry*, *277*(52), 50380–50385. https://doi.org/10.1074/jbc.M204898200

Moser, M., Hippocampus, E. M.-, & 1998, undefined. (1998). Functional differentiation in the hippocampus. *Wiley Online Library*. Retrieved from https://onlinelibrary.wiley.com/doi/abs/10.1002/(SICI)1098-1063(1998)8:6%3C608::AID-HIPO3%3E3.0.CO;2-7?casa_token=r4U3B7EMYFgAAAAA:ztru9D8RSRwzQF9gXaQm8ijX9e8bAPI5OFOuO4y2Mwzg6c25i2UpPJdPIWwV19dxywZQDRwOxB0

MOUNTCASTLE, V. B. (1957). Modality and topographic properties of single neurons of cat's somatic sensory cortex. *Journal of Neurophysiology*, *20*(4), 408–434. https://doi.org/10.1152/jn.1957.20.4.408

Muller, C., & Remy, S. (2014). Dendritic inhibition mediated by O-LM and bistratified interneurons in the hippocampus. *Frontiers in Synaptic Neuroscience*, *6*(SEP), 23. https://doi.org/10.3389/fnsyn.2014.00023

Muñoz, S. S., Garner, B., & Ooi, L. (2019). Understanding the Role of ApoE Fragments in Alzheimer's Disease. *Neurochemical Research*, *44*(6), 1297–1305. https://doi.org/10.1007/s11064-018-2629-1

Nai, Q., Li, S., Wang, S. H., Liu, J., Lee, F. J. S., Frankland, P. W., & Liu, F. (2010). Uncoupling the D1-N-Methyl-D-Aspartate (NMDA) Receptor Complex Promotes NMDA-Dependent Long-Term

Potentiation and Working Memory. *Biological Psychiatry*, *67*(3), 246–254. https://doi.org/10.1016/J.BIOPSYCH.2009.08.011

Najm, R., Jones, E. A., & Huang, Y. (2019, June 11). Apolipoprotein E4, inhibitory network dysfunction, and Alzheimer's disease. *Molecular Neurodegeneration*. BioMed Central Ltd. https://doi.org/10.1186/s13024-019-0324-6

Nakajima, C., Kulik, A., Frotscher, M., Herz, J., Schäfer, M., Bock, H. H., & May, P. (2013). Low Density Lipoprotein Receptor-related Protein 1 (LRP1) Modulates N-Methyl-d-aspartate (NMDA) Receptor-dependent Intracellular Signaling and NMDA-induced Regulation of Postsynaptic Protein Complexes. *Journal of Biological Chemistry*, *288*(30), 21909–21923. https://doi.org/10.1074/JBC.M112.444364

Nakazawa, K., Sun, L. D., Quirk, M. C., Rondi-Reig, L., Wilson, M. A., & Tonegawa, S. (2003). Hippocampal CA3 NMDA Receptors Are Crucial for Memory Acquisition of One-Time Experience. *Neuron*, *38*(2), 305–315. https://doi.org/10.1016/S0896-6273(03)00165-X

Neustadtl, A. L., Winston, C. N., Parsadanian, M., Main, B. S., Villapol, S., & Burns, M. P. (2017). Reduced cortical excitatory synapse number in APOE4 mice is associated with increased calcineurin activity. *Neuroreport*, *28*(10), 618. https://doi.org/10.1097/WNR.0000000000000811

Nguyen, D., Dhanasekaran, P., Nickel, M., Nakatani, R., Saito, H., Phillips, M. C., & Lund-Katz, S. (2010). No Title. *Biochemistry*, *49*(51), 10881–10889. https://doi.org/10.1021/BI1017655

Nichol, K., Deeny, S. P., Seif, J., Camaclang, K., & Cotman, C. W. (2009). Exercise improves cognition and hippocampal plasticity in APOE ϵ4 mice. *Alzheimer's and Dementia*, *5*(4), 287–294. https://doi.org/10.1016/j.jalz.2009.02.006

Nonaka, M., Fitzpatrick, R., Lapira, J., Wheeler, D., Spooner, P. A., Corcoles-Parada, M., … Morris, R. G. M. (2017). Everyday memory: towards a translationally effective method of modelling the encoding, forgetting and enhancement of memory. *European Journal of Neuroscience*, *46*(4), 1937–1953. https://doi.org/10.1111/EJN.13637

Notter, T., Panzanelli, P., Pfister, S., Mircsof, D., & Fritschy, J. M. (2014). A protocol for concurrent high-quality immunohistochemical and biochemical analyses in adult mouse central nervous system. *European Journal of Neuroscience*, *39*(2), 165–175. https://doi.org/10.1111/ejn.12447

Nuriel, T., Angulo, S. L., Khan, U., Ashok, A., Chen, Q., Figueroa, H. Y., … Duff, K. E. (2017). Neuronal hyperactivity due to loss of inhibitory tone in APOE4 mice lacking Alzheimer's disease-like pathology. *Nature Communications*, *8*(1), 1–14. https://doi.org/10.1038/s41467-017-01444-0

Nwabuisi-Heath, E., William Rebeck, G., LaDu, M. J., & Yu, C. (2014). ApoE4 delays dendritic spine formation during neuron development and accelerates loss of mature spines in vitro. *ASN Neuro*, *6*(1), 21–28. https://doi.org/10.1042/AN200130043

Oh, M. M., Oliveira, F. A., Waters, J., & Disterhoft, J. F. (2013). Altered calcium metabolism in aging CA1 hippocampal pyramidal neurons. *Journal of Neuroscience*, *33*(18), 7905–7911. https://doi.org/10.1523/JNEUROSCI.5457-12.2013

Oh, M. M., Simkin, D., & Disterhoft, J. F. (2016). Intrinsic hippocampal excitability changes of opposite signs and different origins in CA1 and CA3 pyramidal neurons underlie aging-related cognitive deficits. *Frontiers in Systems Neuroscience*, *10*(JUN), 52.

Ohkubo, N., Mitsuda, N., Tamatani, M., Yamaguchi, A., Lee, Y. D., Ogihara, T., … Tohyama, M. (2001). Apolipoprotein E4 Stimulates cAMP Response Element-binding Protein Transcriptional Activity through the Extracellular Signal-regulated Kinase Pathway *. *Journal of Biological Chemistry*, *276*(5), 3046–3053. https://doi.org/10.1074/JBC.M005070200

O'Keefe, J., & Nadel, L. (1978). *The hippocampus as a cognitive map*. Oxford University Press (OUP). Retrieved from https://discovery.ucl.ac.uk/id/eprint/10103569/1/HCMComplete.pdf

Olajide, O. J., Suvanto, M. E., & Chapman, C. A. (2021). Molecular mechanisms of neurodegeneration in the entorhinal cortex that underlie its selective vulnerability during the pathogenesis of Alzheimer's disease. *Biology Open*, *10*(1). https://doi.org/10.1242/BIO.056796/237244

Olaya, B., Bobak, M., Haro, J. M., & Demakakos, P. (2017). Trajectories of Verbal Episodic Memory in Middle-Aged and Older Adults: Evidence from the English Longitudinal Study of Ageing. *Journal of the American Geriatrics Society*, *65*(6), 1274–1281. https://doi.org/10.1111/JGS.14789

O'Leary, T. P., & Brown, R. E. (2012). The effects of apparatus design and test procedure on learning and memory performance of C57BL/6J mice on the Barnes maze. *Journal of Neuroscience Methods*, *203*(2), 315–324. https://doi.org/10.1016/j.jneumeth.2011.09.027

O'Leary, T. P., & Brown, R. E. (2013). Optimization of apparatus design and behavioral measures for the assessment of visuo-spatial learning and memory of mice on the Barnes maze. *Learning and Memory*, *20*(2), 85–96. https://doi.org/10.1101/lm.028076.112

O'Leary, T. P., & Brown, R. E. (2009). Visuo-spatial learning and memory deficits on the Barnes maze in the 16-month-old APPswe/PS1dE9 mouse model of Alzheimer's disease. *Behavioural Brain Research*, *201*(1), 120–127. https://doi.org/10.1016/J.BBR.2009.01.039

Oomen, C. A., Hvoslef-Eide, M., Heath, C. J., Mar, A. C., Horner, A. E., Bussey, T. J., & Saksida, L. M. (2013). The touchscreen operant platform for testing working memory and pattern separation in rats and mice. *Nature Protocols*, *8*(10), 2006–2021. https://doi.org/10.1038/nprot.2013.124

Orth, M., & Bellosta, S. (2012). Cholesterol: Its regulation and role in central nervous system disorders. *Cholesterol*, *2012*. https://doi.org/10.1155/2012/292598

Ossendorf, M., & Prellwitz, W. (2000). Rapid and easy apolipoprotein E genotyping using an improved PCR-RFLP technique. *Prenatal Diagnosis*, (1), 11–13. Retrieved from www.qiagen.com/clinical/

Otgaar, H., Memory, M. H.-, & 2014, undefined. (2013). What kind of memory has evolution wrought? Introductory Article for the Special Issue of Memory: Adaptive memory: The emergence and nature of proximate. *Taylor & Francis*, *22*(1), 1–8. https://doi.org/10.1080/09658211.2013.800355

Packard, M., memory, J. M.-N. of learning and, & 1996, undefined. (1996). Inactivation of hippocampus or caudate nucleus with lidocaine differentially affects expression of place and response learning. *Elsevier*, *65*, 65–72. https://doi.org/10.1006/nlme.1996.0007

Pan, Y.-W., Chan, G. C. K., Kuo, C. T., Storm, D. R., & Xia, Z. (2012). Inhibition of adult neurogenesis by inducible and targeted deletion of ERK5 mitogen-activated protein kinase specifically in adult neurogenic regions impairs. *Soc Neuroscience*. https://doi.org/10.1523/JNEUROSCI.6076-11.2012

Parslow, D. M., Morris, R. G., Fleminger, S., Rahman, Q., Abrahams, S., & Recce, M. (2005). Allocentric spatial memory in humans with hippocampal lesions. *Acta Psychologica*, *118*(1–2), 123–147. https://doi.org/10.1016/J.ACTPSY.2004.10.006

Patil, S. S., Sunyer, B., Höger, H., & Lubec, G. (2009). Evaluation of spatial memory of C57BL/6J and CD1 mice in the Barnes maze, the Multiple T-maze and in the Morris water maze. *Behavioural Brain Research*, *198*(1), 58–68. https://doi.org/10.1016/J.BBR.2008.10.029

Pause, B. M., Zlomuzica, A., Kinugawa, K., Mariani, J., Pietrowsky, R., & Dere, E. (2013). Perspectives on episodic-like and episodic memory. *Frontiers in Behavioral Neuroscience*, *0*(APR 2013), 33. https://doi.org/10.3389/FNBEH.2013.00033/BIBTEX

Pelkey, K. A., Chittajallu, R., Craig, M. T., Tricoire, L., Wester, J. C., & McBain, C. J. (2017). Hippocampal gabaergic inhibitory interneurons. *Physiological Reviews*, *97*(4), 1619–1747. https://doi.org/10.1152/physrev.00007.2017

Peng, X., Thierry-Mieg, J., Thierry-Mieg, D., Nishida, A., Pipes, L., Bozinoski, M., … Mason, C. E. (2015). Tissue-specific transcriptome sequencing analysis expands the non-human primate reference transcriptome resource (NHPRTR). *Nucleic Acids Research*, *43*(D1), D737–D742. https://doi.org/10.1093/NAR/GKU1110

Penner, M. R., Roth, T. L., Chawla, M. K., Hoang, L. T., Roth, E. D., Lubin, F. D., … Barnes, C. A. (2011). Age-related changes in Arc transcription and DNA methylation within the hippocampus. *Neurobiology of Aging*, *32*(12), 2198–2210. https://doi.org/10.1016/J.NEUROBIOLAGING.2010.01.009

Peris-Sampedro, F., Basaure, P., Reverte, I., Cabré, M., Domingo, J. L., & Colomina, M. T. (2015). Chronic exposure to chlorpyrifos triggered body weight increase and memory impairment depending on human apoE polymorphisms in a targeted replacement mouse model. *Physiology and Behavior*, *144*, 37–45. https://doi.org/10.1016/j.physbeh.2015.03.006

Pezze, M., & Bast, T. (2012). Dopaminergic modulation of hippocampus-dependent learning: Blockade of hippocampal D1-class receptors during learning impairs 1-trial place memory at a 30-min retention delay. *Neuropharmacology*, *63*(4), 710–718. https://doi.org/10.1016/J.NEUROPHARM.2012.05.036

Pignatelli, M., Ryan, T. J., Roy, D. S., Lovett, C., Smith, L. M., Muralidhar, S., & Tonegawa, S. (2019). Engram Cell Excitability State Determines the Efficacy of Memory Retrieval. *Neuron*, *101*(2), 274–284.e5. https://doi.org/10.1016/J.NEURON.2018.11.029

Piolino, P., Desgranges, B., Benali, K., & Eustache, F. (2002). Episodic and semantic remote autobiographical memory in ageing. *Memory*, *10*(4), 239–257. https://doi.org/10.1080/09658210143000353

Pitas, R. E., Boyles, J. K., Lee, S. H., Hui, D., & Weisgraber, K. H. (1987). Lipoproteins and their receptors in the central nervous system. Characterization of the lipoproteins in cerebrospinal fluid and identification of apolipoprotein B,E(LDL) receptors in the brain. *Journal of Biological Chemistry*, *262*(29), 14352–14360. https://doi.org/10.1016/s0021-9258(18)47945-8

Pohlkamp, T., Xian, X., Wong, C. H., Durakoglugil, M., Saido, T., Evers, B. M., … Herz, J. (2021). Endosomal Acidification by NHE6-depletion Corrects ApoE4-mediated Synaptic Impairments and Reduces Amyloid Plaque Load. *BioRxiv*, 2021.03.22.436385. https://doi.org/10.1101/2021.03.22.436385

Poll, S., Mittag, M., Musacchio, F., Justus, L. C., Giovannetti, E. A., Steffen, J., … Fuhrmann, M. (2020). Memory trace interference impairs recall in a mouse model of Alzheimer's disease. *Nature Neuroscience*, *23*(8), 952–958. https://doi.org/10.1038/s41593-020-0652-4

Pontifex, M. G., Martinsen, A., Saleh, R. N. M., Harden, G., Tejera, N., Müller, M., … Minihane, A. M. (2021). APOE4 genotype exacerbates the impact of menopause on cognition and synaptic plasticity in APOE-TR mice. *FASEB Journal*, *35*(5), e21583. https://doi.org/10.1096/fj.202002621RR

Poo, M., Pignatelli, M., Ryan, T. J., Tonegawa, S., Bonhoeffer, T., Martin, K. C., … Stevens, C. (2016). What is memory? The present state of the engram. *BMC Biology 2016 14:1*, *14*(1), 1–18. https://doi.org/10.1186/S12915-016-0261-6

Prasad, H., & Rao, R. (2018). Amyloid clearance defect in ApoE4 astrocytes is reversed by epigenetic correction of endosomal pH. *Proceedings of the National Academy of Sciences of the United States of America*, *115*(28), E6640–E6649. https://doi.org/10.1073/pnas.1801612115

Pravosudov, V. V., & Roth, T. C. (2013). Cognitive ecology of food hoarding: The evolution of spatial memory and the hippocampus. *Annual Review of Ecology, Evolution, and Systematics*, *44*, 173–193. https://doi.org/10.1146/annurev-ecolsys-110512-135904

Preibisch, S., Saalfeld, S., & Tomancak, P. (2009). Globally optimal stitching of tiled 3D microscopic image acquisitions. *Bioinformatics*, *25*(11), 1463–1465. https://doi.org/10.1093/bioinformatics/btp184

Prut, L., Abramowski, D., Krucker, T., Levy, C. L., Roberts, A. J., Staufenbiel, M., & Wiessner, C. (2007). Aged APP23 mice show a delay in switching to the use of a strategy in the Barnes maze. *Behavioural Brain Research*, *179*(1), 107–110. https://doi.org/10.1016/J.BBR.2007.01.017

Pyapali, G. K., Sik, A., Penttonen, M., Buzsaki, G., & Turner, D. A. (1998). Dendritic properties of hippocampal CA1 pyramidal neurons in the rat: Intracellular staining in vivo and in vitro. *Journal of Comparative Neurology*, *391*(3), 335–352. https://doi.org/10.1002/(SICI)1096-9861(19980216)391:3<335::AID-CNE4>3.0.CO;2-2

Qiao, F., Gao, X. P., Yuan, L., Cai, H. Y., & Qi, J. S. (2014). Apolipoprotein E4 impairs in vivo hippocampal long-term synaptic plasticity by reducing the phosphorylation of CaMKIIα and CREB. *Journal of Alzheimer's Disease*, *41*(4), 1165–1176. https://doi.org/10.3233/JAD-140375

Qin, Y., Qi, J. S., & Qiao, J. T. (2006). Apolipoprotein E4 suppresses delayed-rectifier potassium channels in membrane patches excised from hippocampal neurons. *Synapse*, *59*(2), 82–91. https://doi.org/10.1002/SYN.20201

Qiu, Z., Hyman, B. T., & Rebeck, G. W. (2004). Apolipoprotein E Receptors Mediate Neurite Outgrowth through Activation of p44/42 Mitogen-activated Protein Kinase in Primary Neurons. *Journal of Biological Chemistry*, *279*(33), 34948–34956. https://doi.org/10.1074/jbc.M401055200

Raber, J. (2008). AR, apoE, and cognitive function. *Hormones and Behavior*, *53*(5), 706–715. https://doi.org/10.1016/J.YHBEH.2008.02.012

Raber, J., Bongers, G., LeFevour, A., Buttini, M., & Mucke, L. (2002). Androgens Protect against Apolipoprotein E4-Induced Cognitive Deficits. *Journal of Neuroscience*, *22*(12), 5204–5209. https://doi.org/10.1523/jneurosci.22-12-05204.2002

Raber, J., Huang, Y., & Ashford, J. W. (2004). ApoE genotype accounts for the vast majority of AD risk and AD pathology. *Neurobiology of Aging*, *25*(5), 641–650. https://doi.org/10.1016/J.NEUROBIOLAGING.2003.12.023

Raber, J., Wong, D., Buttini, M., Orth, M., Bellosta, S., Pitas, R. E., … Mucke, L. (1998). Isoform-specific effects of human apolipoprotein E on brain function revealed in ApoE knockout mice: Increased susceptibility of females. *Neurobiology*, *95*, 10914–10919. Retrieved from www.pnas.org.

Raber, J., Wong, D., Yu, G. Q., Buttini, M., Mahley, R. W., Pitas, R. E., & Mucke, L. (2000). Apolipoprotein E and cognitive performance. *Nature 2000 404:6776*, *404*(6776), 352–354. https://doi.org/10.1038/35006165

Raffaï, R. L., Dong, L.-M., Farese, R. V, & Weisgraber, K. H. (2001). Introduction of human apolipoprotein E4 "domain interaction" into mouse apolipoprotein E. *Proceedings of the National Academy of Sciences*, *98*(20), 11587–11591.

Rajavashisth, T. B., Kaptein, J. S., Reue, K. L., & Lusis, A. J. (1985). *Evolution of apolipoprotein E: Mouse sequence and evidence for an 11-nucleotide ancestral unit*. *Proceedings of the National Academy of Sciences of the United States of America* (Vol. 82). https://doi.org/10.1073/pnas.82.23.8085

Ramakrishna, S., Jhaveri, V., Konings, S. C., Nawalpuri, B., Chakraborty, S., Holst, B., … Muddashetty, R. S. (2021). Apoe4 affects basal and nmdar-mediated protein synthesis in neurons by perturbing calcium homeostasis. *Journal of Neuroscience*, *41*(42), 8686–8709. https://doi.org/10.1523/JNEUROSCI.0435-21.2021

Ramaswamy, G., Xu, Q., Huang, Y., & Weisgraber, K. H. (2005). Effect of Domain Interaction on Apolipoprotein E Levels in Mouse Brain. *The Journal of Neuroscience*, *25*(46), 10658. https://doi.org/10.1523/JNEUROSCI.1922-05.2005

Ramirez, S., Liu, X., Lin, P. A., Suh, J., Pignatelli, M., Redondo, R. L., … Tonegawa, S. (2013). Creating a false memory in the hippocampus. *Science*, *341*(6144), 387–391. https://doi.org/10.1126/science.1239073

Rasia-Filho, A. R.-F. (2010). Dendritic spines observed by extracellular DiI dye and immunolabeling under confocal microscopy. *Protocol Exchange*. https://doi.org/10.1038/nprot.2010.153

Raulin, A. C., Kraft, L., Al-Hilaly, Y. K., Xue, W. F., McGeehan, J. E., Atack, J. R., & Serpell, L. (2019). The Molecular Basis for Apolipoprotein E4 as the Major Risk Factor for Late-Onset Alzheimer's Disease. *Journal of Molecular Biology*, *431*(12), 2248–2265. https://doi.org/10.1016/j.jmb.2019.04.019

Rebeck, G. W. (2017). The role of APOE on lipid homeostasis and inflammation in normal brains: Thematic Review Series: ApoE and Lipid Homeostasis in Alzheimer's Disease. *Journal of Lipid Research*, *58*(8), 1493–1499. https://doi.org/10.1194/JLR.R075408

Rebeck, G. W., Alonzo, N. C., Berezovska, O., Harr, S. D., Knowles, R. B., Growdon, J. H., … Mendez, A. J. (1998). Structure and Functions of Human Cerebrospinal Fluid Lipoproteins from Individuals of Different APOE Genotypes. *Experimental Neurology*, *149*(1), 175–182. https://doi.org/10.1006/EXNR.1997.6710

Reverte, I., Klein, A. B., Domingo, J. L., & Colomina, M. T. (2013). Long term effects of murine postnatal exposure to decabromodiphenyl ether (BDE-209) on learning and memory are dependent upon APOE polymorphism and age. *Neurotoxicology and Teratology*, *40*, 17–27. https://doi.org/10.1016/J.NTT.2013.08.003

Reverte, I., Klein, A. B., Ratner, C., Domingo, J. L., & Colomina, M. T. (2012). Behavioral phenotype and BDNF differences related to apoE isoforms and sex in young transgenic mice. *Experimental Neurology*, *237*(1), 116–125. https://doi.org/10.1016/J.EXPNEUROL.2012.06.015

Revilla, V., & Jones, A. (2002). Cryostat sectioning of brains. *International Review of Neurobiology*, *47*, 61–70. https://doi.org/10.1016/S0074-7742(02)47052-3

Riddell, D. R., Zhou, H., Atchison, K., Warwick, H. K., Atkinson, P. J., Jefferson, J., … Reinhart, P. H. (2008). Impact of Apolipoprotein E (ApoE) polymorphism on brain ApoE levels. *Journal of Neuroscience*, *28*(45), 11445–11453. https://doi.org/10.1523/JNEUROSCI.1972-08.2008

Riedel, G., Robinson, L., & Crouch, B. (2018). Spatial learning and flexibility in 129S2/SvHsd and C57BL/6J mouse strains using different variants of the Barnes maze. *Behavioural Pharmacology*, *29*(8), 688–700. https://doi.org/10.1097/FBP.0000000000000433

Robitsek, J., Ratner, M. H., Stewart, T., Eichenbaum, H., & Farb, D. H. (2015). Combined administration of levetiracetam and valproic acid attenuates age-related hyperactivity of CA3 place cells, reduces place field area, and increases spatial information content in aged rat hippocampus. *Hippocampus*, *25*(12), 1541–1555. https://doi.org/10.1002/HIPO.22474

Rodriguez, G. A., Burns, M. P., Weeber, E. J., & Rebeck, G. W. (2013). Young APOE4 targeted replacement mice exhibit poor spatial learning and memory, with reduced dendritic spine density in the medial entorhinal cortex. *Learning and Memory*, *20*(5), 256–266. https://doi.org/10.1101/lm.030031.112

Rolls, E. T. (2013). The mechanisms for pattern completion and pattern separation in the hippocampus. *Frontiers in Systems Neuroscience*, *7*(OCT), 74. https://doi.org/10.3389/FNSYS.2013.00074/BIBTEX

Rolls, E. T., & Kesner, R. P. (2006). A computational theory of hippocampal function, and empirical tests of the theory. *Progress in Neurobiology*, *79*(1), 1–48. https://doi.org/10.1016/j.pneurobio.2006.04.005

Rosenfeld, C. S., & Ferguson, S. A. (2014). Barnes maze testing strategies with small and large rodent models. *Journal of Visualized Experiments : JoVE*, (84), e51194. https://doi.org/10.3791/51194

Roy, D. S., Arons, A., Mitchell, T. I., Pignatelli, M., Ryan, T. J., & Tonegawa, S. (2016). Memory retrieval by activating engram cells in mouse models of early Alzheimer's disease. *Nature*, *531*(7595), 508–512. https://doi.org/10.1038/nature17172

Ruediger, S., Spirig, D., Donato, F., & Caroni, P. (2012). Goal-oriented searching mediated by ventral hippocampus early in trial-and-error learning. *Nature Neuroscience*, *15*(11), 1563–1571. https://doi.org/10.1038/nn.3224

Ruediger, S., Vittori, C., Bednarek, E., Genoud, C., Strata, P., Sacchetti, B., & Caroni, P. (2011). Learning-related feedforward inhibitory connectivity growth required for memory precision. *Nature*, *473*(7348), 514–518. https://doi.org/10.1038/nature09946

Ruiz, J., Kouiavskaia, D., Migliorini, M., Robinson, S., Saenko, E. L., Gorlatova, N., … Strickland, D. K. (2005). The apoE isoform binding properties of the VLDL receptor reveal marked differences from LRP and the LDL receptor. *Journal of Lipid Research*, *46*(8), 1721–1731. https://doi.org/10.1194/jlr.M500114-JLR200

Rusted, J. M., Evans, S. L., King, S. L., Dowell, N., Tabet, N., & Tofts, P. S. (2013). APOE e4 polymorphism in young adults is associated with improved attention and indexed by distinct neural signatures. *NeuroImage*, *65*, 364–373. https://doi.org/10.1016/J.NEUROIMAGE.2012.10.010

Ryan, T. J., de San Luis, C. O., Pezzoli, M., & Sen, S. (2021). Engram cell connectivity: an evolving substrate for information storage. *Current Opinion in Neurobiology*, *67*, 215–225. https://doi.org/10.1016/J.CONB.2021.01.006

Ryan, T. J., Roy, D. S., Pignatelli, M., Arons, A., & Tonegawa, S. (2015). Engram cells retain memory under retrograde amnesia. *Science*, *348*(6238), 1007–1013. https://doi.org/10.1126/science.aaa5542

Rydbirk, R., Folke, J., Winge, K., Aznar, S., Pakkenberg, B., & Brudek, T. (2016). Assessment of brain reference genes for RT-qPCR studies in neurodegenerative diseases. *Scientific Reports*, *6*(1), 1–11. https://doi.org/10.1038/srep37116

Sakamoto, T., Tanaka, M., Vedhachalam, C., Nickel, M., Nguyen, D., Dhanasekaran, P., … Saito, H. (2008). Contributions of the Carboxyl-Terminal Helical Segment to the Self-Association and Lipoprotein Preferences of Human Apolipoprotein E3 and E4 Isoforms†. *Biochemistry*, *47*(9), 2968–2977. https://doi.org/10.1021/BI701923H

Salomon-Zimri, S., Liraz, O., & Michaelson, D. M. (2015). Behavioral testing affects the phenotypic expression of APOE ε3 and APOE ε4 in targeted replacement mice and reduces the differences between them

Sasaguri, H., Nilsson, P., Hashimoto, S., Nagata, K., Saito, T., Strooper, B. De, … Saido, T. C. (2017). APP mouse models for Alzheimer's disease preclinical studies. *The EMBO Journal*, *36*(17), 2473–2487. https://doi.org/10.15252/EMBJ.201797397

Sasaki, T., Piatti, V. C., Hwaun, E., Ahmadi, S., Lisman, J. E., Leutgeb, S., & Leutgeb, J. K. (2018). Dentate network activity is necessary for spatial working memory by supporting CA3 sharp-wave ripple generation and prospective firing of CA3 neurons. *Nature Neuroscience*, *21*(2), 258–269. https://doi.org/10.1038/s41593-017-0061-5

Schachtele, S. J., Losh, J., Dailey, M. E., & Green, S. H. (2011). Spine Formation and Maturation in the Developing Rat Auditory Cortex. *The Journal of Comparative Neurology*, *519*(16), 3327. https://doi.org/10.1002/CNE.22728

Scharfman, H. E. (2016). The enigmatic mossy cell of the dentate gyrus. *Nature Reviews Neuroscience*, *17*(9), 562–575. https://doi.org/10.1038/nrn.2016.87

Scharfman, H. E., & Myers, C. E. (2012). Hilar mossy cells of the dentate gyrus: A historical perspective. *Frontiers in Neural Circuits*, *0*(DEC), 106. https://doi.org/10.3389/FNCIR.2012.00106/BIBTEX

Schmitt, J., Paradis, A. L., Boucher, M., Andrieu, L., Barnéoud, P., & Rondi-Reig, L. (2021). Flexibility as a marker of early cognitive decline in humanized apolipoprotein E ε4 (ApoE4) mice. *Neurobiology of Aging*, *102*, 129–138. https://doi.org/10.1016/J.NEUROBIOLAGING.2021.01.013

Schott, J. M., Fox, N. C., & Rossor, M. N. (2002). Genetics of the dementias. *Journal of Neurology, Neurosurgery & Psychiatry*, *73*(suppl 2), ii27-ii31. https://doi.org/10.1136/JNNP.73.SUPPL_2.II27

Schultz, C., & Engelhardt, M. (2014). Anatomy of the hippocampal formation. *The Hippocampus in Clinical Neuroscience*, *34*, 6–17. https://doi.org/10.1159/000360925

Segev, A., Yanagi, M., Scott, D., Southcott, S. A., Lister, J. M., Tan, C., … Tamminga, C. A. (2018). Reduced GluN1 in mouse dentate gyrus is associated with CA3 hyperactivity and psychosis-like behaviors. *Molecular Psychiatry*, *25*(11), 2832–2843. https://doi.org/10.1038/s41380-018-0124-3

Selkoe, D. J. (2001). Alzheimer's disease: Genes, proteins, and therapy. *Physiological Reviews*, *81*(2), 741–766. https://doi.org/10.1152/PHYSREV.2001.81.2.741/ASSET/IMAGES/LARGE/9J0210134004.JPEG

Semon, R. (1921). *The mneme*. *G. Allen & Unwin Limited*. Retrieved from https://books.google.co.uk/books?hl=en&lr=&id=rFfuAgAAQBAJ&oi=fnd&pg=PA17&ots=4e3J8klgP-&sig=VJWSufFMBbCUF9SF41fE3umntus

Serino, S., Cipresso, P., Morganti, F., & Riva, G. (2014). The role of egocentric and allocentric abilities in Alzheimer's disease: A systematic review. *Ageing Research Reviews*, *16*(1), 32–44. https://doi.org/10.1016/J.ARR.2014.04.004

Shang, Y., Mishra, A., Wang, T., Wang, Y., Desai, M., Chen, S., … Brinton, R. D. (2020). Evidence in support of chromosomal sex influencing plasma based metabolome vs APOE genotype influencing brain metabolome profile in humanized APOE male and female mice. *PLoS ONE*, *15*(1), e0225392. https://doi.org/10.1371/journal.pone.0225392

Sharma, S., Rakoczy, S., & Brown-Borg, H. (2010). Assessment of spatial memory in mice. *Life Sciences*, *87*(17–18), 521–536. https://doi.org/10.1016/J.LFS.2010.09.004

Shaw, K., Bell, L., Boyd, K., Grijseels, D. M., Clarke, D., Bonnar, O., … Hall, C. N. (2021). Neurovascular coupling and oxygenation are decreased in hippocampus compared to neocortex because of microvascular differences. *Nature Communications*, *12*(1). https://doi.org/10.1038/S41467-021-23508-Y

Shea, Y. F., Chu, L. W., Chan, A. O. K., Ha, J., Li, Y., & Song, Y. Q. (2016). A systematic review of familial Alzheimer's disease: Differences in presentation of clinical features among three mutated genes and potential ethnic differences. *Journal of the Formosan Medical Association*, *115*(2), 67–75. https://doi.org/10.1016/j.jfma.2015.08.004

Sheppard, D. P., Graves, L. V., Holden, H. M., Delano-Wood, L., Bondi, M. W., & Gilbert, P. E. (2016). Spatial pattern separation differences in older adult carriers and non-carriers for the apolipoprotein E epsilon 4 allele. *Neurobiology of Learning and Memory*, *129*, 113–119. https://doi.org/10.1016/J.NLM.2015.04.011

Sherry, D. F., & Schacter, D. L. (1987). The Evolution of Multiple Memory Systems. *Psychological Review*, *94*(4), 439–454. https://doi.org/10.1037/0033-295X.94.4.439

Shi, L., Du, X., Zhou, H., Tao, C., Liu, Y., Meng, F., … Zhou, J.-N. (2014). Cumulative effects of the ApoE genotype and gender on the synaptic proteome and oxidative stress in the mouse brain. *The International Journal of Neuropsychopharmacology*, *17*(11), 1863–1879. https://doi.org/10.1017/S1461145714000601

Shi, Y., Yamada, K., Liddelow, S. A., Smith, S. T., Zhao, L., Luo, W., … Holtzman, D. M. (2017). ApoE4 markedly exacerbates tau-mediated neurodegeneration in a mouse model of tauopathy. *Nature 2017 549:7673*, *549*(7673), 523–527. https://doi.org/10.1038/nature24016

Shinohara, M. M., Kanekiyo, T., Yang, L., Linthicum, D., Shinohara, M. M., Fu, Y., … Bu, G. (2016). APOE2 eases cognitive decline during Aging: Clinical and preclinical evaluations. *Annals of Neurology*, *79*(5), 758–774. https://doi.org/10.1002/ANA.24628

Shukitt-Hale, B., McEwen, J. J., Szprengiel, A., & Joseph, J. A. (2004). Effect of age on the radial arm water maze—a test of spatial learning and memory. *Neurobiology of Aging*, *25*(2), 223–229. https://doi.org/10.1016/S0197-4580(03)00041-1

Siegel, J. A., Haley, G. E., & Raber, J. (2012). Apolipoprotein E isoform-dependent effects on anxiety and cognition in female TR mice. *Neurobiology of Aging*, *33*(2), 345–358. https://doi.org/10.1016/J.NEUROBIOLAGING.2010.03.002

Sinclair, L. I., Button, K. S., Munafò, M. R., Day, I. N. M., & Lewis, G. (2015). Possible association of APOE genotype with working memory in young adults. *PLoS ONE*, *10*(8), e0135894. https://doi.org/10.1371/journal.pone.0135894

Singer, B. F., Bubula, N., Li, D., Przybycien-Szymanska, M. M., Bindokas, V. P., & Vezina, P. (2016). Drug-Paired Contextual Stimuli Increase Dendritic Spine Dynamics in Select Nucleus Accumbens Neurons. *Neuropsychopharmacology 2016 41:8*, *41*(8), 2178–2187. https://doi.org/10.1038/npp.2016.39

Singh, P., Singh, M., biology, S. M.-A. of human, & 2006, undefined. (2006). APOE distribution in world populations with new data from India and the UK. *Taylor & Francis*, *33*(3), 279–308. https://doi.org/10.1080/03014460600594513

Šišková, Z., Justus, D., Kaneko, H., Friedrichs, D., Henneberg, N., Beutel, T., … Remy, S. (2014). Dendritic Structural Degeneration Is Functionally Linked to Cellular Hyperexcitability in a Mouse Model of Alzheimer's Disease. *Neuron*, *84*(5), 1023–1033. https://doi.org/10.1016/J.NEURON.2014.10.024

Small, B. J., Rosnick, C. B., Fratiglioni, L., & Bäckman, L. (2004). Apolipoprotein E and cognitive performance: A meta-analysis. *Psychology and Aging*, *19*(4), 592–600. https://doi.org/10.1037/0882-7974.19.4.592

Small, S. A., Tsai, W. Y., Delapaz, R., Mayeux, R., & Stern, Y. (2002). Imaging hippocampal function across the human life span: Is memory decline normal or not? *Annals of Neurology*, *51*(3), 290–295. https://doi.org/10.1002/ANA.10105

Speidell, A. P., Demby, T., Lee, Y., Rodriguez, O., Albanese, C., Mandelblatt, J., & Rebeck, G. W. (2019). Development of a Human APOE Knock-in Mouse Model for Study of Cognitive Function After Cancer Chemotherapy. *Neurotoxicity Research*, *35*(2), 291–303. https://doi.org/10.1007/s12640-018-9954-7

Spiegel, A. M., Koh, M. T., Vogt, N. M., Rapp, P. R., & Gallagher, M. (2013). Hilar interneuron vulnerability distinguishes aged rats with memory impairment. *Journal of Comparative Neurology*, *521*(15), 3508–3523. https://doi.org/10.1002/CNE.23367

Sprague, J. E., Preston, A. S., Leifheit, M., & Woodside, B. (2003). Hippocampal serotonergic damage induced by MDMA (ecstasy): effects on spatial learning. *Physiology & Behavior*, *79*(2), 281–287. https://doi.org/10.1016/S0031-9384(03)00092-1

Squire, L. R. (2004). Memory systems of the brain: A brief history and current perspective. *Neurobiology of Learning and Memory*, *82*(3), 171–177. https://doi.org/10.1016/J.NLM.2004.06.005

Stark, S. M., Yassa, M. A., Lacy, J. W., & Stark, C. E. L. (2013). A task to assess behavioral pattern separation (BPS) in humans: Data from healthy aging and mild cognitive impairment. *Neuropsychologia*, *51*(12), 2442–2449. https://doi.org/10.1016/J.NEUROPSYCHOLOGIA.2012.12.014

Steele, R. J., & Morris, R. G. M. (1999). Delay-dependent impairment of a matching-to-place task with chronic and intrahippocampal infusion of the NMDA-antagonist D-AP5. *Hippocampus*, *9*(2), 118–136. https://doi.org/10.1002/(SICI)1098-1063(1999)9:2<118::AID-HIPO4>3.0.CO;2-8

Stefanelli, T., Bertollini, C., Lüscher, C., Muller, D., & Mendez, P. (2016). Hippocampal Somatostatin Interneurons Control the Size of Neuronal Memory Ensembles. *Neuron*, *89*(5), 1074–1085. https://doi.org/10.1016/j.neuron.2016.01.024

Stranahan, A. M., & Mattson, M. P. (2010). Selective vulnerability of neurons in layer II of the entorhinal cortex during aging and Alzheimer's disease. *Neural Plasticity*, *2010*. https://doi.org/10.1155/2010/108190

Strange, B. A., Witter, M. P., Lein, E. S., & Moser, E. I. (2014). Functional organization of the hippocampal longitudinal axis. *Nature Reviews Neuroscience*, *15*(10), 655–669. https://doi.org/10.1038/nrn3785

Sullivan, P. M., Han, B., Liu, F., Mace, B. E., Ervin, J. F., Wu, S., … Bales, K. R. (2011). Reduced levels of human apoE4 protein in an animal model of cognitive impairment. *Neurobiology of Aging*, *32*(5), 791–801. https://doi.org/10.1016/J.NEUROBIOLAGING.2009.05.011

Sullivan, P. M., Mace, B. E., Maeda, N., & Schmechel, D. E. (2004). Marked regional differences of brain human apolipoprotein e expression in targeted replacement mice. *Neuroscience*, *124*(4), 725–733. https://doi.org/10.1016/J.NEUROSCIENCE.2003.10.011

Sullivan, P. M., Mezdour, H., Aratani, Y., Knouff, C., Najib, J., Reddick, R. L., … Maeda, N. (1997). Targeted Replacement of the Mouse Apolipoprotein E Gene with the Common Human APOE3 Allele Enhances Diet-induced Hypercholesterolemia and Atherosclerosis. *Journal of Biological Chemistry*, *272*(29), 17972–17980. https://doi.org/10.1074/JBC.272.29.17972

Sun, G. Z., He, Y. C., Ma, X. K., Li, S. T., Chen, D. J., Gao, M., … Wu, J. (2017). Hippocampal synaptic and neural network deficits in young mice carrying the human APOE4 gene. *CNS Neuroscience and Therapeutics*, *23*(9), 748–758. https://doi.org/10.1111/cns.12720

Sun, Y., Wu, S., Bu, G., Onifade, M. K., Patel, S. N., LaDu, M. J., … Holtzman, D. M. (1998). Glial Fibrillary Acidic Protein–Apolipoprotein E (apoE) Transgenic Mice: Astrocyte-Specific Expression and Differing Biological Effects of Astrocyte-Secreted apoE3 and apoE4 Lipoproteins. *Journal of Neuroscience*, *18*(9), 3261–3272. https://doi.org/10.1523/JNEUROSCI.18-09-03261.1998

Sung, H. Y., Park, K. A., Kwon, S., Woolley, C. S., Sullivan, P. M., Pasternak, J. F., & Trommer, B. L. (2007). Estradiol enhances long term potentiation in hippocampal slices from aged ApoE4-TR mice. *Hippocampus*, *17*(12), 1153–1157. https://doi.org/10.1002/hipo.20357

Tai, L. M., Balu, D., Avila-Munoz, E., Abdullah, L., Thomas, R., Collins, N., … LaDu, M. J. (2017). EFAD transgenic mice as a human APOE relevant preclinical model of Alzheimer'ns disease [S]. *Journal of Lipid Research*, *58*(9), 1733–1755. https://doi.org/10.1194/JLR.R076315

Tai, L. M., Maldonado Weng, J., LaDu, M. J., & Brady, S. T. (2021). Relevance of transgenic mouse models for Alzheimer's disease. *Progress in Molecular Biology and Translational Science*, *177*, 1–48. https://doi.org/10.1016/bs.pmbts.2020.07.007

Tai, L. M., Youmans, K. L., Jungbauer, L., Yu, C., & LaDu, M. J. (2011). Introducing human APOE into Aβ transgenic mouse models. *International Journal of Alzheimer's Disease*. https://doi.org/10.4061/2011/810981

Takeuchi, T., Duszkiewicz, A. J., Sonneborn, A., Spooner, P. A., Yamasaki, M., Watanabe, M., … Morris, R. G. M. (2016). Locus coeruleus and dopaminergic consolidation of everyday memory. *Nature*, *537*(7620), 357–362. https://doi.org/10.1038/nature19325

Tamboli, I. Y., Heo, D., & Rebeck, G. W. (2014). Extracellular proteolysis of apolipoprotein e (apoE) by secreted serine neuronal protease. *PLoS ONE*, *9*(3). https://doi.org/10.1371/journal.pone.0093120

Tanaka, K. Z., He, H., Tomar, A., Niisato, K., Huang, A. J. Y., & McHugh, T. J. (2018). The hippocampal engram maps experience but not place. *Science*, *361*(6400), 392–397. https://doi.org/10.1126/science.aat5397

Tanaka, K. Z., Pevzner, A., Hamidi, A. B., Nakazawa, Y., Graham, J., & Wiltgen, B. J. (2014). Cortical Representations Are Reinstated by the Hippocampus during Memory Retrieval. *Neuron*, *84*(2), 347–354. https://doi.org/10.1016/J.NEURON.2014.09.037

Tang, K. F., Cai, L., & Zhou, J. N. (2009). Observation of the density and size of cells in hippocampus and vascular lesion in thalamus of GFAP-apoE transgenic mice. *Neuroscience Bulletin*, *25*(4), 167. https://doi.org/10.1007/S12264-009-0324-6

Taylor, S. C., Nadeau, K., Abbasi, M., Lachance, C., Nguyen, M., & Fenrich, J. (2019). The Ultimate qPCR Experiment: Producing Publication Quality, Reproducible Data the First Time. *Trends in Biotechnology*, *37*(7), 761–774. https://doi.org/10.1016/J.TIBTECH.2018.12.002

Taylor, S., Wakem, M., Dijkman, G., Alsarraj, M., & Nguyen, M. (2010). A practical approach to RT-qPCR-Publishing data that conform to the MIQE guidelines. *Methods*, *50*(4), S1. https://doi.org/10.1016/j.ymeth.2010.01.005

Tensaouti, Y., Stephanz, E. P., Yu, T. S., & Kernie, S. G. (2018). ApoE Regulates the Development of Adult Newborn Hippocampal Neurons. *ENeuro*, *5*(4). https://doi.org/10.1523/ENEURO.0155-18.2018

Tensaouti, Y., Yu, T. S., & Kernie, S. G. (2020). Apolipoprotein e regulates the maturation of injury-induced adult-born hippocampal neurons following traumatic brain injury. *PLoS ONE*, *15*(3), e0229240. https://doi.org/10.1371/journal.pone.0229240

Tesseur, I., Van Dorpe, J., Bruynseels, K., Bronfman, F., Sciot, R., Van Lommel, A., & Van Leuven, F. (2000). Prominent axonopathy and disruption of axonal transport in transgenic mice expressing human apolipoprotein E4 in neurons of brain and spinal cord. *American Journal of Pathology*, *157*(5), 1495–1510. https://doi.org/10.1016/S0002-9440(10)64788-8

Theendakara, V., Peters-Libeu, C. A., Bredesen, D. E., & Rao, R. V. (2018). Transcriptional Effects of ApoE4: Relevance to Alzheimer's Disease. *Molecular Neurobiology*, *55*(6), 5243–5254. https://doi.org/10.1007/s12035-017-0757-2

Theendakara, V., Peters-Libeu, C. A., Spilman, P., Poksay, K. S., Bredesen, D. E., & Rao, R. V. (2016). Direct transcriptional effects of apolipoprotein E. *Journal of Neuroscience*, *36*(3), 685–700. https://doi.org/10.1523/JNEUROSCI.3562-15.2016

Thinakaran, G., & Koo, E. H. (2008). Amyloid Precursor Protein Trafficking, Processing, and Function. *Journal of Biological Chemistry*, *283*(44), 29615–29619. https://doi.org/10.1074/JBC.R800019200

Thomas, G. M., & Huganir, R. L. (2004). MAPK cascade signalling and synaptic plasticity. *Nature Reviews Neuroscience*, *5*(3), 173–183. https://doi.org/10.1038/nrn1346

Tilley, L., Morgan, K., & Kalsheker, N. (1998). Genetic risk factors in Alzheimer's disease. *Molecular Pathology*, *51*(6), 293. https://doi.org/10.1136/MP.51.6.293

Tokuda, T., Calero, M., Matsubara, E., Vidal, R., Kumar, A., Permanne, B., … Ghiso, J. (2000). Lipidation of apolipoprotein E influences its isoform-specific interaction with Alzheimer's amyloid β peptides. *Biochemical Journal*, *348*(2), 359–365. https://doi.org/10.1042/0264-6021:3480359

Tolar, M., Keller, J. N., Chan, S., Mattson, M. P., Marques, M. A., & Crutcher, K. A. (1999). *Truncated apolipoprotein E (ApoE) causes increased intracellular calcium and may mediate ApoE neurotoxicity*. *Journal of Neuroscience* (Vol. 19). https://doi.org/10.1523/jneurosci.19-16-07100.1999

Tonegawa, S., Liu, X., Ramirez, S., & Redondo, R. (2015). Memory Engram Cells Have Come of Age. *Neuron*, *87*(5), 918–931. https://doi.org/10.1016/J.NEURON.2015.08.002

Tonegawa, S., Pignatelli, M., Roy, D. S., & Ryan, T. J. (2015). Memory engram storage and retrieval. *Current Opinion in Neurobiology*, *35*, 101–109. https://doi.org/10.1016/J.CONB.2015.07.009

Tong, L. M., Djukic, B., Arnold, C., Gillespie, A. K., Yoon, S. Y., Wang, M. M., … Huang, Y. (2014). Inhibitory interneuron progenitor transplantation restores normal learning and memory in ApoE4 knock-in mice without or with Aβ accumulation. *Journal of Neuroscience*, *34*(29), 9506–9515. https://doi.org/10.1523/JNEUROSCI.0693-14.2014

Tong, L. M., Yoon, S. Y., Andrews-Zwilling, Y., Yang, A., Lin, V., Lei, H., & Huang, Y. (2016). Enhancing GABA signaling during middle adulthood prevents age-dependent GABAergic interneuron decline and learning and memory deficits in ApoE4 mice. *Soc Neuroscience*. https://doi.org/10.1523/JNEUROSCI.3815-15.2016

Tran, T. T., Speck, C. L., Pisupati, A., Gallagher, M., & Bakker, A. (2017). Increased hippocampal activation in ApoE-4 carriers and non-carriers with amnestic mild cognitive impairment. *NeuroImage: Clinical*, *13*, 237–245. https://doi.org/10.1016/j.nicl.2016.12.002

Trivino-Paredes, J. S., Nahirney, P. C., Pinar, C., Grandes, P., & Christie, B. R. (2019). Acute slice preparation for electrophysiology increases spine numbers equivalently in the male and female juvenile hippocampus: A DiI labeling study. *Journal of Neurophysiology*, *122*(3), 958–969. https://doi.org/10.1152/jn.00332.2019

Trommer, B. L., Shah, C., Yun, S. H., Gamkrelidze, G., Pasternak, E. S., Ye, G. L., … LaDu, M. J. (2004). ApoE isoform affects LTP in human targeted replacement mice. *NeuroReport*, *15*(17), 2655–2658. https://doi.org/10.1097/00001756-200412030-00020

Tuckwell, H. C. (2019). *Transcription of Fos family genes in nucleus accumbens: roles of AP-1, epigenetics and stochasticity*. *Researchgate preprint*. Retrieved from https://www.researchgate.net/publication/337085551

Tulving, E. (1972). 12. Episodic and Semantic Memory. *Academic Press*, 381–403. Retrieved from http://alumni.media.mit.edu/~jorkin/generals/papers/Tulving_memory.pdf

Tulving, E. (2002). Episodic memory: From mind to brain. *Annual Review of Psychology*, *53*, 1–25. https://doi.org/10.1146/annurev.psych.53.100901.135114

Tulving, E., & Markowitsch, H. J. (1998). Episodic and declarative memory: Role of the hippocampus. *Hippocampus*, *8*(3), 198–204. https://doi.org/10.1002/(SICI)1098-1063(1998)8:3<198::AID-HIPO2>3.0.CO;2-G

Twine, N. A., Janitz, K., Wilkins, M. R., & Janitz, M. (2011). Whole transcriptome sequencing reveals gene expression and splicing differences in brain regions affected by Alzheimer's disease. *PLoS ONE*, *6*(1), e16266. https://doi.org/10.1371/journal.pone.0016266

Tzioras, M., Davies, C., Newman, A., Jackson, R., & Spires-Jones, T. (2019). Invited Review: APOE at the interface of inflammation, neurodegeneration and pathological protein spread in Alzheimer's disease. *Neuropathology and Applied Neurobiology*, *45*(4), 327–346. https://doi.org/10.1111/NAN.12529

Uhlen, M., Lindskog, C., Lundberg, E., Ponten, F., Mulder, J., Nielsen, J., … Ahlen, I. (2015). Tissue-based map of the human proteome. *Science*, *347*, 1260419. Retrieved from https://www.proteinatlas.org/

Ulrich, J. D., Burchett, J. M., Restivo, J. L., Schuler, D. R., Verghese, P. B., Mahan, T. E., … Holtzman, D. M. (2013). In vivo measurement of apolipoprotein E from the brain interstitial fluid using microdialysis. *Molecular Neurodegeneration*, *8*(1), 13. https://doi.org/10.1186/1750-1326-8-13

Uriarte, M., Ogundele, O. M., & Pardo, J. (2017). Long-lasting training in the Barnes maze prompts hippocampal spinogenesis and habituation in rats. *NeuroReport*, *28*(6), 307–312. https://doi.org/10.1097/WNR.0000000000000755

van Groen, T., Miettinen, P., & Kadish, I. (2003). The entorhinal cortex of the mouse: Organization of the projection to the hippocampal formation. *Hippocampus*, *13*(1), 133–149. https://doi.org/10.1002/hipo.10037

van Meer, P., Acevedo, S., & Raber, J. (2007). Impairments in spatial memory retention of GFAP-apoE4 female mice. *Behavioural Brain Research*, *176*(2), 372–375. https://doi.org/10.1016/J.BBR.2006.10.024

Van Strien, N. M., Cappaert, N. L. M., & Witter, M. P. (2009). The anatomy of memory: An interactive overview of the parahippocampal- hippocampal network. *Nature Reviews Neuroscience*, *10*(4), 272–282. https://doi.org/10.1038/nrn2614

VanElzakker, M., Fevurly, R. D., Breindel, T., & Spencer, R. L. (2008). Environmental novelty is associated with a selective increase in Fos expression in the output elements of the hippocampal formation and the perirhinal cortex. *Learning and Memory*, *15*(12), 899–908. https://doi.org/10.1101/lm.1196508

Vazdarjanova, A., Guzowski,J. of,. (2004). Differences in hippocampal neuronal population responses to modifications of an environmental context: evidence for distinct, yet complementary, functions of CA3. *Soc Neuroscience*. https://doi.org/10.1523/JNEUROSCI.0350-04.2004

Veinbergs, I., Mallory, M., Mante, M., Rockenstein, E., Gilbert, J. R., & Masliah, E. (1999). Differential neurotrophic effects of apolipoprotein E in aged transgenic mice. *Neuroscience Letters*, *265*(3), 218–222. https://doi.org/10.1016/S0304-3940(99)00243-8

Verghese, P. B., Castellano, J. M., Garai, K., Wang, Y., Jiang, H., Shah, A., … Holtzman, D. M. (2013). ApoE influences amyloid-β (Aβ) clearance despite minimal apoE/Aβ association in physiological conditions. *Proceedings of the National Academy of Sciences of the United States of America*, *110*(19). https://doi.org/10.1073/pnas.1220484110

Villasana, L. E., Benice, T. S., & Raber, J. (2011). Long-Term Effects of 56Fe Irradiation on Spatial Memory of Mice: Role of Sex and Apolipoprotein E Isoform. *International Journal of Radiation*, *80*(2), 567–573. https://doi.org/10.1016/J.IJROBP.2010.12.034

Villasana, L. E., Weber, S., Akinyeke, T., & Raber, J. (2016). Genotype differences in anxiety and fear learning and memory of WT and ApoE4 mice associated with enhanced generation of hippocampal reactive oxygen species. *Journal of Neurochemistry*, *138*(6), 896–908. https://doi.org/10.1111/JNC.13737

Villasana, L., Acevedo, S., Poage, C., & Raber, J. (2006). Sex- and APOE isoform-dependent effects of radiation on cognitive function. *Radiation Research*, *166*(6), 883–891. https://doi.org/10.1667/RR0642.1

Viola, H., Ballarini, F., Martínez, M. C., & Moncada, D. (2014). The Tagging and Capture Hypothesis from Synapse to Memory. *Progress in Molecular Biology and Translational Science*, *122*, 391–423. https://doi.org/10.1016/B978-0-12-420170-5.00013-1

Vitale, P., Salgueiro-Pereira, A. R., Lupascu, C. A., Willem, M., Migliore, R., Migliore, M., & Marie, H. (2021). Analysis of Age-Dependent Alterations in Excitability Properties of CA1 Pyramidal Neurons in an APPPS1 Model of Alzheimer's Disease. *Frontiers in Aging Neuroscience*, *13*, 302. https://doi.org/10.3389/FNAGI.2021.668948/BIBTEX

Vorhees, C. V., & Williams, M. T. (2014). Assessing Spatial Learning and Memory in Rodents. *ILAR Journal*, *55*(2), 310–332. https://doi.org/10.1093/ILAR/ILU013

Vorhees, C. V., & Williams, M. T. (2006). Morris water maze: Procedures for assessing spatial and related forms of learning and memory. *Nature Protocols*, *1*(2), 848–858. https://doi.org/10.1038/nprot.2006.116

Vorhees, C. V., & Williams, M. T. (2014). Value of water mazes for assessing spatial and egocentric learning and memory in rodent basic research and regulatory studies. *Neurotoxicology and Teratology*, *45*, 75–90. https://doi.org/10.1016/J.NTT.2014.07.003

Vyleta, N. P., Borges-Merjane, C., & Jonas, P. (2016). Plasticity-dependent, full detonation at hippocampal mossy fiber–CA3 pyramidal neuron synapses. *ELife*, *5*. https://doi.org/10.7554/eLife.17977

Wahrle, S. E., Jiang, H., Parsadanian, M., Legleiter, J., Han, X., Fryer, J. D., … Holtzman, D. M. (2004). ABCA1 Is Required for Normal Central Nervous System ApoE Levels and for Lipidation of Astrocyte-secreted apoE. *Journal of Biological Chemistry*, *279*(39), 40987–40993. https://doi.org/10.1074/JBC.M407963200

Wang, C., Chen, X., & Knierim, J. J. (2020). Egocentric and allocentric representations of space in the rodent brain. *Current Opinion in Neurobiology*, *60*, 12–20. https://doi.org/10.1016/J.CONB.2019.11.005

Wang, C., Najm, R., Xu, Q., Jeong, D. E., Walker, D., Balestra, M. E., … Huang, Y. (2018). Gain of toxic Apolipoprotein E4 effects in Human iPSC-Derived Neurons Is Ameliorated by a Small-Molecule Structure Corrector. *Nature Medicine*, *24*(5), 647. https://doi.org/10.1038/S41591-018-0004-Z

Wang, C., Wilson, W. A., Moore, S. D., Mace, B. E., Maeda, N., Schmechel, D. E., & Sullivan, P. M. (2005). Human apoE4-targeted replacement mice display synaptic deficits in the absence of neuropathology. *Neurobiology of Disease*, *18*(2), 390–398. https://doi.org/10.1016/J.NBD.2004.10.013

Wang, S. H. (2018). Novelty enhances memory persistence and remediates propranolol-induced deficit via reconsolidation. *Neuropharmacology*, *141*, 42–54. https://doi.org/10.1016/J.NEUROPHARM.2018.08.015

Wang, X. shu, Ciraolo, G., Morris, R., & Gruenstein, E. (1997). Identification of a neuronal endocytic pathway activated by an apolipoprotein E (apoE) receptor binding peptide. *Brain Research*, *778*(1), 6–15. https://doi.org/10.1016/S0006-8993(97)00877-9

Ward, A., Crean, S., Mercaldi, C. J., Collins, J. M., Boyd, D., Cook, M. N., & Arrighi, H. M. (2012). Prevalence of Apolipoprotein E4 genotype and homozygotes (APOE e4/4) among patients diagnosed with alzheimer's disease: A systematic review and meta-analysis. *Neuroepidemiology*, *38*(1), 1–17. https://doi.org/10.1159/000334607

Weisgraber, K. H., Innerarity, T. L., & Mahley, R. W. (1982). Abnormal lipoprotein receptor-binding activity of the human E apoprotein due to cysteine-arginine interchange at a single site. *Journal of Biological Chemistry*, *257*(5), 2518–2521. https://doi.org/10.1016/S0021-9258(18)34954-8

Weisgraber, K. H., Rall, S. C., & Mahley, R. W. (1981). Human E apoprotein heterogeneity. Cysteine-arginine interchanges in the amino acid sequence of the apo-E isoforms. *Journal of Biological Chemistry*, *256*(17), 9077–9083. https://doi.org/10.1016/s0021-9258(19)52510-8

Weisgraber, K. H. (1994). Apolipoprotein E: Structure-Function Relationships. *Advances in Protein Chemistry*, *45*, 249–302. https://doi.org/10.1016/S0065-3233(08)60642-7

Weisgraber, K. H., & Mahley, R. W. (1996). Human apolipoprotein E: the Alzheimer's disease connection. *The FASEB Journal*, *10*(13), 1485–1494. https://doi.org/10.1096/FASEBJ.10.13.8940294

Wenk, G. L. (2004). Assessment of Spatial Memory Using the Radial Arm Maze and Morris Water Maze. *Current Protocols in Neuroscience*, *26*(1). https://doi.org/10.1002/0471142301.ns0805as26

Whitaker, L. R., & Hope, B. T. (2018). Chasing the addicted engram: Identifying functional alterations in Fos-expressing neuronal ensembles that mediate drug-related learned behavior. *Learning and Memory*, *25*(9), 455–460. https://doi.org/10.1101/lm.046698.117

White, F., Horsburgh, K., Nicoll, J. A. R., Horsburgh, K., & Roses, A. D. (2001). Impaired Neuronal Plasticity in Transgenic Mice Expressing Human Apolipoprotein E4 Compared to E3 in a Model of Entorhinal Cortex Lesion. *Neurobiology of Disease*, *8*(4), 611–625. https://doi.org/10.1006/NBDI.2001.0401

Wiesmann, M., Zerbi, V., Jansen, D., Haast, R., Lütjohann, D., Broersen, L. M., … Kiliaan, A. J. (2016). A Dietary Treatment Improves Cerebral Blood Flow and Brain Connectivity in Aging apoE4 Mice. *Neural Plasticity*, *2016*. https://doi.org/10.1155/2016/6846721

Williams, J. G., Huppert, F. A., Matthews, F. E., & Nickson, J. (2003). Performance and normative values of a concise neuropsychological test (CAMCOG) in an elderly population sample. *International Journal of Geriatric Psychiatry*, *18*(7), 631–644. https://doi.org/10.1002/GPS.886

Wilson, B., Cockburn, J., Baddeley, A., & Hiorns, R. (1989). The development and validation of a test battery for detecting and monitoring everyday memory problems. *Journal of Clinical and Experimental Neuropsychology*, *11*(6), 855–870. https://doi.org/10.1080/01688638908400940

Wisniewski, T., & Drummond, E. (2020). APOE-amyloid interaction: Therapeutic targets. *Neurobiology of Disease*, *138*, 104784. https://doi.org/10.1016/J.NBD.2020.104784

Wu, M. V., Luna, V. M., & Hen, R. (2015). Running rescues a fear-based contextual discrimination deficit in aged mice. *Frontiers in Systems Neuroscience*, *9*(AUGUST), 114. https://doi.org/10.3389/FNSYS.2015.00114/BIBTEX

Xian, X., Pohlkamp, T., Durakoglugil, M. S., Wong, C. H., Beck, J. K., Lane-Donovan, C., … Herz, J. (2018). Reversal of ApoE4-induced recycling block as a novel prevention approach for Alzheimer's disease. *ELife*, *7*. https://doi.org/10.7554/eLife.40048

Xie, F., Xiao, P., Chen, D., Xu, L., & Zhang, B. (2012). miRDeepFinder: a miRNA analysis tool for deep sequencing of plant small RNAs. *Plant Molecular Biology*, *80*(1), 75–84. https://doi.org/10.1007/S11103-012-9885-2

Xu, P.-T., Gilbert, J. R., Hui-Ling, Q., Ervin, J., Rothrock-Christian, T. R., Hulette, C., & Schmechel, D. E. (1999). Specific regional transcription of apolipoprotein E in human brain neurons. *American Journal of Pathology*, *154*(2), 601–611. https://doi.org/10.1016/s0002-9440(10)65305-9

Xu, Q., Bernardo, A., Walker, D., Kanegawa, T., Mahley, R. W., & Huang, Y. (2006). Profile and Regulation of Apolipoprotein E (ApoE) Expression in the CNS in Mice with Targeting of Green Fluorescent Protein Gene to the ApoE Locus. *The Journal of Neuroscience*, *26*(19), 4985. https://doi.org/10.1523/JNEUROSCI.5476-05.2006

Xu, Q., Brecht, W. J., Weisgraber, K. H., Mahley, R. W., & Huang, Y. (2004). Apolipoprotein E4 domain interaction occurs in living neuronal cells as determined by fluorescence resonance energy transfer. *Journal of Biological Chemistry*, *279*(24), 25511–25516. https://doi.org/10.1074/jbc.M311256200

Xu, Q., Walker, D., Bernardo, A., Brodbeck, J., Balestra, M. E., & Huang, Y. (2008). Intron-3 retention/splicing controls neuronal expression of apolipoprotein E in the CNS. *Journal of Neuroscience*, *28*(6), 1452–1459. https://doi.org/10.1523/JNEUROSCI.3253-07.2008

Yan, K., Gao, L. N., Cui, Y. L., Zhang, Y., & Zhou, X. (2016). The cyclic AMP signaling pathway: Exploring targets for successful drug discovery (review). *Molecular Medicine Reports*, *13*(5), 3715–3723. https://doi.org/10.3892/MMR.2016.5005/HTML

Yassa, M. A., & Stark, C. E. L. (2011). Pattern separation in the hippocampus. *Trends in Neurosciences*, *34*(10), 515. https://doi.org/10.1016/J.TINS.2011.06.006

Yin, J. X., Turner, G. H., Lin, H. J., Coons, S. W., & Shi, J. (2011). Deficits in spatial learning and memory is associated with hippocampal volume loss in aged apolipoprotein e4 mice. *Journal of Alz*

Yin, J., Turner, G., Coons, S., Maalouf, M., Reiman, E., & Shi, J. (2014). Association of Amyloid Burden, Brain Atrophy and Memory Deficits in Aged Apolipoprotein E4 Mice. *Current Alzheimer Research, 11(3), 283–290. https://doi.org/10.2174/1567205011031403292200 07*

Yong, S. M., Lim, M. L., Low, C. M., & Wong, B. S. (2014). Reduced neuronal signaling in the ageing apolipoprotein-E4 targeted replacement female mice*. Scientific Reports, 4(1), 1–9. https://doi.org/10.1038/srep06580*

Youn, J., Ellenbroek, B. A., van Eck, I., Roubos, S., Verhage, M., & Stiedl, O. (2012). Finding the right motivation: Genotype-dependent differences in effective reinforcements for spatial learning. *Behavioural Brain Research, 226(2), 397–403. https://doi.org/10.1016/j.bbr.2011.09.034*

Zalocusky, K. A., Najm, R., Taubes, A. L., Hao, Y., Yoon, S. Y., Koutsodendris, N., … Huang, Y. (2021). Neuronal ApoE upregulates MHC-I expression to drive selective neurodegeneration in Alzheimer's disease. *Nature Neuroscience, 24(6), 786–798. https://doi.org/10.1038/s41593-021-00851-3*

Zannis, V. I., Breslow, J. L., Utermann, G., Mahley, R. W., Weisgraber, K. H., Havel, R. J., … Blum, C. (1982). Proposed nomenclature of apoE isoproteins, apoE genotypes, and phenotypes*. Journal of Lipid Research, 23(6), 911–914. https://doi.org/10.1016/s0022-2275(20)38094-9*

Zannis, V. I., VanderSpek, J., & Silverman, D. (1986). Intracellular modifications of human apolipoprotein E. *Journal of Biological Chemistry, 261(29), 13415–13421. https://doi.org/10.1016/S0021-9258(18)67033-4*

Zannis, V. I., Kardassis, D., Ogami, K., Hadzopoulou-Cladaras, M., & Cladaras, C. (1990). Transcriptional Regulation of the Human Apolipoprotein Genes. *Front Biosc, 1–23. https://doi.org/10.1007/978-1-4684-5904-3_1*

Zerbi, V., Wiesmann, M., Emmerzaal, T. L., Jansen, D., Beek, M. Van, Mutsaers, M. P. C., … Kiliaan, A. J. (2014). Resting-state functional connectivity changes in aging apoe4 and apoe-ko mice. *Journal of Neuroscience, 34(42), 13963–13975. https://doi.org/10.1523/JNEUROSCI.0684-14.2014*

Zhang, J., Lin, L., Dai, X., Xiao, N., Ye, Q., & Chen, X. (2021). ApoE4 increases susceptibility to stress-induced age-dependent depression-like behavior and cognitive impairment. J*ournal of Psychiatric Research, 143, 292–301. https://doi.org/10.1016/J.JPSYCHIRES.2021.09.029*

Zhang, J., Lin, Y., Dai, X., Fang, W., Wu, X., & Chen, X. (2019). Metformin treatment improves the spatial memory of aged mice in an APOE genotype–dependent manner. *FASEB Journal, 33(6), 7748–7757. https://doi.org/10.1096/fj.201802718R*

Zhao, N., Ren, Y., Yamazaki, Y., Qiao, W., Li, F., Felton, L. M., … Bu, G. (2020). Alzheimer's Risk Factors Age, APOE Genotype, and Sex Drive Distinct Molecular Pathways. *Neuron, 106(5), 727–742.e6. https://doi.org/10.1016/J.NEURON.2020.02.034*

Zhong, N., Ramaswamy, G., & Weisgraber, K. H. (2009). Apolipoprotein E4 domain interaction induces endoplasmic reticulum stress and impairs astrocyte function. *Journal of Biological Chemistry, 284(40), 27273–27280. https://doi.org/10.1074/jbc.M109.014464*

Zhu, Y., Nwabuisi-Heath, E., Dumanis, S. B., Tai, L. M., Yu, C., Rebeck, G. W., & Ladu, M. J. (2012). APOE genotype alters glial activation and loss of synaptic markers in mice. *Glia, 60(4), 559–569. https://doi.org/10.1002/GLIA.22289*

Zola-Morgan, S., Squire, L. R., & Amaral, D. G. (1986). Human amnesia and the medial temporal region: Enduring memory impairment following a bilateral lesion limited to field CA1 of the hippocampus. *Journal of Neuroscience, 6(10), 2950–2967. https://doi.org/10.1523/jneurosci.06-10-02950.1986*

Zola-Morgan, S., & Squire, L. R. (1986). Memory Impairment in Monkeys Following Lesions Limited to the Hippocampus*. Behavioral Neuroscience, 100(2), 155–160. https://doi.org/10.1037/0735-7044.100.2.155*

Zott, B., Busche, M. A., Sperling, R. A., & Konnerth, A. (2018). What happens with the circuit in Alzheimer's disease in mice and humans? *Annual Review of Neuroscience, 41, 277–297. https://doi.org/10.1146/annurev-neuro-080317-061725*

APPENDIX

Supplementary materials

Supplementary Table 2.1: Primer efficiency and R^2 values for individual primers used for RT-qPCR assays designed in Chapter five.

Gene target	Efficiency (%)	R2
c-Fos	97.9	0.994
APOE	91.7	0.998
Mto1	104.6	0.990
TRMU	109.4	1.000
ActB	104.1	0.998
CPSF4	109.8	0.999

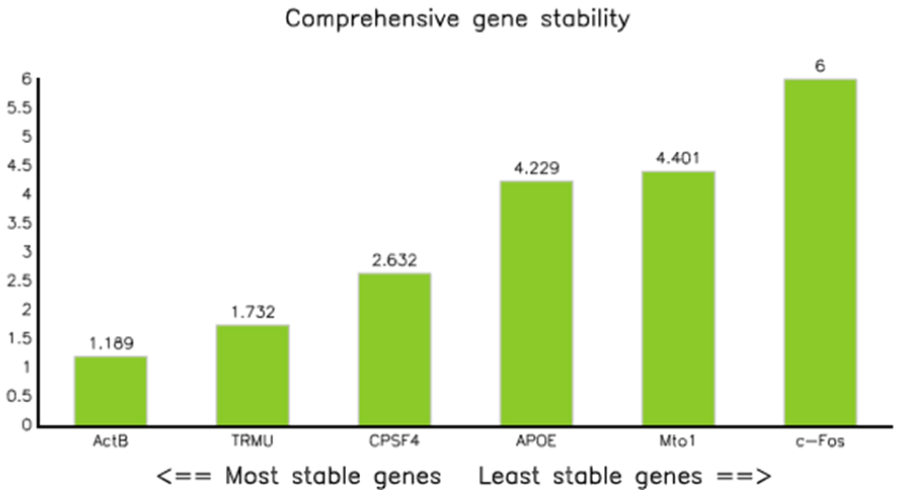

Supplementary Figure 2.1: Example output from Reffinder software using raw Ct values from all samples used in experiments conducted in Chapter five (N = 81), across reference genes (ActB, TRMU, CPSF4, Mto1) and genes of interest (c-Fos, APOE). Y-axis Values represent consensus rank index of stability of genes based on algorithms from Delta Ct, BestKeeper, Normfinder, and Genorm (Xie et al., 2012).

Supplementary Table 3.1: Statistical analysis of place preference during T2 probe trials at each possible target position (32) relative to chance (3.13%) in the mBM task in Chapter three experiment three. Relevant target and foil positions on the maze, statistic, and correction to Holm-Bonferroni criteria is provided. "Above" corresponds to preference for a given position significantly above chance, "Below" corresponds to significantly below chance, and "ND" corresponds to not significantly different from chance. Note, that despite performing analysis at individual positions, only the target and directly adjacent foil remain significantly above chance following correction, with the majority of foils either no different from, or significantly below chance preference, suggesting a specific preference for the target.

Position	*t*	df	*p*	HB survival
Target	7.18	35	<.001	Above
2	5.52	35	<.001	Above
3	2.22	35	0.033	ND
4	3.16	35	0.003	ND
5	3.78	35	0.001	Below
6	2.47	35	0.018	ND
7	1.73	35	0.092	ND
8	3.61	35	0.001	Below
9	2.15	35	0.039	ND
10	1.51	35	0.139	ND
11	1.05	35	0.299	ND
12	2.60	35	0.014	ND
13	2.10	35	0.043	ND
14	2.57	35	0.014	ND
15	3.41	35	0.002	ND
16	3.89	35	<.001	Above
17	-3.69	35	0.001	Below
18	-3.25	35	0.003	ND
19	-4.99	35	<.001	Below
20	-7.25	35	<.001	Below
21	-7.95	35	<.001	Below
22	-8.30	35	<.001	Below
23	-7.37	35	<.001	Below
24	-9.36	35	<.001	Below
25	-9.80	35	<.001	Below
26	-9.48	35	<.001	Below
27	-8.35	35	<.001	Below
28	-11.02	35	<.001	Below
29	-6.17	35	<.001	Below
30	-4.46	35	<.001	Below
31	-3.45	35	0.001	Below
32	-4.53	35	<.001	Below

Supplementary Table 4.1: Model fit parameters for random intercepts and all primary variables and interactions in mixed models of measure variables used in analysis in Chapter four. For each measure the AIC (Akaike information criterion), Log likelihood (LL), and p-values are provided. In each case, significantly lower values of AIC and LL give an indication of better model fit, expected when incorporating variables that significantly predict the given measure variable. Note in place preference, this was not the case, reflected in the lack of significant main effects in primary analyses.

Measure	Trial type	Age	Model	AIC	Log Likelihood	*p*
Path length						
	Training (D1-8)	3-18-months	Random intercept Vs intercept	9962.20	-4978.10	0.010
			Random intercept Vs full model	9737.61	-4850.81	<.001
Errors						
	Training (D1-8)	3-18-months	Random intercept Vs intercept	5169.42	-2581.71	<.001
			Random intercept Vs full model	4980.29	-2472.14	<.001
Learning index						
	Training (D1-8)	3-18-months	Random intercept Vs intercept	1790.06	-893.03	0.002
			Random intercept Vs full model	1782.74	-888.37	<.001
Place preference						
	T2 probe trials	3-18-months	Random intercept Vs intercept	1325.53	-659.77	0.023
			Random intercept Vs full model	1334.01	-657.00	0.596
Separation accuracy						
	T2 probe trials	3-18-months	Random intercept Vs intercept	1003.45	-498.72	<.001
			Random intercept Vs full model	994.06	-479.03	0.001

Supplementary Table 4.2: Statistical analysis of place preference for the target location relative to chance (11.11%) during T2 and T5 probe trials across age in experiments conducted in Chapter four. Trial type, age, and relevant statistical values are provided.

Measure	Trial type	Age	*t*	*p*
Place preference (%)				
	T2 probe trials	3-months	5.21	<.001
		6-months	6.19	<.001
		9-months	6.00	<.001
		12-months	7.54	<.001
		15-months	7.65	<.001
		18-months	6.56	<.001
	T5 probe trials			
		3-months	6.51	<.001
		18-months	6.44	<.001

Supplementary Table 4.3: Statistical analysis of separation accuracy during T2 and T5 probe trials at 18-months age in experiments conducted in Chapter four. The coefficient for the effect of separation is only shown to be significant following extended (4-trial), but not single (1-trial) reinforcement. Corresponds to Figure 4.7D.

Measure	Trial type	Age	Variable	Coefficient	SE	CI lower	CI upper	*t*	*p*
Reward:foil ratio (separation accuracy)									
	T2 probe trials	18-months	Separation	-0.01	0.06	-0.12	0.10	-0.12	0.825
	T5 probe trials	18-months	Separation	0.24	0.09	0.05	0.42	3.00	0.015

Supplementary Table 4.4: Statistical analysis of search errors across trials and age during 4-hour and 12-hour ITI trials in experiments conducted in Chapter four. F and p-values are provided for the effect of trial at each age. Note that the effect of trial is not significant at 12 & 18-months during 4-hour ITI trials, and 9, 12, and 18-months during 12-hour ITI trials. This suggests that within-day learning was not significant during extended ITI trials as a function of age.

Measure	Trial type	Variable	Age	F	*p*
Errors					
	4-hour ITI	Trial	6-months	8.72	<.001
		Trial	9-months	3.69	0.015
		Trial	12-months	1.37	0.258
		Trial	15-months	3.80	0.013
		Trial	18-months	1.86	0.144
	12-hour ITI	Trial	6-months	7.28	0.000
		Trial	9-months	2.23	0.090
		Trial	12-months	1.30	0.281
		Trial	15-months	4.80	0.004
		Trial	18-months	0.76	0.523

Supplementary Table 5.1: Statistical analysis of hippocampal NeuN+ neuron densities by hippocampal subregion in APOE-TR mice in Chapter five experiment one. Relevant main effects are represented. Results correspond to Figure 5.1C and Supplementary Figure 5.1.

Measure	Subregion	Variable	Statistic
Estimated NeuN density	**CA1**	Sex	F(1,69) = 0.21, p = .814
		Genotype	F(2,69) = 0.07, p = .931
		Age	F(1,69) = 0.38, p = .539
	CA3	Sex	F(1,69) = 0.46, p = .499
		Genotype	F(2,69) = 0.47, p = .629
		Age	F(1,69) = 0.61, p = .439
	DGS	Sex	F(1,69) = 1.62, p = .207
		Genotype	F(2,69) = 0.07, p = .937
		Age	F(1,69) = 0.07, p = .797
	DGI	Sex	F(1,69) = 0.29, p = .595
		Genotype	F(2,69) = 0.20, p = .818
		Age	F(1,69) = 0.01, p = .913

Supplementary Table 5.2: Correlation analysis of hippocampal c-Fos neuron densities between regions corrected for multiple comparisons using Bonferroni criterion. Correction applied to 12 tests at alpha = 0.05, corrected alpha = 0.0042. "s" and "ns" correspond to significant or non-significant according to the corrected alpha criterion. Results correspond to Figure 5.1C and Supplementary Figure 5.15.

Condition	Subregion	*r*	*p*	Bonferroni
E3-TR females 3-12 months				
	CA1-CA3	0.75	0.003	s
	CA1-DG	0.34	0.256	ns
	CA3-DG	0.24	0.431	ns
E4-TR females 3-12 months				
	CA1-CA3	0.85	<.001	s
	CA1-DG	0.78	0.003	s
	CA3-DG	0.60	0.039	ns
E3-TR males 3-12 months				
	CA1-CA3	0.83	<.001	s
	CA1-DG	0.74	0.004	s
	CA3-DG	0.83	<.001	s
E4-TR males 3-12 months				
	CA1-CA3	0.64	0.006	ns
	CA1-DG	0.46	0.061	ns
	CA3-DG	0.55	0.021	ns

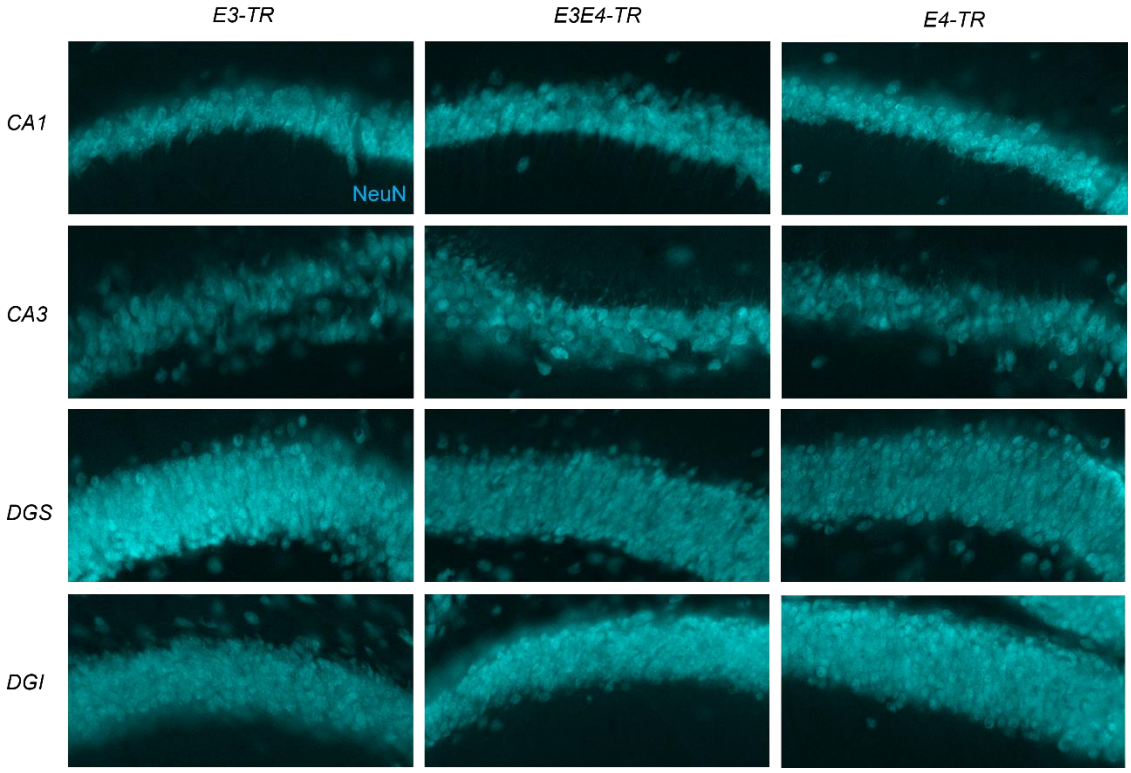

Supplementary Figure 5.1: Representative NeuN immunofluorescence labelling in CA1, CA3, DGS, and DGI primary pyramidal/granule cell layers of APOE-TR mice used in Chapter five, experiment one. No discernible differences were detected between genotypes in estimated NeuN+ neuron density in any individual subregion. Relevant figure and statistics are provided in section 5.8.1.

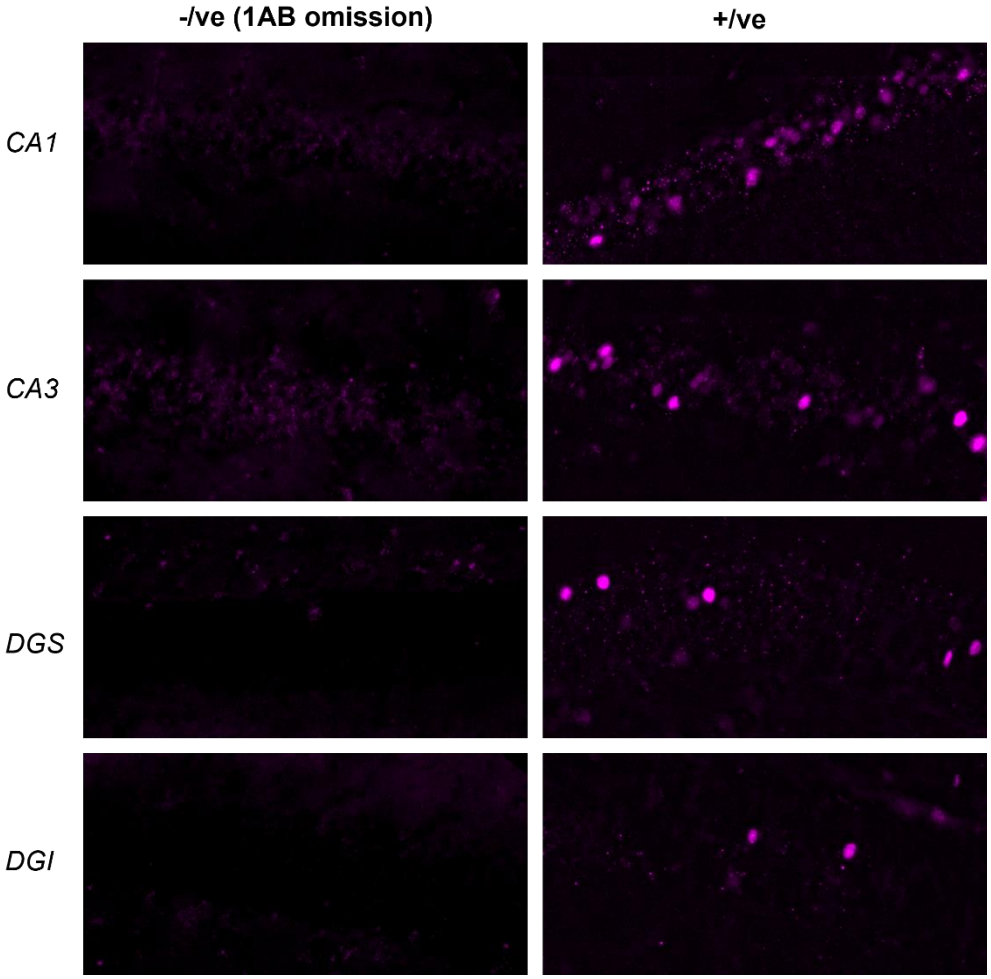

Supplementary Figure 5.2 panel 1: Representative c-Fos immunofluorescence labelling in CA1, CA3, DGS, and DGI primary pyramidal/granule cell layers of APOE-TR mice used in Chapter five experiment one. Panels represent primary antibody omission negative control and positive control, respectively. Note, contrast was enhanced in control images to allow background visibility. Minor tissue autofluorescence (corresponding to 488nm excitation) was visible, particularly within CA3, although intensity was low relative to c-Fos signal, and interference was minimal under contrast standardised conditions.

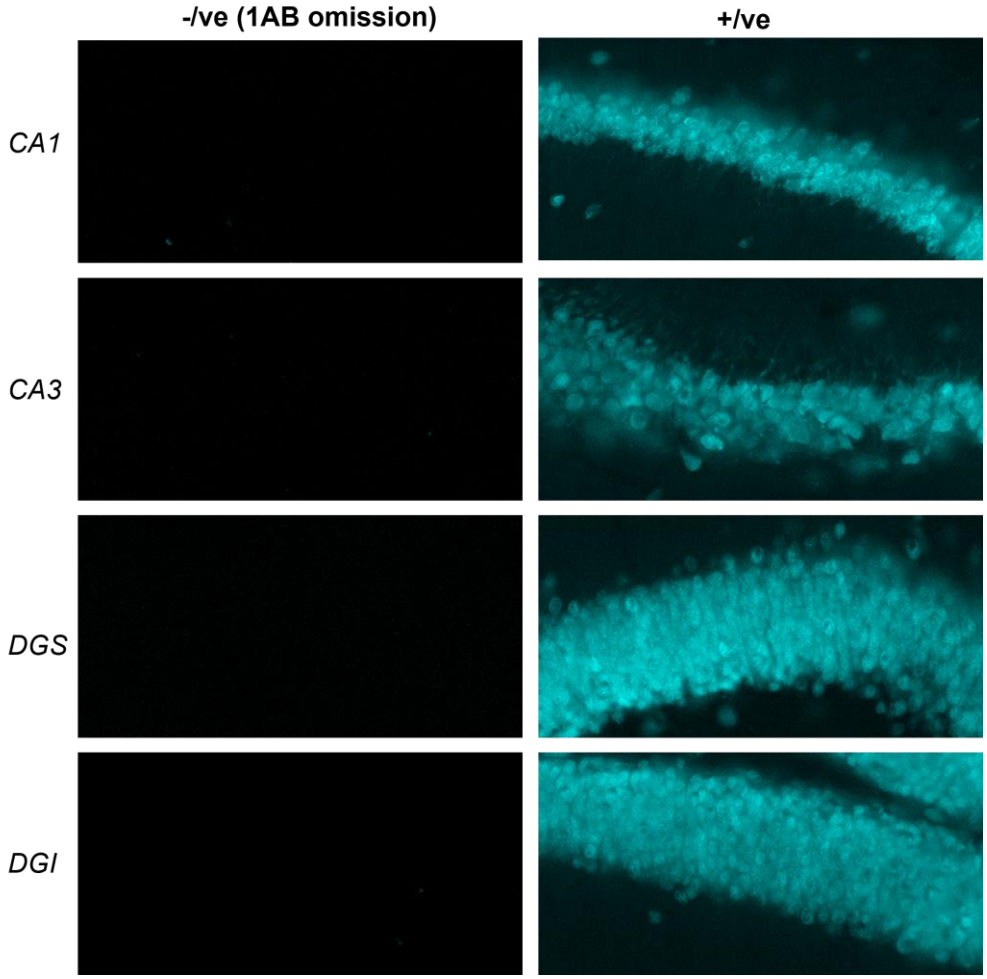

Supplementary Figure 5.2 panel 2: Representative NeuN immunofluorescence labelling in CA1, CA3, DGS, and DGI primary pyramidal/granule cell layers of APOE-TR mice used in Chapter five experiment one. Panels represent primary antibody omission negative control and positive control, respectively. Note, contrast was enhanced in control images to allow background visibility, however background was almost completely absent (corresponding to 633nm excitation).

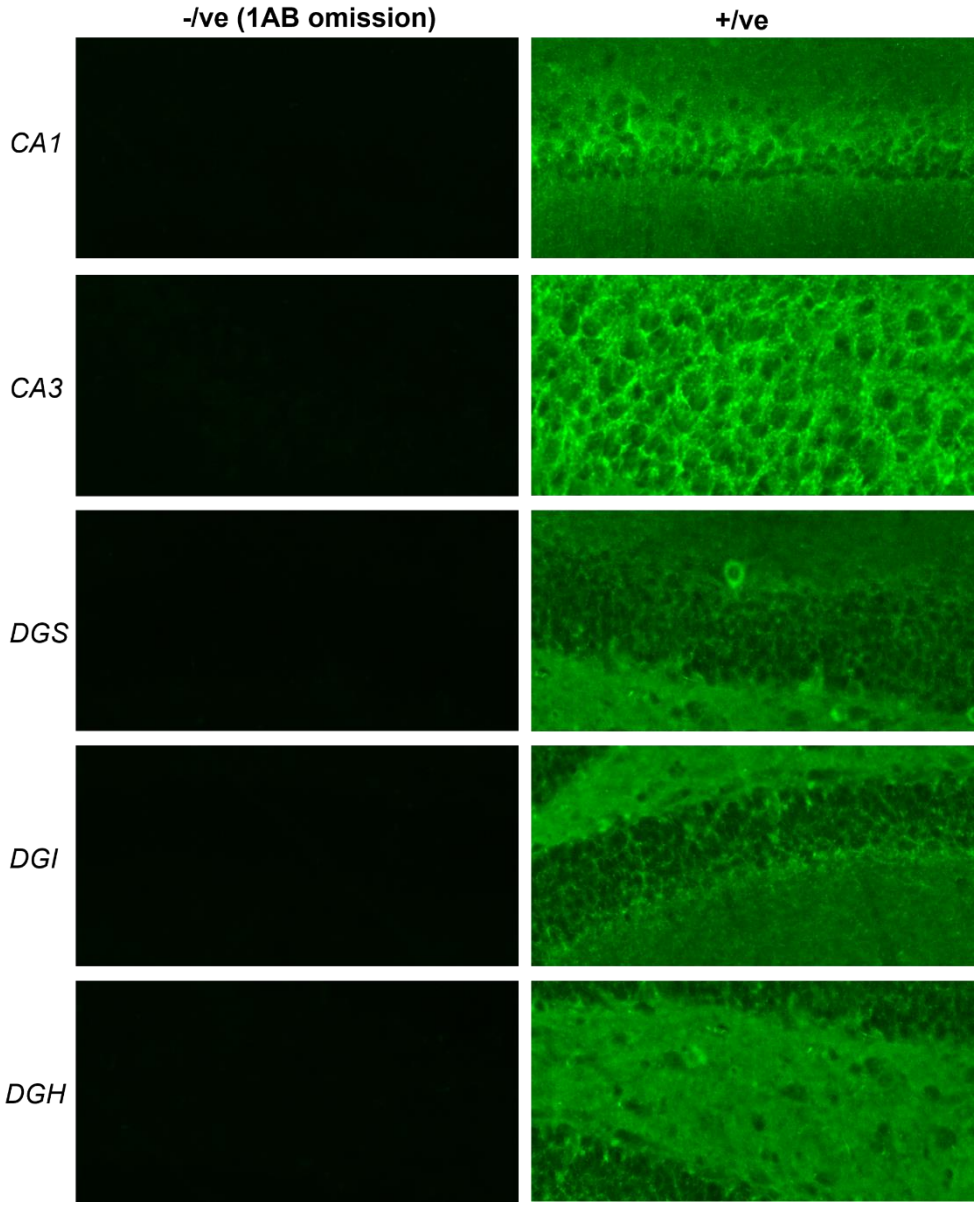

Supplementary Figure 5.2 panel 3: Representative GAD-67 immunofluorescence labelling in CA1, CA3, DGS, DGI, and DGH primary pyramidal/granule/hilar cell layers of APOE-TR mice used in Chapter five experiment one. Panels represent primary antibody omission negative control and positive control, respectively. Background was very low, with some minor elevation outside of primary cell layers (corresponding to 561nm excitation).

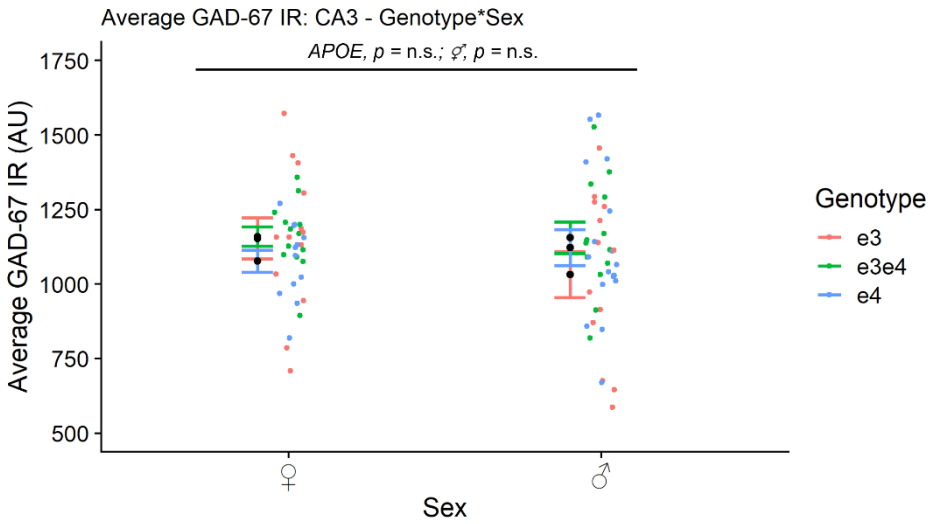

Supplementary Figure 5.3: Average GAD-67 immunoreactivity (IR) in the CA3 pyramidal cell layer of APOE-TR mice, expressed as the mean fluorescence intensity, grouped by genotype and sex. Brackets and labels represent relevant statistical main effects, interactions and pairwise comparisons where appropriate. Individual points represent the IR measurement averaged across sections within a single animal. Error bars represent mean +/- SEM. Sex grouping is represented by "♀" and "♂" overlay.

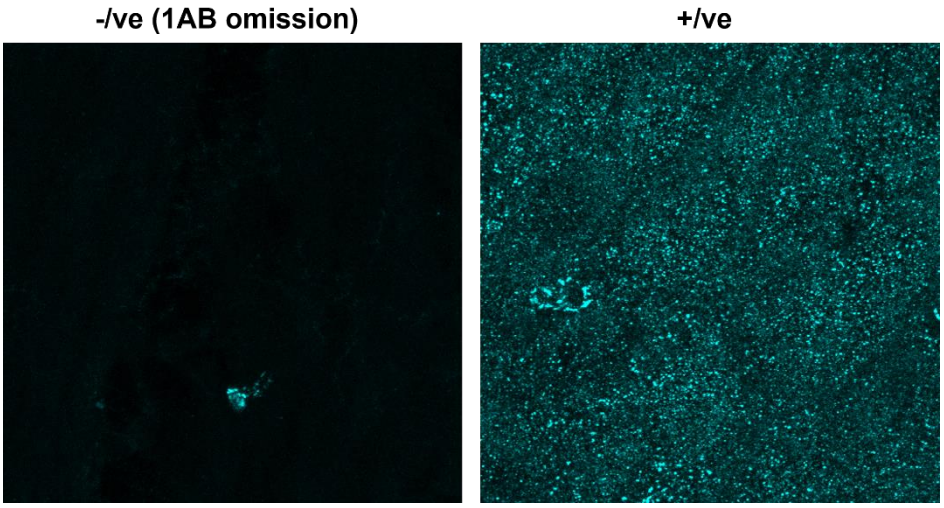

Supplementary Figure 6.1: Representative Bassoon immunofluorescence labelling in CA1 pyramidal and radiatum/oriens layers of APOE-TR mice used in Chapter six experiment three. Panels represent primary antibody omission negative control and positive control, respectively. Image in this case was taken using an SP8 confocal microscope at 63x magnification. Observed background was low, with some minor elevation outside of primary cell layers (corresponding to 633nm excitation).